Dissertation zur Erlangung des Doktorgrades
der Fakultät für Chemie und Pharmazie
der Ludwig-Maximilians-Universität München

Development of helical aromatic oligoamide foldamers for protein recognition

Florian Jean-François Sanchez

aus

Bourgoin-Jallieu, France

2025

Erklärung

Diese Dissertation wurde im Sinne von § 7 der Promotionsordnung vom 28. November 2011 von Herrn Prof. Dr. Ivan Huc betreut.

Eidesstattliche Versicherung

Diese Dissertation wurde eigenständig und ohne unerlaubte Hilfe erarbeitet.

München, den 15.10.2025

Unterschrift: _____

Florian Sanchez

Dissertation eingereicht am 20.10.2025

1. Gutachter: Prof. Dr. Ivan Huc

2. Gutachter: Prof. Dr. Vladimir Torbeev

Mündliche Prüfung am 12.12.2025

Acknowledgments

First and foremost, I would like to express my deepest gratitude to Prof. Dr. Ivan Huc for giving me the opportunity to pursue my PhD within his group. His unwavering support, insightful guidance, and scientific rigor have been crucial throughout this journey, and I am truly thankful for the trust he placed in me.

I am also sincerely grateful to Dr. Céline Douat for her generous advice and encouragement throughout these years. Your patience, and kindness have played a vital role in my progress, many of my successes would not have been possible without you.

I would also like to extend my gratitude to Dr. Lucile Fischer for her valuable insights and support, especially during my time in Bordeaux.

I am very grateful to have worked with very nice colleagues in this group, Jiaojiao Wu, Dr. Lizeth Bodero, Nikolas Schneider, Niklas Böcher, Giorgio Del Castello, Ilaria Guissani, Dr. Alexandru Grozavu, Dr. Tulika Chakrabortty, Dr. Lisa Gourdon-Grünewaldt, Dr. Lars Allmendinger, Ivan Alonso, Dr. Arundhati Roy, Dr. Shuhe Wang, Dr. Vasilii Morozov, Dr. Ryan Howard, Dr. Daniel Gill, Dr. Robin Hess, Dr. Kathrin Aftahy, Dr. Deepak and Dr. Sebastian Dengler, their support and help carried me through my journey.

Specially, our Boyz group, thanks again so much to Dr. Mathieu Denis, Manuel Loos, Ignacio Muñoz-Alonso and Johannes Sigl for the guidance and help, the laughs and for our strict 1pm lunches together.

Collaborative work played a significant role in shaping the various projects I undertook during my PhD. I am especially grateful to the team in Budapest, Dr. Petra Sőregi, Dr. Márton Zwillinger, Dr. Márton Csékei, and Dr. András Kotschy, for the engaging discussions and fruitful collaboration. I also deeply appreciated the opportunity to work with the team in Stockholm, and I would like to warmly thank Dr. Johan Nilvebrant and Prof. Dr. Per-Åke Nygren for their valuable input and support.

I am deeply grateful to my friends, both near and far, who have been a constant source of encouragement, laughter, and perspective throughout this journey. Your support, whether through late-night conversations, spontaneous distractions, or simply being there, has helped me stay grounded and reminded me of the joy beyond the lab bench.

Last but certainly not least, I want to thank my husband for his wholehearted support throughout this chapter of our lives. Your patience, encouragement, and steady presence have carried me through the most challenging moments of this journey. I leaned on you more times than I can count, and I am deeply grateful to have you by my side.

Table of Contents

Acknowledgments 3
1. List of publications 7
2. Abstract 8
3. Introduction 9
3.1. Targeting protein surfaces through molecular recognition 9
3.1.1. Targeting protein surfaces: a key strategy for modulating protein-protein and protein-nucleic acid interactions 9
3.1.2. Occurrence of PPIs and PNIs in natural systems 10
3.1.2.1. Protein-protein interactions 10
3.1.2.2. Antibodies and Nanobodies 10
3.1.2.3. Protein-nucleic acid interactions 12
3.2. Protein-mediated surface recognition 14
3.2.1. Mini immunoglobulin-based scaffolds 15
3.2.2. Non-immunoglobulin scaffolds 17
3.3. Synthetic molecules to recognise protein surfaces 18
3.3.1. Nucleic acids 18
3.3.2. α-Helices 19
3.3.2.1. Stabilisation of α-helices 19
3.3.2.2. Mimicry of α-helices 21
3.3.3. Macrocyclic peptides 23
3.3.3.1. Use of peptide macrocycles with non-canonical amino acids 23
3.3.3.2. m-RNA display selection 24
3.3.3.3. Flexible *in vitro* translation and RaPID selection 25
3.3.4. Molecular glues 26
3.4. Aromatic oligoamides foldamers for protein surface recognition 27
3.4.1. Generalities on AOFs 27
3.4.2. Peptide-foldamers macrocycle hybrids 30
3.4.3. AOFs as DNA mimics 31
3.4.4. AOFs as α-helix mimics 33
4. Objectives 35
5. References 37
6. Development of a vast library of abiotic aromatic building blocks and implementation of automated solid phase foldamer synthesis 44
6.1. Publication: Development of aromatic foldamer building blocks bearing multiple biogenic side chains 46
6.2. Supporting information: Development of aromatic foldamer building blocks bearing multiple biogenic side chains 57

6.3. Publication: Optimisation and automation of of helical aromatic oligoamide foldamer solid-phase-synthesis 180
6.4. Supporting information: Optimisation and automation of of helical aromatic oligoamide foldamer solid-phase-synthesis 191
7. Decoding aromatic helix recognition: β-sheets vs. α-helices 222
7.1. Introduction 223
7.2. Results and discussion 224
7.2.1. Phage display selection, characterisation of the selected clone and structural comparison with C10 224
7.2.2. X-ray crystal structure and characterisation of the binding 226
7.2.3. Structural comparison with affitin C10 227
7.2.4. Ala-scan mutagenesis of affibody clone G02 229
7.2.5. Foldamer mutagenesis study and binding affinity 229
7.3. Conclusion and perspectives 233
7.4. Supporting information: chemical synthesis 235
7.4.1. Materials 235
7.4.2. General methods for HPLC analysis and purification, LCMS and NMR analyses 235
7.4.3. Generalities on solid phase foldamer synthesis (SPFS) 236
7.4.4. Syntheses of oligomers 238
7.4.5. Characterisation data 249
7.5. Supporting information: biochemistry, biophysical measurements, and binding analyses 279
7.5.1. Material and general methods 279
7.5.2. Expression and purification of proteins 281
7.5.3. Protein expressions and characterisation 283
7.6. Crystallography 309
7.7. References 310
8. Targeting the NEMO-di-ubiquitin complex by mimicking the interaction of the coiled-coil NEMO with AOFs 312
8.1. Introduction 313
8.2. Structural information on coiled-coil NEMO and linear di-ubiquitin 314
8.3. Design and strategy for the mimicry 315
8.3.1. Protein construct choice Ub(H68C) 315
8.3.2. AOF designs for mimicry 317
8.4. Results and discussion 318
8.4.1. Syntheses of AOF candidates 318
8.4.2. Protein overexpression and purification 321
8.4.3. Ligation chemistry and adduct formation 322

8.4.4. Structural elucidation of adducts via NMR analysis 324
8.4.5. Structural elucidation of covalent adducts via crystallisation assays 325
8.5. Conclusion and perspectives 326
8.6. Experimental part : chemical synthesis 328
8.6.1. Materials 328
8.6.2. General methods for HPLC analysis and purification, LCMS and NMR analyses 328
8.6.3. Generalities on solid phase foldamer synthesis (SPFS) 330
8.6.4. AOFs syntheses and characterisation 332
8.6.5. Characterisation data 336
8.7. Experimental part: protein expression 346
8.7.1. Material and general methods 346
8.7.2. Expression and purification of proteins 347
8.7.3. Protein expressions and adduct characterisation 349
8.7.4. Adduct characterisation via NMR 356
8.8. References 360
9. Conclusion and perspectives 362
9.1. Summary of the thesis projects 362
9.2. Perspectives 363

1. List of publications

Published:

V. Corvaglia, F. Sanchez, F. S. Menke, C. Douat and I. Huc, Optimization and Automation of Helical Aromatic Oligoamide Foldamer Solid-Phase Synthesis. *Chem. Eur. J*. **2023**, 29, e202300898. (doi.org/10.1002/chem.202300898).

(**Section 6.3.**)

M. Zwillinger[#], P. Sőregi[#], F. Sanchez[#], C. Douat, M. Csékei, I. Huc* and A. Kotschy*, Development of Aromatic Foldamer Building Blocks Bearing Multiple Biogenic Side Chains. *J. Org. Chem*. **2025**, 90, 8, 3043-3052. (doi.org/10.1021/acs.joc.4c02900).

[#]Equal contributors

(**Section 6.1.**)

2. Abstract

Protein-protein interactions (PPIs) are key regulators of cellular signaling and represent promising yet complex therapeutic targets. Advances in chemical biology and structural computational tools now enable the design of molecules to modulate these interfaces. Inspired by natural biopolymer folding, aromatic oligoamide foldamers (AOFs) offer synthetically accessible, stable helical frameworks with predictable side-chain orientation, making them attractive candidates for functional design and drug discovery.

This thesis presents the design and synthesis of novel building blocks for AOFs, enhancing the chemical diversity of the quinoline (**Q**) scaffold through targeted substitutions at positions 4, 5, 6, and 4,6. New methodologies enabled the incorporation of diverse biogenic side chains: cationic, anionic, polar, and hydrophobic. These new building blocks broaden the capabilities of AOFs for biomolecular recognition. Mechanistic studies of solid phase foldamer synthesis (SPFS) led to optimised protocols for automated synthesiser, allowing efficient parallel production of up to three AOF sequences. Making use of the newly established protocols and biogenic side chains, an AOF was designed and synthesised to randomly recognise a library of protein (affitin and affibody), clones were identified and submicromolar binding was observed for the racemic Q_{12} AOF candidate. We discovered an AOF capable of binding two structurally distinct protein scaffolds: β-sheet-based (affitin) and α-helical (affibody) selected via mRNA and phage display, respectively. Solution studies enabled truncation of the AOF to its minimal binding epitope. Notably, the AOF exhibits enantioselective recognition of both targets, driven by its intrinsic *P*-handedness. In an attempt to target the bio-relevant interaction between linear di-ubiquitin and the coiled-coil domain of NEMO, AOFs candidates were designed to mimic the interaction of the coiled-coil on the surface of the ubiquitin. Each AOF incorporated covalent linkers via triphosgene activation and an activated disulphide for site-specific ligation. Solution-state NMR confirmed local environmental perturbations upon ligation, although initial crystallisation attempts were unsuccessful. Modifications to linker length and side-chain composition enabled reproducible crystal formation, yet structural resolution remained limited due to poor diffraction and asymmetric unit complexity.

In conclusion, this work highlights the synthetic versatility and functional potential of aromatic oligoamide foldamers (AOFs). The integration of diverse biogenic side chains and streamlined automated protocols enabled the generation of AOFs with submicromolar affinities for distinct protein targets. These findings underscore the promise of AOFs as adaptable molecular tools for protein recognition and interface mimicry in biologically relevant contexts.

3. Introduction

3.1. Targeting protein surfaces through molecular recognition

3.1.1. Targeting protein surfaces: a key strategy for modulating protein-protein and protein-nucleic acid interactions

Protein-protein interactions referred as PPIs play a central role in regulating cellular signalling pathways, making them highly attractive targets for therapeutic applications. PPIs were often considered as challenging or “undruggable”, but recent advances in chemical biology, structural analysis, or screening technologies have improved the ability to design molecules which can target these interactions. The increasing number of validated PPI modulators has shown that targeting protein interfaces is not only feasible but now also showing significant attention. Some compounds are even progressing beyond discovery into clinical trials.[1-3] With these developments, PPIs have emerged as a promising option for innovative drug design, offering new strategies to modulate complex biological processes.

PPIs take place on the protein surface, known as interface domains. These interfaces can form either stable complexes or more transient, dynamic associations, depending on the biological context and function.[4] Although hydrogen bonds and electronic interactions are important, PPIs are mostly driven by hydrophobic effects.[5] Unlike enzymes, PPIs often lack well-defined structural features such as deep binding pockets or clefts that typically guide drug design. Because of this, enzyme active sites, though they involve protein interactions, are generally not classified as PPIs when it comes to drug discovery efforts. Studies have shown that large hydrophobic or uncharged polar residues are more often involved in the interface of interaction between proteins. These residues are usually qualified as “hot spots”, whereas charged residues are more frequently exposed to the solvent.[6]

The interfaces are the results of clusters of hot spots residues in close proximity either exposed at the surface of the proteins or isolated in pockets. Although tools for prediction have become extremely reliable, notably with the recent application of computational protein design which got awarded by the Nobel Prize of Chemistry in 2024[7-9], numerous proteins possess disordered regions or are completely disordered in solution. It is only upon binding to their partner that these proteins are stabilised enough so that they can be studied.[10] More than half of the eukaryotic proteome is estimated to consist of natively unfolded proteins, with many containing significant intrinsically disordered regions under normal physiological conditions.[11]

In order to understand PPIs, a range of structural and biophysical techniques can be used. X-ray crystallography[12] and cryo-electron microscopy (cryo-EM)[13] offer high-resolution snapshots of protein complexes, while NMR spectroscopy can reveal binding sites in solution

via chemical shift perturbation.[14] To measure binding affinities, isothermal titration calorimetry (ITC)[15] and surface plasmon resonance (SPR)[16] are commonly applied. ITC quantifies heat changes during binding, making it suitable for soluble, natural proteins, but less reliable for hydrophobic ligands or interactions with low enthalpy changes. SPR as well as biolayer interferometry (BLI)[17] usually involve immobilised proteins on sensor chips or tips and provide reproducible measurements across a wide concentration range.

3.1.2. Occurrence of PPIs and PNIs in natural systems

3.1.2.1. Protein-protein interactions

More than 30% of protein secondary structures are α-helices, making them the most common structural motif. Given their abundance, many PPIs involve α-helices, making them a broadly relevant and useful scaffold for designing inhibitors.[18] Consequently, if a α-helix is present at a PPI interface, a synthetic mimetic that reproduces its key recognition features could serve as a competitive inhibitor. A well-known example to illustrate this strategy is the binary complex between p53 and hDM2 proteins. The essential p53 transcription factor protein is a tumour suppressor protein that is often referred as the guardian of the genome. Under normal conditions, the p53 protein levels are evaluated in cell by hDM2/X proteins, which together ubiquitinate p53 to trigger its proteasome degradation.[19] Developing molecules that can inhibit the p53-hDM2 binary complex formation is therefore a promising strategy for new treatments in cancer therapy. Structural studies revealed that the recognition of $p53_{17\text{-}29}$ by $MDM2_{25\text{-}109}$ involves three helix turns equivalent to twelve residues. The three hot spots residues are all located on the same helix face and are hydrophobic in nature: Phe19, Trp23 and Leu26 (**Figure 1**).

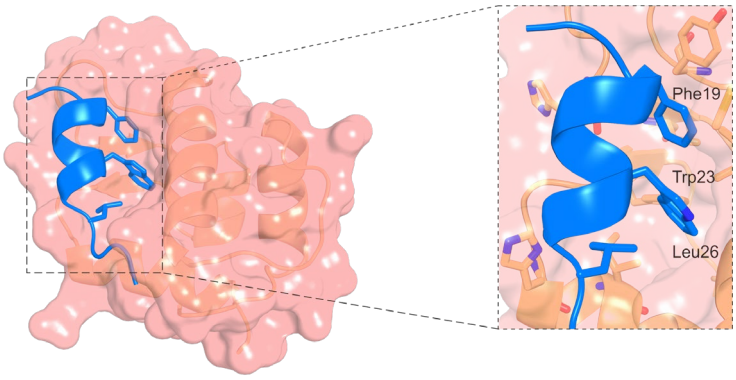

Figure 1. Crystal structure of MDM2 represented in orange and p53 fragment in blue with the three key residues for the binding labelled (PDB#1YCR).[20]

3.1.2.2. Antibodies and Nanobodies

Antibodies, also known as immunoglobulins, are secreted by plasma cells in response to invading pathogens. Their role is to bind to specific antigens on bacteria or viruses, blocking

the infection, tagging them for immune destruction, and promoting their clearance from the body.[21] Structurally, an antibody is a large Y-shaped protein (~150 kDa) and consists of two identical heavy and light chains. Disulphide bonds are bridging the heavy chains together while also linking the light chains to the heavy ones. Both the light and heavy chains possess variable regions (V_L and V_H), which are essential for antigen binding, as well as constant region (C_L and C_H). Antibodies can also be classified into two main parts: the antigen-binding fragments (Fab) as well as the crystallisable fragment (Fc). In the Fab region lies the variable domain (Fv) which interacts with an antigen. This is the most variable part of an antibody. Upon folding, three β-sheets are exposed on the tip of the Y-shaped antibody. These β-sheets are the complementarity-determining regions (CDRs) (**Figure 2a**). These CDRs are in direct interaction with antigens, from large surface antigens to smaller ones.[22]

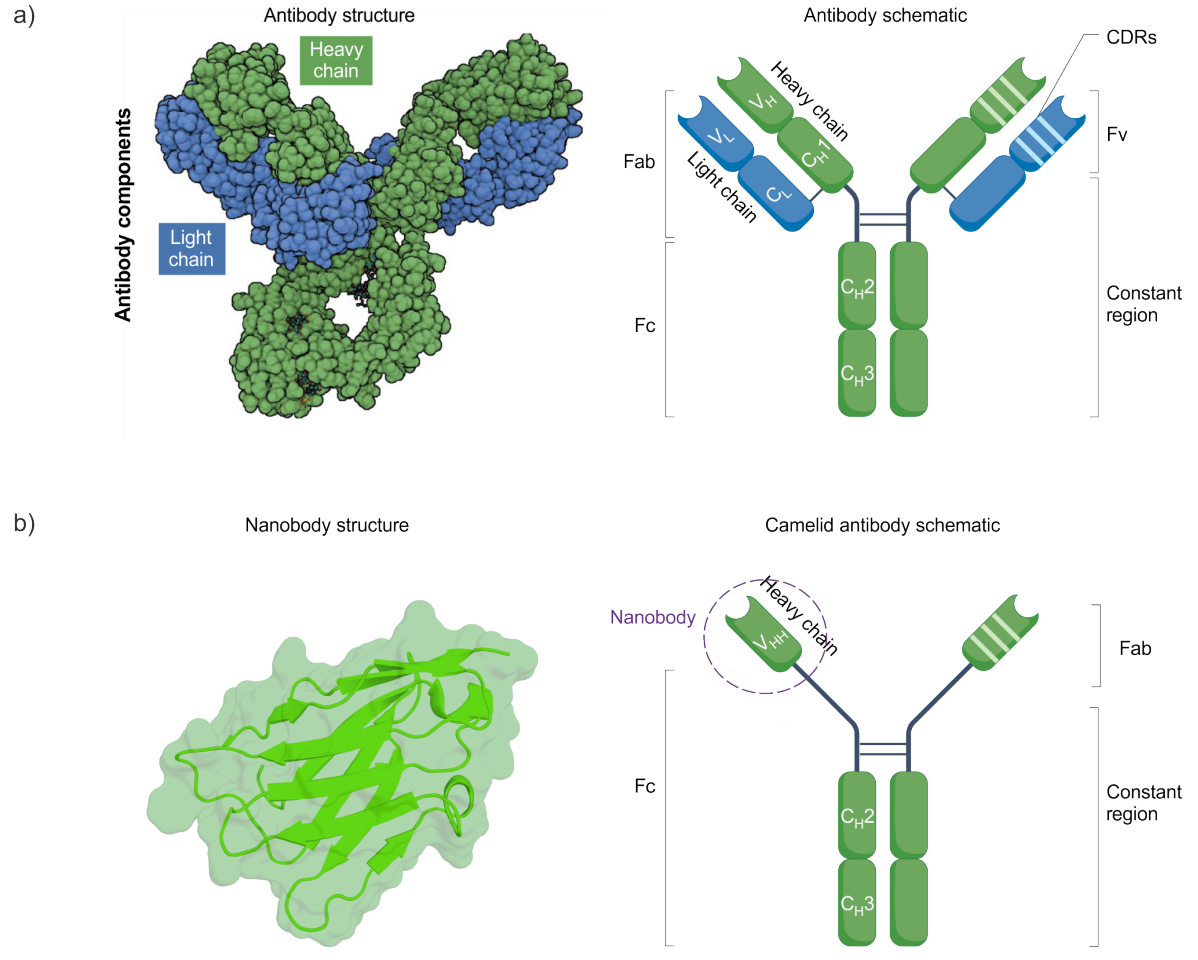

Figure 2. a) Schematic representation of an antibody with its different sections. b) Schematic representation of a camelid antibody and X-ray structure of a nanobody (PDB#2XV6). Schematics adapted from Paul. S *et al.* (2024) [22]

Another class of antibodies, smaller, was discovered 30 years ago in camelids (**Figure 2b**). They consist of heavy-chain only antibodies or hcAbs. They lack light chains and C_H1 domains, but function through their heavy chains only, leaving these biomolecular architectures with a

significant lower molecular weight (~90 kDa).[23] While being smaller, they can bind through a single variable domain called V_{HH} or nanobody.[24] Natural nanobodies usually contain one or two disulphide bonds, which can enhance stability and binding in some cases. However, these bonds are often not essential for proper folding, allowing nanobodies to stay stable and soluble even in reducing environments like the cytosol.[25] This makes them ideal for use in intracellular targeting or modulation of protein function.

3.1.2.3. Protein-nucleic acid interactions

Interactions between DNA and proteins are crucial to numerous cellular processes. This very specific class of proteins is referred as DNA-binding proteins (DBPs); known examples are transcription factors, histones or DNA polymerases.[26] DBPs can be classified into three main categories:

- Binding via α-helices: leucine zippers or helix-turn-helix motifs
- Binding via β-sheets: beta-ribbons or immunoglobulin fold
- Binding via a combination of both: zinc fingers

A common example of DBPs via α-helices are basic leucine zipper or bZIP. This structural motif is composed of two α-helices which interact with each other through hydrophobic contacts between leucine residues. Thanks to their stabilising repeating pattern of leucine or isoleucine every seventh position, or heptad repeat, the α-helices form a coiled-coil domain, and because of this arrangement, the bZIPs function as dimers. The N-terminal region of bZIPs are rich in basic amino-acids residues, responsible for DNA recognition and binding. When unbound, the basic region of bZIPs is mostly disordered, it is only upon binding DNA that one of the helices interacts with DNA base pairs while the other interacts with the phosphate backbone and thus folds into an helical arrangement.[27] The transcriptional factor GCN4 is a well-studied example of bZIPs; its structure is composed of a leucine zipper directing the coiled-coil formation followed by a basic-residues region interacting specifically with the major groove of a DNA (**Figure 3**).[28]

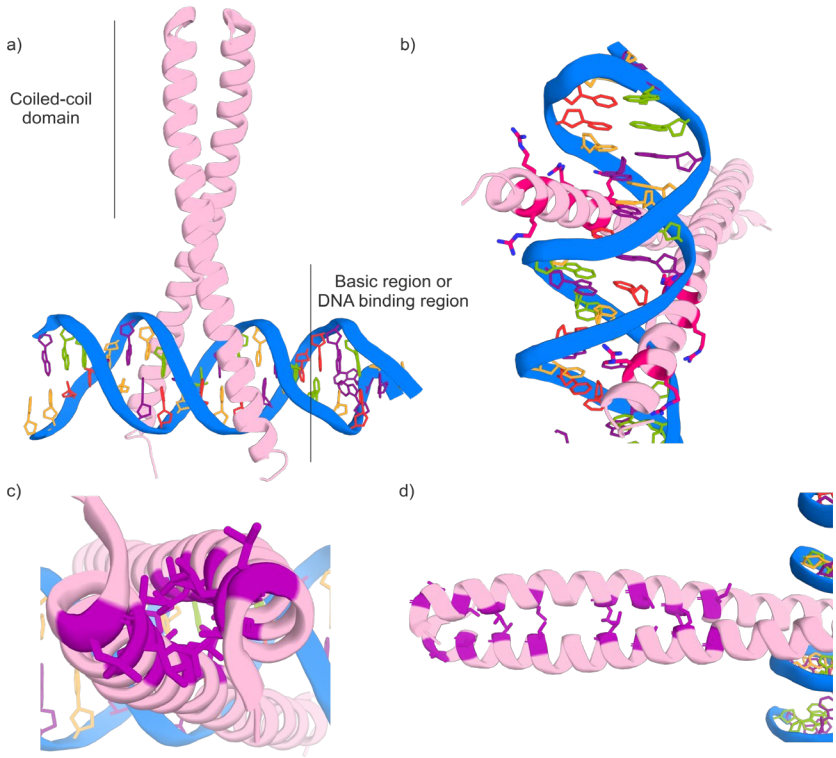

Figure 3. a) Basic leucine zipper motif of GCN4 bound to DNA segment (PDB#1YSA). b) Basic region of zipper with pink arginine residues highlighted in contact with the phosphodiester backbone. c) Top view of the coiled-coil domain with leucine, valine and methionine residues highlighted in purple. d) Side view of the coiled-coil domain.

While many proteins bind DNA through α-helices, some rely on β-ribbon. It is a common feature found in bacteriophage and prokaryotes. A classic example is the TATA-binding protein (TBP), which uses β-ribbons to bind the TATA box in DNA. To do this, it bends the DNA by 80 degrees, which helps to expose the sequence and makes the binding more effective.[29] The HU protein is a small, DNA-binding protein found in prokaryotes which helps organise and compact the bacterial chromosome. It binds non-specifically to DNA through β-ribbons (**Figure 4**).[30]

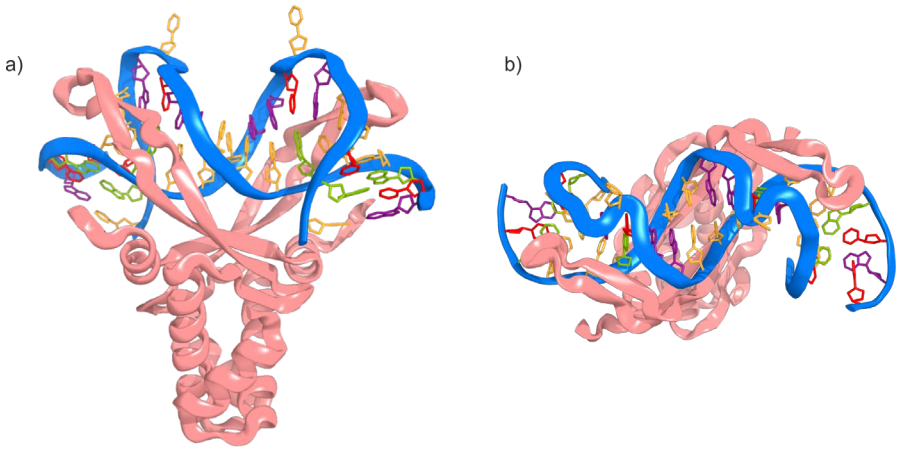

Figure 4. a) X-ray structure of Anabena HU-DNA complex (PDB#1P71). b) Top view of the complex exposing the DNA sequence.

Zinc finger motifs represent about 3% of the human genome. It is a small motif composed of, on average thirty amino acid residues. Usually, a zinc cation is coordinating to two cysteines and two histidines which stabilises the fold. This motif provides the protein with a specific shape that allows it to fit into the major groove of DNA and bind to it.

One of the first zinc finger discovered was in the transcription factor IIIA of TFIIIA from *Xenopus leavis* oocytes. It was shown that nine tandem zinc fingers motifs recognise specifically DNA sequences of the 5S RNA gene (**Figure 5**).[31-33] Structural data revealed a complex between $TFIIIA_{10\text{-}188}$ with six zinc fingers. Fingers 1-3 bind to the major groove of a 31 bp duplex DNA, fingers 4 and 6 play the role of spacers while finger 5 makes contact with bases in the major groove.[34]

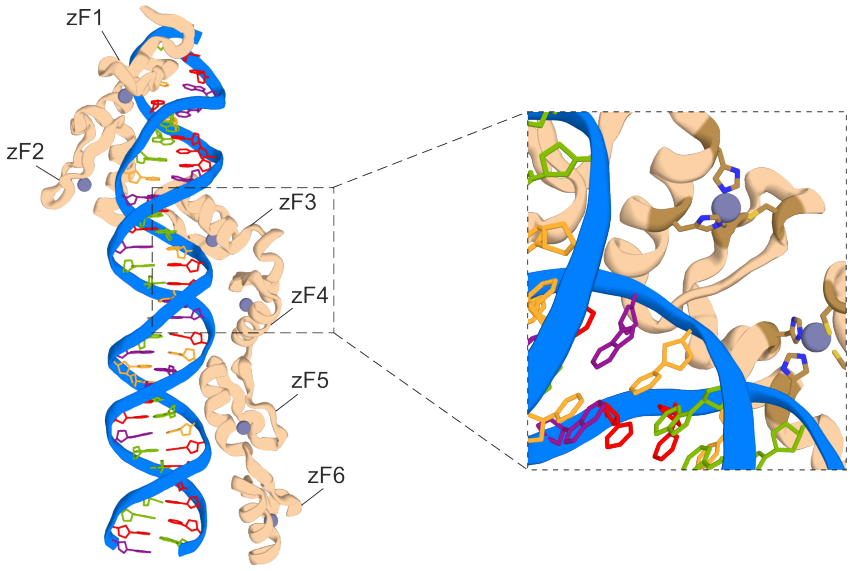

Figure 5. X-ray structure of TFIIIA with 6 zinc fingers, in brown are highlighted the residues in contact with the zinc cations (PDB#1TF6).

3.2. Protein-mediated surface recognition

Identifying protein binders for a specific target remains a central objective in research, but achieving this is often challenging and complex. Various technologies and methods have been developed and used extensively to achieve this goal. Phage display selection is a well-established technique first described by George Smith in 1985 and was recognised in 2018 with the Nobel Prize in Chemistry.[35]

Phage display selection is a cyclic *in vitro* process used to identify peptides or proteins (*e.g.* antibodies) that specifically bind to a target molecule (**Figure 6**). The process starts with the expression of a very diverse library by bacteriophages (~10^{10} individuals) displaying various peptides or antibody fragments. These phages convey the genetic material of the unique peptides. The library is then incubated with the immobilised target, allowing specific binders

to attach. Unbound or weakly bound phages are removed through washing, and the tightly bound phages are eluted. These selected phages are amplified in *E. coli*, and the process is repeated for multiple rounds to enrich high-affinity binders. Finally, individual clones are screened, sequenced, and characterised for binding specificity and affinity, enabling the discovery of target-specific molecules.[36] Among the high-affinity antibody fragments discovered using this technique is adalimumab, known for being the first humanised antibody approved for clinical use.[37]

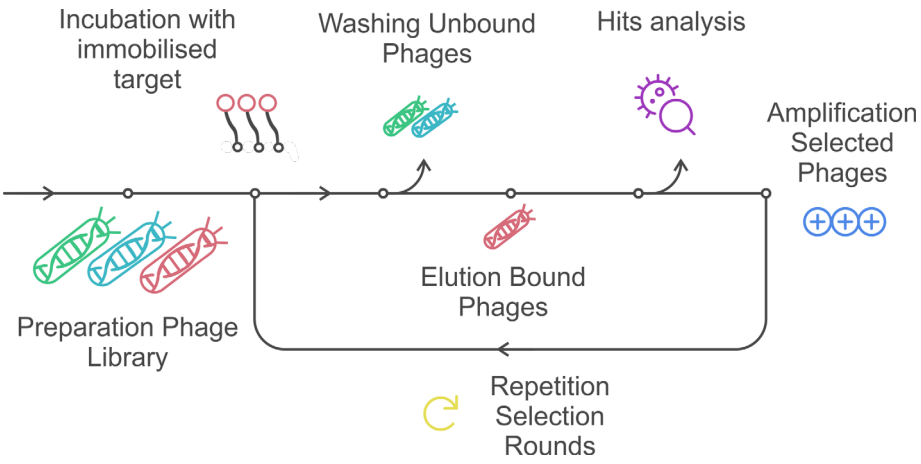

Figure 6. Schematic representation of the phage display selection technique. The immobilised target is incubated with the phage library, unbound phages are washed away. Phages carrying binders are eluted and can be amplified in *E.Coli*. They are then re-utilised in the next round of selection.

3.2.1. Mini immunoglobulin-based scaffolds

Despite their broad usefulness, whole antibodies possess numerous limitations. Their structure, which relies on disulphide bonds, renders them unsuitable for expression within the reducing environment of the cytoplasm, thereby limiting intracellular applications. Furthermore, their relatively large binding sites are not able to access certain hidden epitopes, such as enzyme active sites.[38] Only a few kinase inhibitors such as imatinib and the EGFR inhibitor lapatinib, exhibit high selectivity. In contrast, most approved kinase inhibitors interact with 10 to 100 off-targets, which may include other kinases, enzymes, and even proteins from unrelated families.[39] Antibodies are also typically monospecific, which may reduce therapeutic versatility. Additionally, they are difficult to produce in microbial systems, often requiring costly mammalian cell lines for expression.[40]

Even if immunoglobulins possess some drawbacks, they are still a natural scaffold for protein recognition. Studies demonstrated that out of the twelve CDRs displayed on an antibody, only the third CDR of the heavy chain in the variable domain makes large contact surface.[41] These findings indicate that it is possible to design antibody-like binding proteins using scaffolds smaller than the traditional V_H-V_L domains (~25 kDa). Smaller scaffolds not only retain binding

potential but also fall within the size range compatible with current NMR techniques, making structural characterisation more feasible.

In this sense, several scaffolds derived from the essential part for recognition of antibodies were studied. The following scaffolds are all accessible via phage-display selection. The fragment antigen-binding region or Fab (**Figure 7a**) is composed of both constant and variable regions of an antibody. While they are still heavy scaffolds (~50 kDa), several therapeutics are derived from these scaffolds. For example, abciximab is a FDA-approved drug which acts as an antiplatelet.[42] The single-chain variable fragment or scFv (**Figure 7b**) is an engineered fusion between the variable regions V_H and V_L of an antibody. They are linked with a short peptide chain which allows for more flexibility and solubility. The scFv size range is around 25 kDa. They have shown promising results in cancer gene therapy by improving the specificity of gene delivery vectors.[43-44] A smaller category, which was introduced earlier in section **3.1.2.2**, are the nanobodies (**Figure 7c**). Many researches are currently focusing on nanobodies and their potential therapeutic applications.[45]

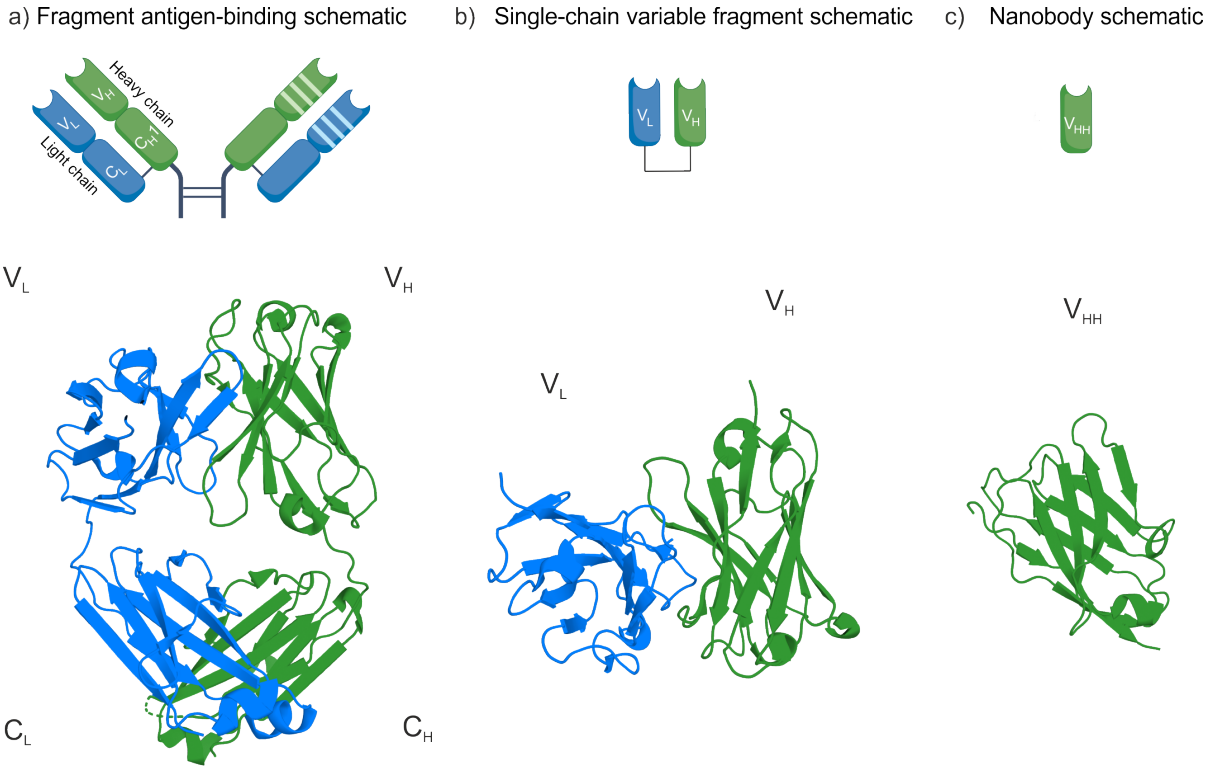

Figure 7. a) Schematic representation of a Fab with X-ray structure (PDB#8FAB). b) Schematic representation of a scFv with X-ray structure (PDB#6J9O). c) Schematic representation of a Nanobody with X-ray structure (PDB#2XV6). Notably, the scale of the structures was kept consistent to better illustrate the relative sizes of the scaffolds. Schematics adapted from Paul. S *et al.* (2024) [22]

3.2.2. Non-immunoglobulin scaffolds

Although monoclonal antibodies (mAbs) offer high potency and greater specificity compared to small-molecule drugs and can be engineered to bind almost any protein epitope, their large size and hydrophilic nature prevent them from accessing intracellular targets. Furthermore, their ability to penetrate solid tumour tissue is often limited, which can reduce therapeutic efficacy. Several engineered non-antibody scaffolds, on which high-affinity binders can be selected are being explored as promising alternatives in cancer therapy. The aim is to overcome some of the limitations of antibody-based scaffolds.

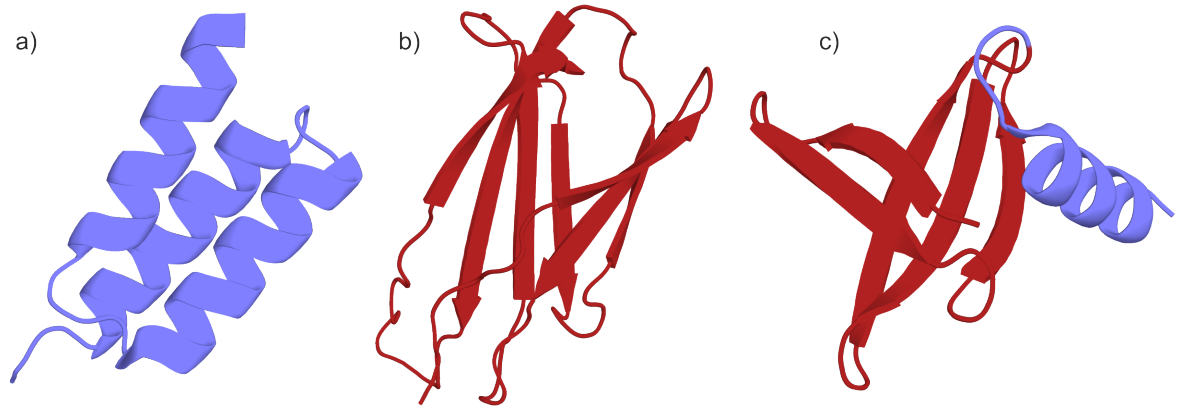

Figure 8. a) Structure of an affibody (PDB#3MZW). b) Structure of a monobody (PDB#1TTG). c) Structure of a nanofitin (PDB#4CJ2). α-helices are represented in blue and β-sheets in dark red.

The affibody scaffold is derived from the B domain of *Staphylococcal* protein A, a small (~6.5 kDa) three α-helix structure originally involved in binding the Fc region of immunoglobulin G (**Figure 8a**).[46] Researchers engineered a version called the Z domain by synthesising the B domain and randomising 13 surface residues in the first two helices to create a library for target-specific binder selection via phage display.[47] Recently, researchers have made significant progress in developing affibodies that specifically target the Human Epidermal Growth Factor Receptor 2 (HER2) for personalised cancer treatment.[48]

Monobodies are small engineered scaffold based on the fibronectin type III domain, FN3 (~10 kDa).[49] Fibronectin is a central structural protein made of repeating I, II, and III domains. The human FN3 domain possess 15 repeating units. Monobodies are based on the tenth unit of human FN3. It is a small, monomeric unit that folds into a β-sheet (**Figure 8b**) similar to antibody V_H domains but with seven β-strands instead of nine.[41] Monobodies have been developed to target SH2 domains, which mediate central phosphorylated-tyrosine-dependent interactions in cell growth and immune signalling. They have shown specificity against SH2 domains in BCR-ABL, SHP2, and the Src kinase family.[39]

The nanofitin scaffold (~7 kDa), also called affitin, is composed of a β-sheet and a short α-helix (**Figure 8c**). It originated from the DNA binding protein Sac7d family and was first commercialised by the ‘‘Affilogic’’ company.[50] Obtained from a thermophile organism they are usually heat resistant proteins. Studies showed the application of a nanofitin combined to a dye as a non-invasive imaging agent for HER2-positive tumours. In both *in vitro* and *in vivo* models, it demonstrated strong binding specificity and affinity for HER2, along with effective internalisation into HER2-expressing cancer cells.[51]

These engineered scaffolds present several advantages compared to mAbs. They are much smaller, usually around a tenth of the size of regular mAbs, they do not contain any disulphide bridges, which ensures a better recombinant expression yield as well as stability in the reducing environment of cells. They also have been designed so that their stability will not suffer from mutations. In this sense, they can all be used in phage display selection (even ribosome- or yeast- display selections) against targets to find potential strong binders.

3.3. Synthetic molecules to recognise protein surfaces

While nature fabricates with defined shape and finely tuned surfaces for molecular recognition, synthetic molecules are increasingly being designed to replicate or even surpass these bimolecular interactions. Over the past two decades, nucleic acids, α-helix mimics, macrocyclic peptides, or molecular glues have emerged as powerful tools to target protein surfaces. Each of these synthetic strategies offers a distinct way to mimic natural recognition elements or introduce new binding modes. This chapter explores how these molecules are engineered to achieve specificity, stability, and functional activity in complex biological environments.

3.3.1. Nucleic acids

The central role of protein-DNA interactions in the regulation of cell mechanisms has made them interesting targets in drug development, gene therapy and biotechnology. By carefully adjusting how these molecules interact, it can be possible to regulate gene expression or develop innovative treatments.

A major breakthrough in this field was the discovery of the Systematic Evolution of Ligands by Exponential Enrichment or SELEX technique in 1990.[52] This selection method allows for the identification of short single-stranded DNA or RNA sequences (usually <100mer) called aptamers, which can bind with high specificity and affinity to a particular target (**Figure 9**). Just like other selection methods, the first step consists in the creation of a large, randomised library (>10^{10} sequences), in the case of oligonucleotides, presenting a constant region used for amplification afterwards. The entire library is then incubated in the presence of the immobilised target of interest. After a first selection cycle, the unbound sequences are washed

away while the aptamer-target remains bound. These bound aptamers are, in a second phase, detached from the target by elution processes, often by changing salt concentration, pH or temperature. They then go through an amplification step either by PCR for DNA or by reverse transcription and then PCR for RNA. This step allows for an enrichment of the selected aptamers before starting the selection process over multiple times. After each round, the pool of selected aptamers is enriched with the highest affinity binders. Once the enrichment is sufficient enough, the selected aptamers are sequenced and characterised to quantify their binding affinity with the target.[53-54]

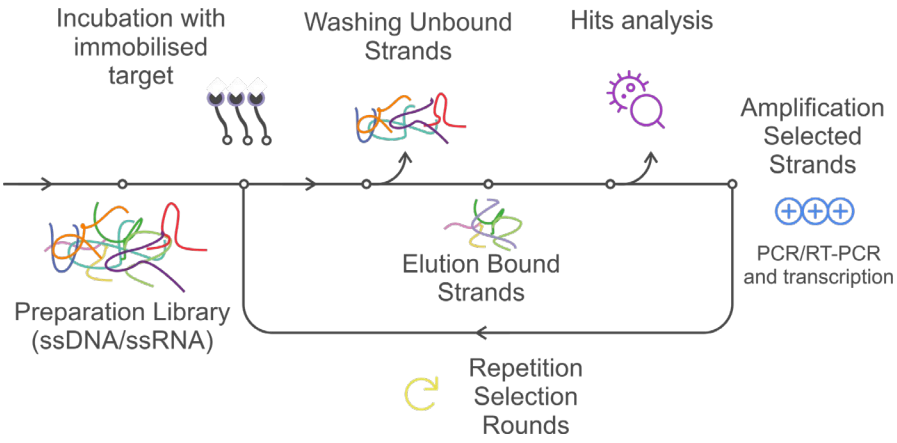

Figure 9. Schematic representation of the SELEX technique. The immobilised target is incubated with a diverse oligonucleotide library. Bound sequences are separated, amplified by PCR, and reintroduced in repeated cycles to enrich for high-affinity binders.

An early example of a variant of the SELEX technique called the toggle SELEX was introduced in 2001.[55] It was developed to generate aptamers, which could recognise homologous species of the same protein. The human thrombin is a key enzyme in the blood coagulation pathway, making the research of antithrombin therapeutics of great interest to prevent or to treat thrombosis. Using the toggle SELEX technique, scientists were able, by alternating rounds of selection between human and porcine thrombin, to find aptamers exhibiting high affinity for both proteins. One of them showed binding affinity in low nanomolar range for both proteins and effectively inhibited clot formation. A truncated derivative of this aptamer exhibited tight binding in addition to improved pharmacological properties, supporting its therapeutic utility.[55]

3.3.2. α-Helices

3.3.2.1. Stabilisation of α-helices

As mentioned before, α-helices are the most common type of secondary structure in proteins. Interestingly, these α-helices regions are often quite short, typically just two to three helical turns long, or about eight to twelve amino acids.[56] This structural observation has inspired the idea that short helical peptides could be engineered to selectively interact with biological

targets. However, when extracted from their native protein context, peptides often lose their defined conformation and exhibit high degree of conformational flexibility. Additionally, small peptides are typically unstable in biological environments, as they are rapidly degraded by proteases. Stabilising peptides in their α-helical conformation could help to address both of these challenges by promoting a defined secondary structure and rendering them less prone to enzymatic degradation.[57]

An approach to stabilise peptides consists in using olefin metathesis chemistry to covalently bind two side chains.[58] Verdine and his team developed a hydrocarbon-stapled version of the p53 transactivation domain using non-natural α-methyl,α-vinyl-disubstituted amino-acid[59] with the aim to restore its function in cancer cells. The chemical staple and the methyl groups lock the peptide into its native α-helical conformation, enhancing its stability and improving its affinity for hDM2. One stapled peptide demonstrated a higher α-helical conformation, stronger binding for hDM2 (410 nM for p53 compared to 55 nM for the stapled peptide) and was able to efficiently enter cells. In cancer cell models overexpressing hDM2, treatment with the stapled peptide reactivated p53-dependent transcriptional pathways and induced apoptosis. This work illustrates how α-helix stabilisation can improve both the structural integrity and intracellular activity of peptides, offering a promising strategy for targeting intracellular protein-protein interactions.[59]

More recently, Arora and his team developed a new approach to stabilise α-helices, the Hydrogen Bond Surrogate strategy or HBS. Unlike the stabilisation method presented before, which can obscure solvent-exposed recognition surfaces or even eliminate key side-chain functionalities, in this strategy the faces of the helix remain accessible. It uses the key stabilising intramolecular hydrogen bond network between the carbonyl oxygen of an amino acid at the *i* position and the hydrogen amide of the amino acid residue at the position *i+4* in a peptide by replacing the hydrogen bond with a carbon-carbon bond synthesised via ring closing metathesis (RCM) chemistry.[60] The authors have further demonstrated the power of this strategy by targeting the gp41 fusion protein of HIV-1, which is a critical mediator of viral entry into host cells. They started by synthesising a peptide version of gp41 containing the known hot spot residues described before[61], Trp628, Trp631 and Ile635, for the formation of the six-helix bundle of gp41 which drives membrane fusion between the virus and the cell. They observed that the 14-residues long peptide did bind weakly with a K_D around 37 μM but Circular Dichroism (CD) measurement demonstrated that the peptide was only 10% helical in nature. By using the HBS strategy and creating a covalent bond between the N-terminus and the Trp at *i+4*, they could not only enhance the helicity of their peptide but also reach similar affinity, around 47 μM and by designing and modifying more their peptide, they could obtain K_D values below 5 μM, proving the strength of their strategy.[62]

3.3.2.2. Mimicry of α-helices

While the stabilisation of α-helices relies predominantly on natural, biotic amino acids, branched or non-natural residues are introduced at defined positions to achieve optimal stapling and helix stabilisation. Many α-helix mimicry strategies employ extensive abiotic or non-peptide scaffold. The main advantage of these abiotic scaffolds is their inherent biological and conformation stability compared to peptides and the possibility to conceive large libraries of building blocks since chemistry could be applied easier on abiotic molecules compared to natural amino acids. The mimicry of α-helices with abiotic scaffolds does not aim to resemble an α-helix but to mimic the projection in space of the natural residues on an abiotic backbone.

Pioneer in this field, Hamilton used terphenyl scaffolds as non-peptide α-helix mimetics. This scaffold was designed to expose side chains on one helical face in *i*, *i+3* or *i+4* and *i+7* (**Figure 10a**). They used these mimics in several PPIs cases and successfully showed the disruption of the interaction for example in the case of p53 with hDM2 with the compound **1** (**Figure 10b**). The binding affinity of this compound with hDM2 was determined by fluorescence polarisation assay at 0.182 μM.^{15}N-HSQC NMR spectroscopy showed that the aryl compound was strongly affecting the residues of hDM2 involved in the binding demonstrating that **1** was indeed recognising the surface of the protein in a similar manner as p53. The stronger binding of **1** can be explained by the addition of a hydrophobic contact in the pocket where normally Trp23 of p53 lies. [63][64]

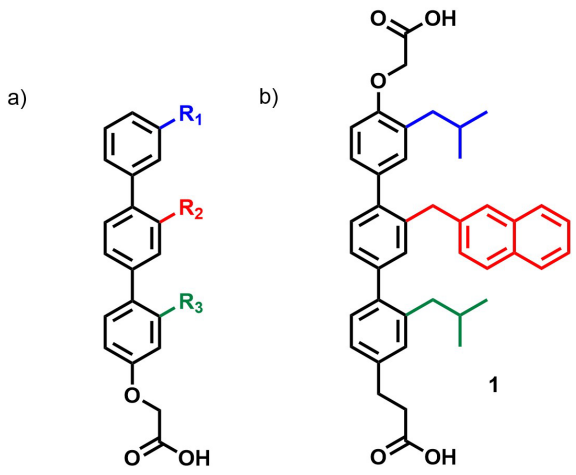

Figure 10. a) Terphenyl scaffold introduced by Hamilton with b) Compound **1** exhibiting a binding of 0.182 μM to the target protein hDM2.

These examples highlight how modifying the side chains on the terphenyl scaffold allows to selectively target various PPIs, much like natural α-helices, which share a common backbone but achieve specificity through diverse side-chain compositions. While terphenyl scaffolds have proven to be valuable for mimicking α-helices, it is not without drawbacks. Their

hydrophobic character makes it difficult to dissolve in water, and their aromatic structure can be challenging to synthesise. To work around these issues, Hamilton mutated some of the aryl rings for pyridines, thus creating a terpyridine version which is easier to synthesise and also more water soluble, all while still effectively providing the right orientation for the exposition of the side chains.[65]

Later, the group of Wilson developed solid-phase synthesis (SPS) of an amide-based aromatic backbone by adapting the conditions developed for solid phase peptide synthesis (SPPS). They first synthesised *N*-alkylated aromatic oligoamides based on *N*-alkylated Fmoc benzoic acid units. Each unit was synthesised to bear hydrophobic, aromatic, and protected cationic side chains. The units were pre-activated into acyl chloride using Ghosez's reagent and coupled overnight. Using this method, they were able to synthesise candidates and tested their inhibition via fluorescence anisotropy competition titration (FAC) and found for compound **2** a half maximal inhibitory concentrating value (IC_{50}) of 2.8 µM for $p53_{15\text{-}31}$/hDM2 complex compared to 1.2 µM for the native truncated $p53_{15\text{-}31}$ (**Figure 11a**).[66] Similarly, they also worked on 3-*O*-alkylated oligoamides, using the same benzamide rigid backbone. A new series of compounds were synthesised on solid support and assessed for their inhibitory properties on hDM2. The authors discovered a promising candidate **3** (**Figure 11b**) with a IC_{50} around 1 µM.[67] However, due to its inherent chemical structure, this candidate was poorly water-soluble which led them to design a more water-soluble substitute bearing a "wet-edge", mainly a hydrophilic triethylene glycol chain. This new candidate **4** showed similar value of IC_{50} compared to the previously discovered compound but with a much higher solubility in aqueous media (**Figure 11b**).

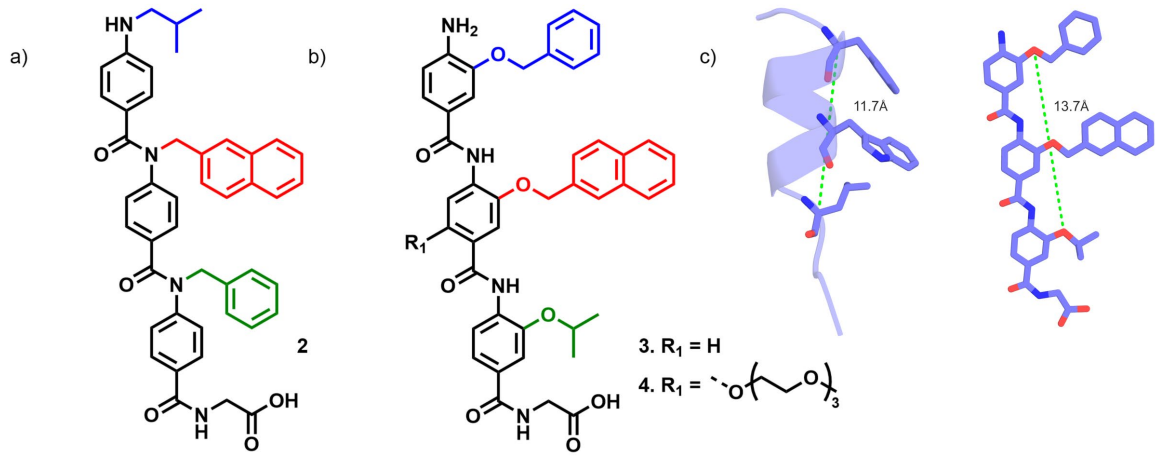

Figure 11. a) Structure of compound **2** used as α-helix mimic for the interaction between $p53_{15\text{-}31}$ and hDM2. b) Structure of compound **3** and its hydrophilic version **4**. c) Structural representation of the segment p53 (on the left) from Glu17 to Asn29. Highlighted are hot-spots residues Phe19, Trp23 and Leu26 (shown in Figure 1). On the right, model of compound **3** displaying its side chains for α-helix mimicry. Highlighted in dashed green lines on both representations are the distances from Cα of Phe19 to Cα of Leu26 and from *exo*-cyclic oxygen atoms on **3**.

3.3.3. Macrocyclic peptides

Linear peptides of middle size are often disordered in water due to their backbone flexibility, leading to higher entropic cost upon binding to their biological target. Constraining their structure makes binding more efficient and selective. In this context, peptide macrocycles have been extensively studied. They offer more rigidity to the backbone which can enhance binding affinity[68], resistance to proteolytic degradation[69] and could also lead to a better cell-permeability.[70] Cyclic peptides can adapt their shape based on the environment. In water, they expose polar groups, but in hydrophobic settings like membranes, they change conformation to hide these groups. This conformational switch enhances membrane permeability and makes them useful for drug delivery.[71] Beyond cyclisation, several chemical strategies improve cyclic peptide permeability, such as N-or Cα-methylation, introducing D-amino acids, or using amide bond isosteres.[72] These modifications enhance stability and help peptides to adopt conformations better suited for crossing cell membranes.

3.3.3.1. Use of peptide macrocycles with non-canonical amino acids

Peptide macrocycles face challenges like poor stability or limited oral bioavailability. To address these, non-natural building blocks such as aromatic heterocycles can be incorporated to enhance structure and function. Inspired by nature's own chemical diversity, synthetic moieties like triazoles, pyrimidines, and furans have been successfully used to fine-tune the properties of macrocycles, expanding their therapeutic potential beyond natural limitations.[73] Replacing certain amino acids in peptides with flat, rigid aromatic groups helps lock the macrocycle into stable conformations, enabling secondary structures not accessible to short linear peptides. These stabilised shapes can mimic natural binding motifs, making them effective at targeting PPIs. Such modifications enhance binding affinity, specificity, enzymatic stability, and lipophilicity aspects that collectively improve biological performance and cell permeability.[74]

Recently, the group of Heinis has reported that bicyclic peptides can be stabilised by small hydrophilic molecules.[75] They explored their previously described method[76], where a small *C*3 symmetrical organic molecule, tris(bromomethyl)benzene (TBMB), was implemented to react with selected peptide libraries against a relevant target containing three cysteine residues. The cysteine residues are positioned at the N-terminus, the C-terminus and in the middle of the peptide sequence. In a later study, they reported new hydrophilic and hydrogen bonding small stabilising molecules 1,3,5-triacryolyl-1,3,5-triazinane (TATA) and *N,N',N''*-(benzene-1,3,5-triyl)-tris(2-bromoacetamide) (TBAB), which can be also tethered to peptide sequences bearing three cysteine residues to form bicycles. A cysteine-rich peptide library

was developed against human uPa, a protein linked to cancer progression and tissue invasion, and the three scaffolds were used to cyclise the selected peptides. Each scaffold yielded unique high-affinity binders with distinct sequences, showing that the core unit influences peptide structure through specific interactions. X-ray crystal structures confirmed scaffold-peptide contacts at atomic resolution (**Figure 12**).

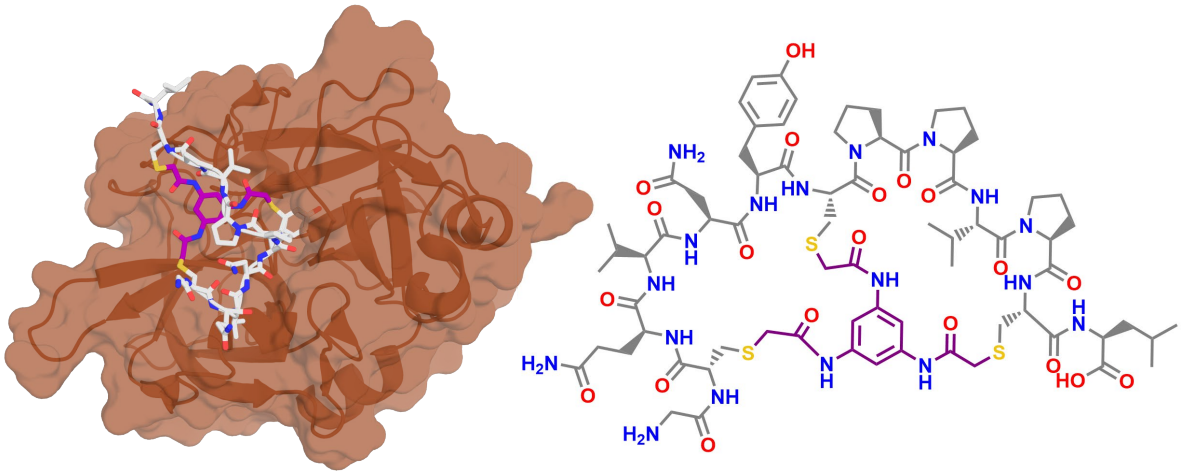

Figure 12. Chemical structure of bicycle UK903 cyclised through three cysteine residues and X-ray crystal structure of UK903 interacting with the protein uPa (PDB#4MNY).

3.3.3.2. m-RNA display selection

First described in 1997 by Roberts and Szostak[77], mRNA display technique is a very powerful *in vitro* selection technique which links each peptide or protein to its own mRNA, allowing the direct identification of high affinity binders for a special target. This technique enables the formation of a physical, covalent linkage between each peptide and the mRNA that encodes its sequence, allowing for a direct identification of the best binders from massive combinatorial libraries often exceeding 10^{12} variants.

The process begins by designing and synthesising a DNA library that encodes a diverse set of peptide or protein sequences. This library is transcribed *in vitro* into mRNA, and a special chemical linker is added at the 3' end of each mRNA. This linker includes a puromycin moiety, a structural mimic of the 3' end of tRNA. During *in vitro* translation, the ribosome moves along the mRNA and synthesises the corresponding peptide. When the ribosome reaches the puromycin at the end of the mRNA, it incorporates the puromycin into the peptide chain, forming a stable covalent bond. This stops the translation and physically links the newly synthesised peptide to its mRNA.

Once the pool of mRNA-peptide fusions is formed, the library is subjected to a selection step. The entire pool is exposed to a target molecule such as a protein, a receptor, or a small molecule immobilised on a solid support. Only the peptides that bind specifically and strongly

to the target remain attached during a series of washing steps, while weaker binders and non-binders are discarded from the selection. After the first round of selection, the mRNA of the bound peptide-mRNA conjugates is recovered and amplified, usually via reverse transcription followed by PCR. This enriched library serves as input for the next round of transcription, translation, selection, and amplification. Multiple iterative rounds allow for the enrichment of the best binders, with increasing strictness applied over successive rounds to favour high-affinity and highly selective peptides.

The first use of mRNA display technique was against ATP, the selection used a large library of more than 10^{12} proteins with a length of 80 randomised amino acids. Through iterative rounds of binding selections, they enriched for proteins that could bind ATP with high affinity. Ultimately, four distinct protein binders were isolated, none bearing resemblance to any known proteins demonstrating that folded, functional protein domains can emerge from completely random sequences. One particularly successful clone exhibited ATP binding with K_D ~100 nM.[78]

3.3.3.3. Flexible *in vitro* translation and RaPID selection

Flexizymes are engineered flexible acylation RNA enzymes, discovered by Suga in 2003[79], they enable the attachment of a wide variety of amino acids including non-canonical ones to specific tRNAs. Combined with the FIT (Flexible *In vitro* Translation) system, they allow the precise incorporation of these amino acids into peptides during *in vitro* protein synthesis.[80] Using the mRNA display technique, acylated tRNAs with non-canonical amino acids can be incorporated into the translation system by removing specific natural components and replacing them with custom ones. The system creates “blank” codons that can be reassigned to new amino acids. These tRNAs recognise specific codons on the mRNA through base pairing, allowing the ribosome to insert the new amino acid into the growing peptide chain. This setup makes it possible to reassign standard genetic codons to custom amino acids, expanding the chemical diversity of the resulting peptides with for example D-amino acids[81], *N*-alkylated amino acids[82] or even β-amino acids.[83] Suga and his team developed a method to induce spontaneous peptide cyclisation by incorporating a chloroacetamide group at the N-terminus of the peptide. This electrophilic moiety selectively reacts with the thiol side chain of the first downstream cysteine, forming a covalent thioether bond and generating a stable macrocyclic structure.[84]

The RaPID (Random non-standard Peptide Integrated Discovery) system generates vast libraries of mRNA-encoded peptide macrocycles by integrating mRNA display with the FIT system (**Figure 13**). This system allows for the creation of a library of peptide macrocycles of more than 10^{12} individuals.[85] An example of this system is its application to the

transmembrane receptor plexin B1 (PlxnB1), which regulates bone cell (osteoblast) differentiation by interacting with semaphorin 4D (Sema4D). Through this selection, Mastunaga *et al.* identified the macrocyclic peptide PB1m6 which binds PlxnB1 with high affinity (K_D = 3.5 nM) and inhibited the interaction with Sema4D. Structural studies demonstrated that PB1m6 binds a site distinct from where Sema4D normally attaches, indicating that the macrocycle acts through an allosteric mechanism to inhibit the receptor.[86]

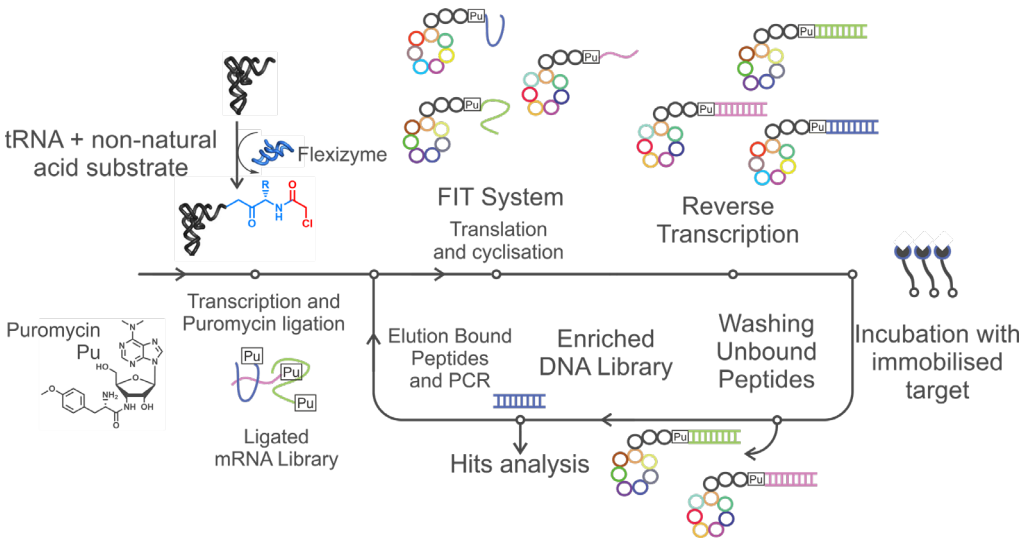

Figure 13. Schematic representation of the RaPID selection. The RaPID selection begins with a semi-randomised DNA library transcribed into a 3'-puromycin mRNA library. Puromycin links the peptide to its encoding mRNA during translation in a FIT reaction, producing peptide-mRNA macrocycle fusions. These are reverse transcribed to cDNA and screened against an immobilised target. High-affinity peptides bound are eluted, then their encoding DNA is recovered by PCR to enrich the library. Repeating this cycle enriches consensus sequences, which are identified by next-generation sequencing.

3.3.4. Molecular glues

Modulating PPIs initially focused on inhibition, a relatively direct strategy. As mentioned before, stabilising PPIs has attracted growing interest due to its unique benefits. Unlike inhibitors, stabilisers enhance naturally occurring interactions rather than competing with existing binding partners, often requiring lower potency. They also tend to bind to specific, transient interfaces formed only when two proteins come together, which can improve selectivity and reduce off-target effects.[87] In this sense, using molecular glues to target PPIs could make accessible the so-called "undruggable" proteins like transcription factors for example.

Immunomodulatory imide drugs (IMiDs) are small molecule acting like molecular glues and protein degraders. Thalidomide, lenalidomide or pomalidomide bind to cereblon (CRBN), which serves as the substrate receptor within the $CRL4^{CRBN}$-E3-ubiquitin ligase complex. Petzold *et al.* showed that lenalidomide redirects this complex to specifically target and degrade CK1α, a process that is crucial to its therapeutic action in certain blood cancers.

Structural studies showed that the drug creates a neosurface which forces the binding to a β-hairpin loop of CK1α.[88] This study emphasises the role of a small drug, which acts as a molecular glue for the degradation of another protein. Another similar example where IMiDs act as molecular glue for the redirection of the ligase to target a new protein is in the presence of the Ikaros zinc-finger transcription factors 1 and 3 (IKZF1 and IKZF3). Lenalidomide redirects the ligase towards IKZF1 and IKZF3 so that the ubiquitination and degradation take place. It is only by the loss of these two proteins that the tumour cell growth can be stopped.[89]

3.4. Aromatic oligoamides foldamers for protein surface recognition

Protein folding has inspired research to design and build synthetic molecules, which could have well-predictable folding features. Seebach introduced β-amino acid oligomers, known as β-peptides in 1996, in which each residue contains an additional α-methylene group compared to α-amino acids. Although this modification might be expected to increase backbone flexibility, β-peptides adopt remarkably well-defined and stable secondary structures, including turns, β-sheet-like arrangement, or helices.[90] Gellman in 1998 was the first to introduce the term of foldamer.[91] Foldamers can go beyond the limitation of the 20 canonical amino-acids that are found in nature. This feature can help providing greater structural diversity and versatility. The building-blocks, to synthesise foldamers, can be assembled via a variety of chemical strategies allowing for the creation of diverse sequences with predictable folding. Foldamer design to mimic natural architectures achieving better predictability while enhancing customisability is currently an expanding field in supramolecular chemistry. The field of foldamers can be divided into two large categories: biotic and abiotic foldamers. Biotic foldamers such as peptoids[92], β-[93], γ-peptides or oligoureas[94] are based on aliphatic backbones derived from α-amino acids while abiotic foldamers are often aromatic backbones such as pyridine[95], benzene[96] or quinoline[97] and offer higher stability.

The following chapter will focus on aromatic oligoamide foldamers (AOFs) and mainly those based on 8-amino-2-quinolinecarboxylic acid units (**Q**).

3.4.1. Generalities on AOFs

Huc and co-workers first described oligomers based on **Q** units for the formation of helical, stable and with high curvature AOFs.[98] Synthetic strategies for AOFs conception generally fall into two categories: solution and solid phase syntheses. While solid-phase synthesis is well-established for peptides, it relies on α-amino acids with reactive amine groups, making its direct application to less reactive aromatic amines more difficult. In this context, early syntheses of AOFs were performed exclusively in solution. Among available methods, acid

chloride activation is typically favoured over classical peptide coupling reagents or reactive esters, as it better accommodates the low nucleophilicity and hindrance of aromatic amines. However, the formation of helical structures during chain elongation significantly reduces reactivity after the first helical turn.

The synthesis of an AOF typically involves repeated deprotection, activation, and coupling cycles (**Figure 14**), often requiring purification after each step, which makes solution-phase synthesis labour-intensive and limits its applicability. In contrast, solid-phase synthesis is well-suited for these targets and has been optimised by the Huc group.[99] For aromatic amines, Fmoc-protected **Q** units are converted to acid chlorides *in situ*, while standard peptide coupling reagents are used for aliphatic amines. Interestingly, the folding of AOFs during synthesis becomes advantageous on solid support, as their helical structure protrudes from the resin and prevents aggregation, which is a common issue in peptide synthesis.

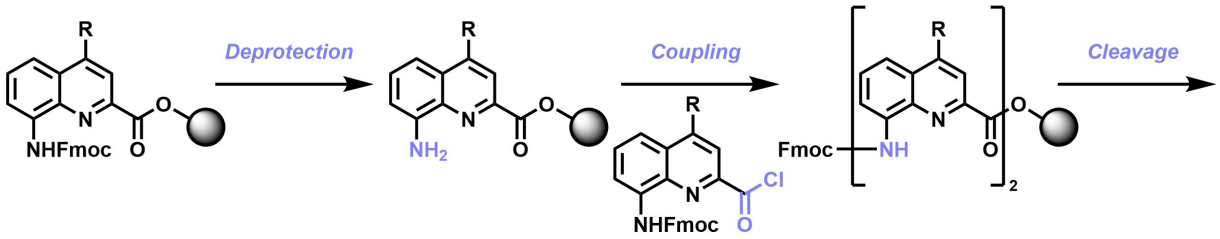

Figure 14. Synthetic route for the synthesis of AOFs on solid support. First step is to add a monomer to a resin; after Fmoc deprotection, the pre-activated monomer can be coupled on the resin-bound amine. Finally, after desired synthesis performed, the AOF is cleaved from the resin.

The helical folding of AOFs is stabilised through the hydrogen bonds connecting each monomer unit between each amide bond and the neighbouring endocyclic nitrogen atom (**Figure 15**). The hydrogen bonding along the inner rim of the helix causes a slight contraction of the helix, resulting in 2.5 units per turn.[98] That is why a dimer remains planar while a trimer bents out of plane due to electrostatic repulsions and adopts a helical structure. Upon elongations of the helix, the stability of AOFs is strengthened by hydrogen bonds as mentioned before but also via π-π stacking between each quinoline units. AOFs are chiral and are necessarily a racemic mixture of right-handed (*P*) or left-handed (*M*) conformations. In solution, they interconvert between these *P*- or *M*- through partially unfolded states. The rate of this inversion is influenced by both oligomer length and solvent polarity, with longer sequences and more polar solvents generally slowing down the process.[100]

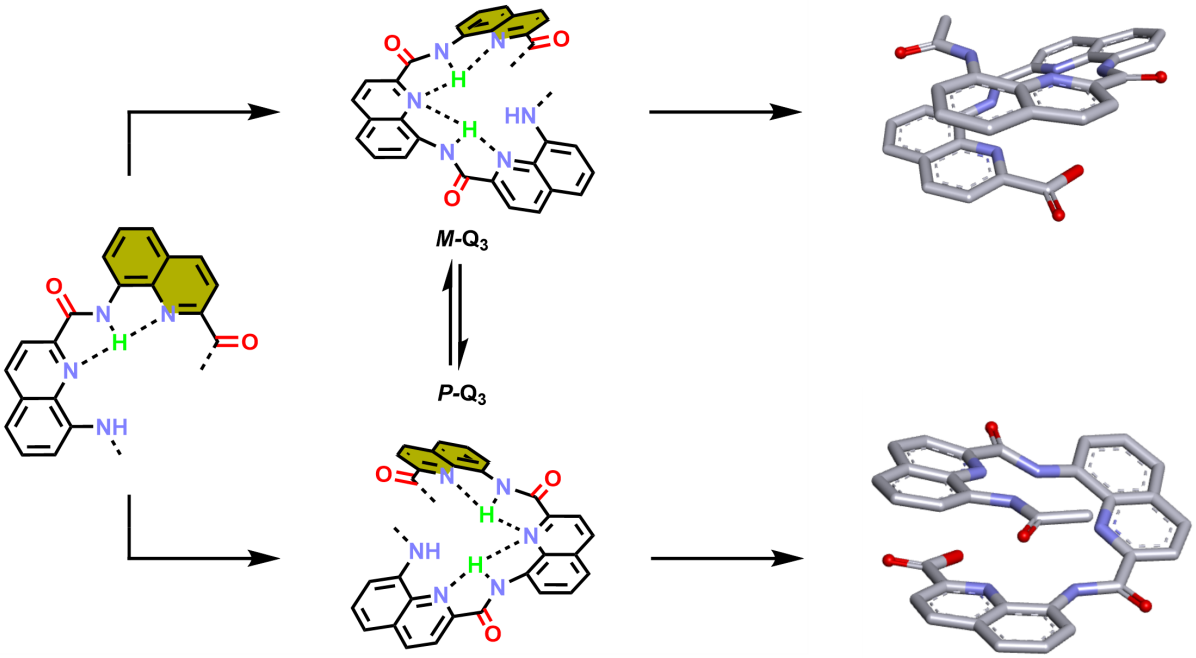

Figure 15. Schematic representation of AOF-helix folding upon elongation. Hydrogen bonds are drawn as dashed lines, nitrogen atoms are depicted in blue and oxygen atoms in red. The helix above represents a *M*-helix trimer while the bottom one shows a *P*-helix trimer.

Q-monomers can be combined with other building blocks, such as 5-methylaminopyridine-2-carboxylic acid unit (**P**) or 2-(2-aminophenoxy)-acetic acid unit (**B**) (**Figure 16**). The **P** and **B** units differ from **Q** monomers by the absence of one aromatic ring but share similar features. They are both aromatic δ-amino acids analogues capable of forming the same hydrogen bonding pattern and imposing comparable helical curvature. Thus, not altering the overall fold of the oligomer. However, the presence of an extra methylene group in **P** increases backbone flexibility which reduces the aromatic stacking area. Incorporating a few **P** or **B** units can be strategically advantageous, for instance, to minimise steric hindrance when designing sequences that interact with protein surfaces. On the other hand, **B** units have been introduced for another purpose, which is helix handedness bias. The aromatic units used to build AOFs are achiral meaning, as mentioned before, that each AOF is necessarily obtained as a racemic of *P*- and *M*- helix. It was previously demonstrated that helix handedness could be biased by adding chiral moieties on each termini of an AOF.[101-103] Recently, it was discovered that by using a chiral derivative from the **B** unit ($\mathbf{B}^{\mathbf{R/SMe}}$), it was possible to bias the handedness of AOFs.[104] This chiral unit possess a stereogenic centre on the carbon atom carrying a methyl group with either the (*S*) or (*R*) configuration. When this unit is incorporated in the middle of a **Q**-oligomer sequence, the bias towards one handedness is quantitative on an NMR-time scale. The (*R)* configuration bias the handedness towards the *M*-helix while the (*S)* configuration towards the *P*-helix. Being able to synthesise chiral AOFs is important especially when helices are designed to interact with a desired target.

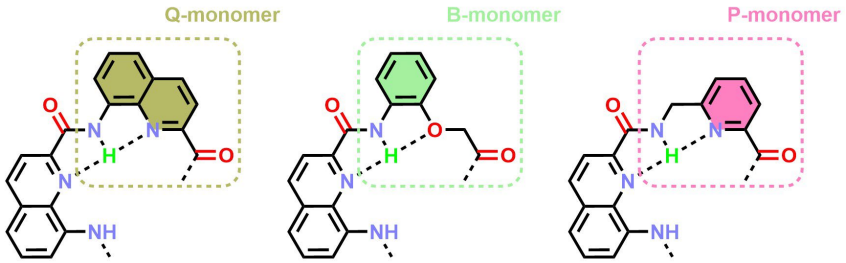

Figure 16. Structure of the different units used to build AOFs. **Q** is the usual quinoline unit, **B** lacks the pyridine ring while **P** lacks an aromatic ring. Hydrogen bonds are represented by dashed lines.

3.4.2. Peptide-foldamers macrocycle hybrids

In a previous section, the FIT technique was introduced (section **3.3.3.3**). This unique technique, enabling the incorporation of non-canonical tRNAs for translation, was introduced to AOFs. Rogers *et al.* demonstrated that the ribosome can initiate translation using AOFs by charging them onto tRNAs thanks to flexizymes.[105] In this study, *in vitro* syntheses of both linear and cyclic foldamer-peptide hybrids were performed. It was demonstrated that, for the cyclic hybrids, the AOFs, when short and flexible enough, could unfold to fit the exit tunnel of the ribosome but refold very fast afterwards while affecting the shape of the peptide. In this study, the peptide segment is forced into a stretched and constrained conformation, but it also biases the AOF handedness. Spectroscopic analyses such as CD, NMR and X-ray crystallography confirmed this mutual conformational influence of the peptide segment and the AOF when cyclised and exhibiting a complementary length. Just like regular peptide macrocycles, it was demonstrated that these hybrid macrocycles have a significant resistance to proteolytic degradation compared to their linear forms.[106]

Thanks to these foundational works, Dengler *et al.* sought to adapt mRNA display selection to find macrocyclic peptide-AOF binders to target the C-lobe segment of the E6AP HECT domain.[107] Using an optimised foldamer-tRNA initiator compatible with ribosomal translation and flexizyme, they incorporated foldamers into peptide libraries within the RaPID system. Different-length peptide libraries were screened and from these high-affinity binders were selected, with one macrocycle showing binding affinity of 28.7 nM to C-lobe domain. X-ray crystallography revealed that the foldamer and peptide helices stabilise each other in a stapled conformation, enabling precise and strong interactions with the protein surface (**Figure 17**).

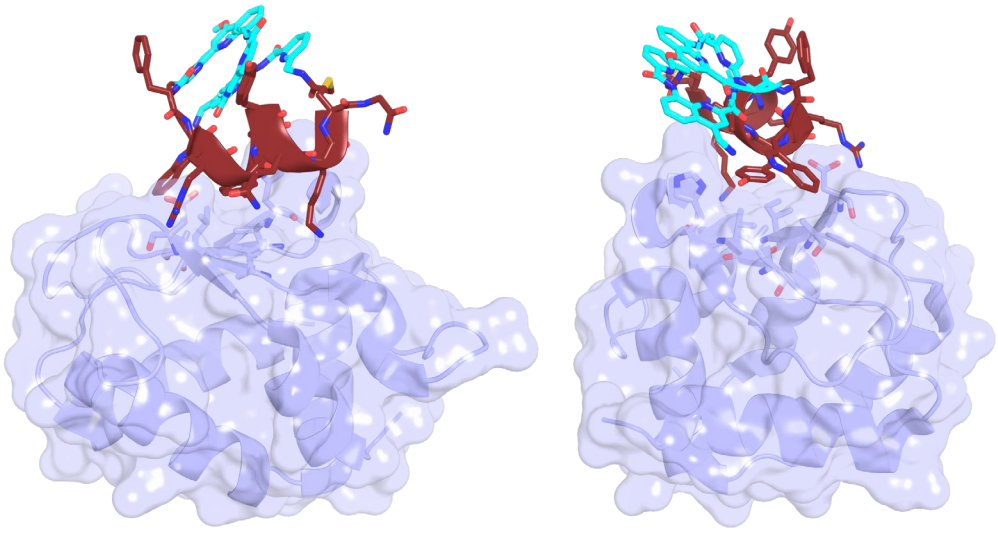

Figure 17. X-ray structure of the complex between foldamer-peptide macrocycle and C-lobe (PDB#7QPB). Peptide segment is highlighted in brown while the foldamer is coloured in cyan.

3.4.3. AOFs as DNA mimics

Despite advances in drug development, transcription factors, as mentioned before, remain hard to target due to their flexible, often disordered structures in absence of their binding partner. Traditional small molecules approaches struggle with the dynamicity of these proteins as their disordered structures lack defined ligand binding pockets.[108-109] A promising alternative is to mimic the structural surfaces of DNA or proteins involved in binding.

Huc and co-workers have explored how AOFs can be utilised as scaffolds for DNA mimics.[110] The starting point was the similarity of some geometric parameters between a single-stranded AOF helix and a double stranded B-DNA. The inner aromatic core of an AOF helix spans around 9.4 Å (between C4 atoms of contiguous **Q** rings) which is very close to the B-DNA base pair core of around 9 Å (between the purine and pyrimidine N1 atoms).

However, in poly-**Q** sequences, two **Q** units encode for 0.8 turns, resulting in a side-chain geometry that does not match the spatial arrangement of phosphate groups in B-DNA. To increase curvature, a **Q** derivative unit with an additional methylene group was introduced: 8-aminomethyl-2-quinoline carboxylic acid **mQ** unit (**Figure 18**). Combined with **Q** units, the resulting (**mQQ**)$_n$ AOF folds with a curvature that resembles B-DNAs rotation per base pair. This causes the negatively charged side chains to align in a double helical pattern mimicking the phosphate arrangement of B-DNA, including their characteristic groove shapes, albeit with a narrower major and wider minor groove than idealised B-DNA. However, each **mQQ** dimer spans 0.9 of a helix turn, which means that each successive dimer in the sequence is rotated backward by one-tenth of a helical turn. Due to this backward shift, the surface double helix

has opposite handedness to the main chain, meaning that an *M*-helix AOF displays a *P*-helical array of its side chains, closely resembling the B-DNA topology.

Overall, the (**mQQ**)$_n$ AOF closely mimics the shape and charge distribution of B-DNA and offers increased degree of freedom to form electronic interactions with their exposed phosphonate side chains, which can in turn be deprotonated twice, increasing charge density.

Studies have shown that (**mQQ**)$_n$ AOFs, as DNA mimics, exhibit strong inhibition of HIV-1 integrase and human Topoisomerase I, with sub-micromolar IC_{50} values, comparable to or better than standard drugs like raltegravir and camptothecin. Their activity depends on foldamer length (32 units) and side-chain positioning. Their flexible, modular design enables selective interference with protein-DNA interactions without relying on sequence recognition.

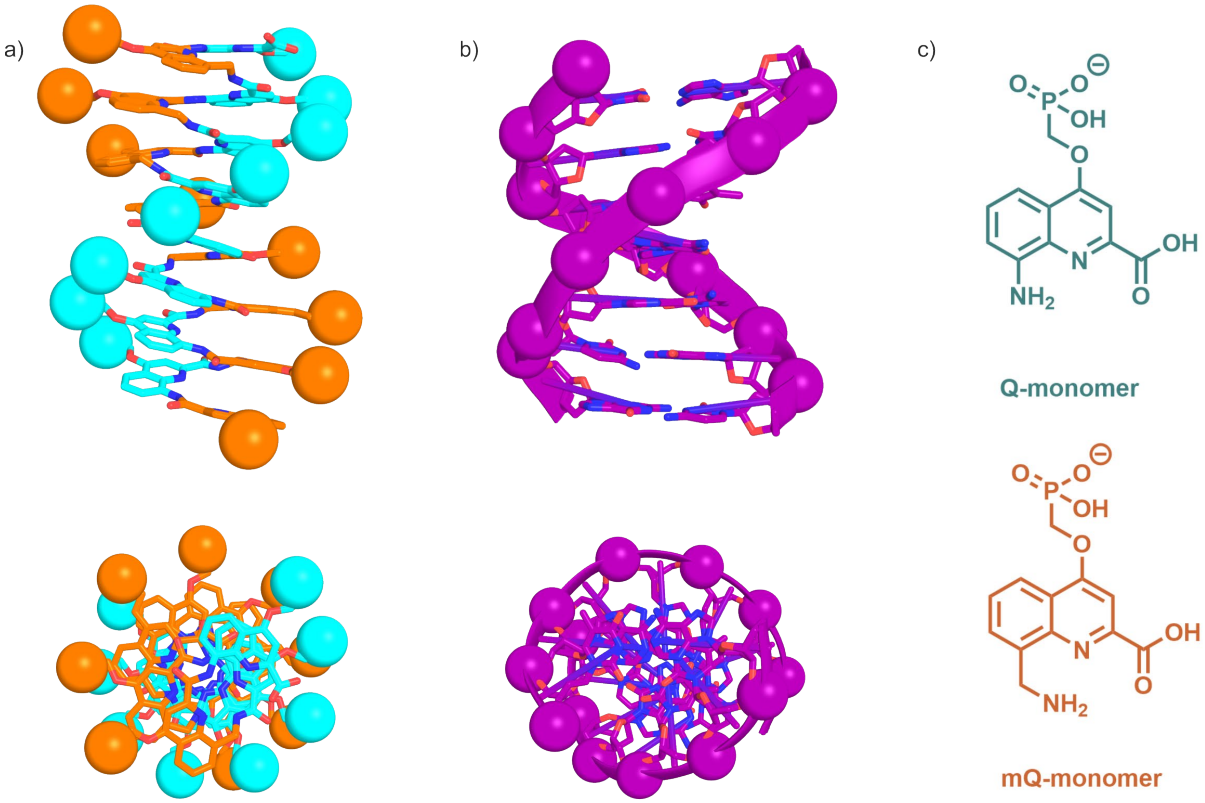

Figure 18. a) X-ray crystal structure of (**mQQ**)$_8$ with appropriate colour code for each monomer unit and its top view. b) X-ray crystal structure of a double-stranded B-DNA with its top view. On both structures, the spheres represent the phosphorus atoms. c) Chemical structures of phosphonate-bearing **Q** and **mQ** monomers.

Recently, these AOF were used to bind to the chromosomal DNA-binding protein Sac7d.[111] Remarkably, the AOF exhibited stronger binding affinity than natural DNA, with clear diastereoselectivity favouring one helical enantiomer. X-ray crystallography revealed that, unlike DNA which bends upon binding, the AOF retains its own rigid conformation within the binding site of the protein (**Figure 19a**). Loos *et al*. went further in the mimicry by synthesising a chimeric structure where B-DNA and DNA mimic AOF are merged.[112] They developed a

novel linker that functions as a hairpin turn in the DNA while anchoring an AOF dimer (**Figure 19b**). Importantly, BLI experiments showed that these artificial hairpin duplexes still bind DBPs just as well as natural DNA.

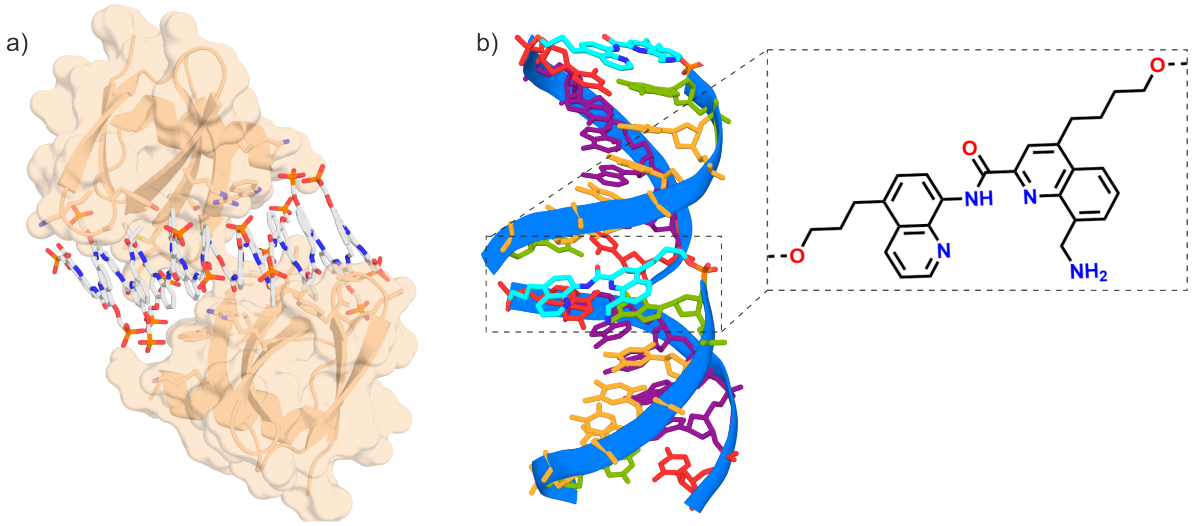

Figure 19. a) X-ray structure of DNA mimic AOF (18mer) interacting with two proteins of Sac7D (PDB#8CMN). b) X-ray structure of chimera B-DNA with AOF dimer represented in cyan (PDB#8Q60) with linker chemical structure highlighted on the right.

3.4.4. AOFs as α-helix mimics

As already explained in the previous paragraphs, AOFs are well-behaved, predictable, and robust scaffolds. In this context, Huc and co-workers tried to make use of these features for α-helix mimicry.

AOFs composed of **Q** units naturally adopt a stable helical conformation with approximately 2.5 residues per turn. Previously, these AOF helices have been sparsely functionalised, with side chains mostly introduced at position 4, occasionally at position 5[113-114], but not in position 6. Upon detailed structural analysis, it was observed that a specific pattern of substitution at both the 4- and 6- position of the quinoline rings could reproduce the spatial side-chain arrangement found on one face of a α-helix. The curvature of natural α-helices typically ranges between the idealised 3.66_{13} helix (three turns per 11 residues) and the more commonly referenced 3.6_{13} helix (five turns per 18 residues).[115]

By aligning these geometries, it was demonstrated that four side chains from a 3.6_{13} α-helix (positions *i*, *i+3*, *i+4*, and *i+7*) can be closely overlaid to four residues on a **Q**-AOF, achieving a root-mean-square deviation (RMSD) of just 0.70–0.95 Å.[116] Notably, the match can be extended to eight side chains, essentially the full interactive face of an 18-residues α-helix.

Interestingly, whereas the peptide presents consecutive side chains, the quinoline helix aligns them using residues spaced two units apart, due to its larger helical pitch.

Even in the idealised 3.66_{13} helix model, a match with eight α-helical side chains is still feasible (to *i+8*, *i+11*, *i+12*, and *i+15* for the last four). Although, the match is less precise with an RMSD ~1.5 Å (**Figure 20**). Nonetheless, this imperfection remains acceptable given the natural variability of both foldamer and peptide geometries, especially under induced fit during binding. Further optimisation is also possible by functionalising quinoline units at position 5, offering finer control over side-chain projection. While AOFs are bulkier than α-helices and might not fit into narrow protein grooves, they are well-suited for mimicking PPIs that involve a single α-helical interface.

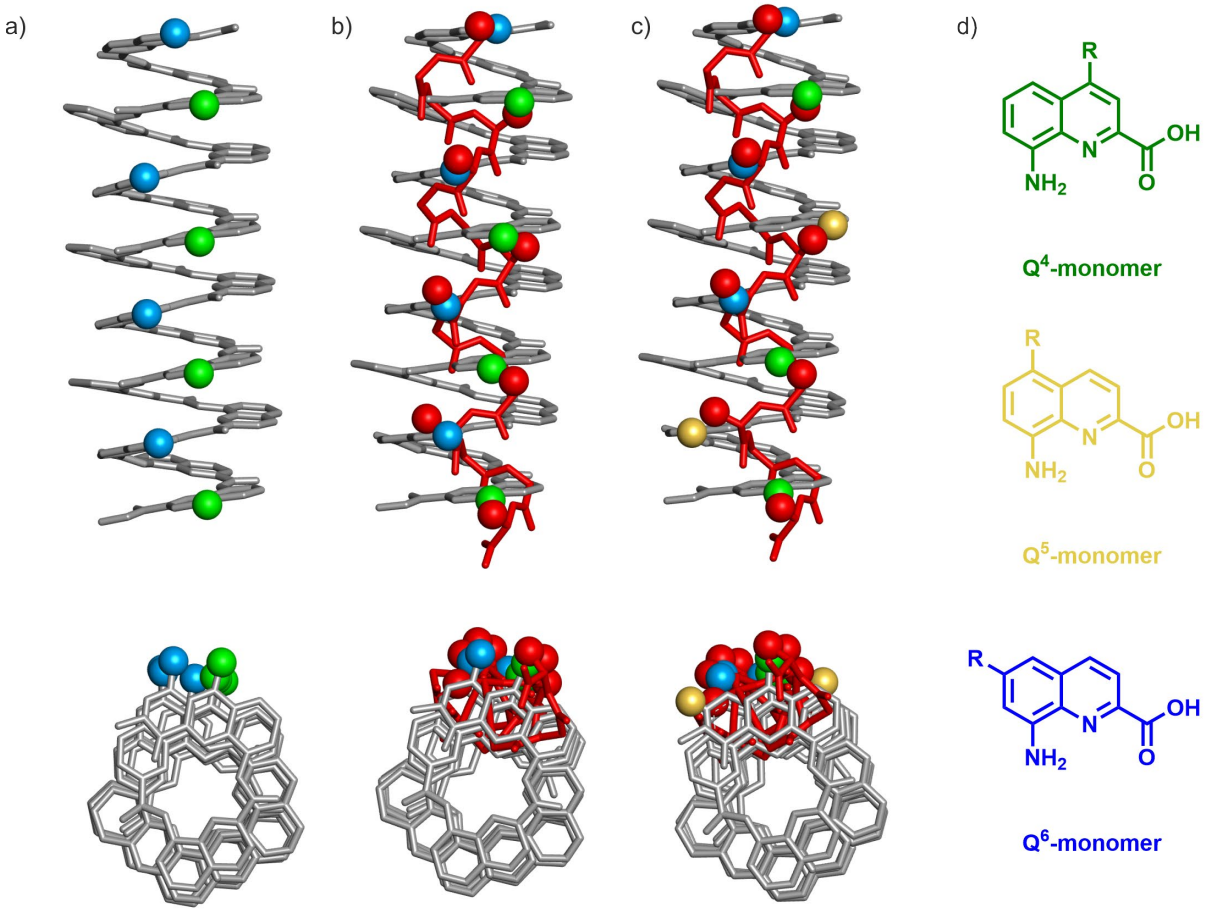

Figure 20. a) Model of a 18mer AOF, side view and top view, green and blue spheres represent **Q** unit substituted in position 4 and 6 respectively. b) Model of a 18mer AOF overlaid with a 3.66_{13} α-helix, side view and top view, green and blue spheres represent **Q** unit substituted in position 4 and 6 respectively while red spheres show β-carbons of residues. c) Same models, this time the golden spheres represent **Q** unit substituted in position 5. d) Structure of **Q** units substituted in 4 (green), 5 (gold) and 6 (blue).

4. Objectives

This thesis presents the design, synthesis, and characterisation of helical aromatic oligoamide foldamers (AOFs) capable of interacting with protein surfaces. A new library of building blocks bearing proteinogenic side chains was developed and used to optimise solid-phase synthesis protocols on an automated system. With these tools, various AOFs were synthesised and applied as candidates for protein recognition.

The guiding objective of **section 6** was to develop new strategies and methodologies to expand and simplify the synthesis of AOFs. One of the main motivation was the production of new building blocks bearing biogenic side chains for protein recognition. Based on recent development in the group, 26 novel Fmoc protected quinoline monomers were synthesised. These include both mono- and di-substituted units bearing cationic, anionic polar and hydrophobic side chains. The diversity of this new library, along with the ability to increase side-chain density, was intended to enhance the capacity of AOFs to interact with protein surfaces with greater specificity and affinity. In parallel, this work sought to overcome the practical limitation that is the labour-intensive and slow process of synthesising long AOF sequences. To address this, *in situ* activation protocols were adapted and optimised on an automated system, enabling the efficient and reproducible solid phase foldamer synthesis (SPFS) of long AOFs.

The aim of **section 7** was to explore how AOFs can recognise and distinguish between protein surfaces, with a deeper goal of designing them into selective molecular tools. The starting point for this investigation was the outcome of different selections experiments with the same AOF which was able to bind two structurally distinct protein scaffolds: one based on a β-sheet, the other on an α-helix. The first goal was to identify which handedness of the AOF was biased for the interaction with the proteins and to figure out the binding mode. High-quality crystals of both complexes were obtained allowing direct comparisons between binding interfaces and revealing recurring features, most notably, the central importance of the hydrophobic aromatic cross-section of the AOF. Another key question was how much of the recognition came from the side chains of the AOF and how much was simply due to the hydrophobic cross-section. Mutations were then introduced on both partners of the interaction. Ala-scan of the protein residues randomised during selection confirmed the key amino-acids for the interaction while a Q^{Gly}-scan of the AOF described how individual side chains influenced the interaction. These experiments revealed a consistent pattern which is that the cross-section of the AOF played the dominant role in the binding, while the side chains acted more like fine-tuners adjusting the interaction rather than driving it. With these insights, the next step was to move from understanding recognition to actively shaping it. Using the crystallographic data and the

mutational analysis, new AOFs variants were designed and synthesised with targeted modifications aiming to discriminate the affinity towards one scaffold or the other. This strategy led to the identification of mutations that could selectively enhance or weaken binding, demonstrating that AOF selectivity can indeed be tuned.

Section 8 of this thesis focuses on designing AOFs that could mimic the spatial arrangement of residues found in biologically relevant complexes, specifically, the linear di-ubiquitin and the coiled-coil NEMO. Drawing on recent findings from the group, single-helix AOF candidates ranging from 10 to 13 units were modelled to replicate the positioning of α-residues within the NEMO coiled-coil. Docking studies explored how different substitution patterns on the quinoline core, at positions 4, 5, and 6, could be used to anchor key interacting residues between NEMO and the ubiquitin surface. To introduce structural variability, both *P*- and *M*-helices were considered. The stability of each complex was assessed through energy minimisation and short molecular dynamics simulations, and only those where the AOF candidates maintained stable associations with the protein were selected for synthesis. These designs were then translated into actual molecules using the newly developed monomer library and optimised protocols for automated SPFS. Chemical ligation of the AOFs to a mutated ubiquitin produced stable protein-AOF adducts. NMR studies provided promising evidence of interaction with the targeted residues. Significant efforts were devoted to crystallisation assays to determine how the AOFs positioned themselves on the protein surface. Although initial attempts did not yield diffracting crystals, adjustments to linker length and solvent-exposed side chains eventually led to reproducible crystals with diffraction quality up to 3.0 Å, though full structural resolution remained out of reach. Returning to the original goal, longer AOF candidates were modelled and synthesised for ligation to linear di-ubiquitin. Broad crystallisation screening has since been carried out, with the long-term aim of capturing the first structural evidence that AOFs can mimic the side-chain arrangement of a coiled-coil.

5. References

[1] S. Kang, T. Tanaka, T. Kishimoto, *International Immunology* **2015**, *27*, 21-29.

[2] H. A. Blair, *Drugs* **2021**, *81*, 1573-1579.

[3] S. S. Lieberman-Blum, H. B. Fung, J. C. Bandres, *Clinical Therapeutics* **2008**, *30*, 1228-1250.

[4] A. G. Ngounou Wetie, I. Sokolowska, A. G. Woods, U. Roy, J. A. Loo, C. C. Darie, *PROTEOMICS* **2013**, *13*, 538-557.

[5] G. C. Kresheck, L. B. Vitello, J. E. Erman, *Biochemistry* **1995**, *34*, 8398-8405.

[6] S. Jones, J. M. Thornton, *Journal of Molecular Biology* **1997**, *272*, 121-132.

[7] M. Baek, D. Baker, *Nature Methods* **2022**, *19*, 13-14.

[8] J. Jumper, R. Evans, A. Pritzel, T. Green, M. Figurnov, O. Ronneberger, K. Tunyasuvunakool, R. Bates, A. Žídek, A. Potapenko, A. Bridgland, C. Meyer, S. A. A. Kohl, A. J. Ballard, A. Cowie, B. Romera-Paredes, S. Nikolov, R. Jain, J. Adler, T. Back, S. Petersen, D. Reiman, E. Clancy, M. Zielinski, M. Steinegger, M. Pacholska, T. Berghammer, S. Bodenstein, D. Silver, O. Vinyals, A. W. Senior, K. Kavukcuoglu, P. Kohli, D. Hassabis, *Nature* **2021**, *596*, 583-589.

[9] J. Abramson, J. Adler, J. Dunger, R. Evans, T. Green, A. Pritzel, O. Ronneberger, L. Willmore, A. J. Ballard, J. Bambrick, S. W. Bodenstein, D. A. Evans, C.-C. Hung, M. O'Neill, D. Reiman, K. Tunyasuvunakool, Z. Wu, A. Žemgulytė, E. Arvaniti, C. Beattie, O. Bertolli, A. Bridgland, A. Cherepanov, M. Congreve, A. I. Cowen-Rivers, A. Cowie, M. Figurnov, F. B. Fuchs, H. Gladman, R. Jain, Y. A. Khan, C. M. R. Low, K. Perlin, A. Potapenko, P. Savy, S. Singh, A. Stecula, A. Thillaisundaram, C. Tong, S. Yakneen, E. D. Zhong, M. Zielinski, A. Žídek, V. Bapst, P. Kohli, M. Jaderberg, D. Hassabis, J. M. Jumper, *Nature* **2024**, *630*, 493-500.

[10] O. Keskin, A. Gursoy, B. Ma, R. Nussinov, *Chemical Reviews* **2008**, *108*, 1225-1244.

[11] S. Zhang, T. C. Owyong, O. Sanislav, L. Englmaier, X. Sui, G. Wang, D. W. Greening, N. A. Williamson, A. Villunger, J. M. White, B. Heras, W. W. H. Wong, P. R. Fisher, Y. Hong, *Nature Methods* **2025**, *22*, 124-134.

[12] J. M. Rini, U. Schulze-Gahmen, I. A. Wilson, *Science* **1992**, *255*, 959-965.

[13] T. Su, T. Izawa, M. Thoms, Y. Yamashita, J. Cheng, O. Berninghausen, F. U. Hartl, T. Inada, W. Neupert, R. Beckmann, *Nature* **2019**, *570*, 538-542.

[14] M. P. Williamson, *Progress in Nuclear Magnetic Resonance Spectroscopy* **2013**, *73*, 1-16.

[15] L. Damian, in *Protein-Ligand Interactions: Methods and Applications* (Eds.: M. A. Williams, T. Daviter), Humana Press, Totowa, NJ, **2013**, pp. 103-118.

[16] R. P. Sparks, J. L. Jenkins, R. Fratti, in *SNAREs: Methods and Protocols* (Ed.: R. Fratti), Springer New York, New York, NY, **2019**, pp. 199-210.
[17] A. Jug, T. Bratkovič, J. Ilaš, *TrAC Trends in Analytical Chemistry* **2024**, *176*, 117741.
[18] V. Azzarito, K. Long, N. S. Murphy, A. J. Wilson, *Nature Chemistry* **2013**, *5*, 161-173.
[19] S. Surget, M. P. Khoury, J.-C. Bourdon, *OncoTargets and Therapy* **2013**, *7*, 57-68.
[20] P. H. Kussie, S. Gorina, V. Marechal, B. Elenbaas, J. Moreau, A. J. Levine, N. P. Pavletich, *Science* **1996**, *274*, 948-953.
[21] D. R. Burton, *Accounts of Chemical Research* **1993**, *26*, 405-411.
[22] S. Paul, M. F. Konig, D. M. Pardoll, C. Bettegowda, N. Papadopoulos, K. M. Wright, S. B. Gabelli, M. Ho, A. van Elsas, S. Zhou, *Nature Reviews Cancer* **2024**, *24*, 399-426.
[23] C. Hamers-Casterman, T. Atarhouch, S. Muyldermans, G. Robinson, C. Hammers, E. B. Songa, N. Bendahman, R. Hammers, *Nature* **1993**, *363*, 446-448.
[24] S. Muyldermans, *Annual Review of Biochemistry* **2013**, *82*, 775-797.
[25] P. Kunz, K. Zinner, N. Mücke, T. Bartoschik, S. Muyldermans, J. D. Hoheisel, *Scientific Reports* **2018**, *8*, 7934.
[26] W. H. Hudson, E. A. Ortlund, *Nature Reviews Molecular Cell Biology* **2014**, *15*, 749-760.
[27] T. Alber, *Current Opinion in Genetics & Development* **1992**, *2*, 205-210.
[28] T. E. Ellenberger, C. J. Brandl, K. Struhl, S. C. Harrison, *Cell* **1992**, *71*, 1223-1237.
[29] Y. Kim, J. H. Geiger, S. Hahn, P. B. Sigler, *Nature* **1993**, *365*, 512-520.
[30] K. K. Swinger, K. M. Lemberg, Y. Zhang, P. A. Rice, *The EMBO Journal* **2003**, *22*, 3749-3760-3760.
[31] J. Miller, A. D. McLachlan, A. Klug, *The EMBO Journal* **1985**, *4*, 1609-1614.
[32] M. P. Foster, D. S. Wuttke, I. Radhakrishnan, D. A. Case, J. M. Gottesfeld, P. E. Wright, *Nature Structural Biology* **1997**, *4*, 605-608.
[33] M. A. Searles, D. Lu, A. Klug, *Journal of Molecular Biology* **2000**, *301*, 47-60.
[34] R. T. Nolte, R. M. Conlin, S. C. Harrison, R. S. Brown, *Proceedings of the National Academy of Sciences* **1998**, *95*, 2938-2943.
[35] G. P. Smith, *Science* **1985**, *228*, 1315-1317.
[36] C. M. Y. Lee, N. Iorno, F. Sierro, D. Christ, *Nature Protocols* **2007**, *2*, 3001-3008.
[37] O. H. Brekke, I. Sandlie, *Nature Reviews Drug Discovery* **2003**, *2*, 52-62.
[38] S. Bhatnagar, E. Deschenes, J. Liao, C. Cilliers, G. M. Thurber, *Journal of Pharmaceutical Sciences* **2014**, *103*, 3276-3286.
[39] O. Hantschel, *Swiss Medical Weekly* **2017**, *147*, w14545.
[40] R. Kunert, D. Reinhart, *Applied Microbiology and Biotechnology* **2016**, *100*, 3451-3461.

[41] A. Koide, C. W. Bailey, X. Huang, S. Koide, *Journal of Molecular Biology* **1998**, *284*, 1141-1151.

[42] T. Ibbotson, J. K. McGavin, K. L. Goa, *Drugs* **2003**, *63*, 1121-1163.

[43] J. S. Huston, D. Levinson, M. Mudgett-Hunter, M. S. Tai, J. Novotný, M. N. Margolies, R. J. Ridge, R. E. Bruccoleri, E. Haber, R. Crea, *Proceedings of the National Academy of Sciences* **1988**, *85*, 5879-5883.

[44] Z. A. Ahmad, S. K. Yeap, A. M. Ali, W. Y. Ho, N. B. M. Alitheen, M. Hamid, *Journal of Immunology Research* **2012**, *2012*, 980250.

[45] I. Jovčevska, S. Muyldermans, *BioDrugs* **2020**, *34*, 11-26.

[46] B. Nilsson, T. Moks, B. Jansson, L. Abrahmsén, A. Elmblad, E. Holmgren, C. Henrichson, T. A. Jones, M. Uhlén, *Protein Engineering* **1987**, *1*, 107-113.

[47] K. Nord, J. Nilsson, B. Nilsson, M. Uhlén, P.-Å. Nygren, *Protein Engineering* **1995**, *8*, 601-608.

[48] S. Li, Y. Jin, Y. Su, W. Li, Y. Xing, F. Wang, Z. Hong, *Molecular Pharmaceutics* **2020**, *17*, 1546-1557.

[49] A. Pessi, E. Bianchi, A. Crameri, S. Venturini, A. Tramontano, M. Sollazzo, *Nature* **1993**, *362*, 367-369.

[50] G. Béhar, M. Bellinzoni, M. Maillasson, L. Paillard-Laurance, P. M. Alzari, X. He, B. Mouratou, F. Pecorari, *Protein Engineering, Design and Selection* **2013**, *26*, 267-275.

[51] M. Iaboni, F. Crivellin, F. Arena, F. La Cava, A. Cordaro, F. Stummo, D. Faletto, S. Huet, L. Candela, J. Pedrault, E. R. Zanella, A. Bertotti, F. Blasi, A. Maiocchi, L. Poggi, E. Reitano, *Scientific Reports* **2025**, *15*, 9832.

[52] C. Tuerk, L. Gold, *Science* **1990**, *249*, 505-510.

[53] A. D. Ellington, J. W. Szostak, *Nature* **1990**, *346*, 818-822.

[54] S. Catuogno, C. L. Esposito, in *Biomedicines, Vol. 5*, **2017**.

[55] R. White, C. Rusconi, E. Scardino, A. Wolberg, J. Lawson, M. Hoffman, B. Sullenger, *Molecular Therapy* **2001**, *4*, 567-573.

[56] D. J. Barlow, J. M. Thornton, *Journal of Molecular Biology* **1988**, *201*, 601-619.

[57] J. D. A. Tyndall, T. Nall, D. P. Fairlie, *Chemical Reviews* **2005**, *105*, 973-1000.

[58] F. Bernal, A. F. Tyler, S. J. Korsmeyer, L. D. Walensky, G. L. Verdine, *Journal of the American Chemical Society* **2007**, *129*, 2456-2457.

[59] C. E. Schafmeister, J. Po, G. L. Verdine, *Journal of the American Chemical Society* **2000**, *122*, 5891-5892.

[60] J. Liu, D. Wang, Q. Zheng, M. Lu, P. S. Arora, *Journal of the American Chemical Society* **2008**, *130*, 4334-4337.

[61] D. C. Chan, D. Fass, J. M. Berger, P. S. Kim, *Cell* **1997**, *89*, 263-273.

[62] D. Wang, M. Lu, P. S. Arora, *Angewandte Chemie International Edition* **2008**, *47*, 1879-1882.

[63] H. Yin, A. D. Hamilton, *Angewandte Chemie International Edition* **2005**, *44*, 4130-4163.

[64] I. Saraogi, Andrew D. Hamilton, *Biochemical Society Transactions* **2008**, *36*, 1414-1417.

[65] J. M. Davis, A. Truong, A. D. Hamilton, *Organic Letters* **2005**, *7*, 5405-5408.

[66] F. Campbell, J. P. Plante, T. A. Edwards, S. L. Warriner, A. J. Wilson, *Org. Biomol. Chem.* **2010**, *8*, 2344-2351.

[67] J. P. Plante, T. Burnley, B. Malkova, M. E. Webb, S. L. Warriner, T. A. Edwards, A. J. Wilson, *Chem. Commun.* **2009**, 5091-5093.

[68] K. E. Duncan, B. R. Dempsey, L. E. Killip, J. Adams, M. L. Bailey, G. A. Lajoie, D. W. Litchfield, C. J. Brandl, G. S. Shaw, B. H. Shilton, *Journal of Medicinal Chemistry* **2011**, *54*, 3854-3865.

[69] T. B. Andrew, M. M. Cayla, R. S. Lokey, *Current Topics in Medicinal Chemistry* **2013**, *13*, 821-836.

[70] D. A. Price, H. Eng, K. A. Farley, G. H. Goetz, Y. Huang, Z. Jiao, A. S. Kalgutkar, N. M. Kablaoui, B. Khunte, S. Liras, C. Limberakis, A. M. Mathiowetz, R. B. Ruggeri, J.-M. Quan, Z. Yang, *Org. Biomol. Chem.* **2017**, *15*, 2501-2506.

[71] L. K. Buckton, M. N. Rahimi, S. R. McAlpine, *Chemistry – A European Journal* **2021**, *27*, 1487-1513.

[72] A. F. B. Räder, M. Weinmüller, F. Reichart, A. Schumacher-Klinger, S. Merzbach, C. Gilon, A. Hoffman, H. Kessler, *Angewandte Chemie International Edition* **2018**, *57*, 14414-14438.

[73] I. V. Smolyar, A. K. Yudin, V. G. Nenajdenko, *Chemical Reviews* **2019**, *119*, 10032-10240.

[74] H. S. Soor, S. D. Appavoo, A. K. Yudin, *Bioorganic & Medicinal Chemistry* **2018**, *26*, 2774-2779.

[75] S. Chen, D. Bertoldo, A. Angelini, F. Pojer, C. Heinis, *Angewandte Chemie International Edition* **2014**, *53*, 1602-1606.

[76] C. Heinis, T. Rutherford, S. Freund, G. Winter, *Nature Chemical Biology* **2009**, *5*, 502-507.

[77] R. W. Roberts, J. W. Szostak, *Proceedings of the National Academy of Sciences* **1997**, *94*, 12297-12302.

[78] A. D. Keefe, J. W. Szostak, *Nature* **2001**, *410*, 715-718.

[79] H. Murakami, H. Saito, H. Suga, *Chemistry & Biology* **2003**, *10*, 655-662.

[80] Y. Goto, T. Katoh, H. Suga, *Nature Protocols* **2011**, *6*, 779-790.

[81] Y. Goto, H. Murakami, H. Suga, *RNA* **2008**, *14*, 1390-1398.

[82] T. Kawakami, H. Murakami, H. Suga, *Chemistry & Biology* **2008**, *15*, 32-42.

[83] Y. Goto, H. Suga, *Journal of the American Chemical Society* **2009**, *131*, 5040-5041.

[84] Y. Goto, A. Ohta, Y. Sako, Y. Yamagishi, H. Murakami, H. Suga, *ACS Chemical Biology* **2008**, *3*, 120-129.

[85] Y. Goto, H. Suga, *Accounts of Chemical Research* **2021**, *54*, 3604-3617.

[86] Y. Matsunaga, Nasir K. Bashiruddin, Y. Kitago, J. Takagi, H. Suga, *Cell Chemical Biology* **2016**, *23*, 1341-1350.

[87] L. Soini, S. Leysen, J. Davis, C. Ottmann, *Current Opinion in Chemical Biology* **2022**, *69*, 102169.

[88] G. Petzold, E. S. Fischer, N. H. Thomä, *Nature* **2016**, *532*, 127-130.

[89] G. Lu, R. E. Middleton, H. Sun, M. Naniong, C. J. Ott, C. S. Mitsiades, K.-K. Wong, J. E. Bradner, W. G. Kaelin, *Science* **2014**, *343*, 305-309.

[90] D. H. Appella, L. A. Christianson, I. L. Karle, D. R. Powell, S. H. Gellman, *Journal of the American Chemical Society* **1996**, *118*, 13071-13072.

[91] S. H. Gellman, *Accounts of Chemical Research* **1998**, *31*, 173-180.

[92] R. N. Zuckermann, *Peptide Science* **2011**, *96*, 545-555.

[93] D. Seebach, J. L. Matthews, *Chem. Commun.* **1997**, 2015-2022.

[94] A. Violette, M. C. Averlant-Petit, V. Semetey, C. Hemmerlin, R. Casimir, R. Graff, M. Marraud, J.-P. Briand, D. Rognan, G. Guichard, *Journal of the American Chemical Society* **2005**, *127*, 2156-2164.

[95] I. Huc, V. Maurizot, H. Gornitzka, J.-M. Léger, *Chem. Commun.* **2002**, 578-579.

[96] B. Gong, *Chemistry – A European Journal* **2001**, *7*, 4336-4342.

[97] I. Huc, *European Journal of Organic Chemistry* **2004**, *2004*, 17-29.

[98] H. Jiang, J.-M. Léger, I. Huc, *Journal of the American Chemical Society* **2003**, *125*, 3448-3449.

[99] B. Baptiste, C. Douat-Casassus, K. Laxmi-Reddy, F. Godde, I. Huc, *The Journal of Organic Chemistry* **2010**, *75*, 7175-7185.

[100] T. Qi, V. Maurizot, H. Noguchi, T. Charoenraks, B. Kauffmann, M. Takafuji, H. Ihara, I. Huc, *Chem. Commun.* **2012**, *48*, 6337-6339.

[101] A. M. Kendhale, L. Poniman, Z. Dong, K. Laxmi-Reddy, B. Kauffmann, Y. Ferrand, I. Huc, *The Journal of Organic Chemistry* **2011**, *76*, 195-200.

[102] L. Yang, C. Ma, B. Kauffmann, D. Li, Q. Gan, *Org. Biomol. Chem.* **2020**, *18*, 6643-6650.

[103] C. Dolain, H. Jiang, J.-M. Léger, P. Guionneau, I. Huc, *Journal of the American Chemical Society* **2005**, *127*, 12943-12951.

[104] D. Bindl, E. Heinemann, P. K. Mandal, I. Huc, *Chem. Commun.* **2021**, *57*, 5662-5665.

[105] J. M. Rogers, S. Kwon, S. J. Dawson, P. K. Mandal, H. Suga, I. Huc, *Nature Chemistry* **2018**, *10*, 405-412.

[106] S. Dengler, P. K. Mandal, L. Allmendinger, C. Douat, I. Huc, *Chemical Science* **2021**, *12*, 11004-11012.

[107] S. Dengler, R. T. Howard, V. Morozov, C. Tsiamantas, W.-E. Huang, Z. Liu, C. Dobrzanski, V. Pophristic, S. Brameyer, C. Douat, H. Suga, I. Huc, *Angewandte Chemie International Edition* **2023**, *62*, e202308408.

[108] Y. Zhang, G. Sicot, X. Cui, M. Vogel, C. A. Wuertzer, K. Lezon-Geyda, J. Wheeler, D. A. Harki, K. A. Muzikar, D. A. Stolper, P. B. Dervan, A. S. Perkins, *Biochemistry* **2011**, *50*, 10431-10441.

[109] J. S. Kang, J. L. Meier, P. B. Dervan, *Journal of the American Chemical Society* **2014**, *136*, 3687-3694.

[110] K. Ziach, C. Chollet, V. Parissi, P. Prabhakaran, M. Marchivie, V. Corvaglia, P. P. Bose, K. Laxmi-Reddy, F. Godde, J.-M. Schmitter, S. Chaignepain, P. Pourquier, I. Huc, *Nature Chemistry* **2018**, *10*, 511-518.

[111] D. Deepak, J. Wu, V. Corvaglia, L. Allmendinger, M. Scheckenbach, P. Tinnefeld, I. Huc, *Angewandte Chemie International Edition* **2025**, *64*, e202422958.

[112] M. Loos, F. Xu, P. K. Mandal, T. Chakrabortty, C. Douat, D. B. Konrad, M. Cabbar, J. Singer, V. Corvaglia, T. Carell, I. Huc, *Angewandte Chemie International Edition* **2025**, *64*, e202505273.

[113] X. Hu, S. J. Dawson, P. K. Mandal, X. de Hatten, B. Baptiste, I. Huc, *Chemical Science* **2017**, *8*, 3741-3749.

[114] V. Corvaglia, D. Carbajo, P. Prabhakaran, K. Ziach, P. K. Mandal, V. D. Santos, C. Legeay, R. Vogel, V. Parissi, P. Pourquier, I. Huc, *Nucleic Acids Research* **2019**, *47*, 5511-5521.

[115] D. J. Kuster, C. Liu, Z. Fang, J. W. Ponder, G. R. Marshall, *PLOS ONE* **2015**, *10*, e0123146.

[116] M. Zwillinger, P. S. Reddy, B. Wicher, P. K. Mandal, M. Csékei, L. Fischer, A. Kotschy, I. Huc, *Chemistry – A European Journal* **2020**, *26*, 17366-17370.

[117] L. Wang, C. Douat, J. Sigl, P. Sai Reddy, L. Fischer, B. L. d'Estaintot, Z. Liu, V. Pophristic, Y. Yang, Y. Zhang, I. Huc, *Chemical Science* **2025**, *16*, 12385-12396.

[118] M. Vallade, M. Jewginski, L. Fischer, J. Buratto, K. Bathany, J.-M. Schmitter, M. Stupfel, F. Godde, C. D. Mackereth, I. Huc, *Bioconjugate Chemistry* **2019**, *30*, 54-62.

[119] D. M. Hoover, J. Lubkowski, *Nucleic Acids Research* **2002**, *30*, e43-e43.

[120] A. F. Sandahl, T. J. D. Nguyen, R. A. Hansen, M. B. Johansen, T. Skrydstrup, K. V. Gothelf, *Nature Communications* **2021**, *12*, 2760.

[121] I. Sarac, C. Meier, *Chemistry – A European Journal* **2015**, *21*, 16421-16426.

[122] N. Hartrampf, A. Saebi, M. Poskus, Z. P. Gates, A. J. Callahan, A. E. Cowfer, S. Hanna, S. Antilla, C. K. Schissel, A. J. Quartararo, X. Ye, A. J. Mijalis, M. D. Simon, A. Loas, S. Liu, C. Jessen, T. E. Nielsen, B. L. Pentelute, *Science* **2020**, *368*, 980-987.

[123] M. D. Simon, P. L. Heider, A. Adamo, A. A. Vinogradov, S. K. Mong, X. Li, T. Berger, R. L. Policarpo, C. Zhang, Y. Zou, X. Liao, A. M. Spokoyny, K. F. Jensen, B. L. Pentelute, *ChemBioChem* **2014**, *15*, 713-720.

[124] F. S. Menke, B. Wicher, V. Maurizot, I. Huc, *Angewandte Chemie International Edition* **2023**, *62*, e202217325.

[125] L. Wang, J. M. Rogers, S. J. Dawson, L. M. Langhorn, R. T. Howard, S. Kwon, C. Douat, H. Suga, I. Huc, *Org. Biomol. Chem.* **2025**, *23*, 4641-4647.

6. Development of a vast library of abiotic aromatic building blocks and implementation of automated solid phase foldamer synthesis

Thanks to their spatially defined side chain orientation, aromatic oligoamide foldamers, composed of 8-amino-2-quinoline carboxylic acid (**Q**) as monomeric unit, have been recently applied to target proteins domains.[111, 117-118] However, the exclusive use of mono-substituted monomers in helical AOFs for protein surface recognition or mimicry might find limited applications due to low density and dispersed distribution of side chains along the helix axis.

Due to their structure, the **Q** units monomers can be considered as δ-amino acids that share the same number of backbone atoms as a biotic Gly-Gly dipeptide. Therefore, acquiring the ability to install and thus expose two side chains on a single **Q** unit would allow for an increased side chain density on the aromatic helix. This should result into higher biomolecule surface contacts and consequently improved binding affinity towards biological targets.

A novel chemistry, notable relying on palladium-based cross couplings, was recently developed, which gave access to novel **Q** units functionalised in position 4, 5, 6.[113-114, 116] Using this methodology, we could successfully expand our building-block library not only with **Q** monomers bearing one side chain but also with di-substituted **Q** units, resulting in 26 new Fmoc-protected monomers including protected cationic, anionic, and polar neutral side chains as well as hydrophobic side chains (**Figure 1**).

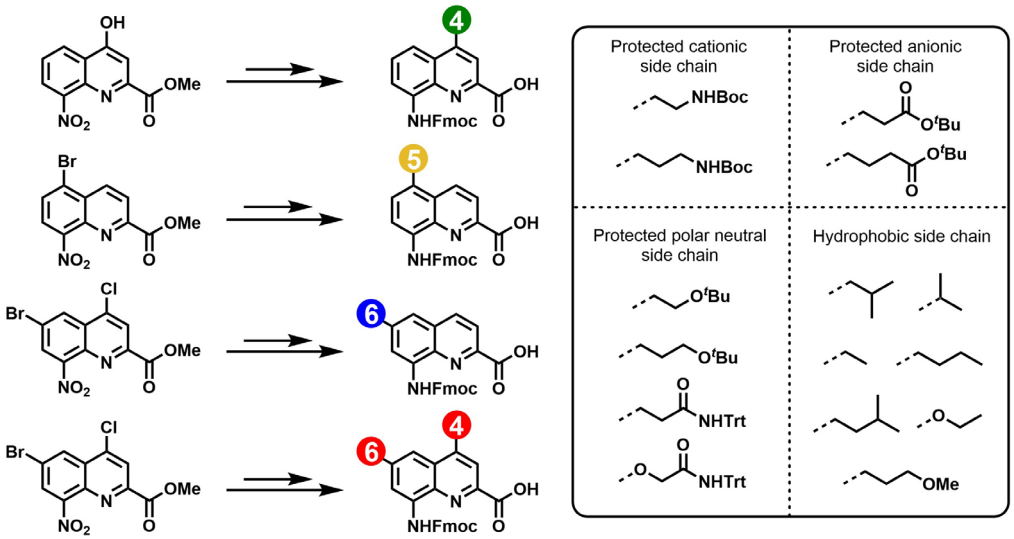

Figure 1. Representation of each building block precursor and end position of substitution on the quinoline ring. In green, the substitution is in position 4, gold is in 5, blue is in 6 and red is di-substituted monomer in positions 4 and 6. On the right are represented the side chains introduced on this quinoline derivatives and classified according to their common characteristic.

Another key synthetic challenge that we turned into a success was the full automation of our solid phase foldamer synthesis (SPFS) and the possibility to run several syntheses in parallel. Automated solid phase peptide synthesis (SPPS) is nowadays very accessible to any laboratory thanks to the variety of instruments available and methods making SPPS a very robust and reliable technique.[119-121] The, sometimes, tedious syntheses of long peptides or proteins have even proven to be facilitated by using automated flow chemistry.[122-123] Efficient solid phase synthesis (SPS) has thus become of an interest for numerous laboratories in diverse fields of research.

Over the years, the Huc group has successfully mastered the concept of SPS to build middle to long size AOFs.[99, 124-125] However, the syntheses of long aromatic oligomers have proven to be more challenging and time consuming. Moving from the previous use of Ghosez's reagent for acid chloride activation of Fmoc-protected Q-monomers, which required tedious dry conditions and short storage, to an *in situ* pre-activation using the Appel's reaction conditions was already a true improvement in terms of handling and efficiency in SPFS. However, for every monomer installation on solid support, a coupling cycle requires a Fmoc deprotection step, followed by a coupling step which must be repeated once to guarantee quasi quantitative coupling yields and series of resin washings, which makes a coupling cycle of about an hour for a well-trained scientist. In the hope of reaching wider surface protein target, the foldamer designs had to also get longer, making the synthesis time spent only in building the foldamer on solid support not negligible.

Aiming to make use of the robustness of the *in situ* SPFS protocols, the Huc group has sought a way to automate the production of AOFs by SPS. The Pure-Pep® Chorus peptide synthesizer from Gyros Protein Technologies has proven to meet all the requirements for SPFS. Not only does this synthesizer offer the possibility of a tandem *in situ* pre-activation-reaction vessel but it allows to perform up to three SPS in parallel.

The different works and results presented in the following publications show the efforts in Q-monomers synthesis to offer a broader range of biogenic building blocks for AOF synthesis with twenty-six new monomers compatible with SPS as well as the development and optimisation of the automated SPFS on long aromatic oligoamide foldamers in high purity and yield.

6.1. Publication: Development of aromatic foldamer building blocks bearing multiple biogenic side chains

Authors: Márton Zwillinger[#], Petra Sőregi[#], Florian Sanchez[#], Céline Douat, Márton Csékei, Ivan Huc[*] and András Kotschy[*].

[#]Equal contributors

Contributions: This project is a joint collaboration between two groups. It was planned by A. Kotschy and I. Huc. Building blocks syntheses were performed by M. Zwillinger, P. Sőregi and me. Foldamer synthesis performed by F. Sanchez and C. Douat. Project was co-supervised by C. Douat, M. Csékei, I. Huc and A. Kotschy. The manuscript was written in collaboration with M. Zwillinger, P. Sőregi, F.,Sanchez, C. Douat, M. Csékei, I. Huc, A. Kotschy.

Publication: *J. Org. Chem*. **2025**, 90, 8, 3043-3052.

DOI: https://doi.org/10.1021/acs.joc.4c02900

JOC The Journal of Organic Chemistry

pubs.acs.org/joc Article

Development of Aromatic Foldamer Building Blocks Bearing Multiple Biogenic Side Chains

Márton Zwillinger,[#] Petra Sőregi,[#] Florian Sanchez,[#] Céline Douat, Márton Csékei, Ivan Huc,* and András Kotschy*

Cite This: J. Org. Chem. 2025, 90, 3043−3052 Read Online

ACCESS | Metrics & More | Article Recommendations | Supporting Information

ABSTRACT: Aromatic oligoamides, with their intrinsic rigidity and well-defined conformations, are recognized for their potential in medical applications. Similar structures are present in several naturally occurring antibiotics and have been explored for their ability to bind to various proteins and B-DNA (canonical right-handed DNA helix). This study introduces a synthetic approach to produce quinoline amino acid monomers bearing diversified side chain combinations in positions 4, 5, and 6 of the quinoline ring, designed to enhance the side chain density on helical foldamers. By increasing the number of side chains on each monomer, we aim to mimic the dense side chain presentation of α-peptides, thus improving the potential for protein surface recognition. This synthetic strategy involves efficient functionalization through cross-coupling reactions, enabling the installation of diverse side chains at strategic positions on the quinoline ring. The process has been optimized for automated solid-phase synthesis, successfully producing a 20-unit oligoamide with good purity. This foldamer, featuring multiple cationic, anionic, polar, and hydrophobic side chains, demonstrates the potential for molecular recognition in drug discovery and therapeutic applications. The methodology described here represents a significant advancement in the construction of aromatic oligoamide foldamers, providing a robust platform for further exploration of biological systems.

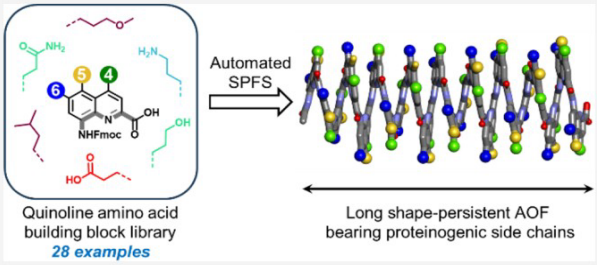

INTRODUCTION

Thanks to their intrinsic rigidity and well-defined conformations, aromatic oligoamides are considered privileged structures for medical applications.[1−8] Several naturally occurring antibiotics contain aromatic amide units, including cystobactamids[9] and albicidin,[10,11] as well as distamycin A and its analogues, netropsin and anthelvencin C.[12−14] The latter family has been the object of considerable development toward sequence-specific oligo-pyrrole-imidazole minor groove binders of B-DNA.[15,16] Along the same line, the old arylamide antiparasitic drug suramin has been shown to bind to a large number of proteins[5−8] and the design of suramin analogs is the object of current investigations.[17−19]

In parallel, along with other rigid backbones,[20−26] aromatic oligoamide foldamers have been developed as scaffolds to display proteinogenic side chains at defined positions in space. These may be divided into short rod-like oligomers with amphipathic structures that may have antibiotic activity,[27,28] rod-like oligomers that mimic α-helices,[29−35] and helically folded oligoarylamides that may cover large surface areas of proteins,[36−38] interfere with amyloid aggregation,[39,40] or mimic the B-DNA structure and competitively inhibit DNA−protein interactions.[41−44]

The field of aromatic oligoamide foldamers is driven by the continuous development of new monomers, and particularly by the availability of a variety of side chains that can be tethered at various positions of the aromatic units (Figure 1). In the case of 8-amino-2-quinoline carboxylic acid (Figure 1), one of the most frequently employed δ-amino acid building blocks of the helically folded oligoarylamides mentioned above, efforts have already been made toward producing main chain variations using pyridine- or benzene-based monomers,[45] and to control helix handedness.[46−50] Methods to install various proteinogenic side chains in positions 4, 5, or 6 of the quinoline ring are also available.[51,52] However, such δ-amino acid monomers may be considered as equivalents to dipeptides, and a dipeptide possesses two side chains. It follows that helices of 8-amino-2-quinoline carboxylic acid-derived oligoamides bearing only one side chain per monomer have a relatively scattered side chain presentation at their surface and largely expose their main chain to the solvent, thus reducing opportunities for interactions with biological targets. Installing additional side chains on each monomer would instead enable a high side chain density at the

Received: November 25, 2024
Revised: January 21, 2025
Accepted: January 30, 2025
Published: February 18, 2025

https://doi.org/10.1021/acs.joc.4c02900
J. Org. Chem. 2025, 90, 3043−3052

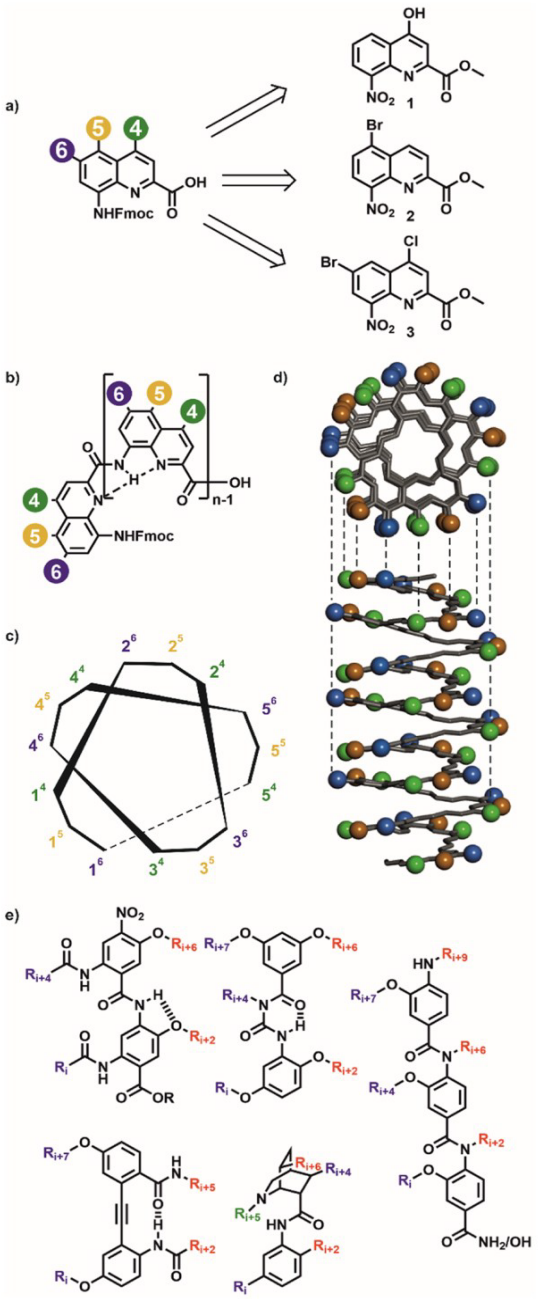

Figure 1. (a) Representation of the different precursors for the synthesis of monomer building blocks bearing side chains in positions 4 (green), 5 (gold), and 6 (blue). (b) Chain elongation of an aromatic oligoamide foldamer. Hydrogen bonds on the inner rim of the helix are indicated as dashed lines. (c) Schematic representations of an 8-amino-2-quinolinecarboxylic acid oligoamide helix showing the density of side chains in position 4 (green), 5 (gold), and 6 (blue). Numbers indicate monomer unit position in the sequence, while superscript numbers indicate side chain position on a given quinoline monomer. (d) Top view and side view of a molecular model of an aromatic oligoamide foldamer showing the substitution position in 4 (green spheres), 5 (gold spheres), and 6 (blue spheres). (e) Examples of multifacial α-helix mimetics having two side chains per monomer taken from ref 31. The side chain numbers correspond to equivalent residue positions in an α-helical α-peptide sequence.

surface of such helices (Figure 1). The issue of low side chain density has already been addressed for rod-like oligoamides, leading to the design and synthesis of multifacial α-helix mimetics bearing two side chains per monomer (Figure 1d).[31,53,54]

Here, we describe an efficient synthetic approach to produce 4,6-disubstituted 8-amino-2-quinoline carboxylic acid monomers. We also expand the diversity of monomers bearing a single side chain at positions 4, 5 or 6. Combined with previously described monomers,[41,42,51,52] the new monomers offer innumerable combinations for side chain presentation on helically folded oligoarylamides.

RESULTS AND DISCUSSION

General Concept. It has been illustrated that a single face of an aromatic foldamer helix, constructed using 4- and 6-substituted quinoline building blocks, can effectively project side chains at positions mimicking those of a polypeptide's α-helix.[51] A crucial aspect in achieving this lies in the increased density of side chains, which create a potential binding motif on one face of the foldamer helix. While relocating specific side chains by altering the substitution pattern of a few monomers within a sequence can result in a localized increase in side chain density, a broader adjustment would be achieved by raising the number of residues carried by the same backbone. We surmised that doubling the number of side chains carried by each quinoline unit would result in a side chain density resembling that observed in α-peptides and proteins. The surface of helices with increased side chain density would be richer in information and better suited for protein surface recognition (Figure 1).

To enable the creation of helical foldamers with modified surface substitution patterns, we designed an array of novel quinoline-based monomers. The designed building blocks feature suitably protected cationic, anionic, polar neutral, and hydrophobic side chains attached to positions 4, 5, or 6 of the quinoline, respectively. To introduce side chains at these positions, three previously described, easily accessible quinoline derivatives were used as starting materials: methyl-4-hydroxy-8-nitro-quinoline-2-carboxylate (**1**),[55] methyl-5-bromo-8-nitro-quinoline-2-carboxylate (**2**)[52] and methyl-6-bromo-4-chloro-8-nitro-quinoline-2-carboxylate (**3**).[51] The 4-hydroxy group of **1** can be utilized in nucleophilic substitutions to yield monomers with oxygen-linked side chains. It can also be converted to a 4-chloro or 4-bromo group. Chloro or bromo substituents in position 4, 5, or 6 can be engaged in carbon−carbon cross-coupling reactions. Efficient functionalization was achieved by sp^2-sp^3 (Suzuki), sp^2-sp^2 (Suzuki, Heck), or sp^2-sp (Sonogashira) cross-couplings. The choice of method depended on the nature of the side chain and the availability of its precursor. Notably, side chain synthons could be either alkynes, alkenes, or alkenyl- or alkyl-boron reagents, thus offering a broad spectrum of potential precursors. Compound **3** possesses both a 4-chloro and a 6-bromo substituent, which can be involved in cross-coupling reactions sequentially, giving access to 4,6-difunctionalized monomers. Finally, the monomers were all delivered in a protected form, ready for solid-phase foldamer synthesis,[56] that is, with a free carboxylic acid in position 2, a Fmoc-protected amine in position 8, and suitable acid-labile protecting groups on their side chains. We discuss below the different routes and the synthetic hurdles with which we had to cope.

Preparation of 4-Monosubstituted Quinoline Derivatives. Several 4-monosubstituted monomers have been

https://doi.org/10.1021/acs.joc.4c02900
J. Org. Chem. 2025, 90, 3043−3052

designed and synthesized, utilizing key intermediates **1** and **4** as starting materials (Scheme 1). The diversity of the new side

Scheme 1. Synthetic Pathway of 4-Monosubstituted *N*-Fmoc Quinoline Monomers 7a−d[a]

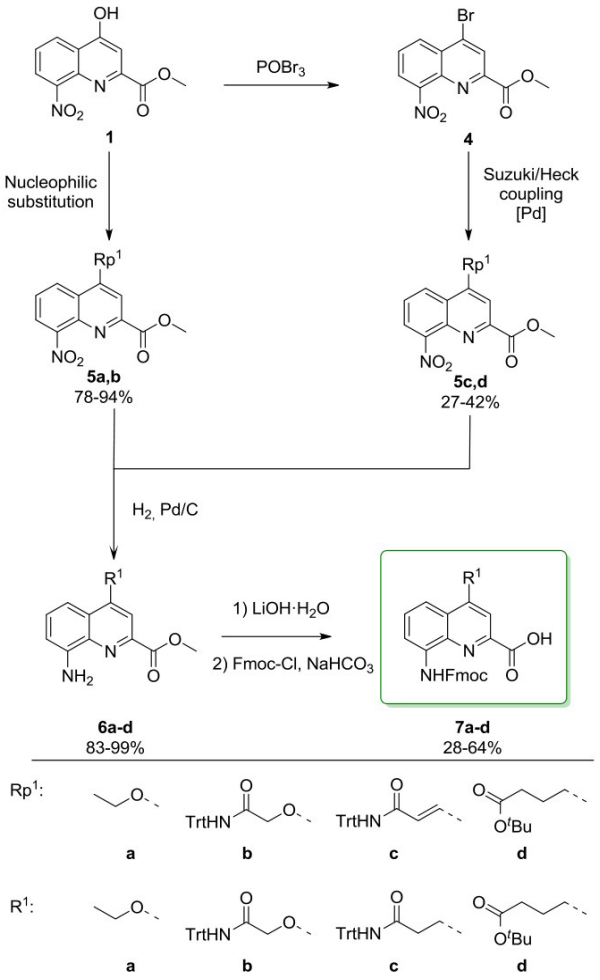

[a]$Pd(OAc)_2$ and tris(*o*-tolyl)phosphine $P(oTol)_3$ were used to obtain intermediate **5c**. Intermediate **5d** was synthesized using bis(di-*tert*-butyl(4-dimethylaminophenyl)phosphine)dichloropalladium(II) Pd-$(AtaPhos)_2Cl_2$.

chains is not extensive, as they simply complement a broad range of hydrophobic, anionic, cationic, and polar neutral side chains already introduced in position 4.[41,42,51,52] Side chains with primary amide functions were desirable as asparagine and glutamine analogues. The synthon **1** has been previously used to prepare a variety of quinoline-based monomers, where the hydroxyl group in position 4 could participate in nucleophilic substitution reactions, leading to aryl-alkyl ether linkages.[52] As depicted in Scheme 1, the nucleophilic substitution of ethyl iodide with **1** furnished intermediate **5a** in good yield, and then the nitro group was reduced by catalytic hydrogenation to give **6a** in quantitative yield. For the preparation of intermediate **5b**, the primary amide was protected with a trityl group.[57] The nucleophilic substitution of 2-bromo-*N*-tritylacetamide with **1** proceeded smoothly, and **6b** was isolated in good yield after subsequent catalytic hydrogenation of **5b** (Scheme 1).

The 4-bromo group of precursor **4**[31] served as the aryl halide in cross-coupling reactions. For the introduction of *N*-tritylpropionamide (**5c**) and *tert*-butyl-butyrate (**5d**) side chains, a Heck coupling of the corresponding alkene derivative with **4**, followed by saturation of the double bond, was envisaged. In the case of the *N*-trityl-protected acrylamide, Heck coupling furnished intermediate **5c** in moderate yield (42%), which was then hydrogenated to give **6c** in 83% yield. In contrast, attempts to perform Heck coupling with *tert*-butyl-but-3-enoate failed. An alternative approach could have been to perform a Sonogashira coupling in the presence of *tert*-butyl-but-3-ynoate, but purchasing or synthesizing this reactant was not practical. A third approach consisted of using boron derivatives in Suzuki coupling.

Since the appropriate alkenyl boronate derivative was not available, we generated the alkyl analog *in situ* from the alkene and 9-BBN.[51] Indeed, the hydroboration of *tert*-butyl-but-3-enoate with 9-BBN gave the corresponding trialkylborane precursor, which was successfully used in the following sp^2-sp^3 Suzuki coupling to give **5d** in a moderate yield (27%). Subsequent hydrogenation of the nitro group yielded **6d** with a good yield (87%). Earlier, we reported a one-pot method to convert amino esters to *N*-Fmoc protected amino acids.[51] Starting from **6a−d**, this method gave monomers **7a−d** in moderate to good yields.

Preparation of 5-Monosubstituted Quinoline Monomers. In a second stage, five new 5-monosubstituted monomers were designed, carrying cationic and aliphatic side chains in position 5 (Scheme 2). Again, these side chains are additions to

Scheme 2. Synthetic Pathway of 5-Monosubstituted *N*-Fmoc Quinoline Monomers 10a−e[a]

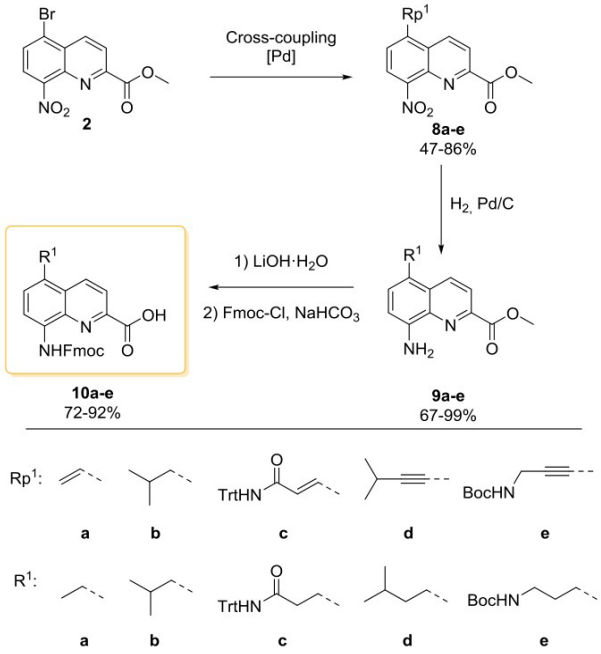

[a]Cross-couplings involved the use of $Pd(OAc)_2$ and SPhos (Dicyclohexyl(2′,6′-dimethoxy[1,1′-biphenyl]-2-yl)phosphine) or P-$(oTol)_3$ for intermediates **8a** and **8c**, respectively. $Pd(PPh_3)_2Cl_2$ was used for the synthesis of intermediates **8b**, **8d**, and **8e**. $P(oTol)_3$ was added for intermediate **8e**.

https://doi.org/10.1021/acs.joc.4c02900
J. Org. Chem. 2025, 90, 3043−3052

an existing series. For example, several anionic side chains containing a carboxylic or phosphonic acid function have been previously introduced in position 5.[41,42,52] Their common starting material was the 5-bromoquinoline derivative **2**, which was converted into intermediates **8a−e** by using various cross-coupling reactions. Hence, **8a** and **8b** were prepared via Suzuki couplings, where potassium vinyltrifluoroborate and isobutylboronic acid were used as side chain synthons, respectively. For the introduction of the *N*-trityl-propionamide side chain, *N*-trityl-acrylamide was employed in a Heck coupling reaction to produce **8c**. Compounds **8d** and **8e** were synthesized via Sonogashira reactions using the appropriate alkynes. Subsequently, all five amino esters **9a−e** were isolated in good to quantitative yields after a catalytic hydrogenation reaction, where both the nitro group and the unsaturated carbon−carbon bonds were reduced. Further hydrolysis of the amino esters and *N*-Fmoc protection of the newly obtained amino acids were performed to obtain the final **10a−e** monomers in good yields.

Selective Functionalization at Position 6 to Furnish 6-Monosubstituted Quinoline Monomers. In a previous work, we reported a robust synthesis allowing the efficient installation of various side chains in position 6 and the production of *N*-Fmoc-protected-6-substituted aminoquinoline carboxylic acid monomers on a gram scale.[51] The approach is based on selective cross-coupling at the 6-position of methyl 6-bromo-4-chloro-8-nitro-2-quinolinecarboxylate (**3**). By adapting this methodology, five new 6-monosubstituted quinoline monomers were prepared, allowing us to broaden the repertoire of side chains available at this position of the quinoline ring (Scheme 3). To introduce the *iso*pentyl and *n*-butyl side chains, we opted for the alkyne synthons 3-methyl-but-1-yne and but-1-yn-1-yltrimethylsilane, respectively. The latter could be easily deprotected *in situ* by using H_2SiF_6. The Sonogashira coupling of these two synthons proceeded smoothly, and the reaction took place regioselectively on the bromine to furnish **11a** and **11b** in good yields, leaving the chlorine untouched. The alkynyl synthons needed for the introduction of isopropyl and isobutyl side chains do not exist, so we started from the appropriate alkenyl boronates, whose Suzuki coupling yielded the desired derivatives **11c** and **11d**. This time, the regioselectivity was poor, and significant amounts of the 4,6-disubstituted products were also obtained in both cases. To introduce a propionate side chain, we attempted to perform the Sonogashira reaction of **3** with *tert*-butyl propiolate, but it failed under several conditions. To overcome this difficulty, we used *tert*-butyl acrylate in Heck coupling. This transformation was selective, and **11e** was isolated in acceptable yield. Intermediates **11a−e** were further transformed by hydrogenation, which allowed the simultaneous (i) dechlorination in position 4, (ii) saturation of the side chains, and (iii) reduction of the nitro group to produce the corresponding amino esters **12a−e** in moderate to good yields. Subsequent hydrolysis and *N*-Fmoc protection were carried out, yielding the *N*-Fmoc-protected-6-substituted amino-quinoline carboxylic acid monomers **13a−e** in fair to good yields.

Scheme 3. Synthetic Pathway of 6-Monosubstituted *N*-Fmoc Quinoline Monomers 13a−11e[a]

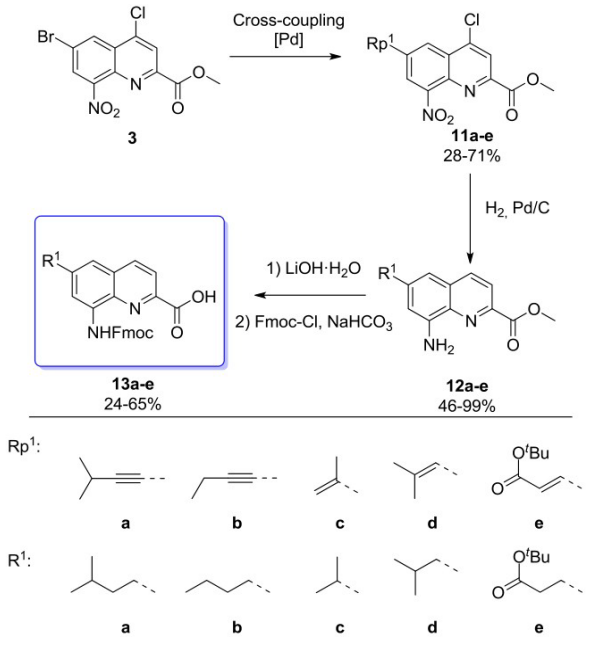

[a]Cross couplings involved different palladium-based catalysts: Pd(PPh$_3$)$_2$Cl$_2$ (**11a−b**), [1,1′-Bis(diphenylphosphino)ferrocene]-palladium(II) dichloride, Pd(dppf)Cl$_2$ (11c and 11d), and Pd(PPh$_3$)$_4$ with P(^{t}Bu)$_3$ (**11e**).

Sequential Side Chain Introduction to Furnish 4,6-Disubstituted Monomers. For 4,6-disubstituted monomers, we wished to install a broad spectrum of side chain characteristics, including hydrophobic, polar neutral, cationic, and anionic moieties, and selected 10 combinations to construct a mini library. Of course, possible combinations are endless. Starting from **3**, functionalization in position 6 afforded **11a** as presented above, as well as previously described **14a** and **14b** (Scheme 4a).[51] The functionalization at position 4 of these compounds was attempted using commercial alkene precursors that were converted to alkylboranes in the presence of 9-BBN to perform sp^2-sp^3 Suzuki couplings. However, these couplings failed, which we attributed to the nitro group that caused undesired side reactions. To circumvent this problem, reduction was brought forward in the synthetic sequence, preceding the cross-coupling. The simultaneous reduction of the side chain triple bond and the 8-nitro group was achieved using mild catalytic hydrogenation over Raney nickel at room temperature, while the chlorine in position 4 remained untouched, yielding **15a−c**. Subsequent two-step, one-pot hydroboration and Suzuki coupling reactions successfully gave access to intermediates **16a−e** in moderate to good yields. The temperature and reaction time for hydroboration and coupling reactions were adjusted for each alkene precursor, as their electronic properties significantly influenced both reactions. Electron-rich alkenes underwent rapid and clean hydroboration, whereas *tert*-butyl acrylate exhibited slower reactivity and produced byproducts. We have also assessed Heck or Sonogashira reactions as potential alternatives, but the Suzuki couplings demonstrated superior performance.

Two other 6-substituted 4-chloroquinolines, **19a** and **19b**, were prepared via regioselective Suzuki coupling from readily available intermediate **18**[51] in moderate to good yields (Scheme 4b). In the subsequent step, **19a** and **19b** were coupled with a second set of alkylboranes to yield *N*-trifluoroacetylated amino esters **20a−e** bearing two different side chains. The one-pot hydrolysis of the amide and ester functions and *N*-Fmoc installation were carried out similarly on intermediates **16a−e** and **20a−e** to obtain the final 4,6-disubstitued monomers **17a−e** and **21a−e** in moderate to good yields.

https://doi.org/10.1021/acs.joc.4c02900
J. Org. Chem. 2025, 90, 3043−3052

Scheme 4. Synthetic Pathways of 4,6-Disubstituted *N*-Fmoc Quinoline Monomers Bearing Different Side Chains[a]

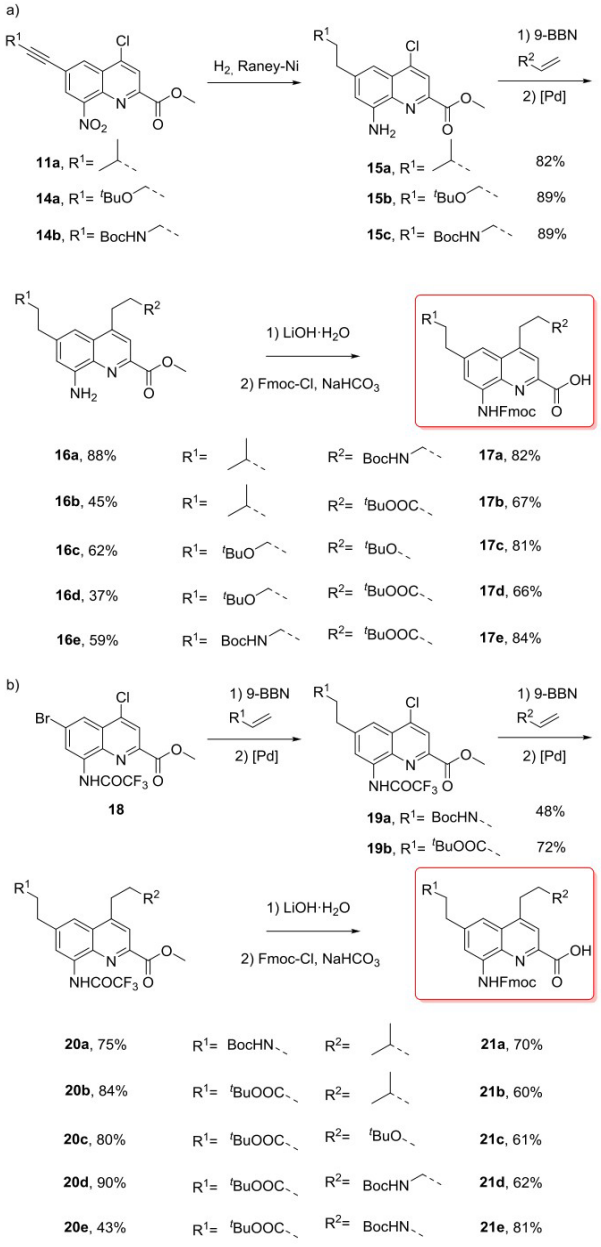

[a]Intermediates **16a−d**, **19b**, and **20a−e** were obtained using $Pd(AtaPhos)_2Cl_2$. Tris(dibenzylideneacetone)dipalladium(0) $Pd_2(dba)_3$ and diethyl(4-dimethylaminophenyl)phosphine were used for intermediate **16e**.

Concomitant Introduction of the Same Side Chain in Positions 4 and 6 of Quinoline Monomers. The presence of the halogen atoms in both the 4- and 6-positions allows for the incorporation of the same side chain at the same time. Coupling of intermediate **18** with the alkylborane derived from *tert*-butylvinyl ether led to the simultaneous production of the monosubstituted product **22a** (which relates to **19a** and **19b**) and the disubstituted product **22b** in 66% and 25% yields, respectively (Scheme 5a). Intermediate **23** was further hydrolyzed to obtain the amino acid, which, after *N*-Fmoc protection, gave monomer **28d** in 50% yield. While the lower reactivity of chlorine at position 4 is advantageous for regioselective couplings, it is disadvantageous when the same side chain is introduced in both positions, as reflected by the low yield of **22b**. To enhance the reactivity at position 4, the 4,6-dibromo quinoline derivative **23** was synthesized from the 6-bromo-4-hydroxy precursor using $POBr_3$.[58] Double Sonogashira couplings gave access to the desired bisalkyne-functionalized quinoline intermediates **24a** and **24b** in good yield (Scheme 5b).

In the case of the propionate side chain, Heck coupling showed significant dehalogenation. When the nitro group of intermediate **23** was carefully reduced over Raney nickel to the amine **25**, the Heck coupling with *tert*-butyl acrylate proceeded smoothly, and intermediate **26** was isolated in 74% yield. Subsequent saturation of the double and triple bonds of **24a−b** and **26** by catalytic hydrogenation gave **27a−c** in a good yield. The one-pot hydrolysis of the obtained amino esters to amino acids, followed by the *N*-Fmoc protection of the 8-amino group, afforded the foldamer building blocks **28a−c** with fair to good yields.

The complete list of the synthesized monomers and the cumulative yields of their synthesis are listed in the Supporting Information Section 3.5. It is difficult to observe any relationship between the efficiency of the synthesis and the nature of the side chain, which is probably not surprising if we consider the fact that all polar side chains are present in a protected form, which masks their differences in character.

Automated Foldamer Synthesis. The development of efficient peptide screening methods in drug discovery, such as display selection, has renewed interest in peptides in both academic and industrial research. Simultaneously, advancements in the automation of peptide synthesis, as well as the release of new synthesizers, have made solid-phase peptide synthesis accessible to many laboratories.[59] In this context, we have developed effective and reliable methods to synthesize helical aromatic oligoamide foldamers on solid phase, and we have recently automated the process.[56] We sought to challenge our automated solid-phase synthesis protocol using the collection of new monomers and set out to build a 20-unit-long, ∼5.3 kDa large sequence comprised of 20 different monomers. For laboratories not equipped with a suitable automated synthesizer, the manual solid-phase synthesis of a 20mer is perfectly doable using microwave heating and *in situ* acid chloride activation protocols adapted from the Appel reaction.[60,61] In contrast, the solution-phase synthesis of such a molecule would be extremely tedious, even to an experienced chemist. To demonstrate the usefulness of the monomers as well as the power of the synthesizer, we selected the 20 building blocks to exhibit multiple cationic, anionic, polar, or hydrophobic moieties on the different faces of the helix and designed foldamer **29** (see Figure 2d). This target foldamer would be comparable to an α-peptide containing each of the 20 natural amino acids in terms of synthetic effort, albeit being twice as large and bearing more than 20 side chains. Note that **29** is achiral and should thus exist as a racemic mixture of right- and left-handed helical conformers. If a one-handed helix is desired, for example, to target a protein diastereoselectively, absolute handedness control can be achieved by introducing chiral residues.[46−50] Alternatively, protein-foldamer interactions may also bias helix handedness of an otherwise achiral foldamer.[37,38,62]

https://doi.org/10.1021/acs.joc.4c02900
J. Org. Chem. 2025, 90, 3043−3052

Scheme 5. Synthetic Pathways of 4,6-Disubstituted *N*-Fmoc Quinoline Monomers Bearing the Same Side Chain[a]

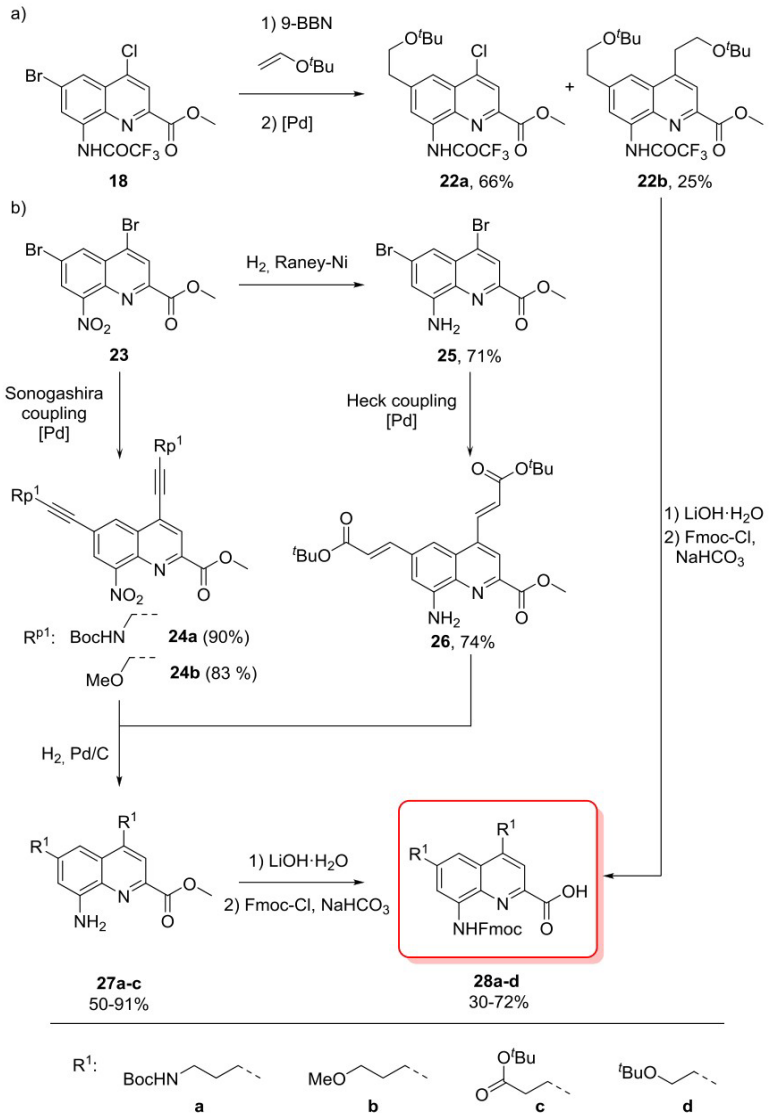

[a]Intermediates **22b** and **24a–b** were obtained using $Pd(AtaPhos)_2Cl_2$. $Pd(OAc)_2$ and $P(o\text{Tol})_3$ were used for the intermediate **26.**

The 4,6-disubstituted monomer **28c** was preloaded on a Tentagel Wang resin (low loading, 15 μmol scale), which allows for better bead swelling and gives cleaner crude profiles for long sequences.[63] The subsequent coupling of 19 different Fmoc-protected quinoline monomers was performed on the automated synthesizer, applying deprotection and coupling conditions as depicted in Figure 2a. Of note, recent optimization of the reaction conditions[64] showed that the Fmoc deprotection using 2% DBU in NMP could be shortened to two times 3 min (previously 2 × 10 min) with no measurable loss of efficiency. Coupling conditions involved, as before, the *in situ* acid chloride formation in the preactivation vessel by relying on the Appel reaction with PPh_3 and trichloroacetonitrile (TCAN), before transferring the solution to the reaction vessel containing the resin swollen in anhydrous THF and 2,4,6-collidine. Couplings were performed twice at 50 °C for 15 min. With that, a coupling/deprotection cycle lasts less than an hour, and the whole 20mer (**29**) could be produced in around 15 h. After final acetylation of the resin-bound 20mer, side chain deprotection and cleavage from the resin were performed in a TFA solution containing 2.5% TIPS and 2.5% water as scavengers.

The reverse-phase HPLC (RP-HPLC) analysis of the recovered crude foldamer was encouraging, showing 55% purity. A second peak with a relatively high intensity was also visible on the chromatogram (marked with a red star in Figure 2b), but we were unable to identify this impurity by mass spectrometry. The 20mer **29** was purified by semi-preparative RP-HPLC, and its final chromatogram confirmed a purity over 95%. The recovered yield after purification was 10%, which is satisfactory when compared to the isolation of an HPLC-purified peptide of comparable size (i.e., 40 residues). The ^{1}H NMR spectrum recorded in DMF-d_7 showed one set of signals spread over a wide range of chemical shifts characteristic of the quinoline carboxamide helices (Figure 2c). Typical indications of helical

https://doi.org/10.1021/acs.joc.4c02900
J. Org. Chem. 2025, 90, 3043−3052

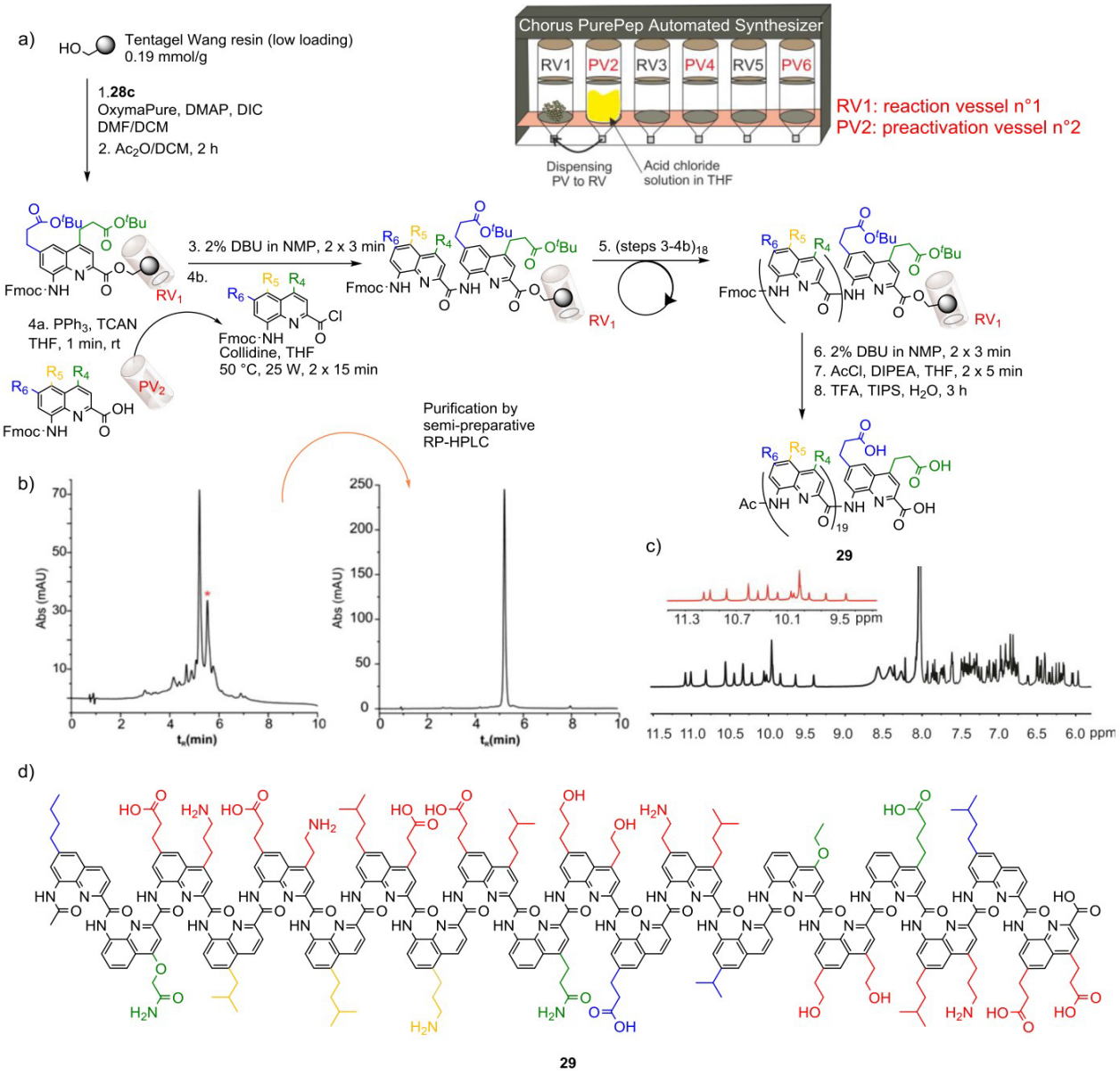

Figure 2. (a) SPFS (solid-phase foldamer synthesis) protocol recently developed, allowing the automation of the deprotection/coupling cycle for each of the 19 different aromatic monomers. The Chorus Purepep synthesizer is depicted to emphasize the *in situ* preactivation step (4a), which is performed in an independent preactivation vessel for 1 min before dispensing the acid chloride solution in the reaction vessel containing the resin swollen in THF with collidine. (b) RP-HPLC chromatograms of the 20mer (**29**), 75 mg as crude and after purification via RP-HPLC (linear gradient from 20% B to 80% B in 15 min, A: H_2O + 0.1% TFA and B: CH_3CN + 0.1% TFA, C8 column. (c) ^1H NMR of purified 20mer (**29**) in DMF-d_7 (500 MHz) at 0.5 mM at 298 K in black, NH amide region highlighted in red. (d) 20mer foldamer representation with position 4 monosubstituted monomer with green side chains, position 5-monosubstituted with golden side chains, position 6 monosubstituted with blue side chains, and position 4,6 disubstituted with red side chains. DIPEA: *N*,*N*-diisopropylethylamine, DIC: diisopropylcarbodiimide.

folding also include the anisochronicity of the diastereotopic CH_2 proton resonances of the side chains in ^1H NMR spectra. Methods to assign these spectra and to demonstrate helical conformations in solution have been reported.[65] An energy-minimized model of **29** is shown in Figure 3 along with a helix-wheel representation of the position of the side chains. Both highlight the side chain density that can be achieved by combining 4-, 5-, and 6-substituted monomers along with 4,6-disubstituted units.

CONCLUSION

Oligoamides built from natural amino acids and their close analogs form an indispensable part of today's research toolbox in medicinal chemistry and chemical biology. This is largely due to the fact that their building blocks are accessible in a large variety and that their construction has been automated, allowing for the efficient preparation of diverse libraries. While aromatic foldamers showed great promise as peptide mimetics due to their inherent self-organization potential and the possibility to

https://doi.org/10.1021/acs.joc.4c02900
J. Org. Chem. 2025, 90, 3043−3052

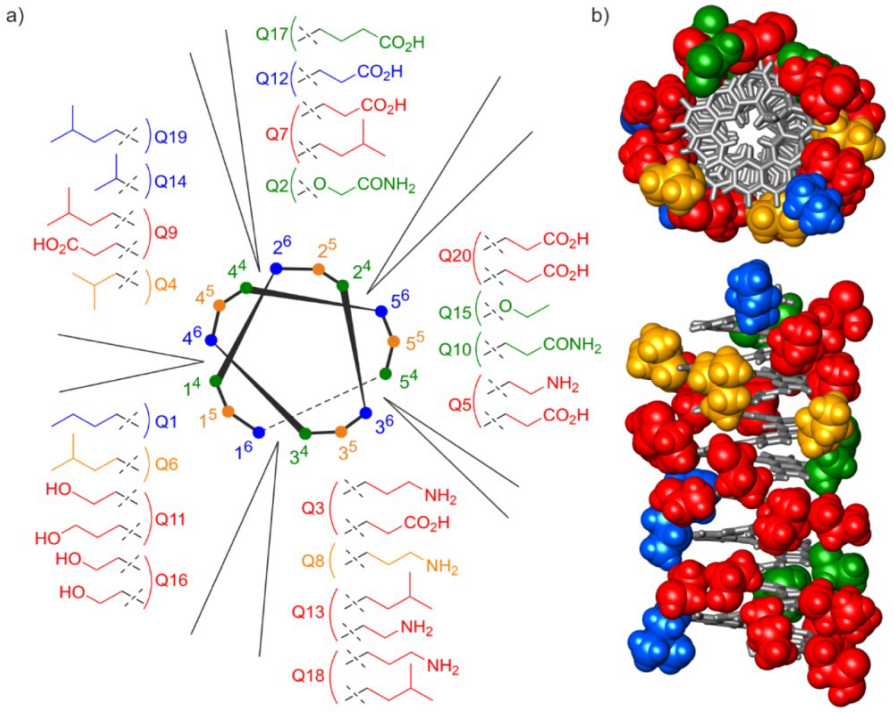

Figure 3. (a) Helix wheel representation of sequence **29**. The numbers around the wheel indicate the five first monomers, and their exponent refers to the possible position of their side chains. Monomers with one side chain in position 4, 5, or 6 are colored in green, gold, or blue, respectively. Monomers with side chains in positions 4 and 6 are shown in red. In all of the cases, the side chain shown on top is in position 4 and that below is in position 6. (b) Top view and side view of an energy minimized (MMFFs force field in Maestro)[66] model of sequence **29**. The main chain is shown in a gray tube representation. The side chains are shown in space-filling representation and are color-coded as in (a).

achieve high pharmacophore density on their surface, their widespread use was hampered both by limited access to building blocks and tedious process of oligomer assembly.

Using some easily accessible common building blocks, we developed a modular synthetic approach that allows for the introduction of various side chains into any of the desired positions on the aromatic foldamer core. The approach was validated through the preparation of 4-, 5-, and 6- mono-substituted, as well as 4,6-disubstituted foldamer building blocks. The prepared compounds carry a collection of side chains—apolar, polar, aromatic, acidic, and basic in nature—that mimic the natural diversity of amino acids. Finally, we demonstrated that a combination of the diverse monomer building blocks with the recently developed automated foldamer synthesis removes the technical barrier from the widespread use of this compound class. A 20mer consisting of 20 different building blocks and carrying a structural design that might be relevant for biological applications (i.e., similar pharmacophores being concentrated on the same part of the foldamer surface) was prepared in less than a day and was isolated in good overall yield and high purity. Expansion of this work to address biological problems is in progress in our laboratories.

■ ASSOCIATED CONTENT

Data Availability Statement

The data underlying this study are available in the published article and its Supporting Information.

Supporting Information

The Supporting Information is available free of charge at https://pubs.acs.org/doi/10.1021/acs.joc.4c02900.

Experimental details, materials, methods, and characterization data, including copies of NMR spectra (PDF)

■ AUTHOR INFORMATION

Corresponding Authors

Ivan Huc − *Ludwig-Maximilians-Universität, München 81377, Germany*; orcid.org/0000-0001-7036-9696; Email: ivan.huc@cup.lmu.de

András Kotschy − *Servier Research Institute of Medicinal Chemistry, Budapest 1031, Hungary*; orcid.org/0000-0002-7675-3864; Email: andras.kotschy@servier.com

Authors

Márton Zwillinger − *Servier Research Institute of Medicinal Chemistry, Budapest 1031, Hungary*

Petra Sőregi − *Servier Research Institute of Medicinal Chemistry, Budapest 1031, Hungary; Hevesy György PhD School of Chemistry, Eötvös Loránd University, Budapest 1117, Hungary*

Florian Sanchez − *Ludwig-Maximilians-Universität, München 81377, Germany*

Céline Douat − *Ludwig-Maximilians-Universität, München 81377, Germany*; orcid.org/0000-0003-2678-1047

Márton Csékei − *Servier Research Institute of Medicinal Chemistry, Budapest 1031, Hungary*; orcid.org/0000-0002-5781-1096

Complete contact information is available at: https://pubs.acs.org/10.1021/acs.joc.4c02900

https://doi.org/10.1021/acs.joc.4c02900
J. Org. Chem. 2025, 90, 3043−3052

Author Contributions

[#]M.Z., P.S., and F.S. contributed equally. The manuscript was written with contributions from all authors.

Notes

The authors declare no competing financial interest.

■ ACKNOWLEDGMENTS

Project C1016600 has been implemented with the support provided by the Ministry of Culture and Innovation of Hungary from the National Research, Development and Innovation Fund, financed under the KDP-2020 funding scheme (P.S.).

■ REFERENCES

(1) Seedorf, T.; Kirschning, A.; Solga, D. Natural and Synthetic Oligoarylamides: Privileged Structures for Medical Applications. *Chem. -Eur. J.* **2021**, *27* (26), 7321−7339.

(2) Zeelen, J.; van Straaten, M.; Verdi, J.; Hempelmann, A.; Hashemi, H.; Perez, K.; Jeffrey, P. D.; Hälg, S.; Wiedemar, N.; Mäser, P.; Papavasiliou, F. N.; Stebbins, C. E. Structure of Trypanosome Coat Protein VSGsur and Function in Suramin Resistance. *Nat. Microbiol.* **2021**, *6* (3), 392−400.

(3) Salvador, G. H. M.; Dreyer, T. R.; Gomes, A. A. S.; Cavalcante, W. L. G.; Dos Santos, J. I.; Gandin, C. A.; De Oliveira Neto, M.; Gallacci, M.; Fontes, M. R. M. Structural and Functional Characterization of Suramin-Bound MjTX-I from Bothrops Moojeni Suggests a Particular Myotoxic Mechanism. *Sci. Rep.* **2018**, *8*, 10317.

(4) Jiao, L.; Ouyang, S.; Liang, M.; Niu, F.; Shaw, N.; Wu, W.; Ding, W.; Jin, C.; Peng, Y.; Zhu, Y.; Zhang, F.; Wang, T.; Li, C.; Zuo, X.; Luan, C.-H.; Li, D.; Liu, Z.-J. Structure of Severe Fever with Thrombocytopenia Syndrome Virus Nucleocapsid Protein in Complex with Suramin Reveals Therapeutic Potential. *J. Virol.* **2013**, *87* (12), 6829−6839.

(5) Murakami, M. T.; Arruda, E. Z.; Melo, P. A.; Martinez, A. B.; Calil-Eliás, S.; Tomaz, M. A.; Lomonte, B.; Gutiérrez, J. M.; Arni, R. K. Inhibition of Myotoxic Activity of Bothrops Asper Myotoxin II by the Anti-Trypanosomal Drug Suramin. *J. Mol. Biol.* **2005**, *350* (3), 416−426.

(6) Salvador, G. H. M.; Dreyer, T. R.; Cavalcante, W. L. G.; Matioli, F. F.; Dos Santos, J. I.; Velazquez-Campoy, A.; Gallacci, M.; Fontes, M. R. M. Structural and Functional Evidence for Membrane Docking and Disruption Sites on Phospholipase A2-like Proteins Revealed by Complexation with the Inhibitor Suramin. *Acta Crystallogr., Sect. D: Biol. Crystallogr.* **2015**, *71*, 2066−2078.

(7) Zhou, X.; Tan, T. -C.; Valiyaveettil, S.; Go, M. L.; Kini, R. M.; Velazquez-Campoy, A.; Sivaraman, J. Structural Characterization of Myotoxic Ecarpholin S from Echis Carinatus Venom. *Biophys. J.* **2008**, *95* (7), 3366−3380.

(8) Mastrangelo, E.; Pezzullo, M.; Tarantino, D.; Petazzi, R.; Germani, F.; Kramer, D.; Robel, I.; Rohayem, J.; Bolognesi, M.; Milani, M. Structure-Based Inhibition of Norovirus RNA-Dependent RNA Polymerases. *J. Mol. Biol.* **2012**, *419* (3−4), 198−210.

(9) Baumann, S.; Herrmann, J.; Raju, R.; Steinmetz, H.; Mohr, K. I.; Hüttel, S.; Harmrolfs, K.; Stadler, M.; Müller, R. Cystobactamids: Myxobacterial Topoisomerase Inhibitors Exhibiting Potent Antibacterial Activity. *Angew. Chem., Int. Ed.* **2014**, *53* (52), 14605−14609.

(10) Michalczyk, E.; Hommernick, K.; Behroz, I.; Kulike, M.; Pakosz-Stępień, Z.; Mazurek, L.; Seidel, M.; Kunert, M.; Santos, K.; von Moeller, H.; Loll, B.; Weston, J. B.; Mainz, A.; Heddle, J. G.; Süssmuth, R. D.; Ghilarov, D. Molecular Mechanism of Topoisomerase Poisoning by the Peptide Antibiotic Albicidin. *Nat. Catal.* **2023**, *6* (1), 52−67.

(11) Hashimi, S. M. Albicidin, a Potent DNA Gyrase Inhibitor with Clinical Potential. *J. Antibiot.* **2019**, *72* (11), 785−792.

(12) Baraldi, P. G.; Del Carmen Nûnez, M.; Espinosa, A.; Romagnoli, R. Distamycin A as Stem of DNA Minor Groove Alkylating Agents. *Curr. Top. Med. Chem.* **2004**, *4*, 231−239.

(13) Hiraku, Y.; Oikawa, S.; Kawanishi, S. Distamycin A, a Minor Groove Binder, Changes Enediyne-Induced DNA Cleavage Sites and Enhances Apoptosis. *Nucleic Acids Res.* **2002**, *2*, 95−96.

(14) Paul, A.; Guo, P.; Boykin, D. W.; Wilson, W. D. A New Generation of Minor-Groove-Binding—Heterocyclic Diamidines That Recognize G·C Base Pairs in an AT Sequence Context. *Molecules* **2019**, *24* (5), 946.

(15) Wang, C. C. C.; Ellervik, U.; Dervan, P. B. Expanding the Recognition of the Minor Groove of DNA by Incorporation of β-Alanine in Hairpin Polyamides. *Bioorg. Med. Chem.* **2001**, *9*, 653−657.

(16) Matsuda, H.; Fukuda, N.; Ueno, T.; Tahira, Y.; Ayame, H.; Zhang, W.; Bando, T.; Sugiyama, H.; Saito, S.; Matsumoto, K.; Mugishima, H.; Serie, K. Development of Gene Silencing Pyrrole-Imidazole Polyamide Targeting the TGF-B1 Promoter for Treatment of Progressive Renal Diseases. *J. Am. Soc. Nephrol.* **2006**, *17* (2), 422−432.

(17) Dey, D.; Ramakumar, S.; Conn, G. L. Targeted Redesign of Suramin Analogs for Novel Antimicrobial Lead Development. *J. Chem. Inf. Model.* **2021**, *61* (9), 4442−4454.

(18) Parveen, N.; Lin, Y. L.; Chou, R. H.; Sun, C. M.; Yu, C. Synthesis of Novel Suramin Analogs With Anti-Proliferative Activity via FGF1 and FGFRD2 Blockade. *Front. Chem.* **2022**, *9*, 764200.

(19) Paulson, C. N.; John, K.; Baxley, R. M.; Kurniawan, F.; Orellana, K.; Francis, R.; Sobeck, A.; Eichman, B. F.; Chazin, W. J.; Aihara, H.; Georg, G. I.; Hawkinson, J. E.; Bielinsky, A. K. The Anti-Parasitic Agent Suramin and Several of Its Analogues Are Inhibitors of the DNA Binding Protein Mcm10. *Open Biol.* **2019**, *9* (8), 1−10.

(20) Roe, W. E.; Warnock, T. M. C.; Knipe, P. C. A Spirocyclic Backbone Accesses New Conformational Space in an Extended, Dipole-Stabilized Foldamer. *Commun. Chem.* **2023**, *6* (71), 1−6.

(21) McCann, S.; Roe, W. E.; Agnew, H. E.; Knipe, P. C. Non-Covalent Interactions Enforce Conformation in Switchable and Water-Soluble Diketopiperazine-Pyridine Foldamers. *Angew. Chem., Int. Ed.* **2023**, *62* (35), 1−5.

(22) Yin, H.; Lee, G. I.; Park, H. S.; Payne, G. A.; Rodriguez, J. M.; Sebti, S. M.; Hamilton, A. D. Terphenyl-Based Helical Mimetics That Disrupt the P53/HDM2 Interaction. *Angew. Chem., Int. Ed.* **2005**, *44* (18), 2704−2707.

(23) Raghuraman, A.; Ko, E.; Perez, L. M.; Ioerger, T. R.; Burgess, K. Pyrrolinone-Pyrrolidine Oligomers as Universal Peptidomimetics. *J. Am. Chem. Soc.* **2011**, *133* (32), 12350−12353.

(24) Moon, H.; Lee, W. S.; Oh, M.; Lee, H.; Lee, J. H.; Im, W.; Lim, H. S. Design, Solid-Phase Synthesis, and Evaluation of a Phenyl-Piperazine-Triazine Scaffold as α-Helix Mimetics. *ACS Comb. Sci.* **2014**, *16* (12), 695−701.

(25) Bayly, A. R.; White, A. J. P.; Spivey, A. C. Design and Synthesis of a Prototype Scaffold for Five-Residue α-Helix Mimetics. *Eur. J. Org. Chem.* **2013**, *2013* (25), 5566−5569.

(26) Jung, K. Y.; Vanommeslaeghe, K.; Lanning, M. E.; Yap, J. L.; Gordon, C.; Wilder, P. T.; Mackerell, A. D.; Fletcher, S. Amphipathic α-Helix Mimetics Based on a 1,2-Diphenylacetylene Scaffold. *Org. Lett.* **2013**, *15* (13), 3234−3237.

(27) Tew, G. N.; Liu, D.; Chen, B.; Doerksen, R. J.; Kaplan, J.; Carroll, P. J.; Klein, M. L.; DeGrado, W. F. De Novo Design of Biomimetic Antimicrobial Polymers. *Proc. NatI. Acad. Sci.* **2002**, *99* (8), 5110−5114.

(28) Lopez, C. F.; Nielsen, S. O.; Srinivas, G.; DeGrado, W. F.; Klein, M. L. Probing Membrane Insertion Activity of Antimicrobial Polymers via Coarse-Grain Molecular Dynamics. *J. Chem. Theory Comput.* **2006**, *2* (3), 649−655.

(29) Plante, J. P.; Burnley, T.; Malkova, B.; Webb, M. E.; Warriner, S. L.; Edwards, T. A.; Wilson, A. J. Oligobenzamide Proteomimetic Inhibitors of the P53-HDM2 Protein-Protein Interaction. *Chem. Commun.* **2009**, No. 34, 5091−5093.

(30) Saraogi, I.; Hebda, J. A.; Becerril, J.; Estroff, L. A.; Miranker, A. D.; Hamilton, A. D. Synthetic α-Helix Mimetics as Agonists and Antagonists of Islet Amyloid Polypeptide Aggregation. *Angew. Chem., Int. Ed.* **2010**, *49* (4), 736−739.

(31) Flack, T.; Romain, C.; White, A. J. P.; Haycock, P. R.; Barnard, A. Design, Synthesis, and Conformational Analysis of Oligobenzanilides as Multifacial α-Helix Mimetics. *Org. Lett.* **2019**, *21* (12), 4433−4438.

https://doi.org/10.1021/acs.joc.4c02900
J. Org. Chem. 2025, 90, 3043−3052

(32) Dohoney, R. A.; Joseph, J. A.; Baysah, C.; Thomas, A. G.; Siwakoti, A.; Ball, T. D.; Kumar, S. "Common-Precursor" Protein Mimetic Approach to Rescue Aβ Aggregation-Mediated Alzheimer's Phenotypes. *ACS Chem. Biol.* **2023**, *18* (7), 1510−1522.
(33) Arrata, I.; Grison, C. M.; Coubrough, H. M.; Prabhakaran, P.; Little, M. A.; Tomlinson, D. C.; Webb, M. E.; Wilson, A. J. Control of Conformation in α-Helix Mimicking Aromatic Oligoamide Foldamers through Interactions between Adjacent Side-Chains. *Org. Biomol. Chem.* **2019**, *17* (15), 3861−3867.
(34) Burslem, G. M.; Kyle, H. F.; Breeze, A. L.; Edwards, T. A.; Nelson, A.; Warriner, S. L.; Wilson, A. J. Small-Molecule Proteomimetic Inhibitors of the HIF-1α-P300 Protein-Protein Interaction. *ChemBioChem* **2014**, *15* (8), 1083−1087.
(35) Kumar, S.; Hamilton, A. D. α-Helix Mimetics as Modulators of Aβ Self-Assembly. *J. Am. Chem. Soc.* **2017**, *139* (16), 5744−5755.
(36) Alex, J. M.; Corvaglia, V.; Hu, X.; Engilberge, S.; Huc, I.; Crowley, P. B. Crystal Structure of a Protein-Aromatic Foldamer Composite: Macromolecular Chiral Resolution. *Chem. Commun.* **2019**, *55* (74), 11087−11090.
(37) Reddy, P. S.; Langlois d'Estaintot, B.; Granier, T.; Mackereth, C. D.; Fischer, L.; Huc, I. Structure Elucidation of Helical Aromatic Foldamer−Protein Complexes with Large Contact Surface Areas. *Chem. -Eur. J.* **2019**, *25* (47), 11042−11047.
(38) Buratto, J.; Colombo, C.; Stupfel, M.; Dawson, S. J.; Dolain, C.; Langlois D'Estaintot, B.; Fischer, L.; Granier, T.; Laguerre, M.; Gallois, B.; Huc, I. Structure of a Complex Formed by a Protein and a Helical Aromatic Oligoamide Foldamer at 2.1 Å Resolution. *Angew. Chem., Int. Ed.* **2014**, *53* (3), 883−887.
(39) Kumar, S.; Birol, M.; Schlamadinger, D. E.; Wojcik, S. P.; Rhoades, E.; Miranker, A. D. Foldamer-Mediated Manipulation of a Pre-Amyloid Toxin. *Nat. Commun.* **2016**, *7*, 11412.
(40) Ahmed, J.; Fitch, T. C.; Donnelly, C. M.; Joseph, J. A.; Ball, T. D.; Bassil, M. M.; Son, A.; Zhang, C.; Ledreux, A.; Horowitz, S.; Qin, Y.; Paredes, D.; Kumar, S. Foldamers Reveal and Validate Therapeutic Targets Associated with Toxic α-Synuclein Self-Assembly. *Nat. Commun.* **2022**, *13*, 2273.
(41) Ziach, K.; Chollet, C.; Parissi, V.; Prabhakaran, P.; Marchivie, M.; Corvaglia, V.; Bose, P. P.; Laxmi-Reddy, K.; Godde, F.; Schmitter, J. M.; Chaignepain, S.; Pourquier, P.; Huc, I. Single Helically Folded Aromatic Oligoamides That Mimic the Charge Surface of Double-Stranded B-DNA. *Nat. Chem.* **2018**, *10* (5), 511−518.
(42) Corvaglia, V.; Carbajo, D.; Prabhakaran, P.; Ziach, K.; Mandal, P. K.; Santos, V. D.; Legeay, C.; Vogel, R.; Parissi, V.; Pourquier, P.; Huc, I. Carboxylate-Functionalized Foldamer Inhibitors of HIV-1 Integrase and Topoisomerase 1: Artificial Analogues of DNA Mimic Proteins. *Nucleic Acid Res.* **2019**, *47* (11), 5511−5521.
(43) Kleene, V.; Corvaglia, V.; Chacin, E.; Forne, I.; Konrad, D. B.; Khosravani, P.; Douat, C.; Kurat, C. F.; Huc, I.; Imhof, A. DNA Mimic Foldamers Affect Chromatin Composition and Disturb Cell Cycle Progression. *Nucleic Acid Res.* **2023**, *51* (18), 9629−9642.
(44) Corvaglia, V.; Wu, J.; Deepak, D.; Loos, M.; Huc, I. Enhancing the Features of DNA Mimic Foldamers for Structural Investigations. *Chem. -Eur. J.* **2024**, *30* (16), No. e202303650.
(45) Bindl, D.; Mandal, P. K.; Huc, I. Generalizing the Aromatic δ-Amino Acid Foldamer Helix. *Chem. -Eur. J.* **2022**, *28*, No. e202200538.
(46) Zheng, L.; Zheng, D.; Wang, Y.; Yu, C.; Zhang, K.; Jiang, H. Chiral Bisphosphine Ligands Based on Quinoline Oligoamide Foldamers: Application in Asymmetric Hydrogenation. *Org. Biomol. Chem.* **2019**, *17* (44), 9573−9577.
(47) Yang, L.; Ma, C.; Kauffmann, B.; Li, D.; Gan, Q. Absolute Handedness Control of Oligoamide Double Helices by Chiral Oxazolylaniline Induction. *Org. Biomol. Chem.* **2020**, *18* (34), 6643−6650.
(48) Dawson, S. J.; Mészáros, Á.; Peth, L.; Colombo, C.; Csékei, M.; Kotschy, A.; Huc, I. Controlling Helix Handedness in Water-Soluble Quinoline Oligoamide Foldamers. *Eur. J. Org. Chem.* **2014**, *2014* (20), 4265−4275.
(49) Liu, Z.; Hu, X.; Abramyan, A. M.; Mészáros; Csékei, M.; Kotschy, A.; Huc, I.; Pophristic, V. Computational Prediction and Rationalization, and Experimental Validation of Handedness Induction in Helical Aromatic Oligoamide Foldamers. *Chem. -Eur. J.* **2017**, *23* (15), 3605−3615.
(50) Bindl, D.; Heinemann, E.; Mandal, P. K.; Huc, I. Quantitative Helix Handedness Bias through a Single H vs. CH3 Stereochemical Differentiation. *Chem. Commun.* **2021**, *57* (46), 5662−5665.
(51) Zwillinger, M.; Reddy, P. S.; Wicher, B.; Mandal, P. K.; Csékei, M.; Fischer, L.; Kotschy, A.; Huc, I. Aromatic Foldamer Helices as α-Helix Extended Surface Mimetics. *Chem. -Eur. J.* **2020**, *26* (72), 17366−17370.
(52) Hu, X.; Dawson, S. J.; Mandal, P. K.; De Hatten, X.; Baptiste, B.; Huc, I. Optimizing Side Chains for Crystal Growth from Water: A Case Study of Aromatic Amide Foldamers. *Chem. Sci.* **2017**, *8* (5), 3741−3749.
(53) Jayatunga, M. K. P.; Thompson, S.; Hamilton, A. D. α-Helix Mimetics: Outwards and Upwards. *Bioorg. Med. Chem. Lett.* **2014**, *24* (3), 717−724.
(54) Lanning, M. E.; Fletcher, S. Multi-Facial, Non-Peptidic α-Helix Mimetics. *Biology* **2015**, *4* (3), 540−555.
(55) Qi, T.; Deschrijver, T.; Huc, I. Large-Scale and Chromatography-Free Synthesis of an Octameric Quinoline-Based Aromatic Amide Helical Foldamer. *Nat. Protoc.* **2013**, *8* (4), 693−708.
(56) Corvaglia, V.; Sanchez, F.; Menke, F. S.; Douat, C.; Huc, I. Optimization and Automation of Helical Aromatic Oligoamide Foldamer Solid-Phase Synthesis. *Chem. -Eur. J.* **2023**, *29* (36), No. e202300898.
(57) Elgaher, W. A. M.; Hamed, M. M.; Baumann, S.; Herrmann, J.; Siebenburger, L.; Krull, J.; Cirnski, K.; Kirschning, A.; Bronstrup, M.; Muller, R.; Hartmann, R. W. Cystobactamid 507: Concise Synthesis, Mode of Action, and Optimization toward More Potent Antibiotics. *Chem. -Eur. J.* **2020**, *26* (32), 7219−7225.
(58) Sőregi, P.; Zwillinger, M.; Vágó, L.; Csékei, M.; Kotschy, A. High Density Information Storage through Isotope Ratio Encoding. *Chem. Sci.* **2024**, *15*, 14938.
(59) Guzmán, F.; Aróstica, M.; Román, T.; Beltrán, D.; Gauna, A.; Albericio, F.; Cárdenas, C. Peptides, Solid-Phase Synthesis and Characterization: Tailor-Made Methodologies. *Electron. J. Biotechnol.* **2023**, *64*, 27−33.
(60) Dengler, S.; Mandal, P. K.; Allmendinger, L.; Douat, C.; Huc, I. Conformational Interplay in Hybrid Peptide-Helical Aromatic Foldamer Macrocycles. *Chem. Sci.* **2021**, *12* (33), 11004−11012.
(61) Baptiste, B.; Douat-Casassus, C.; Laxmi-Reddy, K.; Godde, F.; Huc, I. Solid Phase Synthesis of Aromatic Oligoamides: Application to Helical Water-Soluble Foldamers. *J. Org. Chem.* **2010**, *75* (21), 7175−7185.
(62) Deepak, D.; Wu, J.; Corvaglia, V.; Allmendinger, L.; Scheckenbach, M.; Tinnefeld, P.; Huc, I. DNA Mimic Foldamer Recognition of a Chromosomal Protein. *Angew. Chem., Int. Ed.* **2025**, No. e202422958.
(63) Lee, M. A.; Brown, J. S.; Loas, A.; Pentelute, B. L. Investigation of Commercially Available Resins for the Automated Flow Synthesis of Difficult or Long Peptide Sequences. *Pept. Sci.* **2024**, *116* (3), No. e24344.
(64) Wang, S.; Wicher, B.; Douat, C.; Maurizot, V.; Huc, I. Domain Swapping in Abiotic Foldamers. *Angew. Chem., Int. Ed.* **2024**, *63* (28), No. e202405091.
(65) Dolain, C.; Grélard, A.; Laguerre, M.; Jiang, H.; Maurizot, V.; Huc, I. Solution Structure of Quinoline- and Pyridine-Derived Oligoamide Foldamers. *Chem. -Eur. J.* **2005**, *11* (21), 6135−6144.
(66) Schrödinger, LLC. *Maestro*; Schrödinger, LLC: New York, NY, 2021.

https://doi.org/10.1021/acs.joc.4c02900
J. Org. Chem. 2025, 90, 3043−3052

6.2. Supporting information: Development of aromatic foldamer building blocks bearing multiple biogenic side chains

SUPPORTING INFORMATION

Development of aromatic foldamer building blocks bearing multiple biogenic side chains

Márton Zwillinger[a‡], Petra Sőregi[a,b‡], Florian Sanchez[c‡], Céline Douat[c], Márton Csékei[a], Ivan Huc*[c], Andras Kotschy*[a]

[a] Servier Research Institute of Medicinal Chemistry, Záhony utca 7, 1031 Budapest, Hungary

[b] Hevesy György PhD School of Chemistry, Eötvös Loránd University, Pázmány Péter sétány 1/A, 1117 Budapest, Hungary

[c] Ludwig-Maximilians-Universität, Butenandtstr. 5–13, 81377 München, Germany

Table of Contents

1 Picture of the Purepep® Chorus synthesizer (Protein Technologies) S2

2 General information S2

3 Experimental data S5

3.1 Analytical data of the newly synthesized compounds in this work S5

3.2 Synthetic procedure and analytical data of the newly synthesized compounds in this work S5

3.3 NMR data of newly synthesized compounds S32

3.4 UV and MS spectra of newly synthesized compounds S119

3.5 The cumulative yields of advanced intermediates and final building blocks S120

3.6 Literature: S122

SUPPORTING INFORMATION

1 Picture of the Purepep® Chorus synthesizer (Protein Technologies)

The synthesizer is composed of six reaction vessels in total, meaning with the *in situ* protocols one can perform up to three SPFS in parallel. Each reaction vessel can be heated up independently. Heating is performed by induction. For a detailed procedure and explanation of the use of this instrument please refer to the *Chem. Eur. J.* 2023, e202300898

2 General information

All reagents obtained from commercial sources were used without further purification unless otherwise stated. Anhydrous solvents were obtained from commercial sources and used without further drying. TG R Wang resin was purchased from CEM. Peptide grade *N*,*N*-dimethylformamide (DMF) was purchased from Carlo Erba and peptide grade *N*-methyl-2-pyrrolidone was purchased from Iris. Anhydrous triethylamine (TEA) and *N*,*N*-diisopropylethylamine (DIPEA) were obtained via distillation over CaH_2 prior to use. Anhydrous tetrahydrofuran (THF), dichloromethane (DCM) and toluene were obtained via an MBRAUN SPS-800 solvent purification system. Anhydrous acetonitrile (MeCN), *N*,*N*-dimethylformamide (DMF) were purchased from Fischer Scientific. Nitrogen gas dried on a column of

SUPPORTING INFORMATION

Drierite® was used as inert atmosphere. In hydrogenation reactions H_2 pressure was provided with a balloon. The reactions were monitored using LC-MS and GC-MS instruments or by thin layer chromatography (TLC) on Merck silica gel 60-F254 plates and observed under UV light. Analytical LC-MS: Agilent HP1200 LC with Agilent 6140 quadrupole MS, operating in positive or negative ion electrospray ionisation mode. Molecular weight scan range was 100 to 1350 m/z. Parallel UV detection was done at 210 nm and 254 nm. Samples were supplied as a 1 mM solution in MeCN with 2 µL loop injection, unless stated otherwise. LC-MS analyses were performed on two instruments, one of which was operated with basic, and the other with acidic eluents. Basic LC-MS: Gemini-NX, 3 µm, C18, 50 mm × 3.00 mm i.d. column at 23°C, at a flow rate of 1 mL min^{-1} using 5 mM aq. NH_4HCO_3 solution and MeCN as eluents. Acidic LC-MS: ZORBAX Eclipse XDB-C18, 1.8 µm, 50 mm × 4.6 mm i.d. column at 40°C, at a flow rate of 1 mL min^{-1} using water and MeCN as eluents, both containing 0.07 *V/V%* TFA. Combination gas chromatography and low-resolution mass spectrometry were performed on Agilent 6850 gas chromatograph and Agilent 5975C mass spectrometer using 15 m × 0.25 mm column with 0.25 µm HP-5MS coating and helium as carrier gas. Ion source: EI^+, 70 eV, 230°C, quadrupole: 150°C, interface: 300°C. Flash chromatography was performed on ISCO CombiFlash Rf 200i or ISCO CombiFlash Torrent® with pre-packed silica-gel cartridges (Redi*Sep*®R_f Gold High Performance). Preparative RP-HPLC purifications were performed on an ISCO CombiFlash EZ Prep system with a Gemini-NX® 10 µm C18, 250 mm × 50 mm column running at a flow rate of 118 mL min^{-1} with UV diode array detection or performed on a Thermo Fisher Scientific Ultimate 3000 HPLC System using Macherey-Nagel Nucleodur C8 Gravity columns (4 × 100 mm, 5 µm and 10 × 250 mm, 5 µm) and Macherey-Nagel Nucleodur C8 Gravity columns (4 × 50 mm, 5 µm and 10 × 100 mm, 5 µm).In the latter case, solvent mixture composed of H_2O+0.1% TFA in A and 0.1%TFA+MeCN in B. For RP-HPLC analyses, a flow rate of 1.0 mL/min was applied; semi-preparative RP-HPLC purification were performed at a flow rate of 5.0 mL/min. UV absorbance was monitored at 300 nm if not stated otherwise. ^1H NMR, and proton-decoupled ^{13}C/DEPTQ NMR measurements were performed on Bruker Avance III 500 MHz spectrometer and Bruker Avance III 400 MHz spectrometer, using DMSO-d_6 or $CDCl_3$ as solvent. ^1H and ^{13}C/DEPTQ NMR data are in the form of delta values, given in part per million (ppm), using the residual peak of the solvent as internal standard (DMSO-d_6: 2.50 ppm (^1H) / 39.5 ppm (^{13}C/DEPTQ), $CDCl_3$: 7.26 ppm (^1H) / 77.2 ppm (^{13}C/DEPTQ), DMF-d_7 8.03 ppm (^1H)). Measurements were performed at 298 K unless stated otherwise. NMR spectra of the oligomers were recorded in DMF-d_7. The raw data were evaluated using Mnova version 14.0.0 from Mestrelab Research or Bruker Topspin 3.2 in case of all small molecules, while Mnova version 14.0.0 from Mestrelab Research for the evaluation of the prepared foldamer. Splitting patterns are designated as: s (singlet), d (doublet), t (triplet), m (multiplet), br s (broad singlet), dd (doublet of doublets), dt (doublet of triplets), quintet (quint), sextet (sext), septet (sp). In some cases, due to tautomers or amide rotamers two sets of signals appear in the spectra, which are represented in a format like „6.98/6.64 (t/br s, J = 5.4 Hz for triplet signal, 1H)" meaning that the singlet signal at 6.98 ppm and the triplet signal with J = 5.4 Hz coupling

SUPPORTING INFORMATION

at 6.64 ppm corresponds to the same proton, and together give an integral of 1. LC-HRMS were determined on an Agilent 1290 Infinity II - Agilent 6545 LC-QTOF, ion source temperature 200°C, ESI +/-, ionization voltage: +/-4.5 kV. InfinityLab Poroshell 120 SB-C18, 2.1 mm, 1.9 µm column. Mass resolution: min. 10000. LC-HRMS spectra for some quinoline monomeres were recorded on a Thermo Scientific Dionex UltiMate 3000 equipped with a Nucleodur C18 gravity column (2 x 50 mm, 1.8 µm) with a flow of 0.33 mL min-1. 0.1% of formic acid in water (solvent A) and 0.1% of formic acid in acetonitrile (solvent B) were used as mobile phase for the ionization of the quinoline monomers and the oligomer. Elution was monitored by UV detection at 214, 254 and 300 nm with a diode array detector. The LC system was coupled to a micrOTOF II mass spectrometer by Bruker Daltonics and molecules were ionized by ESI. GC-HRMS were determined on Agilent 7890B gas chromatograph and AccuTOF GCX mass spectrometer using 15 m × 0.25 mm column with 0.25 µm HP-5MS coating and helium as carrier gas. Ion source: FI, 37V, interface: 320°C. Chemical names were generated by BioviaDraw 2021.

SUPPORTING INFORMATION

3 Experimental data

3.1 Analytical data of the newly synthesized compounds in this work

General procedure A for hydrogenation

To a pear-shaped flask and **methyl 8-nitro-quinoline-2-carboxylate** (1.0 equiv.) and Pd/C (10% mol%, 0.1 g/g). were measured, the flask was closed with a rubber septum, evacuated, and charged with dry N_2. Then methanol (100 ml/g, dry, N_2 flushed), dichloromethane (100 mL/g, dry, N_2 flushed) and *N*,*N*-diethylethanamine (10 ml/g) were added. The headspace of the flask was evacuated then backfilled with H_2 gas (1 bar). The reaction mixture was stirred at RT for 1-48 h until full conversion was observed. Catalyst was filtered on a celite pad, washed with DCM, the organic phase dried over Na_2SO_4 and the filtrate was concentrated in *vacuo*. The crude product was purified by normal phase flash chromatography (eluent: DCM/MeOH) to afford **methyl 8-amino-quinoline-2-carboxylate**.

General procedure B for the hydrolysis and Fmoc-protection steps

To a pear-shaped flask **methyl 8-amino-quinoline-2-carboxylate** (1.0 equiv.) was measured and dissolved in 1,4-dioxane (100 mL/g). A solution of LiOH · H_2O (1.5 equiv.) in water (50 mL/g) was added and the reaction mixture was stirred at room temperature until hydrolysis was complete (usually 1 h). Hydrolysis was quenched by addition of 1M aq. HCl solution (1.5 equiv.). The reaction mixture was cooled to 0°C, $NaHCO_3$ (5 equiv.) was added (pH set to ~7-8), and a solution of FmocCl (1.5 equiv.) in 1,4-dioxane (30 mL/g) was introduced dropwise during a 1 h period. Stirring at 0°C was continued for 1h-18h until complete conversion was observed. The reaction mixture was diluted with water, pH was adjusted to 3-4 by the addition of 5% citric acid solution. DCM was added, the organic layer separated and washed with 5% citric acid solution. Organic phase was dried over Na_2SO_4 filtered and the filtrate was concentrated. The crude product was purified by normal phase flash chromatography (eluent: heptane/DCM/MeOH), then was further purified with RP-HPLC purification in (MeCN/25mM aq NH_4HCOO buffer) to afford **8-(9H-fluoren-9-ylmethoxycarbonylamino)-2-carboxylic acid** derivatives.

3.2 Synthetic procedure and analytical data of the newly synthesized compounds in this work

Methyl 5-bromo-8-nitro-quinoline-2-carboxylate (2)

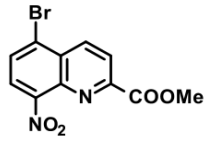

20.8 g **5-bromo-8-nitroquinoline-2-carboxylic acid** (prepared according to [1], 1.0 equiv., 70 mmol) is dissolved in 250 mL of MeOH, then 5 mL of concentrated H_2SO_4 was added and the mixture was heated up to reflux using an oil bath and left stirring overnight. After reaction completion, mixture was cooled down to room temperature, the precipitate was filtered and washed with cold MeOH. The reaction yielded product **2** as a brown solid (16.6 g, 76%).

^{1}H NMR (500 MHz, DMSO-d_6) δ= 8.86 (d, *J* = 8.8 Hz, 1H), 8.41 (d, *J* = 8.8 Hz, 1H), 8.36 (d, *J* = 8.1 Hz, 1H), 8.31 (d, *J* = 8.1 Hz, 1H), 3.97 (s, 3H).^{13}C{^{1}H} NMR (125 MHz, DMSO-d_6): δ = 164.1, 150.1, 147.9, 138.3, 137.7, 131.7, 128.4, 124.8, 124.1, 53.1.

HRMS (ESI) *m/z* calcd for $C_{11}H_7BrN_2O_4$: $[M+Na]^+$: 332.9481; found: 332.9483.

Methyl 4-ethoxy-8-nitro-quinoline-2-carboxylate (5a)

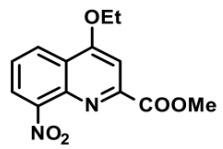

5.00 g **methyl 4-hydroxy-8-nitro-quinoline-2-carboxylate (1)** (prepared according to [2], 1.0 equiv., 20.1 mmol) and 5.55 g K_2CO_3 (2 equiv., 40.2 mmol) were suspended in 100 mL anhydrous DMF under N_2 atmosphere. 2.30 mL **ethyl iodide** (1.4 equiv., 28.6 mmol) was then added and the mixture was heated up to 70°C by a heating block and stirred overnight. Then the mixture was cooled to RT and 500 mL of cold H_2O was added. The precipitate was filtered and washed with 3x100 mL of cold H_2O. The resulting solid was then dried *in vacuo* at 50°C for 2 days. Without further purification, **5a** was obtained as a beige solid (5.23 g, 94%).

^{1}H NMR (500 MHz, DMSO-d_6): δ = 8.45 (dd, *J* = 8.5, 1.4 Hz, 1H), 8.34 (dd, *J* = 7.4, 1.4 Hz, 1H), 7.83 (dd, *J* = 8.5, 7.5 Hz, 1H), 7.67 (s, 1H), 4.47 (q, *J* = 7.0 Hz, 2H), 3.95 (s, 3H), 1.52 (t, *J* = 7.0 Hz, 3H).

SUPPORTING INFORMATION

$^{13}C\{^{1}H\}$ NMR (125 MHz, DMSO-d_6): δ = 164.9, 162.2, 151.0, 148.3, 138.8, 127.0, 125.5, 124.4, 122.2, 102.6, 65.5, 53.0, 14.1.
HRMS (ESI): *m/z* $[M+Na]^+$ calcd. for $C_{13}H_{12}N_2O_5$: 299.0638; found: 299.0638.

2-bromo-*N*-trityl-acetamide (S1)

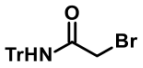

To a 250 mL pear-shaped flask 2.000 g **2-bromoacetamide** (1.0 equiv., 14.497 mmol) and 7.547 g **triphenylmethanol** (2 equiv., 28.994 mmol) were measured were measured, the flask was closed with a rubber septum, evacuated and charged with dry N_2., then 43.49 mL acetic acid (3 mL/mmol), 2.74 mL acetyl acetate (2 equiv., 28.994 mmol) and 0.074 mL sulfuric acid (0.1 equiv., 1.450 mmol). The reaction mixture was heated to 50°C by a heating block and stirred at this temperature for 30 minutes. After 30 minutes, precipitation was observed. The reaction mixture was cooled to 0°C, the formed precipitate was filtered, washed with 10 mL cold water and 10 mL cold Et_2O. The solid was dried *in vacuo* to afford **S1** (2.814 g, 51%) as a white solid.
^{1}H NMR (500 MHz, dmso-d_6) δ 9.07 (s, 1H), 7.33-7.27 (m, 6H), 7.25-7.20 (m, 3H), 7.19-7.15 (m, 6H), 4.03 (s, 2H). $^{13}C\{^{1}H\}$ NMR (125 MHz, dmso-d_6) δ 165.5, 144.3, 128.4, 127.6, 126.6, 69.4, 30.6.
HRMS (ESI): *m/z* $[M+Na]^+$ calcd for $C_{21}H_{18}BrNO$: 402.0469; found: 402.0465.

Methyl 8-nitro-4-[2-oxo-2-(tritylamino)ethoxy]quinoline-2-carboxylate (5b)

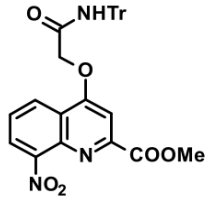

To a 250 mL pear-shaped flask 2.000 g **methyl 4-hydroxy-8-nitro-quinoline-2-carboxylate (1)** (prepared according to [2], 1.0 equiv., 8.058 mmol), 3.800 g **2-bromo-*N*-trityl-acetamide** (1.25 equiv., 9.992 mmol) and 7.877 g Cs_2CO_3 (3 equiv., 24.1749 mmol,) were measured the flask was closed with a rubber septum, evacuated and charged with dry N2., then 40 mL *N*,*N*-dimethylformamide was added and the reaction mixture heated to 50°C by a heating block and stirred for 1 hour. Then 100 mL DCM was added to the reaction mixture, was washed with 20 mL water and 20 mL brine, the organic phase dried over Na_2SO_4 and the filtrate was concentrated *in vacuo*. The crude product was purified by normal phase flash chromatography (220 g silicagel column, DCM/MeOH, gradient elution: 0-100%) to afford **5b** (3.846 g, 78%) as a beige solid.
^{1}H NMR (500 MHz, dmso-d_6) δ 9.14 (s, 1H), 8.42 (dd, *J* = 8.5 Hz, 1.1 Hz, 1H), 8.34 (dd, *J* = 8.5 Hz, 1.1 Hz, 1H), 7.82 (t, *J* = 8.0 Hz, 1H), 7.65 (s, 1H), 7.31-7.17 (m, 15H), 5.29 (s, 2H), 4.00 (s, 3H). $^{13}C\{^{1}H\}$ NMR (125 MHz, dmso-d_6) δ 165.8, 164.8, 162.0, 150.5, 148.2, 144.4, 138.8, 128.5, 127.6, 127.2, 126.6, 125.6, 124.5, 122.1, 103.1, 69.5, 67.4, 53.2.
HRMS (ESI): *m/z* $[M+H]^+$ calcd for $C_{32}H_{25}N_3O_6$: 548.1816; found: 548.1815.

***N*-tritylprop-2-enamide (S2)**

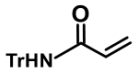

To a 250 mL pear-shaped flask 2.000 g **prop-2-enamide** (1.0 equiv., 28.14 mmol) and 14.650 g **triphenylmethanol** (2 equiv., 56.27 mmol) were measured, the flask was closed with a rubber septum, evacuated and charged with dry N_2., then 84.41 mL acetic acid (3 mL/mmol), 5.32 mL acetyl acetate (2 equiv., 56.27 mmol) and 0.1434 mL sulfuric acid (0.1 equiv., 2.814 mmol). The reaction mixture was heated to 50°C by a heating block and stirred at this temperature for 1 hour. Then the reaction mixture was poured onto 500 g ice, precipitation was observed. The formed precipitate was filtered, washed with 10 mL cold water and taken up in 300 mL EtOAc and was washed with 3 x 100 mL water, the organic phase dried over Na_2SO_4 and the filtrate was concentrated *in vacuo*. The crude product was purified by flash chromatography (220 g silicagel column, heptane/EtOAc, gradient elution: 0-100%) to afford **S2**(6.929 g, 79%) as a white solid.
^{1}H NMR (500 MHz, dmso-d_6) δ 8.88 (s, 1H),), 7.32-7.25 (m, 6H), 7.24-7.16 (m, 9H), 6.67 (dd, *J* = 16.6 Hz, 10.1 Hz, 1H), 5.96 (dd, *J* = 17.1 Hz, 2.3 Hz, 1H), 5.54 (dd, *J* = 10.1 Hz, 2.3 Hz, 1H). $^{13}C\{^{1}H\}$ NMR (125 MHz, dmso-d_6) δ 164.2, 144.7, 132.3, 128.5, 127.5, 126.4, 125.4, 69.4.
HRMS (ESI): *m/z* $[M+H]^+$ calcd for $C_{22}H_{19}NO$: 314.1539; found: 314.1540.

SUPPORTING INFORMATION

Methyl 8-nitro-4-[(E)-3-oxo-3-(tritylamino)prop-1-enyl]quinoline-2-carboxylate (5c)

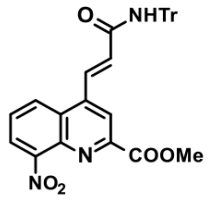

To a 250 mL pear-shaped flask 3.500 g **methyl 4-bromo-8-nitro-quinoline-2-carboxylate (4)** (prepared according to [2], 1.0 equiv., 11.25 mmol), 126 mg diacetoxypalladium (0.05 equiv., 0.5625 mmol), 685 mg tris-*o*-tolylphosphane (0.2 equiv., 2.250 mmol) and 5.289 g ***N*-tritylprop-2-enamide** (1.5 equiv., 16.88 mmol) were measured, the flask was closed with a rubber septum, evacuated, and charged with dry N_2. Then 22.5 mL *N*,*N*-dimethylformamide (2 mL/mmol) and 22.5 mL *N*-ethyl-*N*-*iso*propyl-propan-2-amine (2 mL/mmol, 129.2 mmol) were added and the reaction mixture was heated to 100°C by a heating block and stirred for 1 h. Reaction mixture was partitioned between 250 mL EtOAc and 100 mL water. Organic phase was washed with 30 mL water and 30 mL brine, dried over Na_2SO_4 and the filtrate was concentrated *in vacuo*. The crude product was purified by flash chromatography (220 g silicagel column, DCM/MeOH, gradient elution: 0-20%) to afford **5c** (2.987 g, 42 %) as a yellow solid.

^{1}H NMR (500 MHz, dmso-d_6) δ 9.24 (s, 1H), 8.59 (dd, *J* = 1.1 Hz, 8.8 Hz, 1H), 8.44 (s, 1H), 8.39 (dd, *J* = 1.1 Hz, 7.6 Hz, 1H), 8.07 (d, *J* = 15.5 Hz, 1H), 7.90 (dd, *J* = 7.6 Hz, 8.6 Hz, 1H), 7.66 (d, *J* = 15.5 Hz, 1H), 7.37-7.29 (m, 6H), 7.29-7.22 (m, 9H), 3.98 (s, 3H). ^{13}C{^{1}H} NMR (125 MHz, dmso-d_6) δ 164.5, 163.3, 149.1, 148.8, 144.5, 142.8, 138.5, 131.9, 131.3, 128.6, 128.4, 127.73, 127.67, 127.1, 126.6, 124.2, 118.7, 69.8, 53.1.

HRMS (ESI): *m/z* $[M+H]^+$ calcd for $C_{33}H_{25}N_3O_5$: 544.1867; found: 544.1869.

Methyl 4-(4-*tert*-butoxy-4-oxo-butyl)-8-nitro-quinoline-2-carboxylate (5d)

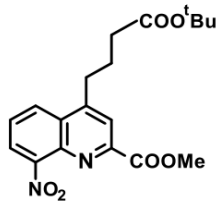

Preparation of alkylboron-reagent:

An oven-dried, 250 mL pear-shaped flask was filled with 738 mg ***tert*-butyl but-3-enoate** (1.2 equiv, 12.85 mmol), closed with a rubber septum, evacuated and charged with dry N_2. Through the septum 27.8 mL 0.50 M solution of 9-borabicyclo[3.3.1]nonane in THF (1.3 equiv., 13.92 mmol) was added at RT, then the resulting mixture was stirred for 12 h. This solution was used in the next step.

Suzuki-coupling:

A 500 mL pear-shaped flask was filled with 3.330 g **methyl 4-bromo-8-nitro-quinoline-2-carboxylate (4)** (prepared according to [2], 1.0 equiv., 10.70 mmol), 379 mg $Pd(AtaPhos)_2Cl_2$ (5.00 mol%, 0.535 mmol) and 10.460 g Cs_2CO_3 (3.00 equiv., 32.11 mmol), closed with a rubber septum, evacuated and charged with dry N_2. Through the septum 0.193 mL (1 equiv., 10.70 mmol) water and the *alkylboron-reagent* were added. The mixture was heated to 50°C by a heating block and stirred for 30 min. After cooling to RT, the reaction mixture was filtered through a celite pad and was washed with 300 mL EtOAc. The filtrate was washed with 2x50 mL water and 50 mL brine, the organic phase was separated and dried over Na_2SO_4, filtered and the filtrate was concentrated *in vacuo*. [SAFETY NOTE: Crude product should be handled under inert gas, as borane residues might be present, causing sudden heating, fuming and fire hazard upon exposition to air.] The crude product was purified by flash chromatography (220 g silicagel column, heptane/DCM, gradient elution: 0-100%) to afford **5d** as a brown, crystalline solid (1206 mg, 27%).

^{1}H NMR (500 MHz, DMSO-d_6) δ= 8.54 (dd, *J* = 8.7 Hz, 1.1 Hz, 1H), 8.36 (dd, *J* = 8.7 Hz, 1.1 Hz, 1H), 8.12 (s, 1H), 7.92 (dd, *J* = 9.0, 7.6 Hz), 3.95 (s, 3H), 2.66 (t, *J* = 7.4 Hz, 2H), 2.34 (t, *J* = 7.4 Hz, 2H), 1.91 (quint, *J* = 7.4 Hz, 2H), 1.38 (s, 9H). ^{13}C{^{1}H} NMR (125 MHz, DMSO-d_6) δ=171.9, 164.7, 150.8, 149.1, 149.0, 138.0, 128.6, 127.9, 127.8, 123.7, 122.3, 79.8, 53.0, 34.0, 30.8, 27.7, 25.3 ppm.

HRMS (ESI) *m/z* calcd for $C_{19}H_{22}N_2O_6$ $[M+H]^+$: 373.1394; found: 373.1397.

Methyl 8-amino-4-ethoxy-quinoline-2-carboxylate (6a)

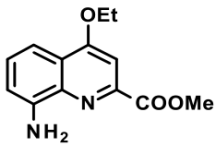

5.230 g **5a** (1.0 equiv., 18.9 mmol) was dissolved in a mixture of 175 mL THF and 175 mL EtOAc. The mixture was bubbled with N_2 for 15 min before 523 mg Pd/C (0.1 equiv., 10 m/m%) was added to the mixture. The mixture was then stirred at room temperature under H_2 atmosphere overnight. The reaction mixture was filtered through celite, washed with EtOAc and the filtrate was concentrated *in vacuo*. Without further purification, **6a** (4.62 g, 99%) was obtained as a yellow solid.

SUPPORTING INFORMATION

^{1}H NMR (500 MHz, DMSO-d6): δ = 7.44 (s, 1H), 7.35 (dd, *J* = 8.2, 7.6 Hz, 1H), 7.25 (dd, *J* = 8.3, 1.4 Hz, 1H), 6.92 (dd, *J* = 7.6, 1.3 Hz, 1H), 6.01 (s, 2H), 4.32 (q, *J* = 6.9 Hz, 2H), 3.93 (s, 3H), 1.47 (t, *J* = 7.0 Hz, 3H). ^{13}C{^{1}H} NMR (125 MHz, DMSO-d6): δ = 165.6, 161.6, 146.0, 145.1, 137.2, 129.0, 122.2, 109.8, 107.0, 100.6, 64.3, 52.5, 14.3.
HRMS (ESI): *m/z* [M+Na]$^+$ calcd. for $C_{13}H_{14}N_2O_3$: 269.0897; found: 269.0896.

Methyl 8-amino-4-[2-oxo-2-(tritylamino)ethoxy]quinoline-2-carboxylate (6b)

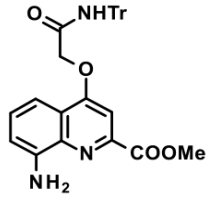

Using **General Procedure A** 3.470 g compound **5b** (1.0 equiv., 6.337 mmol), **6b** (3.379 g, 97%) was obtained as yellow solid.
^{1}H NMR (500 MHz, dmso-*d*$_6$) δ 9.05 (s, 1H), 7.46 (s,H), 7.38-7.14 (m, 15H), 6.91 (dd, *J* = 7.6 Hz, 1.1 Hz), 6.02 (s, 2H), 5.13(s, 2H), 3.98 (s, 3H). ^{13}C{^{1}H} NMR (125 MHz, dmso-*d*$_6$) δ 166.3, 165.5, 161.2, 146.0, 144.7, 144.4, 137.2, 129.1, 128.5, 127.6, 126.6, 122.1, 109.8, 107.0, 101.1, 69.5, 66.9, 52.7.
HRMS (ESI): *m/z* [M+H]$^+$ calcd for $C_{32}H_{27}N_3O_4$: 518.2074; found: 518.2080.

Methyl 8-amino-4-[3-oxo-3-(tritylamino)propyl]quinoline-2-carboxylate (6c)

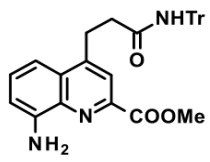

Using **General Procedure A** 2.800 g compound **5c** (1.0 equiv., 5.151 mmol), **6c** (2.405 g, 83%) was obtained as yellow solid
^{1}H NMR (500 MHz, DMSO-d$_6$) δ 8.76 (s, 1H), 7.94 (s, 1H), 7.44 (dd, *J* = 7.8 Hz, 8.3 Hz, 1H), 7.24-7.14 (m, 10H), 7.13-7.09 (m, 6H), 6.93 (dd, *J* = 1.1 Hz, 7.6 Hz, 1H), 6.12 (s, 2H), 3.95 (s, 3H), 3.22 (t, *J* = 7.2 Hz, 2H), 2.81 (t, *J* = 7.2 Hz, 2H). ^{13}C{^{1}H} NMR (125 MHz, DMSO-d$_6$) δ= 170.7, 165.5, 148.4, 146.8, 144.8, 143.3, 136.4, 130.1, 128.9, 128.5, 127.4, 126.3, 119.8, 109.2, 109.0, 69.3, 52.5, 34.8, 27.0 ppm.
HRMS (ESI) *m/z* calcd for $C_{33}H_{29}N_3O_3$ [M+H]$^+$: 516.2282; found: 516.2281.

Methyl 8-amino-4-(4-*tert*-butoxy-4-oxo-butyl)quinoline-2-carboxylate (6d)

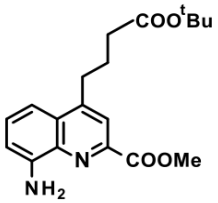

Using **General Procedure A** 1.200 g compound **5d** (1.0 equiv., 3.205 mmol), **6d** (1.090 g, 87%) was obtained as yellow solid.
^{1}H NMR (500 MHz, DMSO-d$_6$) δ 7.89 (s, 1H), 7.44 (t, *J* = 8.1 Hz, 1H), 7.27 (dd, *J* = 8.5 Hz, 1.1 Hz, 1H), 6.93 (dd, *J* = 7.6 Hz, 1.1 Hz), 6.11 (s, 2H), 3.94 (s, 3H), 3.05 (t, *J* = 7.4 Hz, 2H), 2.30 (t, *J* = 7.4 Hz, 2H), 1.88 (quint, *J* = 7.4 Hz, 2H), 1.40 (s, 9H). ^{13}C{^{1}H} NMR (125 MHz, DMSO-d$_6$) δ= 172.0, 165.5, 148.7, 146.8, 143.3, 136.5, 130.1, 128.8, 120.5, 109.2, 109.0, 79.7, 52.5, 34.2, 31.0, 27.7, 25.0 ppm.
HRMS (ESI) *m/z* calcd for $C_{19}H_{24}N_2O_4$ [M+H]$^+$: 345.1809; found: 345.1816.

4-ethoxy-8-(9H-fluoren-9-ylmethoxycarbonylamino)quinoline-2-carboxylic acid (7a)

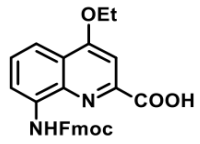

4.62 g **6a** (1.0 equiv., 18.8 mmol) was dissolved in 500 mL 1,4-dioxane. A solution of 1.19 g LiOH · H_2O (1.5 equiv., 28.3 mmol) in 375 mL water was added and the reaction mixture was stirred at room temperature for 1 hour. Hydrolysis was quenched by addition of 28.3 mL 1 M aq. hydrogen chloride solution (1.5 equiv., 28.3 mmol). The reaction mixture was cooled to 0°C, 7.87 g $NaHCO_3$ (5 equiv., 93.7 mmol) was added (pH was set to 7-8), and a solution of 7.28 g FmocCl (1.5 equiv., 28.3 mmol) in 200 mL 1,4-dioxane was introduced dropwise during a 1 h period. After reaction completion, 5% citric acid solution was added until pH 4 was reached. Mixture was then extracted with DCM (3×200mL). Organic layers were combined and dried over $MgSO_4$, filtered and the filtrate was concentrated *in vacuo*. Crude product was suspended in MeOH and sonicated for 1h. After going back to room temperature it was let at -25°C overnight. The suspension was filtered and washed with cold MeOH to afford **7a** as an off-white solid. (5.45 g, 64%).
HPLC-UV purity: 97.9%.
^{1}H NMR (500 MHz, DMSO-*d*$_6$): δ = 13.50 (b s, 1H), 10.44 (s, 1H), 8.34 (b s, 1H), 7.93 (dt, *J* = 7.6, 1.0 Hz, 2H), 7.81 (dd, *J* = 8.4, 1.2 Hz, 1H), 7.78 (dd, *J* = 7.4, 0.6 Hz, 2H), 7.62 (s, 2H), 7.44 (tt, *J* = 7.5, 0.9 Hz, 2H), 7.37 (td, *J* = 7.5, 1.2 Hz, 2H), 4.61 (d, *J* = 6.9 Hz, 2H), 4.44 (quint, *J* = 7.1 Hz, 3H), 2.53 (s, 1H), 1.50 (t, *J* = 7.0 Hz, 3H). ^{13}C{^{1}H} NMR (125 MHz, DMSO-*d*$_6$): δ = 165.5, 162.6, 153.5, 146.7,

SUPPORTING INFORMATION

143.7, 140.8, 137.5, 135.7, 128.4, 127.8, 127.2, 125.2, 121.8, 120.2, 116.5, 114.6, 100.4, 66.4, 64.9, 46.6, 14.2.
HRMS (ESI): *m/z* $[M+H]^+$ calcd. for $C_{27}H_{23}N_2O_5$: 455.1601; found: 455.1596.

8-(9H-fluoren-9-ylmethoxycarbonylamino)-4-[2-oxo-2-(tritylamino)ethoxy]quinoline-2-carboxylic acid (7b)

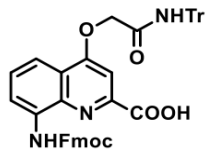

Using General Procedure B 3.200 g **6b** (1.0 equiv., 5.812 mmol), **7b** (1.184 g, 28%) was obtained as an off-white solid.
HPLC-UV purity: 98.8%.
^{1}H NMR (500 MHz, dmso-d_6) δ 10.26 (bs, 1H), 9.10 (s, 1H), 8.31 (bs, 1H), 7.93 (d, *J* = 7.8, 2H), 7.77 (d, *J* = 7.8 Hz, 3H), 7.65 (s, 1H), 7.56 (t, *J* = 7.6 Hz, 1 H), 7.44 (t, *J* = 7.6 Hz, 2H), 7.36 (td, *J* = 7.4, 1.1 Hz, 2H), 7.31-7.17 (m, 15H), 5.21 (s, 1H), 4.60 (d, *J* = 6.6 Hz, 2H), 4.44 (t, *J* = 6.6 Hz, 1H). ^{13}C{^{1}H} NMR (125 MHz, dmso-d_6) δ 166.1, 165.9, 161.9, 153.4, 144.4, 143.7, 140.8, 137.6, 135.4, 128.6, 127.9, 127.8, 127.6, 127.2, 126.6, 125.1, 121.4, 120.3, 116.0, 114.6, 109.8, 101.3, 69.5, 67.1, 66.4, 46.6.
HRMS (ESI): *m/z* $[M+H]^+$ calcd for $C_{46}H_{35}N_3O_6$: 726.2599; found: 726.2603.

8-(9H-fluoren-9-ylmethoxycarbonylamino)-4-[3-oxo-3-(tritylamino)propyl]quinoline-2-carboxylic acid (7c)

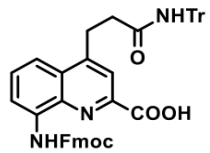

Using **General Procedure B** 2.300 g **6c** (1.0 equiv., 4.104 mmol), **7c** (1.391 g, 45%) was obtained as an off-white solid.
HPLC-UV purity: 96.5%.
^{1}H NMR (500 MHz, dmso-d_6) δ 10.34 (bs, 1H), 8.78 (s, 1H), 8.31 (bs, 1H), 8.10 (s, 1H), 7.93 (d, *J* = 7.6, 2H), 7.79 (d, *J* = 7.6, 1H), 7.77 (dd, *J* = 0.6 Hz, 7.4 Hz, 2H), 7.64 (t, *J* = 7.4 Hz, 1H), 7.44 (t, *J* = 7.4 Hz, 2H), 7.36 (td, *J* = 1.1 Hz, 7.4 Hz, 2H), 7.24-7.19 (m, 6H), 7.19-7.14 (m, 3H), 7.13-7.08 (m, 6H), 4.60 (d, *J* = 6.6 Hz, 2H), 4.44 (t, *J* = 6.6 Hz, 1H), 3.30 (t, *J* = 7.1 Hz, 2H), 2.84 (t, *J* = 7.1 Hz, 2H). ^{13}C{^{1}H} NMR (125 MHz, dmso-d_6) δ 170.6, 165.7, 153.5, 150.2, 144.8, 143.7, 140.8, 136.7, 136.2, 129.2, 128.5, 128.4, 127.8, 127.4, 127.2, 126.3, 125.2, 120.3, 119.8, 117.0, 115.8, 69.3, 66.4, 46.6, 34.8, 26.9.
HRMS (ESI): *m/z* $[M+H]^+$ calcd for $C_{47}H_{37}N_3O_5$: 724.2806; found: 724.2805.

4-(4-*tert*-butoxy-4-oxo-butyl)-8-(9H-fluoren-9-ylmethoxycarbonylamino)quinoline-2-carboxylic acid (7d)

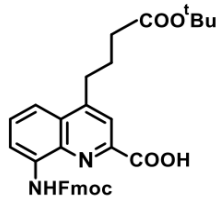

Using General Procedure B 2.900 g **6d** (1.0 equiv., 7.747 mmol), **7d** (2.079 g, 49%) was obtained as an off-white solid.
HPLC-UV purity: 99.5%.
^{1}H NMR (500 MHz, dmso-d_6) δ 10.27 (bs, 1H), 8.29 (bs, 1H), 8.02 (s, 1H), 7.92 (d, *J* = 7.6, 2H), 7.83 (d, *J* = 8.7 Hz, 1H), 7.74 (d, , *J* = 7.6 Hz 2H), 7.64 (t, *J* = 7.6 Hz, 1 H), 7.43 (t, *J* = 7.6 Hz, 2H), 7.34 (dt, *J* = 7.6, 1.1 Hz, 2H), 4.57 (d, *J* = 6.6 Hz, 2H), 4.40 (t, *J* = 6.6 Hz, 1H), 3.12 (t, *J* = 7.4 Hz, 2H), 2.30 (t, *J* = 7.4 Hz, 2H), 1.88 (quint, *J* = 7.4 Hz, 2H), 1.39 (s, 9H). ^{13}C{^{1}H} NMR (125 MHz, dmso-d_6) δ 171.9, 166.2, 153.3, 149.8, 143.7, 140.8, 136.8, 136.0, 128.6, 127.9, 127.8, 127.2, 125.1, 120.8, 120.3, 116.9, 115.3, 79.7, 66.4, 46.5, 34.1, 30.9, 27.8, 25.2.
HRMS (ESI): *m/z* $[M+H]^+$ calcd for $C_{33}H_{32}N_2O_6$: 553.2333; found: 553.2333.

Methyl 8-nitro-5-vinyl-quinoline-2-carboxylate (8a)

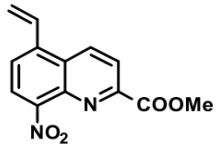

1.00 g **methyl 5-bromo-8-nitroquinoline-2-carboxylate (2)** (1.0 equiv., 3.20 mmol), 0.515 g potassium trifluoro(vinyl)borate (1.2 equiv., 3.84 mmol), 35.9 mg $Pd(OAc)_2$ (0.05 equiv., 0.160 mmol), 131.4 mg SPhos (0.1 equiv., 0.320 mmol) and 1.33 g K_2CO_3 (3.0 equiv., 9.6 mmol) were added in a sealed tube. The combined solids were flushed 3 times with N_2. 8.5 mL toluene and 2.0 mL degassed water were then added and the reaction mixture was heated to 85°C using an oil bath for 18 h. Then H_2O was added and mixture was extracted with DCM. Organic layers were combined and dried over $MgSO_4$, filtered and and the filtrate was concentrated *in vacuo*. Crude product was suspended in MeOH and sonicated for 1h. After going back

SUPPORTING INFORMATION

to RT, it was let to stir at -25°C overnight. The suspension was filtered and washed with cold MeOH to afford **8a** as a brown solid (0.390 g, 47%).
^{1}H NMR (500 MHz, DMSO-d_6): δ = 9.03 (d, *J* = 8.9 Hz, 1H), 8.38 (d, *J* = 7.9 Hz, 1H), 8.28 (d, *J* = 8.9 Hz, 1H), 8.08 (d, *J* = 7.9 Hz, 1H), 7.64 (dd, *J* = 17.2, 11.1 Hz, 1H), 6.14 (dd, *J* = 17.2, 1.0 Hz, 1H), 5.75 (dd, *J* = 11.0, 0.9 Hz, 1H), 3.96 (s, 3H). ^{13}C{^{1}H} NMR (125 MHz, DMSO-d_6): δ = 164.6, 149.3, 147.6, 139.2, 138.1, 135.1, 131.3, 126.9, 124.4, 124.3, 122.6, 122.0, 53.1, 48.7.
HRMS (ESI): *m/z* [M+Na]$^+$ calcd. for $C_{13}H_{10}N_2O_4$: 281.0533; found: 281.0531.

Methyl 5-*iso*butyl-8-nitro-quinoline-2-carboxylate (8b)

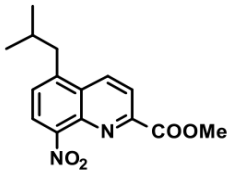

1.87 g **methyl 5-bromo-8-nitroquinoline-2-carboxylate (2)** (1.0 equiv., 6.00 mmol), 253 mg $Pd(PPh_3)_2Cl_2$ (0.06 equiv., 0.36 mmol), 2.93 g Cs_2CO_3 (1.5 equiv., 9.0 mmol), 857 mg ***iso*butylboronic acid** (1.4 equiv., 8.4 mmol) were added in a flask and flushed three times with N_2, then 150 mL dry toluene was added. The mixture was heated up to 80°C using an oil bath and stirred under N_2 overnight. Full conversion was observed, then the mixture was diluted with 300 mL EtOAc, washed with 2x150 mL aq. citric acid 5% and 2x150mL H_2O. The combined aqueous phase were extracted with 3x150 mL EtOAc. Organic layers were combined and dried over $MgSO_4$, filtered and solvent was removed *in vacuo*. Crude product was suspended in iPr_2O and sonicated for 1h. After going back to RT it was stirred at -25°C overnight. The suspension was filtered and washed with cold $^iPr_2O$ to obtain **8b** as a brown solid (1.34 g, 78%).
^{1}H NMR (500 MHz, DMSO-d_6): δ = 8.92 (d, *J* = 8.9 Hz, 1H), 8.31 (d, *J* = 7.6 Hz, 1H), 8.26 (d, *J* = 8.9 Hz, 1H), 7.70 (d, *J* = 7.7 Hz, 1H), 3.96 (s, 3H), 3.05 (d, *J* = 7.2 Hz, 2H), 1.95 (h, *J* = 6.7 Hz, 1H), 0.92 (d, *J* = 6.6 Hz, 6H). ^{13}C{^{1}H} NMR (125 MHz, DMSO-d_6): δ = 164.6, 148.9, 146.9, 143.5, 138.2, 135.5, 128.2, 128.1, 123.9, 122.2, 53.0, 40.5, 29.7, 22.3.
HRMS (ESI): *m/z* [M+Na]$^+$ for $C_{15}H_{16}N_2O_4$: 311.1002; found: 311.1002.

Methyl 8-nitro-5-[(E)-3-oxo-3-(tritylamino)prop-1-enyl]quinoline-2-carboxylate (8c)

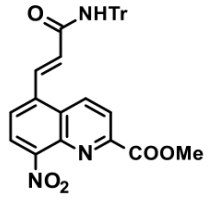

To a 250 mL pear-shaped flask 6.000 g **methyl 5-bromo-8-nitro-quinoline-2-carboxylate (2)** (1.0 equiv., 19.29 mmol), 217 mg diacetoxypalladium (0.05 equiv., 0.9644 mmol), 1.174 g tris-*o*-tolylphosphane (0.2 equiv., 3.857 mmol) and 9.067 g ***N*-tritylprop-2-enamide** (1.5 equiv., 28.93 mmol) were measured, the flask was closed with a rubber septum, evacuated, and charged with dry N_2. Then 38.6 mL N,N-dimethylformamide (2 mL/mmol) and 38.6 mL *N*-ethyl-*N*-*iso*propyl-propan-2-amine (2 mL/mmol) were added and the reaction mixture was heated to 100°C by a heating block and stirred for 2 h. Reaction mixture was partitioned between 500 mL EtOAc and 150 mL water. Organic phase was washed with 50 mL water and 50 mL brine, dried over Na_2SO_4 and the filtrate was concentrated *in vacuo*. The crude product was purified by flash chromatography (330 g silicagel column, DCM/MeOH, gradient elution: 0-100%) to afford **8c** (7.260 g, 69%) as a yellow solid.
^{1}H NMR (500 MHz, dmso-d_6) δ 9.14 (s, 1H), 9.00 (d, *J* = 9.0 Hz, 1H), 8.44 (d, *J* = 8.0 Hz, 1H), 8.27 (d, *J* = 9.0 Hz, 1H), 8.09 (d, *J* = 8.0 Hz, 1H), 8.05 (d, *J* = 15.6 Hz, 1H), 7.40 (d, *J* = 15.6 Hz, 1H), 7.36-7.20 (m, 15H), 3.96 (s, 3H). ^{13}C{^{1}H} NMR (125 MHz, dmso-d_6) δ 164.4, 163.7, 149.4, 148.1, 144.6, 138.1, 136.9, 135.1, 132.4, 130.0, 128.6, 127.6, 127.4, 126.6, 125.6, 124.2, 122.8, 69.7, 53.1.
HRMS (ESI): *m/z* [M+H]$^+$ calcd for $C_{33}H_{25}N_3O_5$: 544.1867; found: 544.1871.

Methyl 5-(3-methylbut-1-ynyl)-8-nitro-quinoline-2-carboxylate (8d)

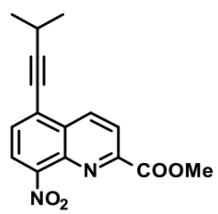

2.50 g **methyl 5-bromo-8-nitroquinoline-2-carboxylate (2)** (1.0 equiv., 8.00 mmol), 337 mg $Pd(PPh_3)_2Cl_2$ (0.06 equiv., 0.480 mmol), 46 mg CuI (0.03 equiv., 0.240 mmol) were added in a flask and flushed 3 times with N_2. To the flask 150 mL of dry MeCN was added followed by 35 mL Et_3N (30 equiv., 240 mmol) and 1.2 mL **3-methylbut-1-yne** (1.4 equiv., 11.3 mmol). The mixture was heated up to 70°C using an oil bath and left stirring under N_2 overnight. After reaction completion, mixture was diluted with 300 mL of DCM, washed with 3x250 mL of 5% aq. citric acid solution. The combined aqueous phase were extracted with 3x200 mL of DCM. Organic layers were combined and dried over $MgSO_4$, filtered and the filtrate was

SUPPORTING INFORMATION

concentrated *in vacuo*. Crude product was suspended in MeCN and sonicated for 1h. After going back to RT it was let at -25°C overnight. The suspension was filtered and washed with cold MeCN to afford **8d** as a off white solid (2.06 g, 86%).

^{1}H NMR (500 MHz, DMSO-d_6): δ = 8.88 (d, *J* = 8.7 Hz, 1H), 8.36 (t, *J* = 9.0 Hz, 2H), 7.95 (d, *J* = 7.8 Hz, 1H), 3.97 (s, 3H), 3.04 (hept, *J* = 6.9 Hz, 1H), 1.35 (d, *J* = 6.9 Hz, 6H). ^{13}C{^{1}H} NMR (125 MHz, DMSO-d_6): δ =164.4, 149.7, 147.3, 137.8, 136.5, 131.0, 129.4, 125.1, 124.3, 123.4, 105.9, 75.3, 53.1, 22.5, 20.8.

HRMS (ESI): *m/z* [M+Na]$^+$ calcd. for $C_{16}H_{14}N_2O_4$: 321.0846; found: 321.0845.

Methyl 5-[3-(*tert*-butoxycarbonylamino)prop-1-ynyl]-8-nitro-quinoline-2-carboxylate (8e)

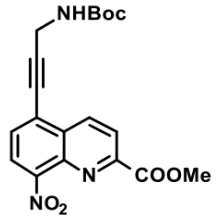

2.00 g **methyl 5-bromo-8-nitroquinoline-2-carboxylate (2)** (1.0 equiv., 6.40 mmol), 140 mg $Pd(PPh_3)_2Cl_2$ (0.03 equiv., 0.19 mmol), 125 mg CuI (0.1 equiv., 0.64 mmol), 200 mg $P(oTol)_3$ (0.1 equiv., 0.64 mmol) and 1.20 g ***N*-Boc-propargylamine** (1.2 equiv., 7.68 mmol) were added to a flask and flushed 3 times with N_2. 50 mL dry DMF was added followed by 8.40 mL DIPEA (7.1 equiv., 45.44 mmol). The mixture was stirred under N_2 atmosphere overnight at RT. Full conversion was observed, then the mixture was diluted with 100 mL DCM, washed with 2x50 mL aq. citric acid 5% and 50 mL sat. aq. $NaHCO_3$ solution. The combined aqueous phase was extracted with 3x200 mL DCM. Organic layers were combined and dried over $MgSO_4$, filtered and solvent was removed *in vacuo*. Crude product was suspended in iPr_2O and sonicated for 1h. After going back to RT it was let at -25°C overnight. The suspension was filtered and washed with cold $^iPr_2O$ to obtain **8e** as a off white solid (1.50 g, 61%).

^{1}H NMR (500 MHz, DMSO-d_6): δ = 8.94 (d, *J* = 8.7 Hz, 1H), 8.38 (d, *J* = 7.8 Hz, 1H), 8.34 (d, *J* = 8.7 Hz, 1H), 8.00 (d, J = 7.8 Hz, 1H), 7.58 (t, J = 5.4 Hz, 1H), 4.18 (d, J = 5.5 Hz, 2H), 3.97 (s, 3H), 1.43 (s, 9H). ^{13}C{^{1}H} NMR (125 MHz, DMSO-d_6): δ = 164.4, 155.5, 149.9, 147.7, 137.7, 136.5, 131.3, 129.5, 124.3, 123.4, 97.3, 78.6, 77.0, 53.1, 30.6, 28.2.

HRMS (ESI): m/z [M+Na]$^+$ for $C_{19}H_{19}N_3O_6$: 408.1166; found: 408.1169.

Methyl 8-amino-5-vinyl-quinoline-2-carboxylate (9a)

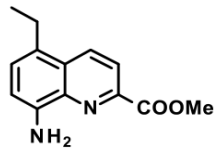

0.390 g **8a** (1.0 equiv., 1.50 mmol) was dissolved in a mixture of 25 mL THF and 25 mL EtOAc. The mixture was bubbled with N_2 for 15 min before 40 mg Pd/C (0.1 equiv., 10 *m/m%*) was added to the mixture. The mixture was then stirred at RT under H_2 atmosphere overnight. The reaction mixture was filtered through celite, washed with EtOAc and solvents were removed *in vacuo*. Without further purification, the **9a** was obtained as a yellow oily solid (0.341g, 99%).

^{1}H NMR (500 MHz, DMSO-d_6): δ = 8.51 (d, *J* = 8.8 Hz, 1H), 8.06 (d, *J* = 8.8 Hz, 1H), 7.29 (d, *J* = 7.8 Hz, 1H), 6.88 (d, *J* = 7.8 Hz, 1H), 5.91 (s, 2H), 3.95 (s, 3H), 2.91 (q, *J* = 7.5 Hz, 2H), 1.22 (t, *J* = 7.5 Hz, 3H). ^{13}C{^{1}H} NMR (125 MHz, DMSO-d_6): δ = 165.4, 144.4, 143.4, 137.0, 133.6, 129.0, 127.8, 125.7, 120.5, 109.1, 52.5, 23.9, 15.5.

HRMS (ESI): *m/z* [M+Na]$^+$ calcd. for $C_{13}H_{14}N_2O_2$: 253.0947; found: 253.0947.

Methyl 8-amino-5-isobutyl-quinoline-2-carboxylate (9b)

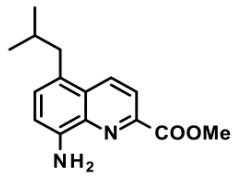

1.34 g **8b** (1.0 equiv., 4.65 mmol) was dissolved in a mixture of 50 mL THF and 50 mL EtOAc. The mixture was bubbled with N_2 for 15 min before 135 mg Pd/C (0.1 equiv. 10% *m/m%*) was added to the mixture. The mixture was then stirred at RT under H_2 atmosphere overnight. The reaction mixture was filtered through celite, washed with EtOAc and solvents were removed *in vacuo*. Without further purification, **9b** was obtained as a yellow solid (1.19 g, 99%).

^{1}H NMR (500 MHz, DMSO-d_6): δ = 8.49 (d, *J* = 8.8 Hz, 1H), 8.04 (d, *J* = 8.8 Hz, 1H), 7.24 (d, *J* = 7.7 Hz, 1H), 6.88 (d, *J* = 7.8 Hz, 1H), 5.93 (s, 2H), 3.95 (s, 3H), 2.74 (d, *J* = 7.2 Hz, 2H), 1.82 (h, *J* = 6.8 Hz, 1H), 0.88 (d, *J* = 6.6 Hz, 6H). ^{13}C{^{1}H} NMR (125 MHz, DMSO-d_6): δ = 165.4, 144.5, 143.3, 136.9, 133.9, 130.9, 128.2, 123.1, 120.3, 108.9, 52.5, 40.2, 29.5, 22.4.

HRMS (ESI): *m/z* [M+Na]$^+$ for $C_{15}H_{18}N_2O_2$: 281.1260; found: 281.1260.

SUPPORTING INFORMATION

Methyl 8-amino-4-[3-oxo-3-(tritylamino)propyl]quinoline-2-carboxylate (9c)

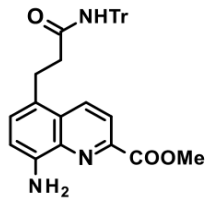

Using **General Procedure A** 7.200 g compound **8c** (1.0 equiv., 13.25 mmol), **9c** (5.686 g, 67%) was obtained as yellow solid.
^{1}H NMR (500 MHz, DMSO-d_6) δ 8.58 (s, 1H), 8.51 (d, *J* = 8.9 Hz, 1H), 8.06 (d, *J* = 8.9 Hz, 1H), 7.30-7.14 (m, 10H), 7.12-7.04 (m, 6H), 6.90 (d, *J* = 7.8 Hz, 1H), 5.97 (s, 2H), 3.95 (s, 3H), 3.07 (t, *J* = 7.3 Hz, 2H), 2.63 (t, *J* = 7.3 Hz, 2H). ^{13}C{^{1}H} NMR (125 MHz, DMSO-d_6) δ= 171.2, 165.4, 144.8, 144.7, 143.3, 136.9, 133.8, 130.2, 128.5, 128.0, 127.4, 126.3, 123.1, 120.5, 108.9, 69.2, 52.5, 37.1, 26.6 ppm.
HRMS (ESI) *m/z* calcd for $C_{33}H_{29}N_3O_3$ [M+H]$^+$: 516.2282; found: 516.2283.

Methyl 8-amino-5-isopentyl-quinoline-2-carboxylate (9d)

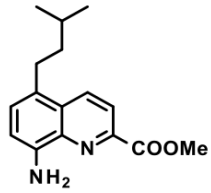

2.06 g **8d** (1.0 equiv., 6.90 mmol) was dissolved in a mixture of 62.5 mL THF and 62.5 mL EtOAc. The mixture was bubbled with N_2 for 15 min before 210 mg Pd/C (0.1 equiv., 10 *m/m%*) was added to the mixture. The mixture was then stirred at RT under H_2 atmosphere overnight. The reaction mixture was filtered through celite, washed with EtOAc and solvents were removed *in vacuo*. Without further purification **9d** (1.86 g, 99%) was obtained as a yellow solid.
^{1}H NMR (500 MHz, DMSO-d_6): δ = 8.47 (d, *J* = 8.8 Hz, 1H), 8.06 (d, *J* = 8.8 Hz, 1H), 7.28 (d, *J* = 7.8 Hz, 1H), 6.87 (d, *J* = 7.7 Hz, 1H), 5.90 (s, 2H), 3.95 (s, 3H), 2.91 – 2.84 (m, 2H), 1.62 (hept, *J* = 6.6 Hz, 1H), 1.50 – 1.42 (m, 2H), 0.94 (d, *J* = 6.6 Hz, 6H). ^{13}C{^{1}H} NMR (125 MHz, DMSO-d_6): δ = 165.3, 144.4, 143.4, 137.0, 133.6, 129.7, 127.8, 124.4, 120.4, 109.0, 52.5, 40.2, 28.8, 27.4, 22.5.
HRMS (ESI): *m/z* [M+Na]$^+$ for $C_{16}H_{20}N_2O_2$: 295.1417; found: 295.1417.

Methyl 8-amino-5-[3-(*tert*-butoxycarbonylamino)propyl]quinoline-2-carboxylate (9e)

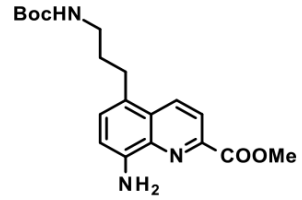

1.50 g **8e** (1.0 equiv., 3.90 mmol) was dissolved in a mixture of 50 mL THF and 50 mL EtOAc. The mixture was bubbled with N_2 for 15 min before 150 mg Pd/C (0.1 equiv.,10 *m/m%*) was added to the mixture. The mixture was then stirred at RT under H_2 atmosphere overnight. The reaction mixture was filtered through celite, washed with EtOAc and solvents were removed *in vacuo*. Without further purification, **9e** was obtained as a yellow solid (1.39 g, 99%).
^{1}H NMR (500 MHz, DMSO-d_6): δ = 8.49 (d, *J* = 8.8 Hz, 1H), 8.04 (d, *J* = 8.8 Hz, 1H), 7.29 (d, *J* = 7.8 Hz, 1H), 6.91 (t, *J* = 5.7 Hz, 1H), 6.87 (d, *J* = 7.8 Hz, 1H), 5.92 (s, 2H), 3.95 (s, 3H), 2.97 (q, *J* = 6.6 Hz, 2H), 2.86 (t, *J* = 7.7 Hz, 2H), 1.68 (quint, *J* = 7.2 Hz, 2H), 1.38 (s, 9H). ^{13}C{^{1}H} NMR (125 MHz, DMSO-d_6): δ = 165.4, 155.7, 144.5, 143.4, 137.0, 133.6, 130.0, 127.9, 123.7, 120.4, 109.0, 77.4, 52.5, 30.9, 28.3, 28.2.
HRMS (ESI): *m/z* [M+Na]$^+$ for $C_{19}H_{25}N_3O_4$: 382.1737; found: 382.1737.

5-ethyl-8-(9H-fluoren-9-ylmethoxycarbonylamino)quinoline-2-carboxylic acid (10a)

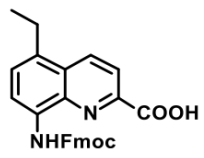

0.348 g **9a** (1.0 equiv., 1.48 mmol) was dissolved in 50 mL 1,4-dioxane and mixed with aqueous solution of 95.0 mg LiOH · H_2O (1.5 equiv., 2.25 mmol) in 30 mL H_2O. After 1 h full conversion was observed, the mixture was quenched with 2.3 mL of 1 M HCl (2.25 mmol) aqueous solution. The mixture was then cooled to 0 °C and 0.630 g $NaHCO_3$ (5.0 equiv., 7.5 mmol) was added (pH was set to 7-8. A solution of 0.580 g Fmoc-Cl (1.5 equiv., 2.25 mmol) in 20 mL 1,4-dioxane was added dropwise to the reaction mixture within 1h. After reaction completion, 5% aq. citric acid solution was added until pH 4 was reached. Then the mixture was extracted with DCM (3×50mL). Organic layers were combined and dried over $MgSO_4$, filtered and the filtrate was concentrated *in vacuo*. Crude product was suspended in MeOH and sonicated for 1h. After going back RT it was stirred at -25°C overnight. The suspension was filtered and washed with cold MeOH to afford **10a** as an off-white solid (0.530 g, 82%).
HPLC-UV purity: 98.9%.
^{1}H NMR (500 MHz, DMSO-d_6): δ = 13.61 (b s, 1H), 10.38 (b s, 1H), 8.74 (d, *J* = 8.8 Hz, 1H), 8.29 (b s, 1H), 8.23 (d, *J* = 8.7 Hz, 1H), 7.93 (d, *J* = 7.5 Hz, 2H), 7.78 (d, *J* = 7.5 Hz, 2H), 7.52 (d, *J* = 8.0 Hz,

1H), 7.44 (t, *J* = 7.3 Hz, 2H), 7.36 (td, *J* = 7.4, 1.2 Hz, 2H), 4.61 (d, *J* = 6.9 Hz, 2H), 4.45 (t, *J* = 6.8 Hz, 1H), 3.05 (q, *J* = 7.5 Hz, 2H), 1.27 (t, *J* = 7.5 Hz, 3H). $^{13}C\{^{1}H\}$ NMR (125 MHz, DMSO-d_6): δ = 165.4, 153.5, 143.7, 140.8, 137.1, 135.0, 133.9, 133.7, 127.9, 127.8, 127.6, 127.2, 125.2, 120.4, 120.3, 116.2, 66.3, 46.6, 24.1, 15.2.
HRMS (ESI): *m/z* $[M+H]^+$ calcd. for $C_{27}H_{22}N_2O_4$: 439.1652; found: 439.1650.

8-(9H-fluoren-9-ylmethoxycarbonylamino)-5-isobutyl-quinoline-2-carboxylic acid (10b)

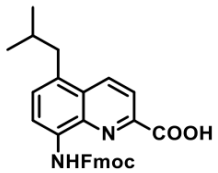

1.19 g **9b** (1.0 equiv., 4.60 mmol) was dissolved in 150 mL 1,4-dioxane and 290 mg LiOH · H_2O (1.5 equiv., 6.90 mmol) in 100 mL H_2O was added. After 1h full conversion was observed, the mixture was quenched with 6.9 mL of 1 M HCl aqueous solution. The mixture was then cooled to 0 °C and 1.93 g $NaHCO_3$ (5.0 equiv., 23.0 mmol) was added (pH was set to 7-8). A solution of 1.78 g FmocCl (1.5 equiv., 6.9 mmol) in 60 mL 1,4-dioxane was added dropwise to the reaction mixture within 1h. After reaction completion, 5% aq. citric acid solution was added until pH 4 was reached. Mixture was then extracted with DCM (3×150mL). Organic layers were combined and dried over $MgSO_4$, filtered and solvent was removed *in vacuo*. Crude product was suspended in MeOH and sonicated for 1h. After going back to rt it was stirred at -25°C overnight. The suspension was filtered and washed with cold MeOH. The reaction yielded product **10b** as an off-white solid (1.63 g, 76%).
HPLC-UV purity: 99.6%.
^{1}H NMR (500 MHz, DMSO-d_6): δ = 13.60 (s, 1H), 10.40 (s, 1H), 8.74 (d, *J* = 8.8 Hz, 1H), 8.28 (b s, 1H), 8.21 (d, *J* = 8.8 Hz, 1H), 7.93 (d, *J* = 7.6 Hz, 2H), 7.78 (d, *J* = 7.5 Hz, 2H), 7.47 (d, *J* = 6.3 Hz, 1H), 7.44 (t, *J* = 7.3 Hz, 2H), 7.36 (td, *J* = 7.4, 1.2 Hz, 2H), 4.61 (d, *J* = 6.9 Hz, 2H), 4.45 (t, *J* = 6.8 Hz, 1H), 2.89 (d, *J* = 7.2 Hz, 2H), 1.89 (h, *J* = 6.8 Hz, 1H), 0.90 (d, *J* = 6.6 Hz, 6H). $^{13}C\{^{1}H\}$ NMR (125 MHz, DMSO-d_6): δ = 165.4, 153.5, 143.7, 140.8, 137.1, 135.4, 134.0, 131.2, 129.9, 128.0, 127.8, 127.2, 125.1, 120.2, 115.9, 66.3, 46.6, 29.5, 22.3.
HRMS (ESI): *m/z* $[M+H]^+$ for $C_{29}H_{26}N_2O_4$: 467.1965; found: 467.1961.

8-(9H-fluoren-9-ylmethoxycarbonylamino)-5-[3-oxo-3-(tritylamino)propyl]quinoline-2-carboxylic acid (10c)

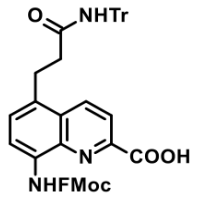

Using **General Procedure B** 5.600 g **9c** (1.0 equiv., 9.558 mmol) **10c** (5.820 g, 77%) was obtained as an off-white solid.
HPLC-UV purity: 95.7%.
^{1}H NMR (500 MHz, dmso-d_6) δ 10.11 (bs, 1H), 8.61 (bs, 1H), 8.58 (d, *J* = 15.4 Hz, 1H), 8.48 (d, *J* = 8.8 Hz, 1H), 8.24 (bs, 1H), 8.15 (d, *J* = 8.8 Hz, 1H), 7.93 (d, *J* = 7.5 Hz, 2H), 7.76 (dd, *J* = 0.6 Hz, 7.5 Hz, 2H), 7.64 (t, *J* = 7.4 Hz, 1H), 7.43 (t, *J* = 7.3 Hz, 2H), 7.36 (dt, *J* = 1.1 Hz, 7.4 Hz, 2H), 7.26-7.14 (m, 9H), 7.11-7.05 (m, 6H), 4.59 (d, *J* = 6.8 Hz, 2H), 4.42 (t, *J* = 6.8 Hz, 1H), 3.18 (t, *J* = 7.1 Hz, 2H), 2.69 (t, *J* = 7.1 Hz, 2H). $^{13}C\{^{1}H\}$ NMR (125 MHz, dmso-d_6) δ 171.0, 153.3, 144.9, 143.7, 140.8, 137.4, 137.0, 134.1, 131.0, 128.9, 128.5, 127.8, 127.4, 127.2, 126.3, 125.1, 121.4, 121.0, 120.3, 120.1, 115.0, 69.2, 66.3, 63.8, 46.6, 36.7, 26.7.

HRMS (ESI): *m/z* $[M+H]^+$ calcd for $C_{47}H_{37}N_3O_5$: 724.2806; found: 724.2804.

8-(9H-fluoren-9-ylmethoxycarbonylamino)-5-isopentyl-quinoline-2-carboxylic acid (10d)

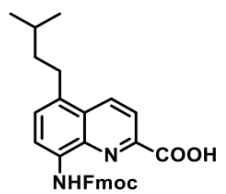

1.86 g **9d** (1.0 equiv., 6.83 mmol) was dissolved in 175 mL 1,4-dioxane and mixed with aqueous solution of 430 mg LiOH · H_2O (1.5 equiv., 10.25 mmol) in 150 mL H_2O. After 1 h, full conversion was observed, the mixture was quenched with 10.3 mL of 1 M HCl aqueous solution. The mixture was then cooled to 0°C and 2.87 g $NaHCO_3$ (5.0 equiv., 34.2 mmol) was added (pH was set to 7-8). A solution of 2.65 g FmocCl (1.5 equiv., 10.25 mmol) in 75 mL 1,4-dioxane was added dropwise to the reaction mixture within 1h. After reaction completion, 5% aq. citric acid solution was added until pH 4 was reached. Mixture was then extracted with DCM (3×100 mL). Organic layers were combined and dried over $MgSO_4$, filtered and solvent was removed *in vacuo*. Crude product was suspended in MeOH and sonicated for 1h. After going back to RT it was let at -25°C

overnight. The suspension was filtered and washed with cold MeOH to afford **10d** as an off-white solid (3.02 g, 92%).
HPLC-UV purity: 99.2%.
^{1}H NMR (500 MHz, DMSO-d_6): δ = 13.55 (b s, 1H), 10.38 (s, 1H), 8.69 (d, *J* = 8.8 Hz, 1H), 8.22 (d, *J* = 8.8 Hz, 2H), 7.93 (d, *J* = 7.6 Hz, 2H), 7.78 (d, *J* = 7.5 Hz, 2H), 7.50 (d, *J* = 8.0 Hz, 1H), 7.43 (t, *J* = 7.5 Hz, 2H), 7.36 (td, *J* = 7.4, 1.2 Hz, 2H), 4.60 (d, *J* = 6.9 Hz, 2H), 4.44 (t, *J* = 6.8 Hz, 1H), 3.04 – 2.97 (m, 2H), 1.63 (hept, *J* = 6.6 Hz, 1H), 1.55 – 1.47 (m, 2H), 0.95 (d, *J* = 6.6 Hz, 6H). ^{13}C{^{1}H} NMR (125 MHz, DMSO-d_6): δ = 165.4, 153.5, 145.0, 143.7, 140.8, 137.1, 135.0, 133.9, 132.5, 128.7, 127.8, 127.6, 127.2, 125.1, 120.4, 120.2, 116.1, 66.3, 46.6, 29.0, 27.5, 22.4.
HRMS (ESI): *m/z* [M+H]$^+$ for $C_{30}H_{28}N_2O_4$: 481.2122; found: 481.2116.

5-[3-(*tert*-butoxycarbonylamino)propyl]-8-(9H-fluoren-9-ylmethoxycarbonylamino)quinoline-2-carboxylic acid (10e)

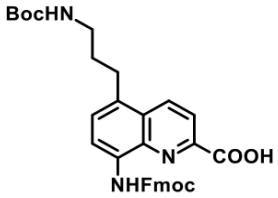

1.39 g **9e** (1.0 equiv., 3.86 mmol) was dissolved in 100 mL 1,4-dioxane and 245 mg LiOH · H_2O (1.5 equiv., 5.79 mmol) in 75 mL H_2O was added. After 1 h full conversion was observed, the mixture was quenched with 6 mL of 1 M HCl aqueous solution. The mixture was then cooled to 0 °C and 1.62 g $NaHCO_3$ (5.0 equiv., 19.3 mmol) was added (pH was set to 7-8). A solution of 1.50 g FmocCl (1.5 equiv., 5.79 mmol) in 50 mL 1,4-dioxane was added dropwise to the reaction mixture within 1 h. After reaction completion, 5% aq. citric acid solution was added until pH 4 was reached. Mixture was then extracted with DCM (3×100mL). Organic layers were combined and dried over $MgSO_4$, filtered and solvent was removed *in vacuo*. Crude product was suspended in MeOH and sonicated for 1h. After going back to RT it was stirred at -25°C overnight. The suspension was filtered and washed with cold MeOH to obtain **10e** as an off-white solid (1.58 g, 72%).
HPLC-UV purity: 98.1%.
^{1}H NMR (500 MHz, DMSO-d_6): δ = 13.62 (s, 1H), 10.43 (s, 1H), 8.74 (d, *J* = 8.8 Hz, 1H), 8.29 (b s, 1H), 8.23 (d, *J* = 8.8 Hz, 1H), 7.94 (dt, *J* = 7.5, 0.9 Hz, 2H), 7.79 (dd, *J* = 7.4, 1.1 Hz, 2H), 7.54 (d, *J* = 7.8 Hz, 1H), 7.45 (t, *J* = 7.4 Hz, 2H), 7.37 (td, *J* = 7.4, 1.2 Hz, 2H), 6.96 (t, *J* = 5.5 Hz, 1H), 4.61 (d, *J* = 6.9 Hz, 2H), 4.46 (t, *J* = 6.8 Hz, 1H), 3.00 (q, *J* = 7.9 Hz, 4H), 1.74 (quint, *J* = 7.1 Hz, 2H), 1.39 (s, 9H). ^{13}C{^{1}H} NMR (125 MHz, DMSO-d_6): δ = 165.4, 155.7, 153.5, 144.9, 143.7, 140.8, 137.1, 135.1, 134.1, 131.8, 129.0, 128.2, 127.8, 127.7, 127.3, 125.2, 120.34, 120.29, 116.1, 77.5, 66.3, 46.6, 30.7, 28.4, 28.3.
HRMS (ESI): *m/z* [M+H]$^+$ for $C_{33}H_{33}N_3O_6$: 568.2442; found: 568.2437.

Methyl 4-chloro-6-(3-methylbut-1-ynyl)-8-nitro-quinoline-2-carboxylate (11a)

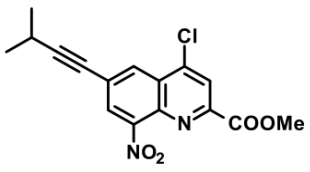

A 1 L pear-shaped flask was filled with 12.00 g compound **methyl 6-bromo-4-chloro-8-nitro-quinoline-2-carboxylate (3)** (prepared according to [2], 1.0 equiv., 25.70 mmol), 489 mg CuI (0.1 equiv., 2.57 mmol) and 902 mg $Pd(PPh_3)_2Cl_2$ (0.05 equiv., 1.29 mmol). The flask was closed with a rubber septum, evacuated and charged with dry N_2, then 385 mL THF (15 mL/mmol methyl 6-bromo-4-chloro-8-nitro-quinoline-2-carboxylate), 51 mL TEA (2 mL/mmol methyl 6-bromo-4-chloro-8-nitro-quinoline-2-carboxylate) and 3.15 mL 3-methylbut-1-yne (1.20 equiv., 30.84 mmol) were added. The reaction mixture was stirred at RT for 24 h, then diluted with 500 mL DCM, washed with 2x100 mL 1 M aq. HCl solution and 100 mL sat. aq. $NaHCO_3$ solution. The combined aq phase was extracted with 2x100 mL DCM. The combined organic phase was dried over Na_2SO_4, filtered and the filtrate was concentrated *in vacuo*. The residue was purified by flash chromatography (220 g column, DCM/MeOH as eluents) to afford 7.157 g **11a** as a beige solid (85% purity, 18.29 mmol, 71%).
^{1}H NMR (500 MHz, DMSO-d$_6$) δ=8.53 (d, *J* = 1.7 Hz, 1H), 8.40 (s, 1H), 8.39 (s, 1H), 3.96 (s, 3H), 2.93 (hept, *J* = 6.9 Hz, 1H), 1.28 ppm (d, *J* = 6.9 Hz, 6H). ^{13}C{^{1}H} NMR (125 MHz, DMSO-d$_6$) δ=163.5, 149.4, 148.7, 143.0, 137.6, 129.2, 127.4, 127.2, 124.1, 123.4, 102.0, 77.7, 53.3, 22.3, 20.6 ppm.
HRMS (ESI) *m/z* calcd for $C_{16}H_{14}ClN_2O_4$ [M+H]$^+$: 333.0642; found: 333.0638.

SUPPORTING INFORMATION

Methyl 6-but-1-ynyl-4-chloro-8-nitro-quinoline-2-carboxylate (11b)

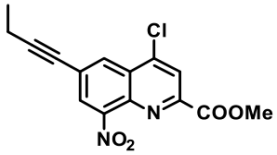

3.46 g **methyl 6-bromo-4-chloro-8-nitroquinoline-2-carboxylate (3)** (prepared according to [2], 1.0 equiv., 10.0 mmol), 211 mg $Pd(PPh_3)_2Cl_2$ (0.03 equiv., 0.30 mmol) and 115 mg CuI (0.06 equiv., 0.60 mmol) were added in a flask and flushed 3 times with N_2. 200 mL of dry THF was added followed by 30.0 mL Et_3N (21.2 equiv., 212 mmol), 1.96 mL **but-1-yn-1-yltrimethylsilane** (1.20 equiv., 12.0 mmol) and 620 mg H_2SiF_6 (0.5 equiv., in 35 *m/m%* aq. solution). The mixture was heated up to 60°C using an oil bathf and was stirred under N_2 for 6h. After reaction completion, mixture was diluted with 300 mL of DCM, washed with 2x200mL of citric acid 5%. The combined aqueous phase were extracted with 3x300mL of DCM. Organic layers were combined and dried over $MgSO_4$, filtered and solvent was removed *in vacuo*. Crude product was suspended in $^{i}Pr_2O$ and sonicated for 1h. After going back to room temperature it was stirred at -25°C overnight. The suspension was filtered and washed with cold $^{i}Pr_2O$. The reaction yielded product **11b** (2.20 g, 69%) as a yellowish solid.

^{1}H NMR (500 MHz, DMSO-d_6): δ = 8.55 (d, *J* = 1.8 Hz, 1H), 8.42 (d, *J* = 1.7 Hz, 1H), 8.40 (s, 1H), 3.96 (s, 3H), 2.56 (q, *J* = 7.5 Hz, 2H), 1.23 (t, *J* = 7.6 Hz, 3H). ^{13}C{^{1}H} NMR (125 MHz, DMSO-d_6): δ = 163.5, 149.4, 148.7, 143.0, 137.7, 129.3, 127.4, 127.2, 124.2, 123.4, 98.4, 77.9, 53.3, 13.3, 12.6.

HRMS (ESI): *m/z* $[M+Na]^+$ for $C_{15}H_{11}ClN_2O_4$: 341.0300; found: 341.0299.

Methyl 4-chloro-6-*iso*propenyl-8-nitro-quinoline-2-carboxylate (11c)

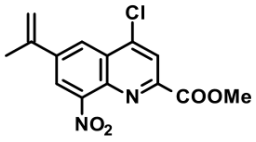

To a 250 mL pear-shaped flask 3.000 g **methyl 6-bromo-4-chloro-8-nitro-quinoline-2-carboxylate (3)** (prepared according to [2], 1.0 equiv., 6.425 mmol), 6.280 g Cs_2CO_3 (3 equiv., 19.27 mmol,), 262 mg cyclopenta-1,3-dien-1-yl(diphenyl)phosphane;dichloromethane;dichloropalladium;iron(2+) (0.05 equiv., 0.3212 mmol) and 1.509 mL **2-*iso*propenyl-4,4,5,5-tetramethyl-1,3,2-dioxaborolane** (1.25 equiv., 1349 mg, 8.031 mmol) were measured. The flask was closed with a rubber septum, evacuated and charged with dry N_2. Then 45 mL 2-methyltetrahydrofuran and 4.5 mL water were added. The reaction mixture was heated to 60°C by a heating block and stirred at this temperature for 6 hours. Full conversion was observed, presence of disubstituted by-product was detected. Then 100 mL EtOAc and 50 ml water were added to the reaction mixture, the phases were separated. The organic phase was washed with 2x20 mL water. The combined aqueous phase was extracted with 20 mL EtOAc. Then the combined organic phase dried over Na_2SO_4, filtered and the filtrate was concentrated *in vacuo*. The crude product was purified by normal phase flash chromatography (220 g silicagel column, DCM/MeOH, gradient elution: 0-40%) to **11c** as a yellow solid (1.333 g, 62%).

^{1}H NMR (400 MHz, dmso-d_6) δ 8.82 (s, 1H), 8.39 (s, 1H), 8.35 (s, 1H) 5.94 (s, 1H), 5.52 (s, 1H), 3.96 (s, 3H), 2.29 (s, 3H). ^{13}C{^{1}H} NMR (100 MHz, dmso-d_6) δ 163.6, 148.9, 143.5, 141.0, 140.0, 137.9, 127.3, 123.2, 122.7, 122.1, 122.0, 118.5, 53.2, 21.0.

HRMS (ESI): *m/z* $[M+H]^+$ calcd for $C_{14}H_{11}ClN_2O_4$: 307.0480; found: 307.0472.

Methyl 4-chloro-6-(2-methylprop-1-enyl)-8-nitro-quinoline-2-carboxylate (11d)

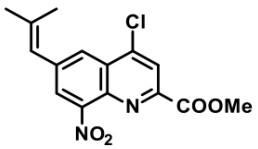

To a 1 L pear-shaped flask 13.000 g **methyl 6-bromo-4-chloro-8-nitro-quinoline-2-carboxylate (3)** (prepared according to [2], 1.0 equiv., 27.841 mmol), 27.214 g Cs_2CO_3 (3 equiv., 83.524 mmol,), 1.137 g cyclopenta-1,3-dien-1-yl(diphenyl)phosphane;dichloromethane;dichloropalladium;iron(2+) (0.05 equiv., 1.3921 mmol) and 6.084 g **4,4,5,5-tetramethyl-2-(2-methylprop-1-enyl)-1,3,2-dioxaborolane** (1.2 equiv., 33.410 mmol) were measured. The flask was closed with a rubber septum, evacuated, and charged with dry N_2. Then 418 mL 2-methyltetrahydrofuran and 42 mL water were added. The reaction mixture was heated to 60°C by a heating block and stirred at this temperature for 26 hours. Then the reaction mixture was filtered on a celite pad, 500 mL EtOAc and 100 ml water were added, the phases were separated. The organic phase was washed with 2x150 mL water. Combined aqueous phase was extracted with 100 mL EtOAc. Then the combined organic phase dried over Na_2SO_4, filtered and the filtrate was concentrated *in vacuo*. The crude product was purified by normal phase flash chromatography (220 g silicagel column, DCM/MeOH, gradient elution: 0-15%) to afford **11d** as a yellow solid (3.620 g, 28%).

SUPPORTING INFORMATION

^{1}H NMR (500 MHz, dmso-d_6) δ 8.40 (d, J = 1.5 Hz, 1H), 8.34 (s, 1H), 8.22 (d, J = 1.5 Hz, 1H), 6.56 (bs, 1H), 3.95 (s, 3H), 1.99 (s, 6H). ^{13}C{^{1}H} NMR (125 MHz, dmso-d_6) δ 164.1, 149.0, 148.9, 143.4, 142.2, 140.0, 137.4, 127.6, 126.5, 125.4, 123.3, 123.1, 53.7, 27.6, 20.0.
HRMS (ESI): *m/z* [M+H]$^+$ calcd for $C_{15}H_{13}ClN_2O_4$: 321.0637; found: 321.0640.

Methyl 6-[(E)-3-*tert*-butoxy-3-oxo-prop-1-enyl]-4-chloro-8-nitro-quinoline-2-carboxylate (11e)

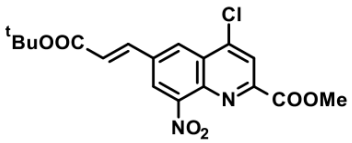

To a 500 mL pear-shaped 7.000 g flask **methyl 6-bromo-4-chloro-8-nitro-quinoline-2-carboxylate (3)** (prepared according to [2], 1.0 equiv., 20.26 mmol) and 1.113 g (1*E*,4*E*)-1,5-diphenylpenta-1,4-dien-3-one;palladium;triphenylphosphane (0.06 equiv., 1.216 mmol) were measured. The flask was closed with a rubber septum, evacuated, and charged with dry N_2. Then 101 mL *N*,*N*-dimethylformamide (dry, degassed), 41 mL *N*-ethyl-*N*-*iso*propyl-propan-2-amine (11.5 equiv., 232.6 mmol), 0.590 mL **tri*tert*-butylphosphane** (0.12 equiv., 2.431 mmol) and 3.56 mL tert-butyl prop-2-enoate (1.2 equiv, 24.31 mmol) were added. The reaction mixture was heated to 100°C by a heating block and stirred at this temperature for 30 min. 300 mL EtOAc and 100 mL water were added to the reaction mixture and the phases were separated. Organic phase was washed with 50 mL water and 50 mL brine. Then the combined organic phase dried over Na_2SO_4, filtered and the filtrate was concentrated *in vacuo*. The crude product was purified by normal phase flash chromatography (220 g silicagel column, heptane/DCM, gradient elution: 30-100%) to afford **11e** as an off-white solid (4.568 g, 57%).
^{1}H NMR (500 MHz, dmso-d_6) δ 8.99 (d, J = 1.7 Hz, 1H), 8.75 (d, J = 1.7 Hz, 1H), 8.39 (s, 1H), 7.91 (d , J = 16.1 Hz, 1H), 6.95 (d , J = 16.1 Hz, 1H), 3.96 (s, 3H), .1.51 (s, 9H). ^{13}C{^{1}H} NMR (125 MHz, dmso-d_6) δ 164.9, 163.5, 149.6, 149.1, 144.0, 140.5, 138.9, 135.5, 128.1, 127.6, 125.1, 123.4, 122.8, 80.6, 53.3, 27.8.
HRMS (ESI): *m/z* [M+H]$^+$ calcd for $C_{18}H_{17}ClN_2O_6$: 393.0848; found: 393.0844.

Methyl 8-amino-6-*iso*pentyl-quinoline-2-carboxylate (12a)

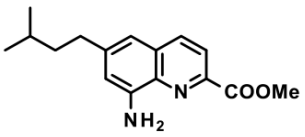

Using **General Procedure A** 6.500 g compound **11a** (1.0 equiv., 16.61 mmol), **12a** (88% purity, 3.328 g, 65%) was obtained as brown solid.
^{1}H NMR (400 MHz, dmso-d_6) δ 8.24 (d, J = 8.6 Hz, 1H), 7.99 (d, J = 8.6 Hz, 1H), 6.95 (d, J = 1.7 Hz, 1H), 6.81 (d, J = 1.7 Hz, 1H), 6.00 (s, 2H), 3.93 (s , 3H), 2.64 (t, 2H), 1.61-1.49 (m, 3 H), 0.92 (d, J = 6.3 Hz, 6H)
^{13}C{^{1}H} NMR (100 MHz, dmso-d_6) δ165.4, 145.8, 145.1, 143.1, 136.4, 135.5, 129.8, 120.9, 112.1, 110.3, 52.4, 33.7, 27.2, 22.4.
HRMS (ESI): *m/z* [M+H]$^+$ calcd for $C_{16}H_{20}N_2O_2$: 273.1598; found: 273.1594.

Methyl 8-amino-6-butyl-quinoline-2-carboxylate (12b)

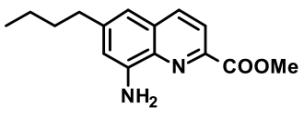

2.20 g **11b** (1.0 equiv., 6.90 mmol) was dissolved in a mixture of 200 mL THF and 200 mL EtOAc. The mixture was bubbled with N_2 for 15 min before 220 mg Pd/C (0.1 g/g., 10% *m*/*m*%), 440 mg $Pd(OH)_2$/C (0.2 g/g, 20% *m*/*m*%) and 4.365 g NH_4COOH (10.0 equiv., 69.0 mmol) were added to the mixture. The mixture was then stirred at rt under H_2 atmosphere overnight. The reaction mixture was filtered through celite, washed with EtOAc. The filtrate was then washed with 2x200 mL water. The combined aqueous phase were extracted with 3x300 mL of DCM. Organic layers were combined and dried over $MgSO_4$, filtered and solvent was removed *in vacuo*. Without further purification, the **12b** was obtained as a yellow solid (1.78 g, 99%).
^{1}H NMR (500 MHz, DMSO-d_6): δ = 8.25 (d, J = 8.6 Hz, 1H), 7.99 (d, J = 8.6 Hz, 1H), 6.94 (d, J = 1.3 Hz, 1H), 6.81 (d, J = 1.7 Hz, 1H), 6.00 (s, 2H), 3.93 (s, 3H), 2.64 (t, J = 7.4 Hz, 2H), 1.66-1.57 (m, 2H), 1.34(sext, 2H), 0.91 (t, J = 7.4 Hz, 3H).^{13}C{^{1}H} NMR (125 MHz, DMSO-d_6): δ = 165.4, 145.8, 144.9, 143.1, 136.4, 135.5, 129.8, 120.9, 112.2, 110.3, 52.5, 35.5, 32.7, 21.9, 13.8.
HRMS (ESI): *m/z* [M+Na]$^+$ for $C_{15}H_{18}N_2O_2$: 281.1260; found: 281.1260.

SUPPORTING INFORMATION

Methyl 8-amino-6-*iso*propyl-quinoline-2-carboxylate (12c)

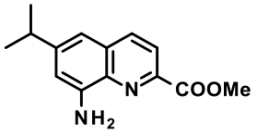

Using **General Procedure A** 1.333 g compound **11c** (1.0 equiv., 3.991 mmol), **12c** (556 mg, 46%) was obtained as brown solid.
^{1}H NMR (500 MHz, dmso-d_6) δ 8.27 (d, J = 8.7 Hz, 1H), 8.00 (d, J = 8.7 Hz, 1H), 6.99 (d, J = 1.7 Hz, 1H), 6.88 (d, J = 1.7 Hz, 1H), 5.99 (bs, 2H), 3.93 (s, 3H), 2.94 (sp, J = 6.9 Hz, 1H), 1.26 (d, J = 6.9 Hz, 6H) ^{13}C{^{1}H} NMR (125 MHz, dmso-d_6) δ 165.4, 150.8, 145.9, 143.2, 136.6, 135.7, 129.8, 120.9, 110.1, 108.7, 52.4, 34.0, 23.6.
HRMS (ESI): *m/z* [M+H]$^+$ calcd for $C_{14}H_{16}N_2O_2$: 245.1284; found: 245.1275.

Methyl 8-amino-6-*iso*butyl-quinoline-2-carboxylate (12d)

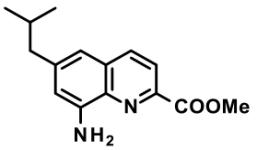

Using **General Procedure A** 330 mg **11d** (1.0 equiv., 0.8952 mmol), **12d** (178 mg, 77%) was obtained as yellow solid.
^{1}H NMR (500 MHz, $CDCl_3$) δ 8.08 (s, 2H), 6.93 (d, J = 1.7 Hz, 1H), 6.80 (d, J = 1.7 Hz, 1H), 5.09 (bs, 2H), 4.03 (s , 3H), 2.55 (d, J = 7.3 Hz, 2H), 1.97 (sp, J = 6.6 Hz, 1H), 0.94 (d, J = 6.6 Hz, 6H). ^{13}C{^{1}H} NMR (125 MHz, $CDCl_3$) δ 166.3, 144.7, 144.3, 144.1, 136.8, 136.4, 130.2, 121.4, 115.2, 52.8, 46.2, 30.1, 25.0, 22.7.
HRMS (ESI): *m/z* [M+H]$^+$ calcd for $C_{15}H_{18}N_2O_2$: 259.1441; found: 259.1430.

Methyl 8-amino-6-(3-*tert*-butoxy-3-oxo-propyl) quinoline-2-carboxylate (12e)

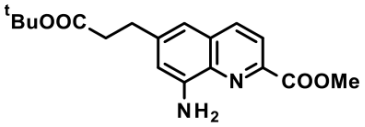

Using **General Procedure A** 4.500 g compound **11e** (1.0 equiv., 11.46 mmol), **12e** (3.159 g, 83%) was obtained as yellow solid.
^{1}H NMR (500 MHz, dmso-d_6) δ 8.25 (d, J = 8.6 Hz, 1H), 8.00 (d, J = 8.6 Hz, 1H), 6.96 (d, J = 1.7 Hz, 1H), 6.81 (d, J = 1.7 Hz, 1H), 6.03 (bs, 2H), 3.93 (s , 3H), 2.88 (tr, J = 7.5 Hz, 2H), 2.57 (tr, J = 7.5 Hz, 2H), 1.35 (s, 9H). ^{13}C NMR (125 MHz, dmso-d_6) δ 171.5, 165.4, 145.8, 143.3, 143.1, 136.5, 135.6, 129.7, 121.0, 112 2, 110.1, 79.7, 52.5, 35 9, 31.1, 27.7.
HRMS (ESI): *m/z* [M+H]$^+$ calcd for $C_{18}H_{22}N_2O_4$: 331.1652; found: 331.1649.

8-(9H-fluoren-9-ylmethoxycarbonylamino)-6-*iso*pentyl-quinoline-2-carboxylic acid (13a)

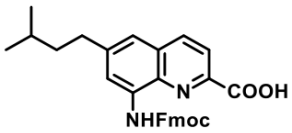

Using **General Procedure B** 3.328 g **12a** (1.0 equiv., 10.76 mmol), **13a** (3.354 g, 65%) was obtained as pale yellow crystals.
HPLC-UV purity: 97.8%.
^{1}H NMR (500 MHz, dmso-d_6) δ 10.32 (bs, 1H), 8.45 (d, J = 8.6 Hz, 1H), 8.30 (bs, 1H), 8.10 (d, J = 8.6 Hz, 1H), 7.93 (d, J = 7.5 Hz, 2H), 7.76 (d, J = 7.5 Hz, 2H), 7.50 (d, J = 1.0 Hz, 1 H), 7.44 (t, J = 7.6 Hz, 2H), 7.36 (td, J = 7.4, 1.0 Hz, 2H), 4.58 (d, J = 6.9 Hz, 2H), 4.43 (t, J = 6.9 Hz, 1H), 2.75 (t, J = 8.0 Hz, 2 H), 1.64-1.50 (m, 3H), 0.93(d, J = 6.4 Hz, 6H) ^{13}C{^{1}H} NMR (125 MHz, dmso-d_6) δ 165.8, 153.4, 143.7, 140.8, 137.5, 135.5, 135.3, 129.1, 127.8, 127.2, 125.1, 121.0, 120.3, 119.2, 117.1, 66.4, 46.6, 33.8, 27.2, 22.4. HR-MS (ESI): *m/z* [M+H]$^+$ calcd for $C_{30}H_{28}N_2O_4$: 481.2122; found: 481.2127.

6-butyl-8-(9H-fluoren-9-ylmethoxycarbonylamino)quinoline-2-carboxylic acid (13b)

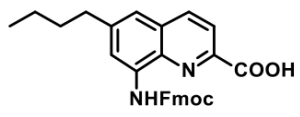

1.78 g **12b** (1.0 equiv., 6.85 mmol) was dissolved in 200 mL 1,4-dioxane and mixed with aqueous solution of 432 mg LiOH · H_2O (1.5 equiv., 10.3 mmol) in 150 mL H_2O. After 1h full conversion was observed, the mixture was quenched with 10.3 mL of 1 M HCl aqueous solution. The mixture was then cooled to 0 °C and 2.88 g $NaHCO_3$ (5.0 equiv., 34.3 mmol) was added. A solution of 2.65 g FmocCl (1.5 equiv., 10.3 mmol) in 75 mL 1,4-dioxane was added dropwise to the reaction mixture within 1h. After full conversion was observed, 5% aq. citric acid solution was added until pH 4 was reached. Mixture was then extracted with 3×200mL DCM. Organic layers were combined and dried over $MgSO_4$, filtered and solvent was removed *in vacuo*. Crude product was suspended in MeOH and sonicated for 1h. After going back to room temperature it was stirred at -25°C overnight. The suspension was filtered and washed with cold MeOH. The reaction yielded **13b** as an off-white solid (2.08 g, 65%).

SUPPORTING INFORMATION

HPLC-UV purity: 96.9%.
^{1}H NMR (500 MHz, DMSO-d_6): δ = 13.53 (b s, 1H), 10.44 (s, 1H), 8.49 (d, *J* = 8.5 Hz, 1H), 8.32 (b s, 1H), 8.17 (d, *J* = 8.5 Hz, 1H), 7.94 (d, *J* = 7.6 Hz, 2H), 7.78 (d, *J* = 7.5 Hz, 2H), 7.52 (d, *J* = 1.8 Hz, 1H), 7.44 (t, *J* = 7.4 Hz, 2H), 7.37 (dt, *J* = 7.4, 1.0 Hz, 2H), 4.61 (d, *J* = 6.7 Hz, 2H), 4.45 (t, *J* = 6.9 Hz, 1H), 2.75 (t, *J* = 7.6 Hz, 2H), 1.64 (m, *J* = 6.8 Hz, 2H), 1.35 (sext, *J* = 7.4 Hz, 2H), 0.91 (t, *J* = 7.4 Hz, 3H).^{13}C{^{1}H} NMR (125 MHz, DMSO-d_6): δ = 165.5, 153.5, 144.1, 143.7, 140.8, 137.8, 135.5, 135.4, 129.3, 127.8, 127.2, 125.1, 120.8, 120.3, 119.3, 117.4, 66.4, 46.6, 40.4, 35.6, 32.7, 21.8, 13.8.
HRMS (ESI): *m/z* [M+H]$^+$ for $C_{29}H_{26}N_2O_4$: 467.1965; found: 467.1961.

8-(9H-fluoren-9-ylmethoxycarbonylamino)-6-*iso*propyl-quinoline-2-carboxylic acid (13c)

Using **General Procedure B** 950 mg **12c** (1.0 equiv., 3.111 mmol), **13c** (333 mg, 24%) was obtained as off-white crystals.
HPLC-UV purity: 98.8%.
^{1}H NMR (500 MHz, dmso-d_6) δ 10.14 (bs, 1H), 8.42 (d, *J* = 8.4 Hz, 1H), 8.32 (bs, 1H), 8.12 (d, *J* = 8.4 Hz, 1H), 7.93 (d, *J* = 7.5 Hz, 2H), 7.76 (d, *J* = 7.5 Hz, 2H), 7.51 (d, *J* = 1.1 Hz, 1 H), 7.44 (t, *J* = 7.5 Hz, 2H), 7.36 (td, *J* = 7.5, 1.1 Hz, 2H), 4.59 (d, *J* = 6.6 Hz, 2H), 4.43 (t, *J* = 6.6 Hz, 1H), 3.04 (quint, *J* = 6.9 Hz, 1 H), 1.28 (d, *J* = 6.9 Hz, 6H) ^{13}C{^{1}H} NMR (125 MHz, dmso-d_6) δ 165.5, 153.6, 149.9, 144.7, 143.7, 140.8, 138.0, 135.7, 135.6, 129.4, 127.8, 127.2, 125.2, 120.7, 120.3, 117.2, 115.9, 66.4, 46.6, 34.1, 23.5.
HRMS (ESI): *m/z* [M+H]$^+$ calcd for $C_{28}H_{24}N_2O_4$: 453.1809; found: 453.1810.

8-(9H-fluoren-9-ylmethoxycarbonylamino)-6-*iso*butyl-quinoline-2-carboxylic acid (13d)

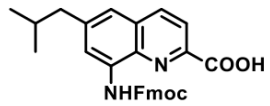

Using **General Procedure B** 2.100 g **12d** (1.0 equiv., 7.154 mmol), **13d** (1.985 g, 57%) was obtained as an off-white solid.
HPLC-UV purity: 98.8%.
^{1}H NMR (500 MHz, dmso-d_6) δ 10.41(s, 1H) 8.48 (d, *J* = 8.6 Hz, 1H), 8.30 (bs, 1H), 8.16 (d, *J* = 8.6 Hz, 1H), 7.93 (d, *J* = 7.5 Hz, 2H), 7.77 (d, *J* = 7.5 Hz, 2H), 7.48 (d, *J* = 1.1 Hz, 1 H), 7.44 (t, *J* = 7.6 Hz, 2H), 7.36 (td, *J* = 7.4, 1.1 Hz, 2H), 4.59 (d, *J* = 6.6 Hz, 2H), 4.44 (t, *J* = 6.6 Hz, 1H), 2.66-2.60 (m, 2H) , 1.94 (sp, *J* = 6.5 Hz, 1 H), 0.90 (d, *J* = 6.5 Hz, 6H) ^{13}C{^{1}H} NMR (125 MHz, dmso-d_6) δ 165.4, 153.6, 144.6, 143.7, 143.1, 140.8, 137.9, 135.5, 135.4, 129.2, 127.8, 127.2, 125.2, 120.7, 120.3, 120.2, 117.9, 66.4, 46.6, 45.2, 29.6, 22.2.
HRMS (ESI): *m/z* [M+H]$^+$ calcd for $C_{29}H_{26}N_2O_4$: 467.1965; found: 467.1968.

6-(3-*tert*-butoxy-3-oxo-propyl)-8-(9H-fluoren-9-ylmethoxycarbonylamino)quinoline-2-carboxylic acid (13e)

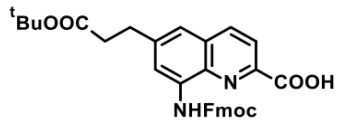

Using **General Procedure B** 4.100 g **12e** (1.0 equiv., 11.29 mmol), **13e** (1.595 g, 26%) was obtained as an off-white solid.
HPLC-UV purity: 99.5%.
^{1}H NMR (500 MHz, dmso-d_6) δ 10.18 (bs, 1H), 8.40 (d, *J* = 8.6 Hz, 1H), 8.24 (bs, 1 H), 8.12 (d, *J* = 8.6 Hz, 1H), 7.93 (d, *J* = 7.5 Hz, 2H), 7.76 (dd, *J* = 0.6 Hz, 7.5 Hz, 2H), 7.49 (d, *J* = 0.6 Hz, 1 H), 7.44 (t, *J* = 7.6 Hz, 2H), 7.36 (td, *J* = 7.4, 1.1 Hz, 2H), 4.60 (d, *J* = 6.6 Hz, 2H), 4.44 (t, *J* = 6.6 Hz, 1H), 2.97 (t, *J* = 6.9 Hz, 2H), 2.60 (t, *J* = 6.9 Hz, 2H), 1.34 (s, 9H). ^{13}C{^{1}H} NMR (125 MHz, dmso-d_6) δ 171.7, 166.7, 153.7, 144.1, 142.0, 141.2, 137.7, 136.0, 135.6, 129.4, 129.2, 128.2, 127.7, 125.6, 121.8, 120.7, 119.8, 117.1, 80.3, 66.8, 47.0, 36.4, 31.6, 28.2.
HRMS (ESI): *m/z* [M+H]$^+$ calcd for $C_{32}H_{30}N_2O_6$: 539.2177; found: 539.2177.

Methyl 8-amino-4-chloro-6-isopentyl-quinoline-2-carboxylate (15a)

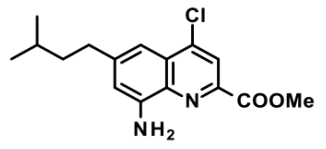

A 2 L pear-shaped flask was filled with 1.10 g Raney nickel (1.94 equiv., 11.8 mmol) under N_2 atmosphere, then washed with 3x20 mL water and 2x20 mL MeOH. 2.02 g compound **11a** (6.06 mmol) and 403 mL MeOH were added and the atmosphere was changed to H_2 (1 bar). The reaction mixture was stirred at RT for 1 week and then filtered through a short pad of celite. The filtrate was concentrated *in vacuo* and the obtained residue was purified by flash chromatography (40 g silicagel column, heptane/EtOAc, gradient elution: 20-50%) to afford compound

SUPPORTING INFORMATION

15a as an orange crystalline solid (1.53 g, 82%).
^{1}H NMR (500 MHz, DMSO-d_6) δ=8.10 (s, 1H), 7.10 (d, *J* = 1.7 Hz, 1H), 6.91 (d, *J* = 1.7 Hz, 1H), 6.22 (s, 2H), 3.94 (s, 3H), 2.69 (t, *J* = 7.8 Hz, 2H), 1.62-1.50 (m, 3H), 0.93 ppm (d, *J* = 6.4 Hz, 6H). ^{13}C{^{1}H} NMR (125 MHz, DMSO-d_6) δ=164.4, 147.0, 146.7, 142.5, 141.1, 135.9, 127.4, 121.0, 111.2, 107.6, 52.7, 40.0, 34.0, 27.2, 22.4 ppm.
HRMS (ESI) *m/z* calcd for $C_{16}H_{20}ClN_2O_2$ [M+H]$^+$: 307.1213; found: 307.1209.

Methyl 8-amino-6-(3-*tert*-butoxypropyl)-4-chloro-quinoline-2-carboxylate (15b)

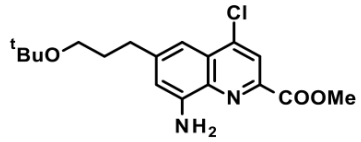

A 2 L pear-shaped flask was filled with 720 mg Raney nickel (2.20 equiv., 8.38 mmol) under N_2 atmosphere, then washed with 3x20 mL water and 2x20 mL MeOH. 1.44 g **14a** (prepared according to [2], 1.0 equiv., 3.81 mmol) and 1.12 L MeOH were added and the atmosphere was changed to H_2 (1 bar). The reaction mixture was stirred at RT for 27 h and then filtered through a short pad of celite. The filtrate was concentrated *in vacuo* and the obtained residue was purified by flash chromatography (40 g silicagel column, heptane/EtOAc, gradient elution: 35-60%) to afford compound **15b** as an orange crystalline solid (1.19 g, 89%).
^{1}H NMR (500 MHz, DMSO-d_6) δ=8.10 (s, 1H), 7.10 (d, *J* = 1.5 Hz, 1H), 6.91 (d, *J* = 1.6 Hz, 1H), 6.23 (s, 2H), 3.94 (s, 3H), 3.32 (t, *J* = 6.3 Hz, 2H), 2.73 (t, *J* = 7.6 Hz, 2H), 1.80 (quint, *J* = 6.7 Hz, 2H), 1.13 ppm (s, 9H). ^{13}C{^{1}H} NMR (125 MHz, DMSO-d_6) δ=164.4, 146.7, 146.4, 142.5, 141.1, 135.9, 127.3, 121.0, 111.3, 107.9, 72.0, 59.8, 52.7, 32.7, 31.4, 27.4 ppm.
HRMS (ESI) *m/z* calcd for $C_{18}H_{24}ClN_2O_3$ [M+H]$^+$: 351.1475; found: 351.1476.

Methyl 8-amino-6-[3-(*tert*-butoxycarbonylamino)propyl]-4-chloro-quinoline-2-carboxylate (15c)

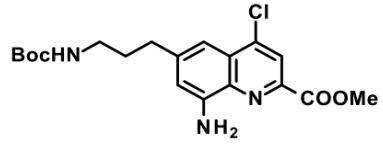

A 2 L pear-shaped flask was filled with 490 mg Raney nickel (2.45 equiv., 5.72 mmol) under N_2 atmosphere, then washed with 3x20 mL water and 2x20 mL MeOH. 980 mg **14b** (prepared according to [2], 1.0 equiv., 2.33 mmol), 49.0 mL DCM and 392 mL MeOH were added and the atmosphere was changed to H_2 (1 bar). The reaction mixture was stirred at RT for 24 h and then filtered through a short pad of celite. The filtrate was concentrated *in vacuo* and the obtained residue was purified by flash chromatography (40 g silicagel column, heptane/EtOAc, gradient elution: 20-60%) to afford compound **15c** as an orange crystalline solid (695 mg, 76%).
^{1}H NMR (500 MHz, DMSO-d_6) δ=8.10 (s, 1H), 7.11 (d, *J* = 1.5 Hz, 1H), 6.91 (t, *J* = 1.5 Hz, 1H), 6.89 (d, *J* = 1.6 Hz, 1H), 6.24 (s, 2H), 3.94 (s, 3H), 2.97 (q, *J* = 6.6 Hz, 2H), 2.67 (t, *J* = 7.7 Hz, 2H), 1.74 (quint, *J* = 7.4 Hz, 2H), 1.38 ppm (s, 9H). ^{13}C{^{1}H} NMR (125 MHz, DMSO-d_6) δ=164.4, 155.6, 146.7, 146.3, 142.6, 141.1, 135.9, 127.4, 121.0, 111.2, 107.8, 77.4, 52.7, 39.6, 33.4, 31.0, 28.3 ppm.
HRMS (ESI) *m/z* calcd for $C_{19}H_{25}ClN_3O_4$ [M+H]$^+$: 394.1534; found: 394.1528.

Methyl 8-amino-4-[3-(*tert*-butoxycarbonylamino)propyl]-6-isopentyl-quinoline-2-carboxylate (16a)

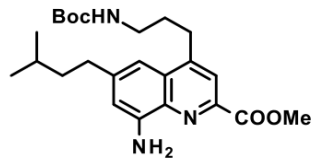

Preparation of alkylboron-reagent:
An oven-dried, 25 mL pear-shaped flask was filled with 738 mg ***tert*-butyl *N*-allylcarbamate** (2.00 equiv, 4.69 mmol), closed with a rubber septum, evacuated and charged with dry N_2. Through the septum 8.21 mL 0.50 M solution of 9-borabicyclo[3.3.1]nonane in THF (1.75 equiv., 4.11 mmol) was added at RT, then the resulting mixture was stirred for 1 h. This solution was used in the next step.
Suzuki-coupling:
A 25 mL pear-shaped flask was filled with 720 mg compound **15a** (1.0 equiv., 2.35 mmol), 83.1 mg $Pd(AtaPhos)_2Cl_2$ (5.00 mol%, 0.12 mmol) and 2.29 g Cs_2CO_3 (3.00 equiv., 7.04 mmol), closed with a rubber septum, evacuated and charged with dry N_2. Through the septum 2.35 mL (1mL/mmol) water and the *alkylboron-reagent* were added. The mixture was heated to 50°C by a heating block and stirred for 20 h. After cooling to RT, the organic phase was separated and dried over Na_2SO_4, filtered and the filtrate was concentrated *in vacuo*. [SAFETY NOTE: Crude product should be handled under inert gas,

as borane residues might be present, causing sudden heating, fuming and fire hazard upon exposition to air.] The residue was triturated with 50 mL heptane, filtered, and the crystals were washed with 3x5 mL heptane. The resulting solid was purified by flash chromatography (120 g silicagel column, DCM/EtOAc, gradient elution: 0-25%) to afford compound **16a** as a pale yellow, crystalline solid (890 mg, 88%).

^{1}H NMR (500 MHz, DMSO-d_6) δ=7.87 (s, 1H), 7.03 (s, 1H), 6.98/6.64 (t/br s, *J* = 5.4 Hz for triplet signal, 1H), 6.80 (d, *J* = 1.3 Hz, 1H), 6.01 (s, 2H), 3.92 (s, 3H), 3.05-2.99 (m, 4H) 2.66 (t, *J* = 7.9 Hz, 2H), 1.78 (quint, *J* = 7.3 Hz, 2H), 1.58 (hept, *J* = 6.2 Hz, 1H), 1.55-1.50 (m, 2H), 1.38/1.32 (s/s, 9H), 0.93 ppm (d, *J* = 6.4 Hz, 6H). (Amide rotamers present at room temperature.) ^{13}C{^{1}H} NMR (125 MHz, DMSO-d_6) δ=165.6, 155.7, 148.2, 146.4, 144.8, 142.5, 135.5, 128.8, 120.2, 109.9, 108.3, 77.5, 52.4, 40.2, 39.7, 34.1, 29.6, 29.1, 28.2, 27.3, 22.4 ppm.

HRMS (ESI) *m/z* calcd for $C_{24}H_{36}N_3O_4$ $[M+H]^+$: 430.2706; found: 430.2704.

Methyl 8-amino-4-(3-*tert*-butoxy-3-oxo-propyl)-6-isopentyl-quinoline-2-carboxylate (16b)

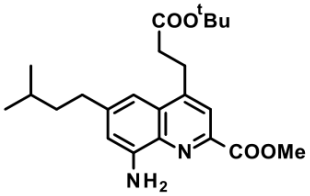

Preparation of alkylboron-reagent:

An oven-dried, 50 mL pear-shaped flask was closed with a rubber septum, evacuated and charged with dry N_2. Through the septum 1.60 mL ***tert*-butyl acrylate** (5.00 equiv., 10.9 mmol), and 21.8 mL 0.50 M solution of 9-borabicyclo[3.3.1]nonane in THF (5.00 equiv., 10.9 mmol) were added at RT, then the resulting mixture was stirred for 2 h. This solution was used in the next step.

Suzuki-coupling:

A 50 mL pear-shaped flask was filled with 670 mg compound **15a** (1.0 equiv., 2.18 mmol), 77.3 mg $Pd(AtaPhos)_2Cl_2$ (5.00 mol%, 0.11 mmol) and 2.14 g Cs_2CO_3 (3.00 equiv., 6.55 mmol), closed with a rubber septum, evacuated and charged with dry N_2. Through the septum 2.18 mL water (1 mL/mmol) and the *alkylboron-reagent* were added. The mixture was heated to 65°C by a heating block and stirred for 2 h. After cooling to RT, the reaction mixture was washed with 2x25 mL brine, the organic phase was dried over Na_2SO_4, filtered and the filtrate was concentrated *in vacuo*. The residue was purified by flash chromatography (80 g silicagel column, heptane/EtOAc, gradient elution: 0-50%) then reversed phase HPLC (EZ Prep system, eluent: 0.1% aq. TFA/MeCN, gradient elution: 70-100%) to afford compound **16b** as a yellow solid (390 mg, 45%).

^{1}H NMR (500 MHz, DMSO-d_6) δ=7.86 (s, 1H), 7.04 (d, *J* = 1.1 Hz, 1H), 6.82 (d, *J* = 1.5 Hz, 1H), 6.03 (s, 2H), 3.92 (s, 3H), 3.25 (t, *J* = 7.2 Hz, 2H), 2.67 (t, *J* = 7.0 Hz, 2H), 1.62-1.50 (m, 3H), 1.36 (s, 9H), 0.94 ppm (d, *J* = 6.3 Hz, 6H). ^{13}C{^{1}H} NMR (125 MHz, DMSO-d_6) δ=171.3, 165.5, 146.6, 146.5, 145.1, 142.4, 135.4, 128.7, 120.0, 110.0, 108.0, 80.0, 52.4, 40.1, 34.2, 34.1, 27.6, 27.2, 26.9, 22.4 ppm.

HRMS (ESI) *m/z* calcd for $C_{23}H_{33}N_2O_4$ $[M+H]^+$: 401.2440; found: 401.2435.

Methyl 8-amino-4-(2-*tert*-butoxyethyl)-6-(3-*tert*-butoxypropyl)quinoline-2-carboxylate (16c)

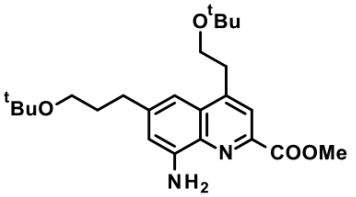

Preparation of alkylboron-reagent:

An oven-dried, 25 mL pear-shaped flask was closed with a rubber septum, evacuated and charged with dry N_2. Through the septum 1.21 mL **2-methyl-2-vinyloxy-propane** (3.50 equiv., 9.18 mmol), and 15.7 mL 0.50 M solution of 9-borabicyclo[3.3.1]nonane in THF (3.00 equiv., 7.87 mmol) were added at RT, then the resulting mixture was stirred for 30 min. This solution was used in the next step.

Suzuki-coupling:

A 50 mL pear-shaped flask was filled with 920 mg compound **15b** (1.0 equiv., 2.62 mmol), 92.9 mg $Pd(AtaPhos)_2Cl_2$ (5.00 mol%, 0.13 mmol) and 2.56 g Cs_2CO_3 (3.00 equiv., 7.87 mmol), closed with a rubber septum, evacuated and charged with dry N_2. Through the septum 2.62 mL water (1 mL/mmol) and the *alkylboron-reagent* were added. The mixture was was heated to 65°C by a heating block and stirred for 20 h. After cooling to RT, the reaction mixture was filtered through a short pad of celite. The filtrate was washed with 2x15 mL brine, and the aqueous phase back-extracted with 2x10 mL THF. The combined organic phase was dried over Na_2SO_4, filtered and the filtrate was concentrated *in vacuo*. The residue was purified by flash chromatography (120 g silicagel column, DCM/EtOAc, gradient elution: 0-40%) to afford compound **16c** as a yellow honey (682 mg, 62%).

SUPPORTING INFORMATION

^{1}H NMR (500 MHz, DMSO-d_6) δ=7.94 (s, 1H), 7.05 (s, 1H), 6.80 (d, *J* = 1.4 Hz, 1H), 6.01 (s, 2H), 3.92 (s, 3H), 3.66 (t, *J* = 6.6 Hz, 2H), 3.33 (t, *J* = 6.3 Hz, 2H), 3.18 (t, *J* = 6.6 Hz, 2H), 2.69 (t, *J* = 7.6 Hz, 2H), 1.80 (quint, *J* = 7.0 Hz, 2H), 1.13 (s, 9H), 1.08 ppm (s, 9H). ^{13}C{^{1}H} NMR (125 MHz, DMSO-d_6) δ=165.6, 146.3, 145.8, 144.2, 142.4, 135.5, 129.1, 121.0, 109.9, 108.5, 72.5, 72.0, 60.3, 60.0, 52.4, 32.9, 32.9, 31.6, 27.4, 27.2 ppm.
HRMS (ESI) *m/z* calcd for $C_{24}H_{37}N_2O_4$ [M+H]$^+$: 417.2753; found: 417.2749.

Methyl 8-amino-4-(3-*tert*-butoxy-3-oxo-propyl)-6-(3-*tert*-butoxypropyl)quinoline-2-carboxylate (16d)

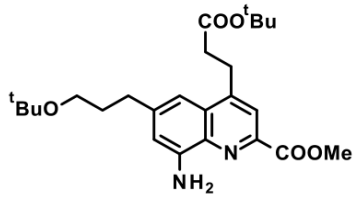

Preparation of alkylboron-reagent:
An oven-dried, 50 mL pear-shaped flask was closed with a rubber septum, evacuated and charged with dry N_2. Through the septum 5.30 mL ***tert*-butyl acrylate** (10.0 equiv., 36.2 mmol), and 36.2 mL 0.50 M solution of 9-borabicyclo[3.3.1]nonane in THF (5.00 equiv., 18.1 mmol) were added at RT, then the resulting mixture was stirred for 20 h. This solution was used in the next step.
Suzuki-coupling:
A 100 mL pear-shaped flask was filled with 1.27 g compound **15b** (1.0 equiv., 3.62 mmol), 128 mg $Pd(AtaPhos)_2Cl_2$ (5.00 mol%, 0.18 mmol) and 3.54 g Cs_2CO_3 (3.00 equiv., 10.9 mmol), closed with a rubber septum, evacuated and charged with dry N_2. Through the septum 3.62 mL water (1 mL/mmol) and the *alkylboron-reagent* were added. The mixture was was heated to 65°C by a heating block and stirred for 20 h. After cooling to RT, the reaction mixture was washed with 2x25 mL brine, the organic phase was dried over Na_2SO_4, filtered and the filtrate was concentrated *in vacuo*. The residue was purified by flash chromatography (330 g silicagel column, heptane/EtOAc/MeOH 89/10/1 as eluent) then reversed phase HPLC (EZ Prep system, eluent: 25mM aq NH_4HCO_3/MeCN, gradient elution: 50-80%) to afford compound **16d** as a yellow solid (596 mg, 37%).
^{1}H NMR (500 MHz, DMSO-d_6) δ=7.86 (s, 1H), 7.03 (d, *J* = 1.1 Hz, 1H), 6.82 (d, *J* = 1.4 Hz, 1H), 6.04 (s, 2H), 3.92 (s, 3H), 3.33 (t, *J* = 6.3 Hz, 2H), 3.25 (t, *J* = 7.2 Hz, 2H), 2.72-2.66 (m, 4H), 1.80 (quint, *J* = 7.1 Hz, 2H), 1.36 (s, 9H), 1.13 ppm (s, 9H). ^{13}C{^{1}H} NMR (125 MHz, DMSO-d_6) δ=171.2, 165.5, 146.7, 146.5, 144.5, 142.4, 135.5, 128.6, 120.1, 110.0, 108.2, 80.0, 72.0, 60.0, 52.4, 34.2, 32.9, 31.5, 27.6, 27.4, 26.9 ppm.
HRMS (ESI) *m/z* calcd for $C_{25}H_{37}N_2O_5$ [M+H]$^+$: 445.2702; found: 445.2706.

Methyl 8-amino-6-[3-(*tert*-butoxycarbonylamino)propyl]-4-(3-*tert*-butoxy-3-oxo-propyl)quinoline-2-carboxylate (16e)

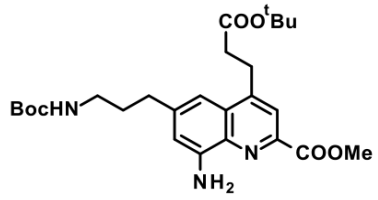

Preparation of alkylboron-reagent:
An oven-dried, 50 mL pear-shaped flask was closed with a rubber septum, evacuated and charged with dry N_2. Through the septum 21.6 mL 0.50 M solution of 9-borabicyclo[3.3.1]nonane in THF (5.00 equiv., 10.8 mmol) and 1.58 mL ***tert*-butyl acrylate** (5.00 equiv., 10.8 mmol) were added at RT, then the resulting mixture was stirred for 2 h. This solution was used in the next step.
Suzuki-coupling:
A 50 mL pear-shaped flask was filled with 850 mg compound **15c** (1.0 equiv., 2.16 mmol), 45.5 mg 4-[bis(1-adamantyl)phosphanyl]-*N*,*N*-dimethyl-aniline (5.00 mol%, 0.11 mmol, prepared according to [2]), 24.7 mg $Pd_2(dba)_3$ (1.25 mol%, 0.03 mmol) and 2.11 g Cs_2CO_3 (3.00 equiv., 6.47 mmol), closed with a rubber septum, evacuated and charged with dry N_2. Through the septum 5.00 mL THF was added and the mixture was stirred at RT for 5 min, then 2.18 mL water (1 mL/mmol) and the *alkylboron-reagent* were added. The mixture was heated to 65°C by a heating block and stirred for 1.5 h. After cooling to RT, the reaction mixture was washed with 2x25 mL brine, the organic phase was dried over Na_2SO_4, filtered and the filtrate was concentrated *in vacuo*. The residue was purified by flash chromatography (80 g silicagel column, heptane/EtOAc, gradient elution: 30-60%) then reversed phase HPLC (EZ Prep system, eluent: 25mM aq NH_4HCO_3/MeCN, gradient elution: 70-90%) to afford compound **16e** as a yellow solid (626 mg, 59%).
^{1}H NMR (400 MHz, DMSO-d_6) δ=7.87 (s, 1H), 7.05 (s, 1H), 6.90 (t, *J* = 5.4 Hz, 1H), 6.80 (s, 1H), 6.05

SUPPORTING INFORMATION

(s, 2H), 3.92 (s, 3H), 3.26 (t, *J* = 7.1 Hz, 2H), 2.97 (q, *J* = 6.5 Hz, 2H), 2.72-2.60 (m, 4H), 1.74 (quint, *J* = 7.3 Hz, 2H), 1.38 (s, 9H), 1.36 ppm (s, 9H). $^{13}C\{^{1}H\}$ NMR (100 MHz, DMSO-d_6) δ=171.3, 165.4, 155.6, 146.7, 146.5, 144.4, 142.4, 135.5, 128.7, 120.1, 110.0, 108.3, 80.0, 77.4, 52.4, 39.4, 34.1, 33.5, 31.1, 28.3, 27.6, 26.9 ppm.
HRMS (ESI) *m/z* calcd for $C_{26}H_{38}N_3O_6$ $[M+H]^+$: 488.2761; found: 488.2760.

4-[3-(*tert*-butoxycarbonylamino)propyl]-8-(9*H*-fluoren-9-ylmethoxycarbonylamino)-6-*iso*pentyl-quinoline-2-carboxylic acid (17a)

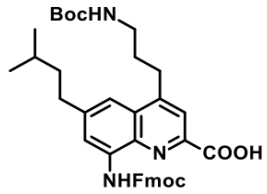

Using **General Procedure B** 865 mg compound **16a** (1.0 equiv., 2.01 mmol), **17a** (1.05 g, 82%) was obtained as pale yellow solid.
HPLC-UV purity: 98.8%.
^{1}H NMR (500 MHz, DMSO-d_6) δ=13.53 (br s, 1H), 10.39 (br s, 1H), 8.32 (br s, 1H), 8.04 (s, 1H), 7.93 (d, *J* = 7.5 Hz, 2H), 7.77 (d, *J* = 7.5 Hz, 2H), 7.60 (s, 1H), 7.44 (t, *J* = 7.4 Hz, 2H), 7.36 (t, *J* = 7.4 Hz, 2H), 6.99/6.65 (t/br s, *J* = 5.4 Hz for triplet signal, 1H), 4.58 (d, *J* = 6.9 Hz, 2H), 4.44 (t, *J* = 7.0 Hz, 1H), 3.11 (t, *J* = 7.7 Hz, 2H), 3.04 (q, *J* = 6.2 Hz, 2H), 2.76 (t, *J* = 7.8 Hz, 2H), 1.80 (quint, *J* = 7.2 Hz, 2H), 1.59 (hept, *J* = 6.5 Hz, 1H), 1.57-1.51 (m, 2H), 1.38/1.32 (s/s, 9H), 0.94 ppm (d, *J* = 6.5 Hz, 6H). (Amide rotamers present at room temperature.) $^{13}C\{^{1}H\}$ NMR (125 MHz, DMSO-d_6) δ=166.1, 155.7, 153.4, 149.7, 145.5, 143.7, 143.7, 140.7, 135.9, 135.6, 128.1, 127.8, 127.2, 125.1, 120.3, 120.2, 116.6, 115.3, 77.5, 66.4, 46.5, 40.1, 39.7, 34.2, 29.7, 29.0, 28.2, 27.3, 22.4 ppm.
HRMS (ESI) *m/z* calcd for $C_{38}H_{44}N_3O_6$ $[M+H]^+$: 638.3230; found: 638.3229.

4-(3-*tert*-butoxy-3-oxo-propyl)-8-(9*H*-fluoren-9-ylmethoxycarbonylamino)-6-*iso*pentyl-quinoline-2-carboxylic acid (17b)

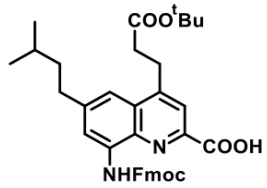

Using **General Procedure B** 390 mg compound **16b** (1.0 equiv., 0.97 mmol), **17b** (400 mg, 67%) was obtained as pale yellow solid.
HPLC-UV purity: 99.6%.
^{1}H NMR (500 MHz, DMSO-d_6) δ=13.52 (br s, 1H), 10.48 (br s, 1H), 8.35 (br s, 1H), 8.05 (s, 1H), 7.93 (d, *J* = 7.5 Hz, 2H), 7.78 (d, *J* = 7.5 Hz, 2H), 7.64 (s, 1H), 7.44 (t, *J* = 7.3 Hz, 2H), 7.36 (td, *J* = 7.5 Hz, *J* = 1.1 Hz, 2H), 4.59 (d, *J* = 7.1 Hz, 2H), 4.45 (t, *J* = 7.0 Hz, 1H), 3.37 (t, *J* = 7.0 Hz, 2H), 2.79 (t, *J* = 7.7 Hz, 2H), 2.72 (t, *J* = 7.1 Hz, 2H), 1.62-1.50 (m, 3H), 1.35 (s, 9H), 0.94 ppm (d, *J* = 6.4 Hz, 6H). $^{13}C\{^{1}H\}$ NMR (125 MHz, DMSO-d_6) δ=171.1, 165.5, 153.5, 148.6, 144.4, 143.7, 140.8, 136.1, 135.5, 128.3, 127.8, 127.2, 125.2, 120.3, 119.9, 117.1, 115.3, 80.1, 66.4, 46.6, 40.0, 34.2, 34.1, 27.6, 27.3, 26.9, 22.4 ppm.
HRMS (ESI) *m/z* calcd for $C_{37}H_{41}N_2O_6$ $[M+H]^+$: 609.2965; found: 609.2963.

4-(2-*tert*-butoxyethyl)-6-(3-*tert*-butoxypropyl)-8-(9*H*-fluoren-9-ylmethoxycarbonylamino)quinoline-2-carboxylic acid (17c)

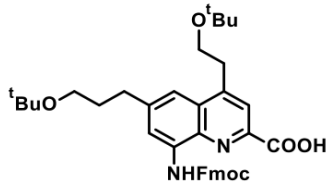

Using **General Procedure B** 658 mg compound **16c** (1.0 equiv., 1.58 mmol), **17c** (798 mg, 81%) was obtained as pale yellow solid.
HPLC-UV purity: 99.2%.
^{1}H NMR (500 MHz, DMSO-d_6) δ=13.58 (br s, 1H), 10.37 (br s, 1H), 8.30 (br s, 1H), 8.09 (s, 1H), 7.93 (d, *J* = 7.5 Hz, 2H), 7.76 (d, *J* = 7.5 Hz, 2H), 7.62 (s, 1H), 7.43 (t, *J* = 7.5 Hz, 2H), 7.35 (td, *J* = 7.5 Hz, *J* = 0.9 Hz, 2H), 4.58 (d, *J* = 6.8 Hz, 2H), 4.43 (t, *J* = 6.9 Hz, 1H), 3.68 (t, *J* = 6.5 Hz, 2H), 3.33 (t, *J* = 6.2 Hz, 2H), 3.28 (t, *J* = 6.5 Hz, 2H), 2.80 (t, *J* = 7.5 Hz, 2H), 1.82 (quint, *J* = 6.9 Hz, 2H), 1.12 (s, 9H), 1.06 ppm (s, 9H). $^{13}C\{^{1}H\}$ NMR (125 MHz, DMSO-d_6) δ=166.0, 153.4, 147.5, 145.1, 143.7, 143.1, 140.7, 135.8, 135.6, 128.5, 127.8, 127.2, 125.1, 121.0, 120.2, 116.8, 115.8, 72.5, 72.0, 66.4, 60.4, 59.9, 46.5, 32.9, 32.8, 31.5, 27.4, 27.2 ppm.
HRMS (ESI) *m/z* calcd for $C_{38}H_{45}N_2O_6$ $[M+H]^+$: 625.3278; found: 625.3279.

SUPPORTING INFORMATION

4-(3-*tert*-butoxy-3-oxo-propyl)-6-(3-*tert*-butoxypropyl)-8-(9H-fluoren-9-ylmethoxycarbonylamino)quinoline-2-carboxylic acid (17d)

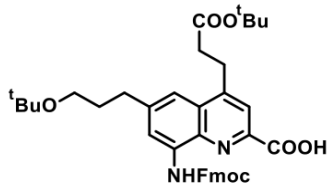

Using **General Procedure B** 575 mg compound **16d** (1.0 equiv., 1.29 mmol), **17d** (559 mg, 66%) was obtained as pale yellow solid.
HPLC-UV purity: 98.4%.
^{1}H NMR (500 MHz, DMSO-d_6) δ=13.58 (br s, 1H), 10.40 (br s, 1H), 8.32 (br s, 1H), 8.03 (s, 1H), 7.93 (d, *J* = 7.5 Hz, 2H), 7.76 (d, *J* = 7.5 Hz, 2H), 7.61 (s, 1H), 7.44 (t, *J* = 7.4 Hz, 2H), 7.36 (t, *J* = 7.4 Hz, 2H), 4.59 (d, *J* = 6.8 Hz, 2H), 4.44 (t, *J* = 6.8 Hz, 1H), 3.36 (t, *J* = 7.3 Hz, 2H), 3.33 (t, *J* = 6.2 Hz, 2H), 2.82 (t, *J* = 7.4 Hz, 2H), 2.70 (t, *J* = 7.2 Hz, 2H), 1.82 (quint, *J* = 6.8 Hz, 2H), 1.35 (s, 9H), 1.12 ppm (s, 9H). ^{13}C{^{1}H} NMR (125 MHz, DMSO-d_6) δ=171.1, 165.8, 153.4, 148.3, 144.9, 143.7, 143.6, 140.8, 136.0, 135.6, 128.0, 127.8, 127.2, 125.1, 120.2, 120.0, 116.9, 115.3, 80.1, 72.0, 66.4, 59.8, 46.5, 34.3, 32.9, 31.5, 27.6, 27.4, 26.9 ppm.
HRMS (ESI) *m/z* calcd for $C_{39}H_{45}N_2O_7$ $[M+H]^+$: 653.3227; found: 653.3226.

6-[3-(*tert*-butoxycarbonylamino)propyl]-4-(3-*tert*-butoxy-3-oxo-propyl)-8-(9*H*-fluoren-9-ylmethoxycarbonylamino)quinoline-2-carboxylic acid (17e)

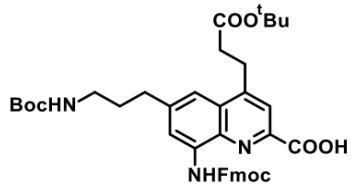

Using **General Procedure B** 800 mg compound **16e** 25 (1.0 equiv., 1.641 mmol), **17e** (960 mg, 84%) was obtained as pale yellow solid.
HPLC-UV purity: 97.5%.
^{1}H NMR (500 MHz, DMSO-d_6) δ=13.52 (br s, 1H), 10.48 (br s, 1H), 8.32 (br s, 1H), 8.05 (s, 1H), 7.93 (d, *J* = 7.5 Hz, 2H), 7.78 (dd, *J* = 7.4 Hz, *J* = 0.6 Hz, 2H), 7.66 (s, 1H), 7.44 (t, *J* = 7.3 Hz, 2H), 7.37 (td, *J* = 7.4 Hz, *J* = 1.1 Hz, 2H), 6.93/6.58 (t/s, *J* = 6.8 Hz for triplet signal, 1H), 4.60 (d, *J* = 6.8 Hz, 2H), 4.46 (t, *J* = 6.9 Hz, 1H), 3.38 (t, *J* = 6.9 Hz, 2H), 2.98 (q, *J* = 6.4 Hz, 2H), 2.77 (t, *J* = 7.4 Hz, 2H), 2.72 (t, *J* = 7.1 Hz, 2H), 1.76 (quint, *J* = 7.1 Hz, 2H), 1.37 (s, 9H), 1.35 ppm (s, 9H). (Amide rotamers present at room temperature.) ^{13}C{^{1}H} NMR (125 MHz, DMSO-d_6) δ=171.1, 165.5, 155.6, 153.5, 148.7, 143.9, 143.7, 140.8, 136.1, 135.6, 128.3, 127.8, 127.2, 125.2, 120.3, 120.0, 117.1, 115.6, 80.1, 77.4, 66.3, 46.6, 39.2, 34.2, 33.5, 31.1, 28.3, 27.6, 26.9 ppm.
HRMS (ESI) *m/z* calcd for $C_{40}H_{46}N_3O_8$ $[M+H]^+$: 696.3285; found: 696.3292.

Methyl 6-(3-*tert*-butoxy-3-oxo-propyl)-4-chloro-8-[(2,2,2-trifluoroacetyl)amino]quinoline-2-carboxylate (19b)

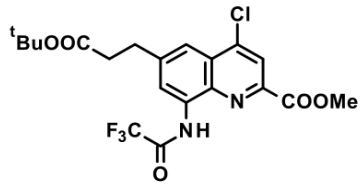

Preparation of alkylboron-reagent:
An oven-dried, 250 mL pear-shaped flask was closed with a rubber septum, evacuated and charged with dry N_2. Through the septum 137 mL 0.50 M solution of 9-borabicyclo[3.3.1]nonane in THF (5.00 equiv., 68.3 mmol) and 20.0 mL ***tert*-butyl acrylate** (10.0 equiv., 137 mmol) were added at RT, then the resulting mixture was stirred for 12 h. This solution was used in the next step.

Suzuki-coupling:
A 250 mL pear-shaped flask was filled with 5.62 g **18** (prepared according to [2], 1.0 equiv., 13.7 mmol), 483 mg $Pd(AtaPhos)_2Cl_2$ (5.00 mol%, 0.68 mmol) and 13.3 g Cs_2CO_3 (3.00 equiv., 41.0 mmol), closed with a rubber septum, evacuated and charged with dry N_2. Through the septum 13.7 mL water (1 mL/mmol) and the *alkylboron-reagent* were added. The mixture was heated to 50°C by a heating block and stirred for 30 min. After cooling to RT, the reaction mixture was washed with 2x25 mL brine, the organic phase was dried over Na_2SO_4, filtered and the filtrate was concentrated *in vacuo*. The residue was was triturated with 90 mL pentane, filtered and washed with 3x10 mL pentane. The obtained solid was purified by flash chromatography (40 g silicagel column, DCM as eluent), then the resulting solid was triturated again with 15 mL pentane, filtered and dried in vacuo to afford **19b** as a white solid (4.52 g, 72%).
^{1}H NMR (400 MHz, DMSO-d_6) δ=11.05 (s, 1H), 8.38 (d, *J* = 1.7 Hz, 1H), 8.32 (s, 1H), 7.97 (d, *J* = 1.7 Hz, 1H), 3.98 (s, 3H), 3.13 (t, *J* = 7.2 Hz, 2H), 2.69 (t, *J* = 7.1 Hz, 2H), 1.35 ppm (s, 9H). ^{13}C{^{1}H} NMR (125 MHz, DMSO-d_6) δ= 171.2, 163.8, 154.7 (q, *J* = 37.4 Hz), 146.1, 144.0, 142.7, 138.7, 132.9, 126.7, 123.9, 122.1, 119.5, 115.6 (q, *J* = 288.4 Hz), 80.0, 53.1, 35.5, 30.9, 27.7 ppm. ^{19}F NMR (376 MHz,

SUPPORTING INFORMATION

DMSO-d_6) δ=-74.5 ppm.
HRMS (ESI) *m/z* calcd for $C_{20}H_{21}ClF_3N_2O_5$ $[M+H]^+$: 461.1091; found: 461.1090.

Methyl 6-[2-(*tert*-butoxycarbonylamino)ethyl]-4-*iso*pentyl-8-[(2,2,2-trifluoroacetyl)amino]quinoline-2-carboxylate (20a)

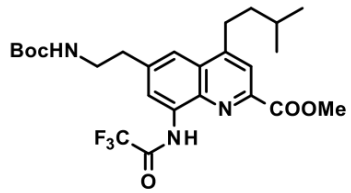

Preparation of alkylboron-reagent:
An oven-dried, 25 mL pear-shaped flask was closed with a rubber septum, evacuated and charged with dry N_2. Through the septum 4.04 mL 1.50 M solution of **3-methylbut-1-ene** in THF (3.0 equiv., 6.05 mmol), and 6.05 mL 0.50 M solution of 9-borabicyclo[3.3.1]nonane in THF (1.5 equiv., 3.03 mmol) were added at RT, then the resulting mixture was stirred for 12 h. This solution was used in the next step.

Suzuki-coupling:
A 50 mL pear-shaped flask was filled with 960 mg compound **methyl 6-[2-(*tert*-butoxycarbonylamino)ethyl]-4-chloro-8-[(2,2,2-trifluoroacetyl)amino]quinoline-2-carboxylate (19a)** (prepared according to [2], 1.0 equiv., 2.02 mmol), 71.4 mg $Pd(AtaPhos)_2Cl_2$ (5.00 mol%, 0.10 mmol) and 1.32 g Cs_2CO_3 (2.00 equiv., 4.04 mmol), closed with a rubber septum, evacuated and charged with dry N_2. Through the septum 2.02 mL (1 mL/mmol) water and the *alkylboron-reagent* were added. The mixture was heated to 50°C by a heating block and stirred for 1 h. After cooling to RT, 15 mL EtOAc was added, the organic phase was separated and washed with 2x5 mL brine. The organic phase was dried over Na_2SO_4, filtered and the filtrate was concentrated *in vacuo*. The residue was purified by flash chromatography (40 g silicagel column, heptane/EtOAc, gradient elution: 0-60%), then the resulting solid was triturated with 20 mL heptane, filtered and dried *in vacuo* to afford compound **20a** as an off-white, crystalline solid (770 mg, 75%).
^{1}H NMR (500 MHz, DMSO-d_6) δ=11.00 (s, 1H), 8.37/8.34 (s/s, 1H), 8.06 (s, 1H), 7.87/7.81 (s, 1H), 6.96/6.60 (t/br s, *J* = 5.6 Hz for triplet signal, 1H), 3.96 (s, 3H), 3.29 (q, *J* = 6.4 Hz, 2H), 3.17 (t, *J* = 8.0 Hz, 2H), 2.97 (t, *J* = 6.8 Hz, 2H), 1.70 (hept, *J* = 6.5 Hz, 1H), 1.60 (q, *J* = 7.6 Hz, 2H), 1.31/1.25 (s, 9H), 1.00 (d, *J* = 6.5 Hz, 6H). (Amide rotamers present at room temperature.) ^{13}C{^{1}H} NMR (125 MHz, DMSO-d_6) δ=164.7, 155.5, 154.1 (q, *J* = 36.8 Hz), 151.2, 145.2, 140.7, 137.1, 132.4, 127.9, 121.1, 121.0, 119.9, 115.6 (q, *J* = 288.5 Hz), 77.5, 52.8, 41.0, 38.6, 36.2, 29.3, 28.1, 27.7, 22.3 ppm. ^{19}F NMR (376 MHz, DMSO-d_6) δ=-74.7 ppm.
HRMS (ESI) *m/z* calcd for $C_{25}H_{33}F_3N_3O_5$ $[M+H]^+$: 512.2372; found: 512.2369.

Methyl 6-(3-*tert*-butoxy-3-oxo-propyl)-4-*iso*pentyl-8-[(2,2,2-trifluoroacetyl)amino]quinoline-2-carboxylate (20b)

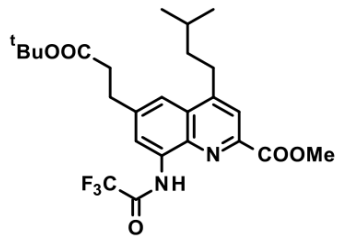

Preparation of alkylboron-reagent:
An oven-dried, 25 mL pear-shaped flask was closed with a rubber septum, evacuated and charged with dry N_2. Through the septum 1.25 mL 1.50M solution of **3-methylbut-1-ene** in THF (3.00 equiv., 2.28 mmol), and 2.28 mL 0.50 M solution of 9-borabicyclo[3.3.1]nonane in THF (1.50 equiv., 1.14 mmol) were added at RT, then the resulting mixture was stirred for 12 h. This solution was used in the next step.
Suzuki-coupling:
A 25 mL pear-shaped flask was filled with 350 mg **19b** (1.0 equiv., 0.76 mmol), 26.9 mg $Pd(AtaPhos)_2Cl_2$ (5.00 mol%, 0.04 mmol) and 495 mg Cs_2CO_3 (2.00 equiv., 1.52 mmol), closed with a rubber septum, evacuated and charged with dry N_2. Through the septum 0.76 mL (1mL/mmol) water and the *alkylboron-reagent* were added. The mixture was heated to 50°C by a heating block and stirred for 1 h. After cooling to RT, the organic phase was separated and washed with 2x2 mL brine. The organic phase was dried over Na_2SO_4, filtered and the filtrate was concentrated in vacuo. The residue was purified by flash chromatography (12 g silicagel column, heptane/EtOAc, gradient elution: 0-40%), then reversed phase HPLC (EZ Prep system, eluent: 25mM aq NH_4HCO_3/MeCN, gradient elution: 80-100%) to afford **20b** as an off-white, crystalline solid (317 mg, 84%).
^{1}H NMR (500 MHz, DMSO-d_6) δ=10.95 (s, 1H), 8.33 (d, *J* = 1.4 Hz, 1H), 8.02 (s, 1H), 7.87 (s, 1H), 3.96 (s, 3H), 3.16-3.10 (m, 2H), 3.08 (t, *J* = 7.3 Hz, 2H), 2.68 (t, *J* = 7.3 Hz, 2H), 1.70 (hept, *J* = 6.6 Hz, 1H), 1.62-1.53 (m, 2H), 1.34 (s, 9H), 0.99 ppm (d, *J* = 6.6 Hz, 6H). ^{13}C{^{1}H} NMR (125 MHz, DMSO-

d_6) δ=171.3, 164.7, 154.2 (q, *J* = 36.9 Hz), 151.2, 145.4, 141.8, 137.2, 132.5, 127.9, 121.1, 121.1, 119.4, 115.6 (q, *J* = 288.5 Hz), 79.9, 52.8, 38.7, 35.7, 31.1, 29.3, 27.7, 27.7, 22.3 ppm. ^{19}F NMR (376 MHz, DMSO-d_6) δ=-74.7 ppm.
HRMS (ESI) *m/z* calcd for $C_{25}H_{32}F_3N_2O_5$ [M+H]$^+$: 497.2260; found: 497.2258.

Methyl 4-(2-*tert*-butoxyethyl)-6-(3-*tert*-butoxy-3-oxo-propyl)-8-[(2,2,2-trifluoroacetyl)amino]quinoline-2-carboxylate (20c)

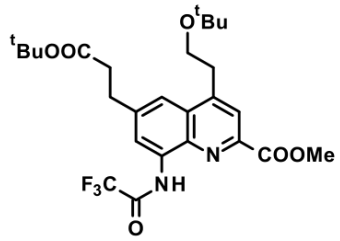

Preparation of alkylboron-reagent:
An oven-dried, 25 mL pear-shaped flask was closed with a rubber septum, evacuated and charged with dry N_2. Through the septum 713 µL **2-methyl-2-vinyloxy-propane** (2.00 equiv., 5.43 mmol), and 10.9 mL 0.50 M solution of 9-borabicyclo[3.3.1]nonane in THF (2.00 equiv., 5.43 mmol) were added at RT, then the resulting mixture was stirred for 30 min. This solution was used in the next step.
Suzuki-coupling:
A 25 mL pear-shaped flask was filled with 1.25 g compound **19b** (1.0 equiv., 2.71 mmol), 96.0 mg $Pd(AtaPhos)_2Cl_2$ (5.00 mol%, 0.14 mmol) and 2.65 g Cs_2CO_3 (3.00 equiv., 8.14 mmol), closed with a rubber septum, evacuated and charged with dry N_2. Through the septum 2.71 mL (1mL/mmol) water and the *alkylboron-reagent* were added. The mixture was stirred atheated to 50°C by a heating block and stirred for 30 min. After cooling to RT, the organic phase was separated and washed with 2x5 mL brine. The organic phase was dried over Na_2SO_4, filtered and the filtrate was concentrated in vacuo. The residue was purified by flash chromatography (80 g silicagel column, heptane/EtOAc, gradient elution: 0-30%), then reversed phase HPLC (EZ Prep system, eluent: 0.1% aq TFA/MeCN, gradient elution: 90-100%) to afford **20c** as an off-white, crystalline solid (1.14 g, 80%).
^{1}H NMR (400 MHz, DMSO-d_6) δ=11.00 (s, 1H), 8.35 (d, *J* = 1.3 Hz, 1H), 8.15 (s, 1H), 7.97 (s, 1H), 3.97 (s, 3H), 3.71 (t, *J* = 6.4 Hz, 2H), 3.34 (t, *J* = 5.2 Hz, 2H), 3.09 (t, *J* = 7.3 Hz, 2H), 2.68 (t, *J* = 7.3 Hz, 2H), 1.35 (s, 9H), 1.05 ppm (s, 9H). ^{13}C{^{1}H} NMR (100 MHz, DMSO-d_6) δ=171.3, 164.8, 154.3 (q, *J* = 36.9 Hz), 148.5, 145.2, 141.6, 137.4, 132.6, 128.5, 122.2, 121.3, 120.0, 115.7 (q, *J* = 291.5 Hz), 79.9, 72.5, 60.4, 52.9, 35.8, 32.5, 31.1, 27.7, 27.2 ppm. ^{19}F NMR (376 MHz, DMSO-d_6) δ=-74.6 ppm.
HRMS (ESI) *m/z* calcd for $C_{26}H_{34}F_3N_2O_6$ [M+H]$^+$: 527.2369; found: 527.2369.

Methyl 4-[3-(*tert*-butoxycarbonylamino)propyl]-6-(3-tert-butoxy-3-oxo-propyl)-8-[(2,2,2-trifluoroacetyl)amino]quinoline-2-carboxylate (20d)

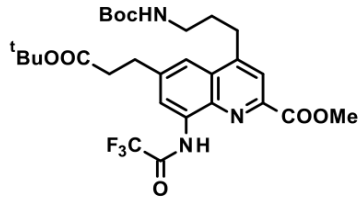

Preparation of alkylboron-reagent:
An oven-dried, 25 mL pear-shaped flask was filled with 880 mg ***tert*-butyl N-allylcarbamate** (3.00 equiv, 5.60 mmol), closed with a rubber septum, evacuated and charged with dry N_2. Through the septum 5.60 mL 0.50 M solution of 9-borabicyclo[3.3.1]nonane in THF (1.50 equiv., 2.80 mmol) was added at RT, then the resulting mixture was stirred for 1 h. This solution was used in the next step.
Suzuki-coupling:
A 25 mL pear-shaped flask was filled with 860 mg compound **19b** (1.0 equiv., 1.87 mmol), 66.1 mg $Pd(AtaPhos)_2Cl_2$ (5.00 mol%, 0.09 mmol) and 1.22 g Cs_2CO_3 (2.00 equiv., 3.73 mmol), closed with a rubber septum, evacuated and charged with dry N_2. Through the septum 1.87 mL (1mL/mmol) water and the *alkylboron-reagent* were added. The mixture was stirred atheated to 50°C by a heating block and stirred for 1 h. After cooling to RT, 10 mL DCM was added, the organic phase was separated and washed with 2x10 mL brine. The organic phase was dried over Na_2SO_4, filtered and the filtrate was concentrated *in vacuo*. [SAFETY NOTE: Crude product should be handled under inert gas, as borane residues might be present, causing sudden heating, fuming and fire hazard upon exposition to air.] The residue was triturated with 25 mL pentane, filtered, and the crystals were washed with 3x5 mL pentane. The resulting solid was purified by flash chromatography (40 g silicagel column, DCM/MeOH, gradient elution: 0-5%) to afford **20d** as an off-white, crystalline solid (977 mg, 90%).
^{1}H NMR (500 MHz, DMSO-d_6) δ=10.99 (s, 1H), 8.35 (d, *J* = 1.6 Hz, 1H), 8.09 (s, 1H), 7.93 (s, 1H), 6.99 (t, *J* = 5.4 Hz, 1H), 3.96 (s, 3H), 3.16 (t, *J* = 7.7 Hz, 2H), 3.09 (t, *J* = 7.5 Hz, 2H), 3.04 (q, *J* = 6.2 Hz, 2H), 2.68 (t, *J* = 7.5 Hz, 2H), 1.82 (quint, *J* = 7.3 Hz, 2H), 1.39 (s, 9H), 1.37 (s, 9H). ^{13}C{^{1}H} NMR

SUPPORTING INFORMATION

(100 MHz, DMSO-d_6) δ=171.3, 164.8, 155.7, 154.3 (q, *J* = 36.8 Hz), 150.6, 145.5, 141.9, 137.4, 132.6, 128.1, 121.5, 121.3, 119.6, 115.6 (q, *J* = 289.8 Hz), 79.9, 77.5, 52.8, 39.6, 35.8, 31.1, 29.8, 28.8, 28.3, 27.7 ppm. ^{19}F NMR (376 MHz, DMSO-d_6) δ=-74.6 ppm.
HRMS (ESI) *m/z* calcd for $C_{28}H_{37}F_3N_3O_7$ [M+H]$^+$: 584.2584; found: 584.2583.

Methyl 4-[2-(*tert*-butoxycarbonylamino)ethyl]-6-(3-*tert*-butoxy-3-oxo-propyl)-8-[(2,2,2-trifluoroacetyl)amino]quinoline-2-carboxylate (20e)

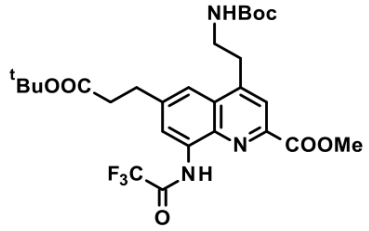

Preparation of alkylboron-reagent:
An oven-dried, 25 mL pear-shaped flask was filled with 699 mg **tert-butyl *N*-vinylcarbamate** (Prepared from *N*-vinyl formamide according to [2].) (1.50 equiv., 4.88 mmol), closed with a rubber septum, evacuated and charged with dry N_2. 13.0 mL 0.50 M solution of 9-borabicyclo[3.3.1]nonane in THF (2.00 equiv., 6.51 mmol) was added at RT, then the resulting mixture was stirred for 1 h. This solution was used in the next step.

Suzuki-coupling:
A 25 mL pear-shaped flask was filled with 1.50 g **19b** (1.0 equiv., 3.26 mmol), 115 mg $Pd(AtaPhos)_2Cl_2$ (5.00 mol%, 0.16 mmol) and 3.18 g Cs_2CO_3 (3.00 equiv., 9.77 mmol), closed with a rubber septum, evacuated and charged with dry N_2. Through the septum 3.26 mL (1mL/mmol) water and the *alkylboron-reagent* were added. The mixture was heated to 50°C by a heating block and stirred for 3 h. After cooling to RT, the organic phase was separated and washed with 2x5 mL brine. The organic phase was dried over Na_2SO_4, filtered and the filtrate was concentrated *in vacuo*. The residue was purified by flash chromatography (120 g silicagel column, heptane/EtOAc, gradient elution: 0-60%). The obtained solid was triturated with 15 mL DIPE, filtered, washed with furter 2x2 mL DIPE and dried in vacuo to afford **20e** as an off-white, crystalline solid (800 mg, 43%).
^{1}H NMR (500 MHz, DMSO-d_6) δ=10.98 (s, 1H), 8.35 (d, *J* = 1.1 Hz, 1H), 8.04 (s, 1H), 8.01/7.93 (s/s, 1H), 7.01/6.60 (t/s, *J* = 5.2 Hz for triplet signal, 1H), 3.96 (s, 3H), 3.32-3.23 (m, 4H), 3.09 (t, *J* = 7.7 Hz, 2H), 2.71 (t, *J* = 7.6 Hz, 2H), 1.37 (s, 9H), 1.30/1.09 ppm (s/s, 9H). (Amide rotamers present at room temperature.) ^{13}C{^{1}H} NMR (125 MHz, DMSO-d_6) δ=171.3, 164.7, 155.5, 154.3 (q, *J* = 36.8 Hz), 148.2, 145.2, 141.8, 137.4, 132.5, 128.4, 122.3, 121.2, 119.7, 115.6 (q, *J* = 288.5 Hz), 79.9, 77.6, 52.8, 40.2, 35.6, 32.1, 31.1, 28.1, 27.7 ppm. ^{19}F NMR (376 MHz, DMSO-d_6) δ=-74.6 ppm.
HRMS (ESI) *m/z* calcd for $C_{27}H_{35}F_3N_3O_7$ [M+H]$^+$: 570.2427; found: 570.2419.

6-[2-(*tert*-butoxycarbonylamino)ethyl]-8-(9H-fluoren-9-ylmethoxycarbonylamino)-4-*iso*pentyl-quinoline-2-carboxylic acid (21a)

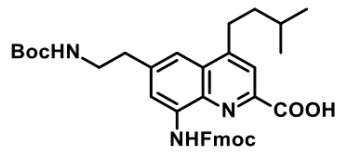

Using **General Procedure B** 730 mg compound **20a** (1.0 equiv., 1.43 mmol), **21a** (625 mg, 70%) was obtained as pale yellow solid.
HPLC-UV purity: 98.3%.
^{1}H NMR (500 MHz, DMSO-d_6) δ=13.58 (br s, 1H), 10.38 (br s, 1H), 8.30 (br s, 1H), 8.03 (s, 1H), 7.94 (d, *J* = 7.5 Hz, 2H), 7.77 (d, *J* = 7.4 Hz, 2H), 7.59/7.55 (s, 1H), 7.44 (t, *J* = 7.4 Hz, 2H), 7.36 (t, *J* = 7.4 Hz, 2H), 6.93/6.56 (t/br s, *J* = 5.5 Hz for triplet signal, 1H), 4.59 (d, *J* = 6.7 Hz, 2H), 4.44 (t, *J* = 6.9 Hz, 1H), 3.24 (q, *J* = 6.5 Hz, 2H), 3.12 (t, *J* = 8.0 Hz, 2H), 2.88 (t, *J* = 6.6 Hz, 2H), 1.68 (hept, *J* = 6.5 Hz, 1H), 1.59 (q, *J* = 8.1 Hz, 2H), 1.32/1.23 (s, 9H), 0.99 ppm (d, *J* = 6.6 Hz, 6H). (Amide rotamers present at room temperature.) ^{13}C{^{1}H} NMR (125 MHz, DMSO-d_6) δ=165.8, 155.5, 153.4, 150.7, 144.8, 143.7, 140.8, 140.7, 136.0, 135.8, 128.2, 127.8, 127.2, 125.1, 120.3, 119.9, 117.2, 116.0, 77.5, 66.4, 46.5, 41.1, 38.5, 36.5, 29.4, 28.2, 27.6, 22.3 ppm.
HRMS (ESI) *m/z* calcd for $C_{37}H_{42}N_3O_6$ [M+H]$^+$: 624.3074; found: 624.3070.

SUPPORTING INFORMATION

6-(3-*tert*-butoxy-3-oxo-propyl)-8-(9*H*-fluoren-9-ylmethoxycarbonylamino)-4-*iso*pentyl-quinoline-2-carboxylic acid (21b)

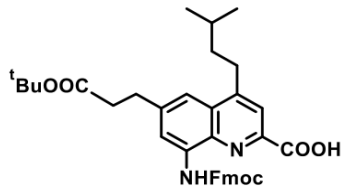

Using **General Procedure B** 800 mg **20b** (1.0 equiv., 1.61 mmol), **21b** (587 mg, 60%) was obtained as pale yellow solid.
HPLC-UV purity: 99.8%.
^{1}H NMR (500 MHz, DMSO-d_6) δ=13.53 (br s, 1H), 10.46 (br s, 1H), 8.29 (br s, 1H), 8.04 (s, 1H), 7.93 (d, *J* = 7.5 Hz, 2H), 7.77 (d, *J* = 7.5 Hz, 2H), 7.63 (s, 1H), 7.44 (t, *J* = 7.4 Hz, 2H), 7.36 (td, *J* = 7.4 Hz, *J* = 1.0 Hz, 2H), 4.61 (d, *J* = 6.6 Hz, 2H), 4.45 (t, *J* = 6.9 Hz, 1H), 3.12 (t, *J* = 8.0 Hz, 2H), 3.01 (t, *J* = 7.1 Hz, 2H), 2.62 (t, *J* = 9.7 Hz, 2H), 1.68 (hept, *J* = 6.6 Hz, 1H), 1.62-1.55 (m, 2H), 1.34 (s, 9H), 0.99 ppm (d, *J* = 6.6 Hz, 6H). ^{13}C{^{1}H} NMR (125 MHz, DMSO-d_6) δ=171.3, 165.6, 153.5, 150.9, 144.4, 143.7, 142.0, 140.8, 136.0, 135.7, 128.2, 127.8, 127.2, 125.1, 120.3, 120.0, 116.9, 115.5, 79.8, 66.4, 46.6, 38.6, 35.8, 31.4, 29.5, 27.7, 27.6, 22.3 ppm.
HRMS (ESI) *m/z* calcd for $C_{37}H_{41}N_2O_6$ [M+H]$^+$: 609.2965; found: 609.2963.

4-(2-*tert*-butoxyethyl)-6-(3-*tert*-butoxy-3-oxo-propyl)-8-(9*H*-fluoren-9-ylmethoxycarbonylamino)quinoline-2-carboxylic acid (21c)

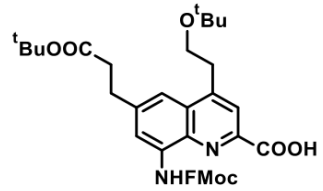

Using **General Procedure B** 1.11 g **20c** (1.0 equiv., 2.11 mmol), **21c** (825 mg, 61%) was obtained as pale yellow solid.
HPLC-UV purity: 99.8%.
^{1}H NMR (500 MHz, DMSO-d_6) δ=13.51 (br s, 1H), 10.46 (br s, 1H), 8.29 (br s, 1H), 8.11 (s, 1H), 7.93 (d, *J* = 7.5 Hz, 2H), 7.78 (d, *J* = 7.5 Hz, 2H), 7.68 (s, 1H), 7.44 (t, *J* = 7.5 Hz, 2H), 7.37 (td, *J* = 7.5 Hz, *J* = 1.0 Hz, 2H), 4.61 (d, *J* = 6.5 Hz, 2H), 4.46 (t, *J* = 6.9 Hz, 1H), 3.70 (t, *J* = 6.5 Hz, 2H), 3.29 (t, *J* = 6.5 Hz, 2H), 3.00 (t, *J* = 7.1 Hz, 2H), 2.62 (t, *J* = 7.7 Hz, 2H), 1.34 (s, 9H), 1.07 ppm (s, 9H). ^{13}C{^{1}H} NMR (125 MHz, DMSO-d_6) δ=171.3, 165.6, 153.5, 148.1, 144.0, 143.7, 142.0, 140.8, 135.9, 135.7, 128.7, 127.8, 127.2, 125.1, 120.9, 120.3, 117.0, 115.9, 79.8, 72.5, 66.4, 60.3, 46.6, 35.9, 32.7, 31.4, 27.7, 27.2 ppm.
HRMS (ESI) *m/z* calcd for $C_{38}H_{43}N_2O_7$ [M+H]$^+$: 639.3070; found: 639.3065.

4-[3-(*tert*-butoxycarbonylamino)propyl]-6-(3-tert-butoxy-3-oxo-propyl)-8-(9H-fluoren-9-ylmethoxycarbonylamino)quinoline-2-carboxylic acid (21d)

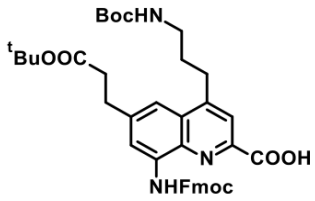

Using **General Procedure B** 942 mg **20d** (1.0 equiv., 1.43 mmol), **21d** (700 mg, 62%) was obtained as pale yellow solid.
HPLC-UV purity: 99.8%.
^{1}H NMR (500 MHz, DMSO-d_6) δ=13.53 (br s, 1H), 10.34 (br s, 1H), 8.26 (br s, 1H), 8.04 (s, 1H), 7.93 (d, *J* = 7.5 Hz, 2H), 7.76 (d, *J* = 7.5 Hz, 2H), 7.63 (s, 1H), 7.44 (t, *J* = 7.4 Hz, 2H), 7.36 (t, *J* = 7.4 Hz, 2H), 6.98 (t, *J* = 5.4 Hz, 1H), 4.60 (d, *J* = 6.6 Hz, 2H), 4.44 (t, *J* = 6.8 Hz, 1H), 3.10 (t, *J* = 7.7 Hz, 2H), 3.03 (q, *J* = 6.4 Hz, 2H), 2.99 (t, *J* = 7.6 Hz, 2H), 2.61 (t, *J* = 7.5 Hz, 2H), 1.80 (quint, *J* = 7.2 Hz, 2H),1.38 (s, 9H), 1.35 ppm (s, 9H). ^{13}C{^{1}H} NMR (125 MHz, DMSO-d_6) δ=171.3, 166.0, 155.7, 153.3, 149.8, 143.7, 141.6, 140.7, 135.9, 135.7, 128.0, 127.8, 127.2, 125.1, 120.5, 120.2, 116.5, 115.5, 79.8, 77.5, 66.4, 46.5, 39.7, 36.0, 31.5, 29.7, 29.0, 28.3, 27.7 ppm.
HRMS (ESI) *m/z* calcd for $C_{40}H_{46}N_3O_8$ [M+H]$^+$: 696.3285; found: 696.3280.

4-[2-(*tert*-butoxycarbonylamino)ethyl]-6-(3-*tert*-butoxy-3-oxo-propyl)-8-(9*H*-fluoren-9-ylmethoxycarbonylamino)quinoline-2-carboxylic acid (21e)

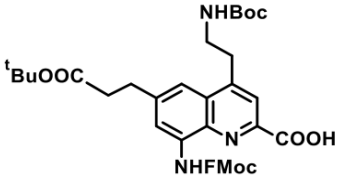

Using **General Procedure B** 780 mg compound **20e** (1.0 equiv., 1.37 mmol), **21e** (760 mg, 81%) was obtained as pale yellow solid.
HPLC-UV purity: 97.9%.
^{1}H NMR (500 MHz, DMSO-d_6) δ=13.50 (br s, 1H), 10.46 (br s, 1H), 8.29 (br s, 1H), 8.02 (s, 1H), 7.93 (d, *J* = 7.5 Hz, 2H), 7.78 (dd, *J* = 7.5 Hz, *J* = 0.5 Hz, 2H), 7.74/7.68 (s/s, 1H), 7.44 (t, *J* = 7.3 Hz, 2H), 7.36 (td, *J* = 7.4 Hz, *J* = 1.0 Hz, 2H), 6.97/6.57 (t/s, *J* = 5.6 Hz for triplet

SUPPORTING INFORMATION

signal, 1H), 4.61 (d, *J* = 6.6 Hz, 2H), 4.46 (t, *J* = 6.9 Hz, 1H), 3.33-3.18 (m, 4H), 3.00 (t, *J* = 7.2 Hz, 2H), 2.65 (t, *J* = 7.6 Hz, 2H), 1.36 (s, 9H), 1.30/1.07 ppm (s/s, 9H). (Amide rotamers present at room temperature.) $^{13}C\{^{1}H\}$ NMR (125 MHz, DMSO-d_6) δ=171.3, 165.5, 155.5, 153.5, 148.0, 144.0, 143.7, 142.1, 140.8, 136.0, 135.8, 128.7, 127.8, 127.2, 125.1, 121.2, 120.3, 116.9, 115.7, 79.8, 77.6, 66.3, 46.6, 40.2, 35.8, 32.3, 31.4, 28.1, 27.7 ppm.
HRMS (ESI) *m/z* calcd for $C_{39}H_{44}N_3O_8$ $[M+H]^+$: 682.3128; found: 682.3126.

Methyl 4,6-bis(2-*tert*-butoxyethyl)-8-[(2,2,2-trifluoroacetyl)amino]quinoline-2-carboxylate (22b)

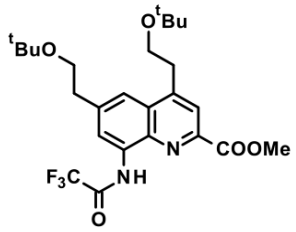

Preparation of alkylboron-reagent:
An oven-dried, 50 mL pear-shaped flask was closed with a rubber septum, evacuated and charged with dry N_2. Through the septum 1.37 mL **2-methyl-2-vinyloxy-propane** (2.00 equiv., 10.5 mmol), and 20.9 mL 0.50 M solution of 9-borabicyclo[3.3.1]nonane in THF (2.00 equiv., 10.5 mmol) were added at RT, then the resulting mixture was stirred for 30 min. This solution was used in the next step.
Suzuki-coupling:
A 100 mL pear-shaped flask was filled with 2.15 g compound **methyl 6-bromo-4-chloro-8-[(2,2,2-trifluoroacetyl)amino]quinoline-2-carboxylate (18)** (1.0 equiv., 5.22 mmol, prepared according to [2]), 116 mg $Pd(AtaPhos)_2Cl_2$ (5.00 mol%, 0.26 mmol) and 3.02 g Cs_2CO_3 (3.00 equiv., 15.7 mmol), closed with a rubber septum, evacuated and charged with dry N_2. Through the septum 5.22 mL water and the *alkylboron-reagent* were added. The mixture was heated to 40°C by a heating block and stirred for 30 min. After cooling to RT, 50 mL DCM and 25 mL water were added, the organic phase was separated. The aqueous phase was extracted with 2x20 mL DCM, the combined organic phase was dried over Na_2SO_4, filtered and the filtrate was concentrated *in vacuo*. The residue was purified by flash chromatography (120 g column, heptane/EtOAc, gradient elution: 0-35%) to afford **22b** as a yellow solid (643 mg, 25%).
^{1}H NMR (500 MHz, DMSO-d_6) δ=10.95 (s, 1H), 8.40 (d, *J* = 1.6 Hz, 1H), 8.12 (s, 1H), 7.96 (d, *J* = 1.5 Hz, 1H), 3.96 (s, 3H), 3.70 (t, *J* = 6.4 Hz, 2H), 3.65 (t, *J* = 6.5 Hz, 2H), 3.32 (t, *J* = 6.4 Hz, 2H), 3.00 (t, *J* = 6.5 Hz, 2H), 1.11 (s, 9H), 1.04 ppm (s,9H). $^{13}C\{^{1}H\}$ NMR (125 MHz, DMSO-d_6) δ=164.8, 154.2 (q, *J* = 36.7 Hz), 148.4, 145.0, 140.8, 137.2, 132.1, 128.4, 122.1, 121.6, 120.5, 115.7 (q, *J* = 287.1 Hz), 72.5, 72.4, 61.4, 60.5, 52.8, 37.0, 32.6, 27.3, 27.2 ppm. ^{19}F NMR (376 MHz, DMSO-d_6) δ=-74.6 ppm.
HRMS (ESI) *m/z* calcd for $C_{25}H_{34}F_3N_2O_5$ $[M+H]^+$: 499.2420; found: 499.2410.

Methyl 4,6-bis[3-(tert-butoxycarbonylamino)prop-1-ynyl]-8-nitro-quinoline-2-carboxylate (24a)

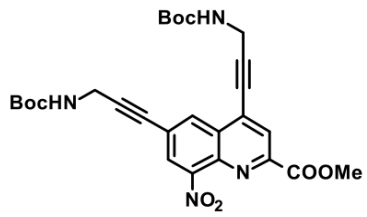

415 mg **methyl 4,6-dibromo-8-nitro-quinoline-2-carboxylate (23)** (prepared according to [3], 1.0 equiv., 1.00 mmol), 466 mg ***tert*-butyl *N*-prop-2-ynylcarbamate** (3.0 equiv., 3.00 mmol), 39 mg copper(I)-iodide (0.2 equiv., 0.20 mmol) were measured into a 50 mL flask. The flask was evacuated then back-filled with N_2 (repeated 3x), then 7.5 mL 1,4-dioxane (dry, degassed) and 2.00 mL *N-iso*propylpropan-2-amine (14.3 equiv., 14.3 mmol) were added at rt while stirring. The reaction mixture was heated to 80°C by a heating block and 35.4 mg dichloropalladium, 4-di*tert*-butylphosphanyl-*N*,*N*-dimethyl-aniline (1:2) (0.05 equiv., 0.05 mmol) was added at this temperature. After 10 min, full conversion was observed and 25 mL DCM was added, the resulting solution was washed with 2x10 mL 5% aq. citric acid solution and 15 mL sat. aq. $NaHCO_3$ solution. Combined aqueous phase was extracted with 2x10 mL DCM. Combined organic phase dried over Na_2SO_4, was filtered and the filtrate was concentrated *in vacuo*. The crude product was purified by normal phase flash chromatography (40 g silicagel column, heptane/DCM, gradient elution: 0-80%) to afford **24a** as an off-white solid (323 mg, 90%).
^{1}H NMR (500 MHz, $CDCl_3$): δ = 8.40 (s, 1H), 8.27 (s, 1H), 8.03 (s, 1H), 5.18 (b s, 1H), 5.04 (b s, 1H), 4.34 (d, *J* = 4.9 Hz, 2H), 4.23 (d, *J* = 4.9 Hz, 2H)) 4.02 (s, 3H), 1.49 (s, 9H), 1.47 (s, 9H). $^{13}C\{^{1}H\}$ NMR

SUPPORTING INFORMATION

(125 MHz, $CDCl_3$): δ = 164.9, 155.6, 149.8, 148.7, 138.7, 132.7, 131.2, 129.4, 127.8, 126.0, 123.1, 99.4, 91.5, 80.7, 77.4, 53.7, 31.6, 31.3, 28.6.
HRMS (ESI): *m/z* $[M+H]^+$ for $C_{27}H_{30}N_4O_8$: 539.2136; found: 539.2137.

Methyl 8-amino-4,6-dibromo-quinoline-2-carboxylate (25)

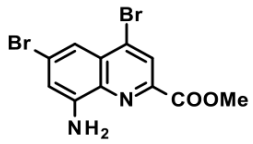

A 2 L pear-shaped flask was filled with 6.74 g Raney nickel (3.14 equiv., 78.7 mmol) under N_2 atmosphere, then washed with 3x20 mL water and 2x20 mL MeOH. 9.77 g compound **methyl 4,6-dibromo-8-nitro-quinoline-2-carboxylate (23)** (prepared according to [3],1.0 equiv., 25.1 mmol) and 1.12 L MeOH were added and the atmosphere was changed to H_2 (1 bar). The reaction mixture was stirred at RT for 18 h and then filtered through a short pad of celite. The filtrate was concentrated *in vacuo* and the obtained residue was purified by flash chromatography (330 g silicagel column, DCM/MeOH, gradient elution: 0-5%) to afford **25** as a yellow solid (6.41 g, 71%).
^1H NMR (500 MHz, DMSO-d_6) δ=8.33 (s, 1H), 7.30 (d, *J* = 2.1 Hz, 1H), 7.11 (d, *J* = 2.1 Hz, 1H), 6.61 (s, 2H), 3.94 ppm (s, 3H). $^{13}C\{^1H\}$ NMR (125 MHz, DMSO-d_6) δ=163.9, 148.5, 143.6, 135.3, 132.3, 130.0, 126.0, 125.8, 112.6, 112.3, 52.8 ppm.
HRMS (ESI) *m/z* calcd for $C_{11}H_9Br_2N_2O_2$ $[M+H]^+$: 358.9031; found: 358.9017.

Methyl 8-amino-4,6-bis[(*E*)-3-*tert*-butoxy-3-oxo-prop-1-enyl]quinoline-2-carboxylate (26)

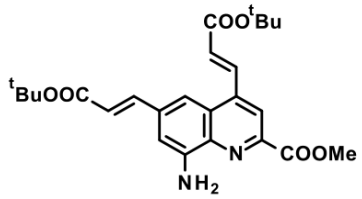

A 25 mL pear-shaped flask was filled with 1.41 g compound **25** (1.0 equiv., 3.92 mmol), 22.0 mg $Pd(OAc)_2$ (2.5 mol%, 0.10 mmol) and 119 mg tris-*o*-tolylphosphane (10.0 mol%, 0.39 mmol), closed with a rubber septum, evacuated and charged with dry N_2. Through the septum 3.92 mL DMF (1 mL/mmol), 3.92 mL DIPEA (1 mL/mmol) and 1.72 mL ***tert*-butyl acrylate** (3.0 equiv., 11.8 mmol) were added. The mixture was heated to 100°C by a heating block and stirred for 1 h. After cooling to RT, 20 mL EtOAc and 20 mL water were added, the organic phase was separated. The organic phase was washed with 20 mL water and 20 mL brine then it was dried over Na_2SO_4, filtered and the filtrate was concentrated in vacuo. The residue was purified by flash chromatography (80 g silicagel column, heptane/EtOAc, gradient elution: 0-60%) to afford compound **26** as an orange solid (1.32 g, 74%).
^1H NMR (500 MHz, DMSO-d_6) δ=8.28 (d, *J* = 15.7 Hz, 1H), 8.27 (s, 1H), 7.69 (d, *J* = 15.9 Hz, 1H), 7.65 (d, *J* = 1.2 Hz, 1H), 7.24 (d, *J* = 1.4 Hz, 1H), 6.81 (d, *J* = 15.8 Hz, 1H), 6.54 (d, *J* = 15.9 Hz, 1H), 6.21 (s, 2H), 3.96 (s, 3H), 1.53 (s, 9H), 1.51 ppm (s, 9H). $^{13}C\{^1H\}$ NMR (125 MHz, DMSO-d_6) δ=165.3, 164.9, 164.7, 146.8, 144.3, 143.8, 140.9, 138.1, 137.6, 136.0, 127.5, 127.0, 121.5, 118.8, 111.3, 106.2, 80.7, 80.2, 52.7, 27.8, 27.8 ppm.
HRMS (ESI) *m/z* calcd for $C_{25}H_{31}N_2O_6$ $[M+H]^+$: 455.2182; found: 455.2181.

Methyl 8-amino-4,6-bis[3-(tert-butoxycarbonylamino)propyl]quinoline-2-carboxylate (27a)

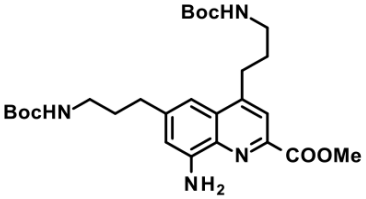

Using **General Procedure A** 90 mg compound **24a** (1.0 equiv., 0.465 mmol), **27a** was obtained as a pale yellow solid (112 mg, 50%).
^1H NMR (500 MHz, DMSO-d_6): δ = 7.88 (s, 1H), 7.05 (s, 1H), 6.97 (t, *J* = 5.5 Hz, 1H), 6.89 (t, *J* = 5.5 Hz, 1H), 6.79 (d, *J* = 1.4 Hz, 1H), 6.03 (b s, 2H), 3.92 (s, 3H), 3.09-2.89 (m, 6H), 2.63 (t, *J* = 7.4 Hz, 2H), 1.83-1.68 (m, 4H), 1.381 (s, 9H), 1.378 (s, 9H).$^{13}C\{^1H\}$ NMR (125 MHz, DMSO-d_6): δ = 165.6, 155.7, 155.6, 148.3, 146.5, 144.1, 142.6, 135.6, 128.8, 120.3, 109.9, 108.5, 77.5, 77.4, 52.4, 33.6, 31.1, 29.5, 29.0, 28.3.
HRMS (ESI): *m/z* $[M+H]^+$ for $C_{27}H_{30}N_4O_8$: 517.3021; found: 517.3022.

SUPPORTING INFORMATION

Methyl 8-amino-4,6-bis(3-*tert*-butoxy-3-oxo-propyl)quinoline-2-carboxylate (27c)

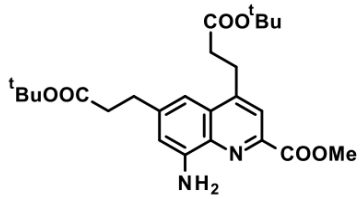

Using **General Procedure A** 1.300 g compound **26** (1.0 equiv., 2.85 mmol), **27c** was obtained as a yellow solid (1.270 g, 97%).
^{1}H NMR (400 MHz, DMSO-d$_6$) δ=7.87 (s, 1H), 7.06 (d, *J* = 1.4 Hz, 1H), 6.81 (d, *J* = 1.6 Hz, 1H), 6.06 (s, 2H), 3.92 (s, 3H), 3.25 (t, *J* = 7.2 Hz, 2H), 2.90 (t, *J* = 7.4 Hz, 2H), 2.67 (t, *J* = 7.2 Hz, 2H), 2.60 (t, *J* = 7.5 Hz, 2H),1.36 (s, 9H), 1.36 ppm (s, 9H). ^{13}C{^{1}H} NMR (125 MHz, DMSO-d$_6$) δ=171.5, 171.2, 165.4, 146.8, 146.5, 143.1, 142.6, 135.5, 128.6, 120.1, 109.9, 108.0, 80.0, 79.7, 52.4, 36.0, 34.1, 31.4, 27.7, 27.6, 26.9 ppm.
HRMS (ESI) *m/z* calcd for $C_{25}H_{35}N_2O_6$ [M+H]$^+$: 459.2495; found: 459.2502.

4,6-bis[3-(tert-butoxycarbonylamino)propyl]-8-(9H-fluoren-9-ylmethoxycarbonylamino)quinoline-2-carboxylic acid (28a)

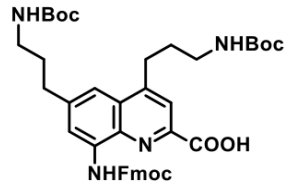

Using **General Procedure B** 160 mg compound **27a** (1.0 equiv., 0.167 mmol), **28a** was obtained as a pale yellow solid (59 mg, 68%).
HPLC-UV purity: 98.2%.
^{1}H NMR (500 MHz, DMSO-*d*$_6$): δ = 10.22 (s, 1H), 8.24 (s, 1H), 8.02 (s, 1H), 7.92 (d, *J* = 7.5 Hz, 1H), 7.74 (d, *J* = 7.5 Hz, 1H), 7.60 (s, 1H), 7.43 (t, *J* = 7.5 Hz, 2H), 7.35 (dt, *J* = 1.0, 7.4 Hz, 2H), 6.97 (t, *J* = 5.1 Hz, 1H), 6.92 (t, *J* = 5.1 Hz, 1H), 4.57 (d, *J* = 6.8 Hz, 2H), 4.41 (t, *J* = 6.8 Hz, 1H), 3.13-2.92 (m, 6H), 2.74 (t, *J* = 7.3 Hz, 2H), 1.86-1.70 (m, 4H), 1.38 (s, 9H), 1.37 (s, 9H).^{13}C{^{1}H} NMR (125 MHz, DMSO-*d*$_6$): δ = 166.3, 155.7, 155.6, 153.3, 149.4, 143.7, 142.5, 140.8, 135.8, 135.6, 127.9, 127.8, 127.24, 127.15, 126.8, 125.2, 125.1, 120.6, 120.3, 119.9, 116.4, 115.6, 77.50, 77.46, 66.4, 46.6, 33.6, 31.2, 29.7, 29.0, 28.3.
HRMS (ESI): *m/z* [M+H]$^+$ for $C_{41}H_{48}N_4O_8$: 725.3545; found: 726.3546.

8-(9H-fluoren-9-ylmethoxycarbonylamino)-4,6-bis(3-methoxypropyl)quinoline-2-carboxylic acid (28b)

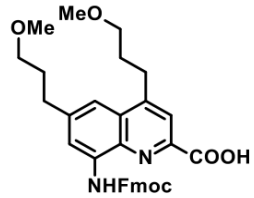

Using **General Procedure B** 188 mg compound **methyl 8-amino-4,6-bis(3-methoxypropyl)quinoline-2-carboxylate (27b)** (prepared according to [3], 1.0 equiv., 0.543 mmol), **28b** was obtained as a pale yellow solid (97 mg, 30%).
HPLC-UV purity: 93.1%
^{1}H NMR (500 MHz, DMSO-*d*$_6$): δ = 13.53 (b s, 1H), 10.45 (s, 1H), 8.31 (b s, 1H), 8.04 (s, 1H), 7.93 (d, *J* = 7.5 Hz, 1H), 7.78 (dd, *J* = 0.6, 7.3 Hz, 1H), 7.63 (d, *J* = 0.7 Hz, 1H), 7.43 (t, *J* = 7.5 Hz, 2H), 7.36 (dt, *J* = 1.2, 7.5 Hz, 2H), 4.60 (d, *J* = 6.7 Hz, 2H), 4.45 (t, *J* = 6.8 Hz, 1H), 3.39 (t, *J* = 6.3 Hz, 2H), 3.36 (t, *J* = 6.3 Hz, 2H), 3.26 (s, 3H), 3.25 (s, 3H), 3.20-3.14 (m, 2H), 2.81 (t, *J* = 7.0 Hz, 2H), 1.97-1.83 (m, 4H).^{13}C{^{1}H} NMR (125 MHz, DMSO-*d*$_6$): δ = 165.7, 153.5, 143.7, 140.8, 136.1, 135.7, 128.4, 127.8, 127.2, 125.2, 120.3, 117.0, 115.6, 71.0, 70.9, 66.4, 57.9, 46.6, 32.8, 30.7, 29.4, 28.3.
HRMS (ESI): *m/z* [M+H]$^+$ for $C_{33}H_{34}N_2O_6$: 555.2490; found: 555.2495.

4,6-bis(3-*tert*-butoxy-3-oxo-propyl)-8-(9*H*-fluoren-9-ylmethoxycarbonylamino)quinoline-2-carboxylic acid (28c)

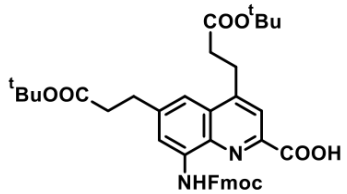

Using **General Procedure B** 1.240 g compound **27c** (1.0 equiv., 2.70 mmol), **28c** (1.300 g, 72%) was obtained as pale yellow solid.
HPLC-UV purity: 99.9%.
^{1}H NMR (500 MHz, DMSO-d$_6$) δ=13.53 (br s, 1H), 10.30 (br s, 1H), 8.25 (br s, 1H), 8.02 (s, 1H), 7.93 (d, *J* = 7.5 Hz, 2H), 7.76 (d, *J* = 7.7 Hz, 2H), 7.63 (s, 1H), 7.43 (t, *J* = 7.3 Hz, 2H), 7.36 (td, *J* = 7.4 Hz, *J* = 1.1 Hz, 2H), 4.60 (d, *J* = 6.2 Hz, 2H), 4.44 (t, *J* = 6.9 Hz, 1H), 3.34 (t, *J* = 7.0 Hz, 2H), 3.00 (t, *J* = 7.0 Hz, 2H), 2.70 (t, *J* = 7.2 Hz,

2H), 2.62 (t, *J* = 7.2 Hz, 2H), 1.36 (s, 9H), 1.35 ppm (s, 9H). $^{13}C\{^1H\}$ NMR (100 MHz, DMSO-d_6) δ=171.3, 171.1, 166.1, 153.3, 148.1, 146.3, 143.7, 141.8, 140.7, 135.9, 135.6, 127.8, 127.7, 127.2, 125.1, 120.3, 120.2, 116.5, 115.3, 80.0, 79.8, 66.4, 46.5, 35.9, 34.2, 31.4, 27.7, 27.6, 26.9 ppm.
HRMS (ESI) *m/z* calcd for $C_{39}H_{43}N_2O_8$ $[M+H]^+$: 667.3019; found: 667.3003.

4,6-bis(2-*tert*-butoxyethyl)-8-(9*H*-fluoren-9-ylmethoxycarbonylamino)quinoline-2-carboxylic acid (28d)

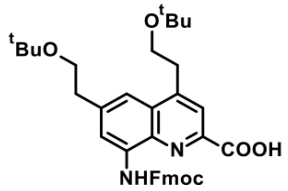

Using **General Procedure B** 624 mg **22b** (1.0 equiv., 1.25 mmol), **4,6-bis(2-*tert*-butoxyethyl)-8-(9*H*-fluoren-9-ylmethoxycarbonylamino)-quinoline-2-carboxylic acid (28d)** (380 mg, 50%) was obtained as pale yellow solid.
HPLC-UV purity: 99.9%.
^1H NMR (500 MHz, DMSO-d_6) δ=13.51 (br s, 1H), 10.45 (br s, 1H), 8.35 (br s, 1H), 8.11 (s, 1H), 7.93 (d, *J* = 7.5 Hz, 2H), 7.78 (d, *J* = 7.5 Hz, 2H), 7.71 (s, 1H), 7.44 (t, *J* = 7.4 Hz, 2H), 7.36 (td, *J* = 7.4 Hz, *J* = 1.2 Hz, 2H), 4.60 (d, *J* = 6.9 Hz, 2H), 4.45 (t, *J* = 7.0 Hz, 1H), 3.69 (t, *J* = 6.5 Hz, 2H), 3.60 (t, *J* = 6.6 Hz, 2H), 3.30 (t, *J* = 6.4 Hz, 2H), 2.92 (t, *J* = 6.5 Hz, 2H), 1.09 (s, 9H), 1.06 ppm (s, 9H). $^{13}C\{^1H\}$ NMR (100 MHz, DMSO-d_6) δ=165.6, 153.5, 148.0, 143.9, 143.7, 141.1, 140.8, 135.7, 135.6, 128.6, 127.8, 127.2, 125.1, 120.9, 120.3, 117.5, 116.6, 72.5, 72.3, 66.3, 61.6, 60.4, 46.6, 37.5, 32.8, 27.3, 27.2 ppm.
HRMS (ESI) *m/z* calcd for $C_{37}H_{43}N_2O_6$ $[M+H]^+$: 611.3121; found: 611.3098.

Oligomer 29

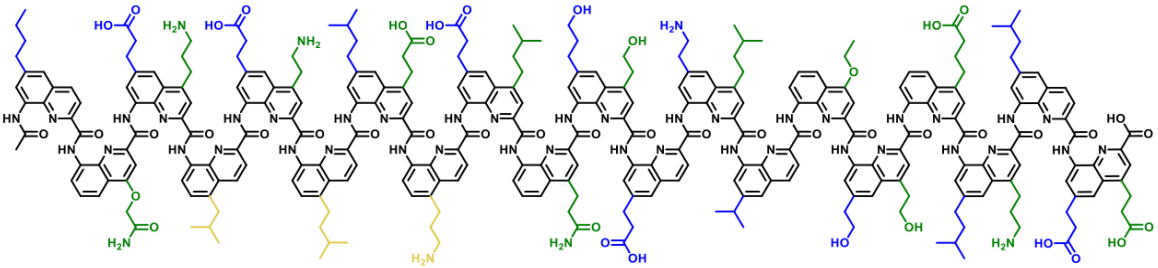

Oligomer **29** was synthesized on TG-R Wang resin (0.19mmol.g^{-1}, 15µmol scale) according to the standard method [4]. Loading of the first monomer: **28c** 0.16mmol.g^{-1} (85%). Unreacted amines were capped using Ac_2O/DCM (1:1) for 2h at room temperature. The final acetyl group was added using the general acetylation method [5]. After purification by semi-preparative HPLC (C8, 20-80B, 50°C, A: H_2O+0.1%TFA, B: MeCN+0.1%TFA), the title compound was obtained as a yellow powder (8.1 mg, 1.54µmol, 10.3%; HPLC purity >95%).
^1H NMR (500 MHz, *d*$_7$-DMF): δ = 12.58 (s, 14H), 11.77 (s, 2H), 11.08 (s, 1H), 11.01 (s, 1H), 10.81 (s, 1H), 10.56 (s, 2H), 10.45 (s, 1H), 10.33 (s, 2H), 10.21 (s, 1H), 10.04 (d, *J* = 15.8 Hz, 2H), 9.95 (d, *J* = 7.1 Hz, 5H), 9.84 (s, 1H), 9.65 (s, 1H), 9.41 (s, 1H), 8.57 (s, 8H), 8.42 (s, 11H), 8.36 (s, 1H), 8.27 (s, 5H), 7.93 (d, *J* = 3.4 Hz, 2H), 7.87 (d, *J* = 8.7 Hz, 2H), 7.81 (d, *J* = 8.3 Hz, 1H), 7.79 – 7.69 (m, 5H), 7.61 (t, *J* = 6.7 Hz, 5H), 7.48 (d, *J* = 7.9 Hz, 3H), 7.46 – 7.39 (m, 4H), 7.38 (s, 1H), 7.37 – 7.31 (m, 3H), 7.30 (d, *J* = 6.9 Hz, 3H), 7.26 (s, 1H), 7.23 (s, 1H), 7.15 (d, *J* = 5.0 Hz, 2H), 7.12 (t, *J* = 3.7 Hz, 2H), 7.08 (s, 1H), 7.06 (s, 1H), 7.04 (s, 1H), 6.98 (t, *J* = 7.4 Hz, 4H), 6.93 (s, 1H), 6.91 (s, 3H), 6.90 – 6.88 (m, 1H), 6.87 (d, *J* = 2.6 Hz, 1H), 6.85 (d, *J* = 4.9 Hz, 4H), 6.82 (s, 2H), 6.80 (d, *J* = 4.7 Hz, 2H), 6.77 (s, 1H), 6.75 (t, *J* = 3.7 Hz, 2H), 6.62 (d, *J* = 7.3 Hz, 1H), 6.51 (s, 1H), 6.49 (s, 1H), 6.46 (s, 1H), 6.45 (s, 1H), 6.40 (t, *J* = 3.8 Hz, 3H), 6.34 (d, *J* = 8.0 Hz, 1H), 6.31 (s, 1H), 6.26 (s, 1H), 6.22 (s, 1H), 6.19 (d, *J* = 8.1 Hz, 1H), 6.16 (d, *J* = 6.0 Hz, 2H), 6.04 (d, *J* = 8.1 Hz, 1H), 5.97 (s, 1H), 5.73 (s, 1H), 4.93 (d, *J* = 3.5 Hz, 2H), 4.84 (s, 1H), 4.45 (s, 1H), 4.39 (s, 1H), 4.09 (s, 3H), 3.86 (s, 2H), 3.74 (s, 2H), 3.31 (s, 5H), 3.25 (s, 6H), 3.12 (s, 4H), 2.99 (s, 1H), 2.67 – 2.49 (m, 36H), 2.45 – 2.34 (m, 3H), 2.15 (t, *J* = 7.4 Hz, 1H), 2.12 – 1.96 (m, 2H), 1.89 – 1.67 (m, 5H), 1.54 (dt, *J* = 21.5, 6.7 Hz, 4H), 1.44 (s, 1H), 1.36 (t, *J* = 8.2 Hz, 5H), 1.32 (d, *J* = 3.9 Hz, 1H), 1.28 (d, *J* = 6.5 Hz, 13H), 1.21 – 1.11 (m, 41H), 1.11 – 1.03 (m, 19H), 0.88 (t, *J* = 6.8 Hz, 2H), 0.79 (t, *J* = 7.5 Hz, 4H).
HRMS (ESI) *m/z* calcd for $C_{297}H_{301}N_{47}O_{46}$ $[M+3H]^{3+}$: 1755.7656; found: 1755.8044.

SUPPORTING INFORMATION

3.3 NMR data of newly synthesized compounds

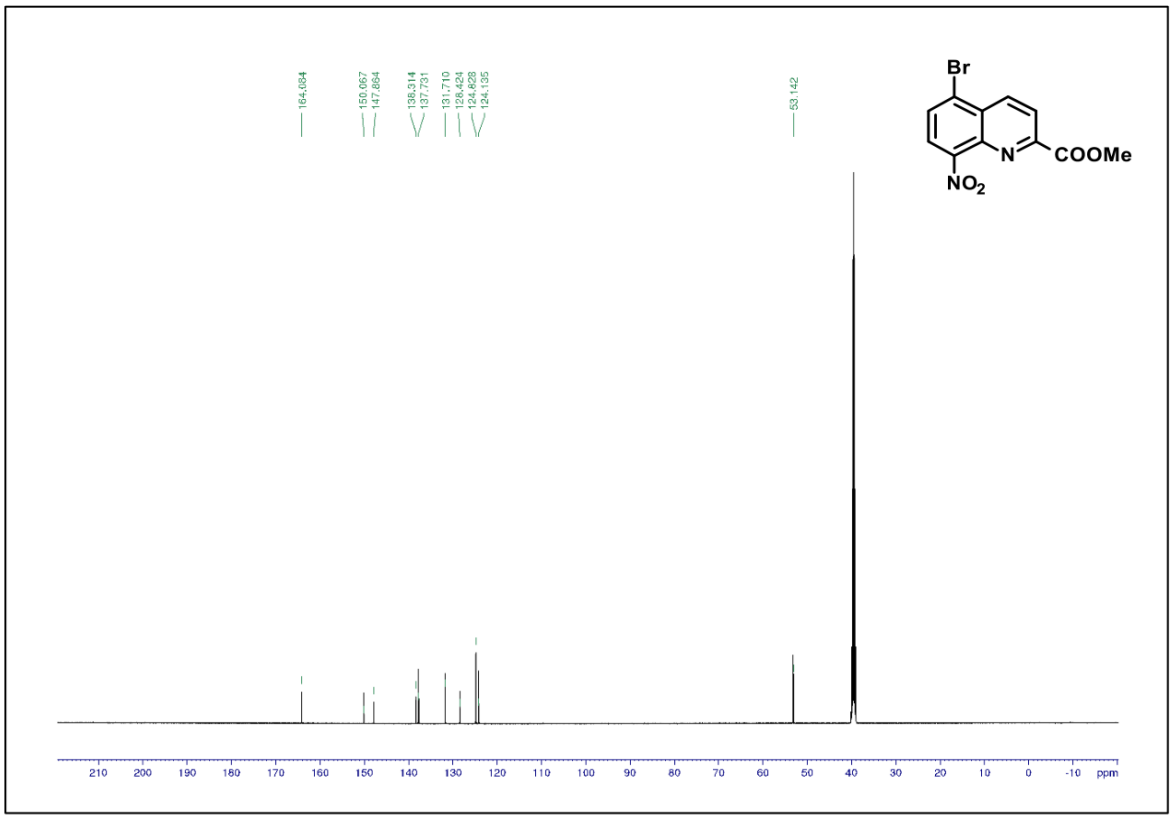

Figure S1. ^{1}H NMR (500 MHz, DMSO-d_6) of compound **2**.

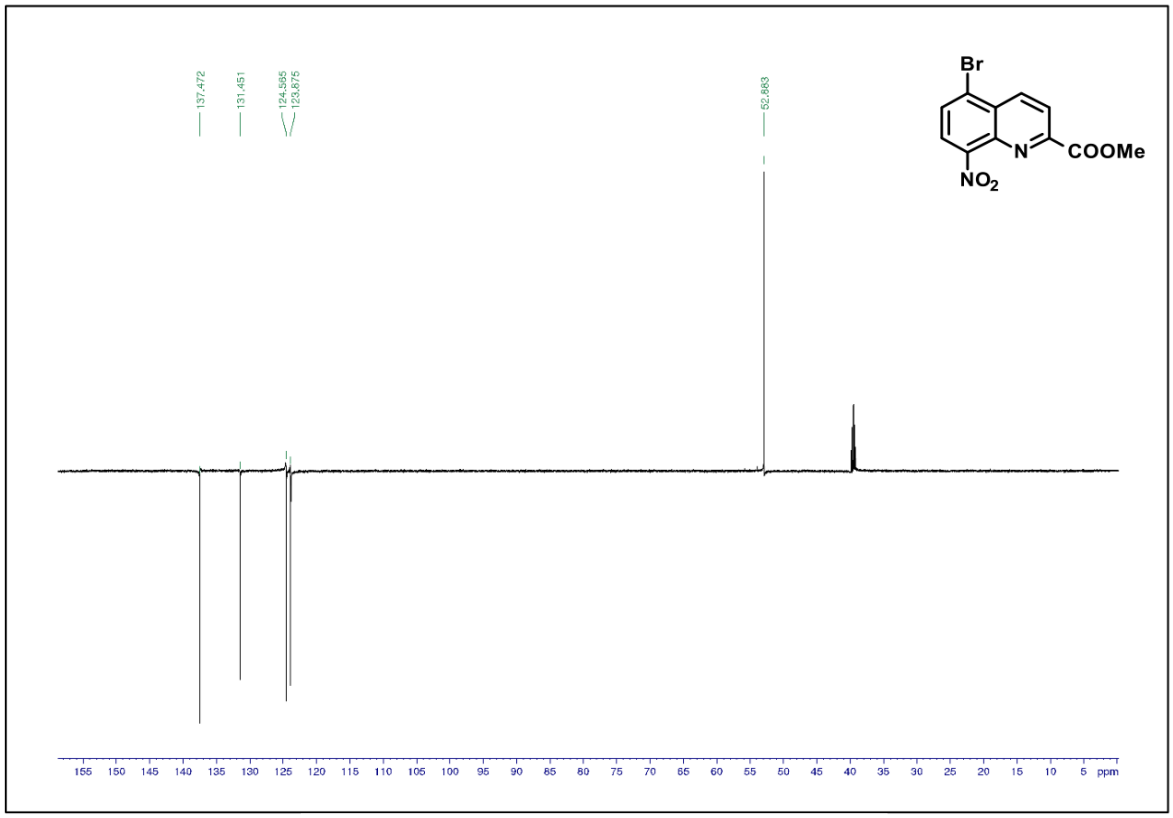

Figure S2. DEPT ^{13}C NMR (125 MHz, DMSO-d_6) of compound **2**.

SUPPORTING INFORMATION

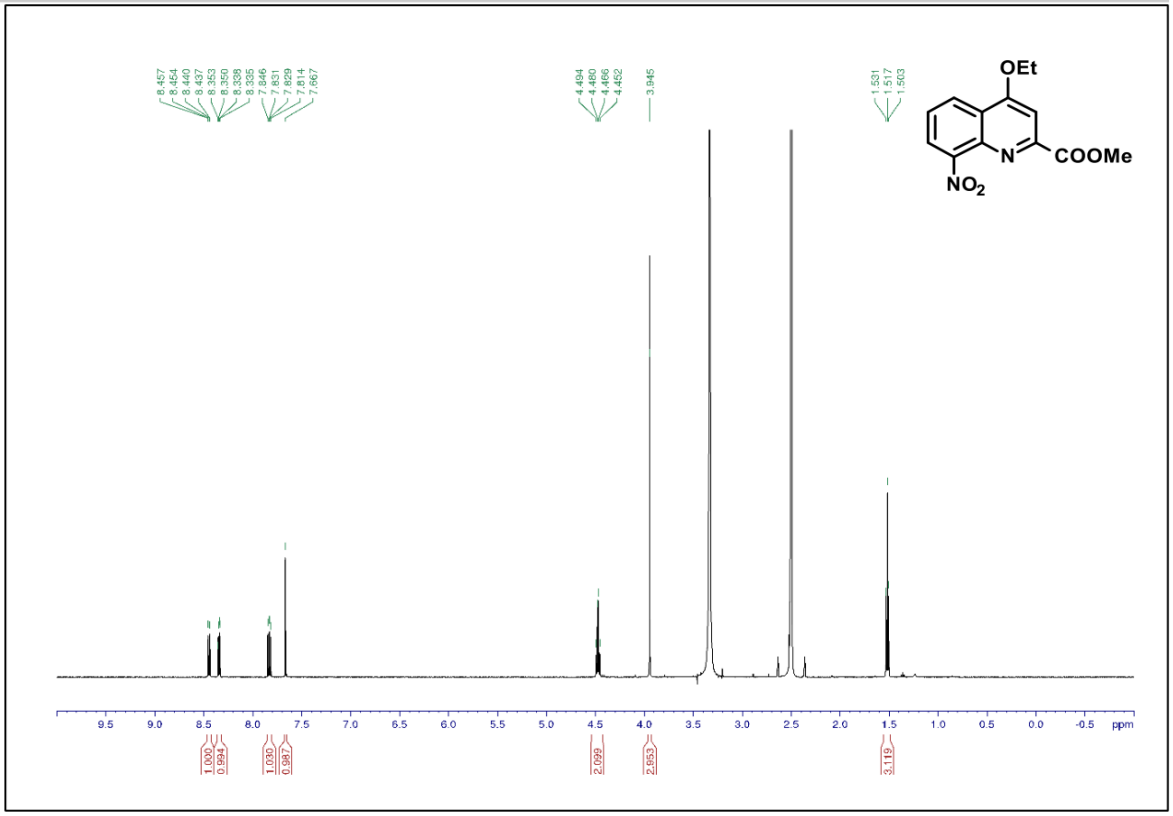

Figure S3. ^{1}H NMR (500 MHz, DMSO-d_6) of compound **5a**.

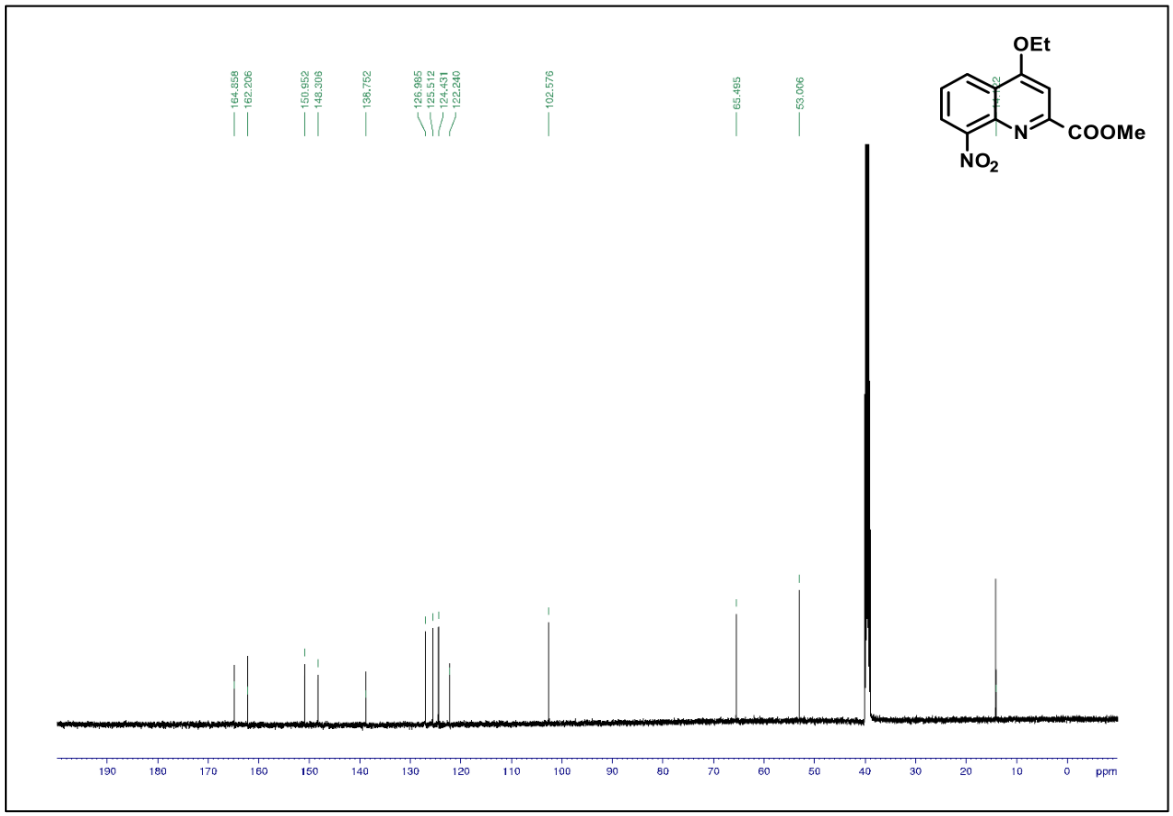

Figure S4. DEPT ^{13}C NMR (125 MHz, DMSO-d_6) of compound **5a**.

SUPPORTING INFORMATION

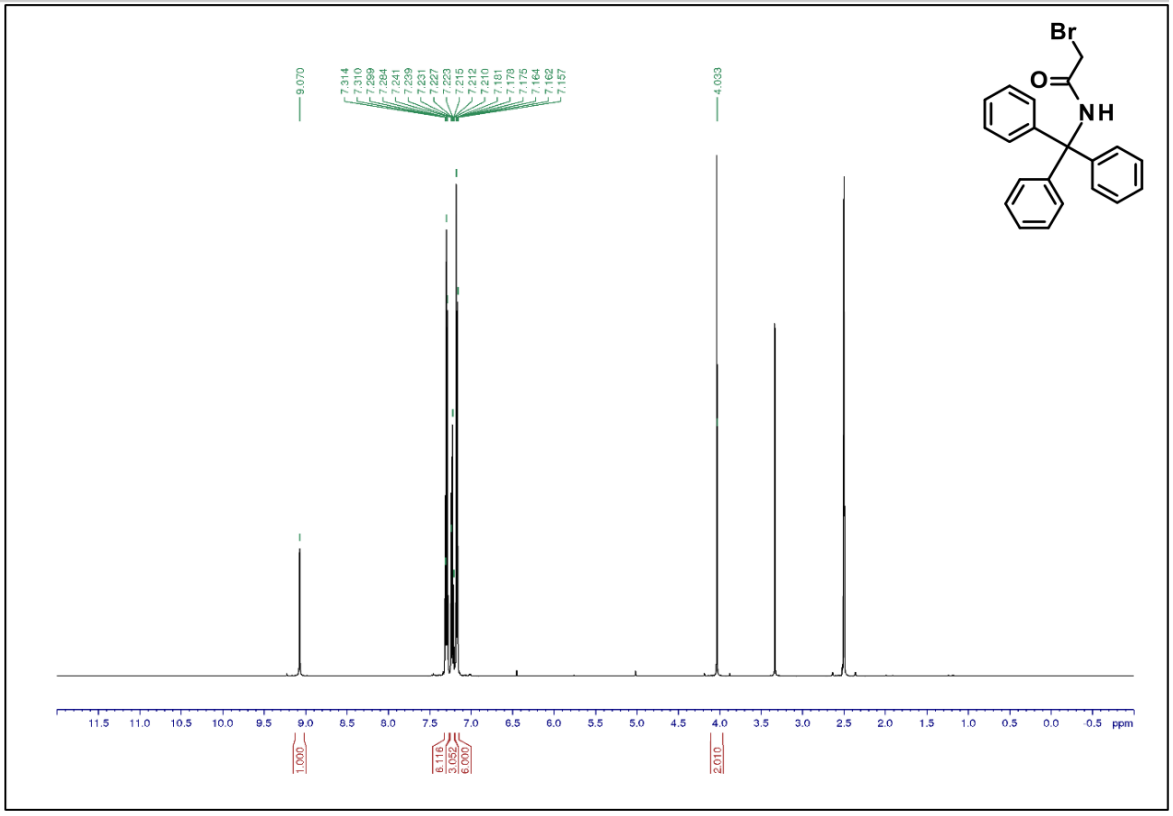

Figure S5. ^{1}H NMR (500 MHz, DMSO-d_6) of compound **S1**.

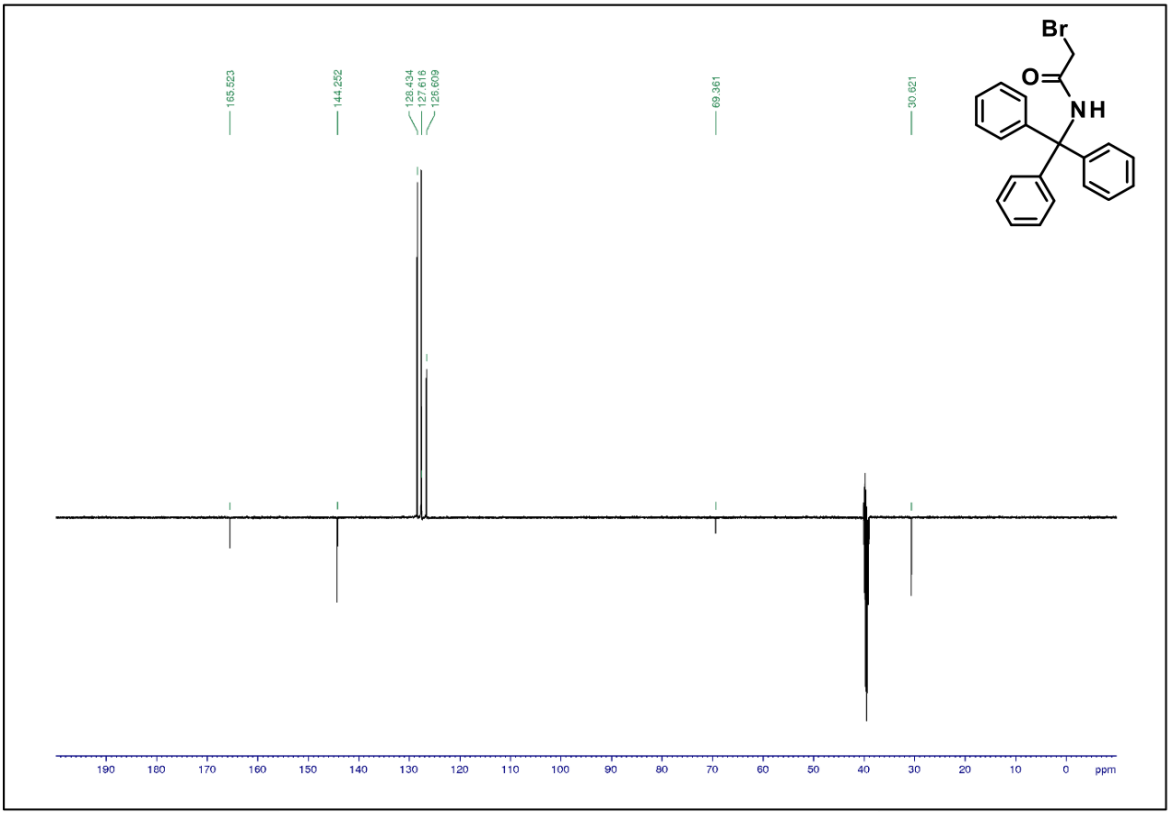

Figure S6. DEPT ^{13}C NMR (125 MHz, DMSO-d_6) of compound **S1**.

SUPPORTING INFORMATION

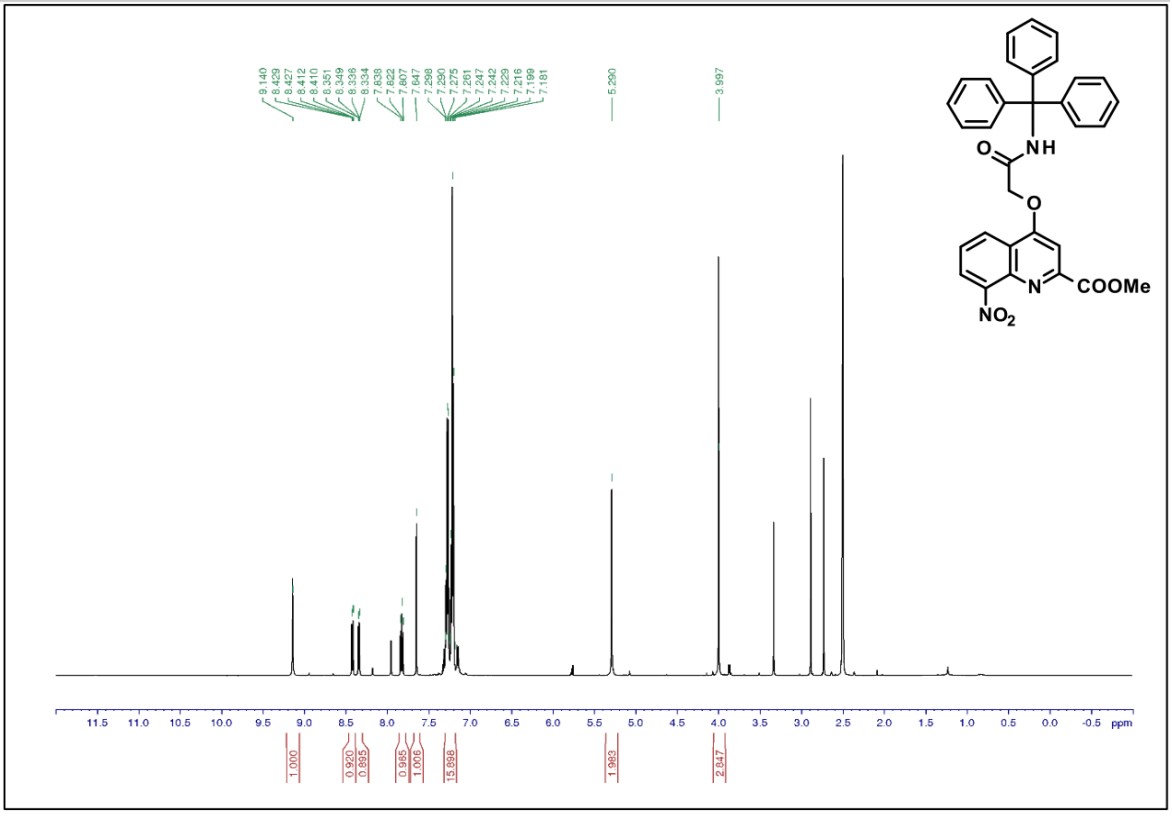

Figure S7. ^{1}H NMR (500 MHz, DMSO-d_6) of compound **5b**.

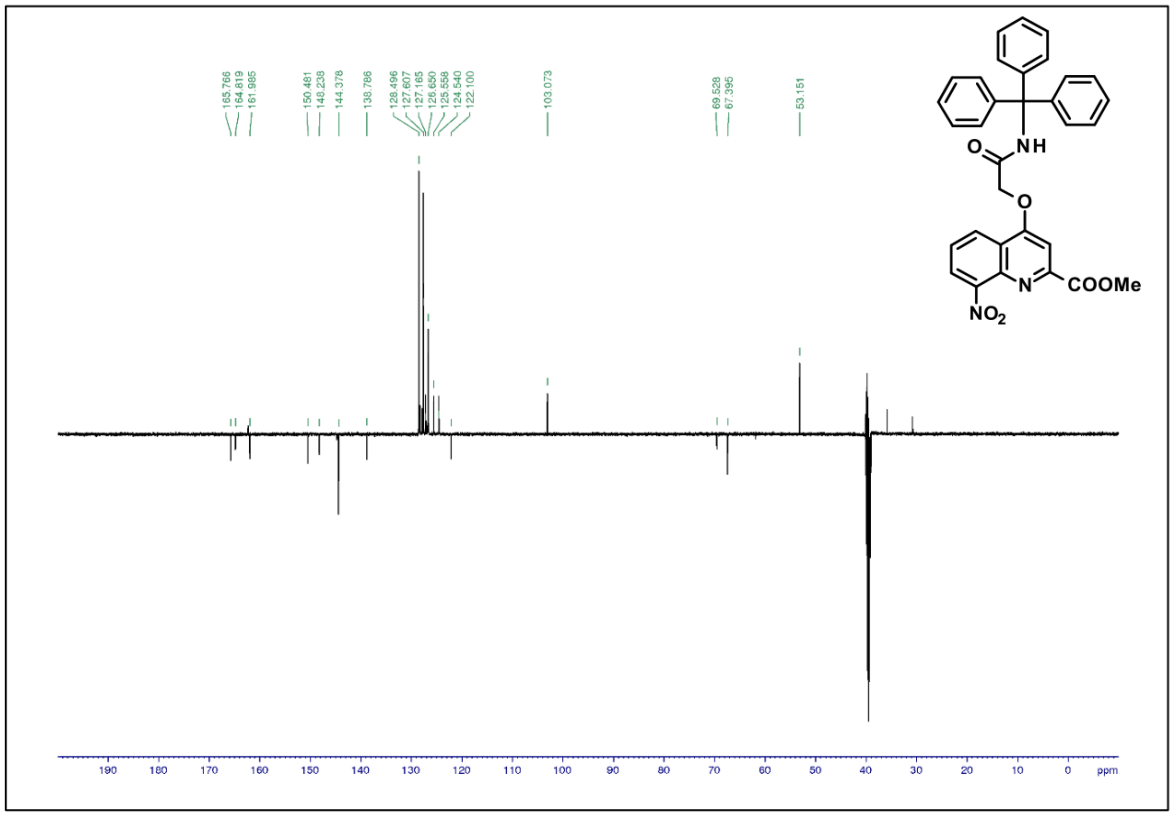

Figure S8. DEPT ^{13}C NMR (125 MHz, DMSO-d_6) of compound **5b**.

SUPPORTING INFORMATION

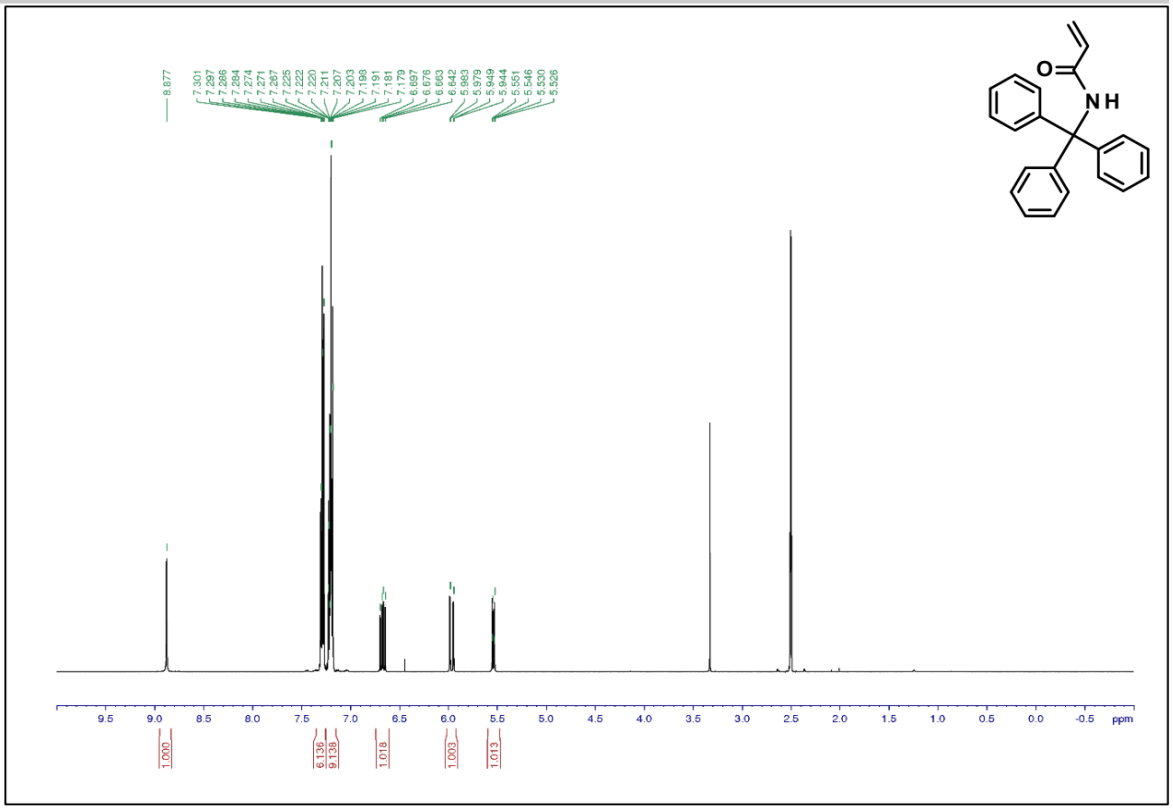

Figure S9. ^{1}H NMR (500 MHz, DMSO-d_6) of compound **S2**.

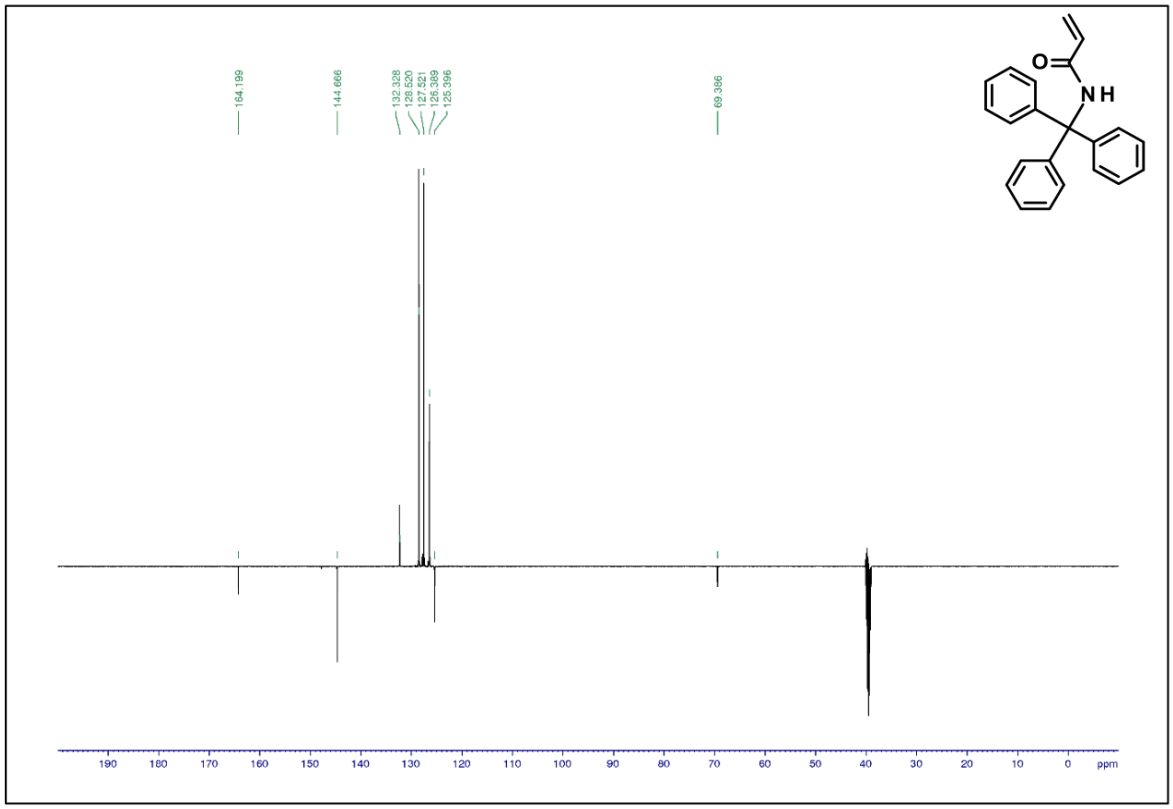

Figure S10. DEPT ^{13}C NMR (125 MHz, DMSO-d_6) of compound **S2**.

SUPPORTING INFORMATION

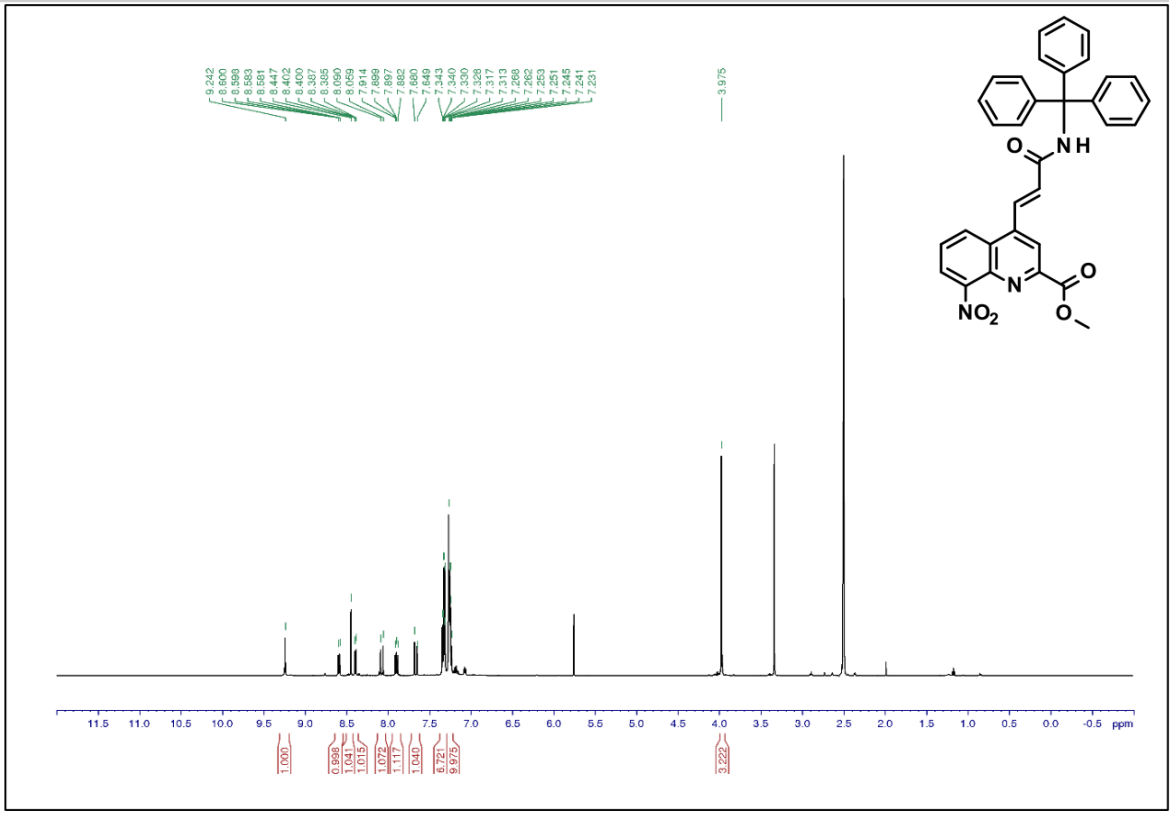

Figure S11. ^{1}H NMR (500 MHz, DMSO-d_6) of compound **5c**.

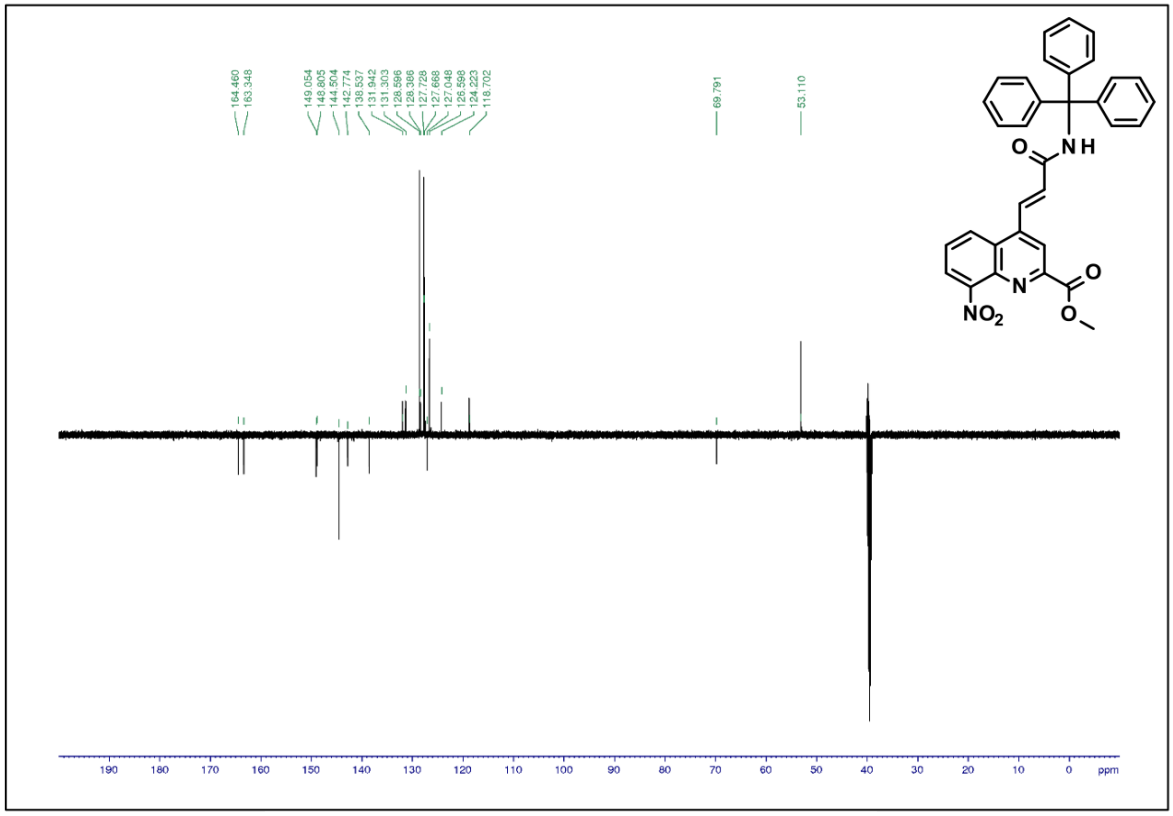

Figure S12. DEPT ^{13}C NMR (125 MHz, DMSO-d_6) of compound **5c**.

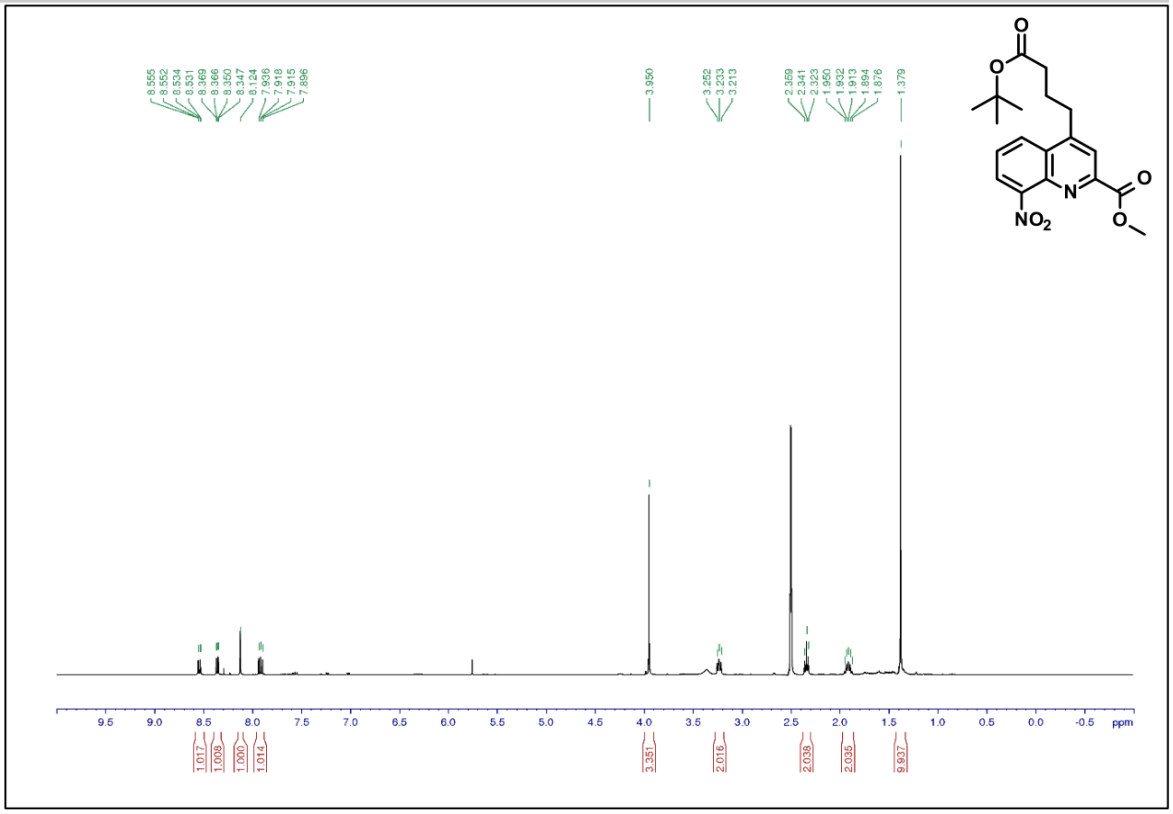

Figure S13. ^{1}H NMR (500 MHz, DMSO-d_6) of compound **5d**.

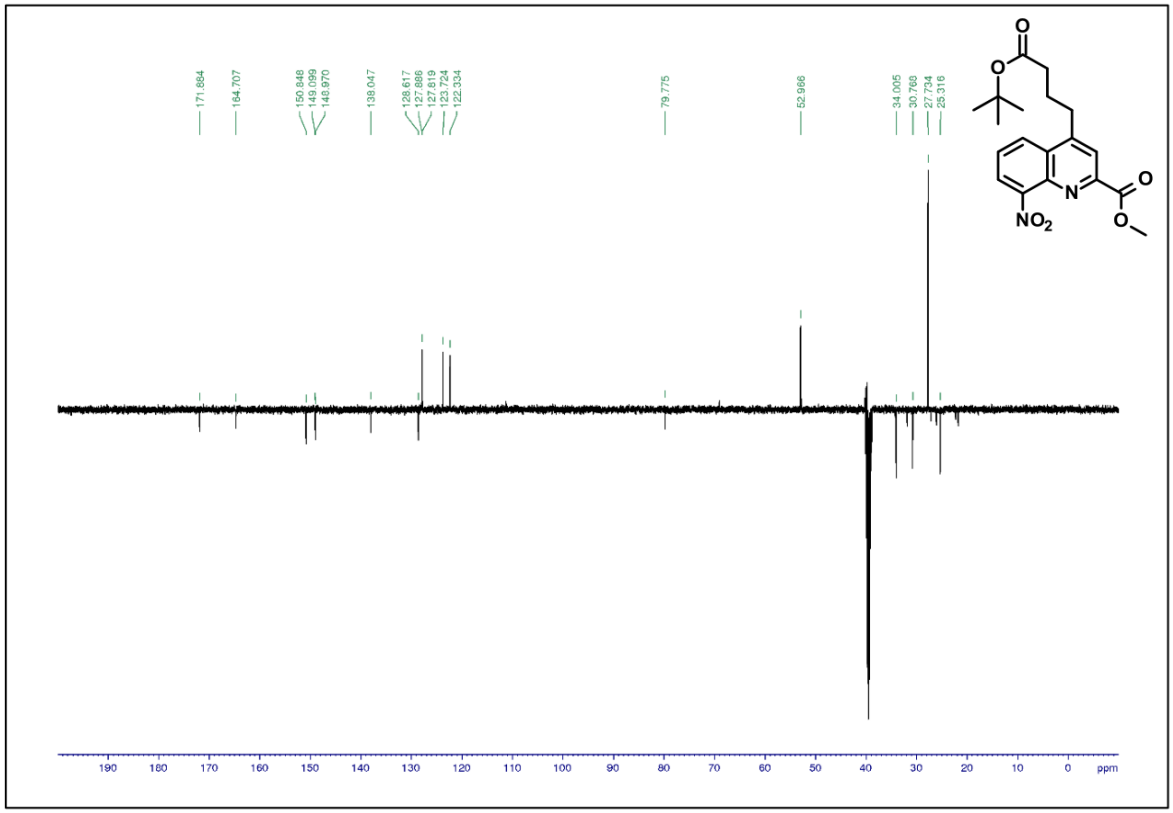

Figure S14. DEPT ^{13}C NMR (125 MHz, DMSO-d_6) of compound **5d**.

SUPPORTING INFORMATION

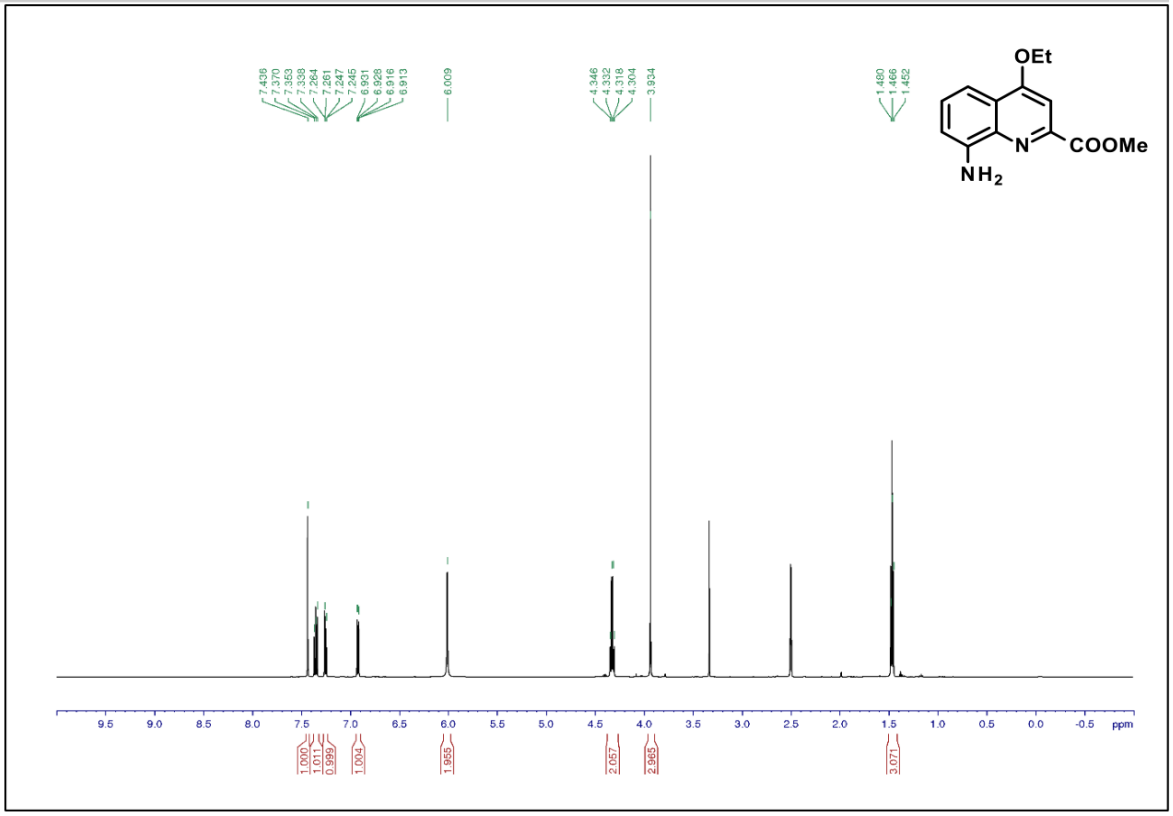

Figure S15. ^{1}H NMR (500 MHz, DMSO-d_6) of compound **6a**.

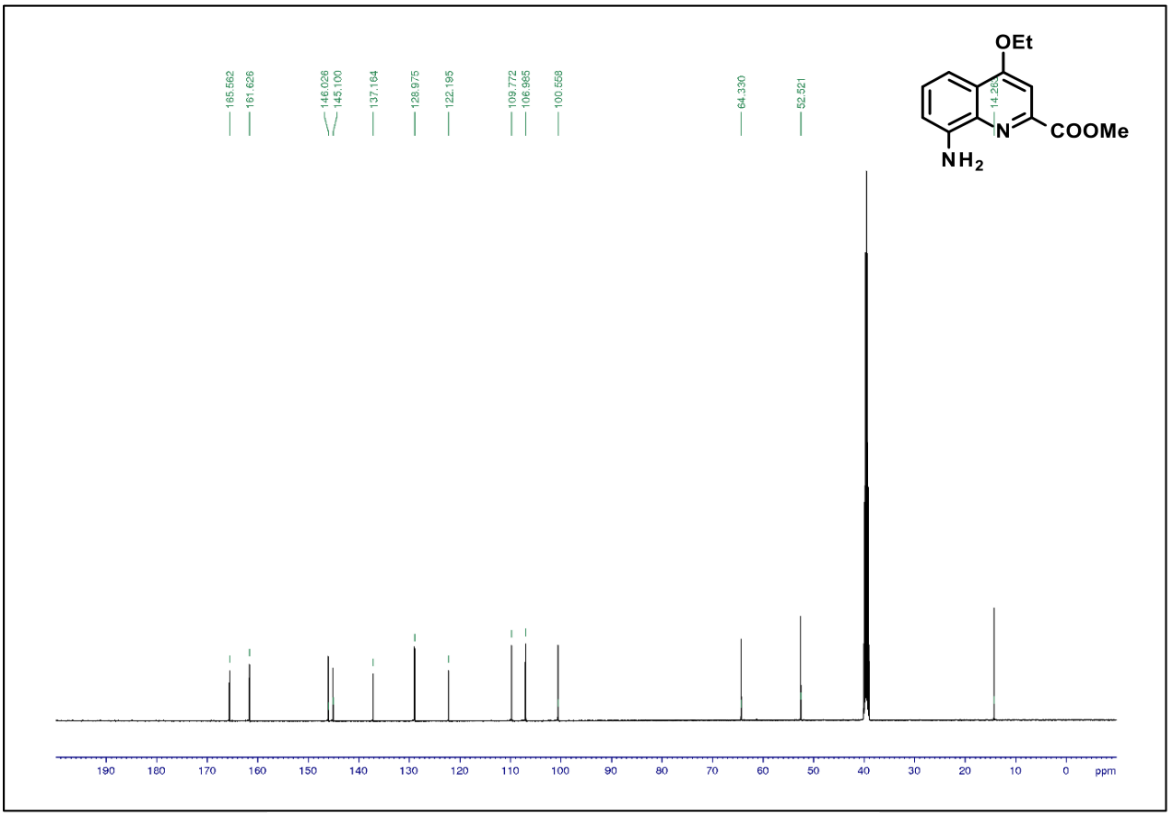

Figure S16. DEPT ^{13}C NMR (125 MHz, DMSO-d_6) of compound **6a**.

SUPPORTING INFORMATION

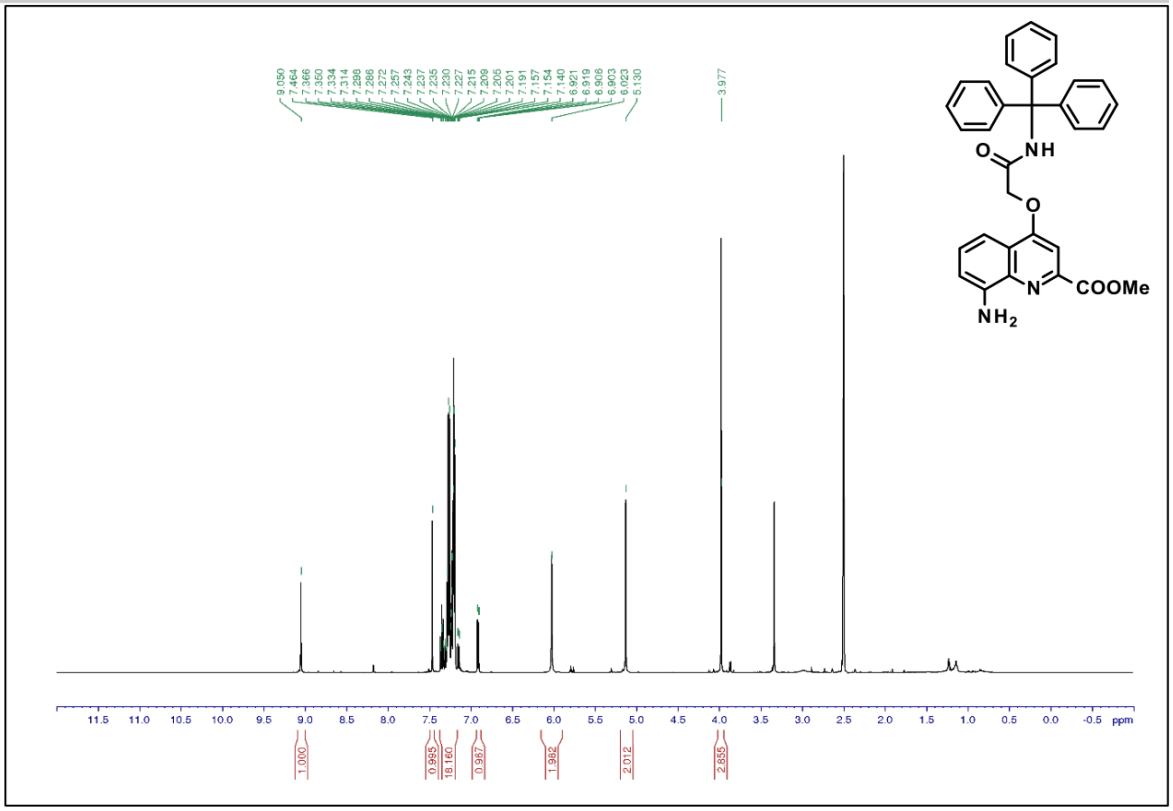

Figure S17. ^{1}H NMR (500 MHz, DMSO-d_6) of compound **6b**.

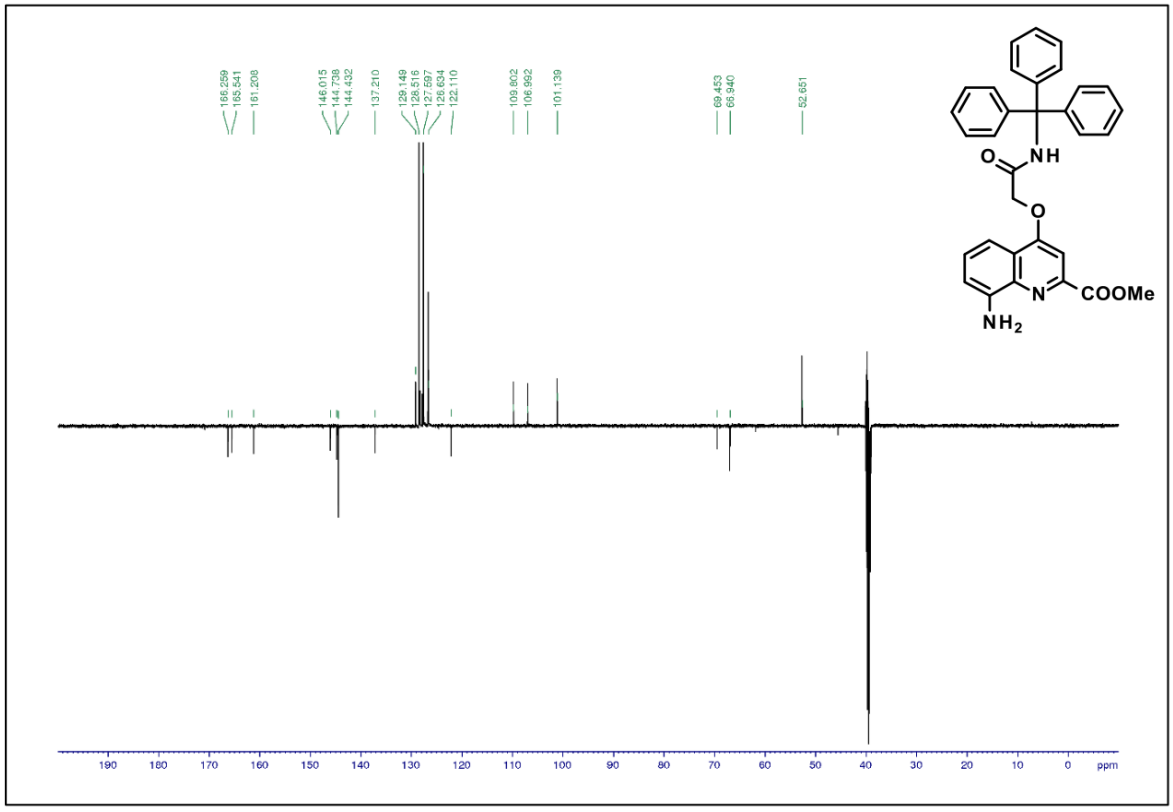

Figure S18. DEPT ^{13}C NMR (125 MHz, DMSO-d_6) of compound **6b**.

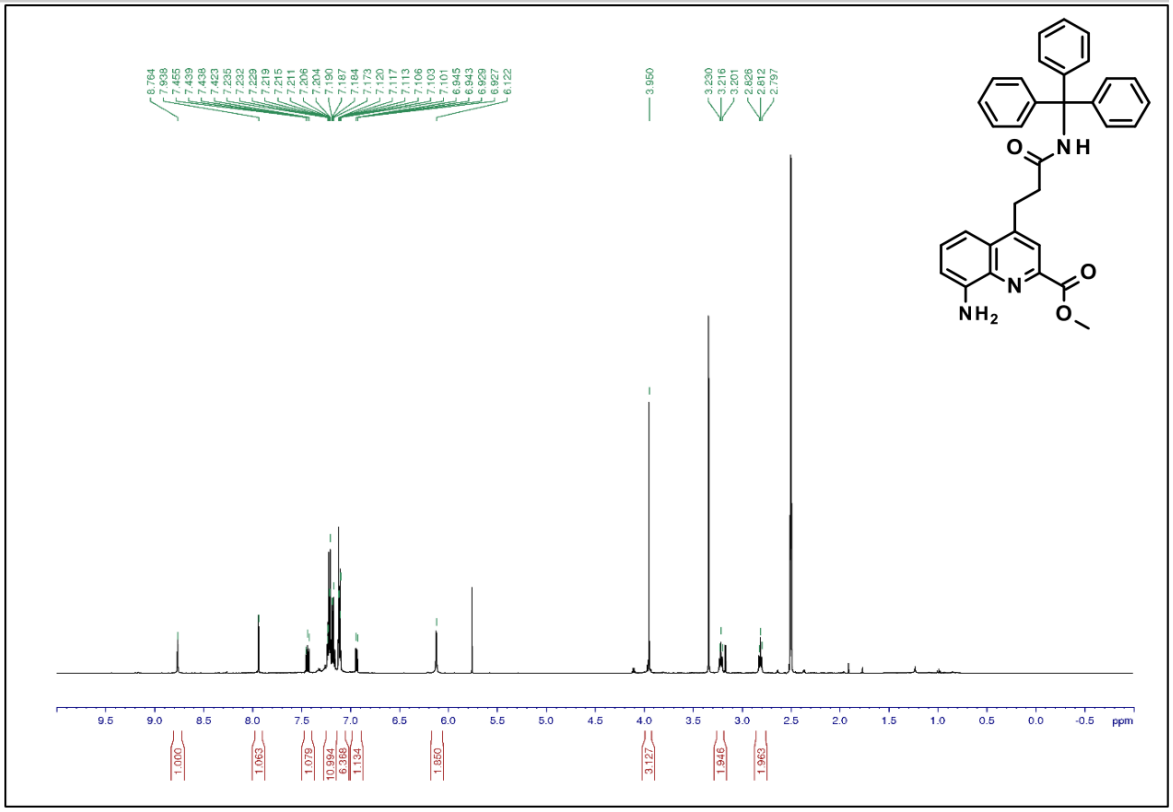

Figure S19. ^{1}H NMR (500 MHz, DMSO-d_6) of compound **6c**.

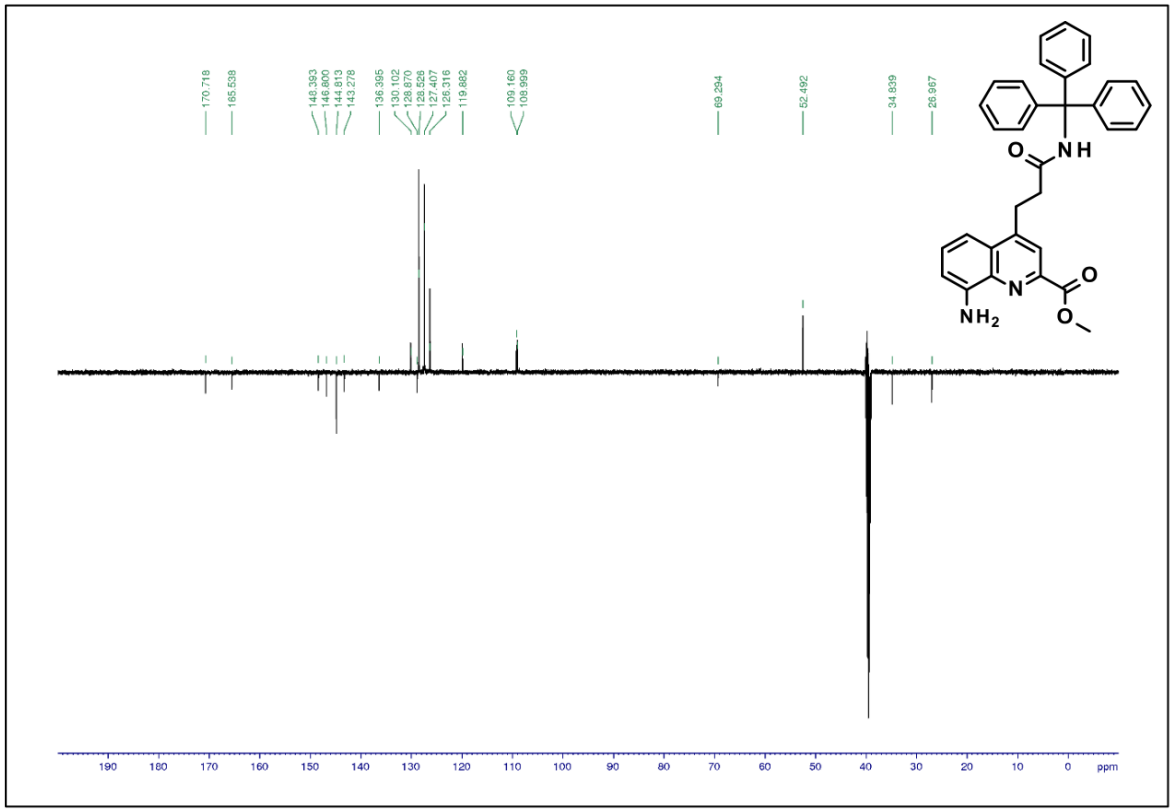

Figure S20. DEPT ^{13}C NMR (125 MHz, DMSO-d_6) of compound **6c**.

SUPPORTING INFORMATION

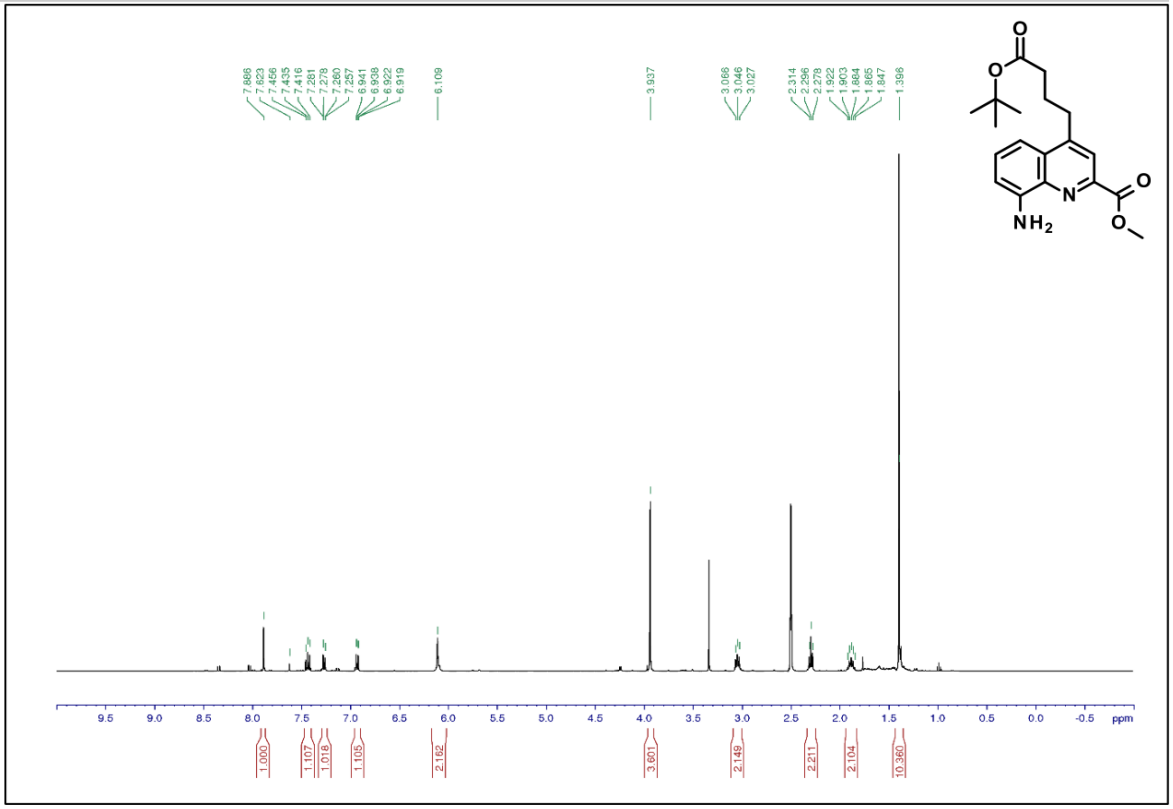

Figure S22. ^{1}H NMR (500 MHz, DMSO-d_6) of compound **6d**.

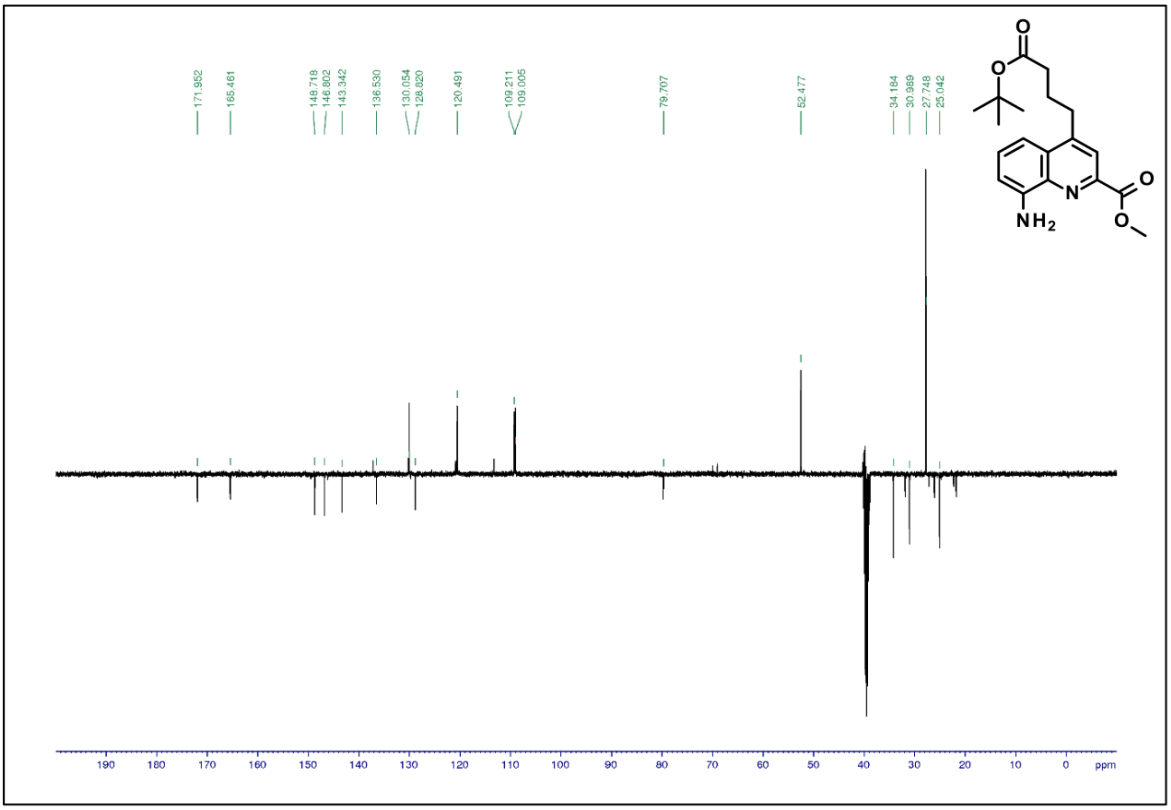

Figure S22. DEPT ^{13}C NMR (125 MHz, DMSO-d_6) of compound **6d**.

SUPPORTING INFORMATION

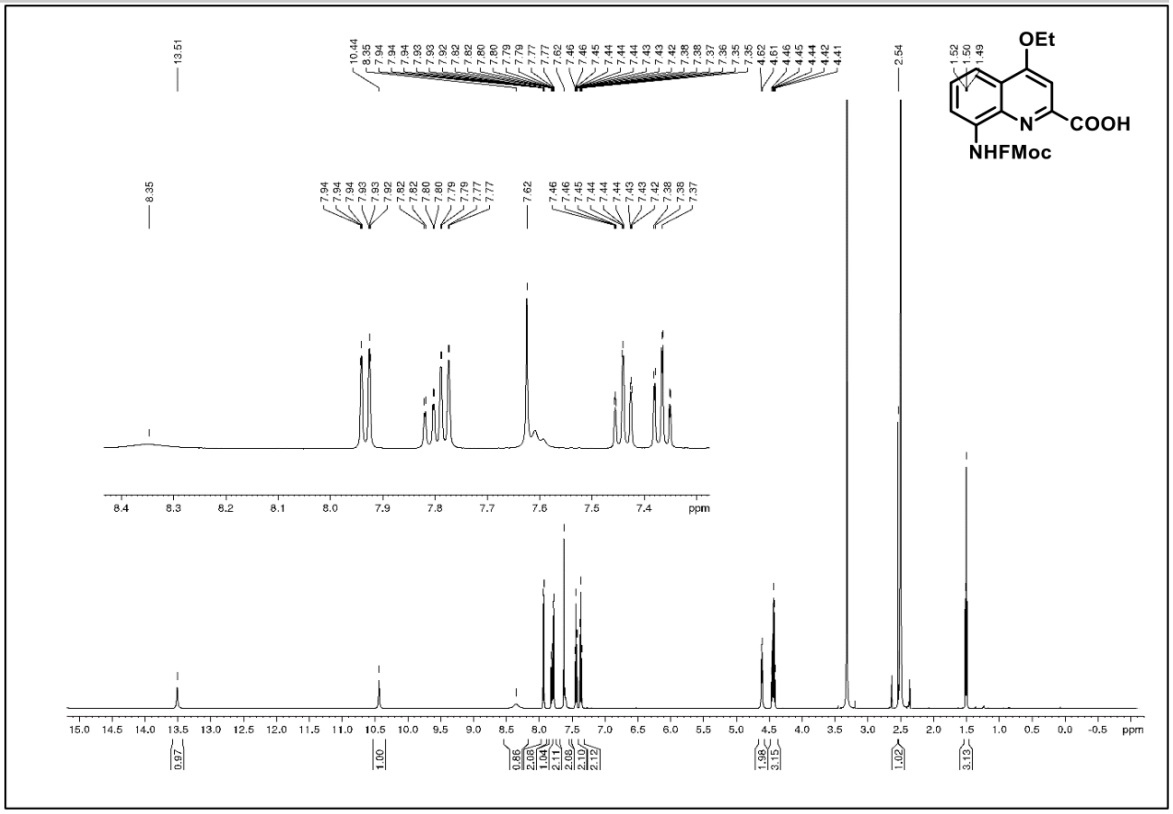

Figure S23. ^{1}H NMR (500 MHz, DMSO-d_6) of compound **7a**.

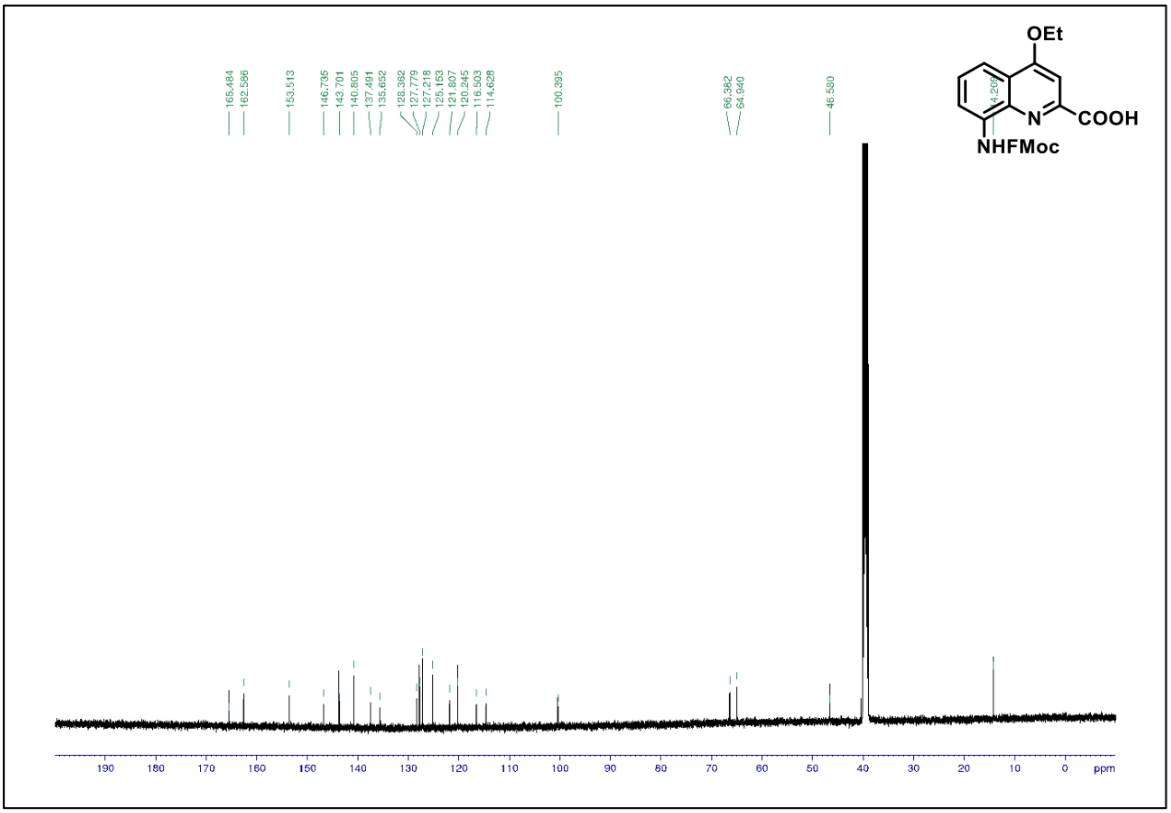

Figure S24. ^{13}C{^{1}H} NMR (125 MHz, DMSO-d_6) of compound **7a**.

SUPPORTING INFORMATION

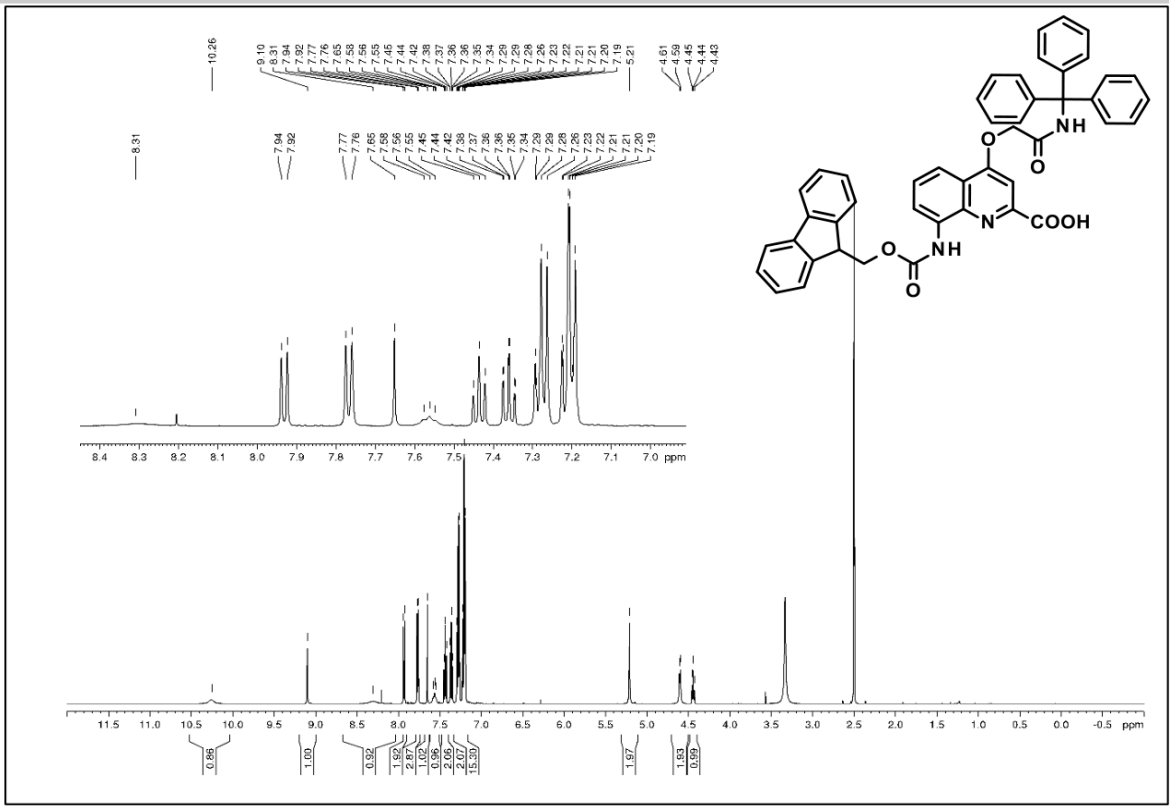

Figure S25. ^{1}H NMR (500 MHz, DMSO-d_6) of compound **7b**.

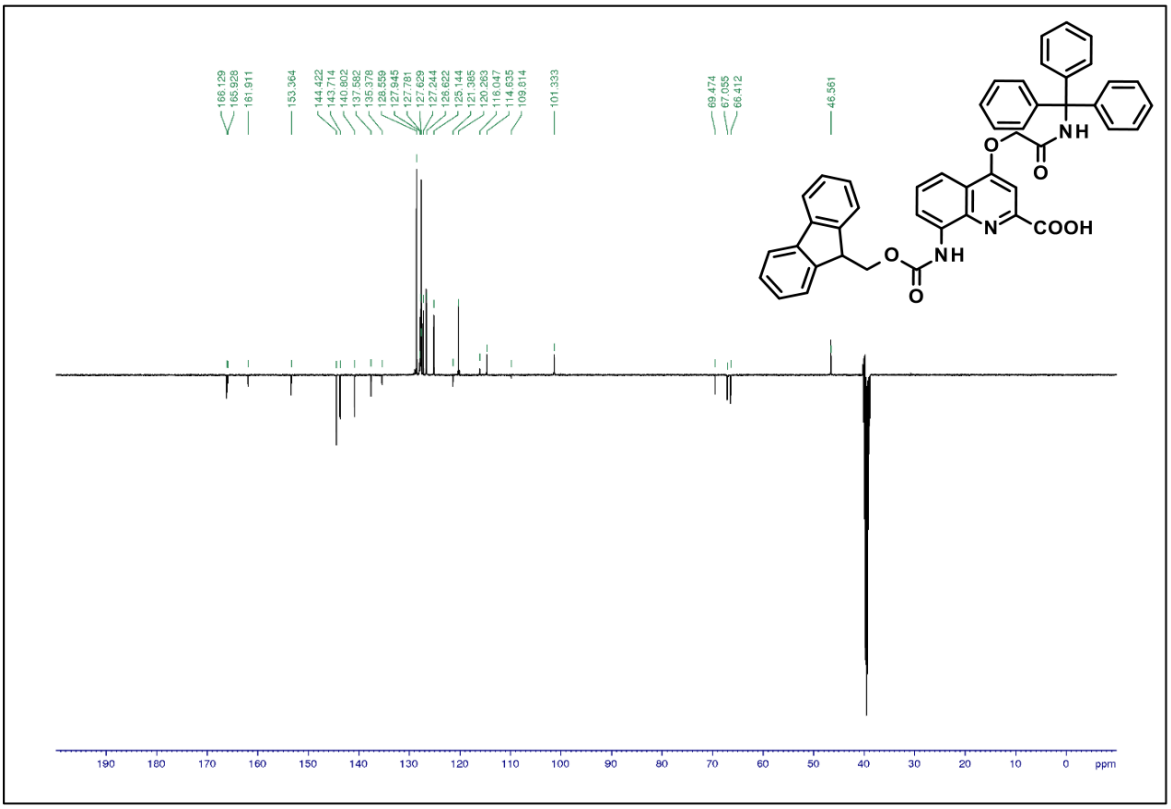

Figure S26. DEPT ^{13}C NMR (125 MHz, DMSO-d_6) of compound **7b**.

SUPPORTING INFORMATION

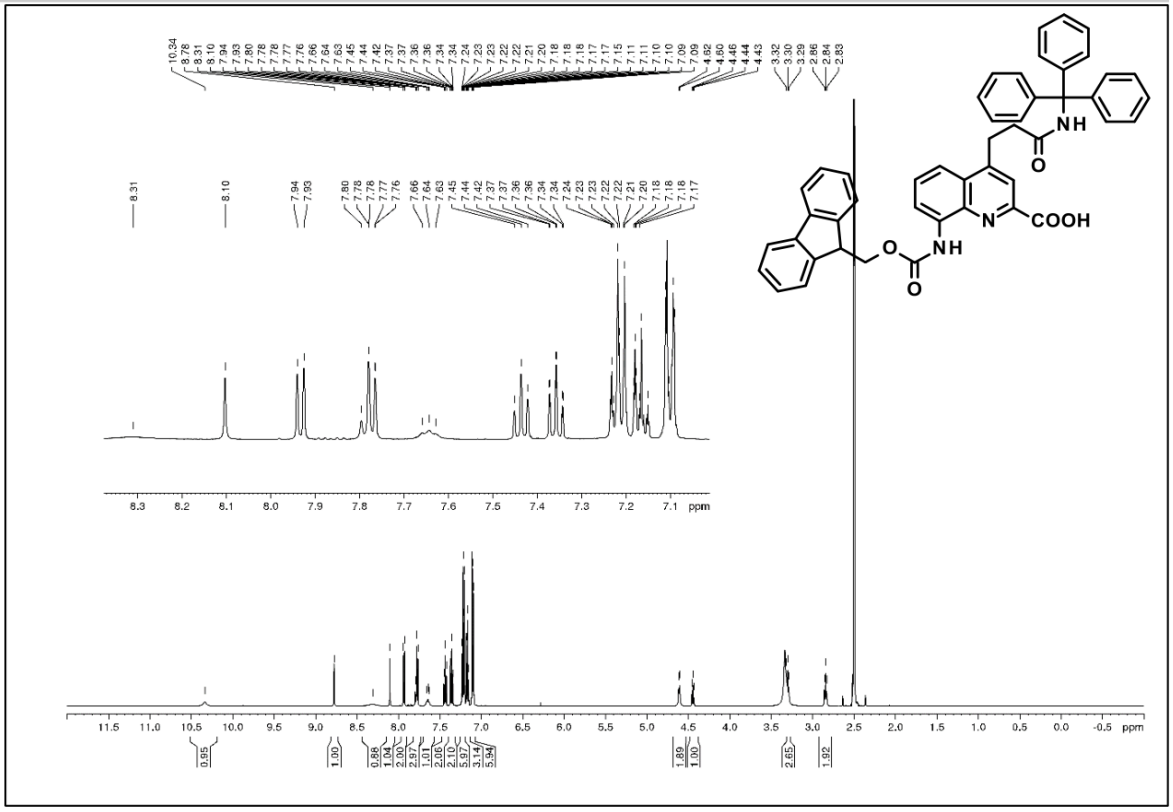

Figure S27. ^{1}H NMR (500 MHz, DMSO-d_6) of compound **7c**.

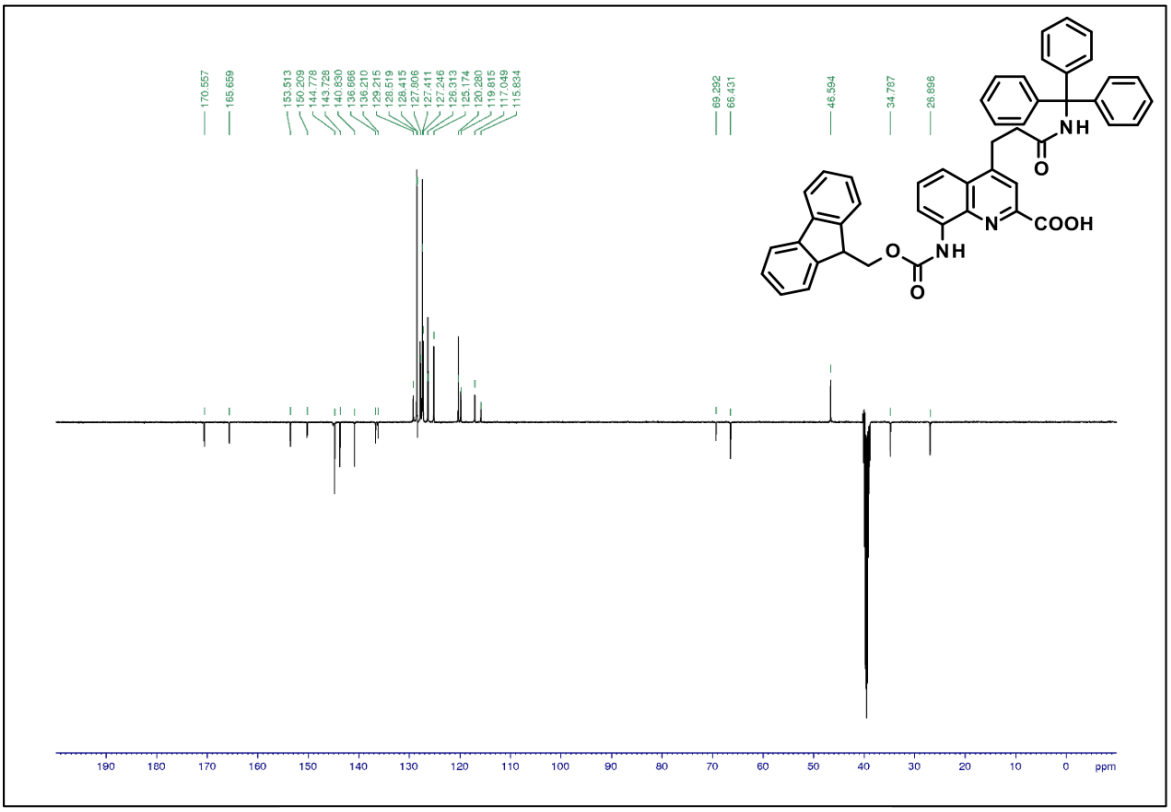

Figure S28. DEPT ^{13}C NMR (125 MHz, DMSO-d_6) of compound **7c**.

SUPPORTING INFORMATION

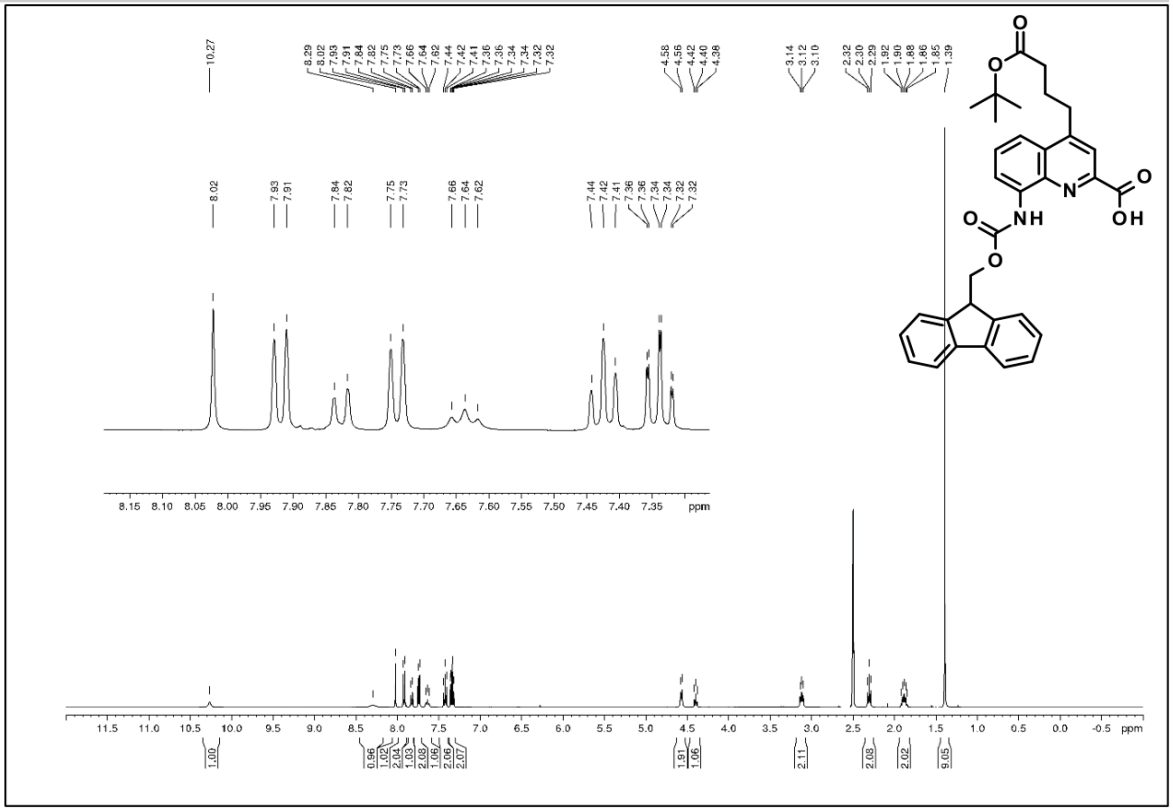

Figure S29. ^{1}H NMR (500 MHz, DMSO-d_6) of compound **7d**.

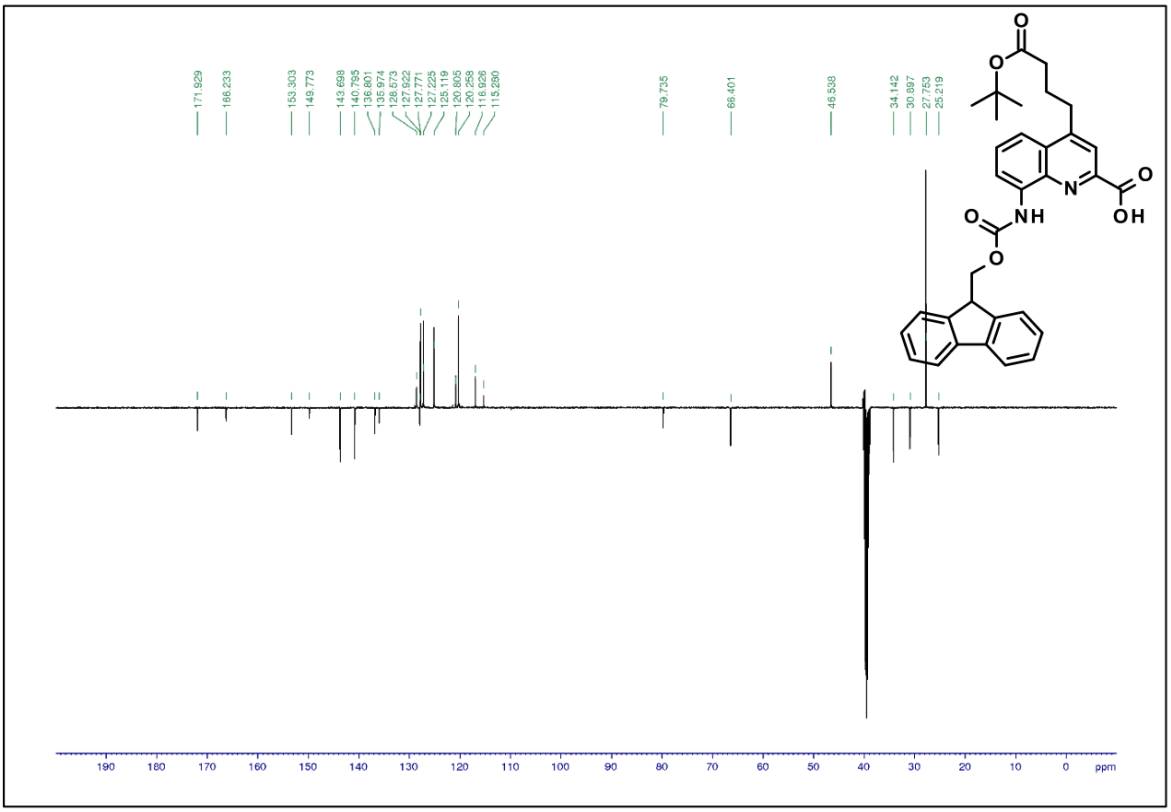

Figure S30. DEPT ^{13}C NMR (125 MHz, DMSO-d_6) of compound **7d**.

SUPPORTING INFORMATION

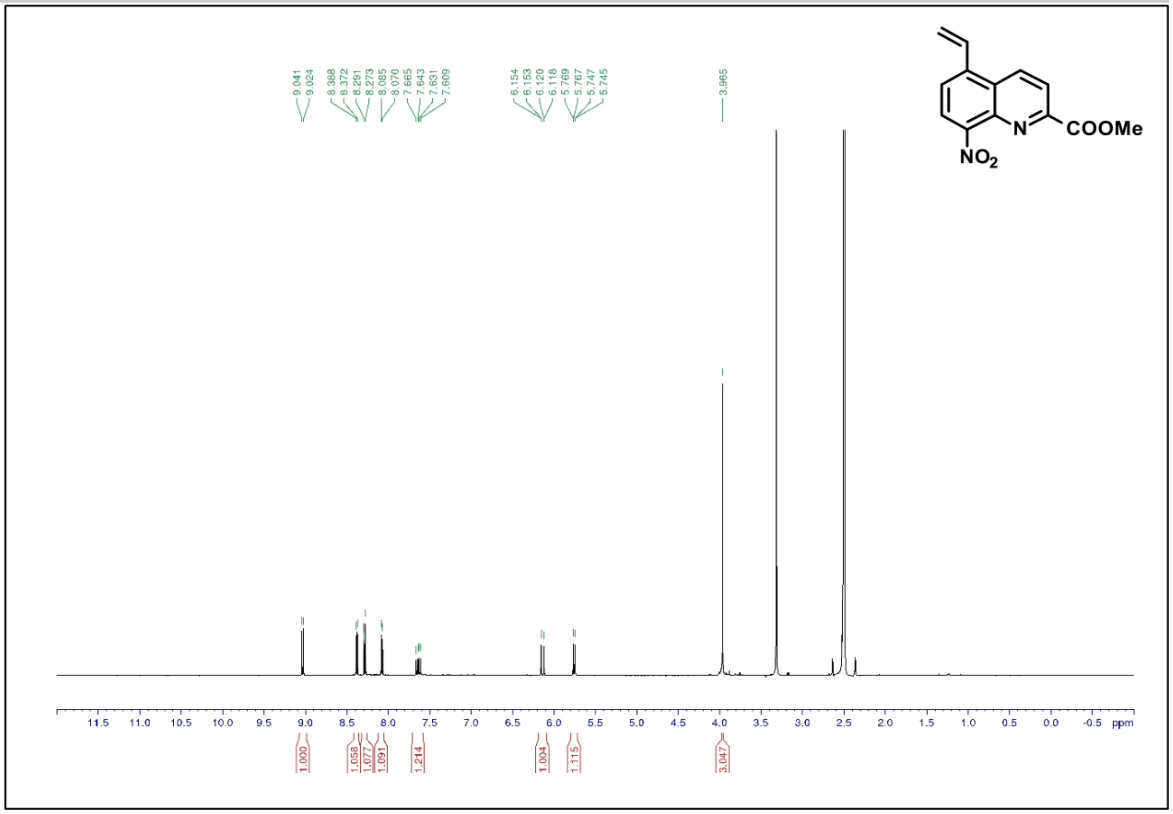

Figure S31. ^{1}H NMR (500 MHz, DMSO-d_6) of compound **8a**.

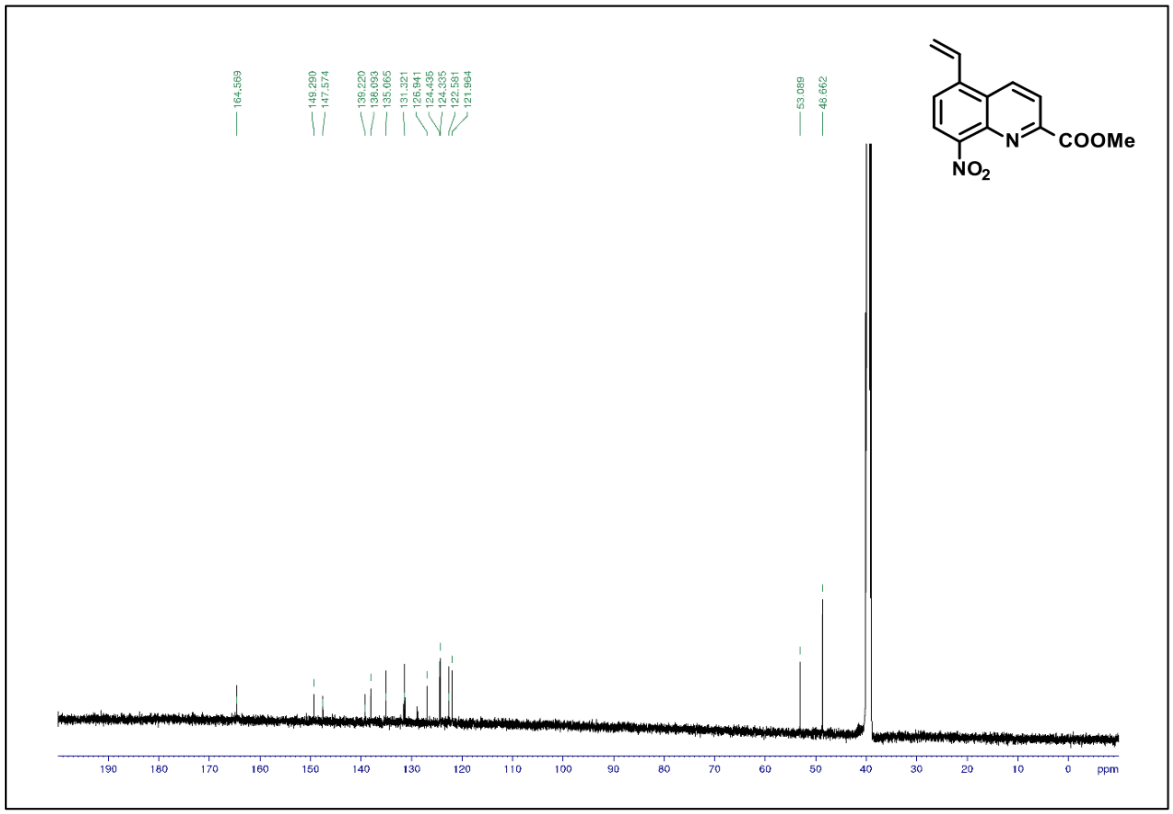

Figure S32. $^{13}C\{^{1}H\}$ NMR (125 MHz, DMSO-d_6) of compound **8a**.

SUPPORTING INFORMATION

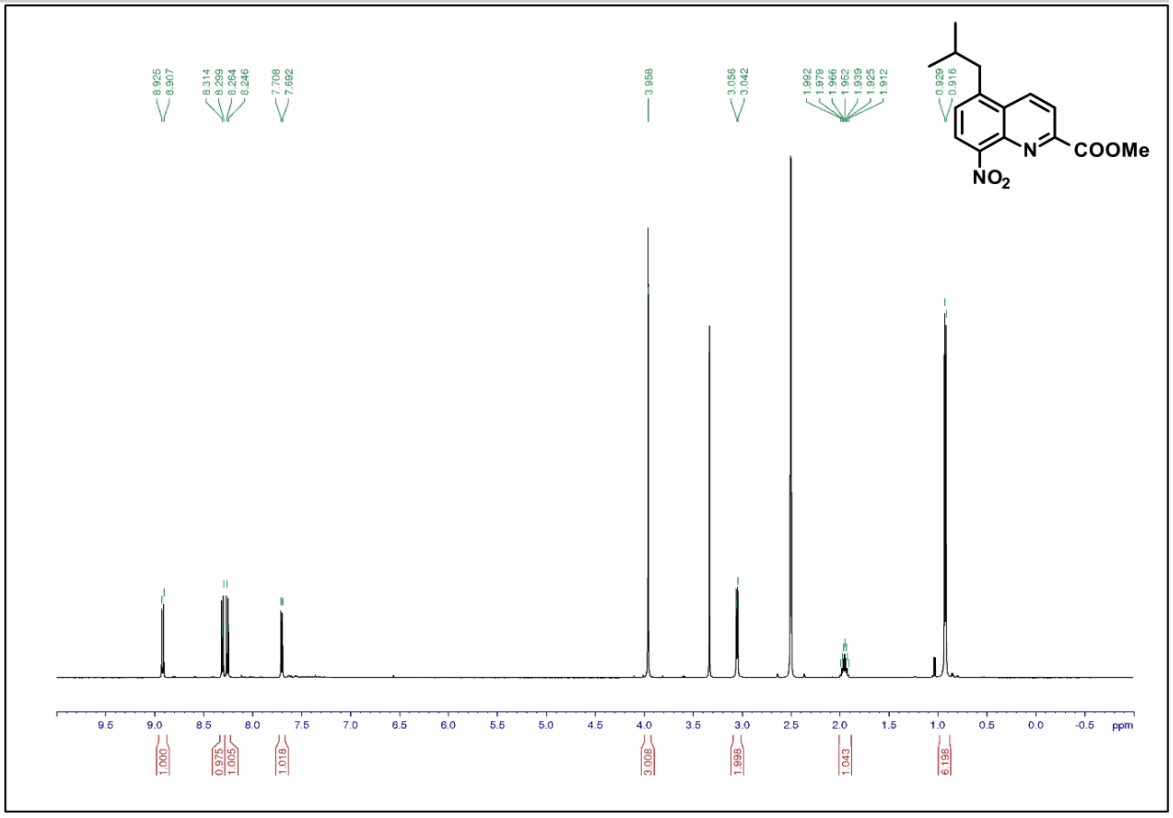

Figure S33. ^{1}H NMR (500 MHz, DMSO-d_6) of compound **8b**.

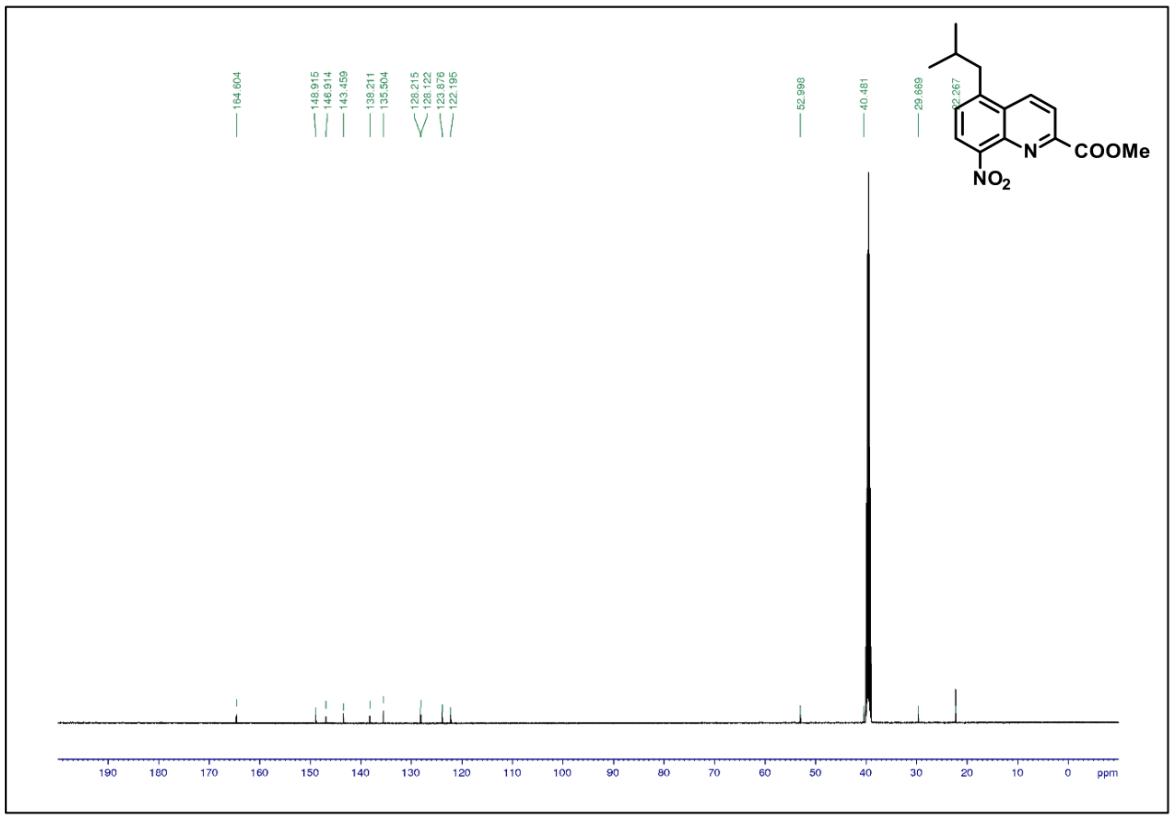

Figure S34. $^{13}C\{^{1}H\}$ NMR (125 MHz, DMSO-d_6) of compound **8b**.

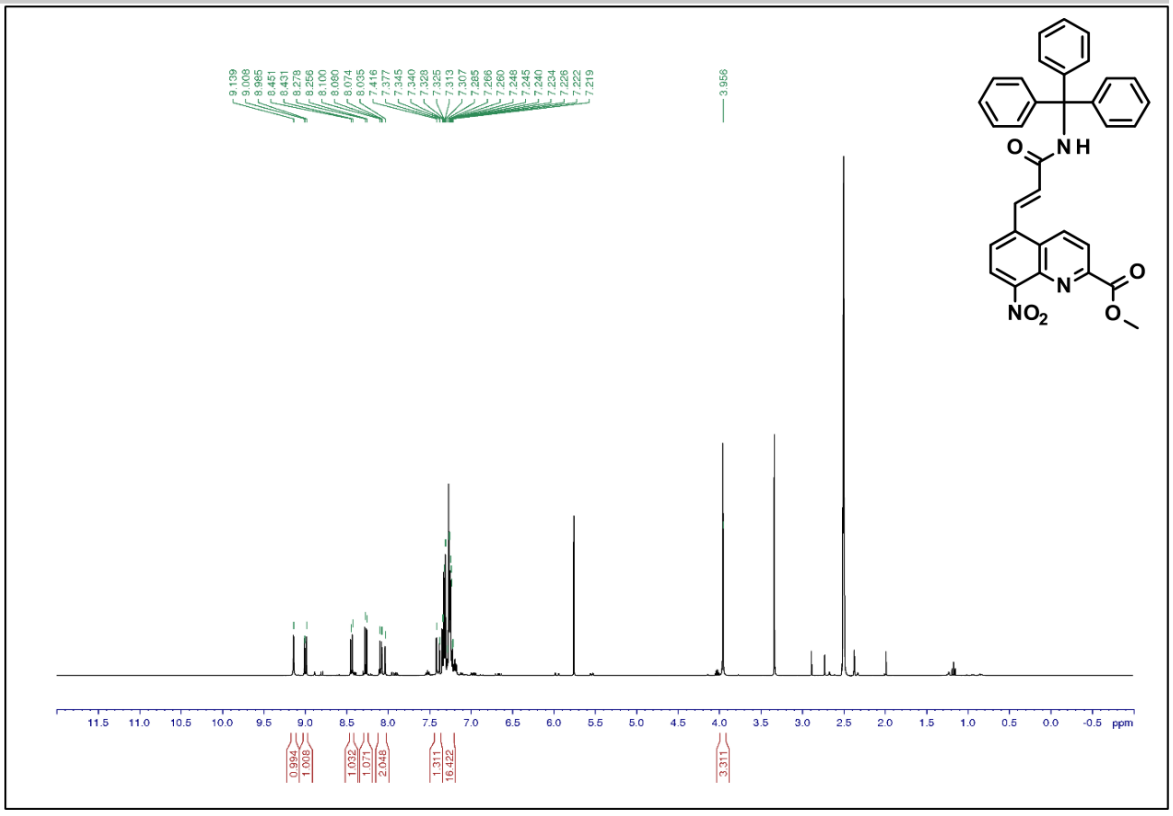

Figure S35. ^{1}H NMR (500 MHz, DMSO-d_6) of compound **8c**.

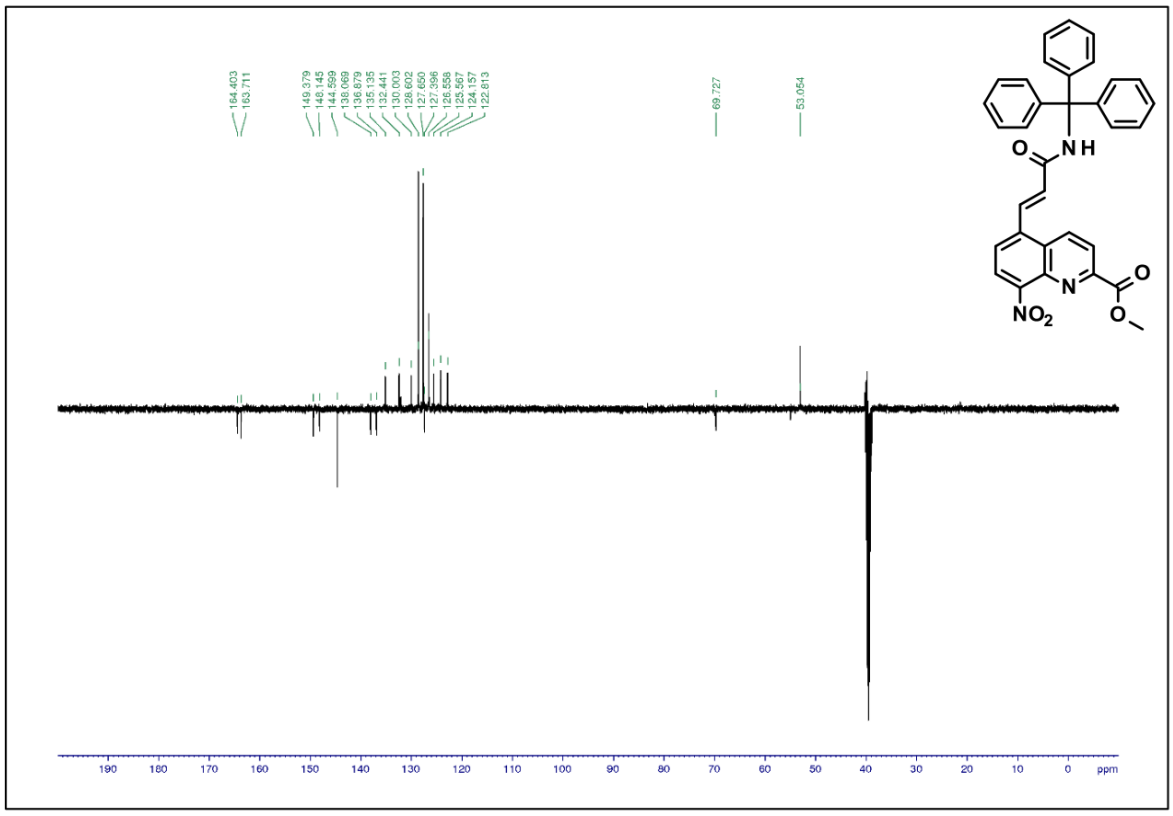

Figure S36. DEPT ^{13}C NMR (125 MHz, DMSO-*d*6) of compound **8c**.

SUPPORTING INFORMATION

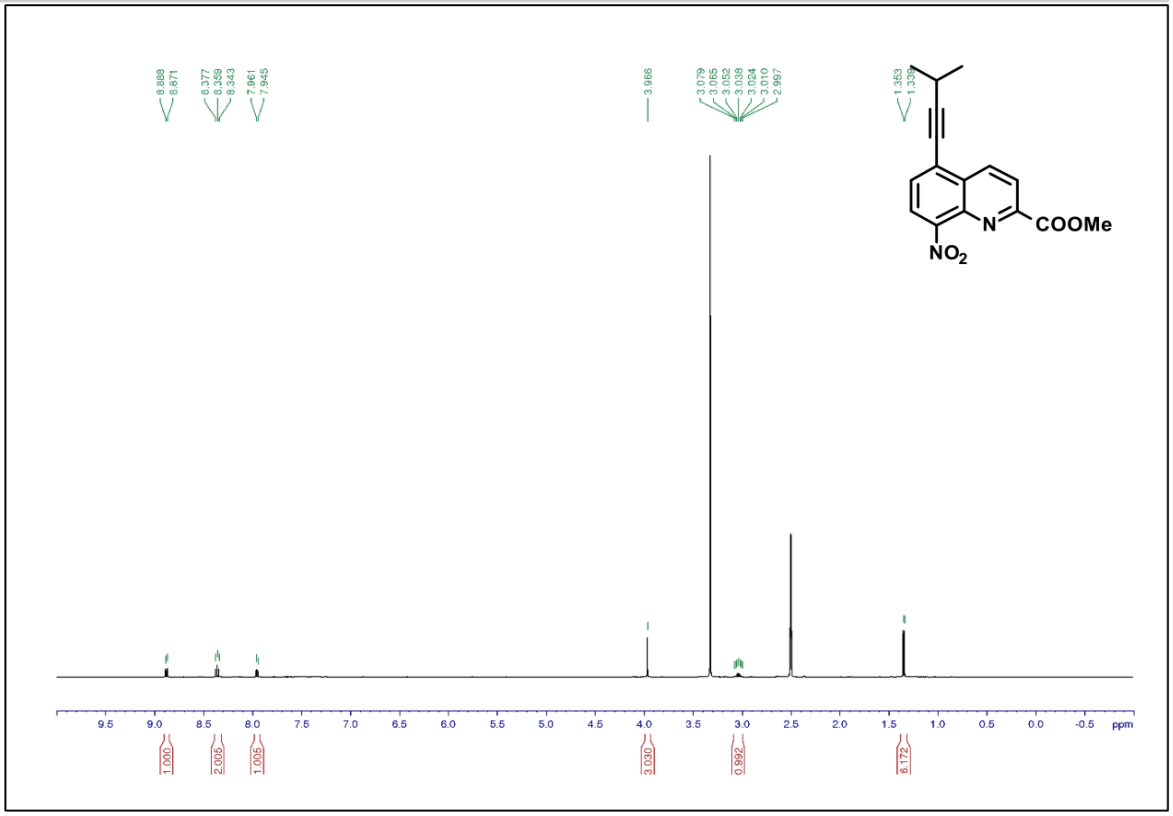

Figure S37. ^{1}H NMR (500 MHz, DMSO-d_6) of compound **8d**.

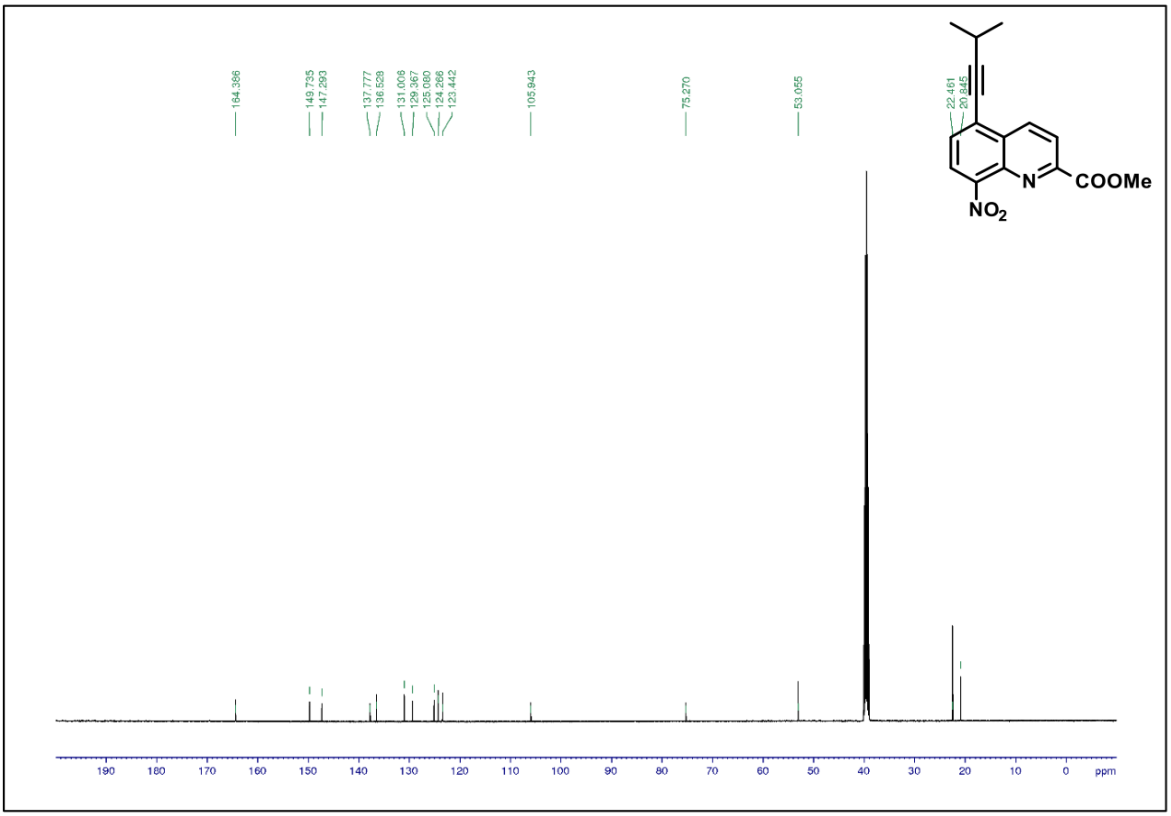

Figure S38. $^{13}C\{^{1}H\}$ NMR (125 MHz, DMSO-d_6) of compound **8d**.

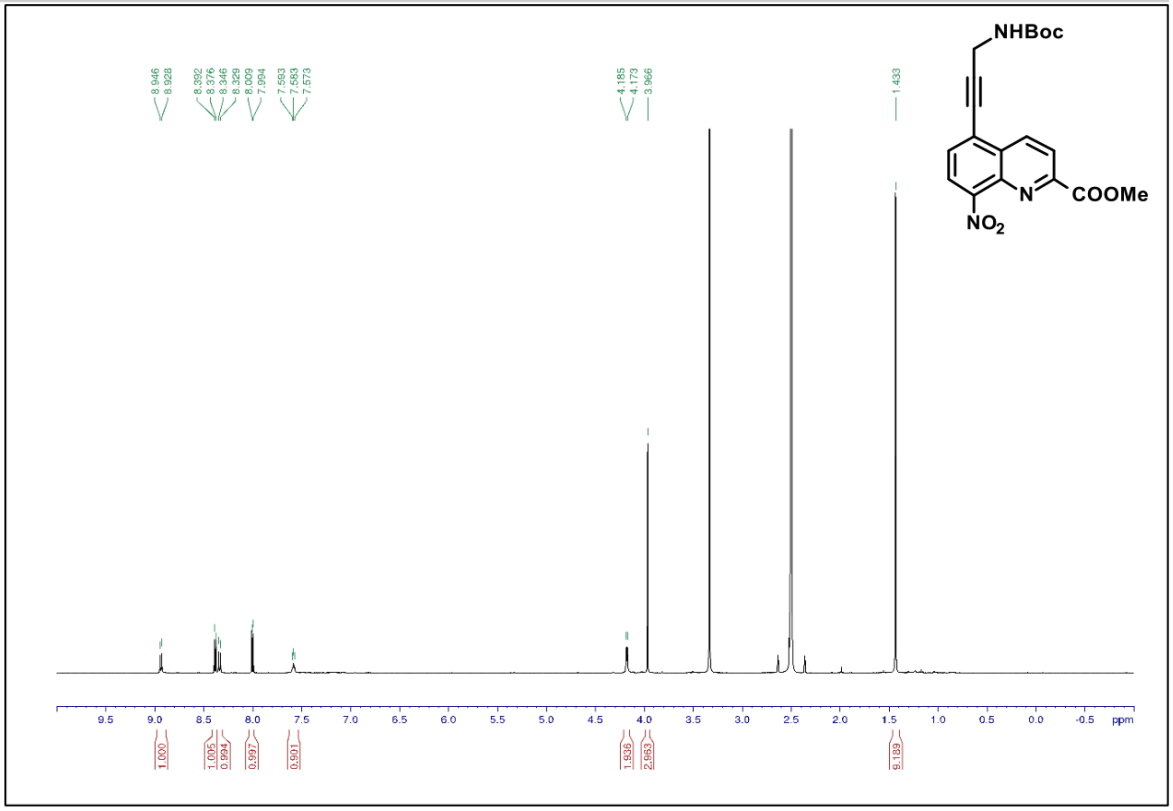

Figure S39. ^{1}H NMR (500 MHz, DMSO-d_6) of compound **8e**.

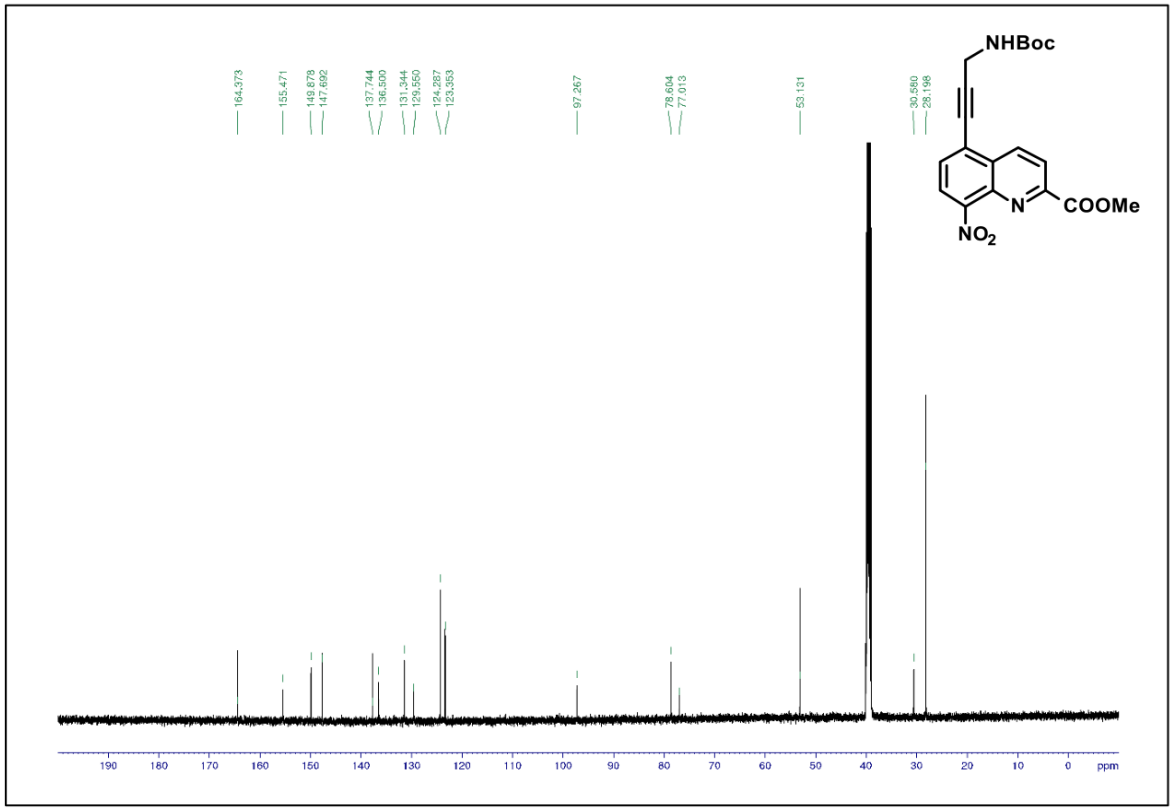

Figure S40. $^{13}C\{^{1}H\}$ NMR (125 MHz, DMSO-d_6) of compound **8e**.

SUPPORTING INFORMATION

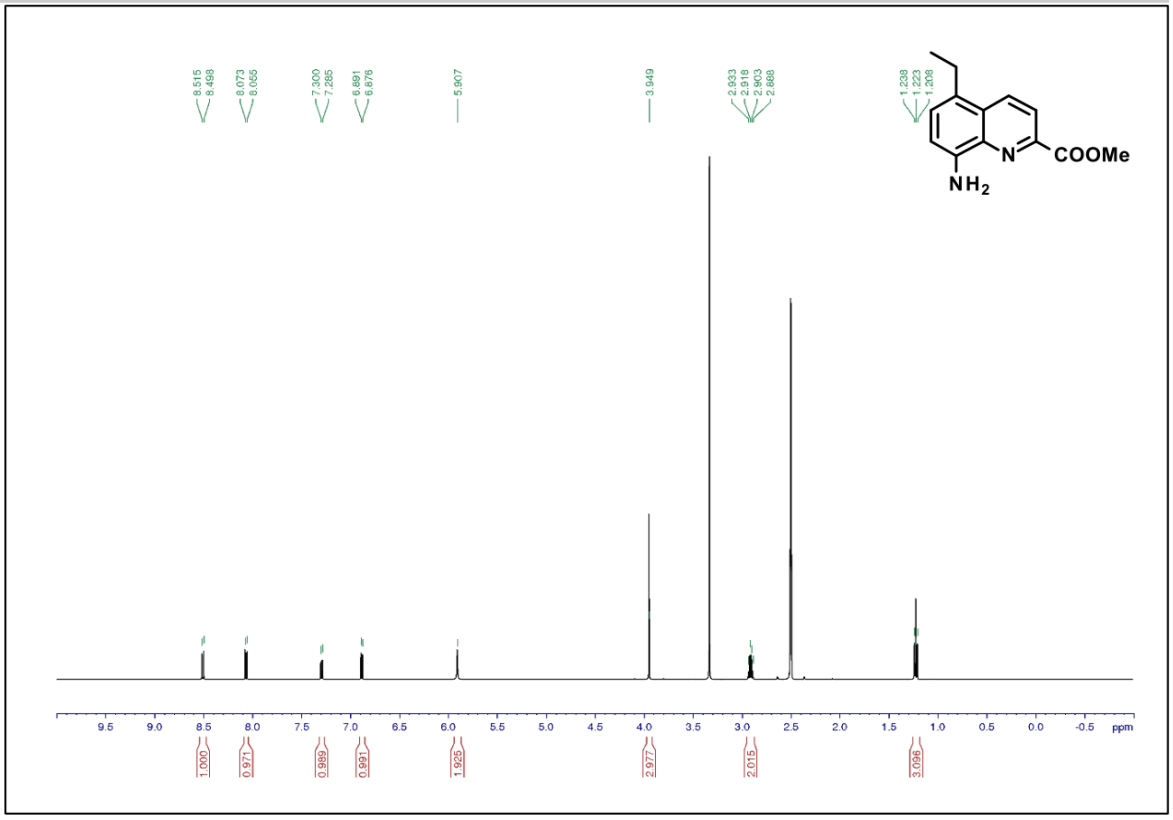

Figure S41. ^{1}H NMR (500 MHz, DMSO-d_6) of compound **9a**.

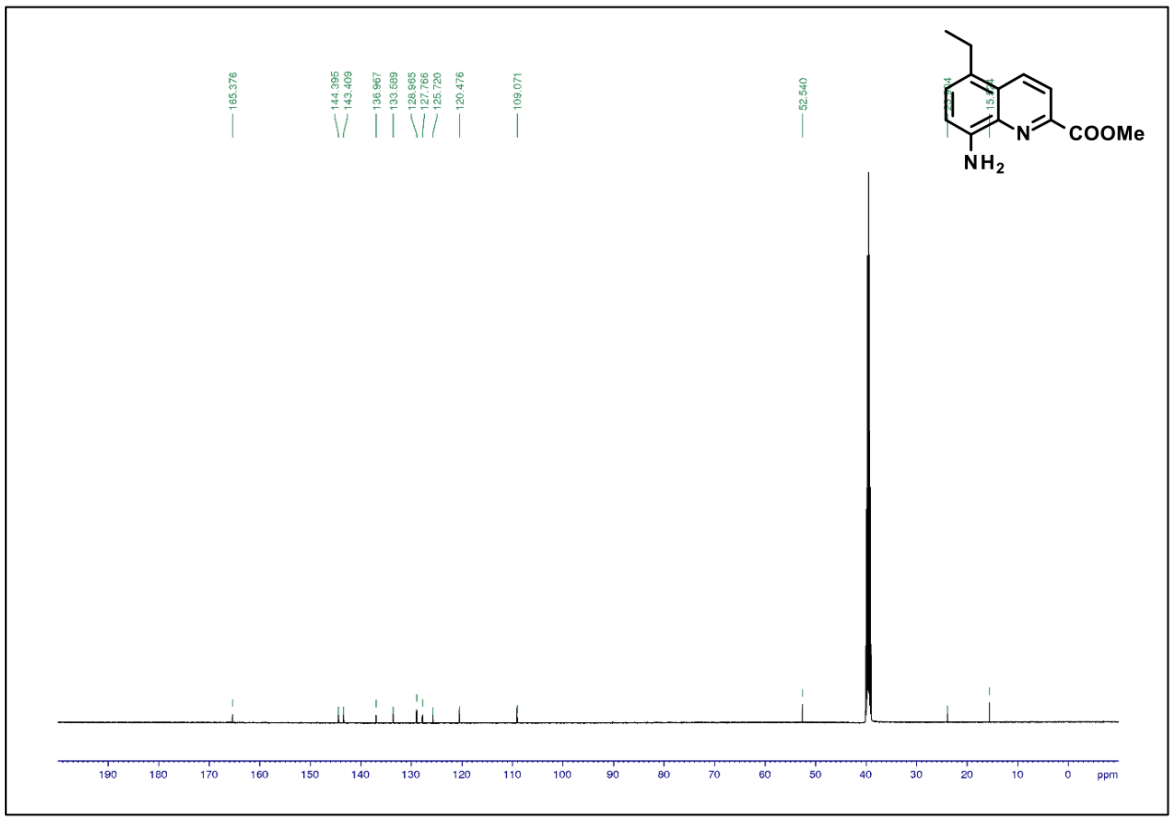

Figure S42. $^{13}C\{^{1}H\}$ NMR (125 MHz, DMSO-d_6) of compound **9a**.

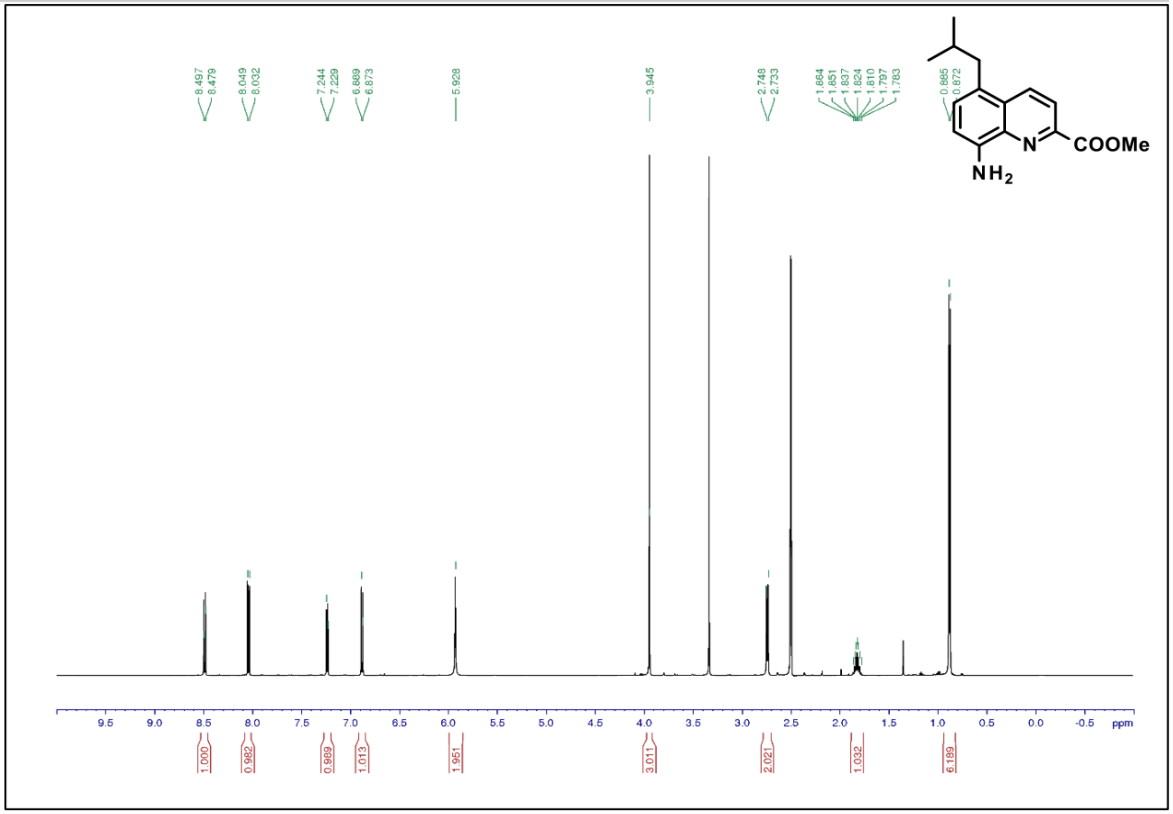

Figure S43. ^{1}H NMR (500 MHz, DMSO-d_6) of compound **9b**.

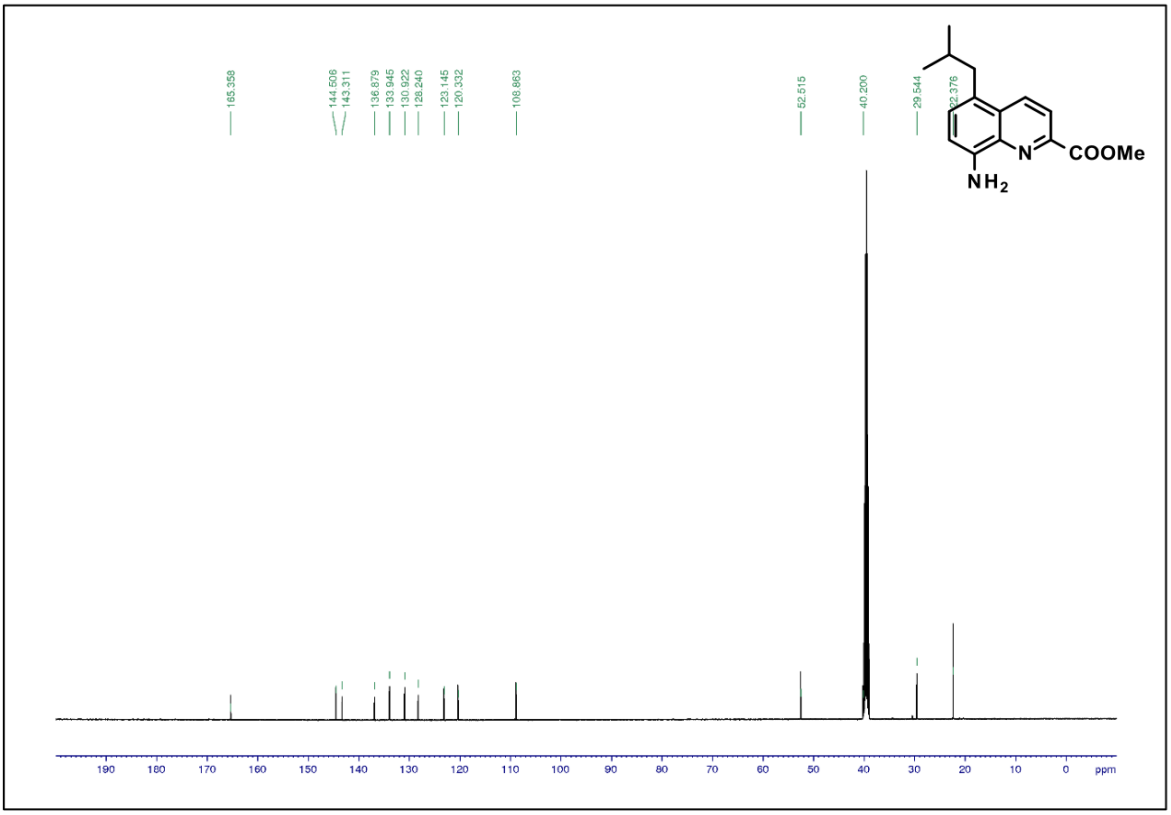

Figure S44. ^{13}C{^{1}H} NMR (125 MHz, DMSO-d_6) of compound **9b**.

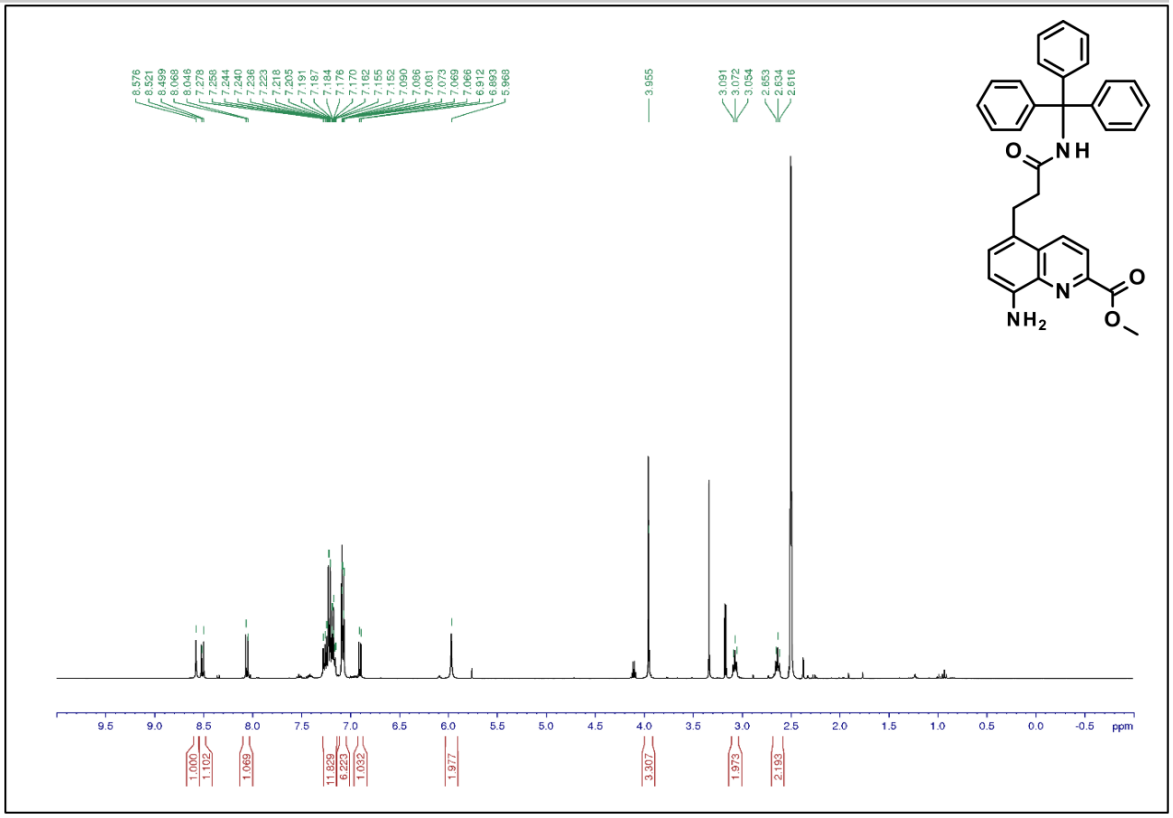

Figure S45. ^{1}H NMR (500 MHz, DMSO-d_6) of compound **9c**.

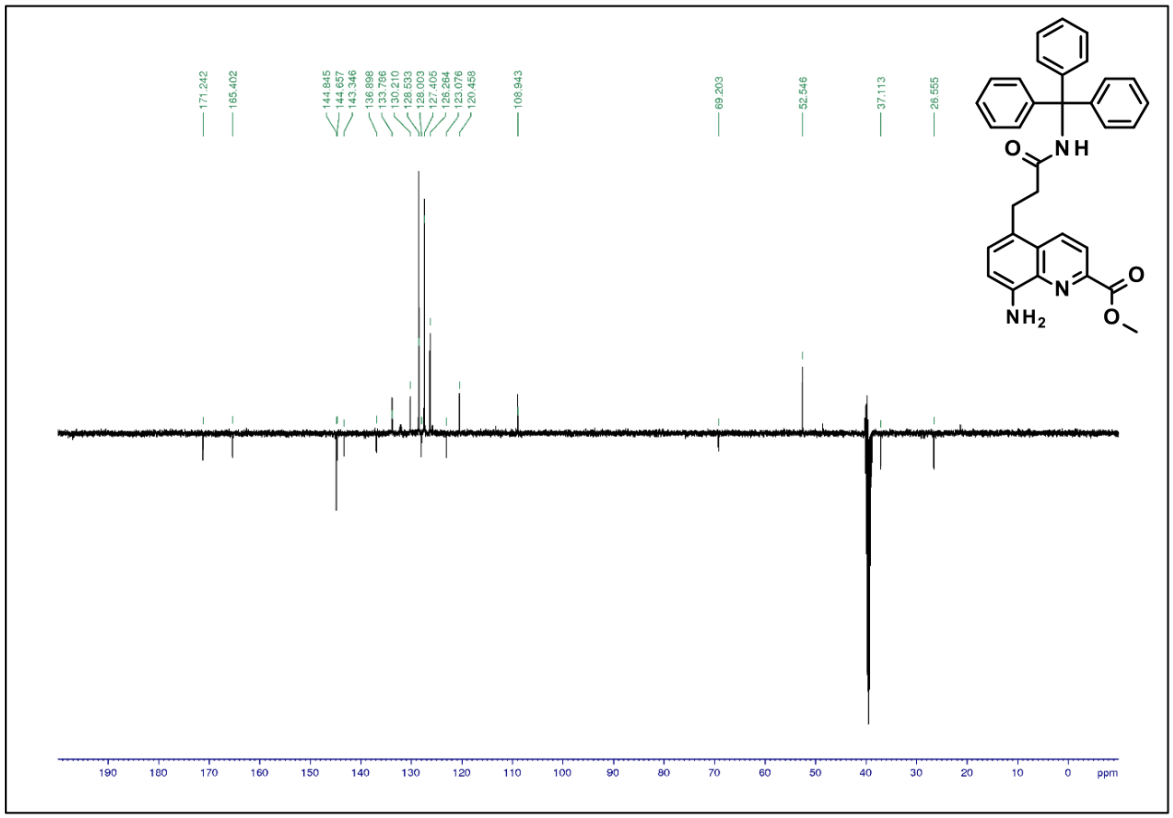

Figure S46. DEPT ^{13}C NMR (125 MHz, DMSO-d_6) of compound **9c**.

SUPPORTING INFORMATION

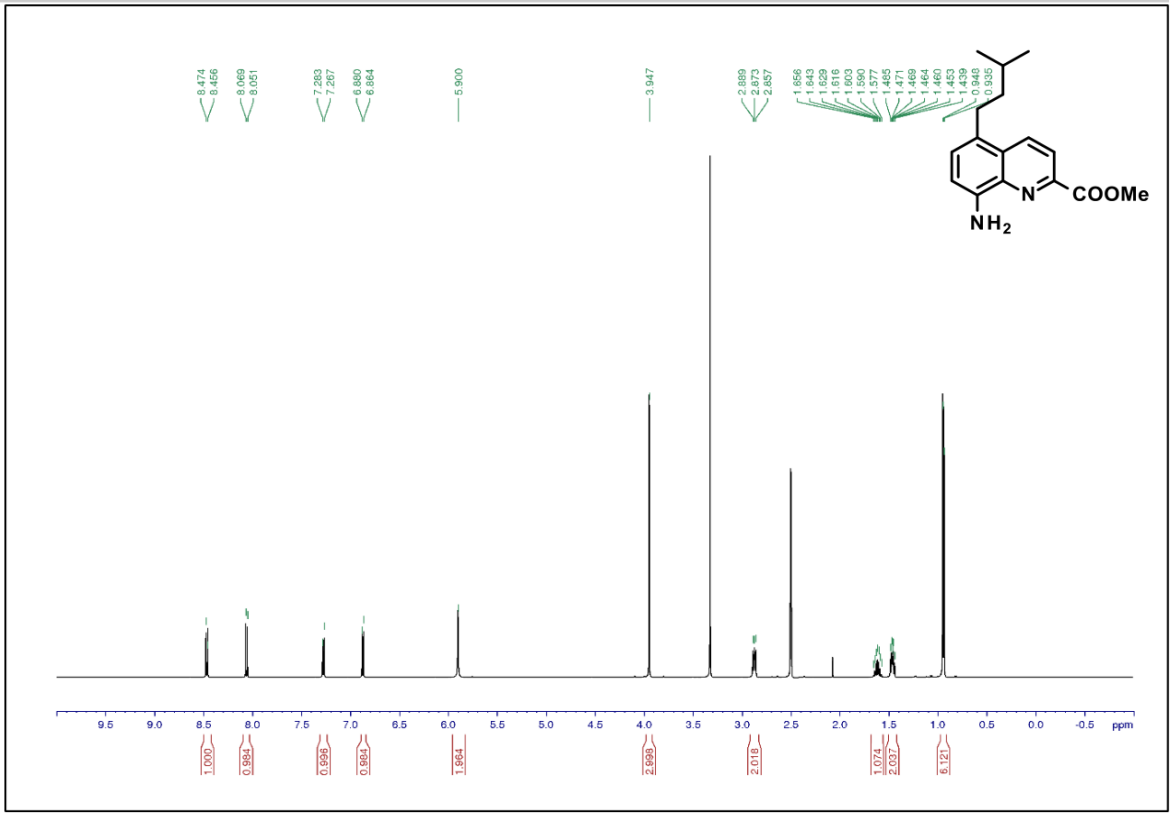

Figure S47. ^{1}H NMR (500 MHz, DMSO-d_6) of compound **9d**.

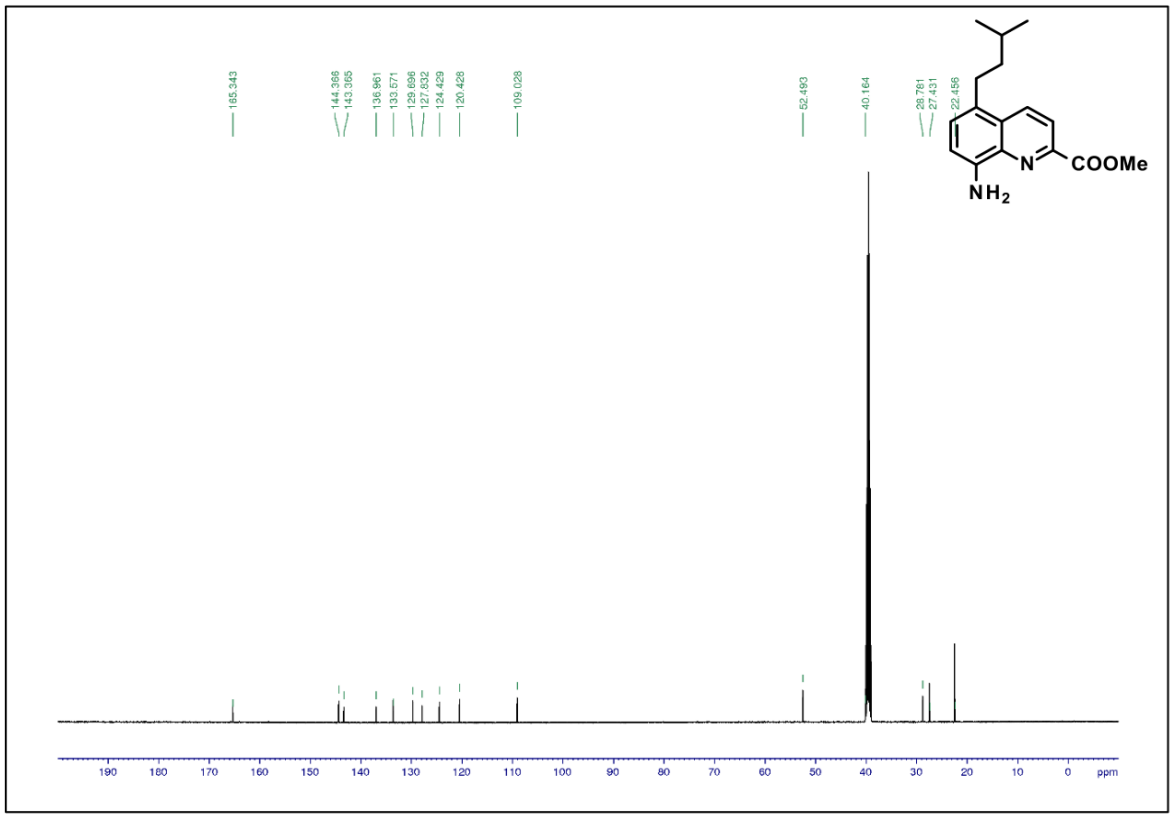

Figure S48. $^{13}C\{^{1}H\}$ NMR (125 MHz, DMSO-d_6) of compound **9d**.

SUPPORTING INFORMATION

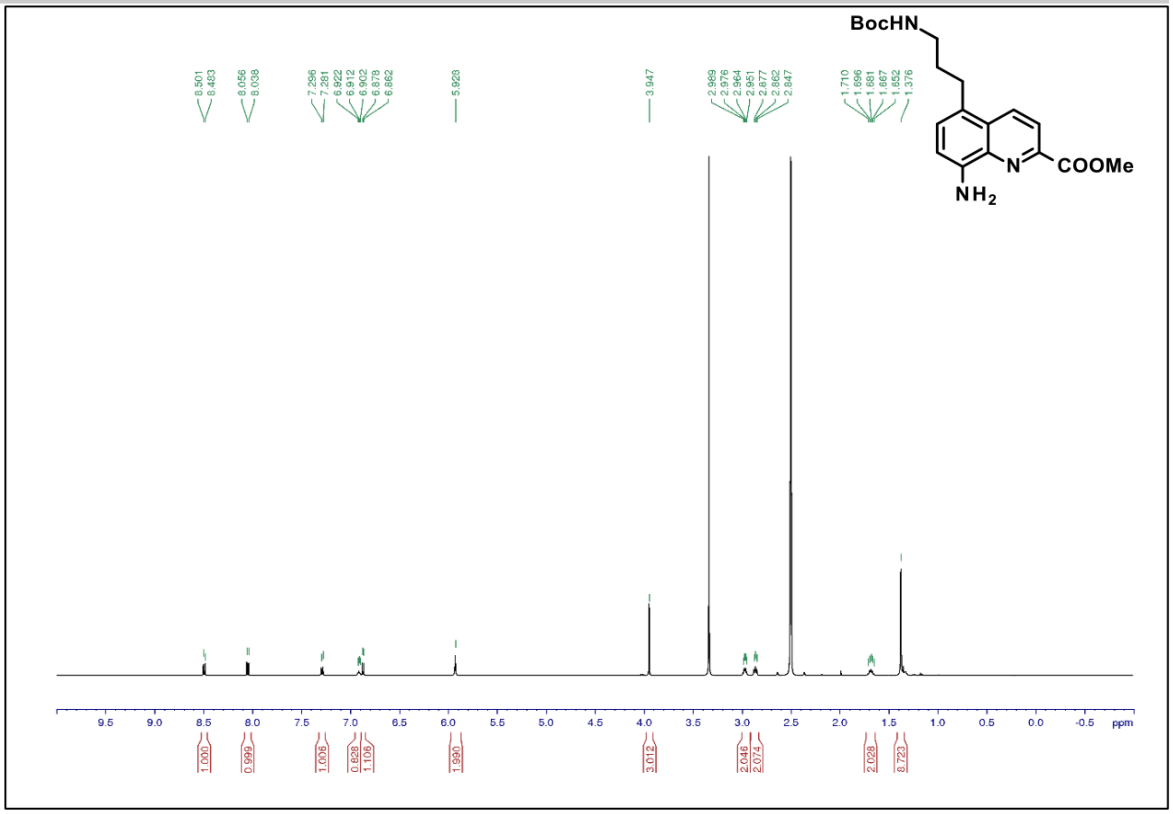

Figure S49. ^{1}H NMR (500 MHz, DMSO-d_6) of compound **9e**.

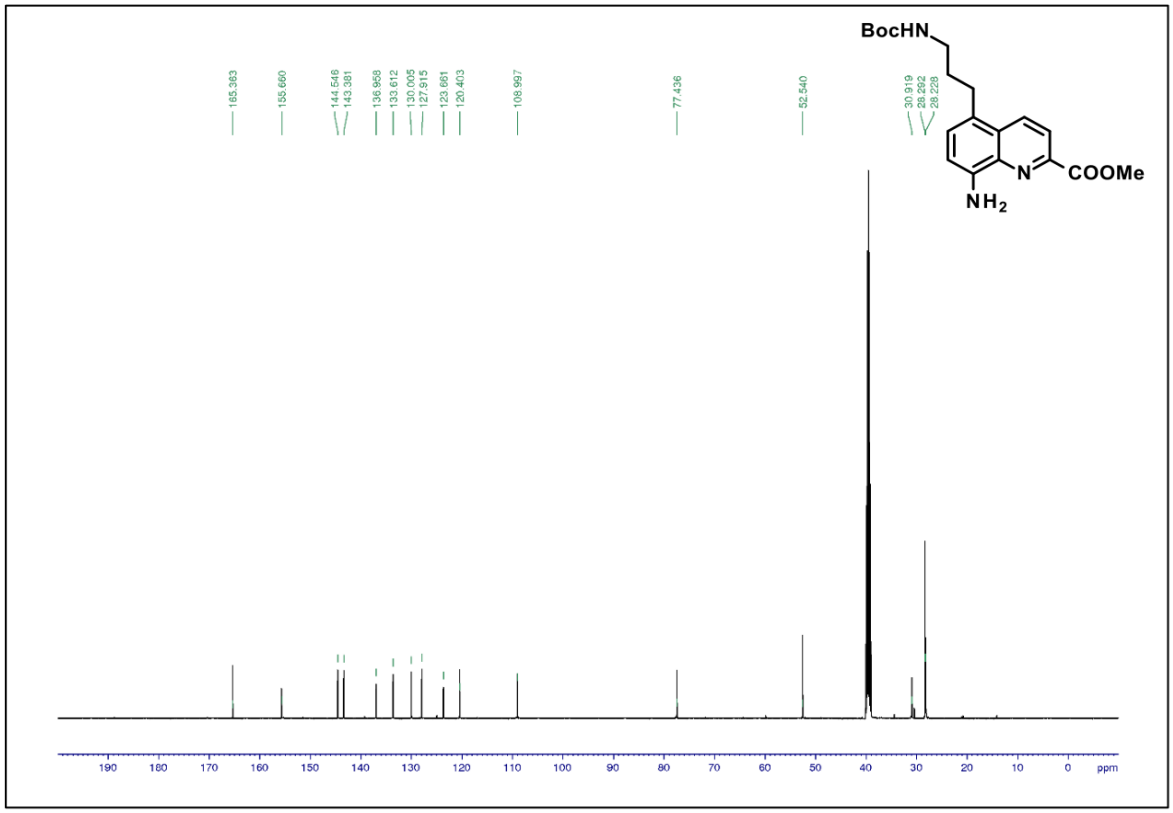

Figure S50. $^{13}C\{^{1}H\}$ NMR (125 MHz, DMSO-d_6) of compound **9e**.

SUPPORTING INFORMATION

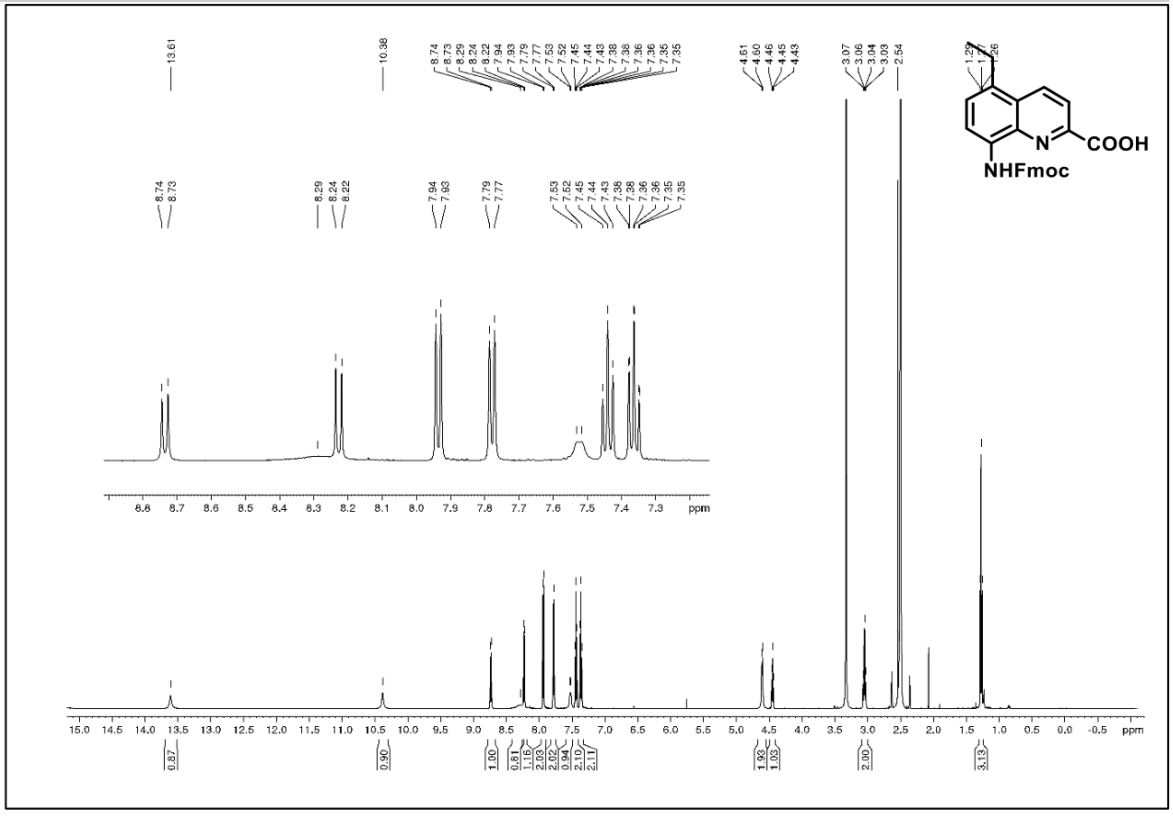

Figure S51. ^{1}H NMR (500 MHz, DMSO-d_6) of compound **10a**.

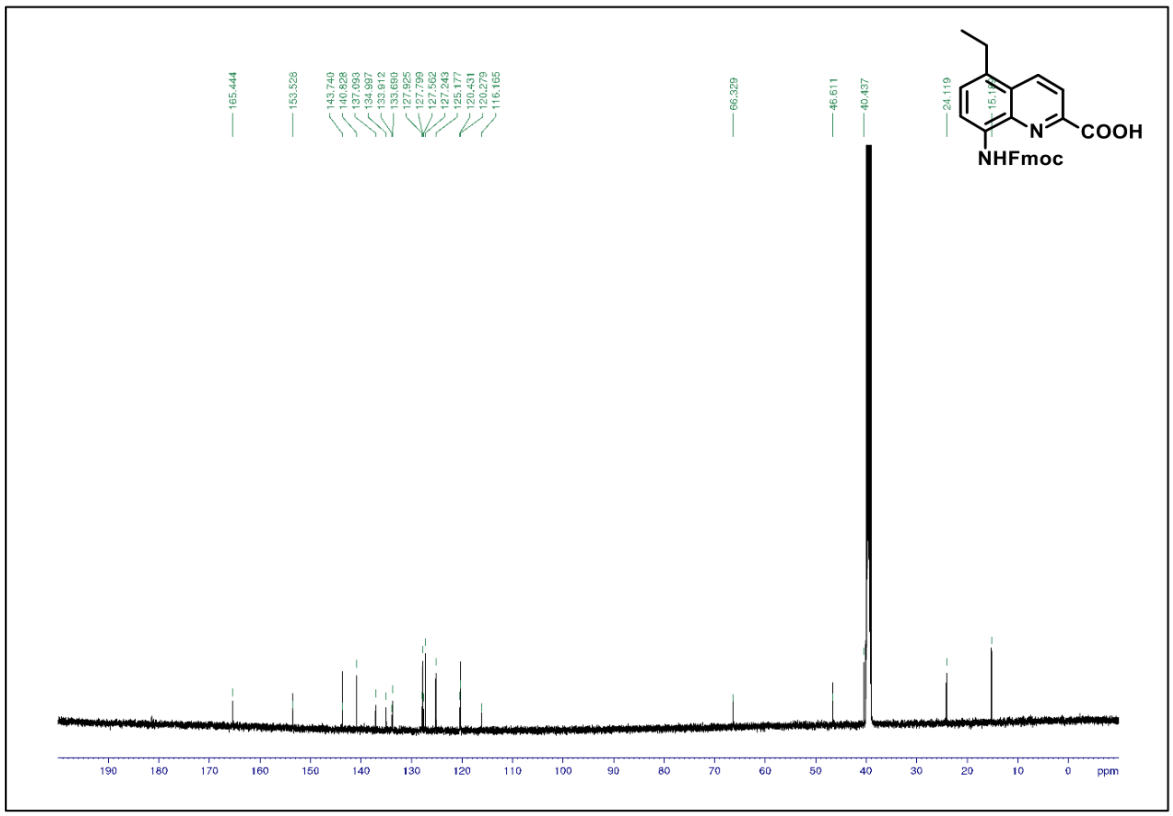

Figure S52. $^{13}C\{^{1}H\}$ NMR (125 MHz, DMSO-d_6) of compound **10a**.

SUPPORTING INFORMATION

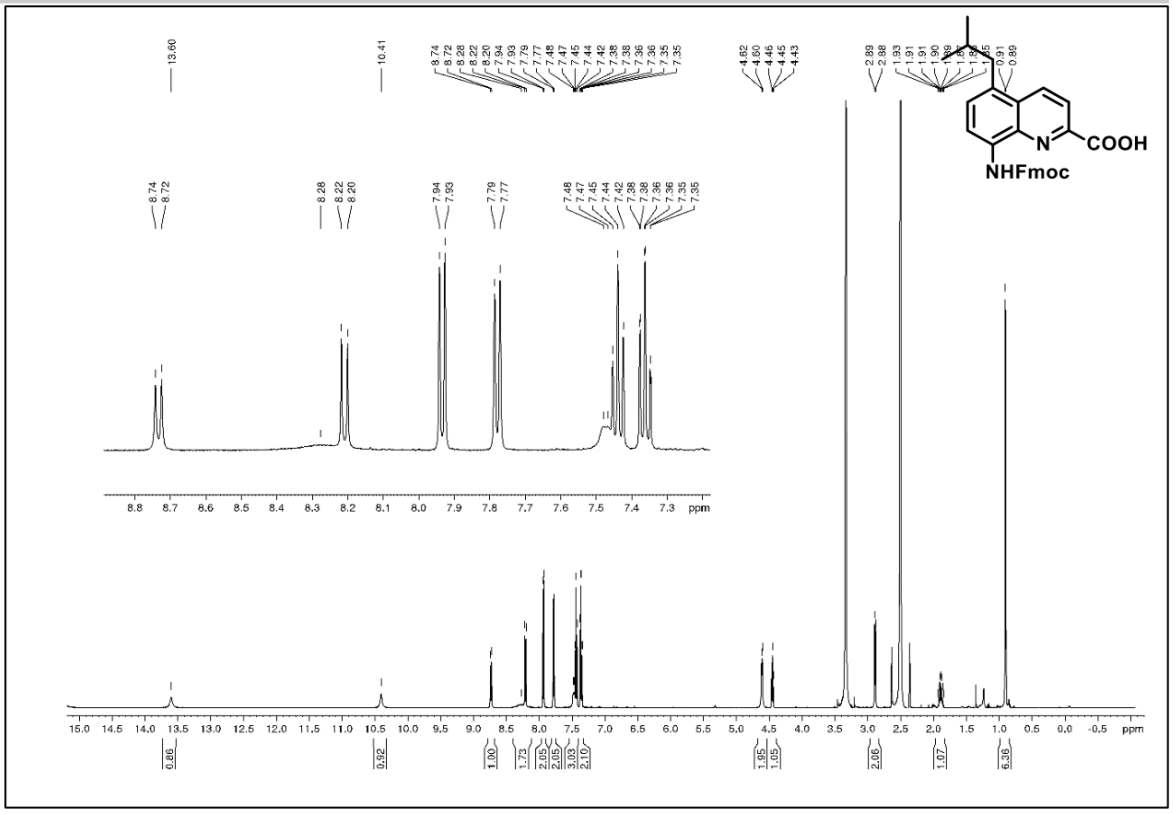

Figure S53. ^{1}H NMR (500 MHz, DMSO-d_6) of compound **10b**.

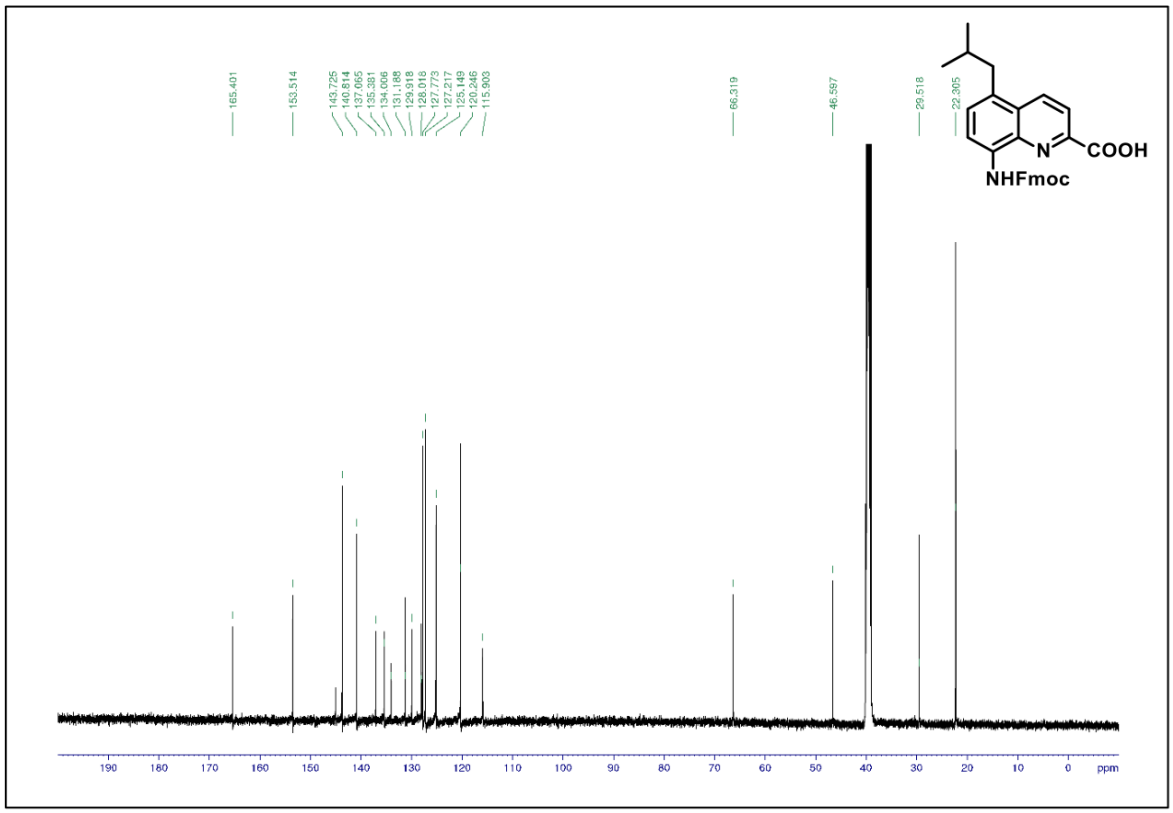

Figure S54. ^{13}C{^{1}H} NMR (125 MHz, DMSO-d_6) of compound **10b**.

SUPPORTING INFORMATION

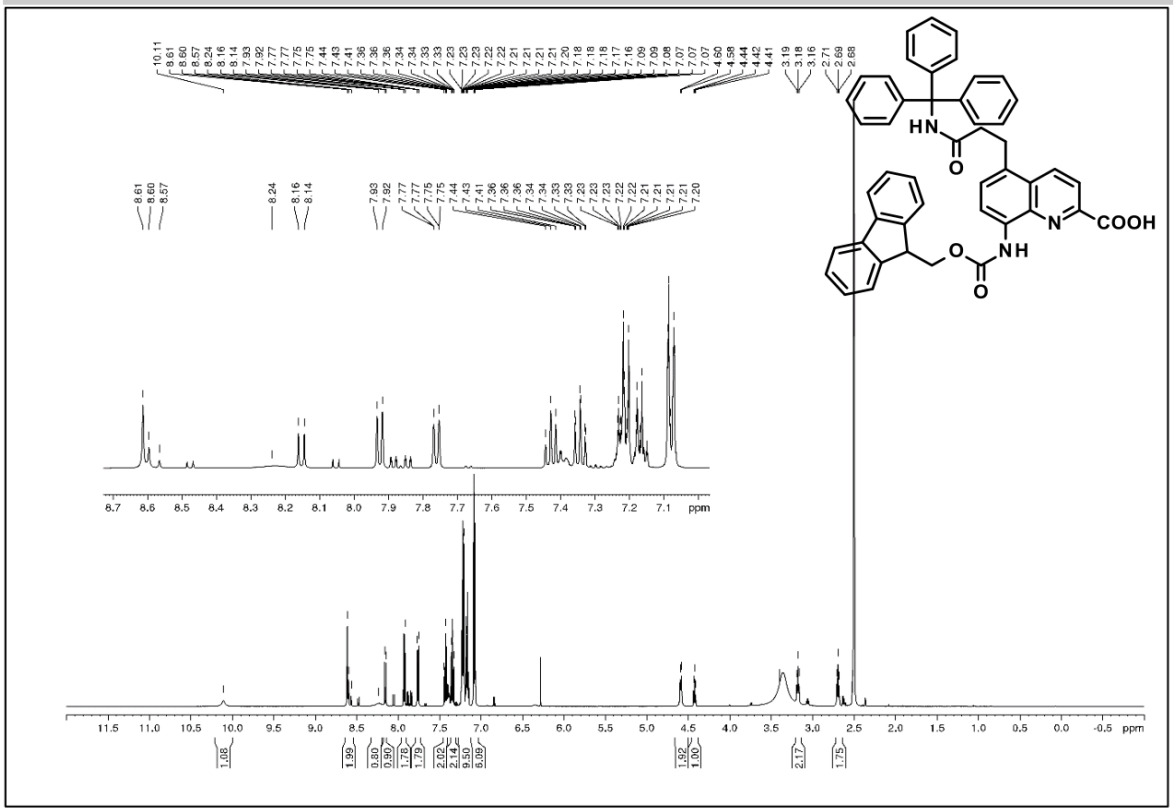

Figure S55. ^{1}H NMR (500 MHz, DMSO-d_6) of compound **10c**.

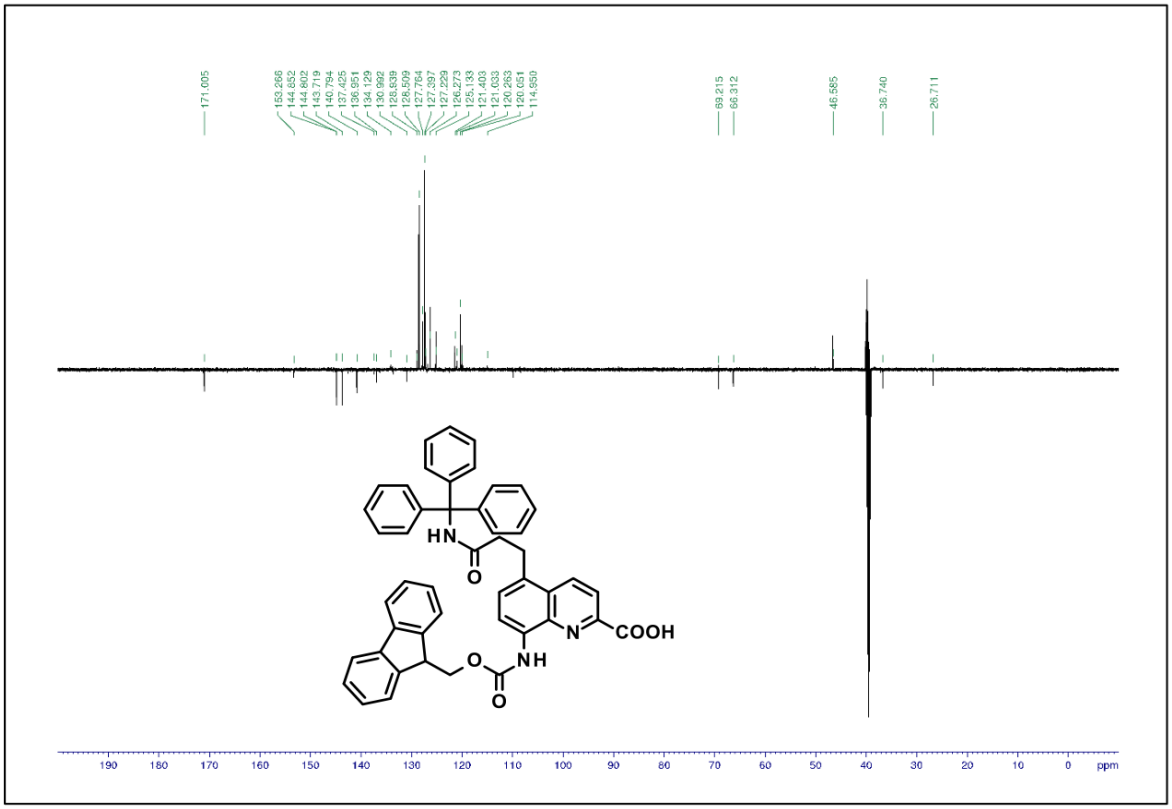

Figure S56. DEPT ^{13}C NMR (125 MHz, DMSO-d_6) of compound **10c**.

SUPPORTING INFORMATION

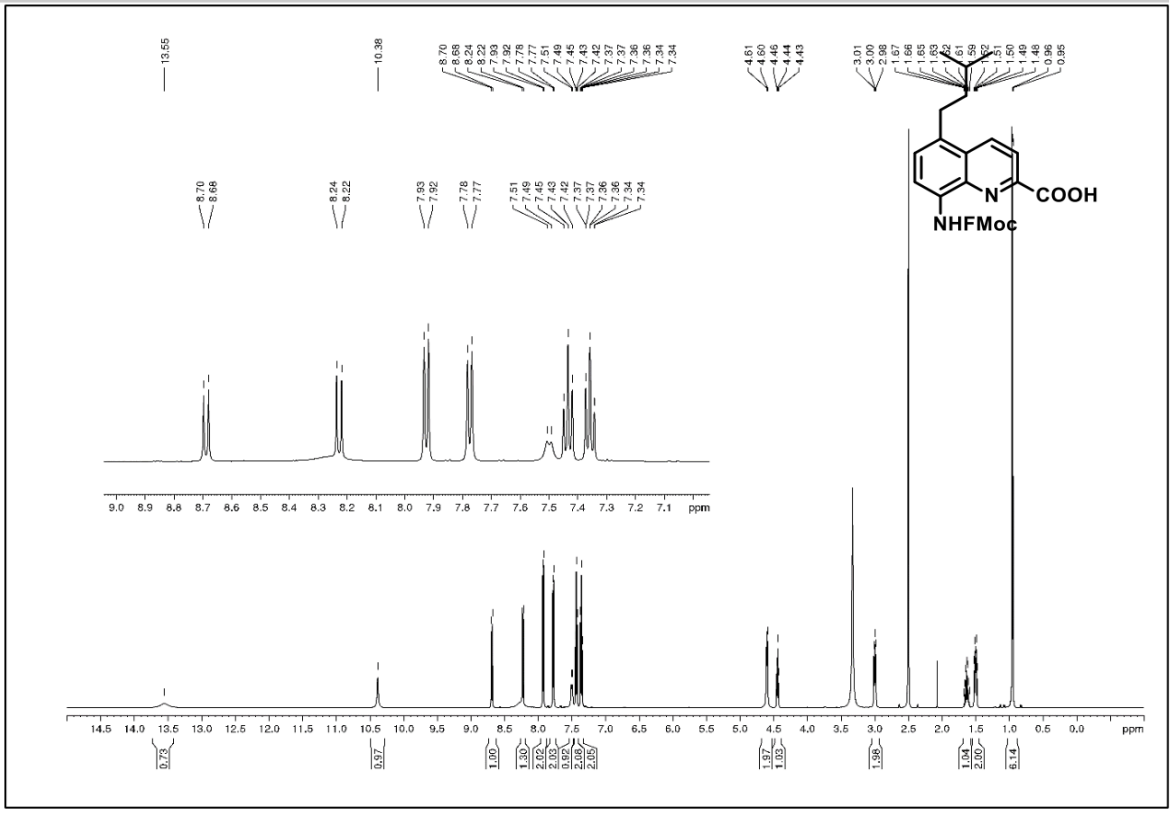

Figure S57. ^{1}H NMR (500 MHz, DMSO-d_6) of compound **10d**.

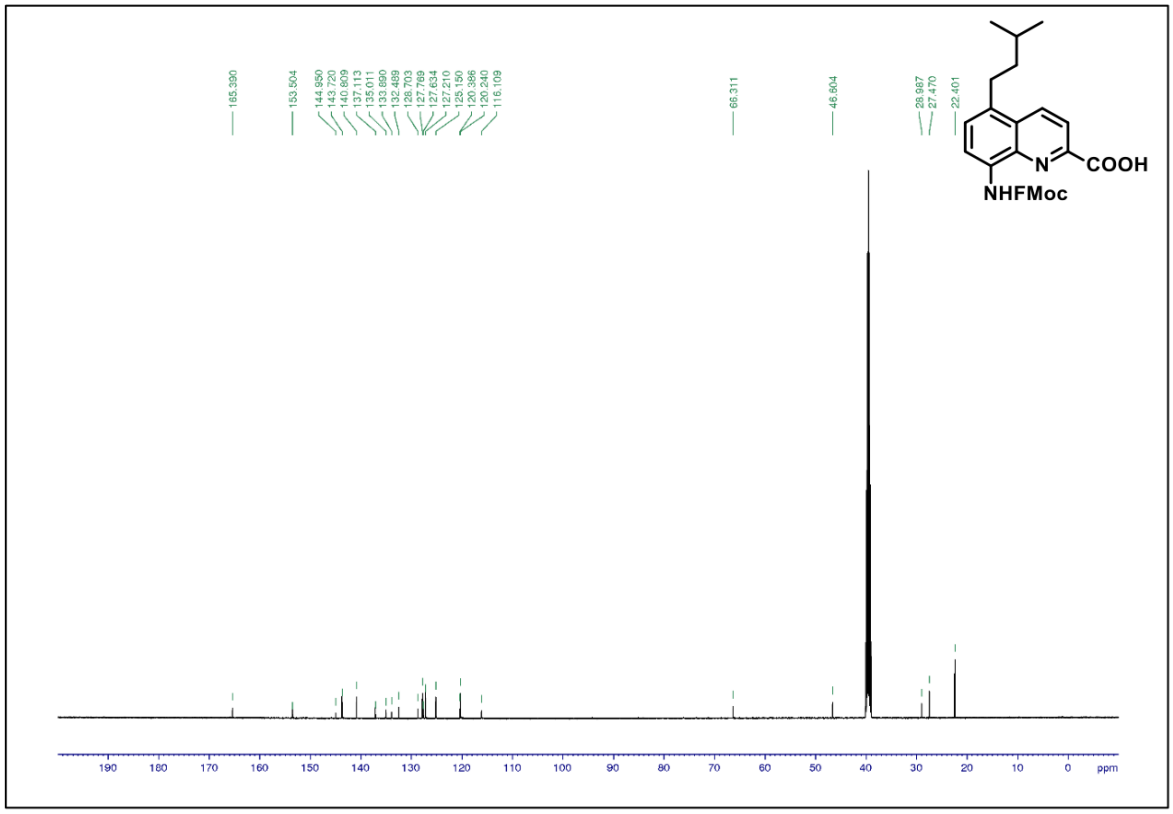

Figure S58. ^{13}C{^{1}H} NMR (125 MHz, DMSO-d_6) of compound **10d**.

SUPPORTING INFORMATION

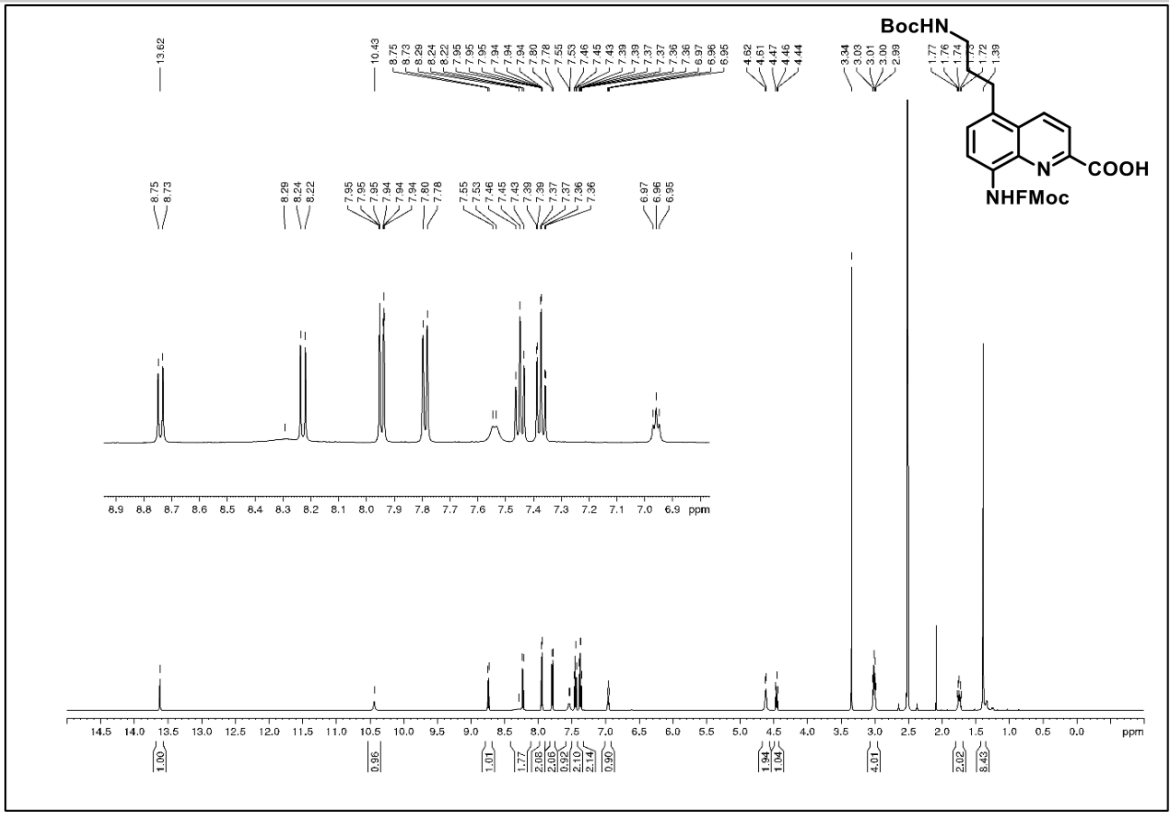

Figure S59. ^{1}H NMR (500 MHz, DMSO-d_6) of compound **10e**.

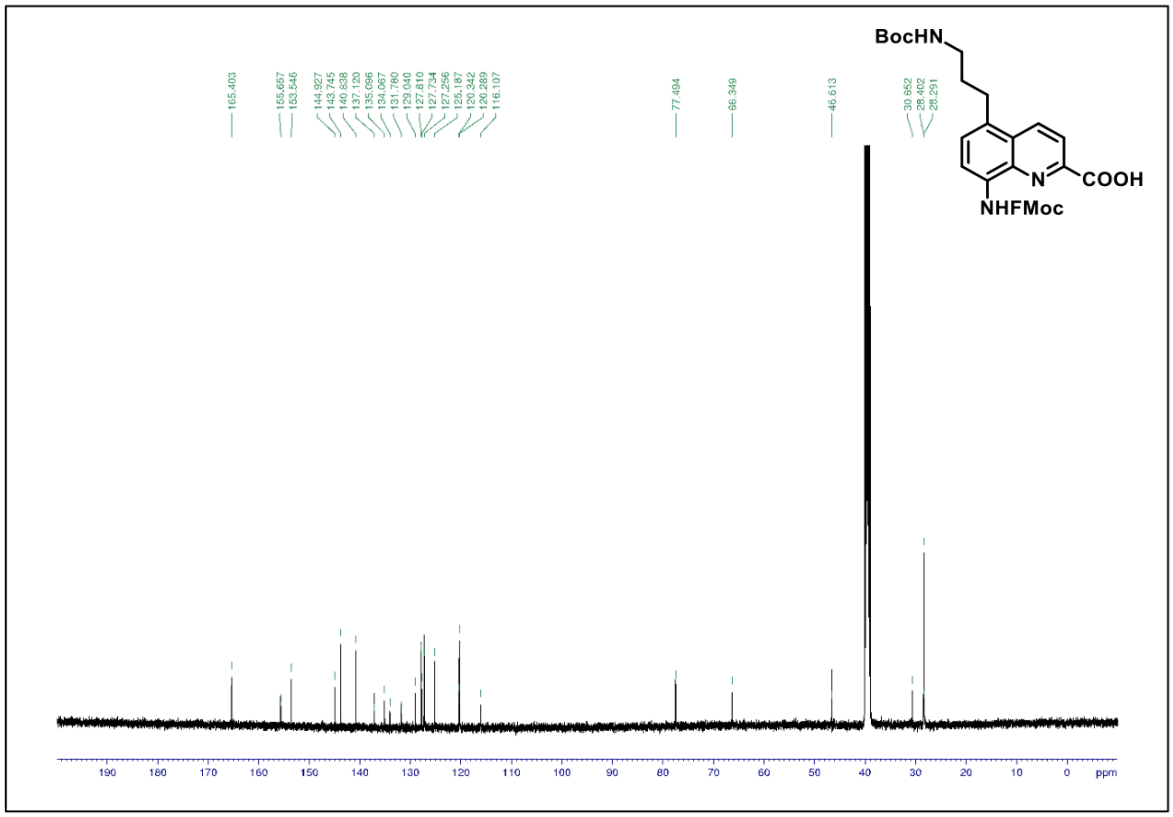

Figure S60. ^{13}C{^{1}H} NMR (125 MHz, DMSO-d_6) of compound **10e**.

SUPPORTING INFORMATION

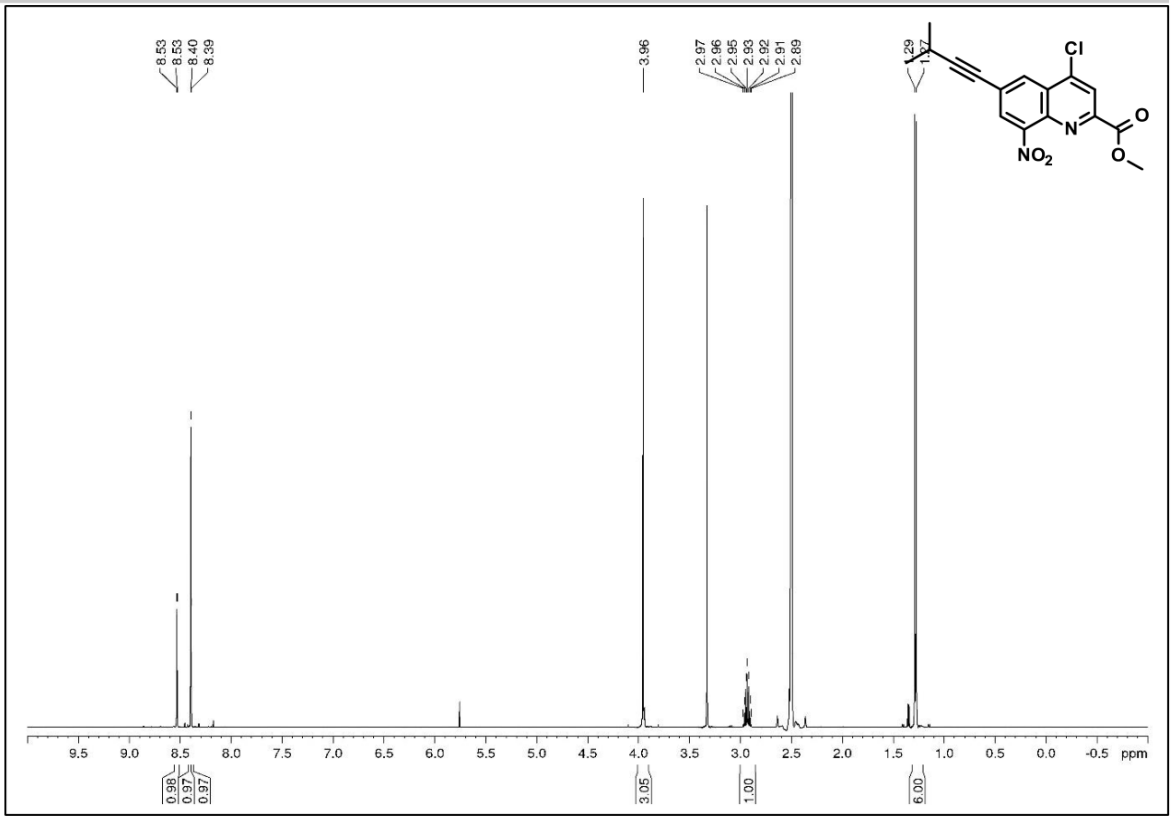

Figure S61. ^{1}H NMR (500 MHz, DMSO-d_6) of compound **11a**.

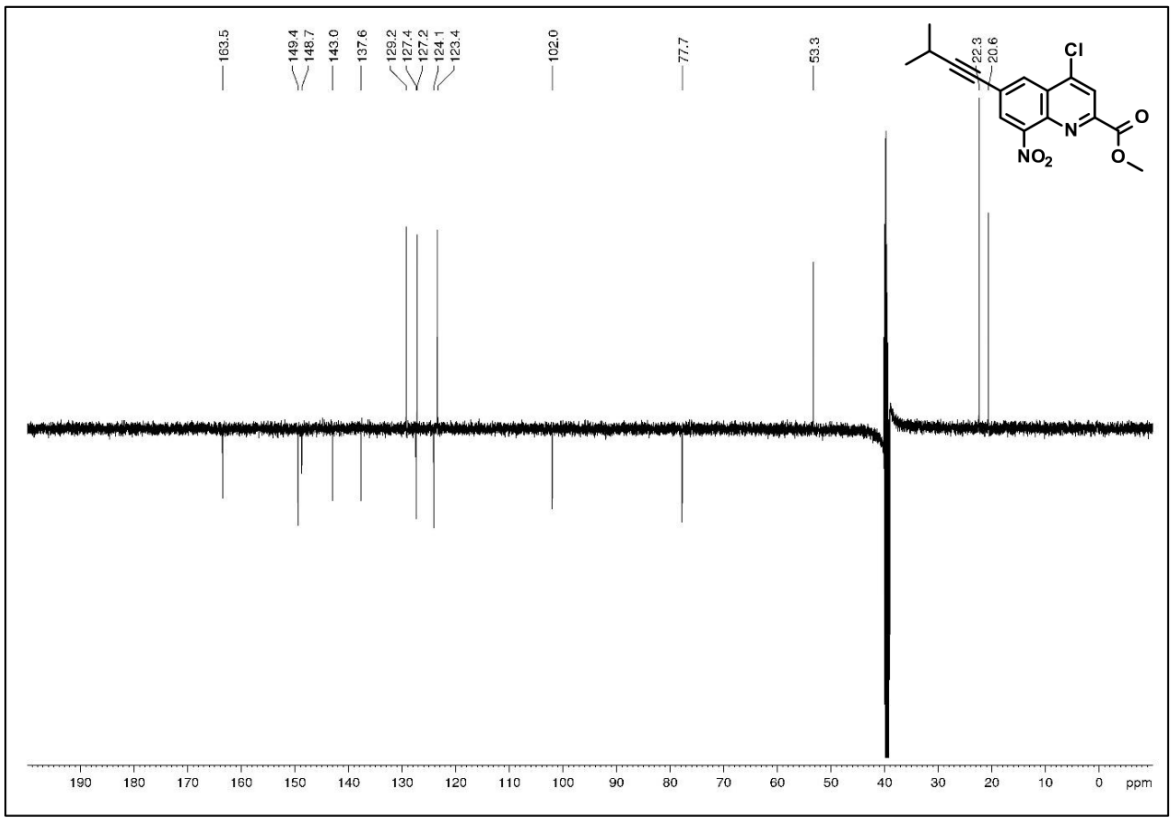

Figure S62. DEPT ^{13}C NMR (125 MHz, DMSO-d_6) of compound **11a**.

SUPPORTING INFORMATION

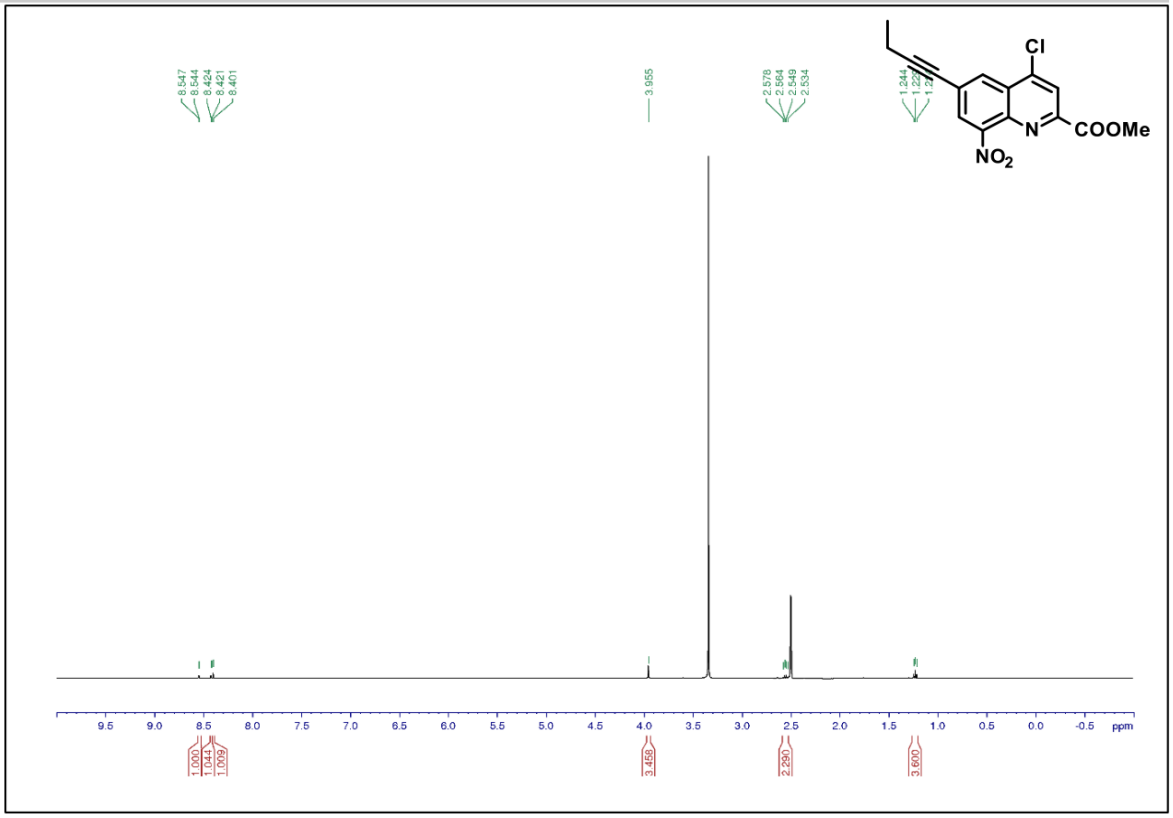

Figure S63. ^{1}H NMR (500 MHz, DMSO-d_6) of compound **11b**.

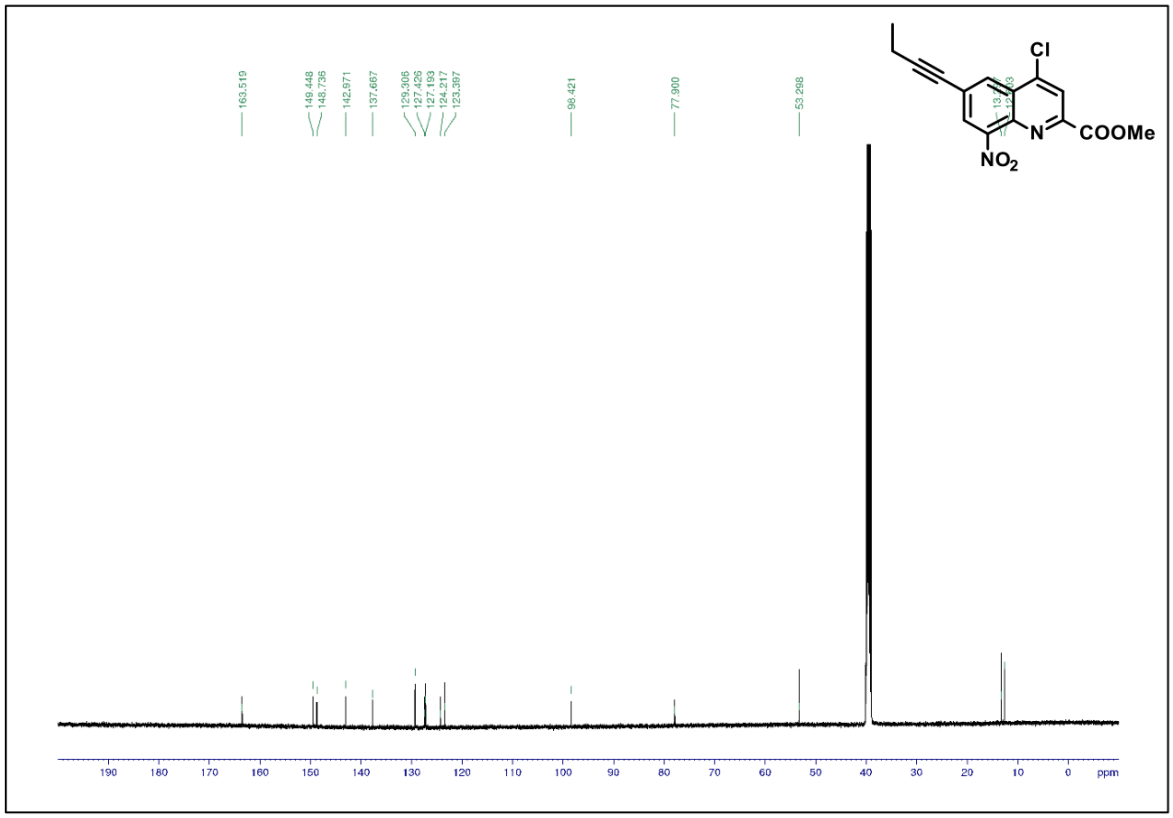

Figure S64. ^{13}C{^{1}H} NMR (125 MHz, DMSO-d_6) of compound **11b**.

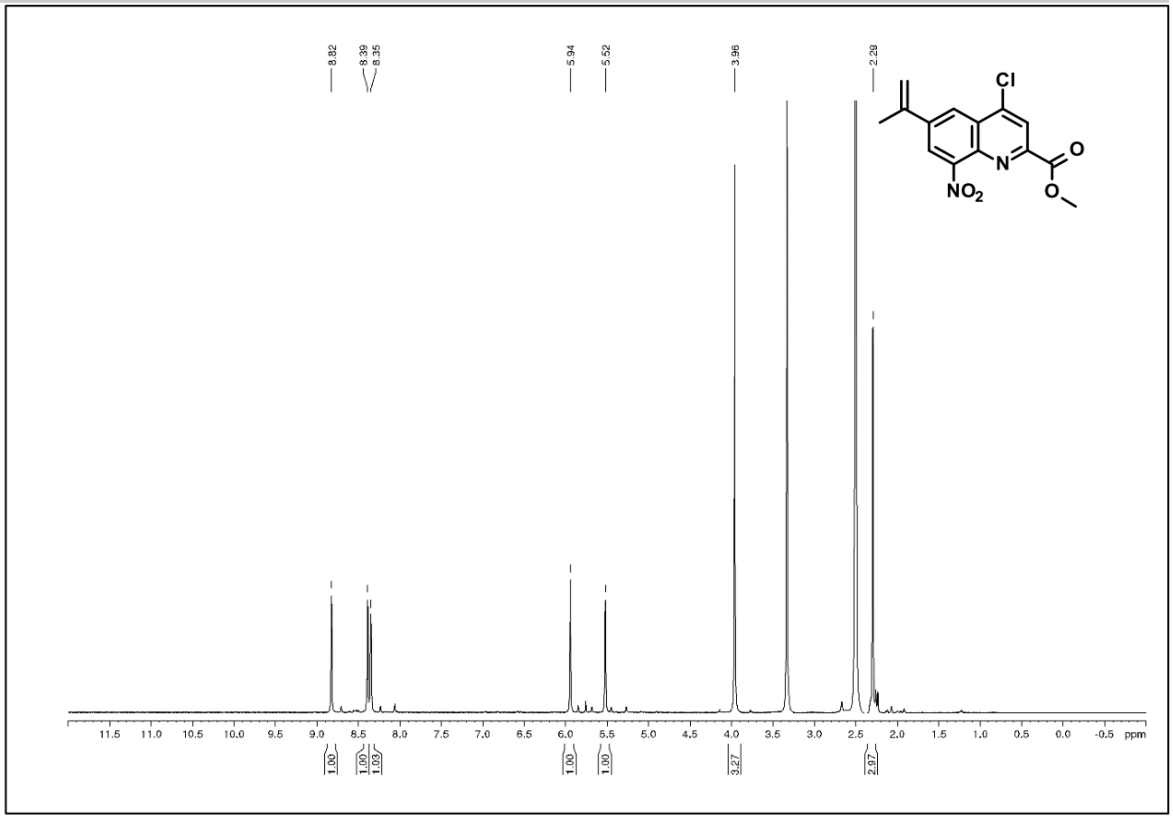

Figure S65. ^{1}H NMR (500 MHz, DMSO-d_6) of compound **11c**.

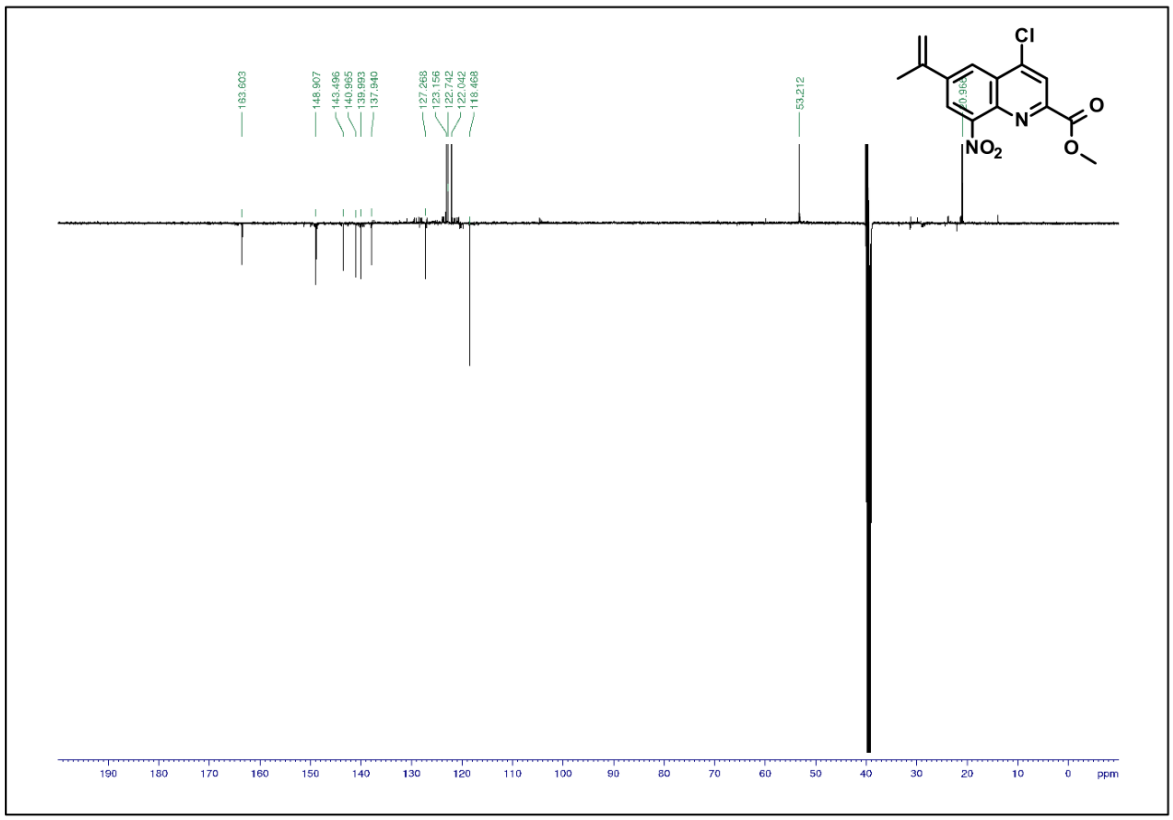

Figure S66. DEPT ^{13}C NMR (125 MHz, DMSO-d_6) of compound **11c**.

SUPPORTING INFORMATION

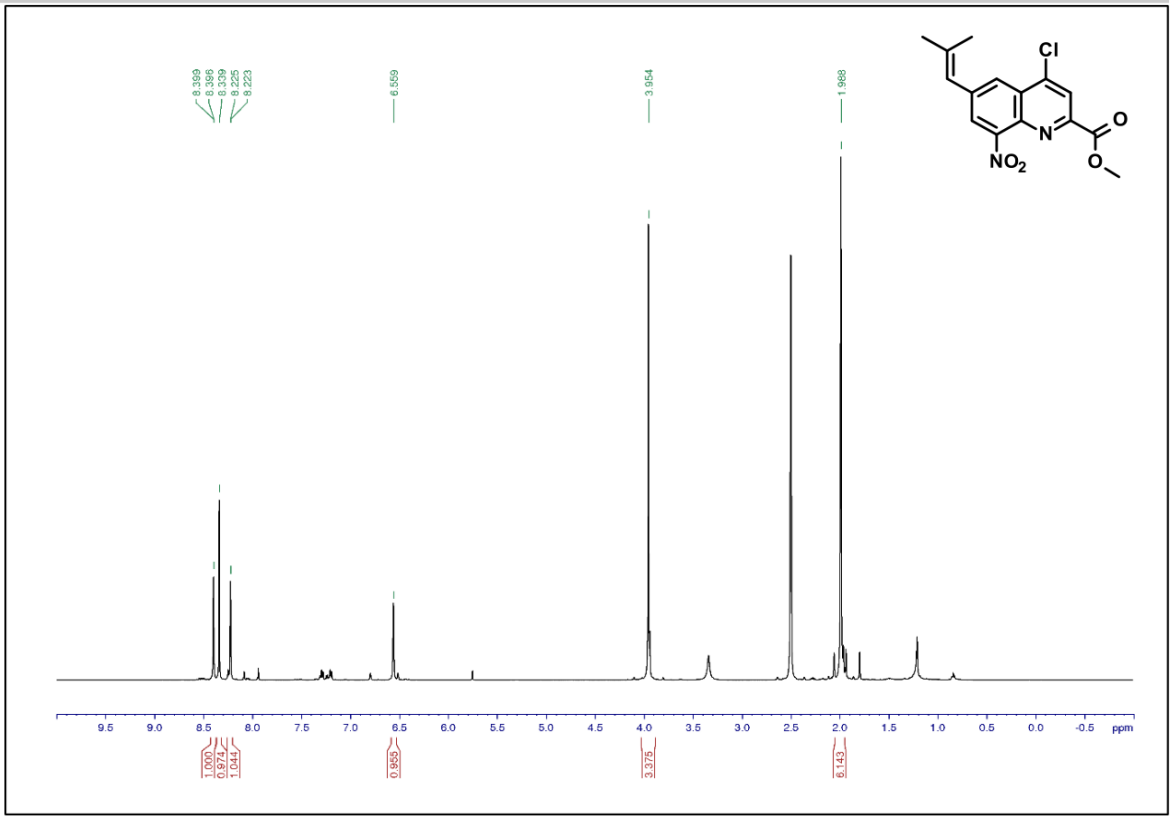

Figure S67. ^{1}H NMR (500 MHz, DMSO-d_6) of compound **11d**.

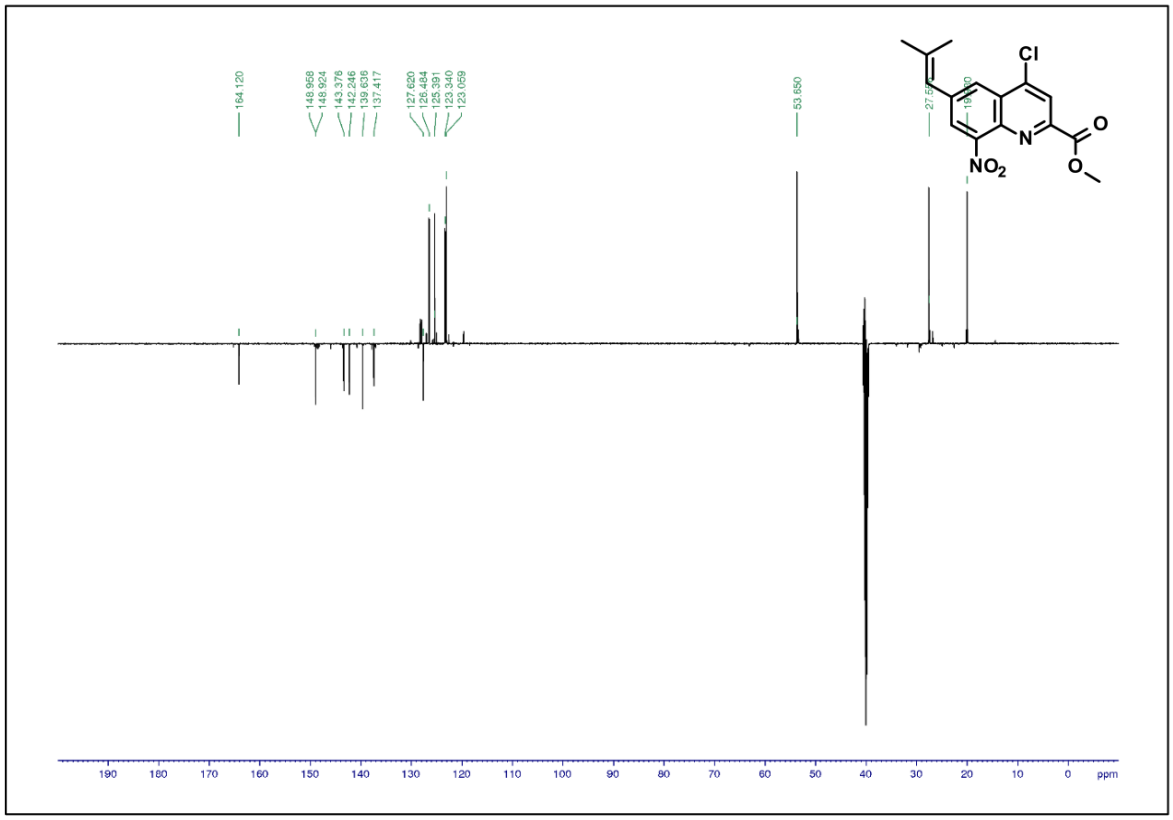

Figure S68. DEPT ^{13}C NMR (125 MHz, DMSO-d_6) of compound **11d**.

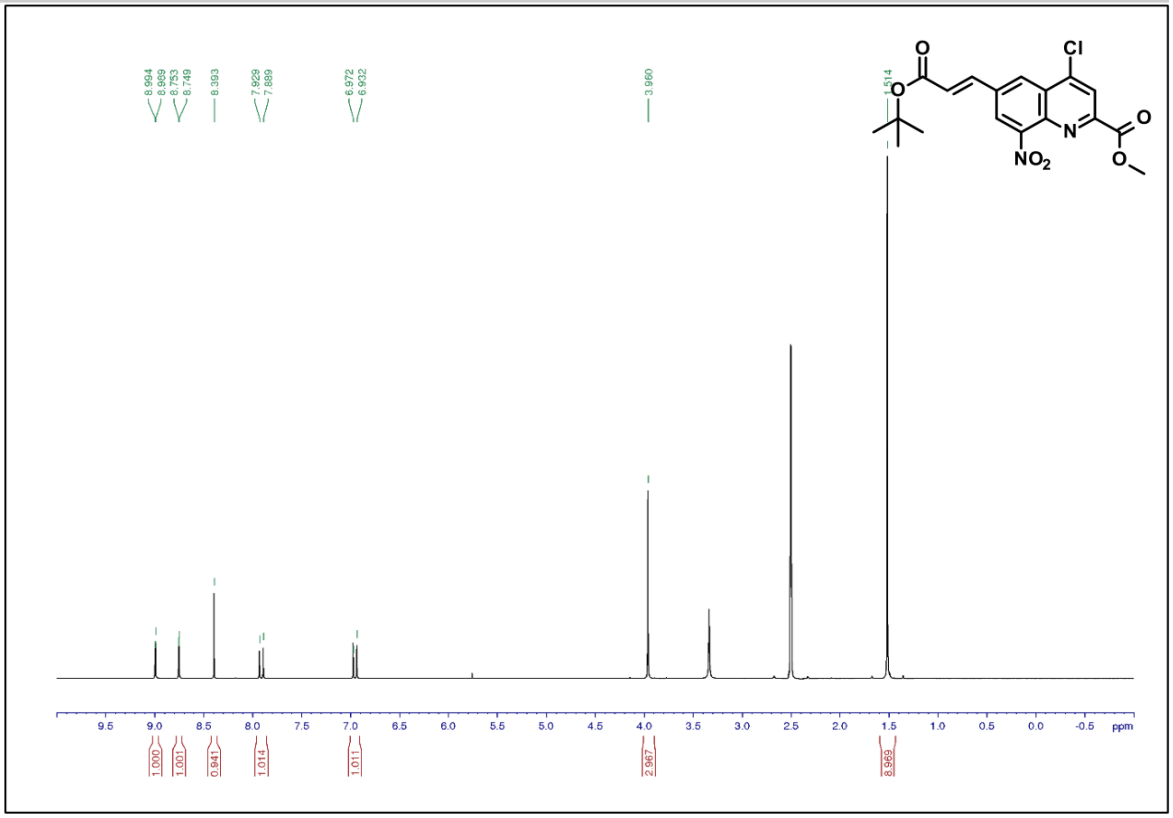

Figure S69. ^{1}H NMR (500 MHz, DMSO-d_6) of compound **11e**.

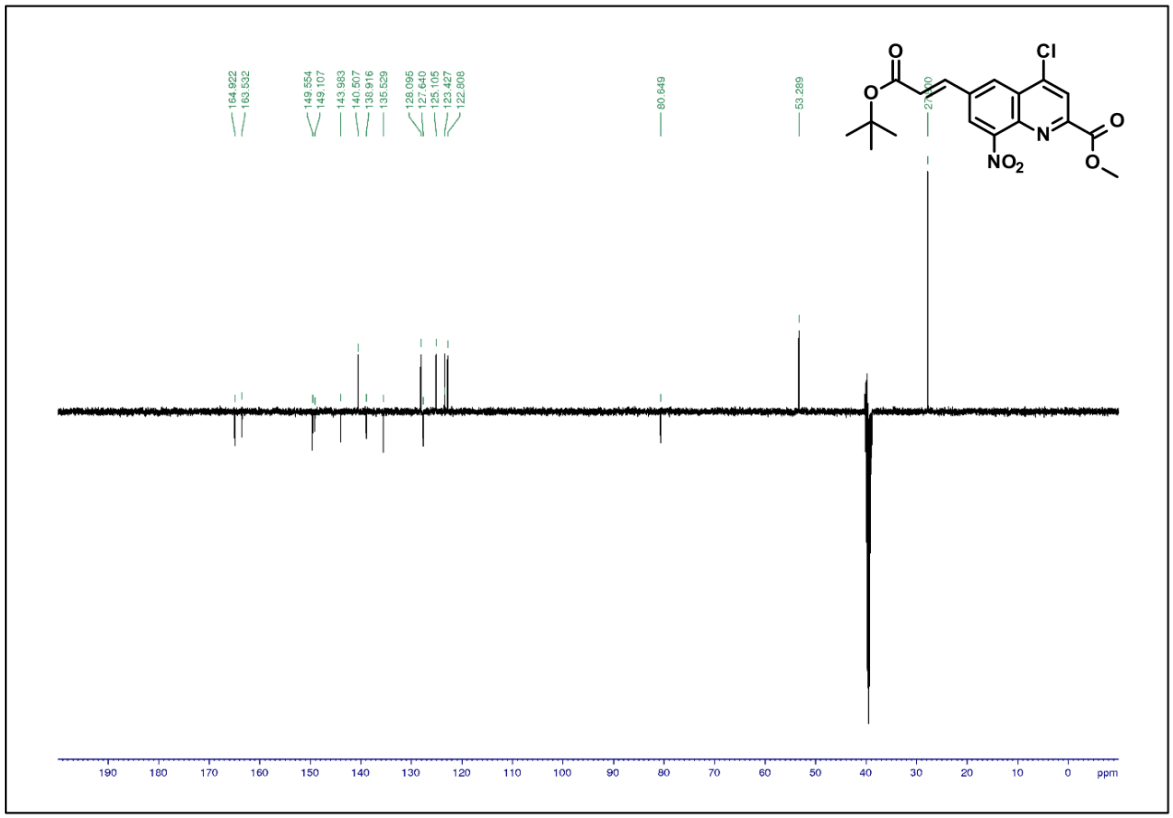

Figure S70. DEPT ^{13}C NMR (125 MHz, DMSO-d_6) of compound **11e**.

SUPPORTING INFORMATION

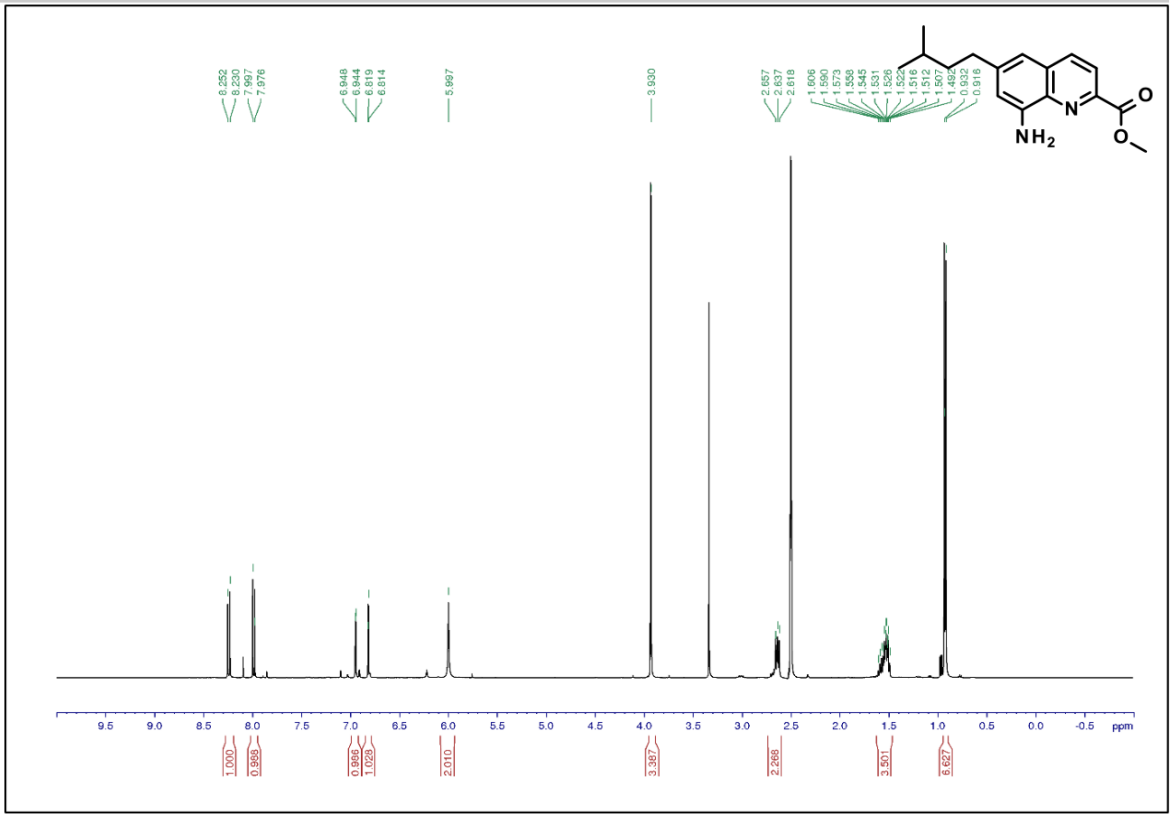

Figure S71. ^{1}H NMR (500 MHz, DMSO-d_6) of compound **12a**.

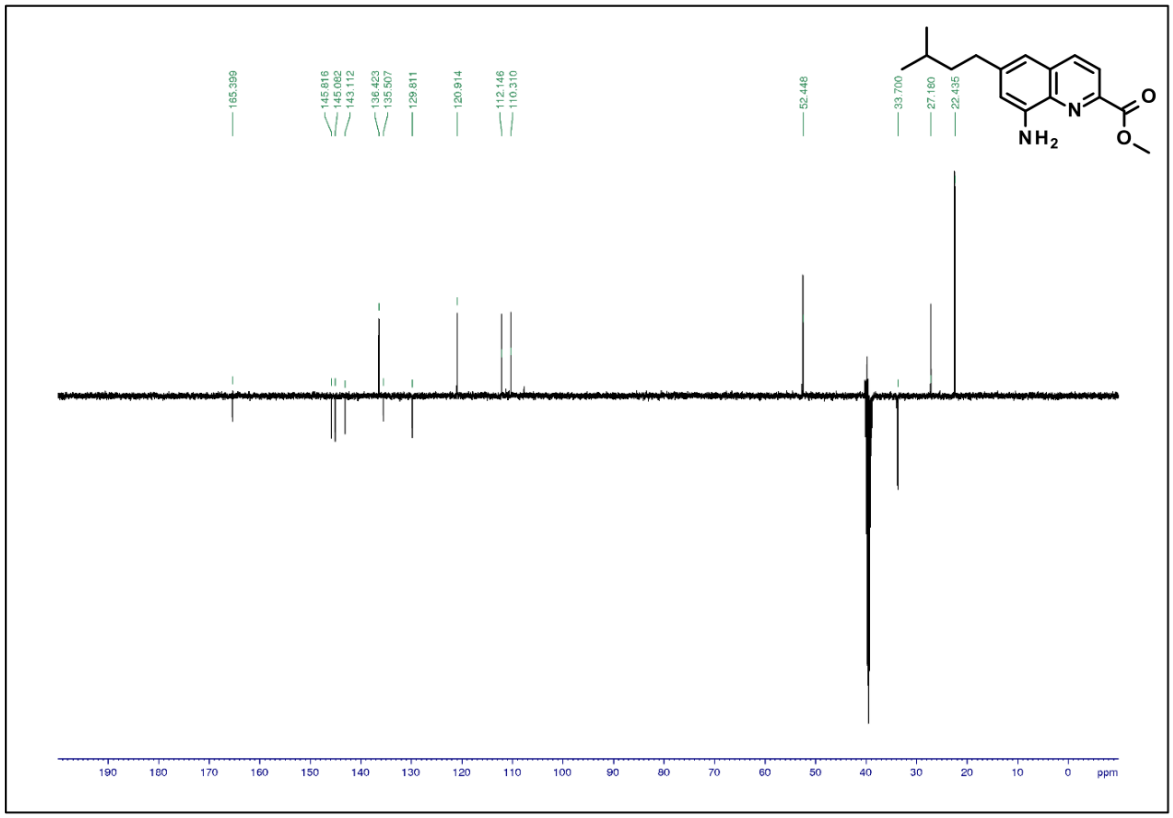

Figure S72. DEPT ^{13}C NMR (125 MHz, DMSO-d_6) of compound **12a**.

SUPPORTING INFORMATION

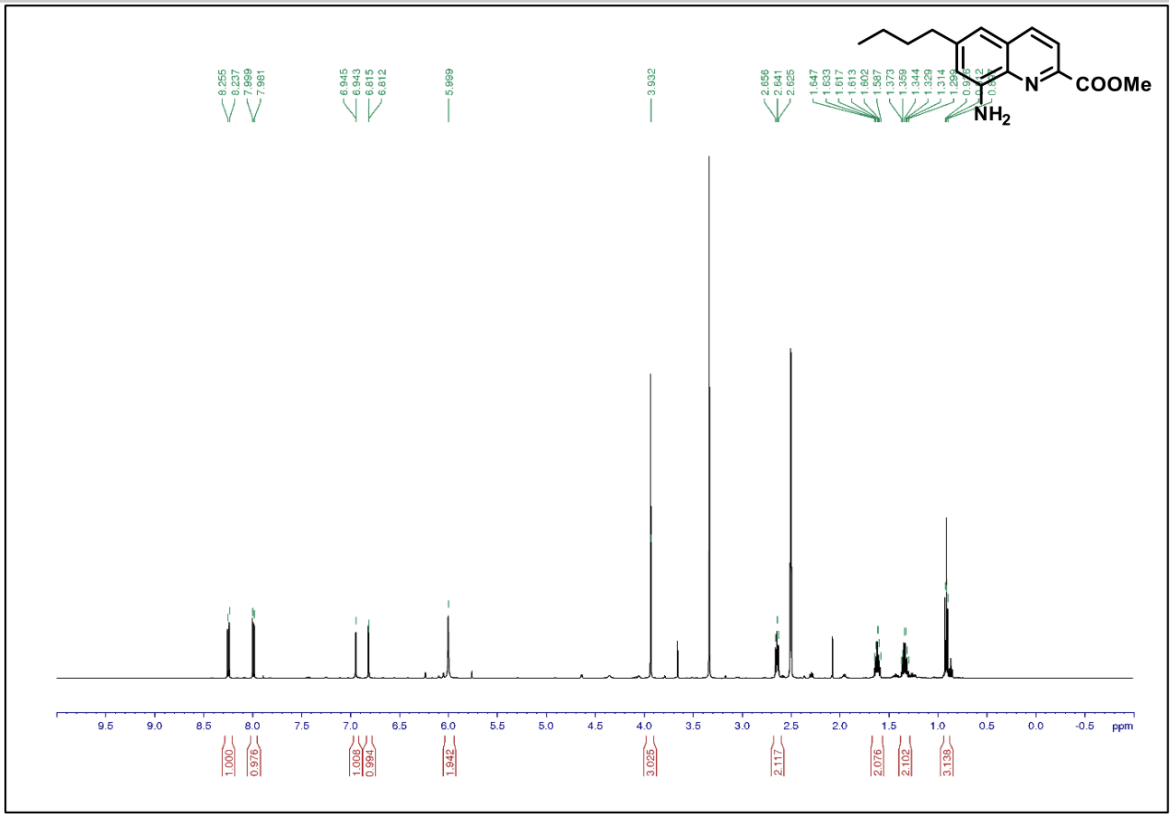

Figure S73. ^{1}H NMR (500 MHz, DMSO-d_6) of compound **12b**.

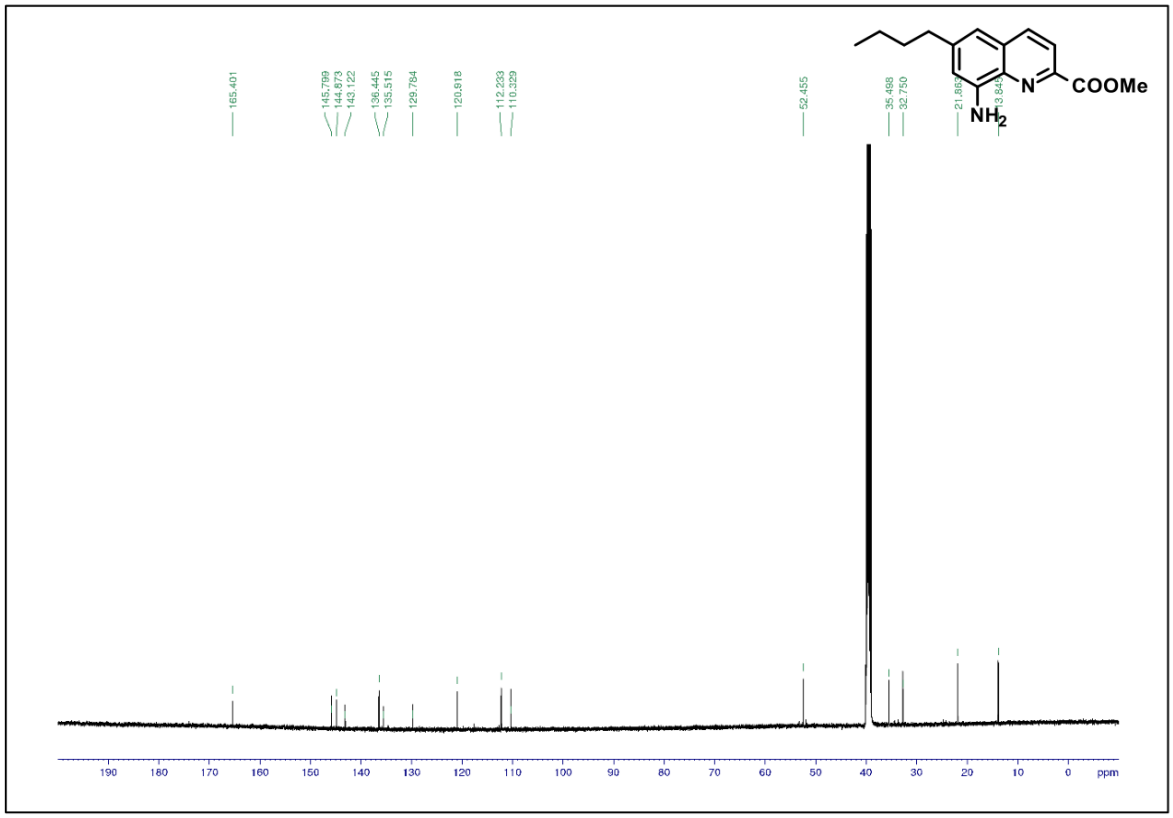

Figure S74. ^{13}C{^{1}H} NMR (125 MHz, DMSO-d_6) of compound **12b**.

SUPPORTING INFORMATION

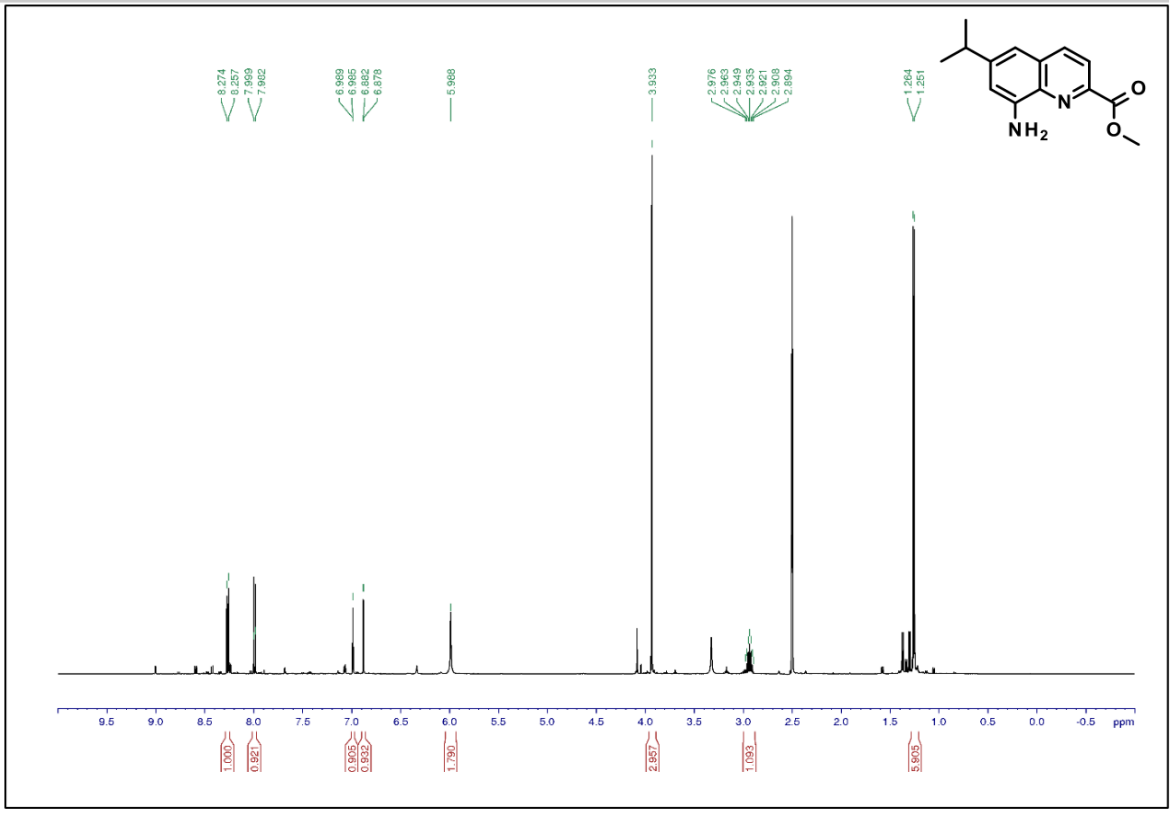

Figure S75. ^{1}H NMR (500 MHz, DMSO-d_6) of compound **12c**.

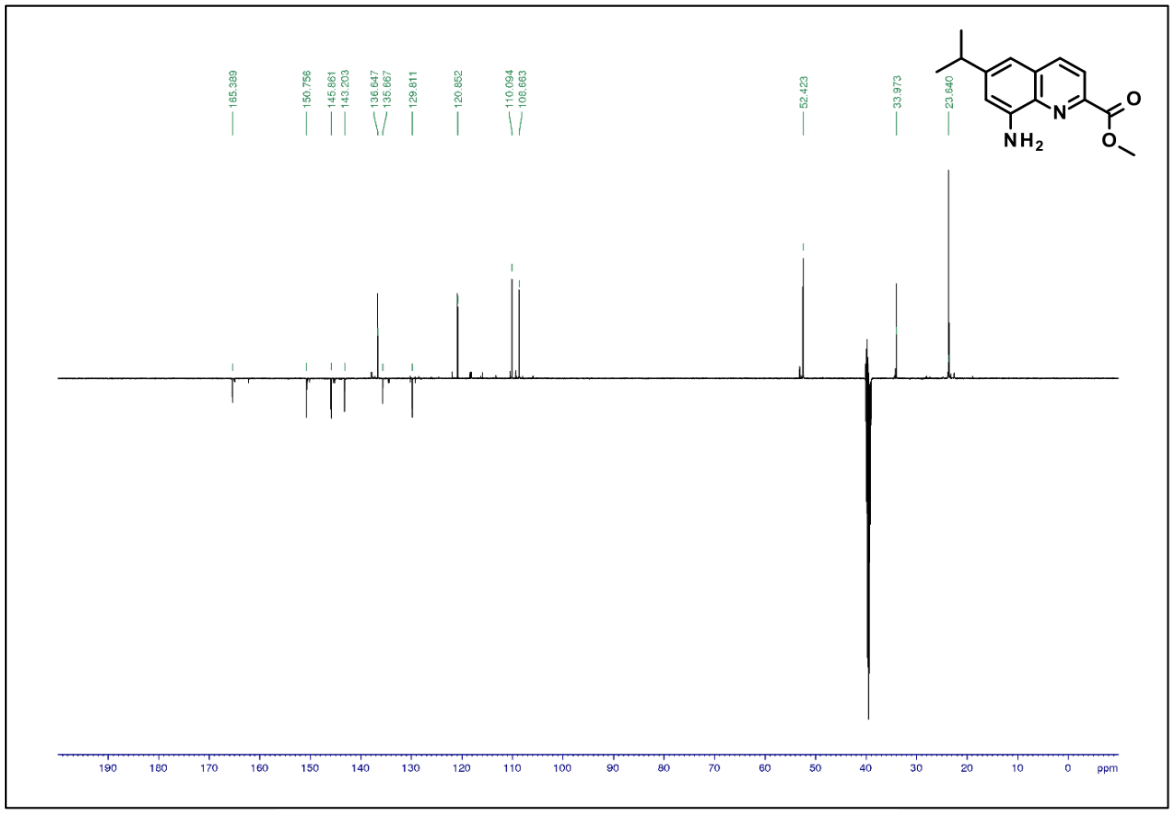

Figure S76. DEPT ^{13}C NMR (125 MHz, DMSO-d_6) of compound **12c**.

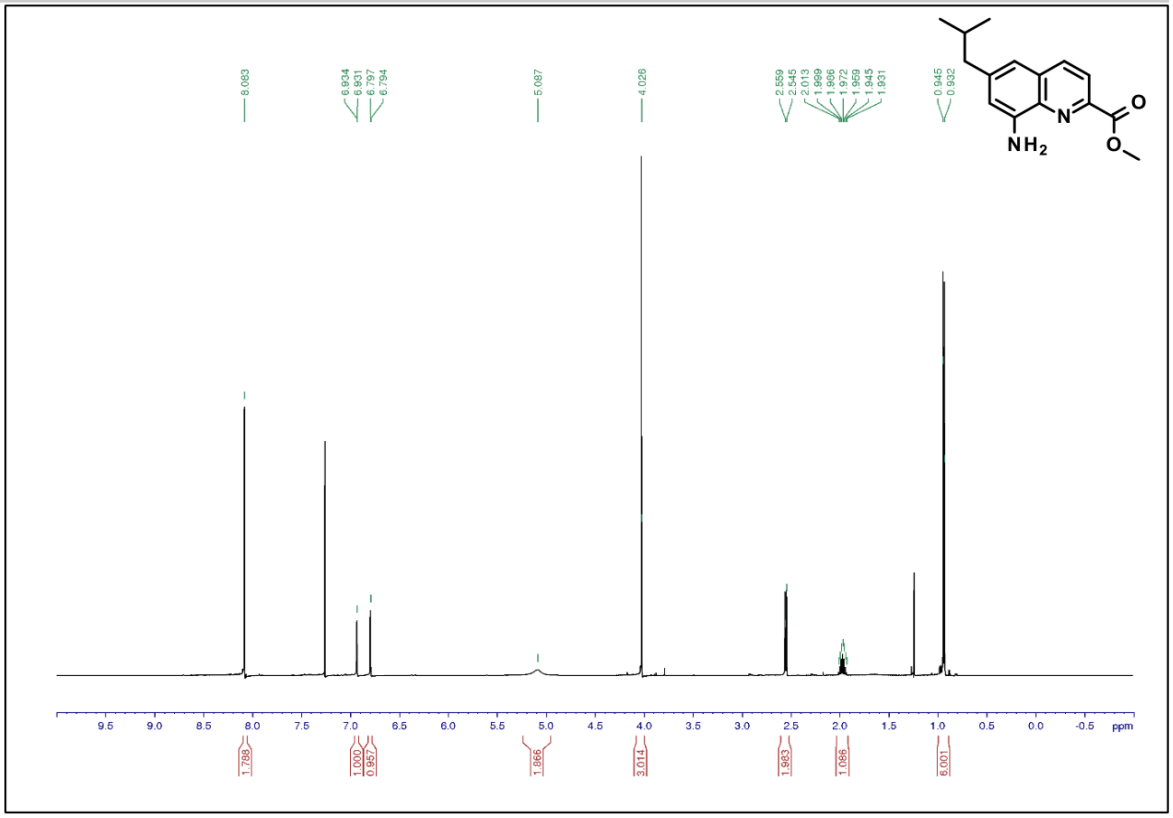

Figure S77. ^{1}H NMR (500 MHz, $CDCl_3$) of compound **12d**.

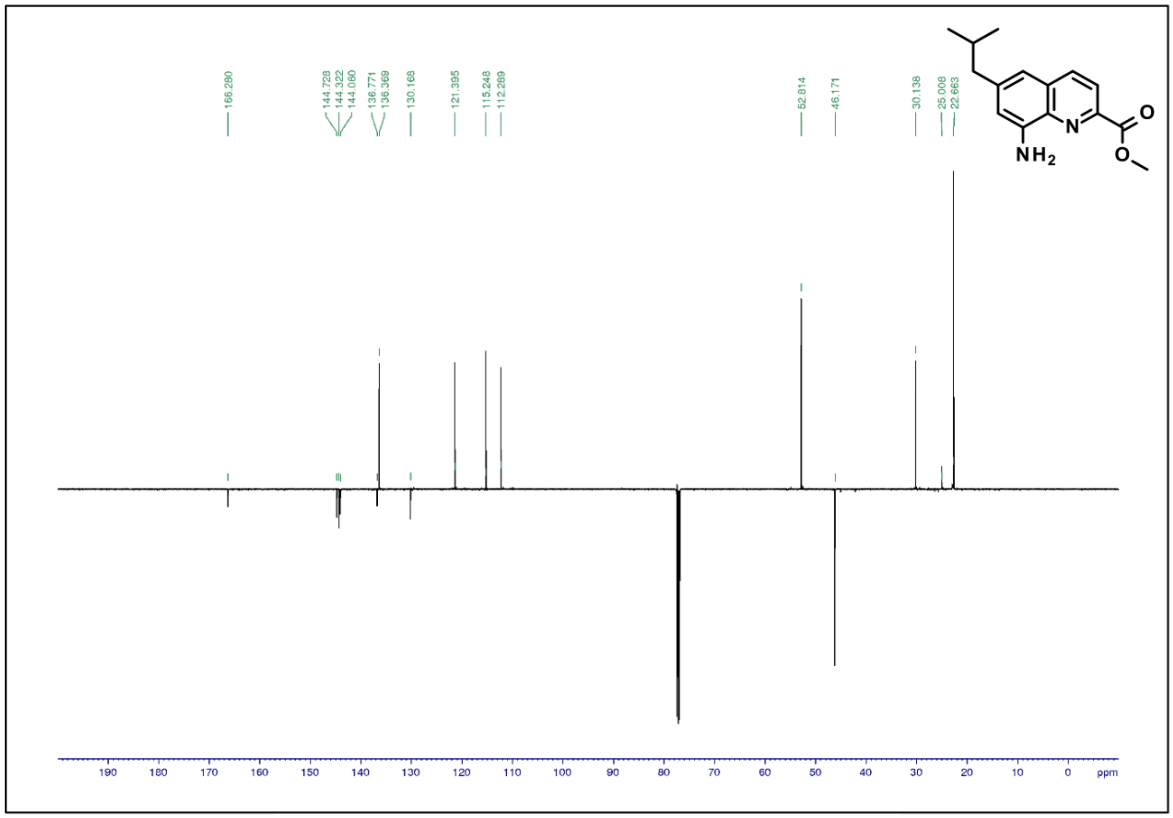

Figure S78. DEPT ^{13}C NMR (125 MHz, DMSO-d_6) of compound **12d**.

SUPPORTING INFORMATION

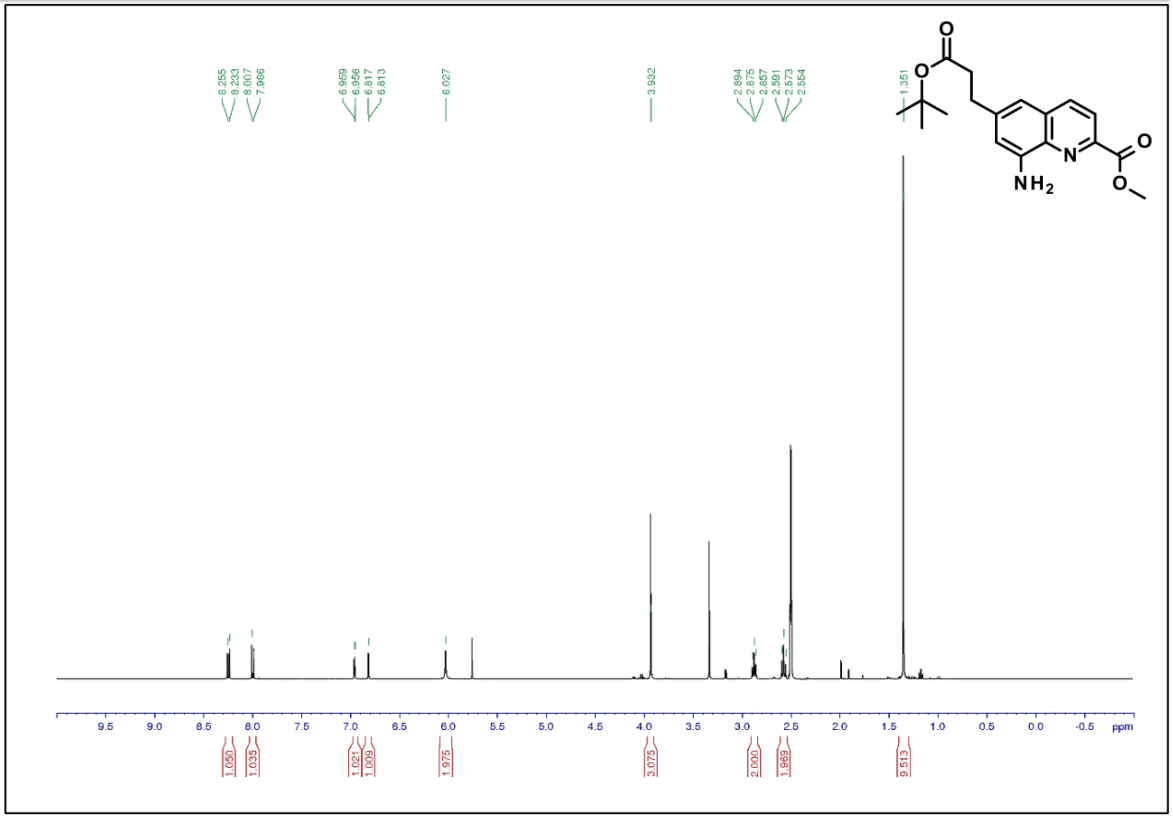

Figure S79. ^{1}H NMR (500 MHz, DMSO-d_6) of compound **12e**.

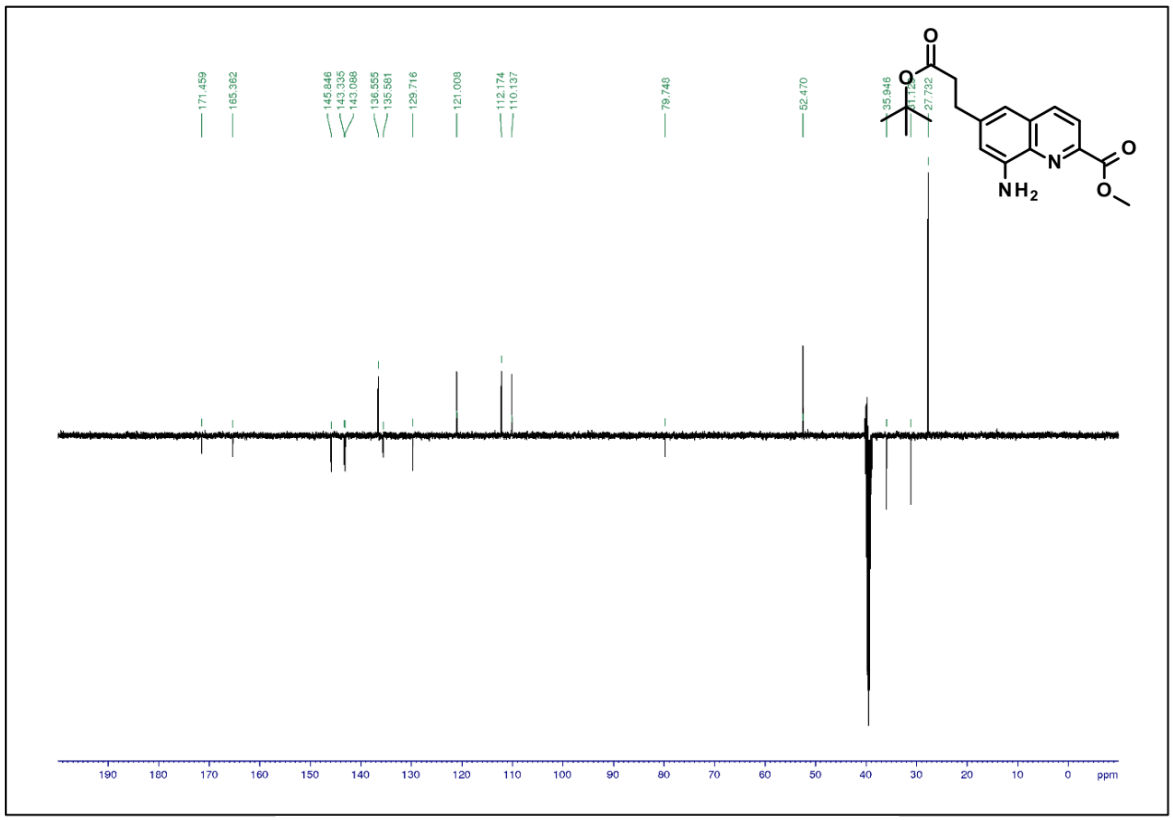

Figure S80. DEPT ^{13}C NMR (125 MHz, DMSO-d_6) of compound **12e**.

SUPPORTING INFORMATION

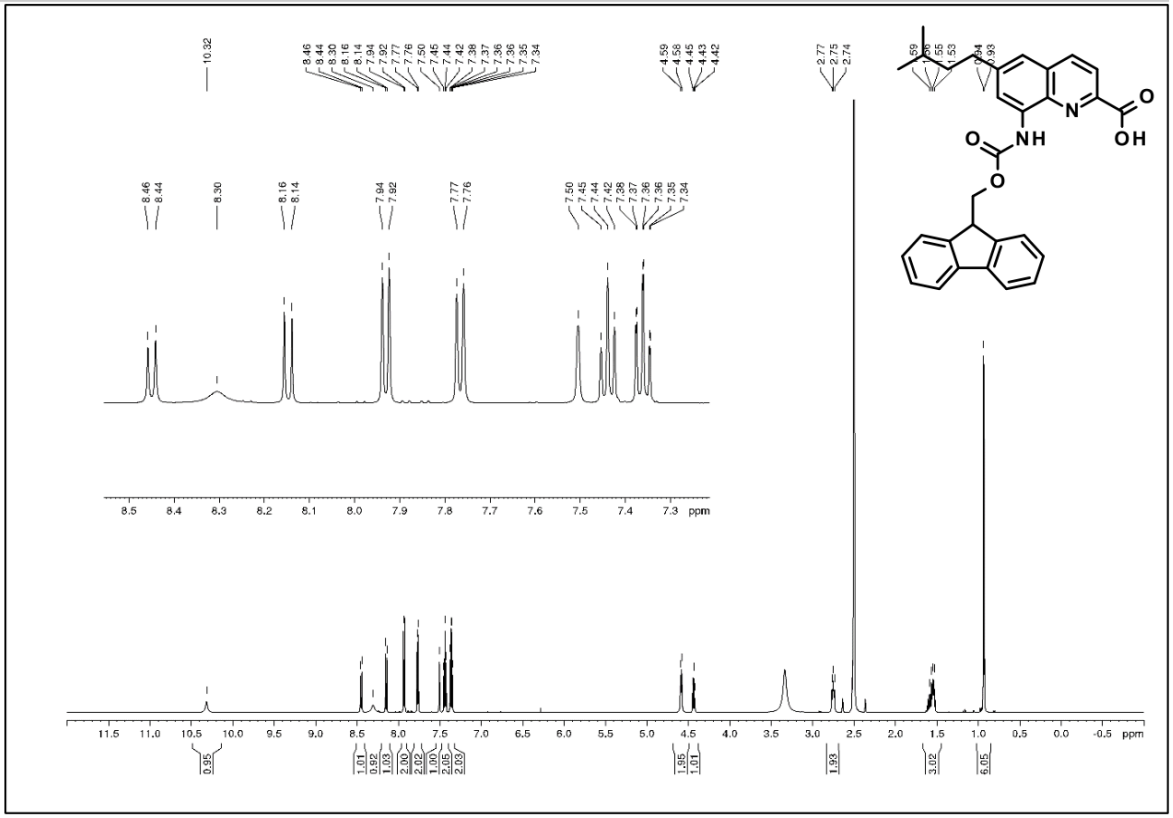

Figure S81. ^{1}H NMR (500 MHz, DMSO-d_6) of compound **13a**.

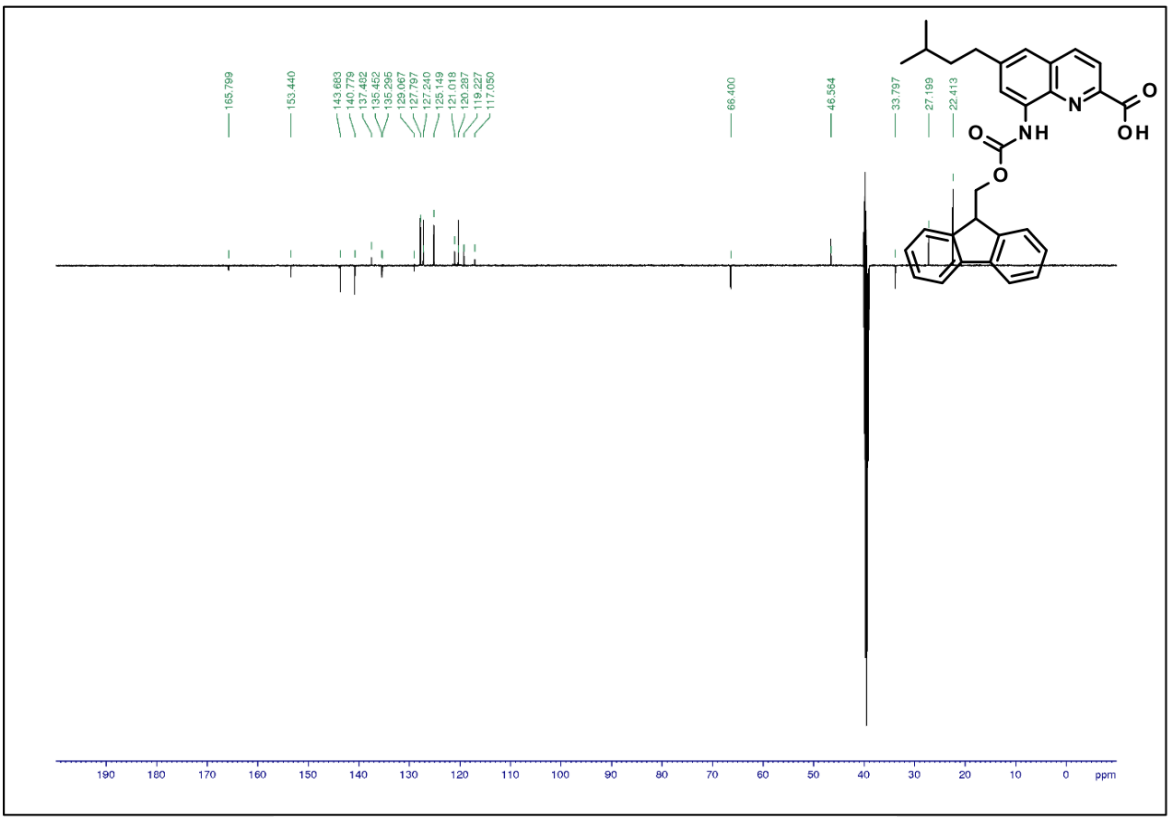

Figure S82. DEPT ^{13}C NMR (125 MHz, DMSO-d_6) of compound **13a**.

SUPPORTING INFORMATION

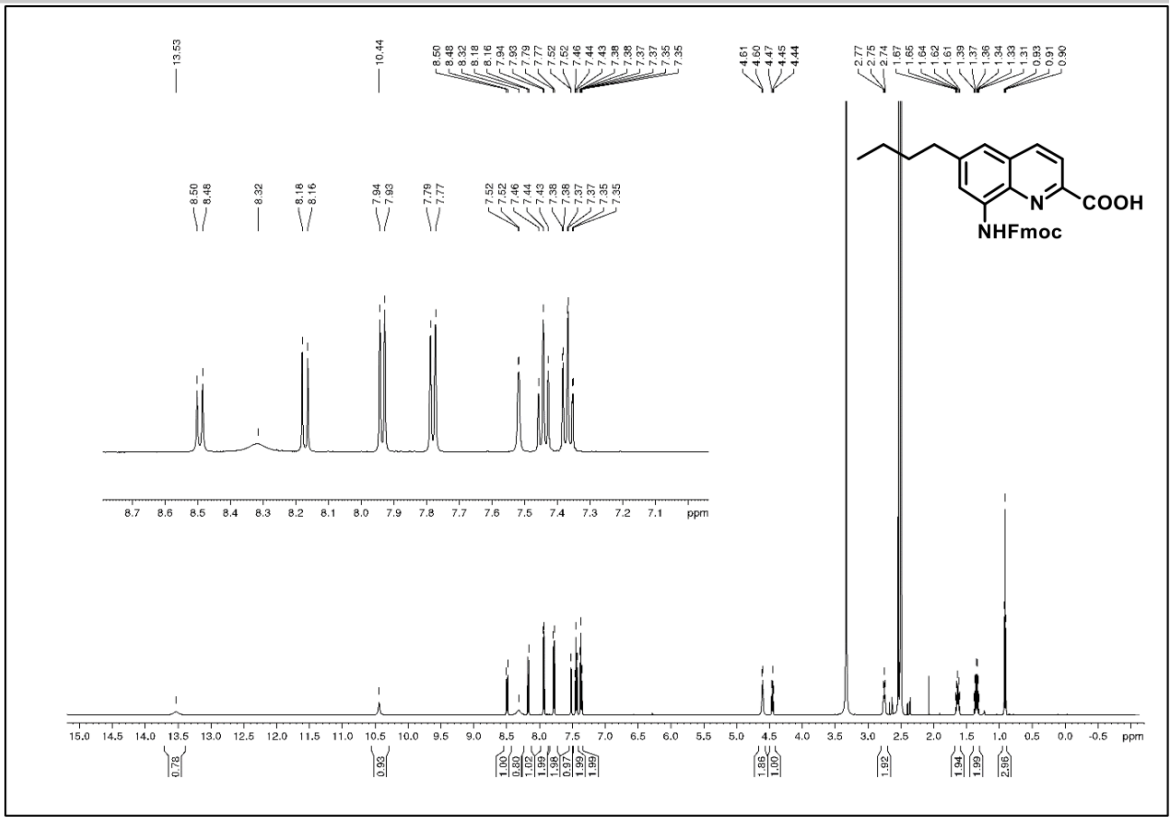

Figure S83. ^{1}H NMR (500 MHz, DMSO-d_6) of compound **13b**.

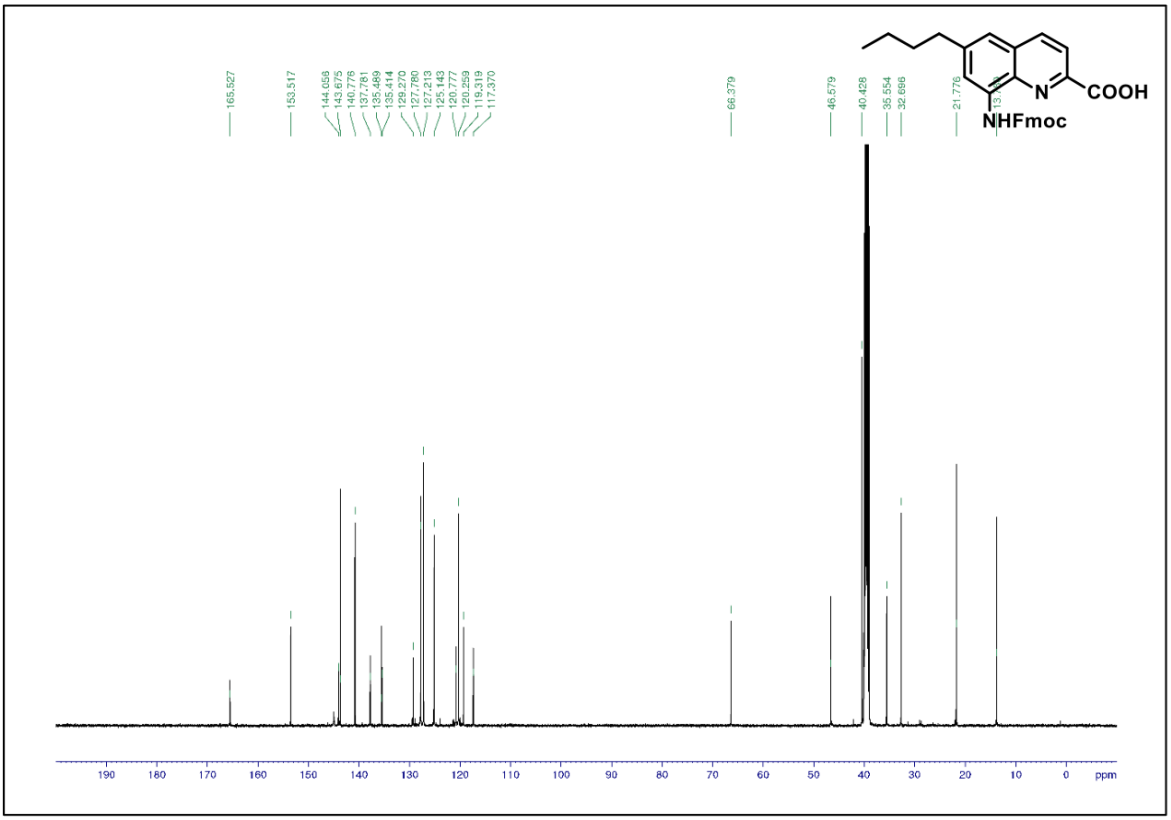

Figure S84. ^{13}C{^{1}H} NMR (125 MHz, DMSO-d_6) of compound **13b**.

SUPPORTING INFORMATION

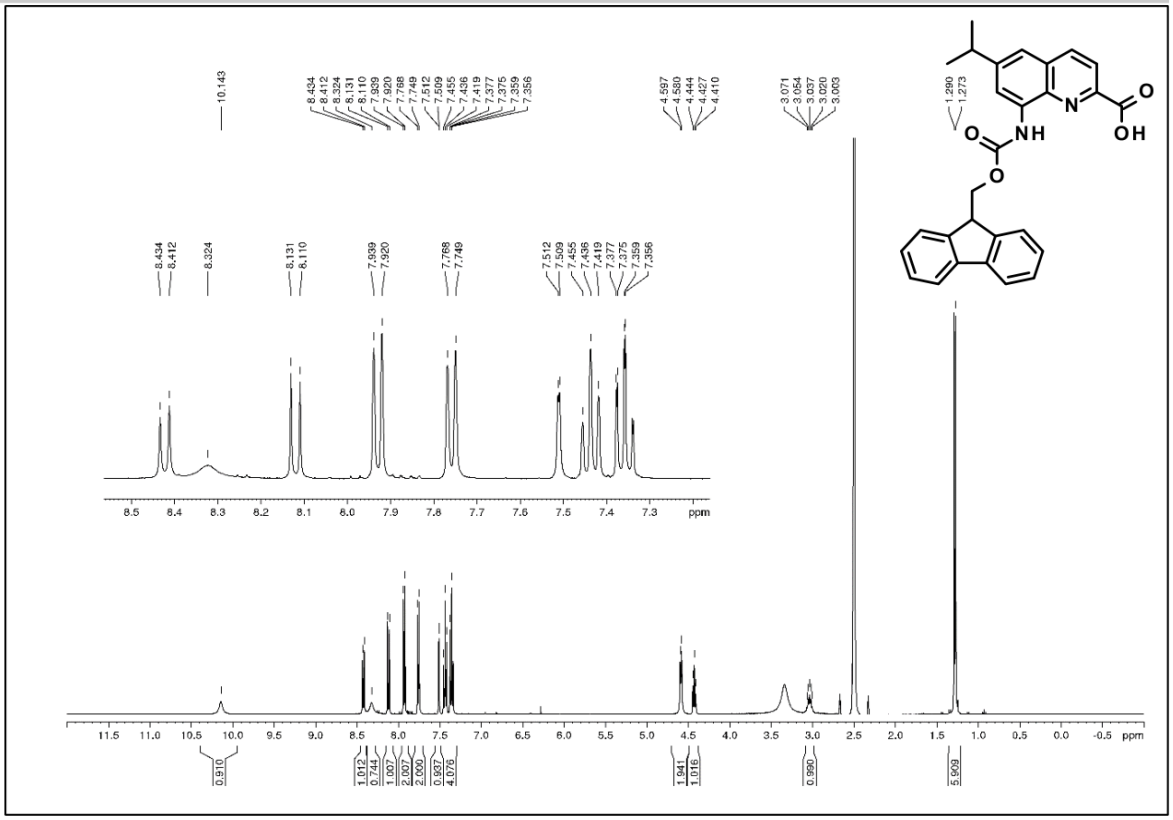

Figure S85. ^{1}H NMR (500 MHz, DMSO-d_6) of compound **13c**.

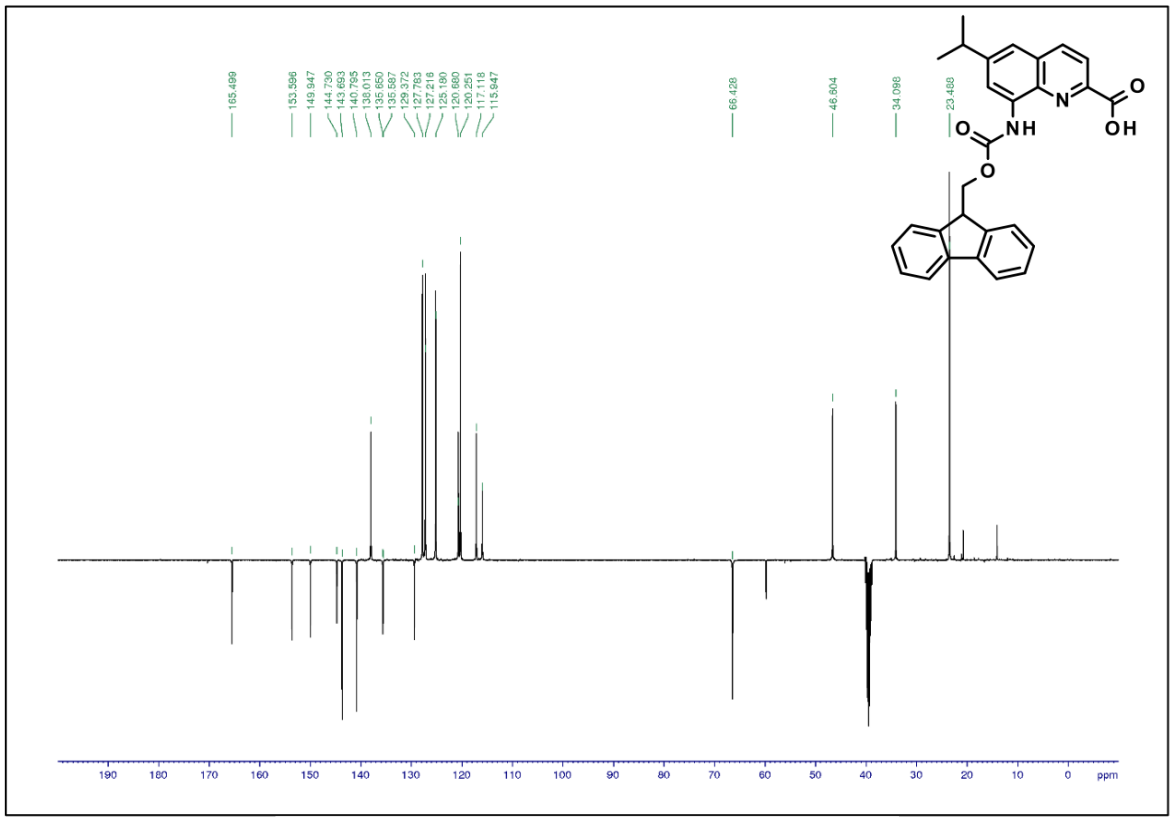

Figure S86. DEPT ^{13}C NMR (125 MHz, DMSO-d_6) of compound **13c**.

SUPPORTING INFORMATION

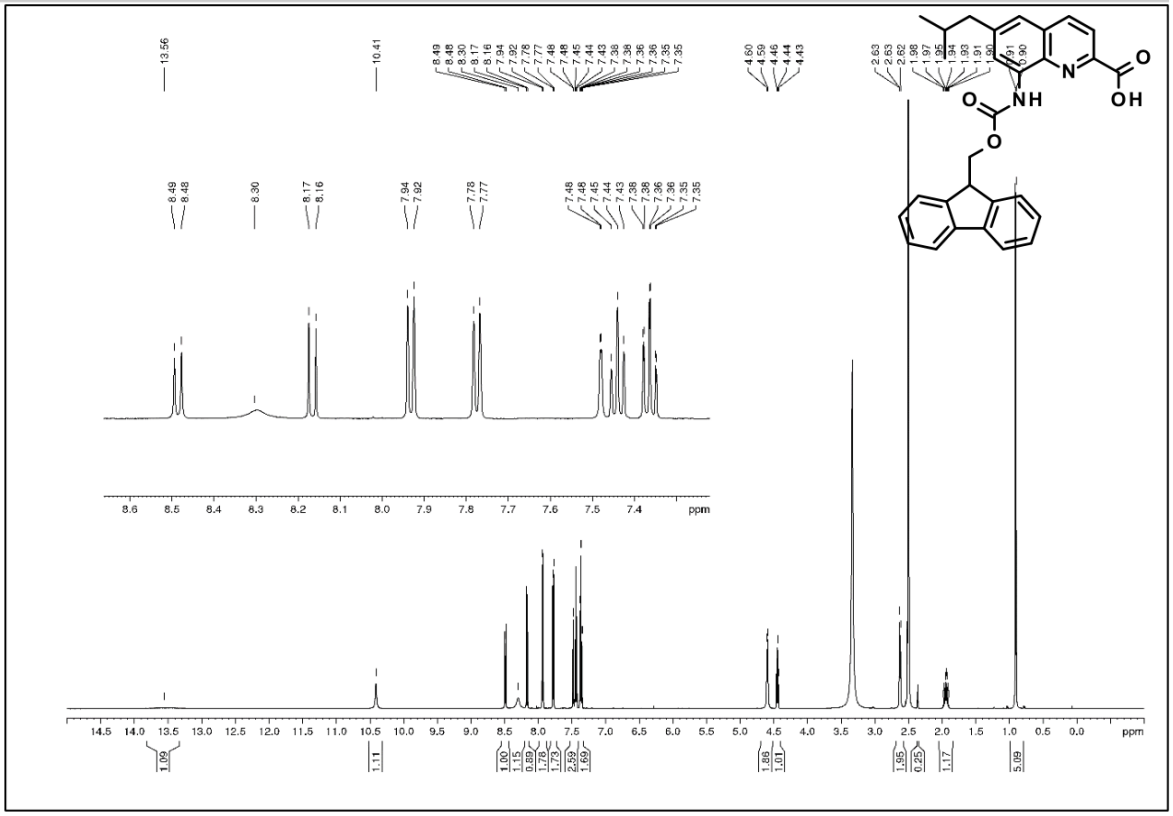

Figure S87. ^{1}H NMR (500 MHz, DMSO-d_6) of compound **13d**.

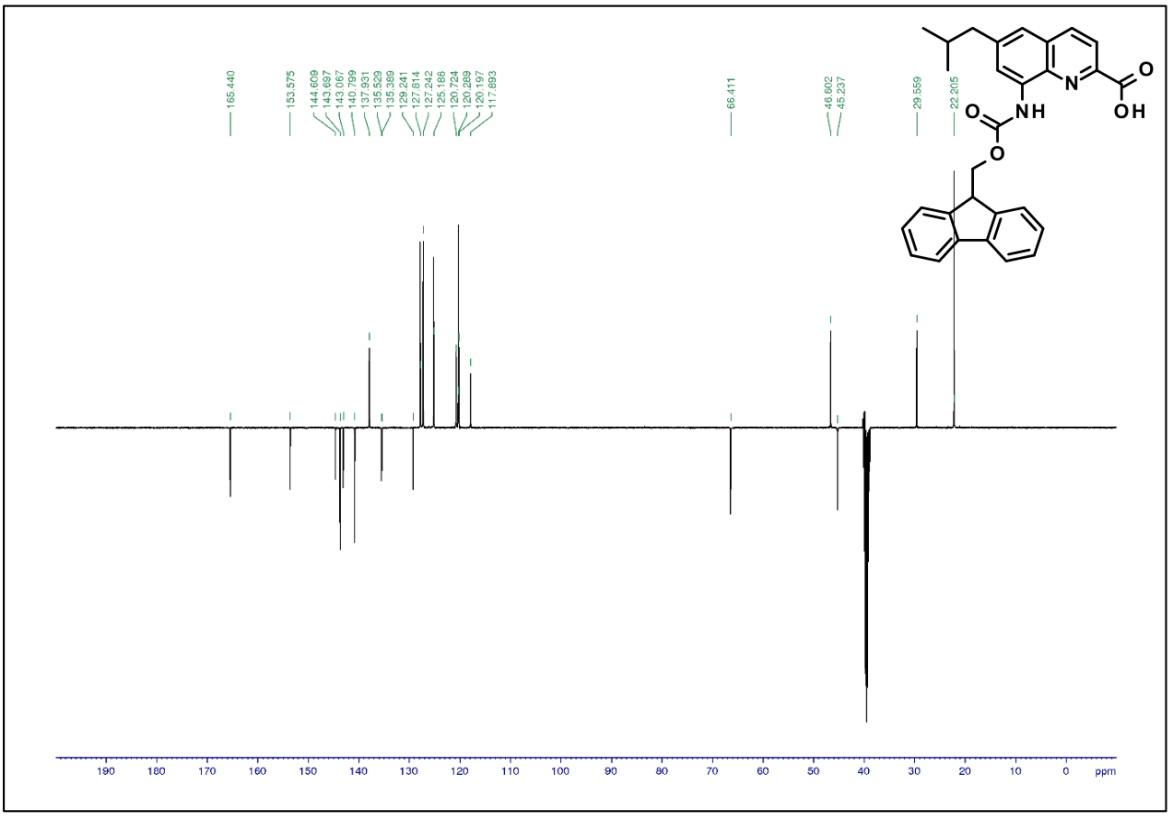

Figure S88. DEPT ^{13}C NMR (125 MHz, DMSO-d_6) of compound **13d**.

SUPPORTING INFORMATION

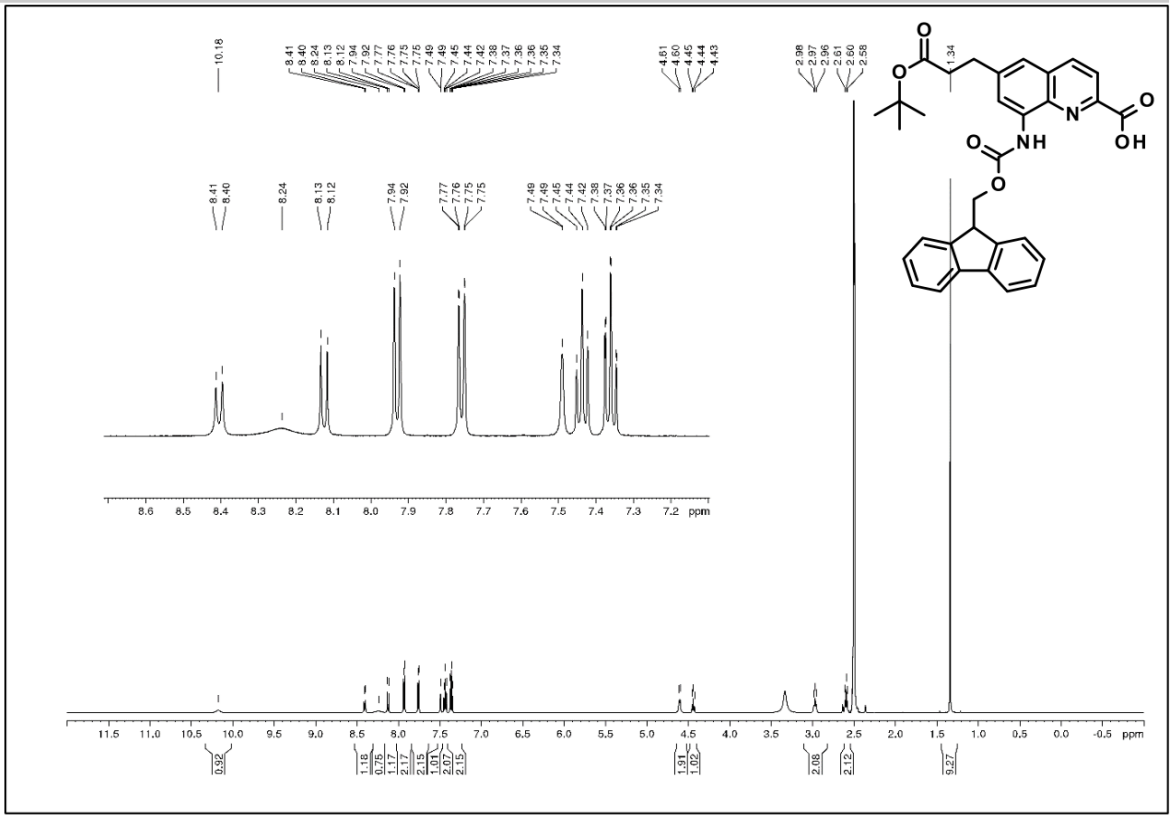

Figure S89. ^{1}H NMR (500 MHz, DMSO-d_6) of compound **13e**.

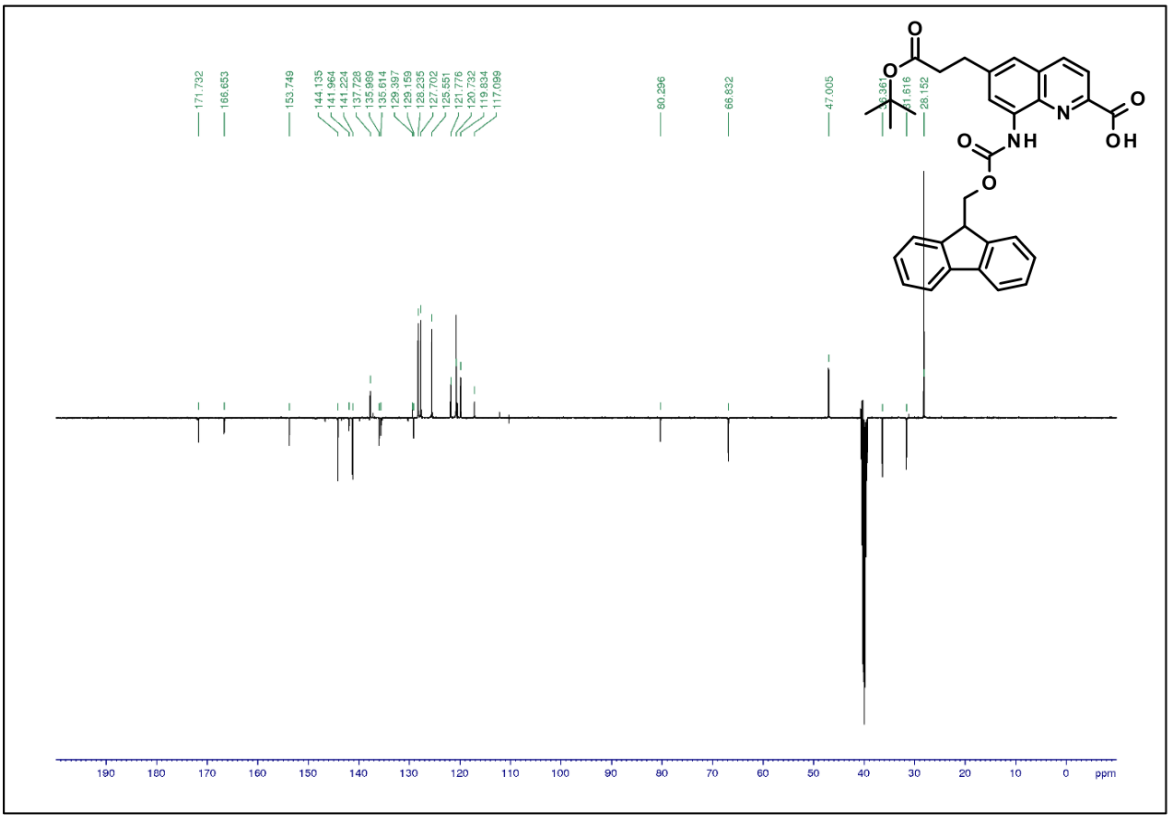

Figure S90. DEPT ^{13}C NMR (125 MHz, DMSO-d_6) of compound **13e**.

SUPPORTING INFORMATION

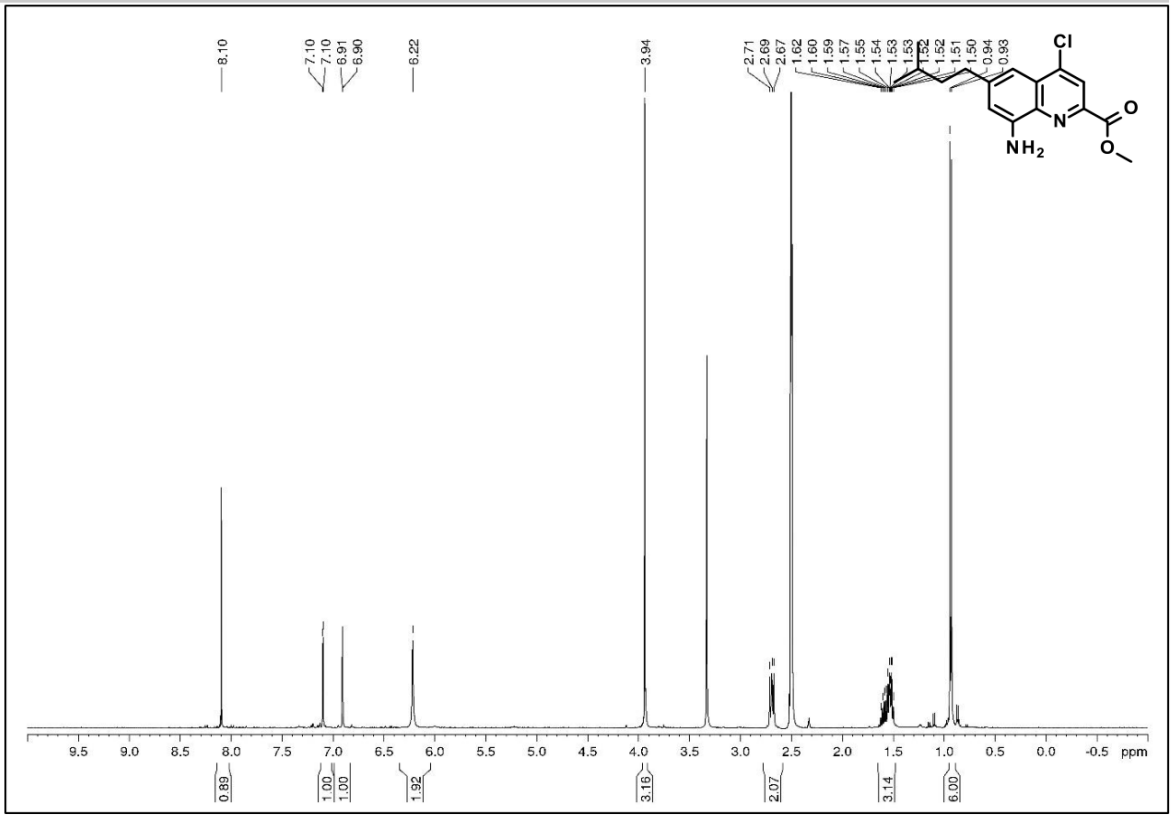

Figure S91. ^{1}H NMR (500 MHz, DMSO-d_6) of compound **13f**.

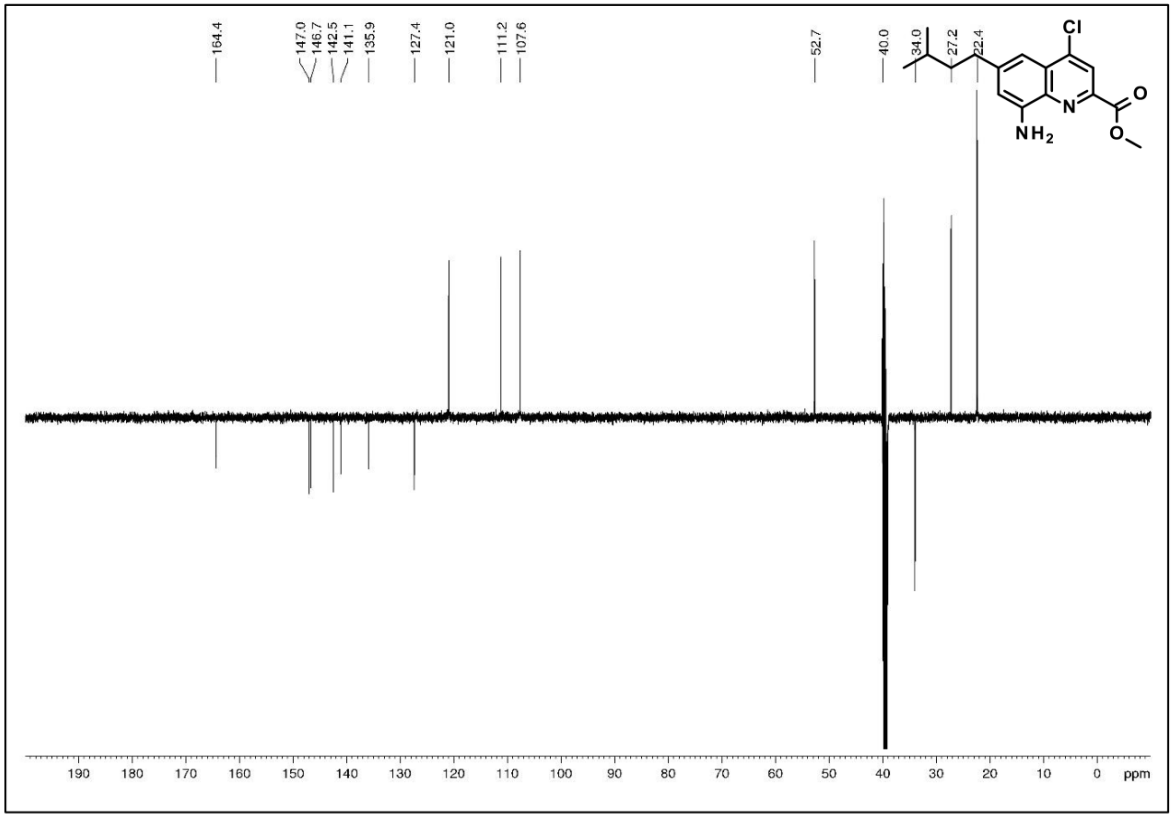

Figure S92. DEPT ^{13}C NMR (125 MHz, DMSO-d_6) of compound **13f**.

SUPPORTING INFORMATION

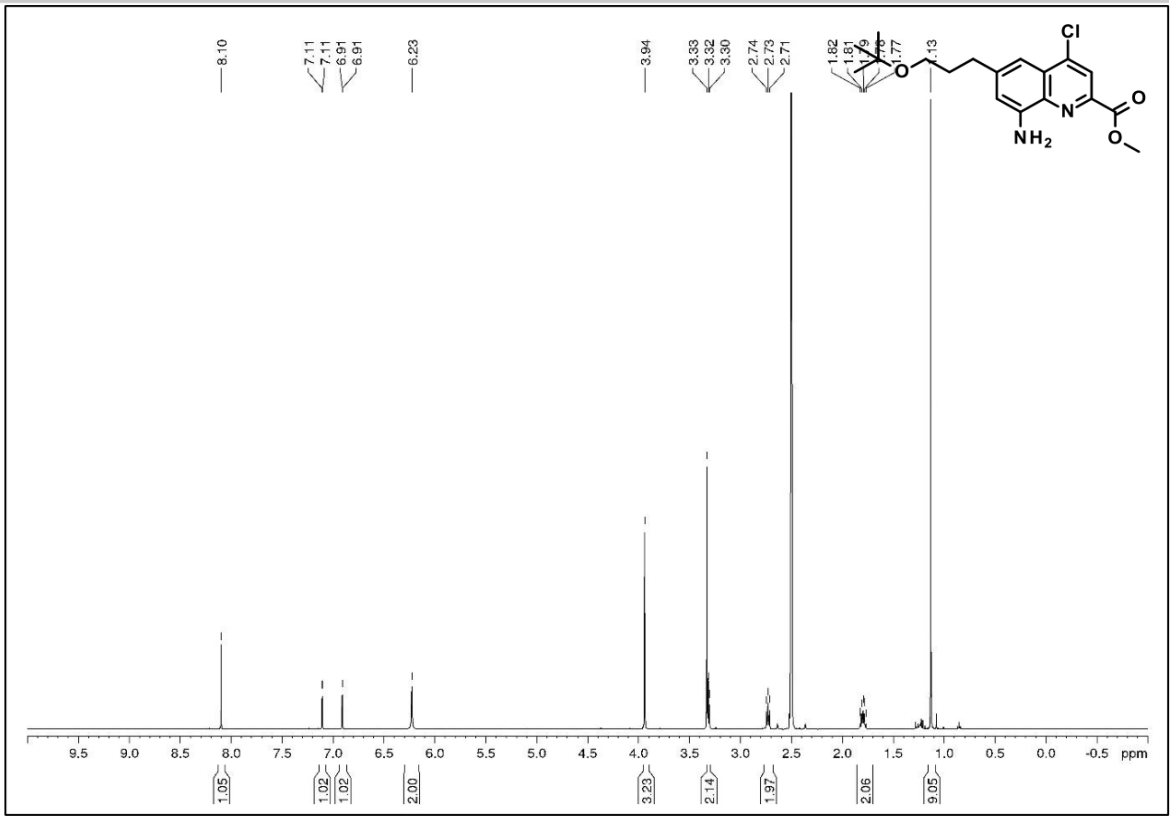

Figure S93. ^{1}H NMR (500 MHz, DMSO-d_6) of compound **15b**.

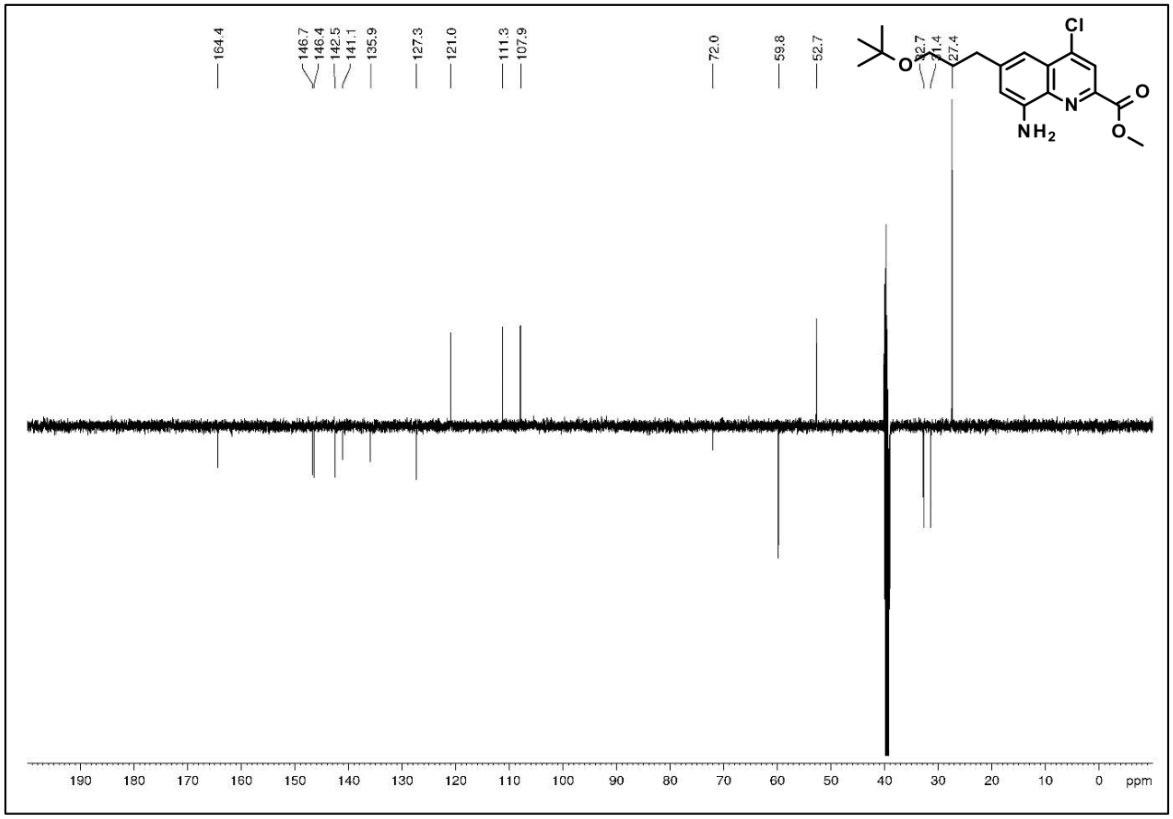

Figure S94. DEPT ^{13}C NMR (125 MHz, DMSO-d_6) of compound **15b**.

SUPPORTING INFORMATION

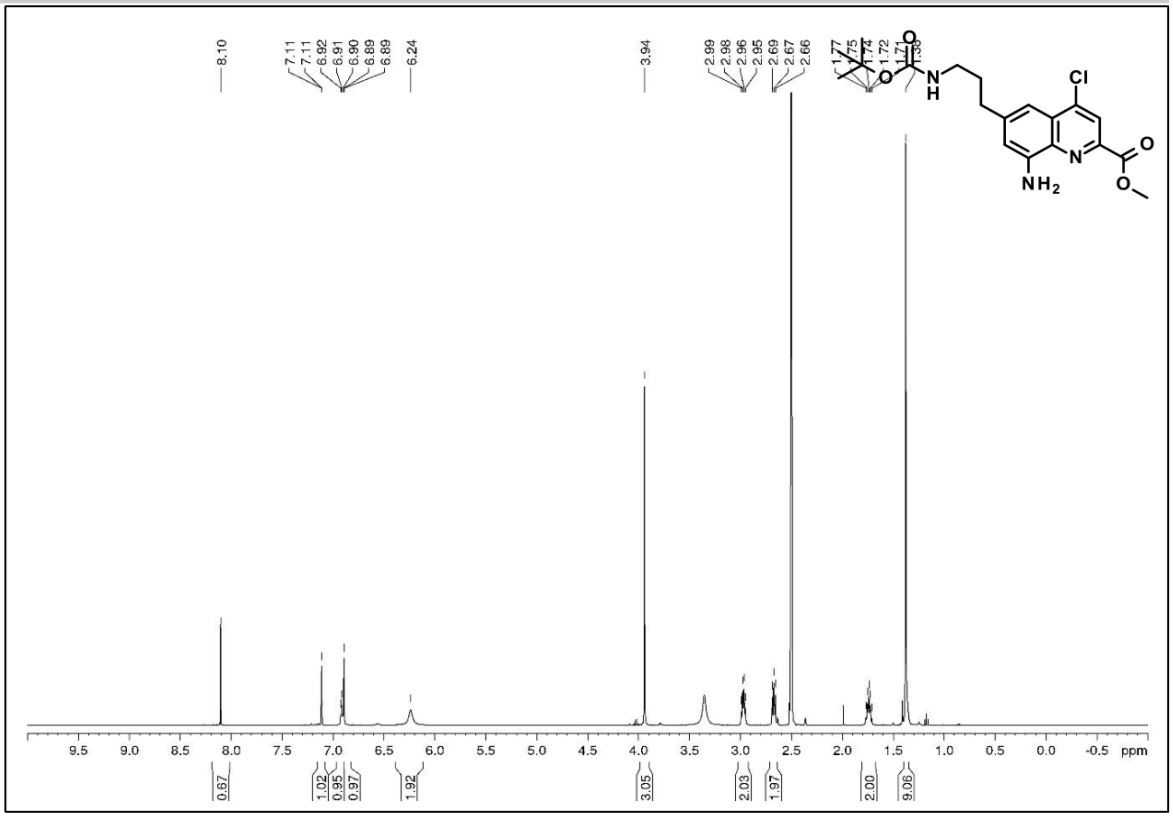

Figure S95. ^{1}H NMR (500 MHz, DMSO-d_6) of compound **15c**.

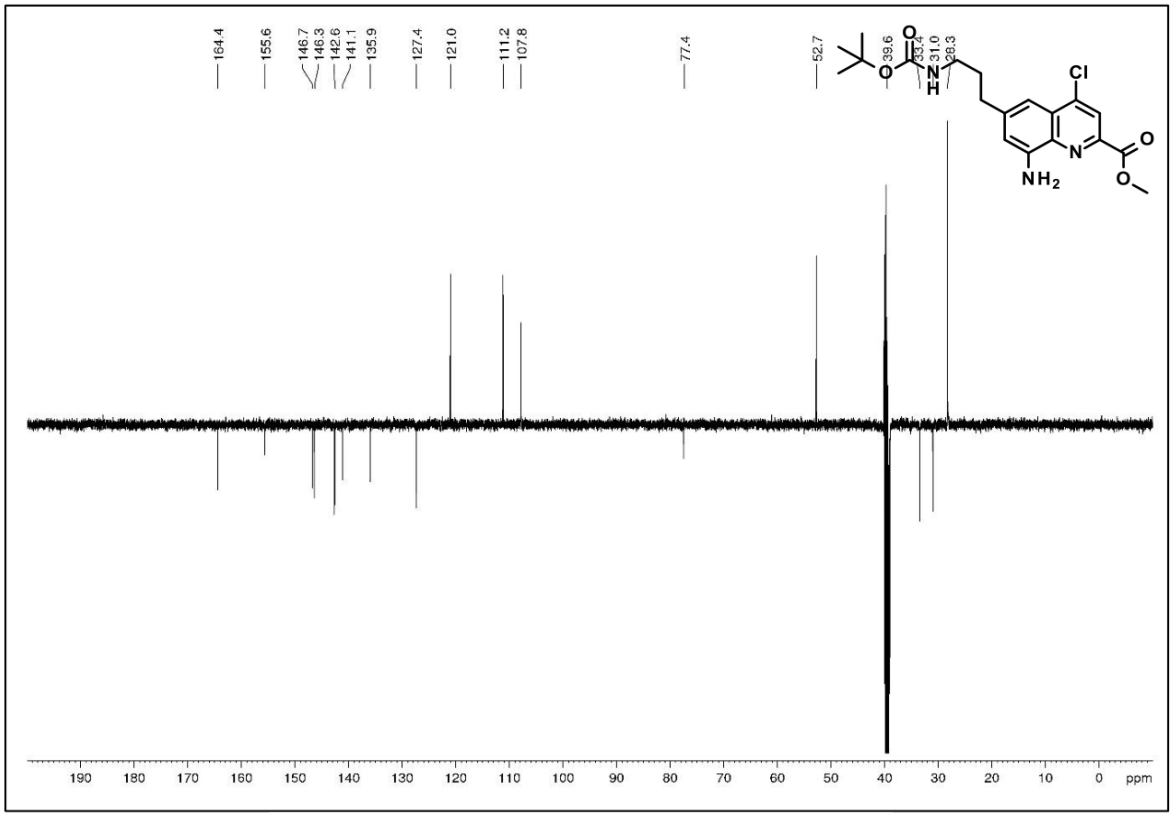

Figure S96. DEPT ^{13}C NMR (125 MHz, DMSO-d_6) of compound **15c**.

SUPPORTING INFORMATION

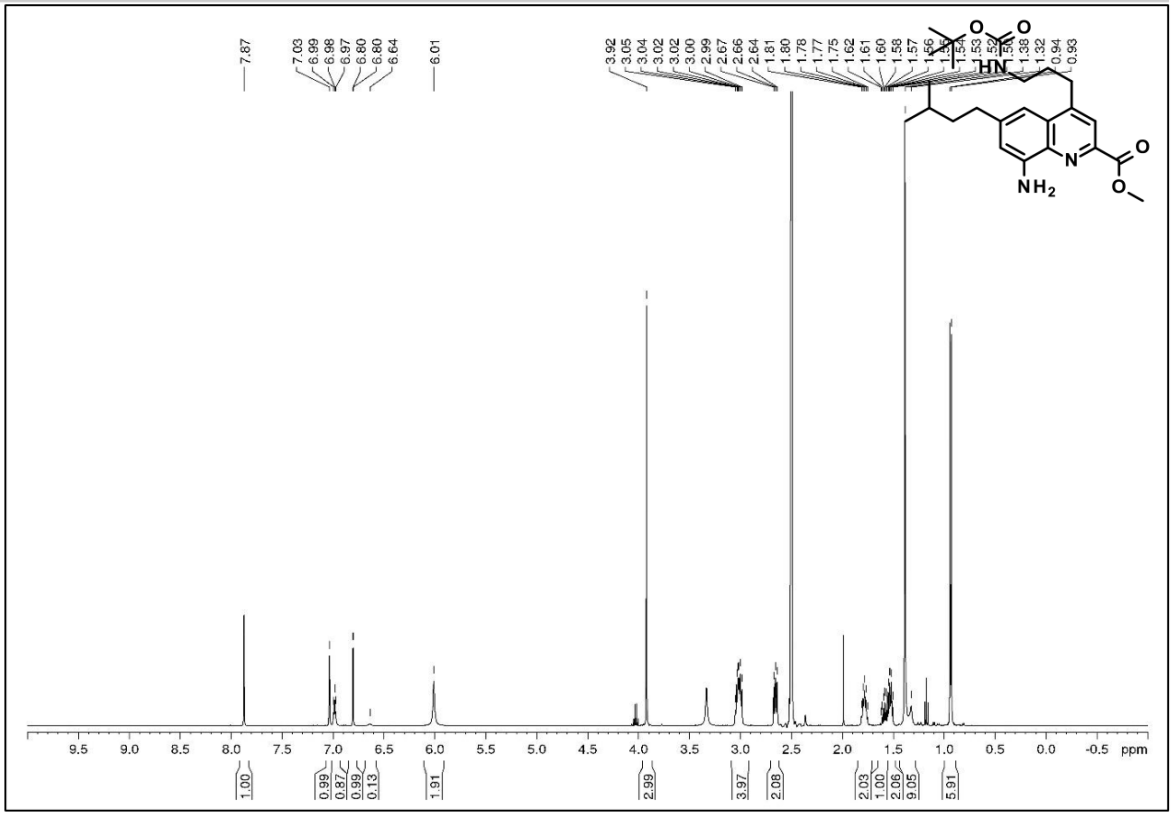

Figure S97. ^{1}H NMR (500 MHz, DMSO-d_6) of compound **16a**.

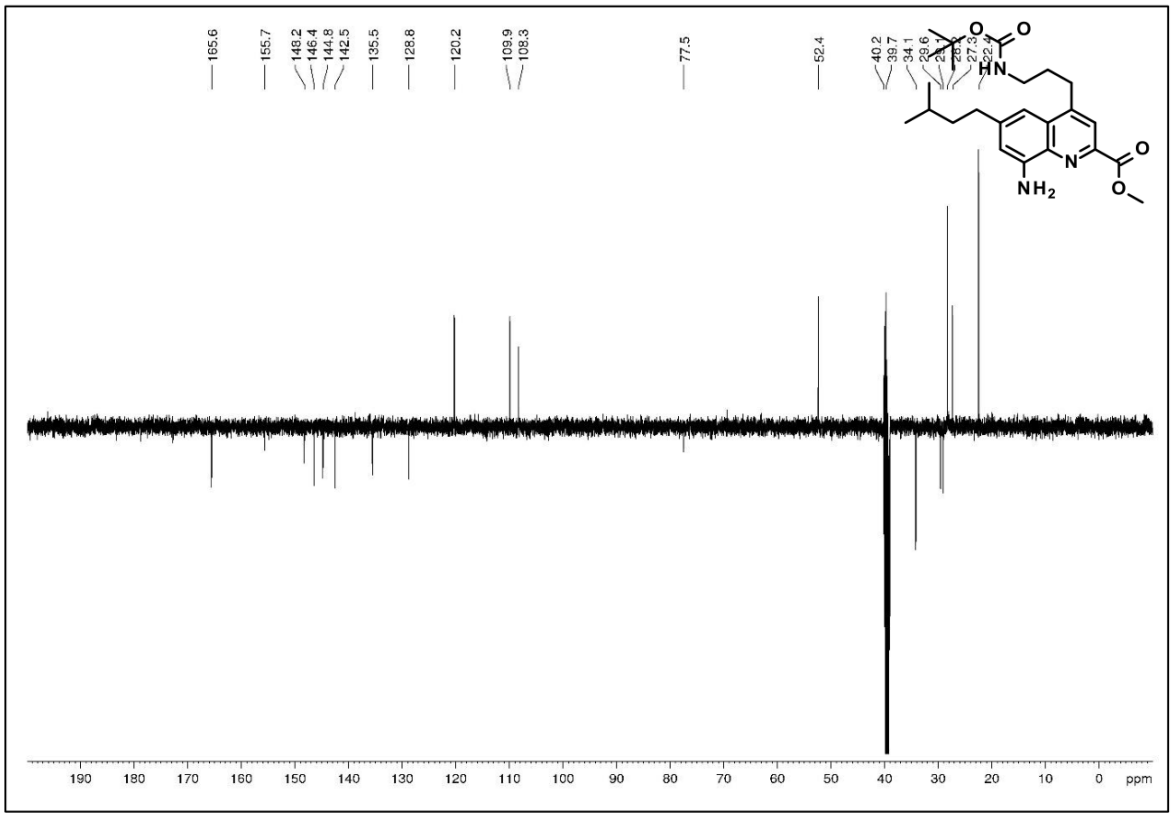

Figure S98. DEPT ^{13}C NMR (125 MHz, DMSO-d_6) of compound **16a**.

SUPPORTING INFORMATION

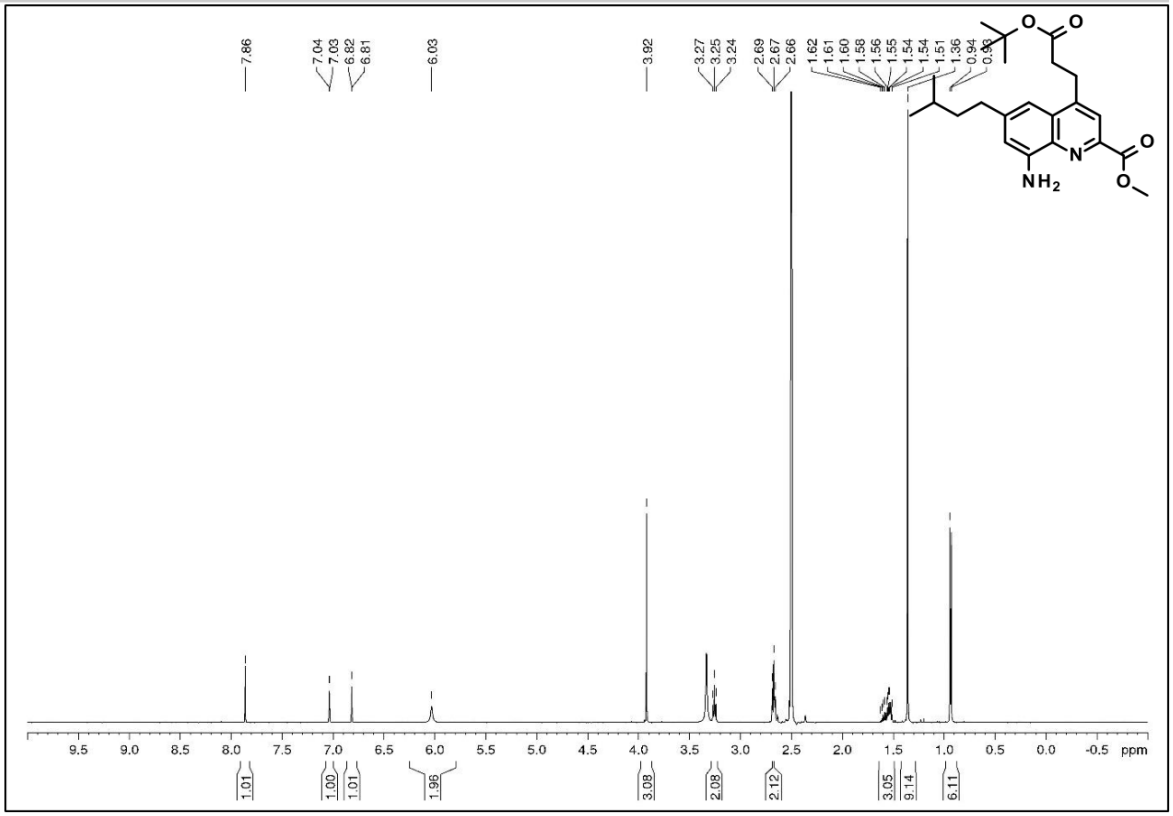

Figure S99. ^{1}H NMR (500 MHz, DMSO-d_6) of compound **16b**.

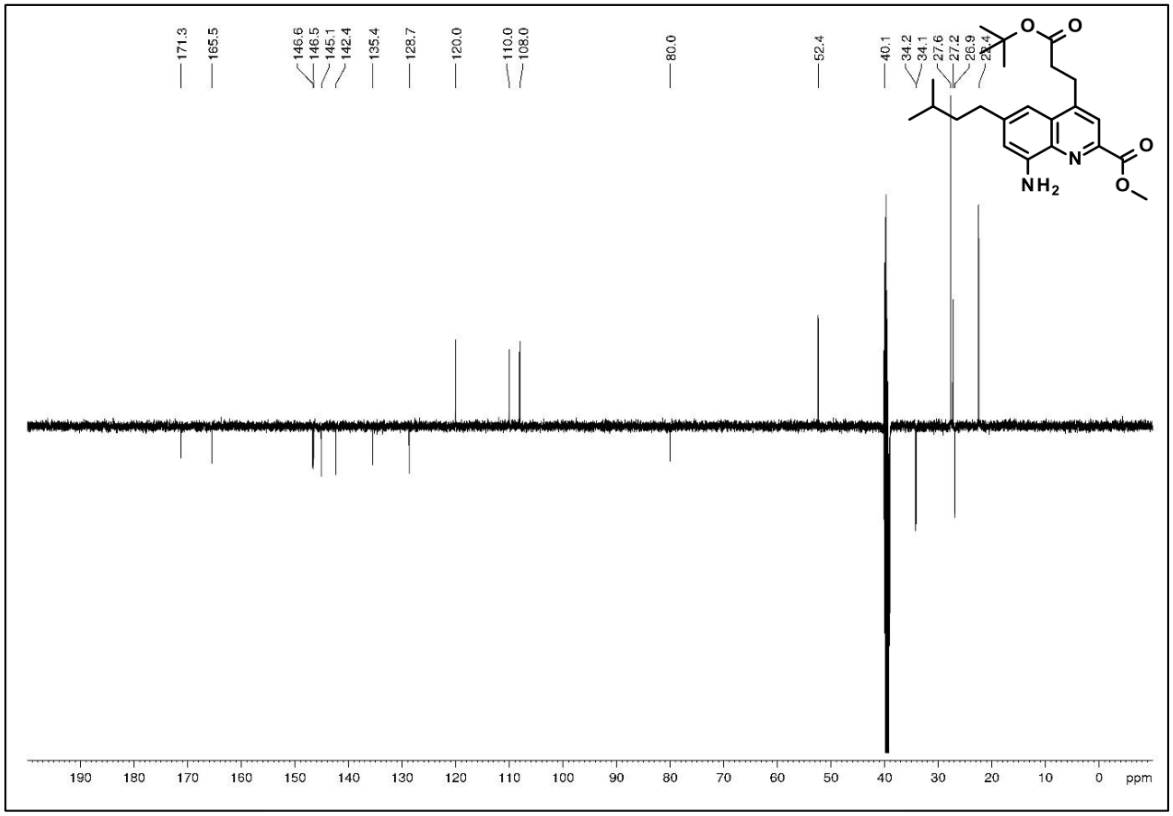

Figure S100. DEPT ^{13}C NMR (125 MHz, DMSO-d_6) of compound **16b**.

SUPPORTING INFORMATION

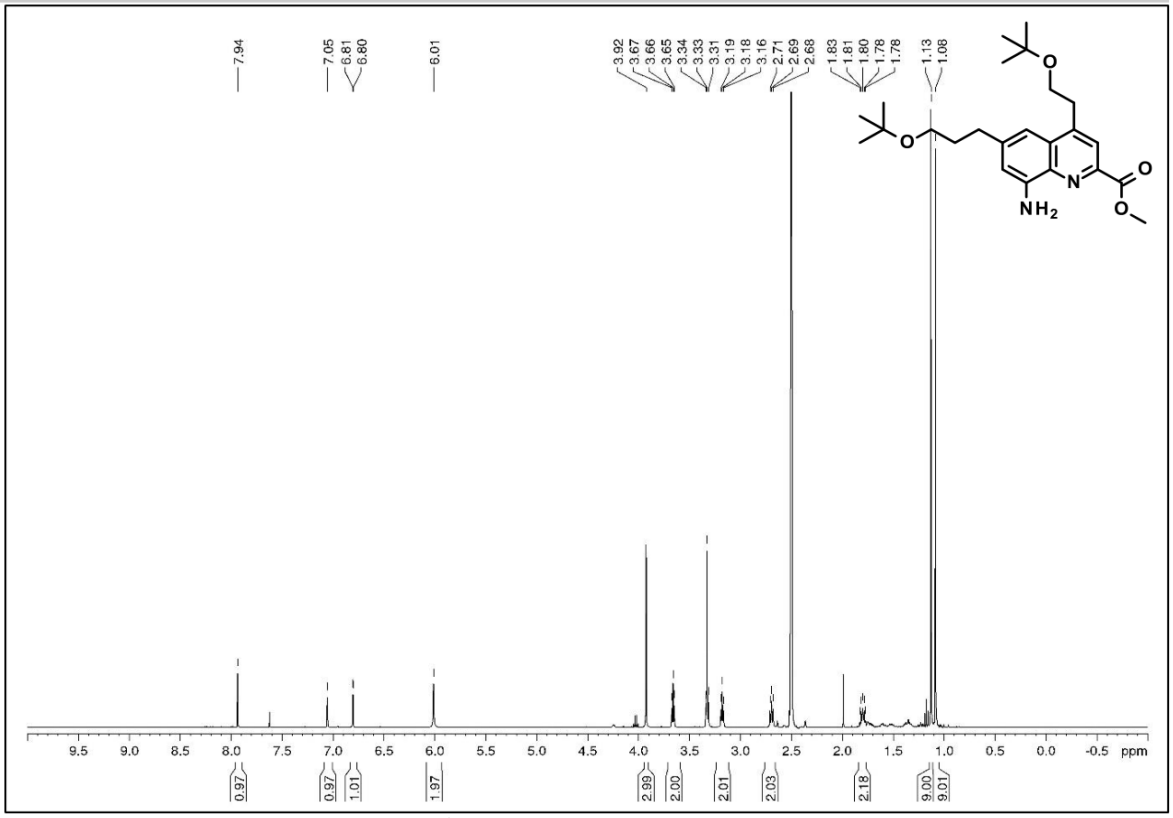

Figure S101. ^{1}H NMR (500 MHz, DMSO-d_6) of compound **16c**.

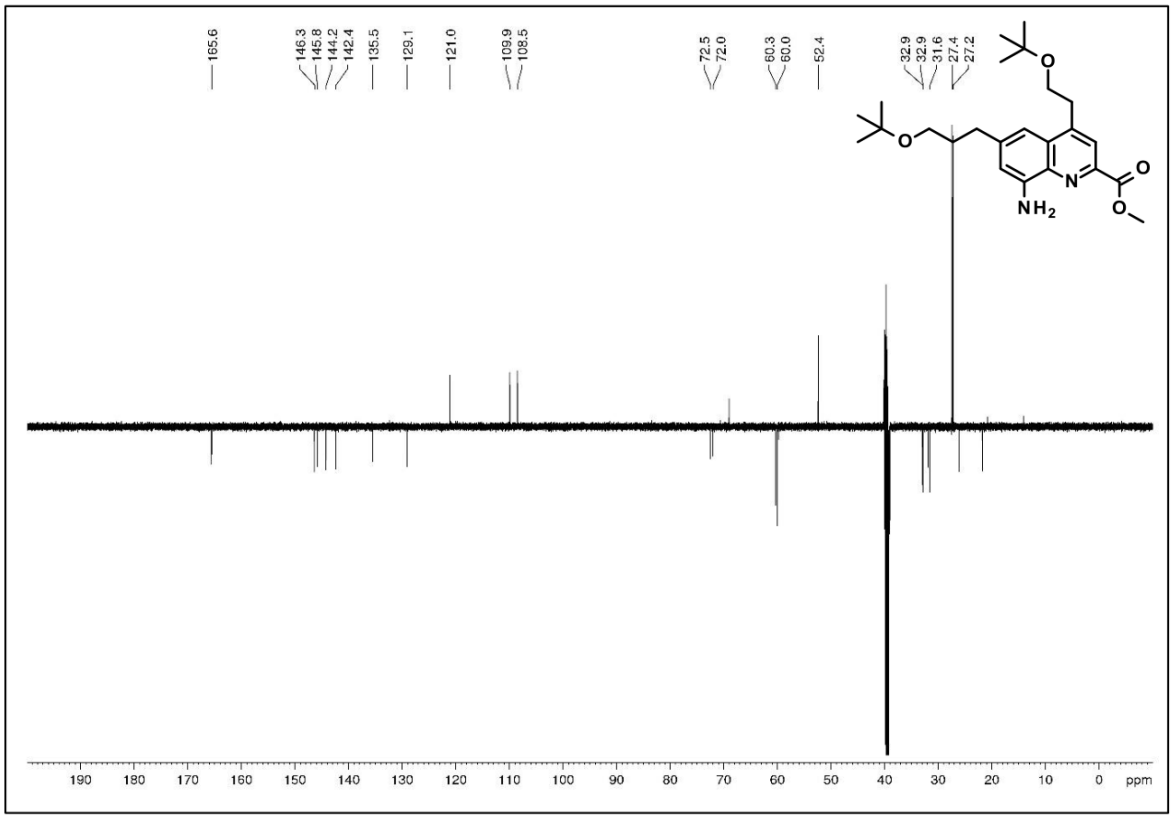

Figure S102. DEPT ^{13}C NMR (125 MHz, DMSO-d_6) of compound **16c**.

SUPPORTING INFORMATION

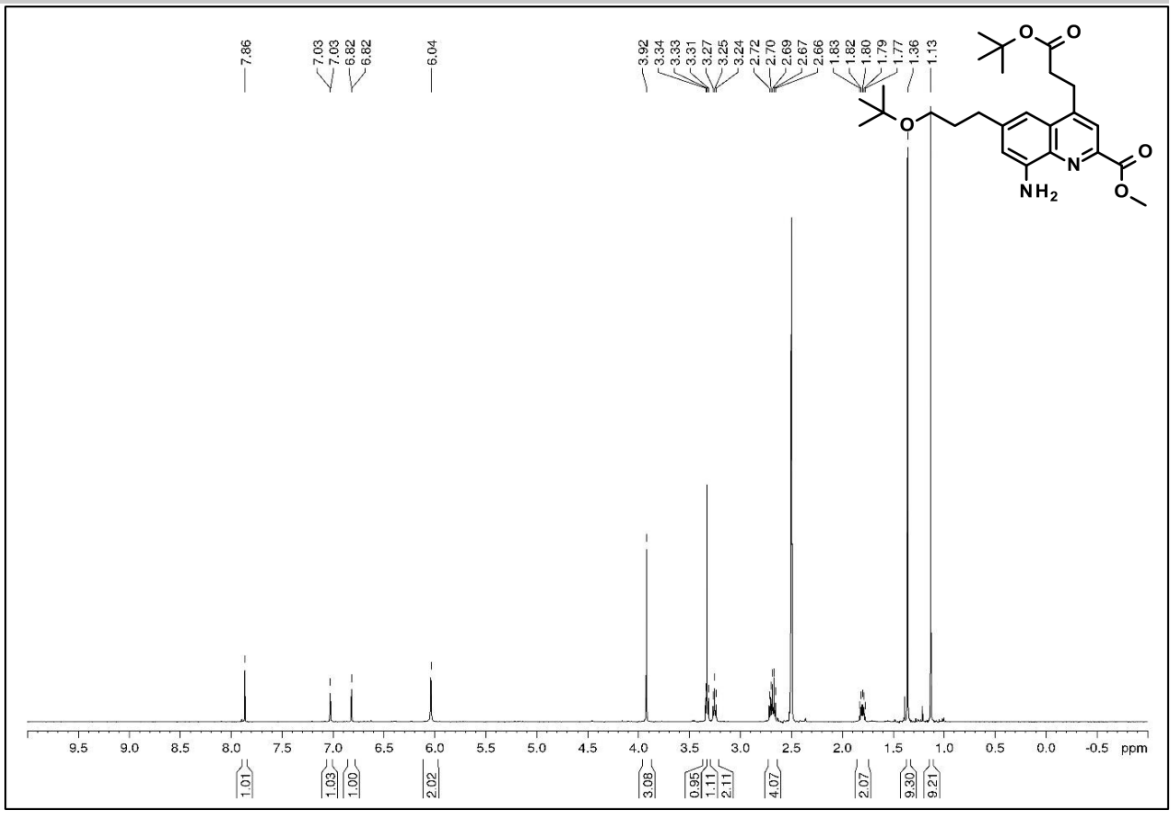

Figure S103. ^{1}H NMR (500 MHz, DMSO-d_6) of compound **16d**.

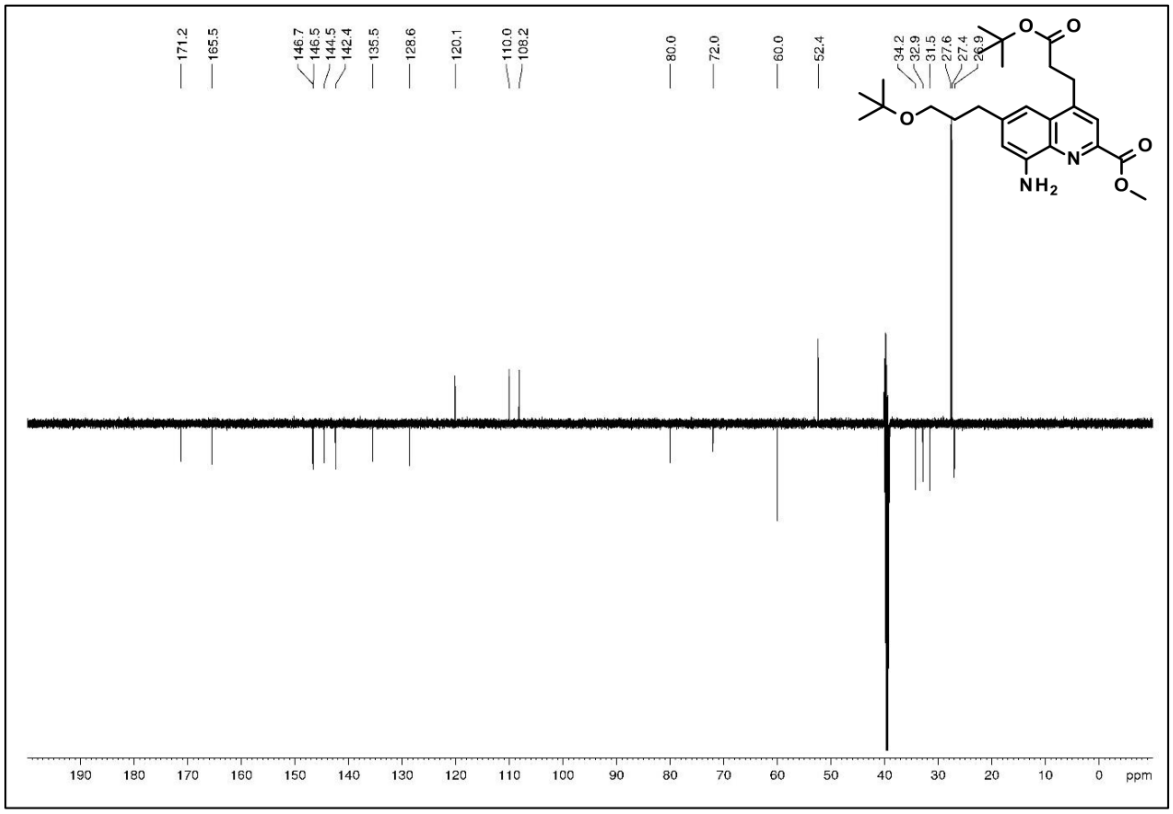

Figure S104. DEPT ^{13}C NMR (125 MHz, DMSO-d_6) of compound **16d**.

SUPPORTING INFORMATION

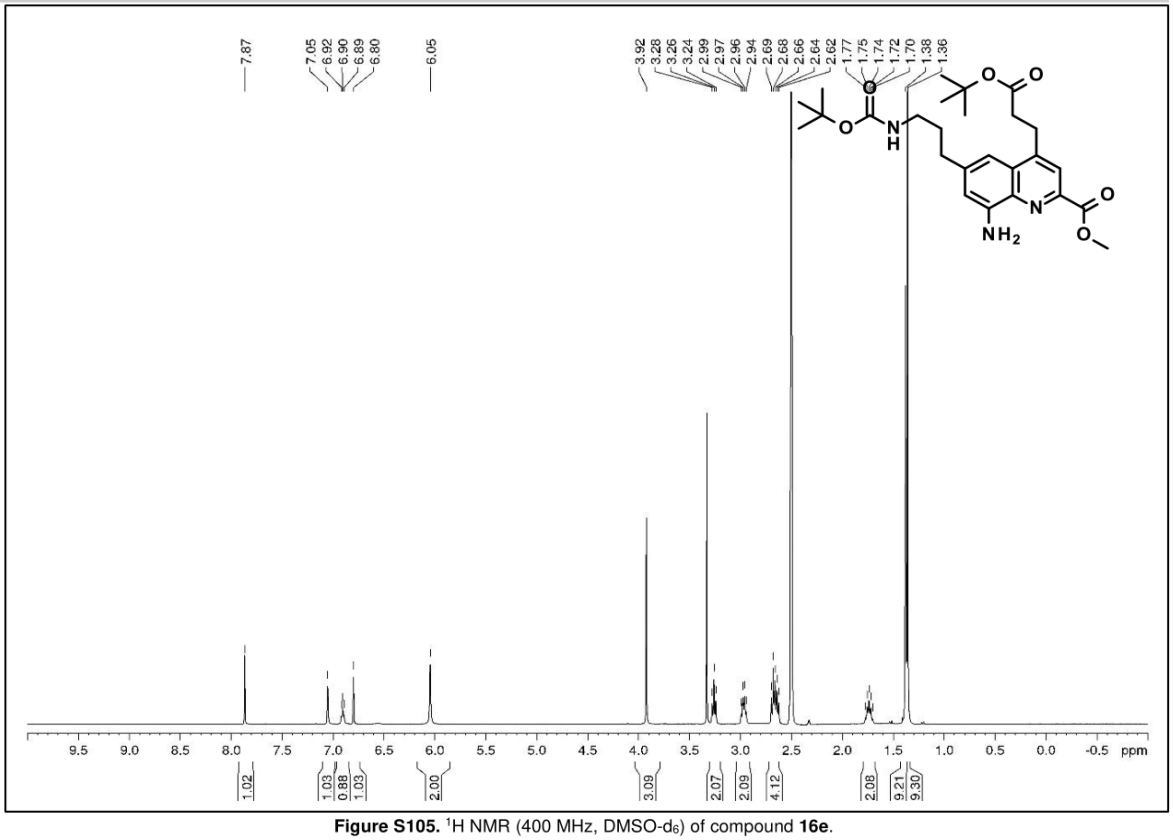

Figure S105. ^{1}H NMR (400 MHz, DMSO-d_6) of compound **16e**.

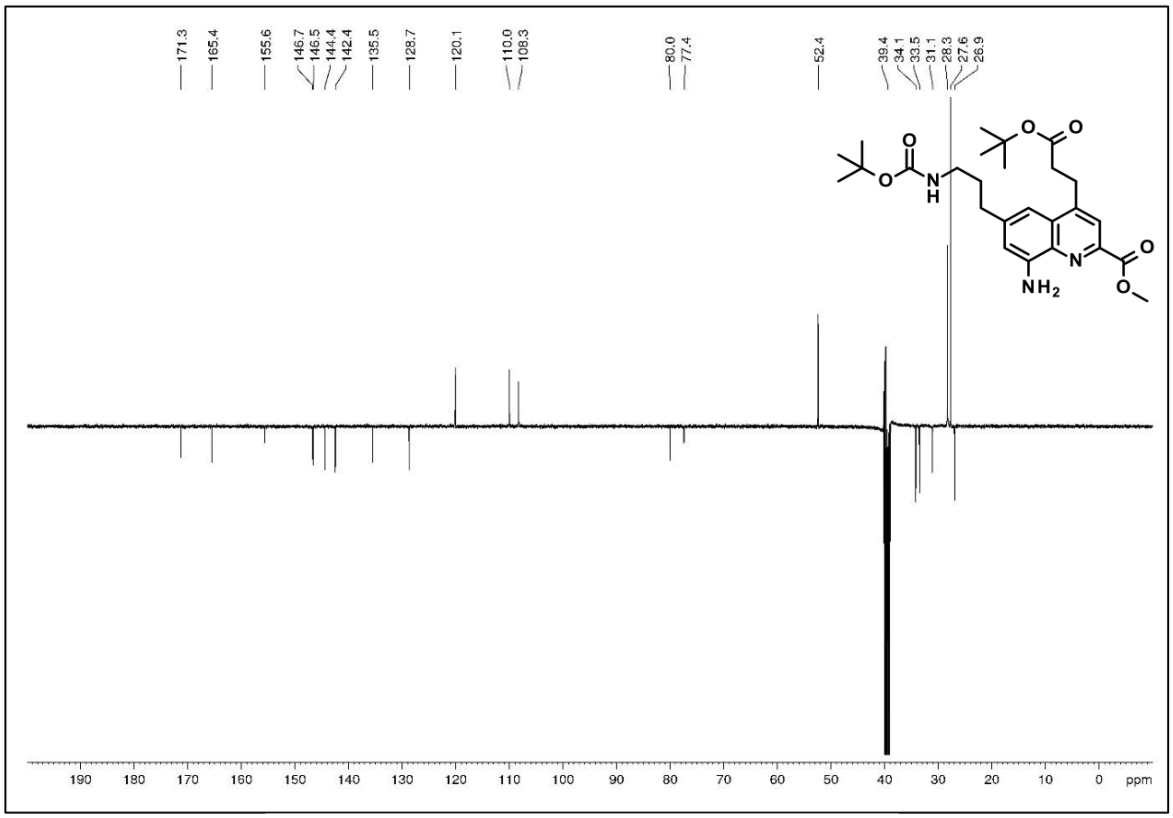

Figure S106. DEPT ^{13}C NMR (125 MHz, DMSO-d_6) of compound **16e**.

SUPPORTING INFORMATION

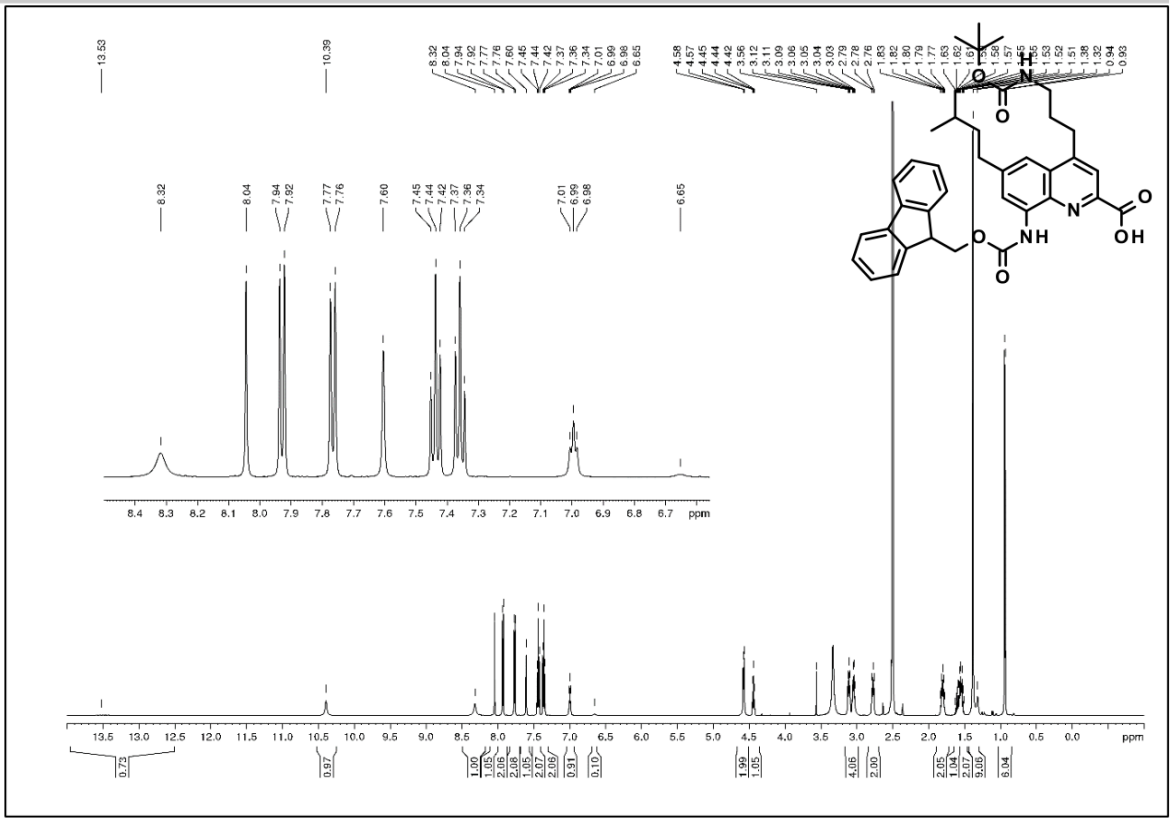

Figure S107. ^{1}H NMR (500 MHz, DMSO-d$_6$) of compound **17a**.

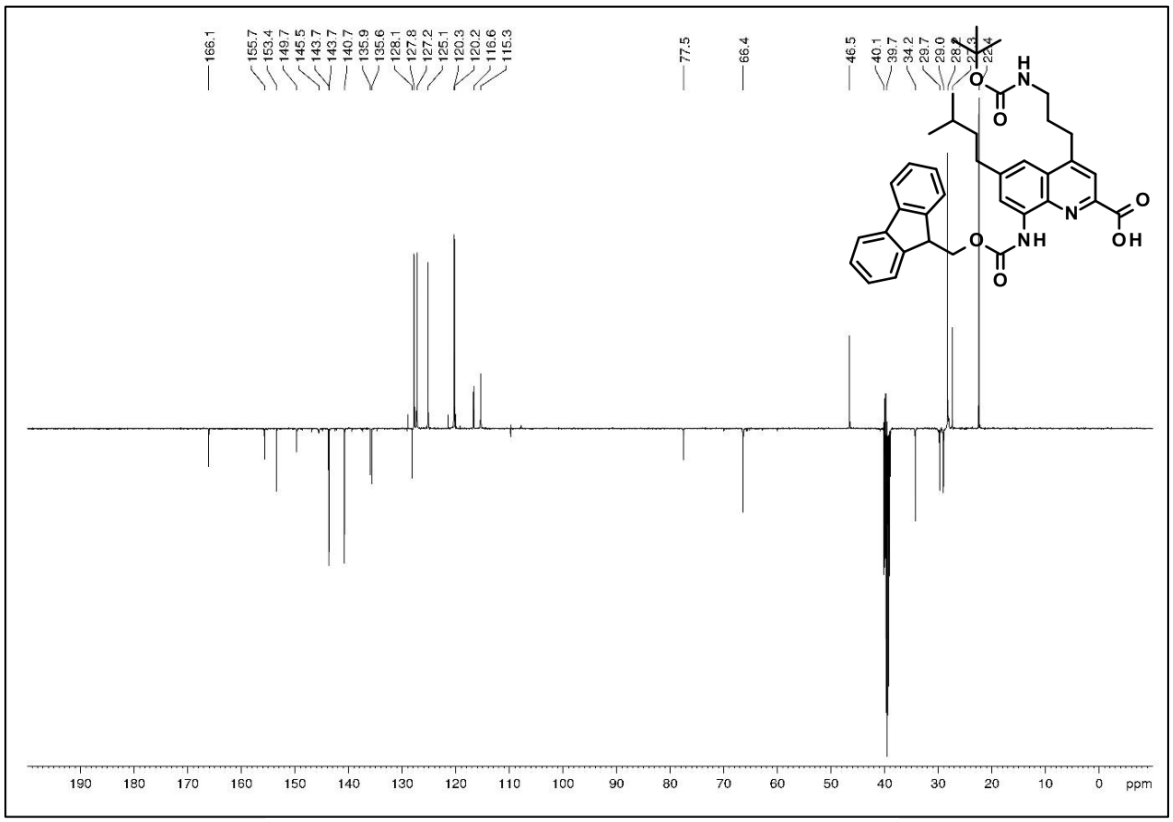

Figure S108. DEPT ^{13}C NMR (125 MHz, DMSO-d_6) of compound **17a**.

SUPPORTING INFORMATION

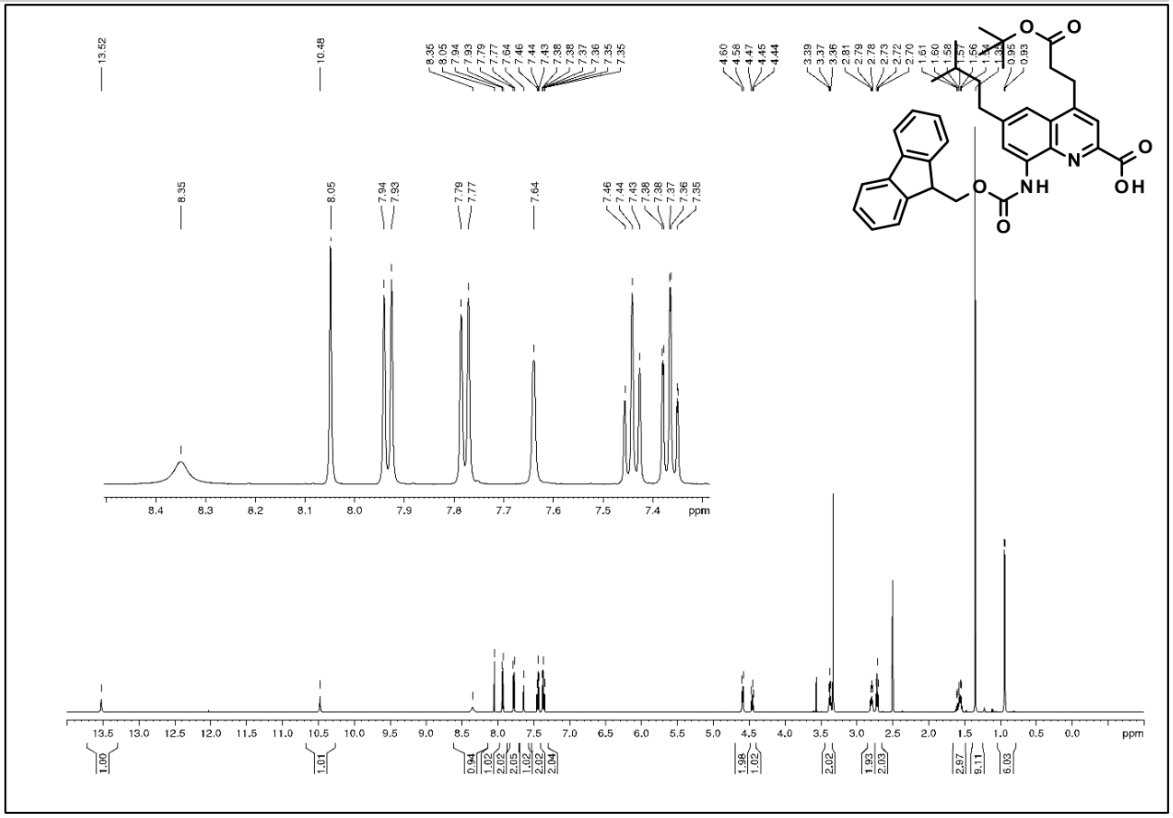

Figure S109. ^{1}H NMR (500 MHz, DMSO-d_6) of compound **17b**.

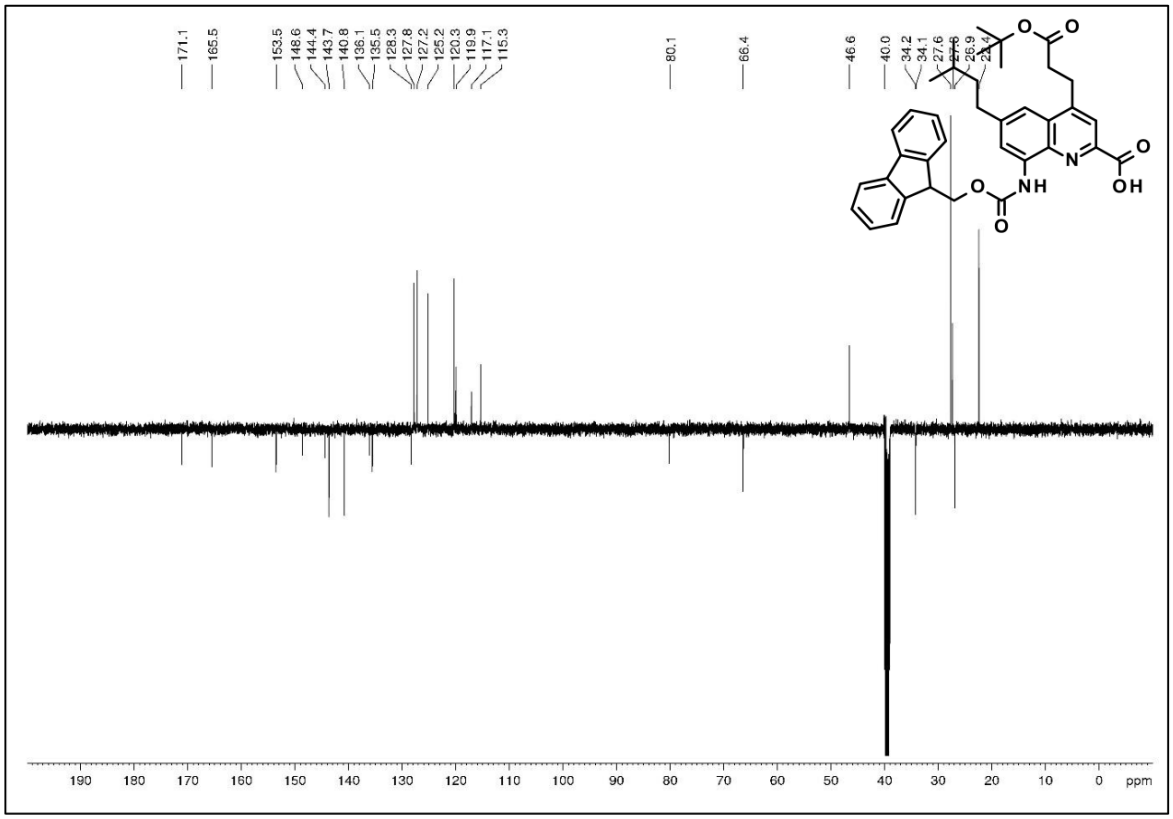

Figure S110. DEPT ^{13}C NMR (125 MHz, DMSO-d_6) of compound **17b**.

SUPPORTING INFORMATION

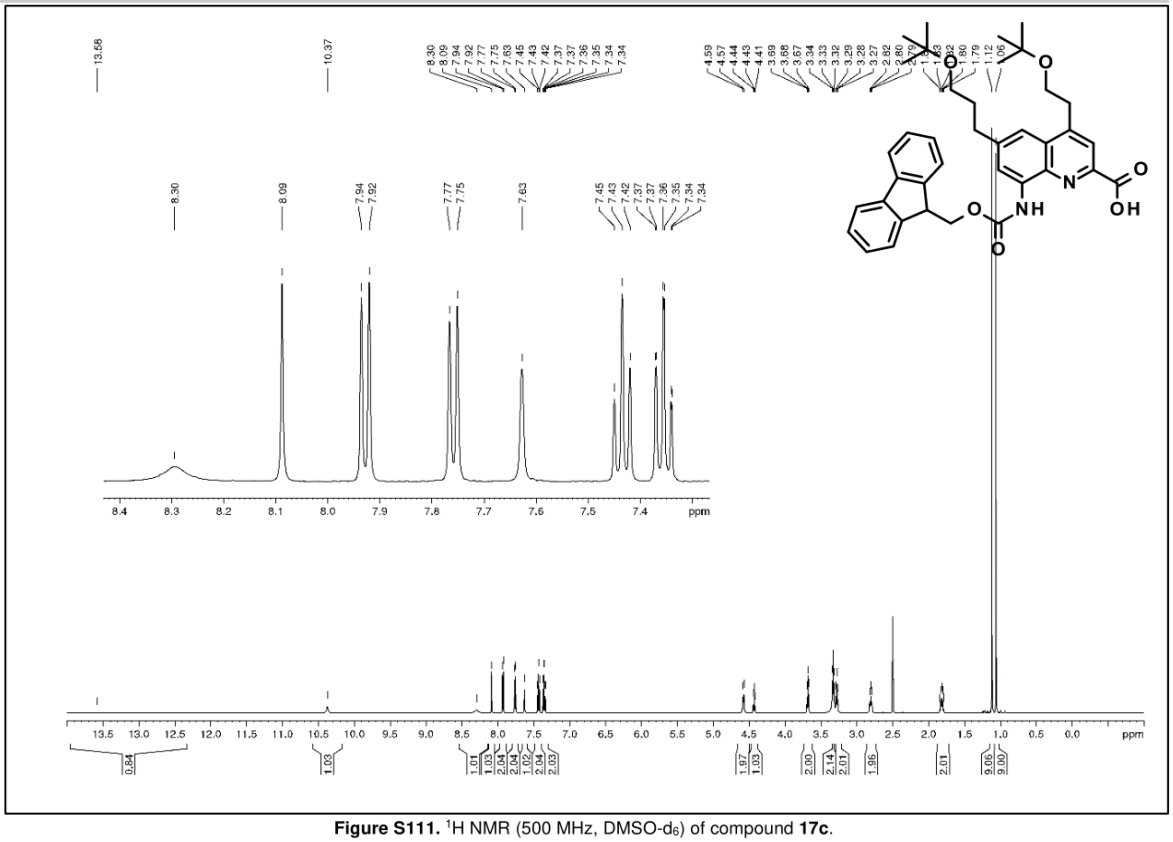

Figure S111. ^{1}H NMR (500 MHz, DMSO-d$_6$) of compound **17c**.

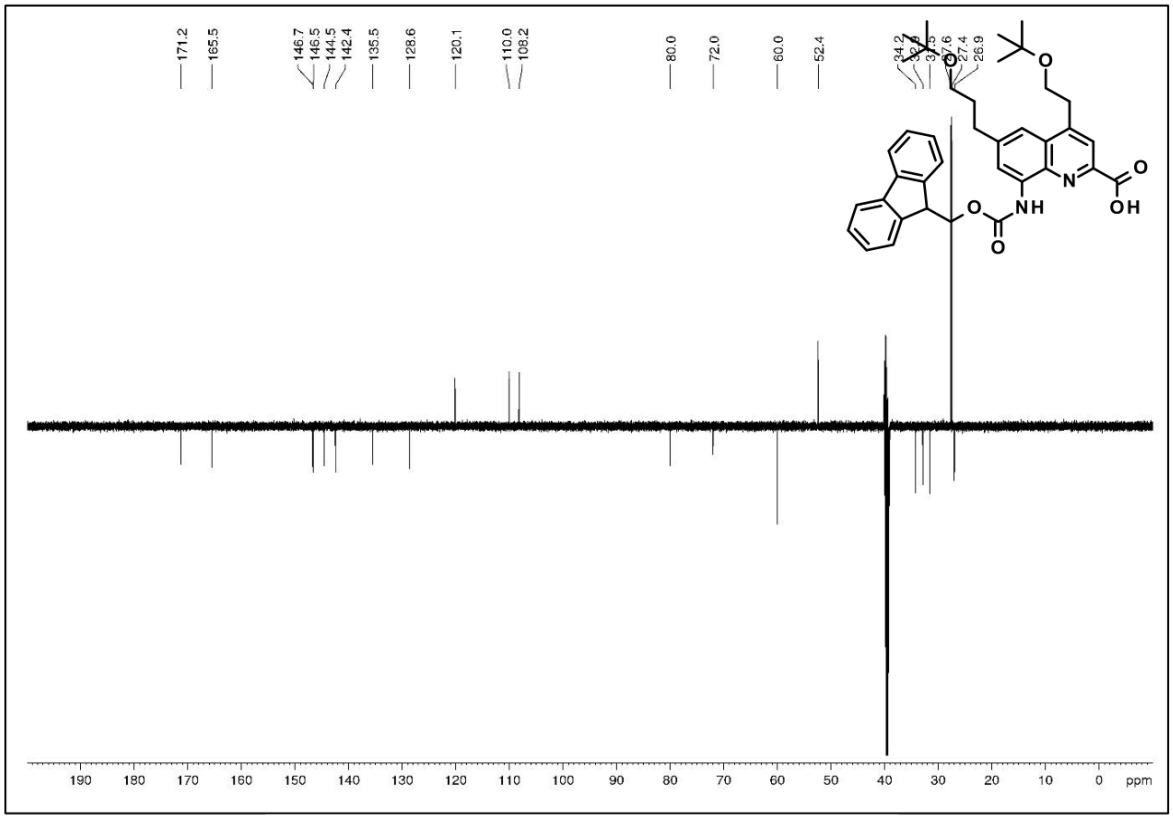

Figure S112. DEPT ^{13}C NMR (125 MHz, DMSO-d_6) of compound **17c**.

SUPPORTING INFORMATION

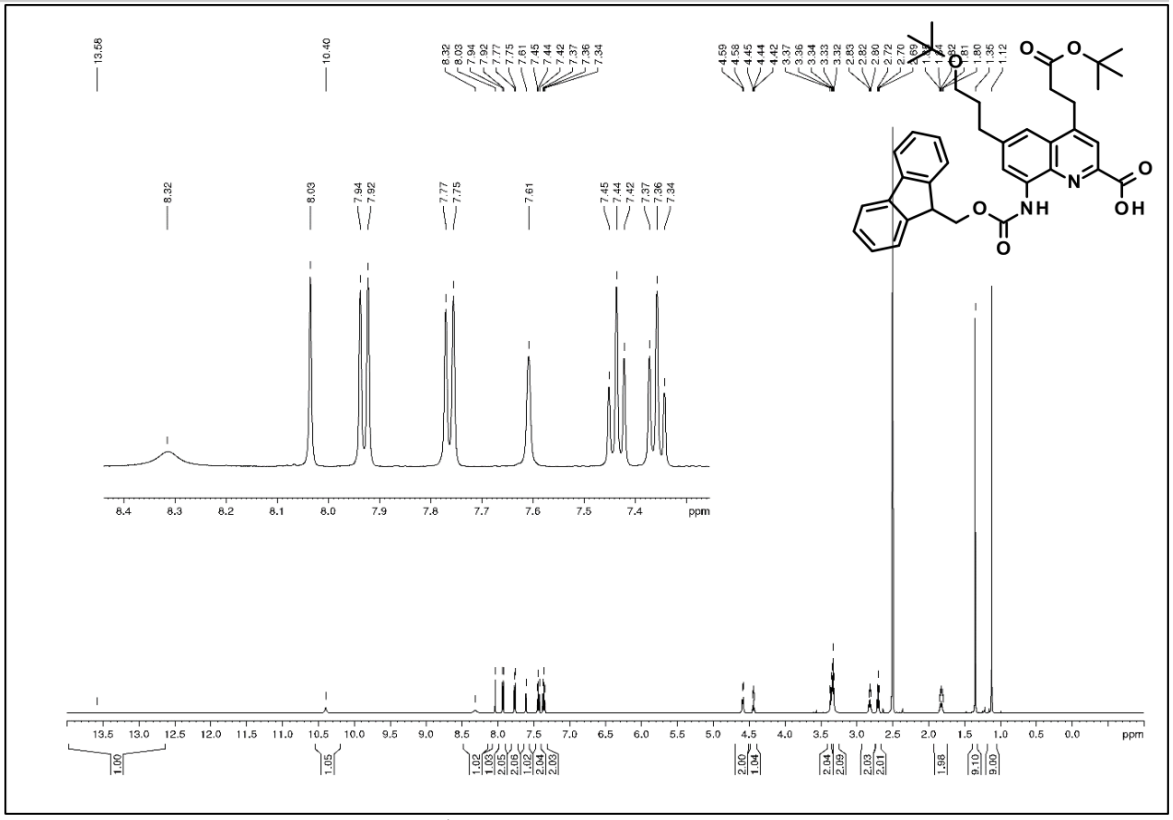

Figure S113. ^{1}H NMR (500 MHz, DMSO-d_6) of compound **17d**.

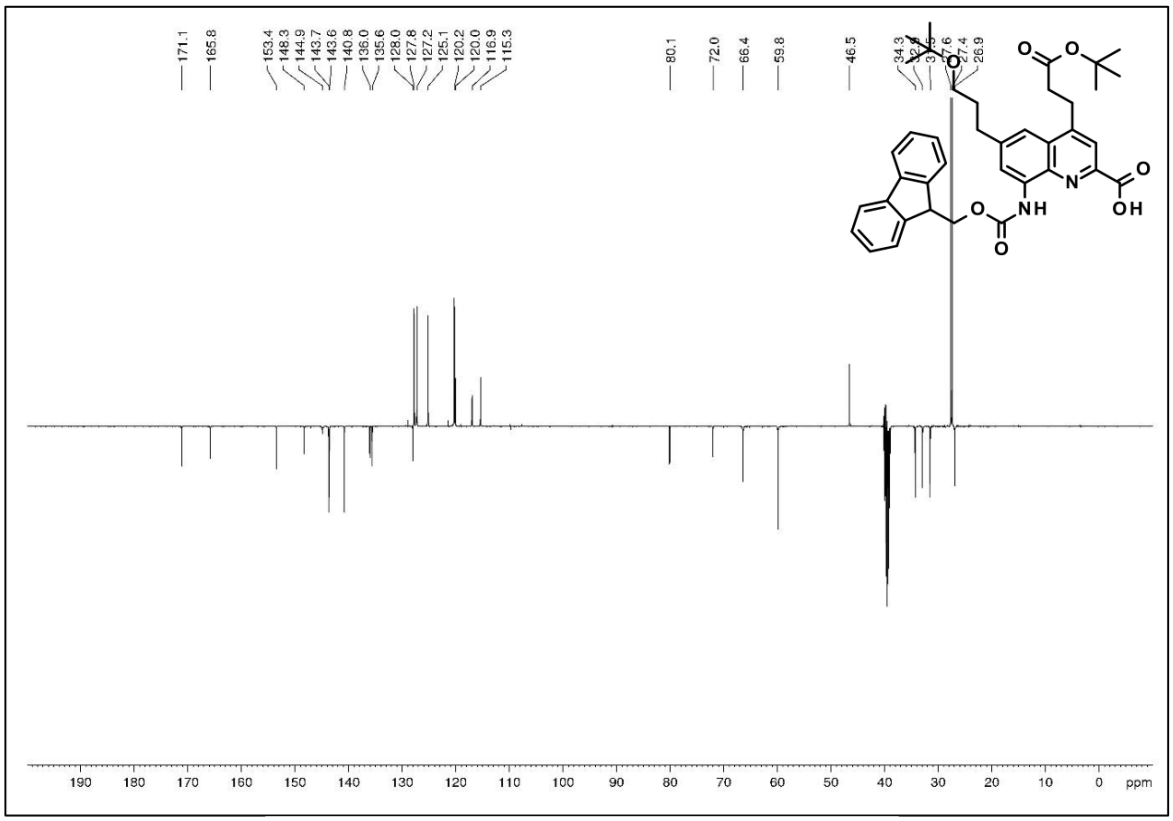

Figure S114. DEPT ^{13}C NMR (125 MHz, DMSO-d_6) of compound **17d**.

SUPPORTING INFORMATION

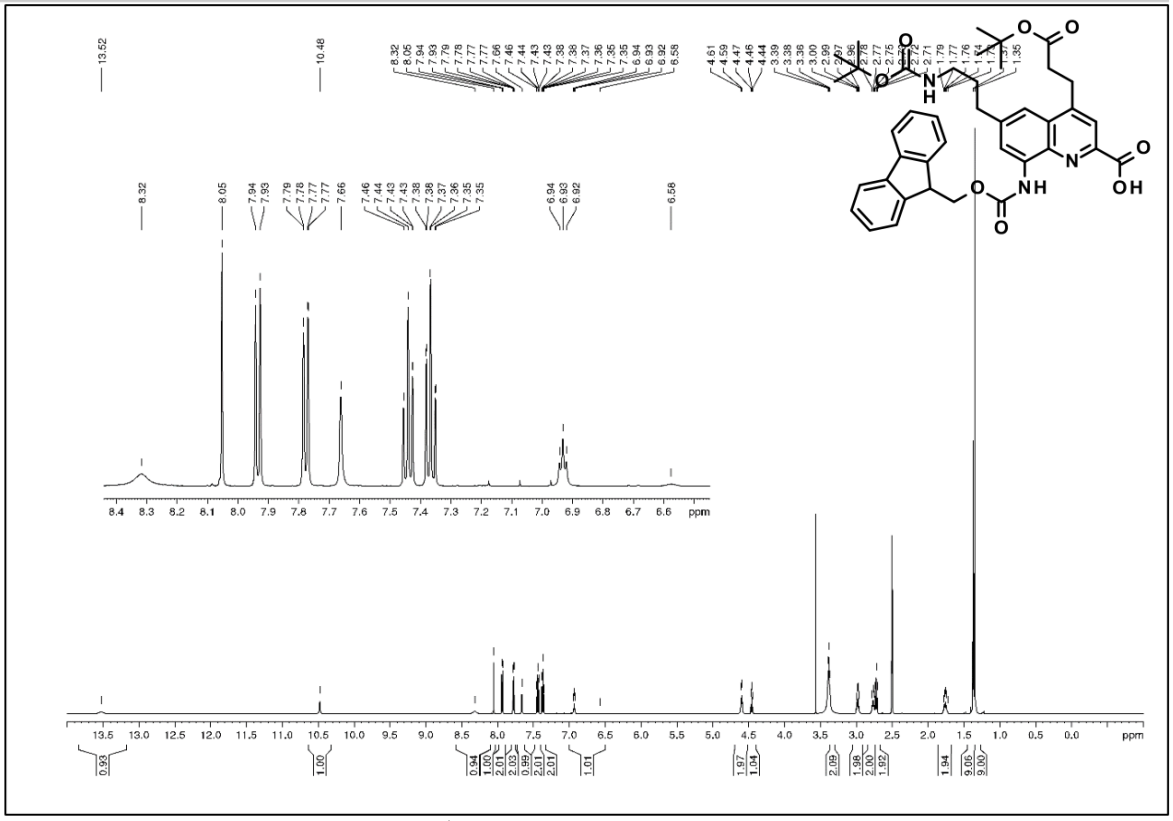

Figure S115. ^{1}H NMR (500 MHz, DMSO-d_6) of compound **17e**.

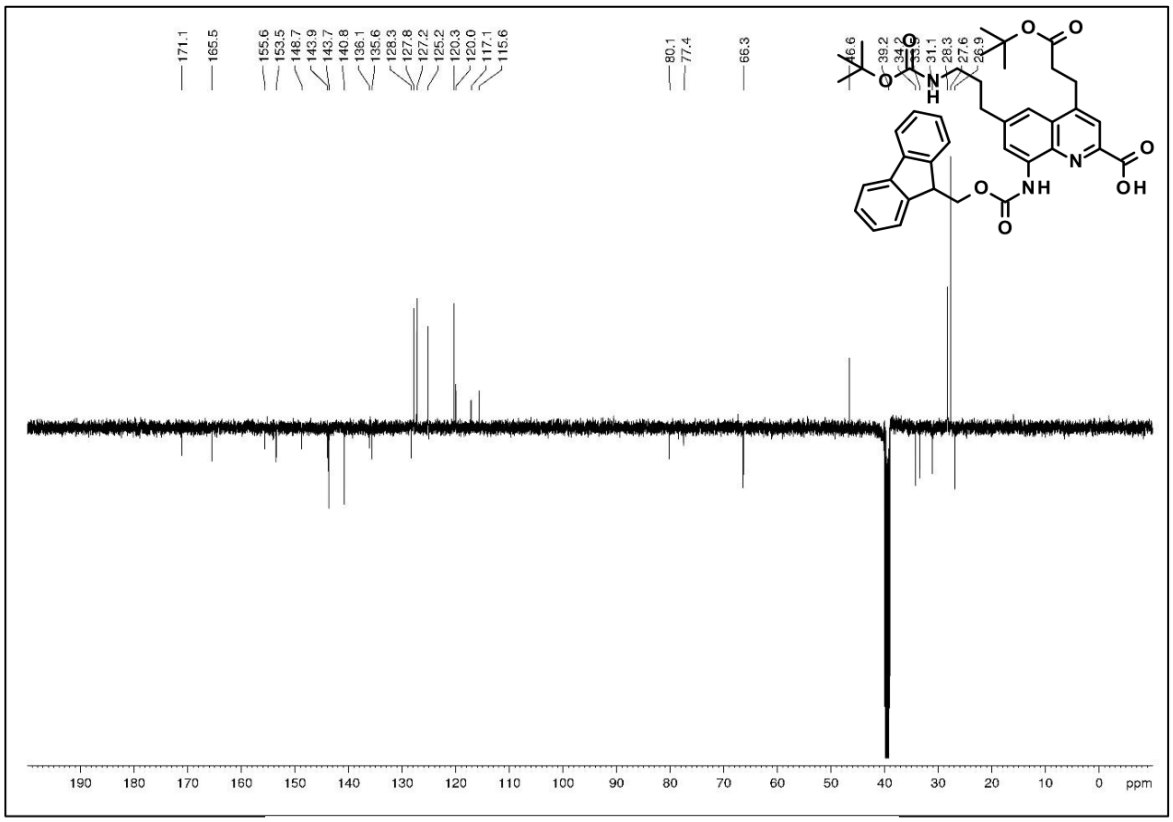

Figure S116. DEPT ^{13}C NMR (125 MHz, DMSO-d_6) of compound **17e**.

SUPPORTING INFORMATION

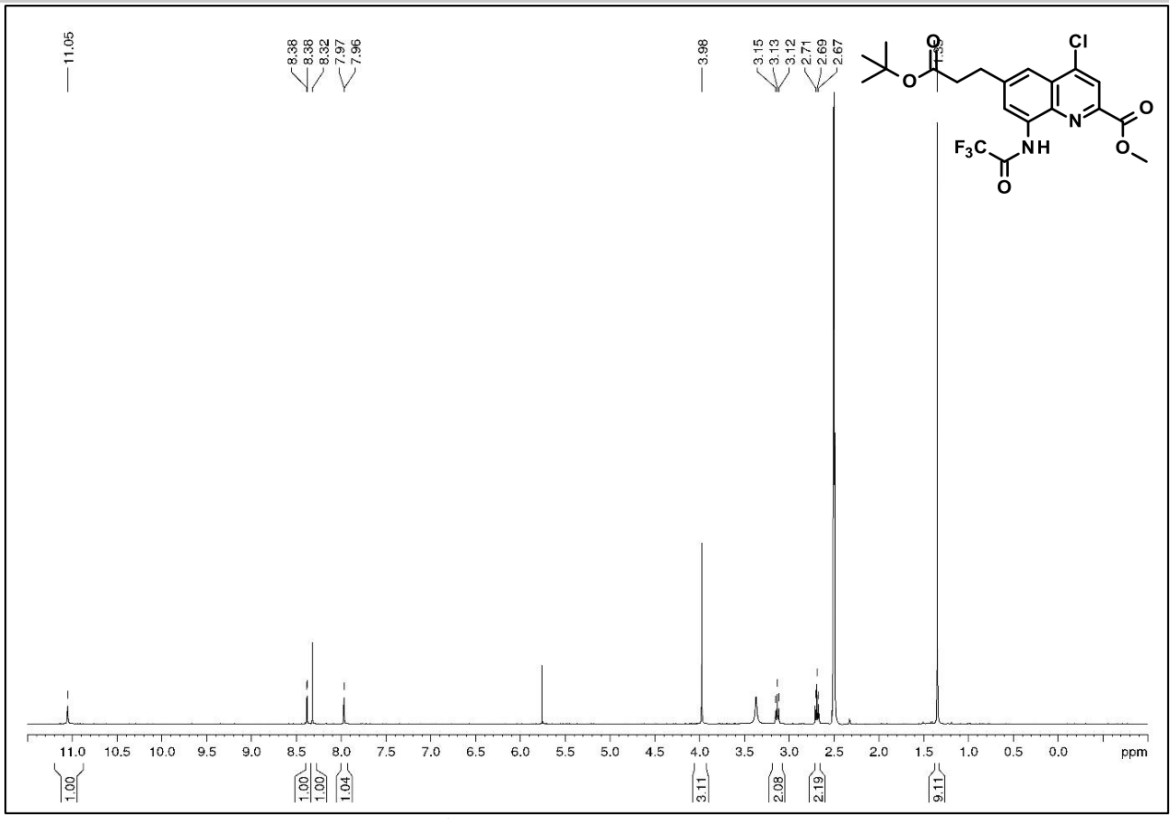

Figure S117. ^{1}H NMR (500 MHz, DMSO-d_6) of compound **19b**.

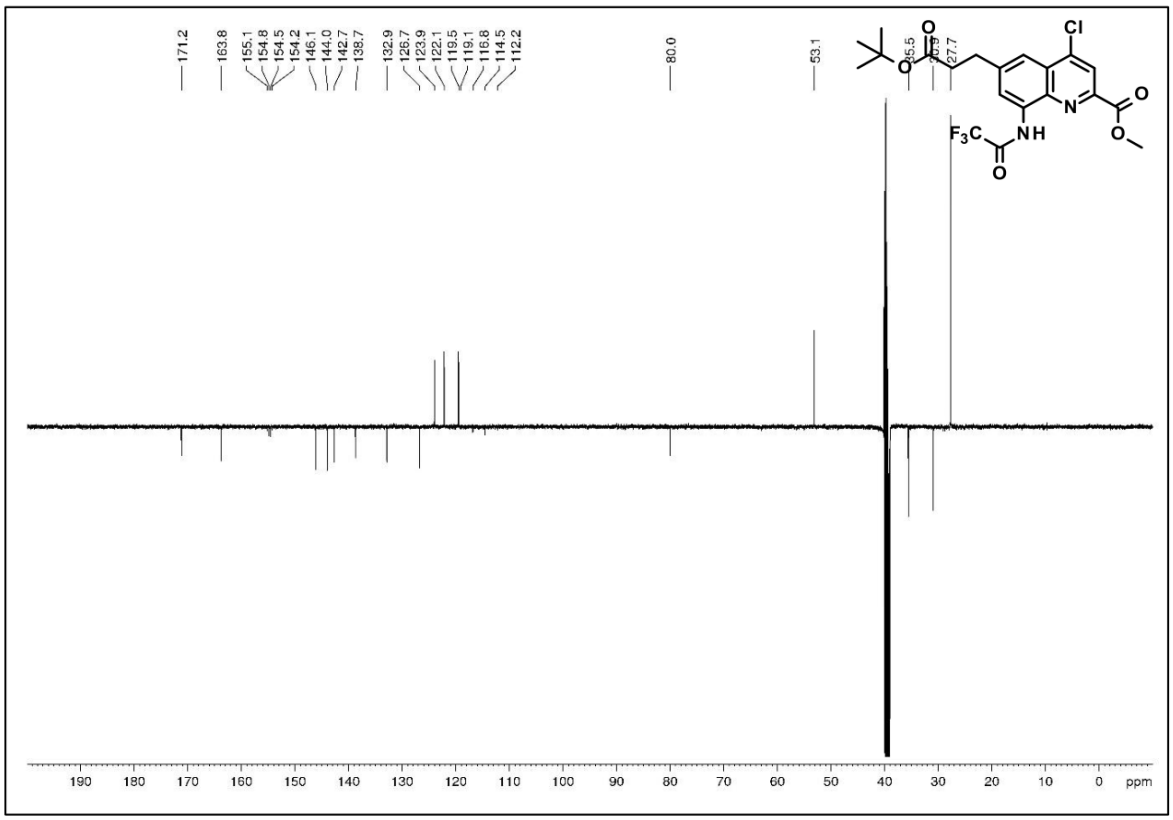

Figure S118. DEPT ^{13}C NMR (125 MHz, DMSO-d_6) of compound **19b**.

SUPPORTING INFORMATION

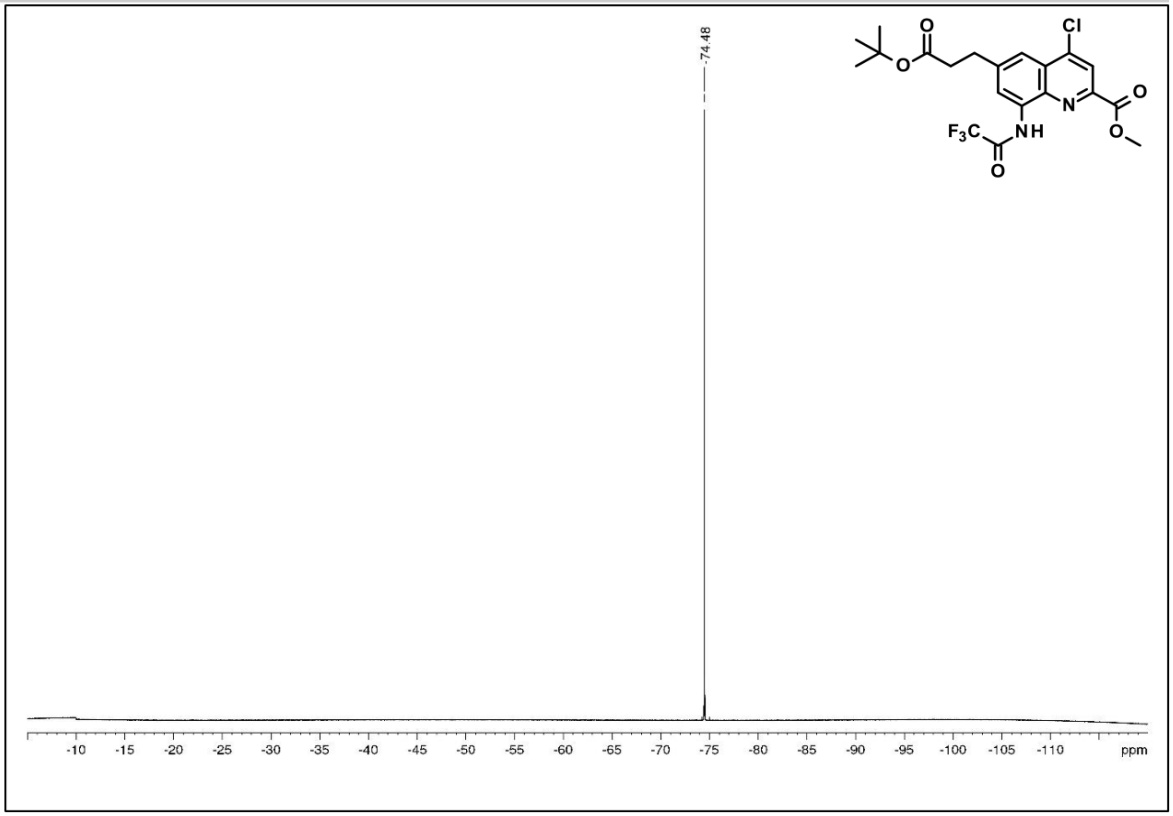

Figure S119. ^{19}F NMR (376 MHz, DMSO-d_6) of compound **19b**.

SUPPORTING INFORMATION

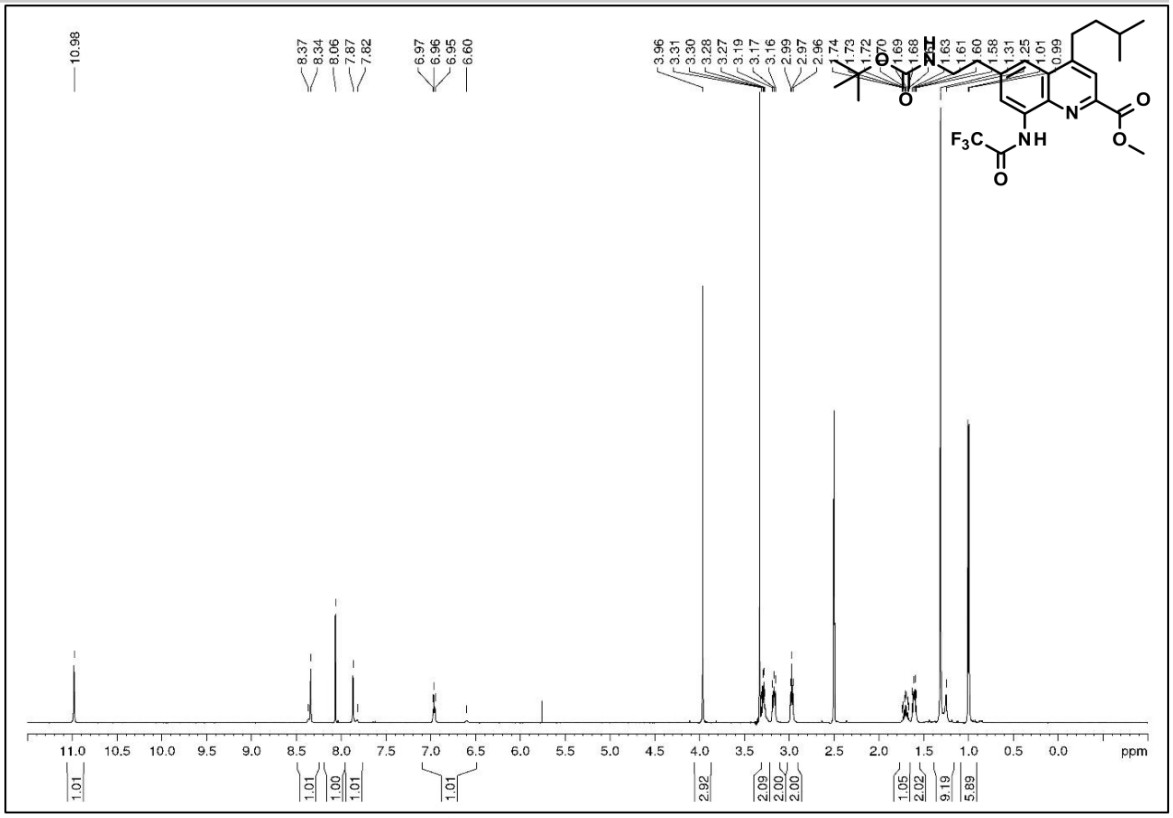

Figure S120. ^{1}H NMR (500 MHz, DMSO-d$_6$) of compound **20a**.

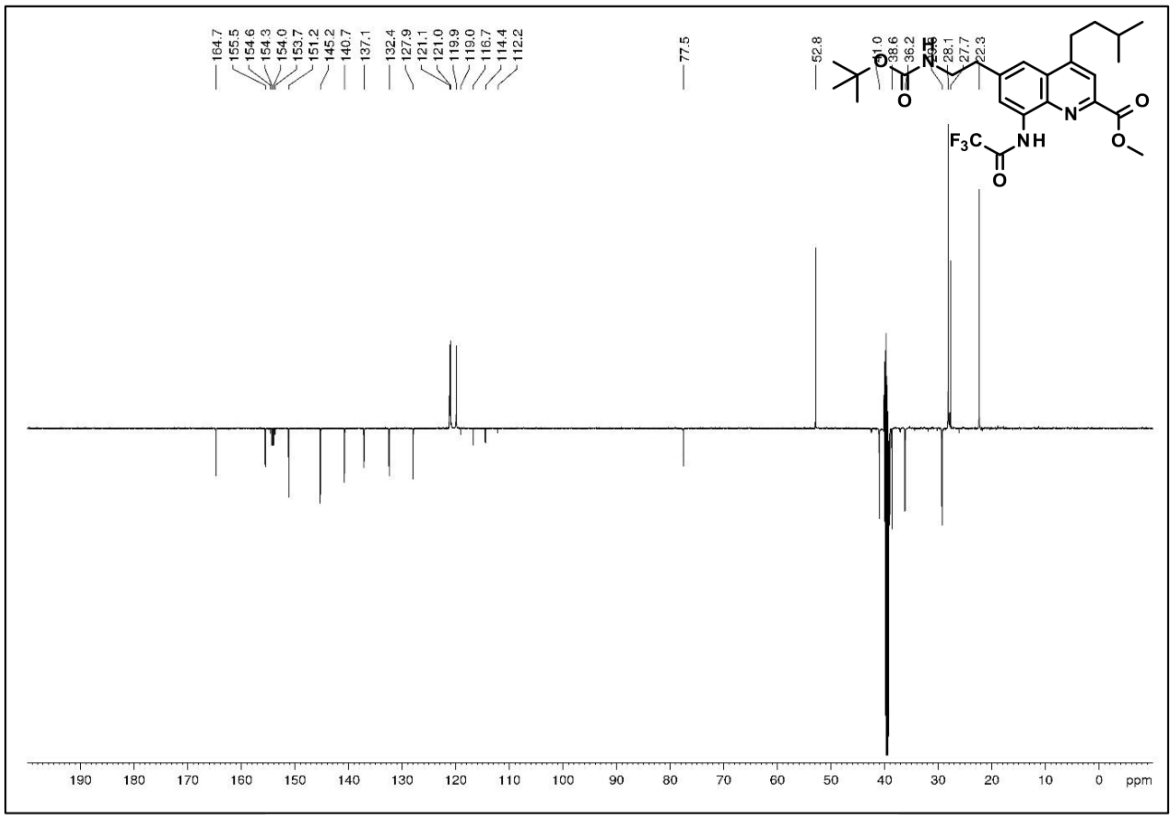

Figure S121. DEPT ^{13}C NMR (125 MHz, DMSO-d_6) of compound **20a**.

SUPPORTING INFORMATION

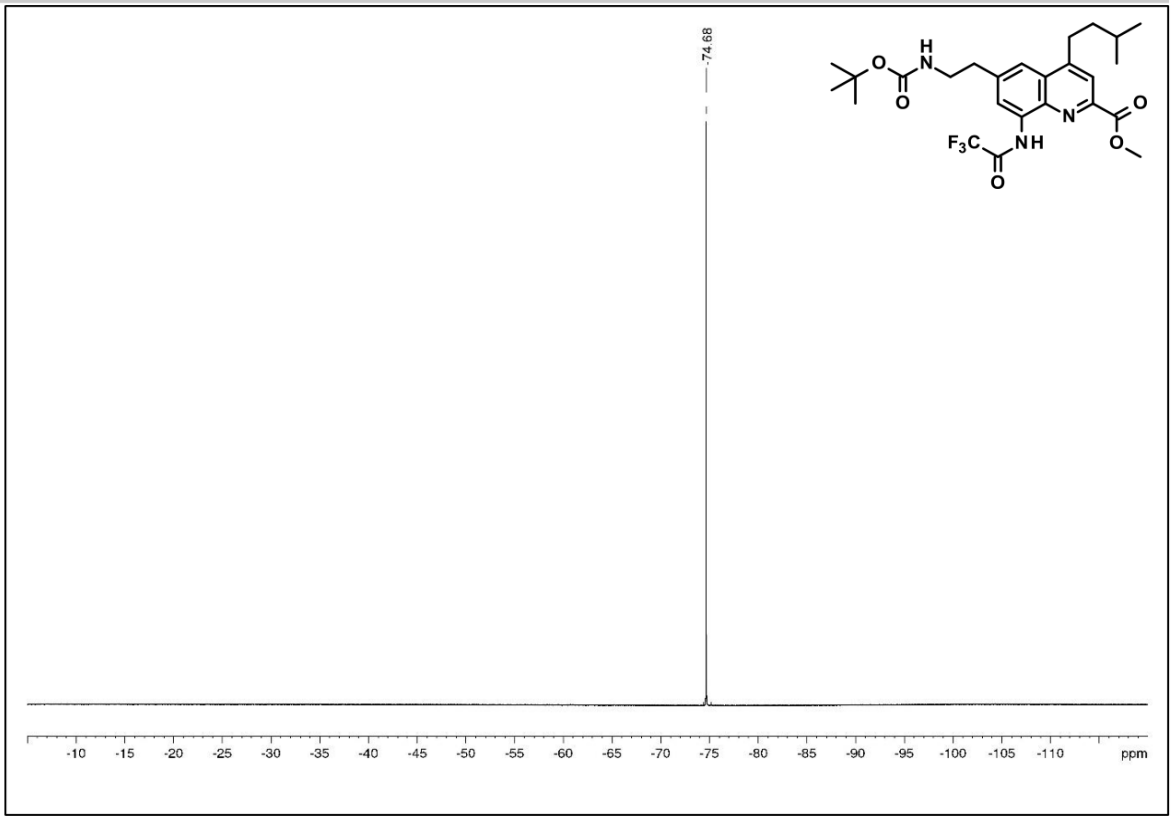

Figure S122. ^{19}F NMR (376 MHz, DMSO-d_6) of compound **20a**.

SUPPORTING INFORMATION

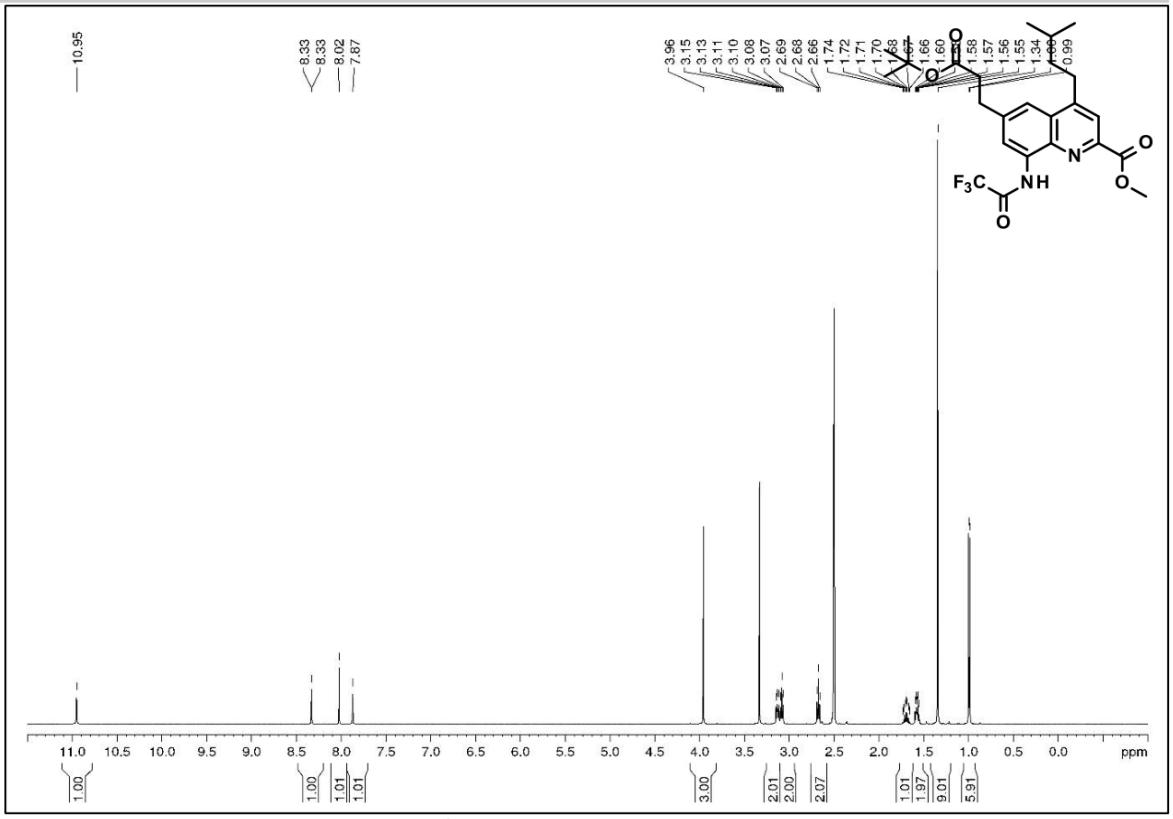

Figure S123. ^{1}H NMR (500 MHz, DMSO-d_6) of compound **20b**.

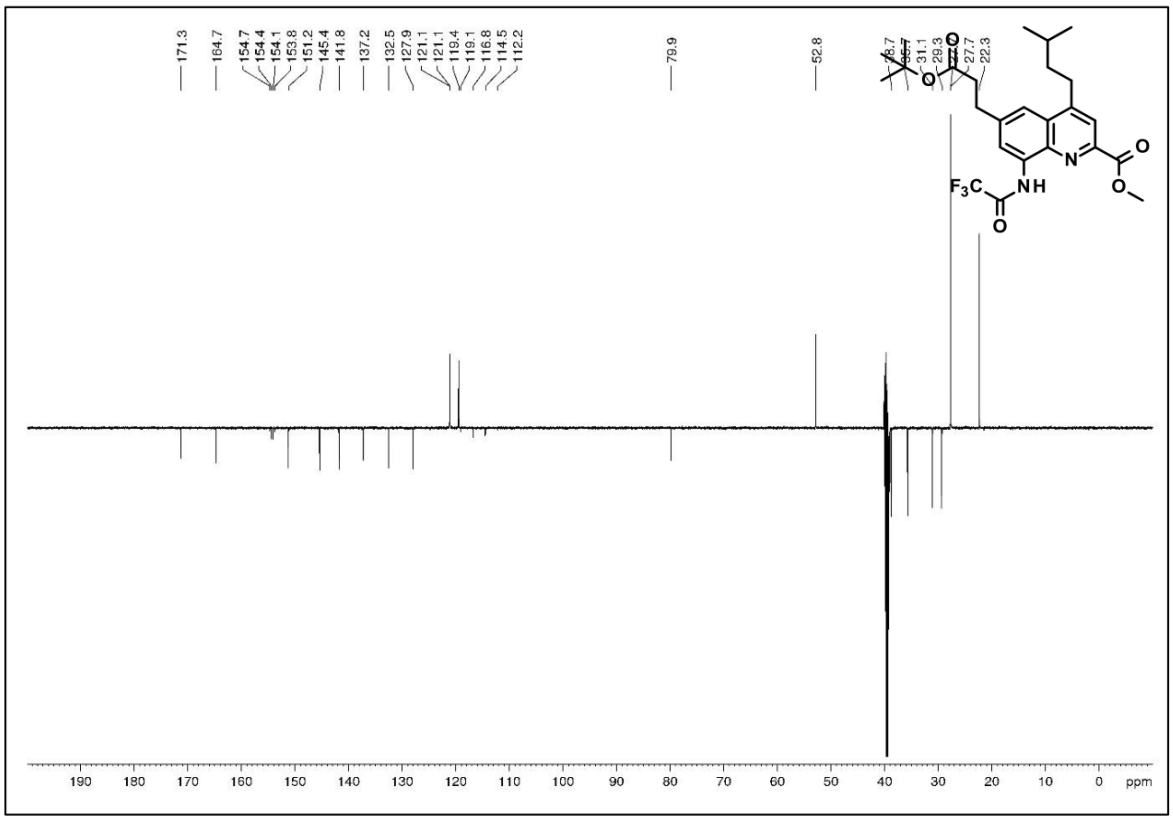

Figure S124. DEPT ^{13}C NMR (125 MHz, DMSO-d_6) of compound **20b**.

SUPPORTING INFORMATION

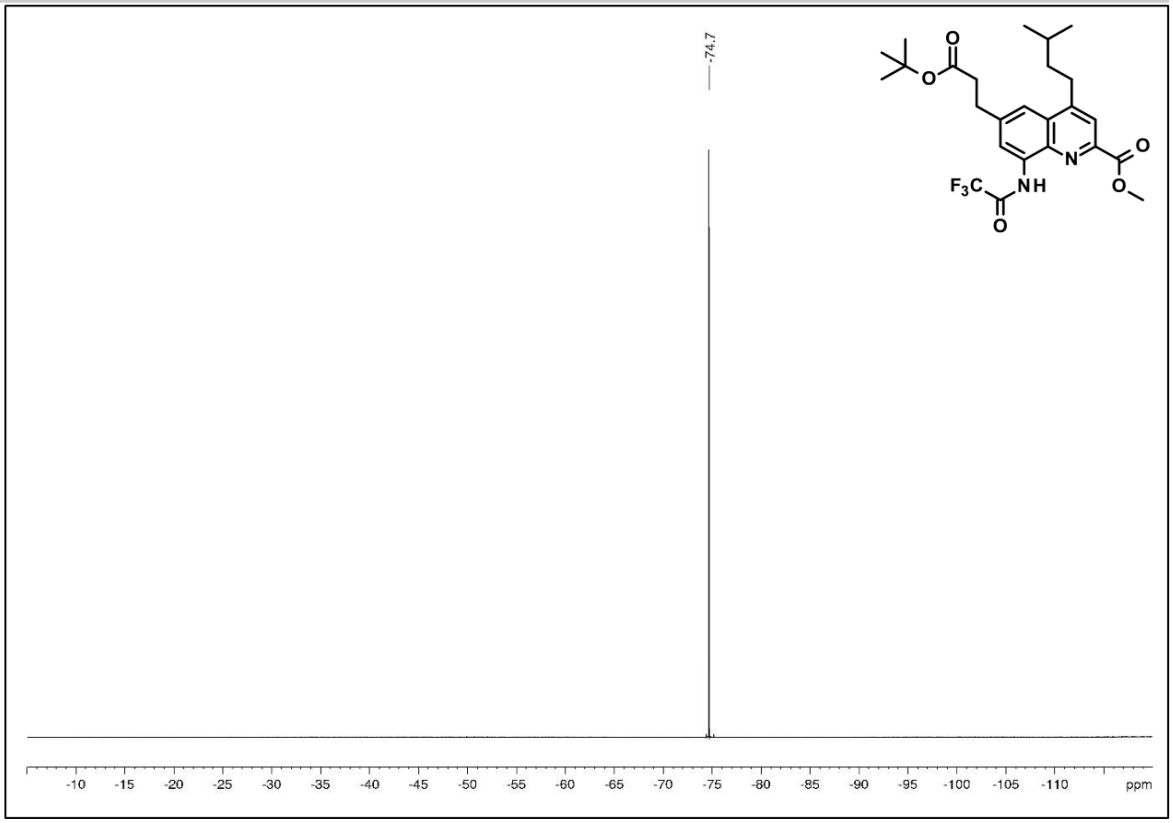

Figure S125. ^{19}F NMR (376 MHz, DMSO-d_6) of compound **20b**.

SUPPORTING INFORMATION

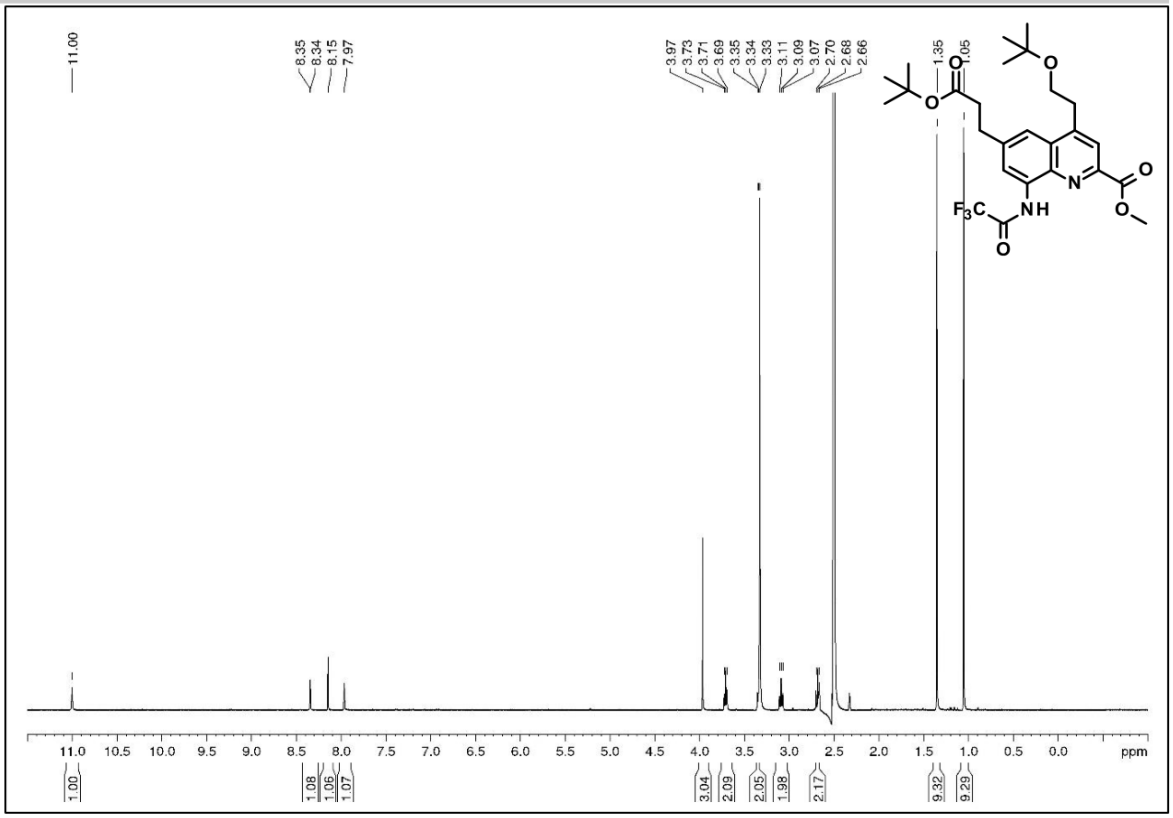

Figure S126. ^{1}H NMR (400 MHz, DMSO-d_6) of compound **20c**.

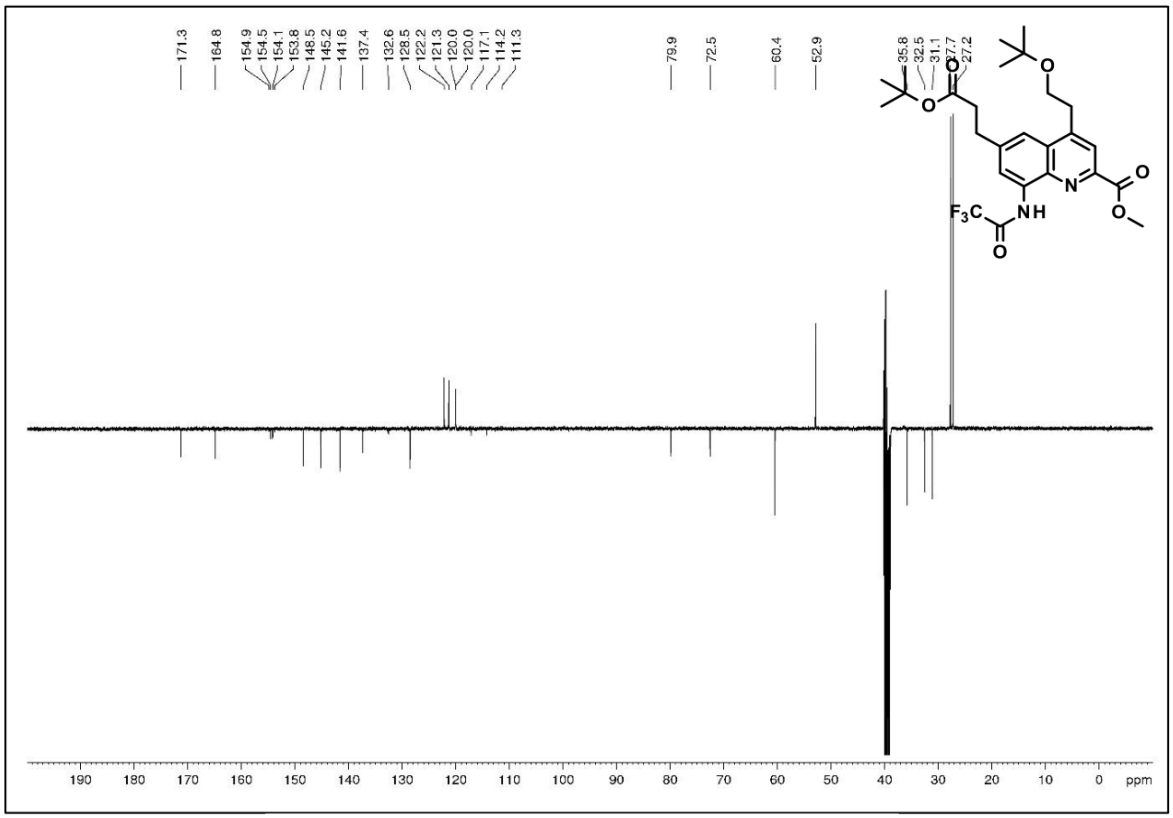

Figure S127. DEPT ^{13}C NMR (125 MHz, DMSO-d_6) of compound **20c**.

SUPPORTING INFORMATION

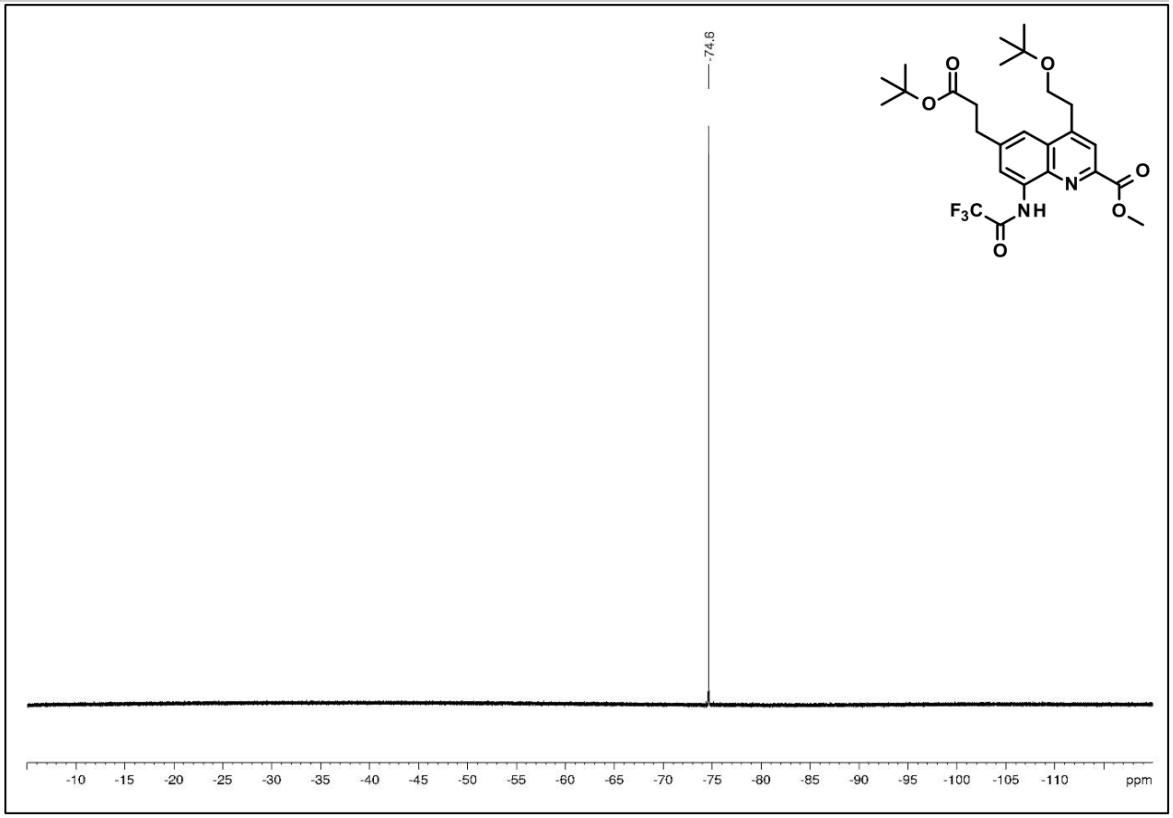

Figure S128. ^{19}F NMR (376 MHz, DMSO-d_6) of compound **20c**.

SUPPORTING INFORMATION

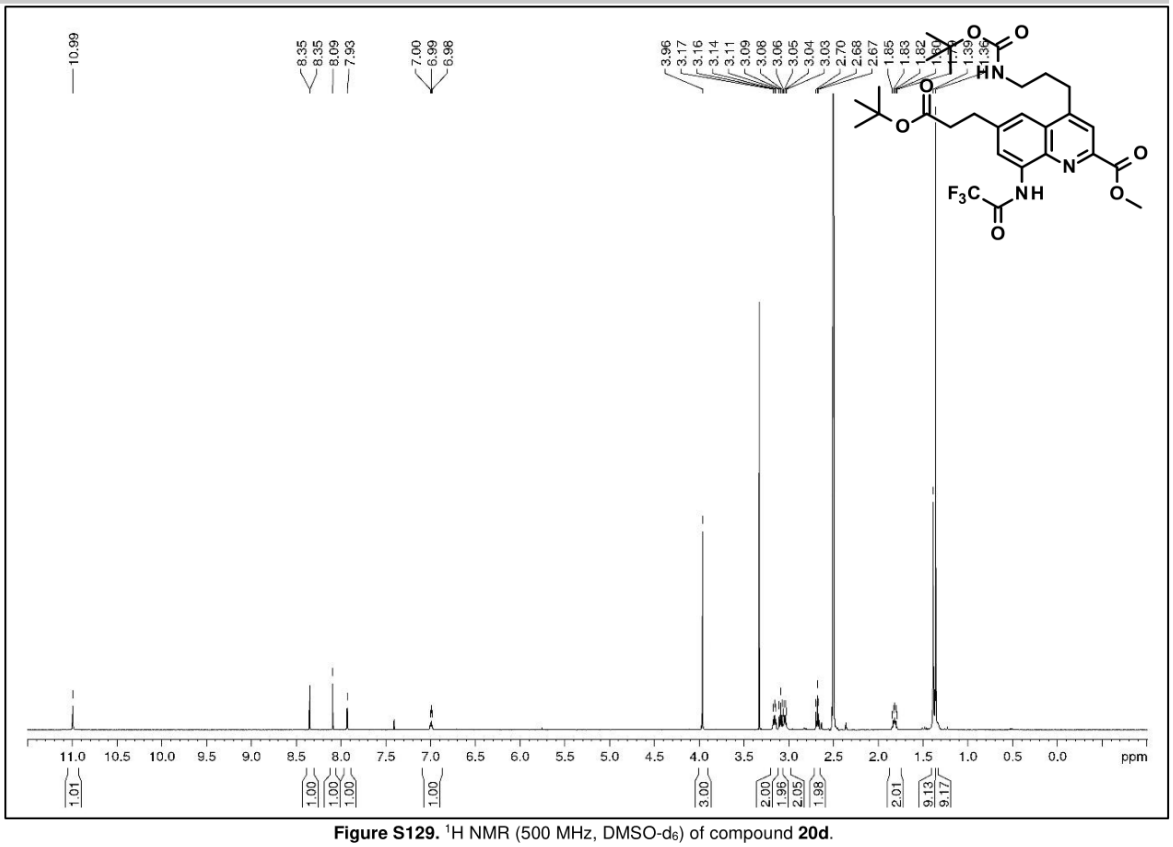

Figure S129. ^{1}H NMR (500 MHz, DMSO-d_6) of compound **20d**.

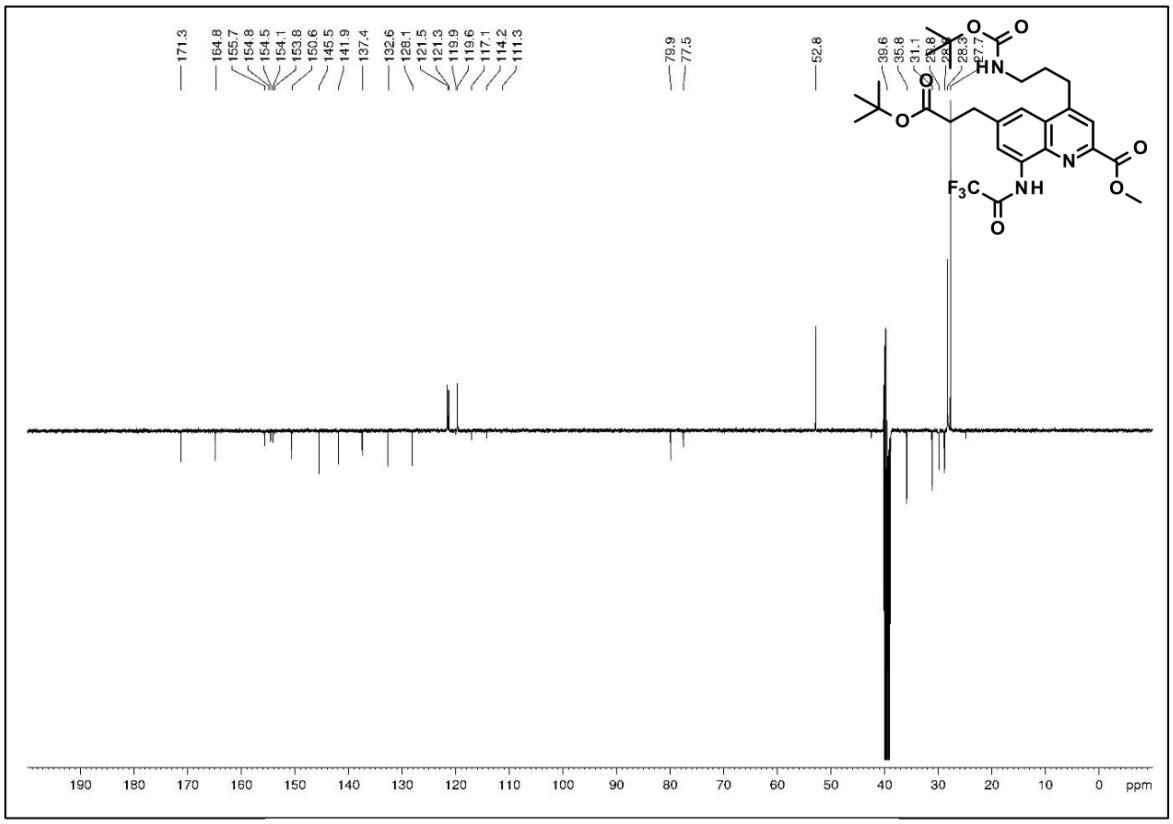

Figure S130. DEPT ^{13}C NMR (125 MHz, DMSO-d_6) of compound **20d**.

SUPPORTING INFORMATION

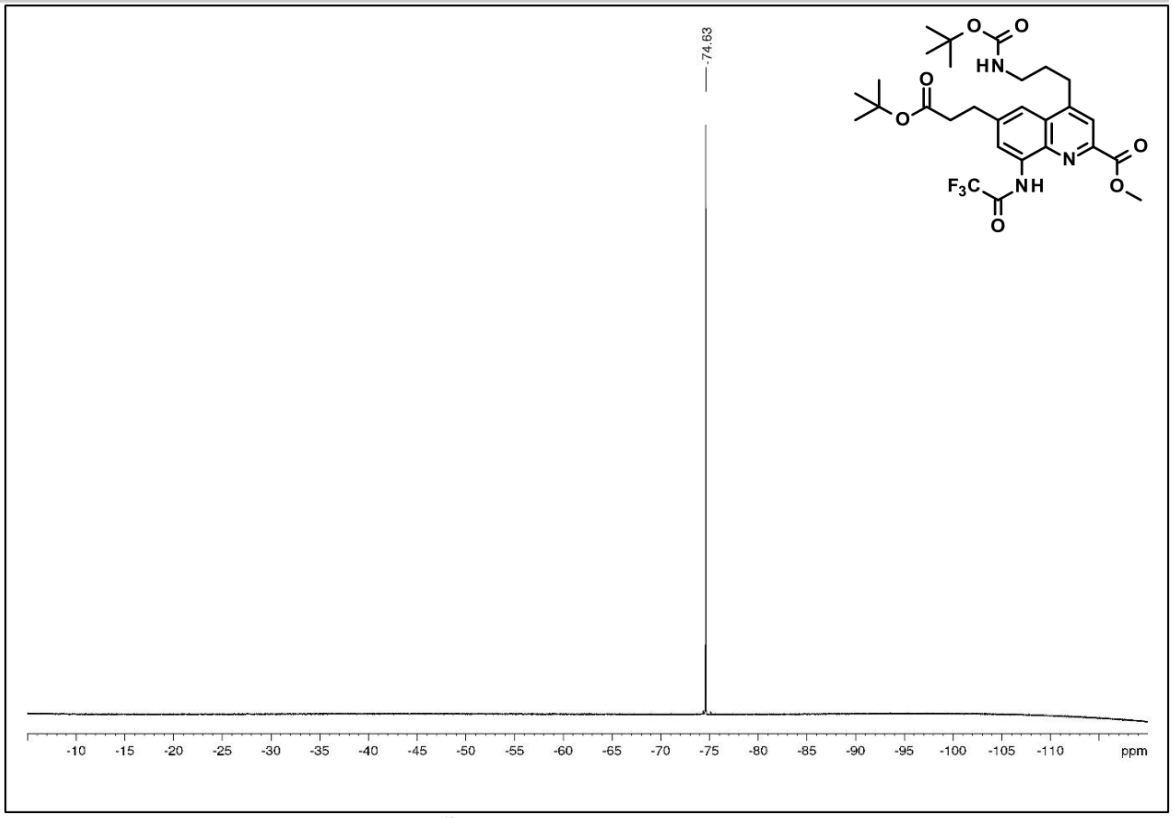

Figure S131. ^{19}F NMR (376 MHz, DMSO-d_6) of compound **20d**.

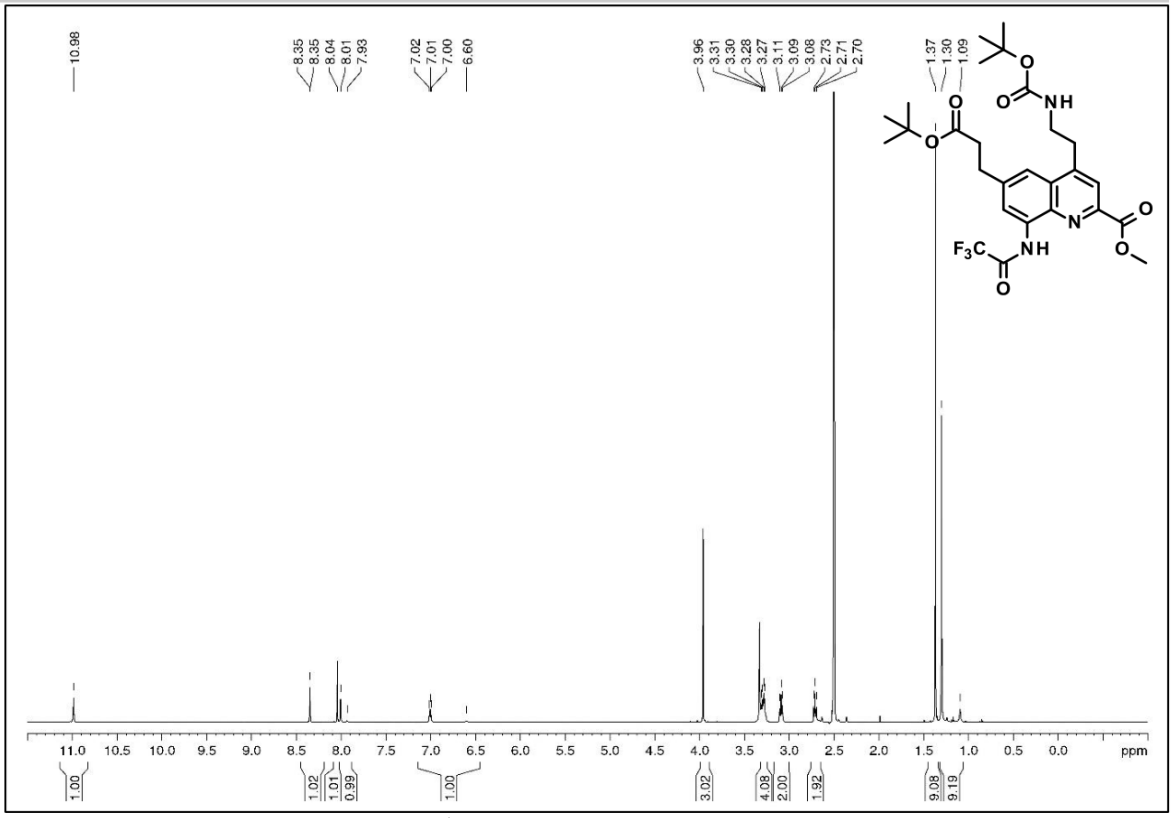

Figure S132. ^{1}H NMR (500 MHz, DMSO-d_6) of compound **20e**.

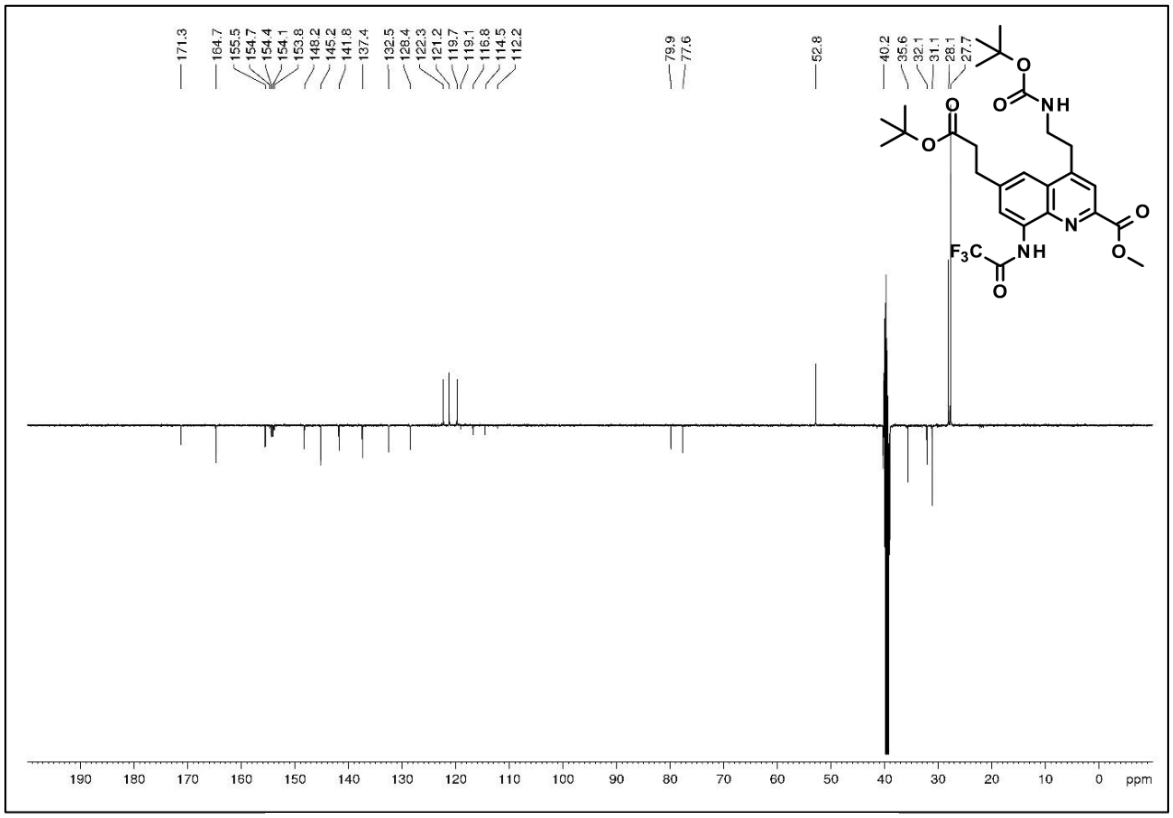

Figure S133. DEPT ^{13}C NMR (125 MHz, DMSO-d_6) of compound **20e**.

SUPPORTING INFORMATION

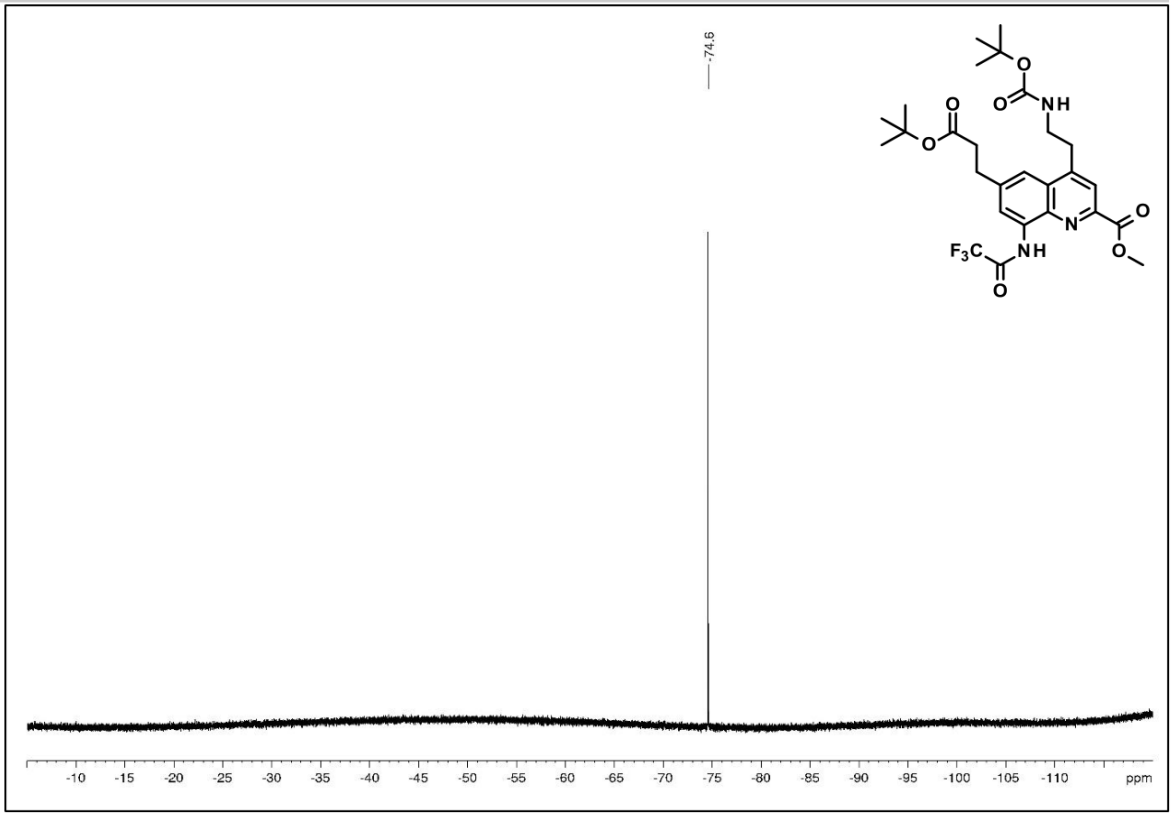

Figure S134. ^{19}F NMR (376 MHz, DMSO-d_6) of compound **20e.**

SUPPORTING INFORMATION

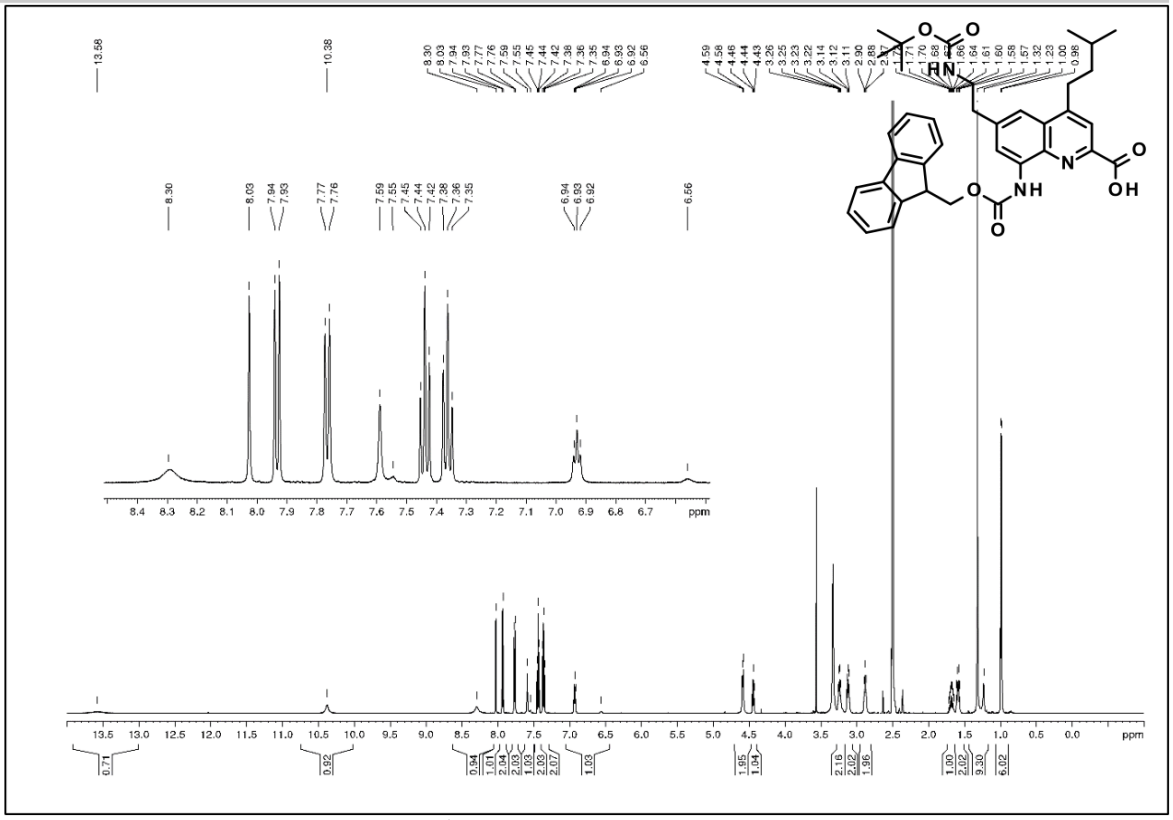

Figure S135. ^{1}H NMR (500 MHz, DMSO-d_6) of compound **21a**.

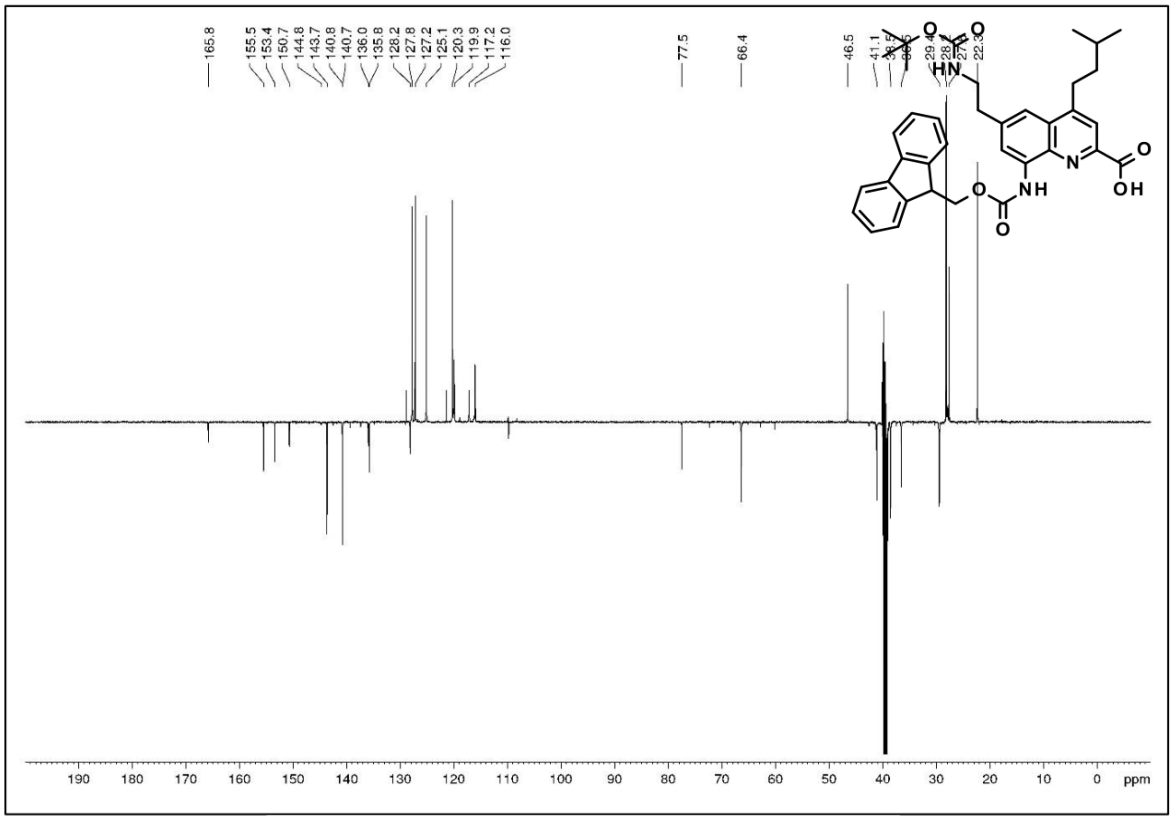

Figure S136. DEPT ^{13}C NMR (125 MHz, DMSO-d_6) of compound **21a**.

SUPPORTING INFORMATION

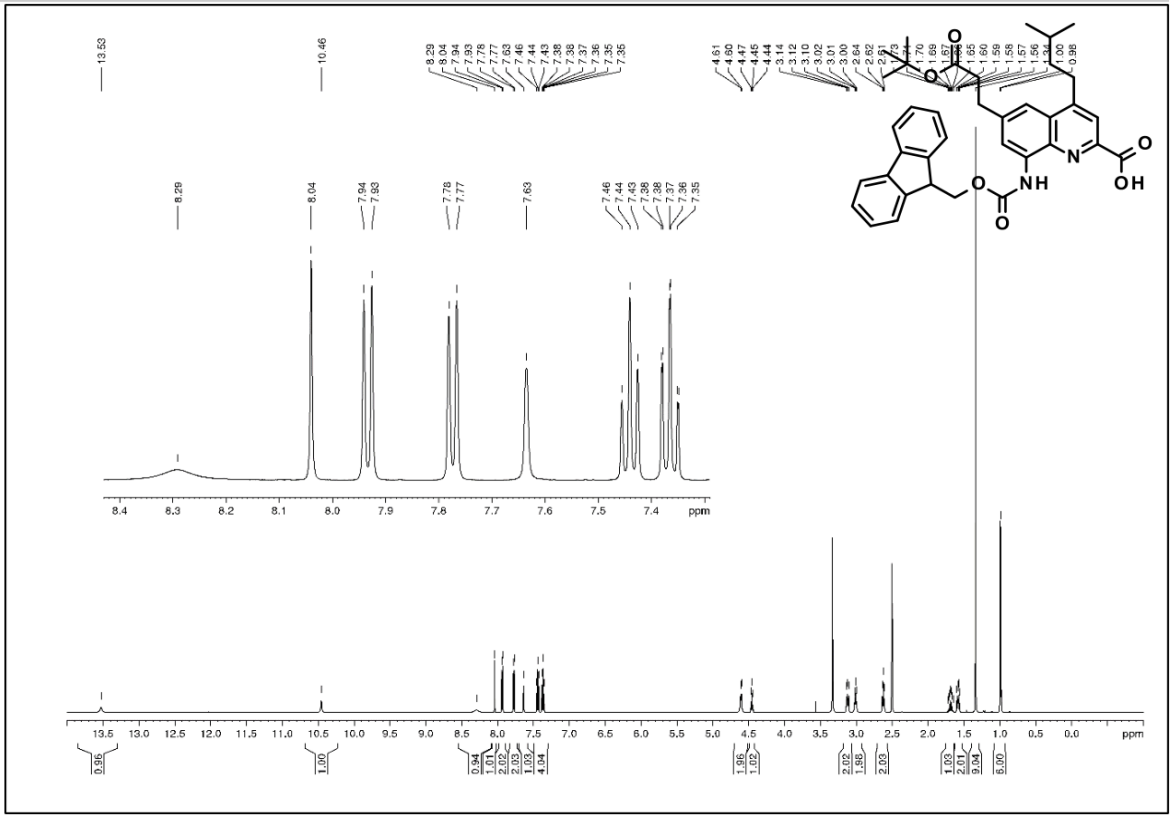

Figure S137. ^{1}H NMR (500 MHz, DMSO-d_6) of compound **21b**.

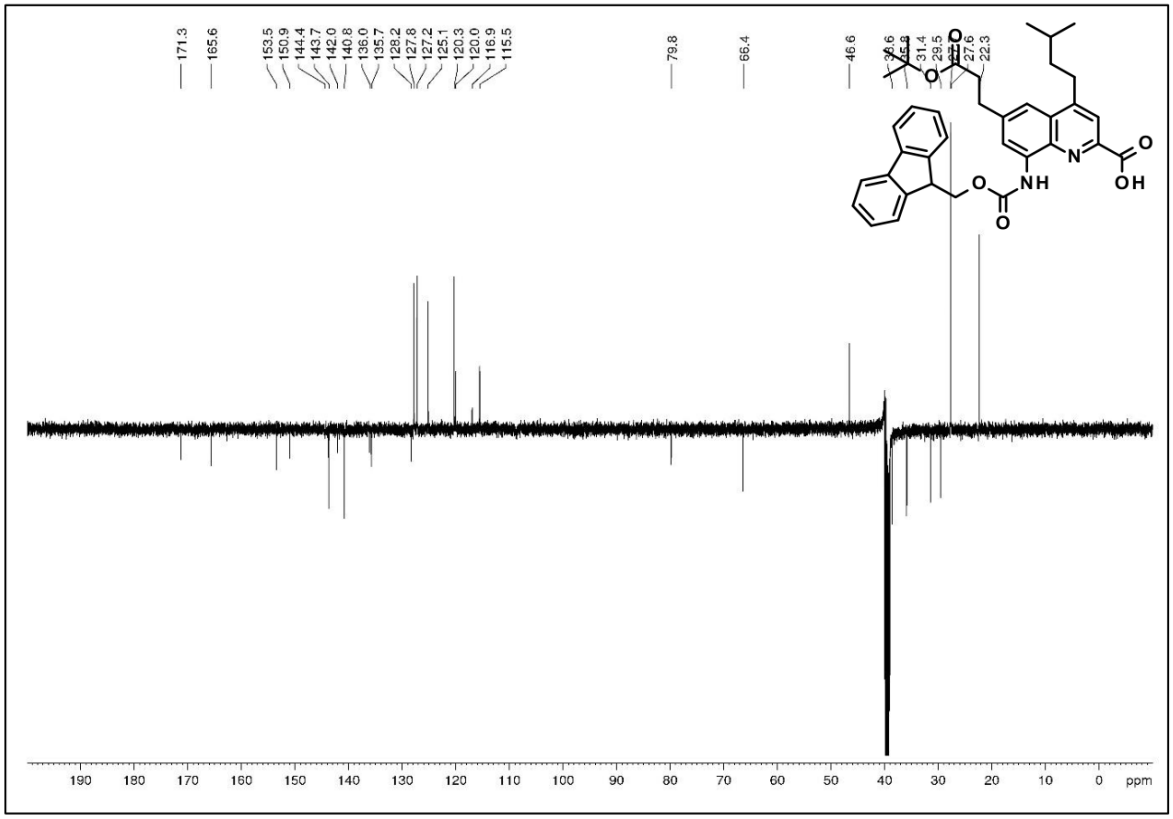

Figure S138. DEPT ^{13}C NMR (125 MHz, DMSO-d_6) of compound **21b**.

SUPPORTING INFORMATION

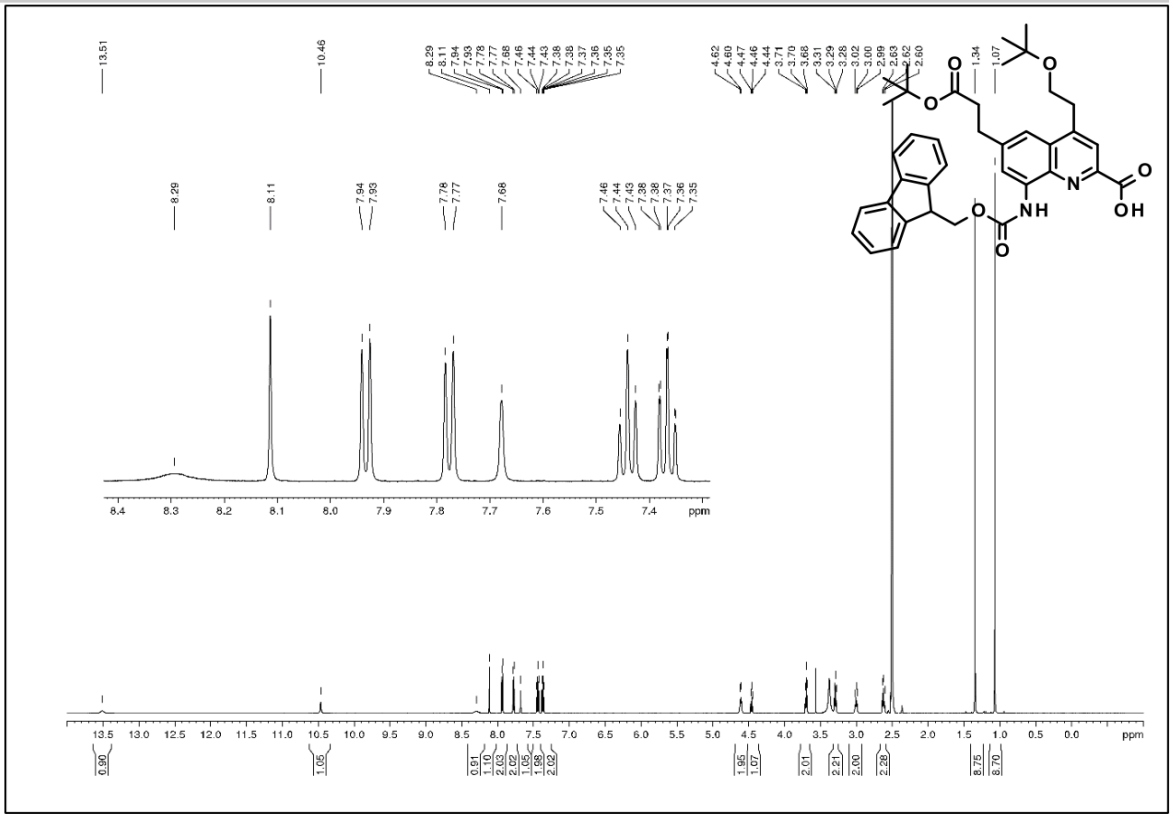

Figure S139. ^{1}H NMR (500 MHz, DMSO-d_6) of compound **21c**.

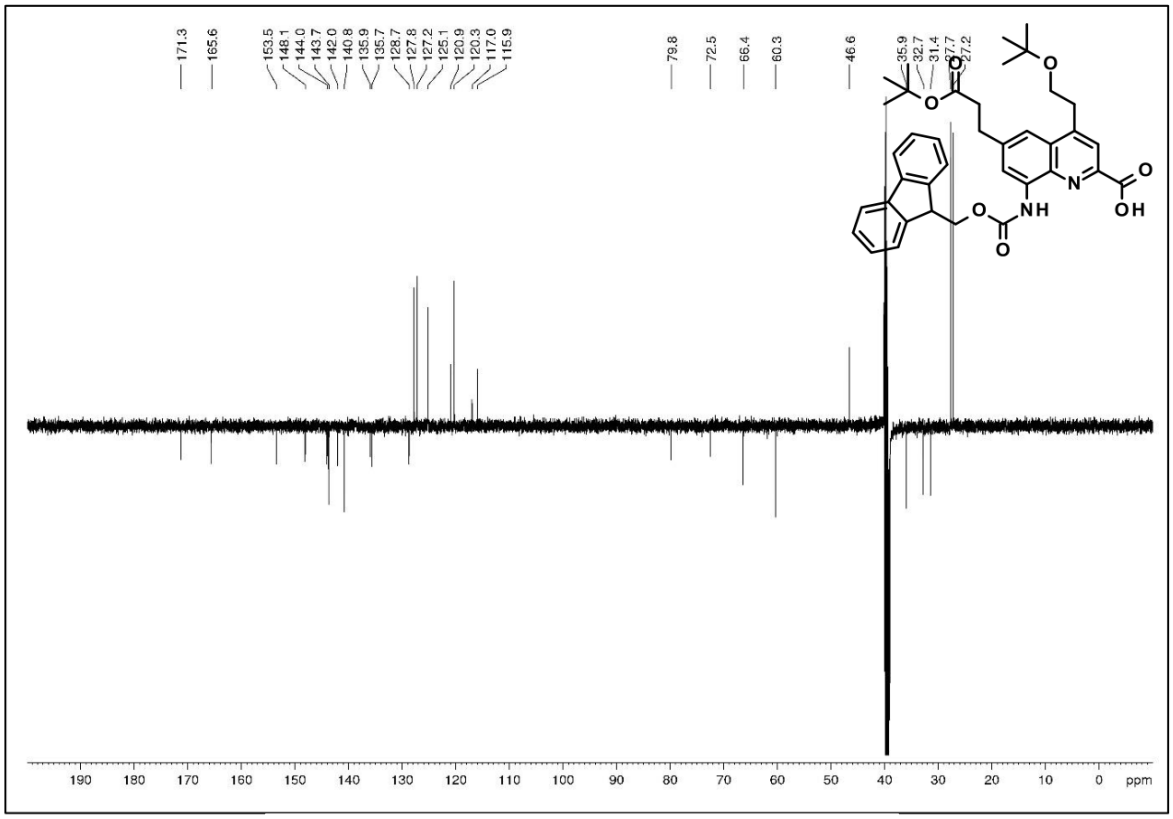

Figure S140. DEPT ^{13}C NMR (125 MHz, DMSO-d_6) of compound **21c**.

SUPPORTING INFORMATION

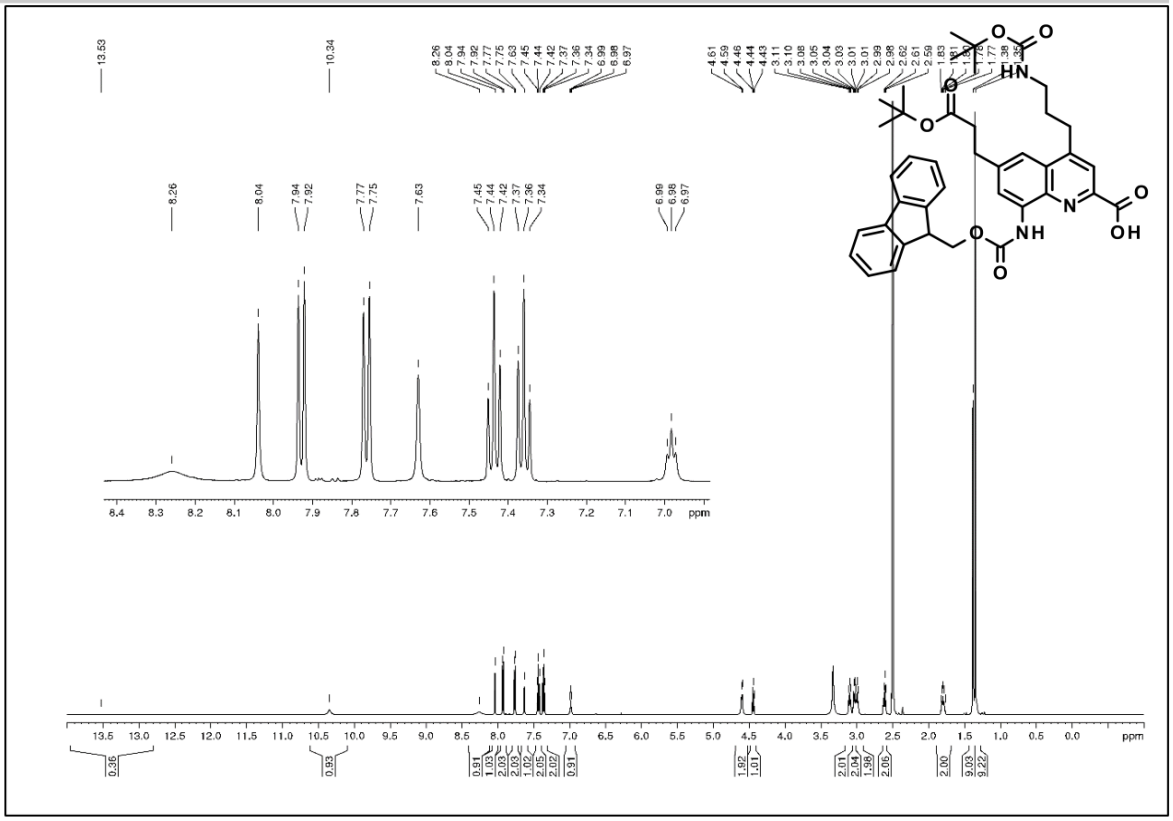

Figure S141. ^{1}H NMR (500 MHz, DMSO-d$_6$) of compound **21d**.

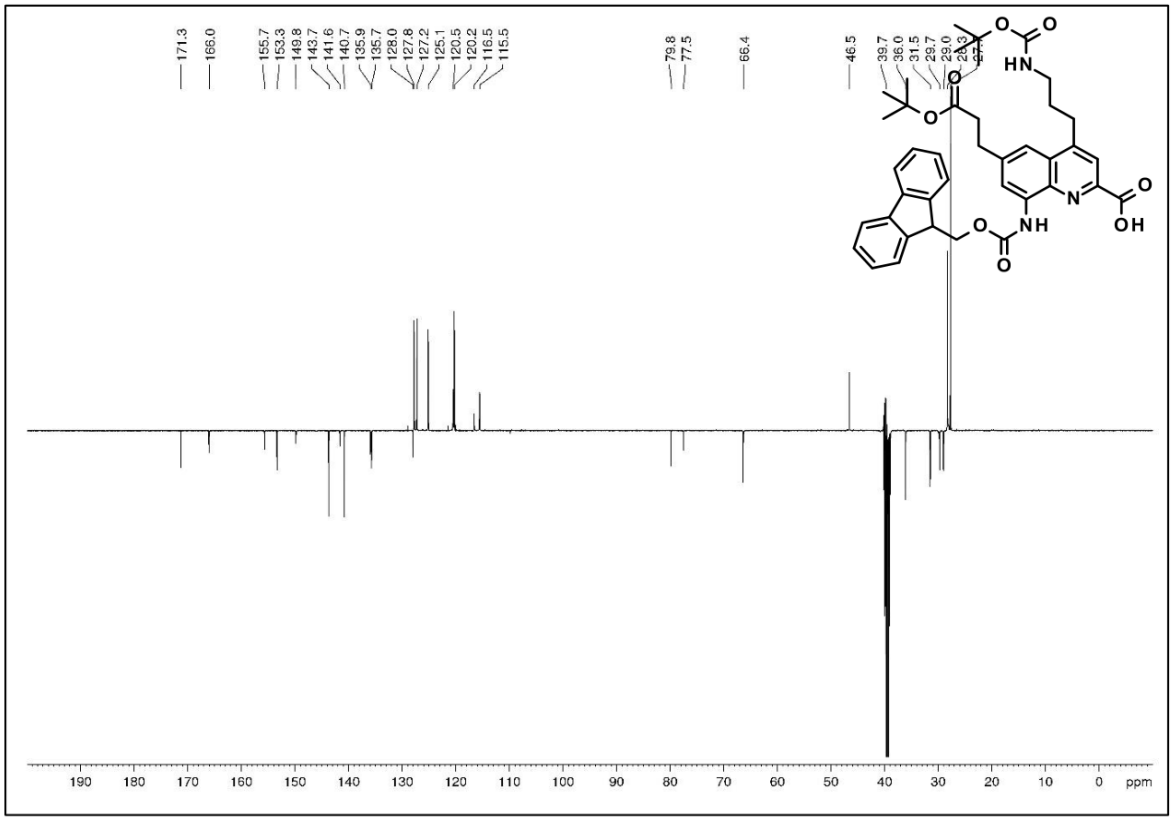

Figure S142. DEPT ^{13}C NMR (125 MHz, DMSO-d_6) of compound **21d**.

SUPPORTING INFORMATION

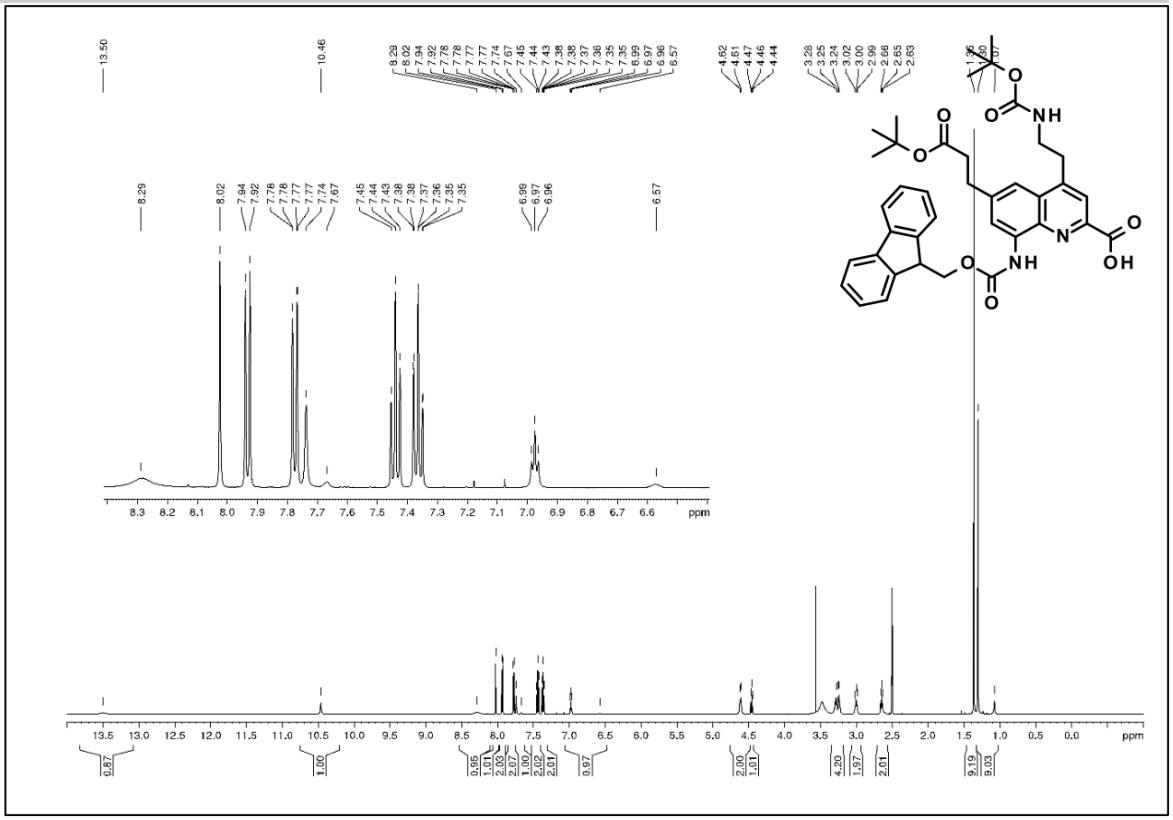

Figure S143. ^{1}H NMR (500 MHz, DMSO-d_6) of compound **21e**.

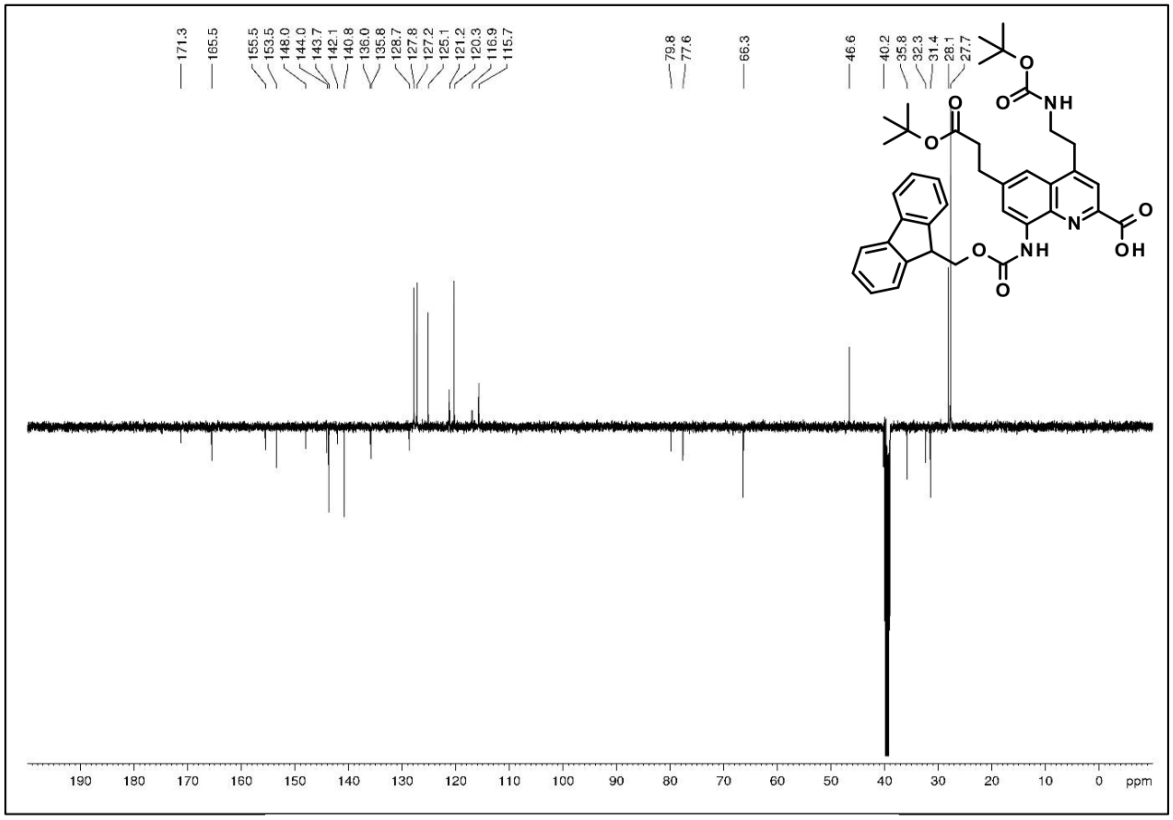

Figure S144. DEPT ^{13}C NMR (125 MHz, DMSO-d_6) of compound **21e**.

SUPPORTING INFORMATION

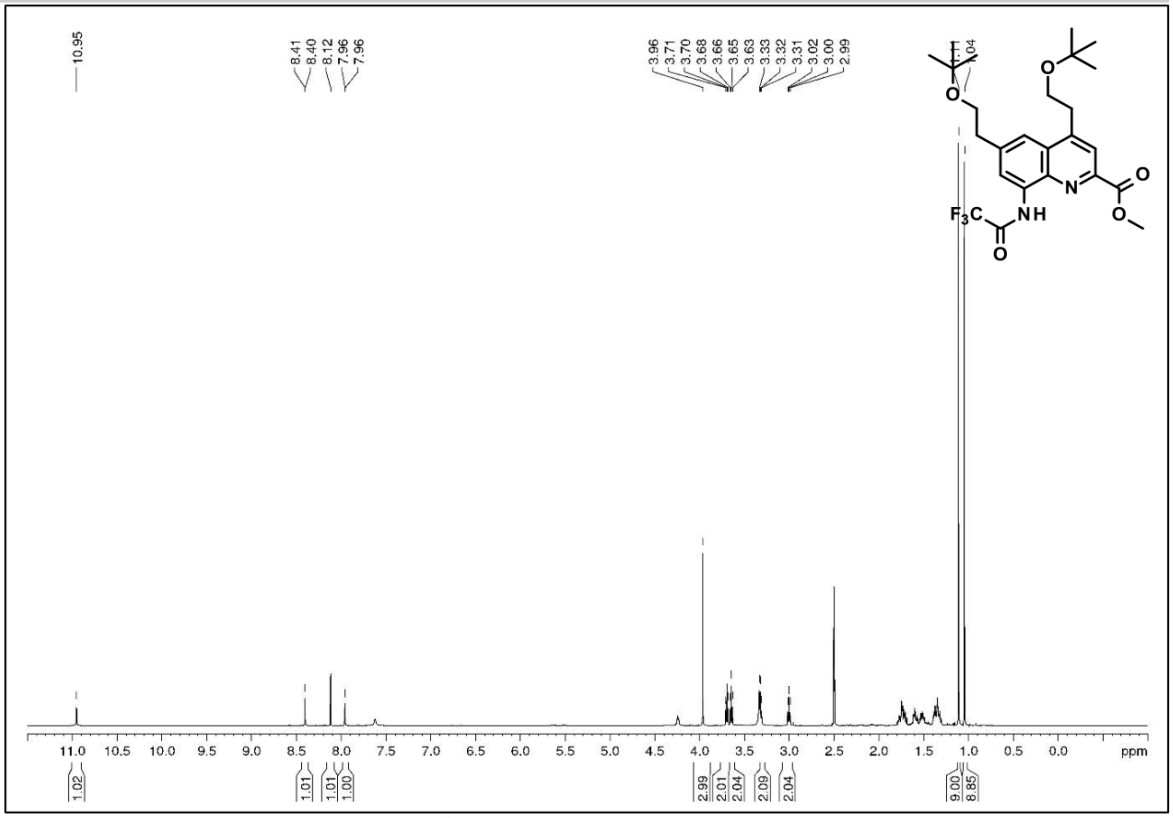

Figure S145. ^{1}H NMR (500 MHz, DMSO-d_6) of compound **22b**.

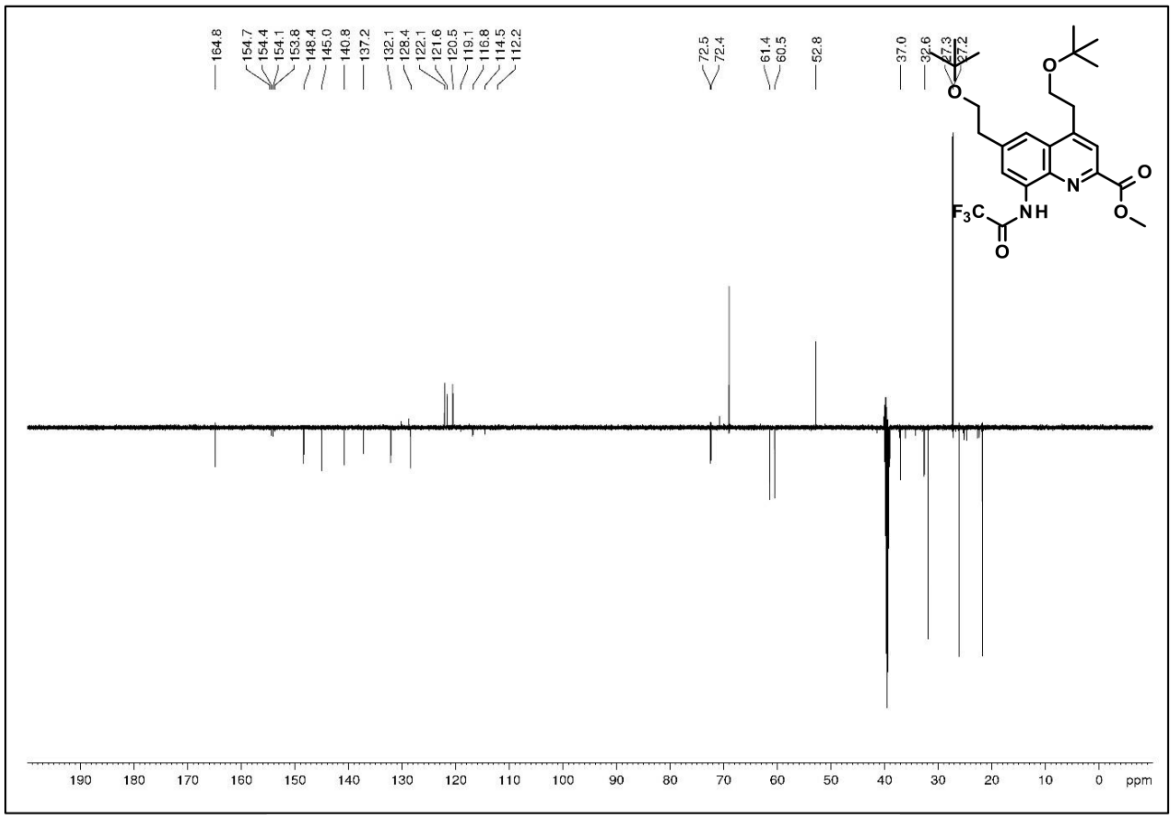

Figure S146. DEPT ^{13}C NMR (125 MHz, DMSO-d_6) of compound **22b**.

SUPPORTING INFORMATION

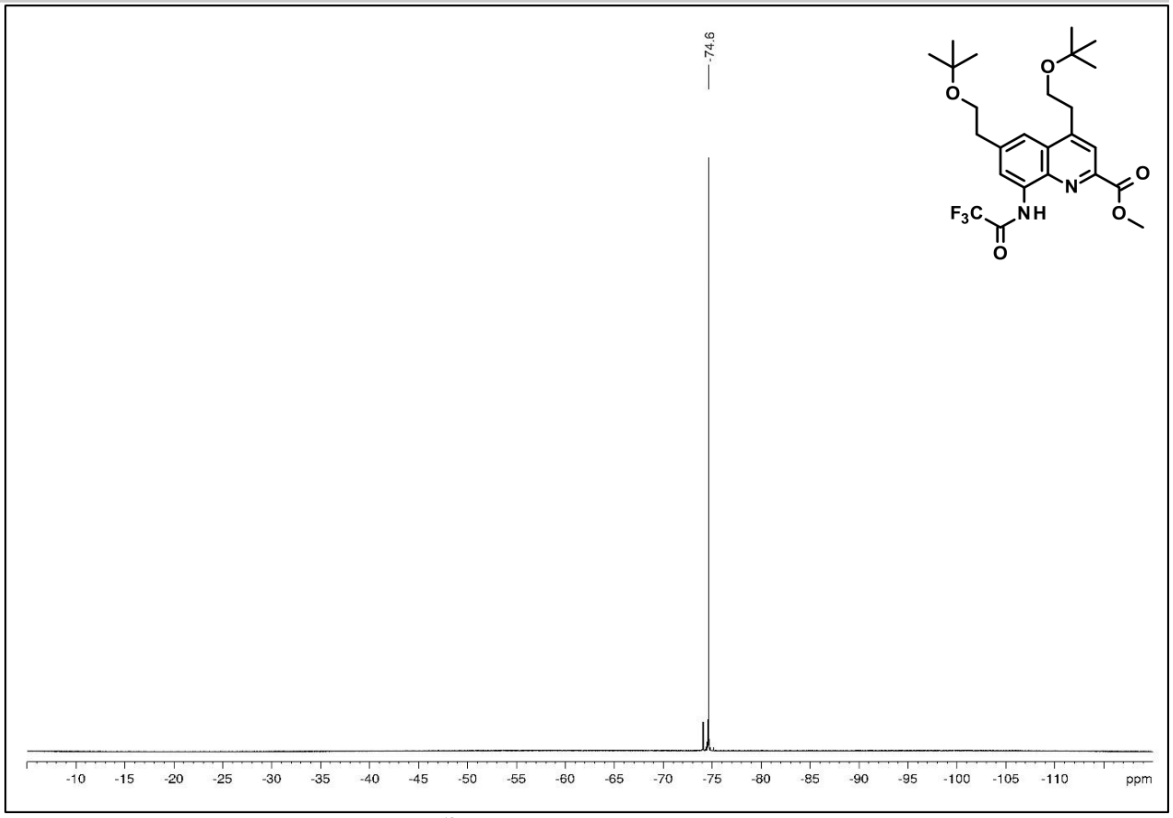

Figure S147. ^{19}F NMR (376 MHz, DMSO-d_6) of compound **22b**.

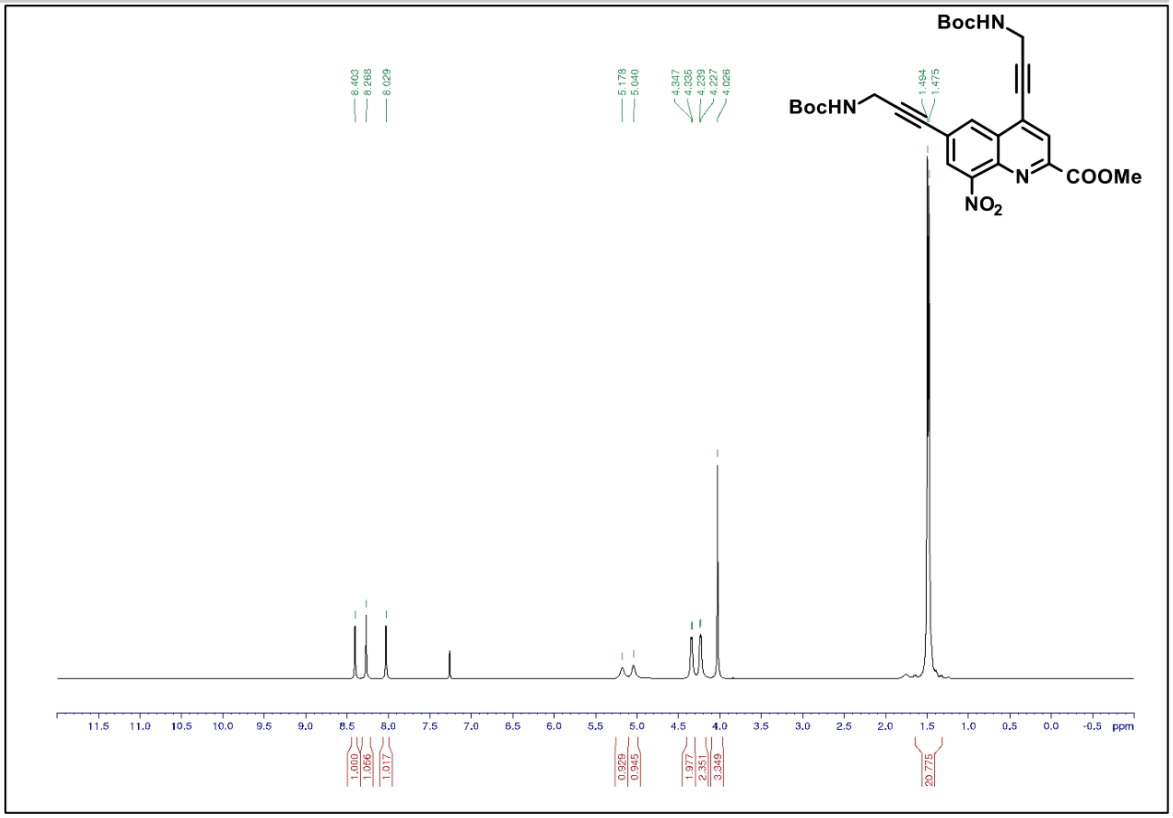

Figure S148. ^{1}H NMR (500 MHz, $CDCl_3$) of compound **24a**.

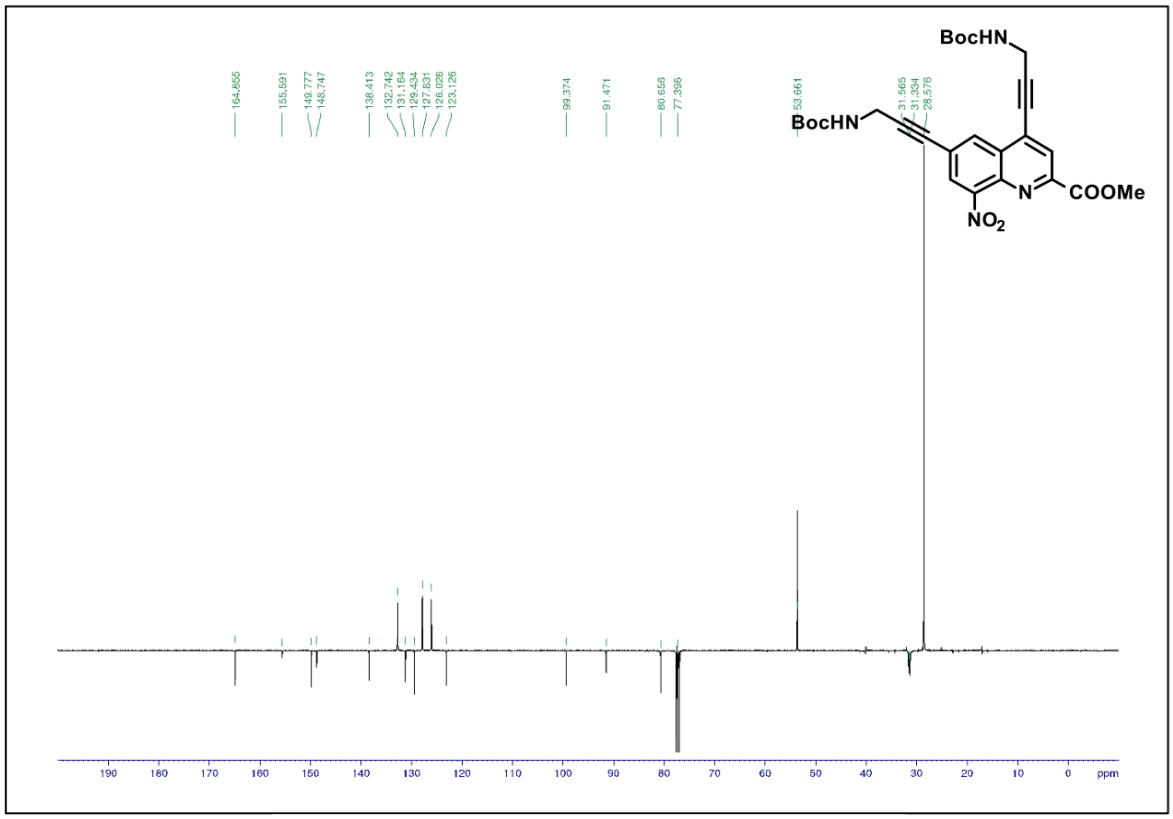

Figure S149. DEPT ^{13}C NMR (125 MHz, DMSO-d_6) of compound **24a**.

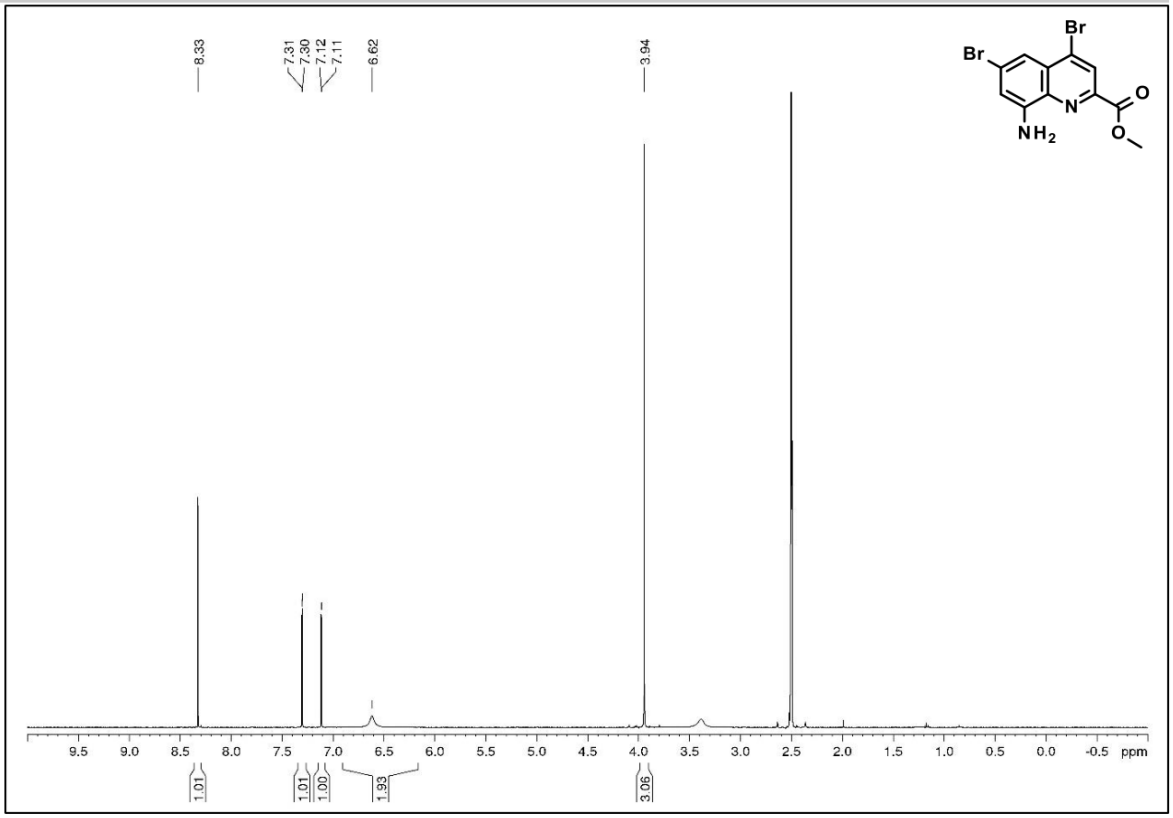

Figure S150. ^{1}H NMR (500 MHz, DMSO-d_6) of compound **25**.

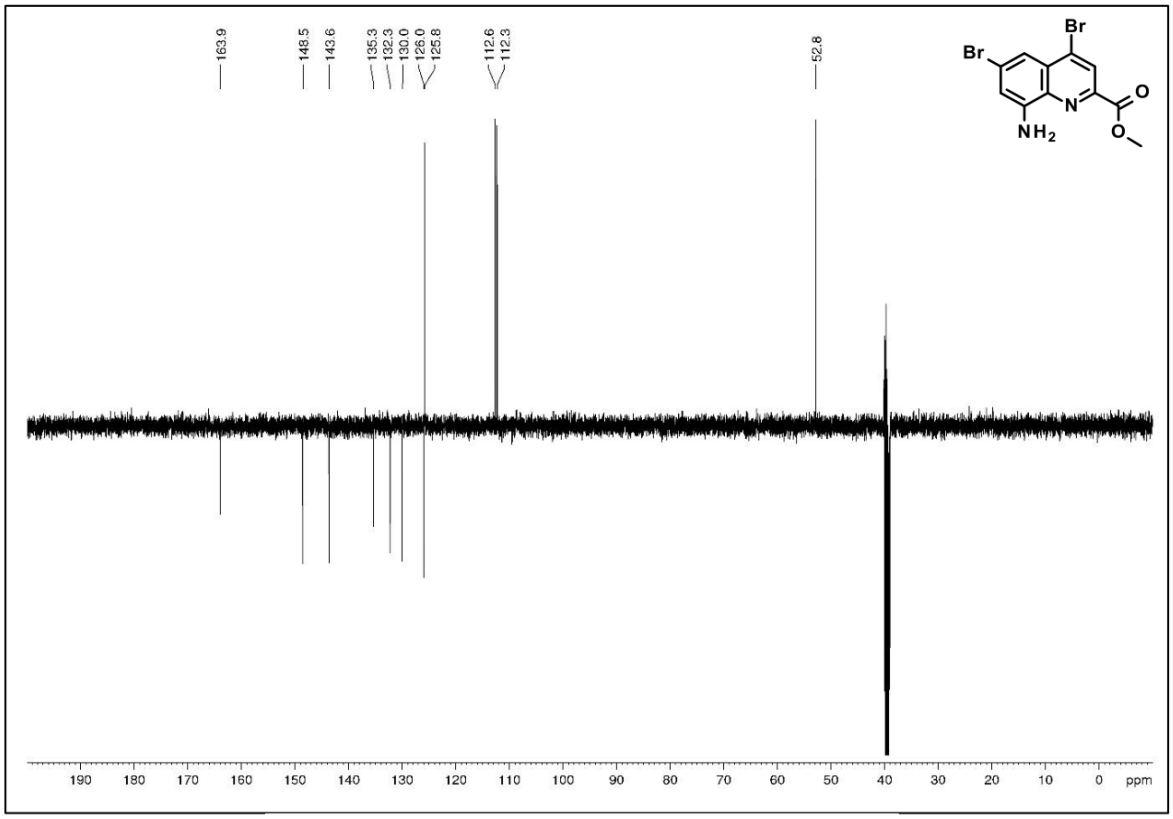

Figure S151. DEPT ^{13}C NMR (125 MHz, DMSO-d_6) of compound **25**.

SUPPORTING INFORMATION

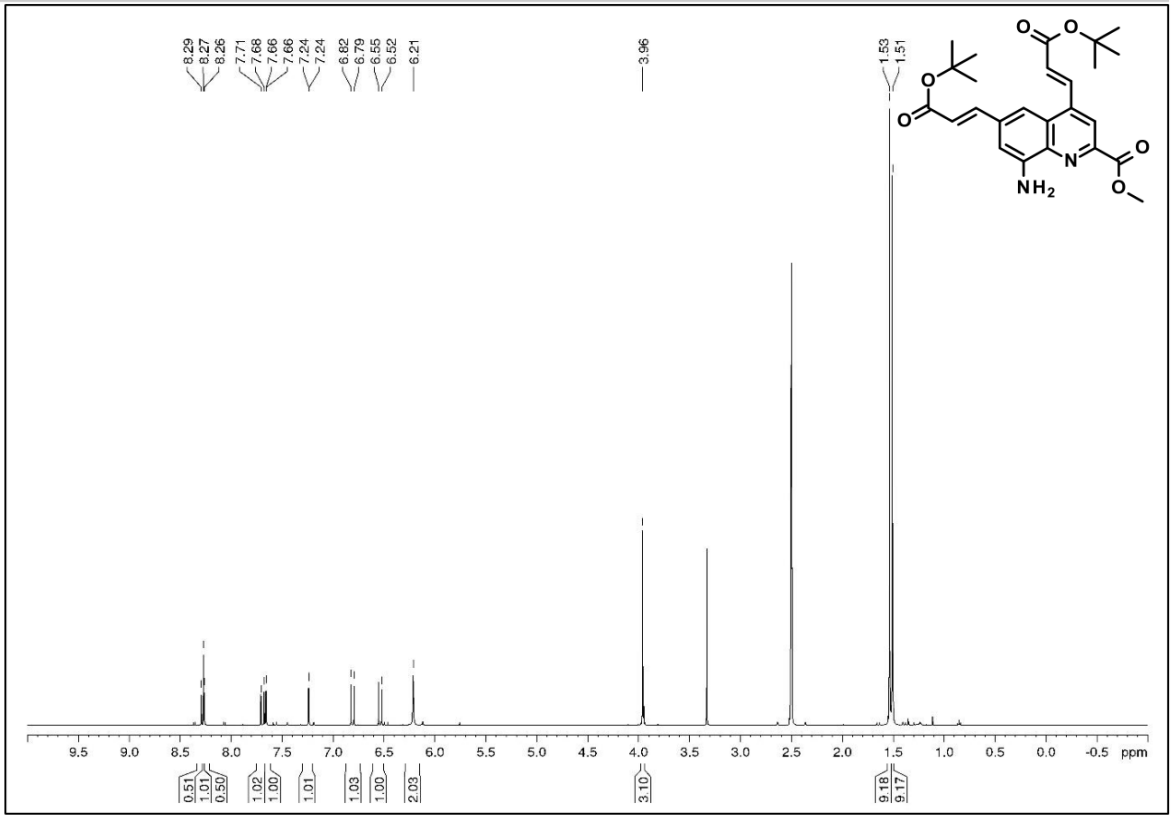

Figure S152. ^{1}H NMR (500 MHz, DMSO-d_6) of compound **26**.

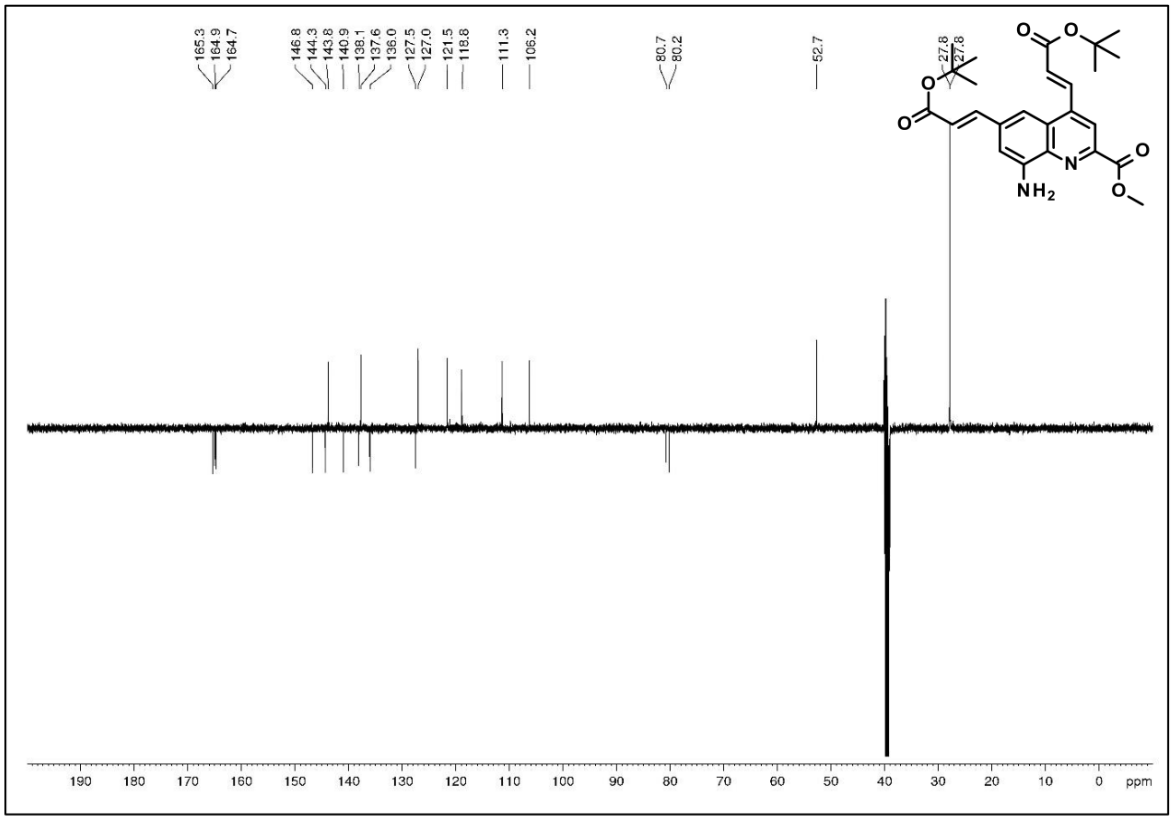

Figure S153. DEPT ^{13}C NMR (125 MHz, DMSO-d_6) of compound **26**.

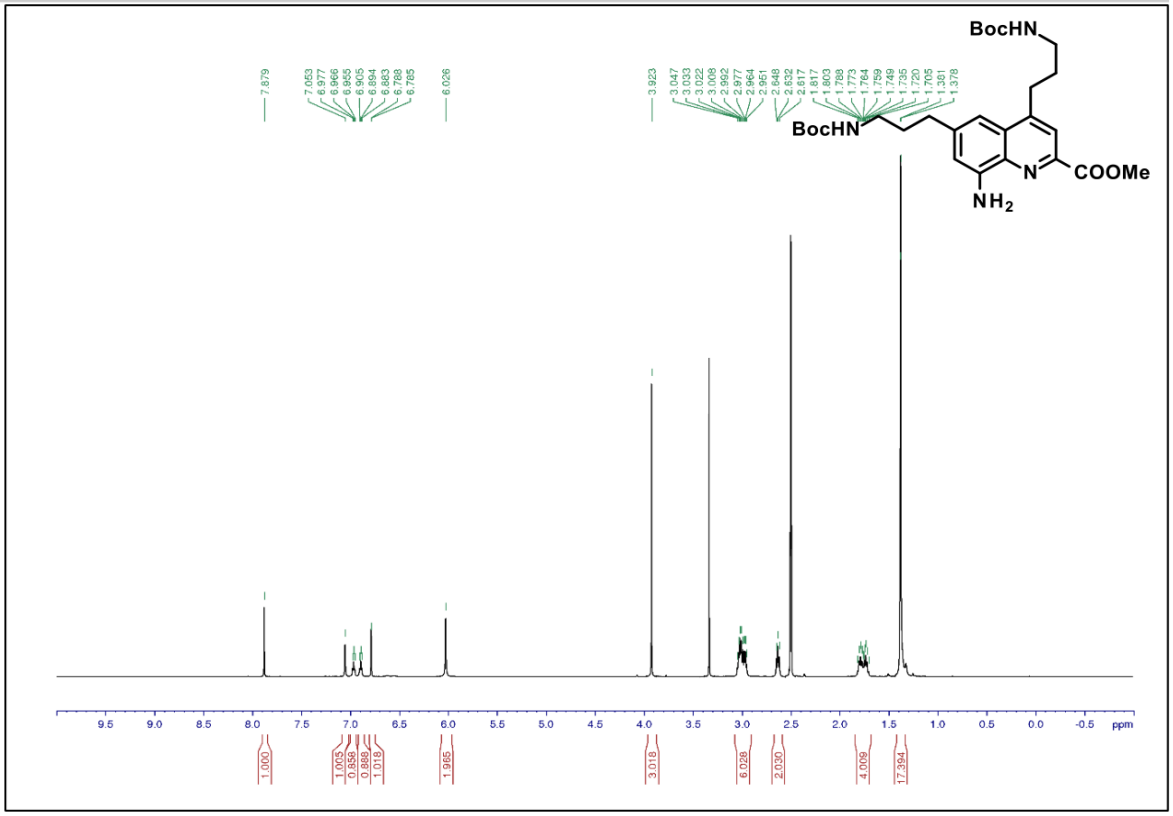

Figure S154. ^{1}H NMR (500 MHz, DMSO-d_6) of compound **27a**.

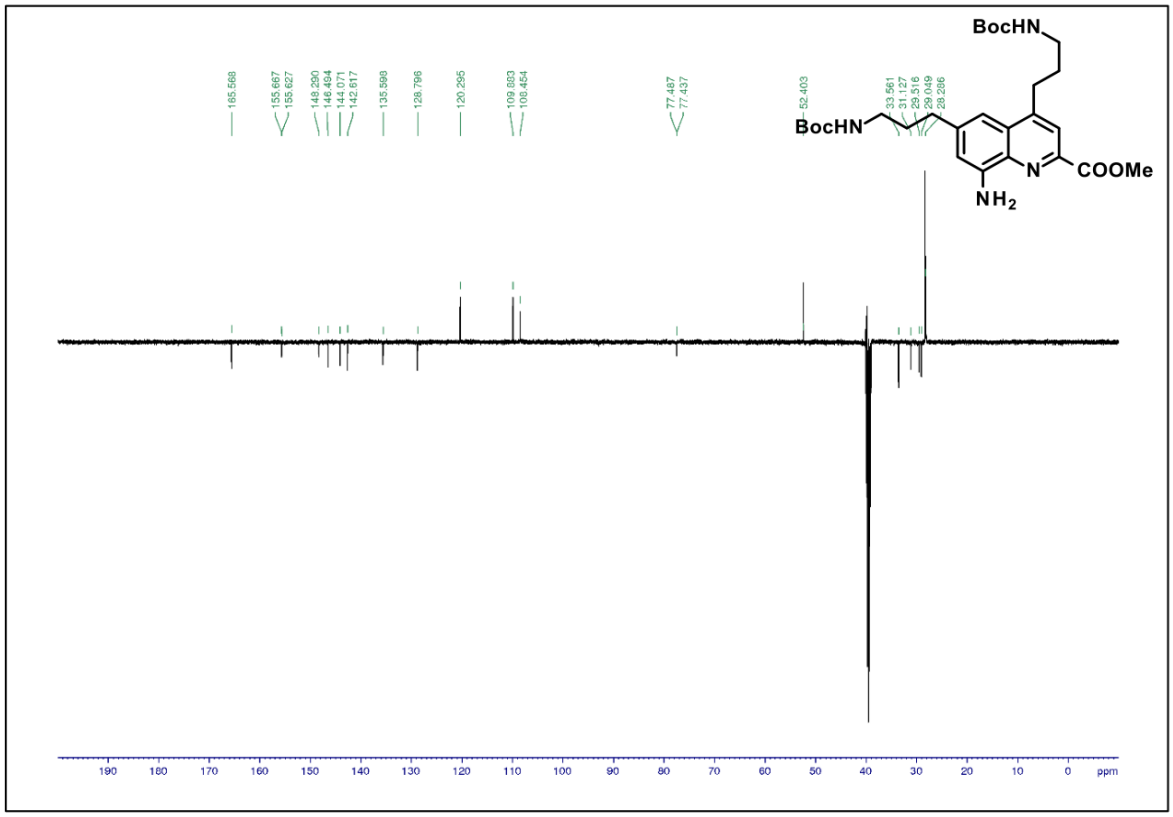

Figure S155. DEPT ^{13}C NMR (125 MHz, DMSO-d_6) of compound **27a**.

SUPPORTING INFORMATION

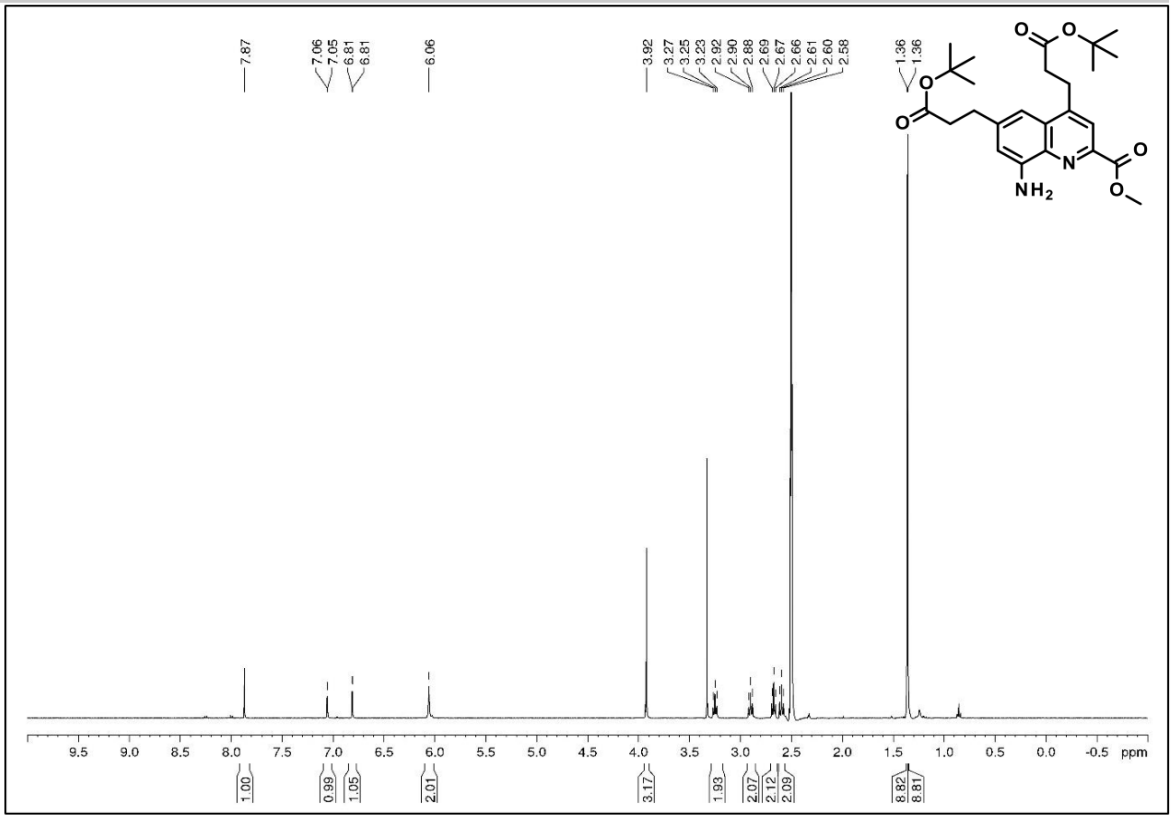

Figure S156. ^{1}H NMR (400 MHz, DMSO-d_6) of compound **27c**.

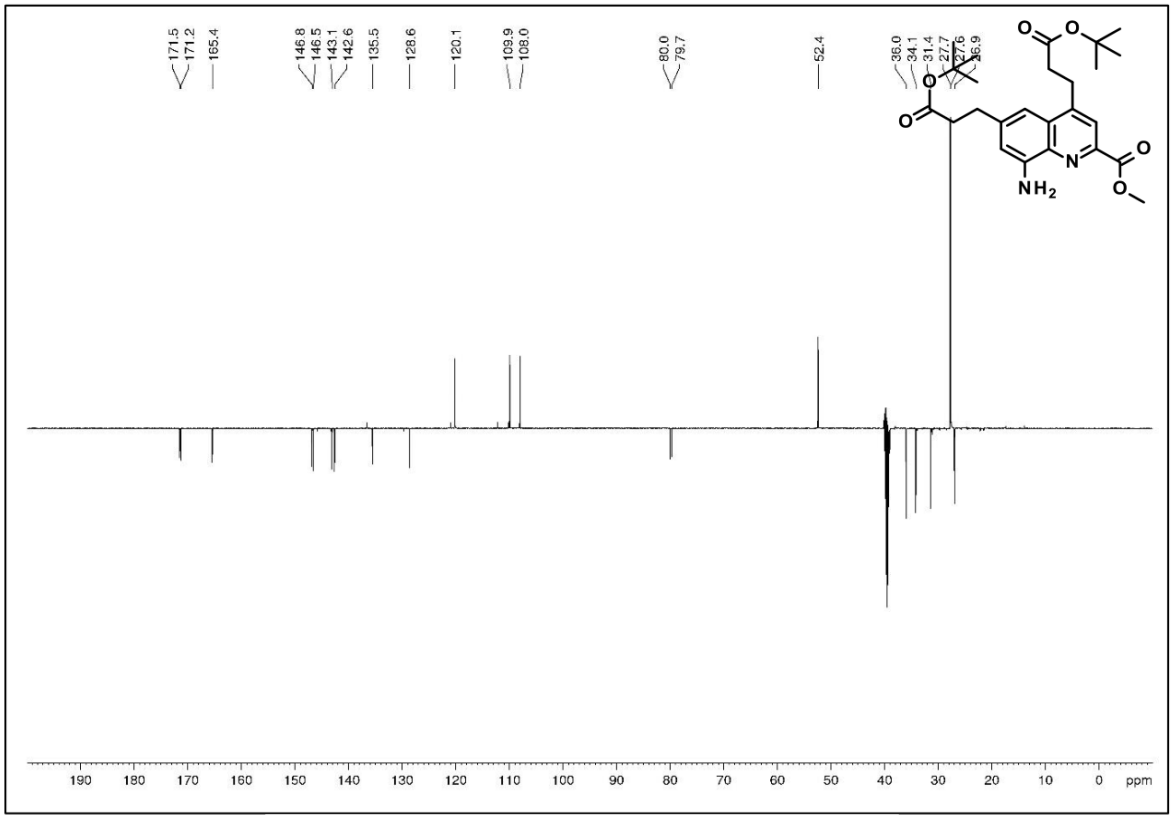

Figure S157. DEPT ^{13}C NMR (125 MHz, DMSO-d_6) of compound **27c**.

SUPPORTING INFORMATION

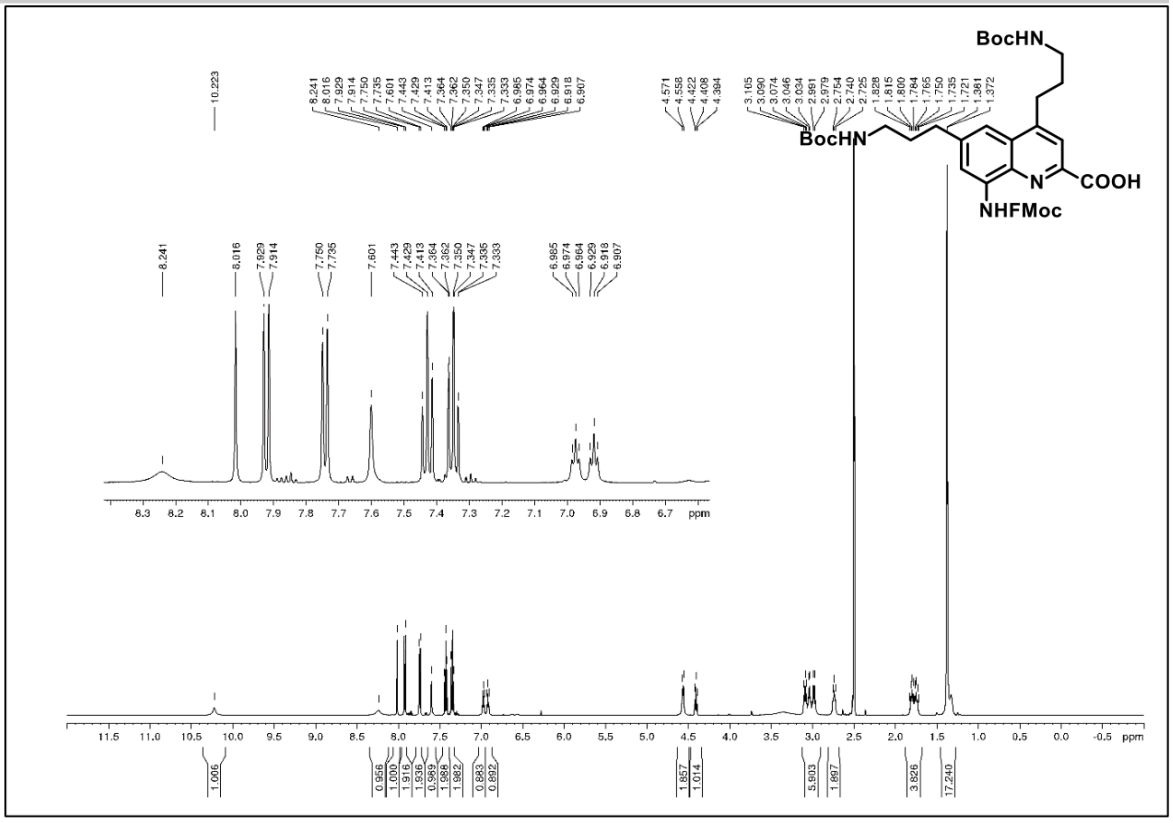

Figure S158. ^{1}H NMR (500 MHz, DMSO-d_6) of compound **28a**.

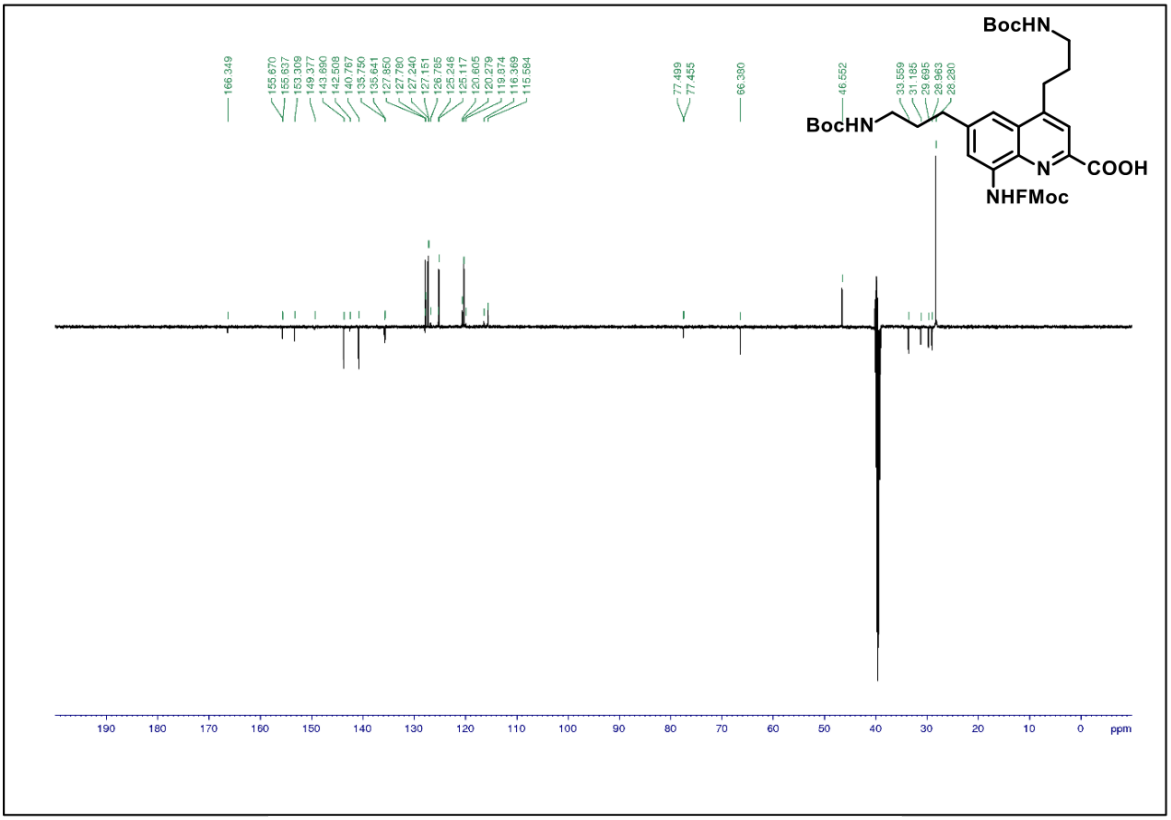

Figure S159. DEPT ^{13}C NMR (125 MHz, DMSO-d_6) of compound **28a**.

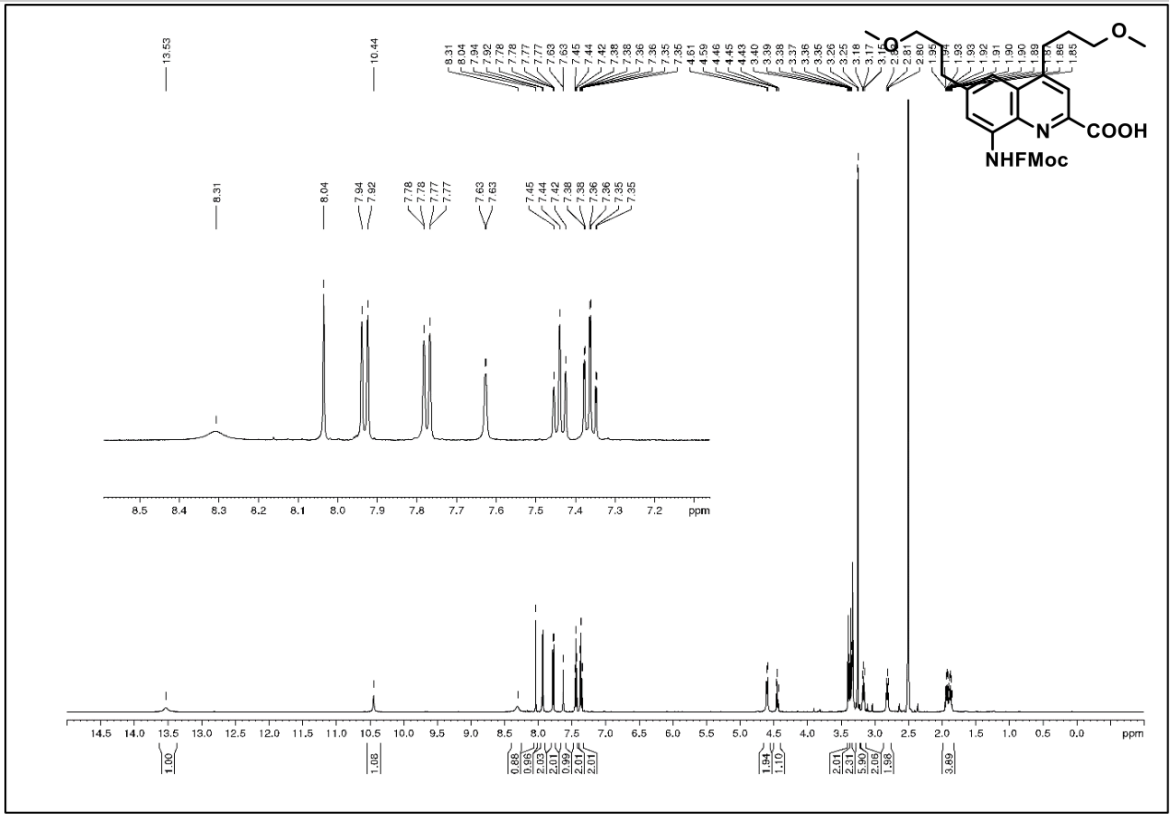

Figure S160. ^{1}H NMR (500 MHz, DMSO-d_6) of compound **28b**.

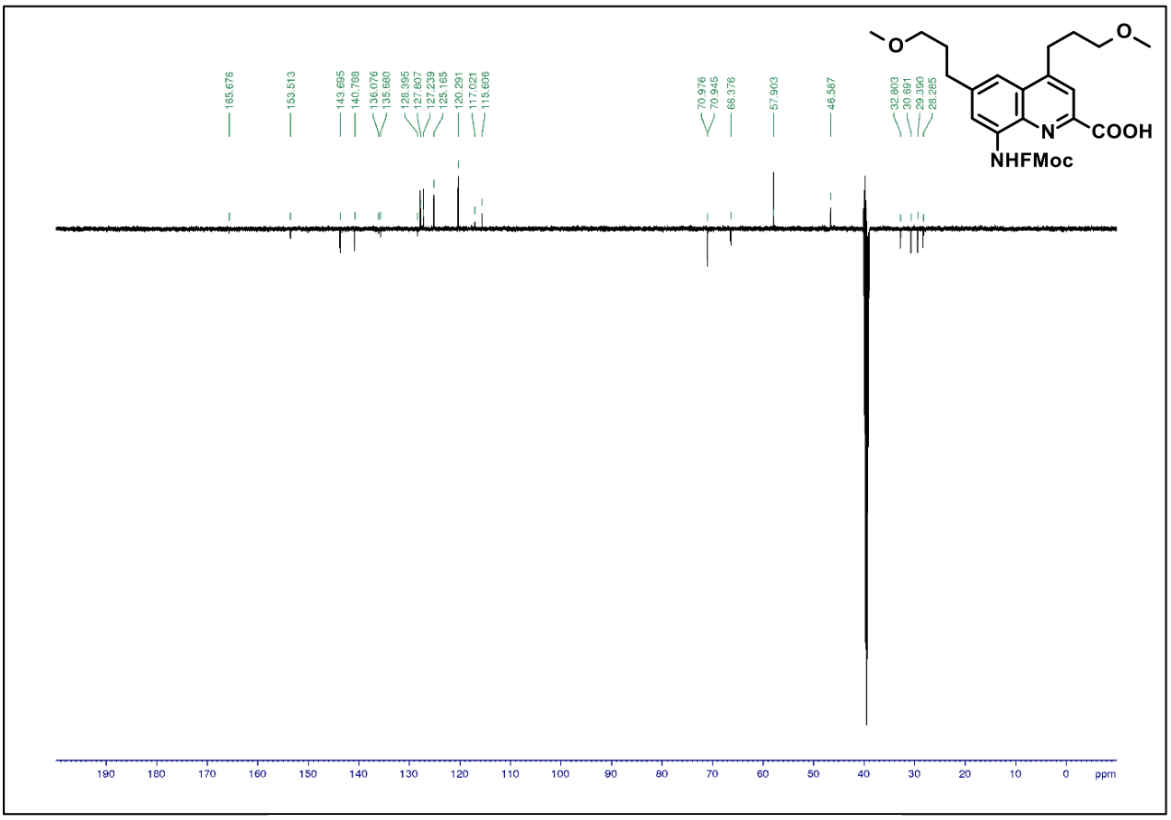

Figure S161. DEPT ^{13}C NMR (125 MHz, DMSO-d_6) of compound **28b**.

SUPPORTING INFORMATION

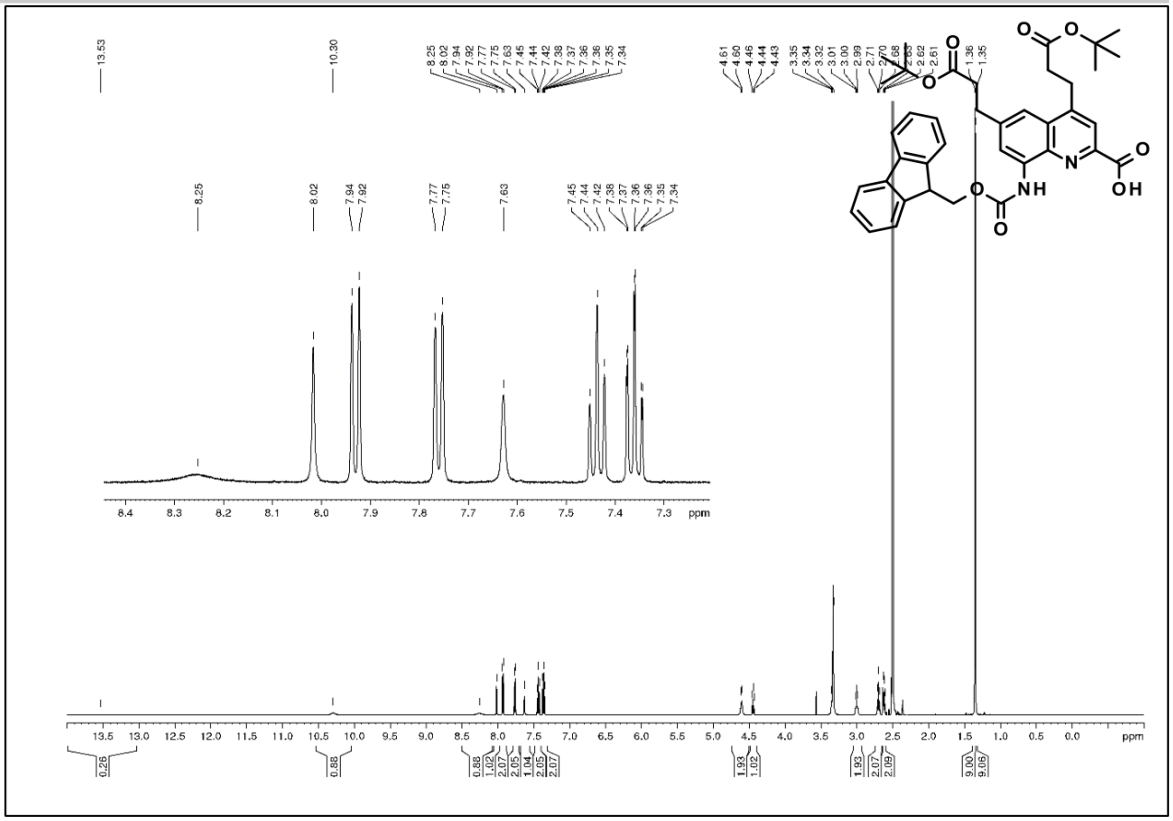

Figure S162. ^{1}H NMR (500 MHz, DMSO-d$_6$) of compound **28c**.

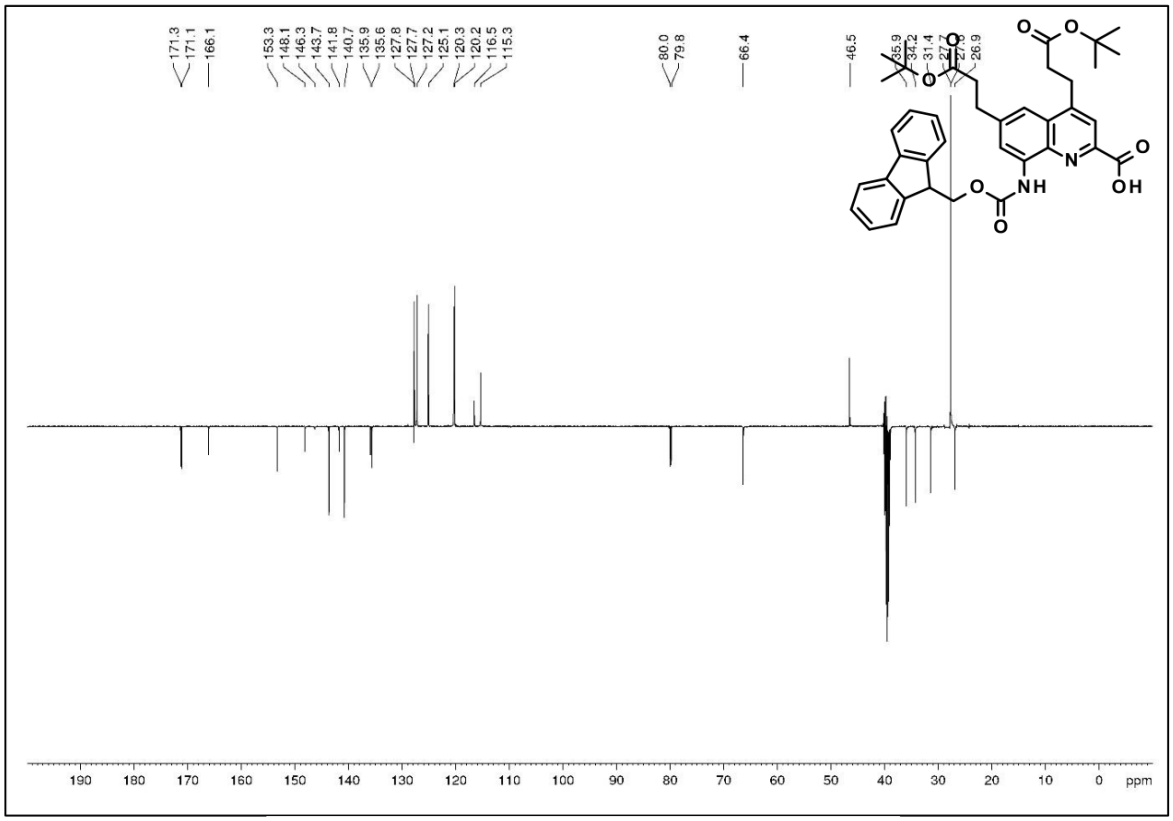

Figure S163. DEPT ^{13}C NMR (125 MHz, DMSO-d_6) of compound **28c**.

SUPPORTING INFORMATION

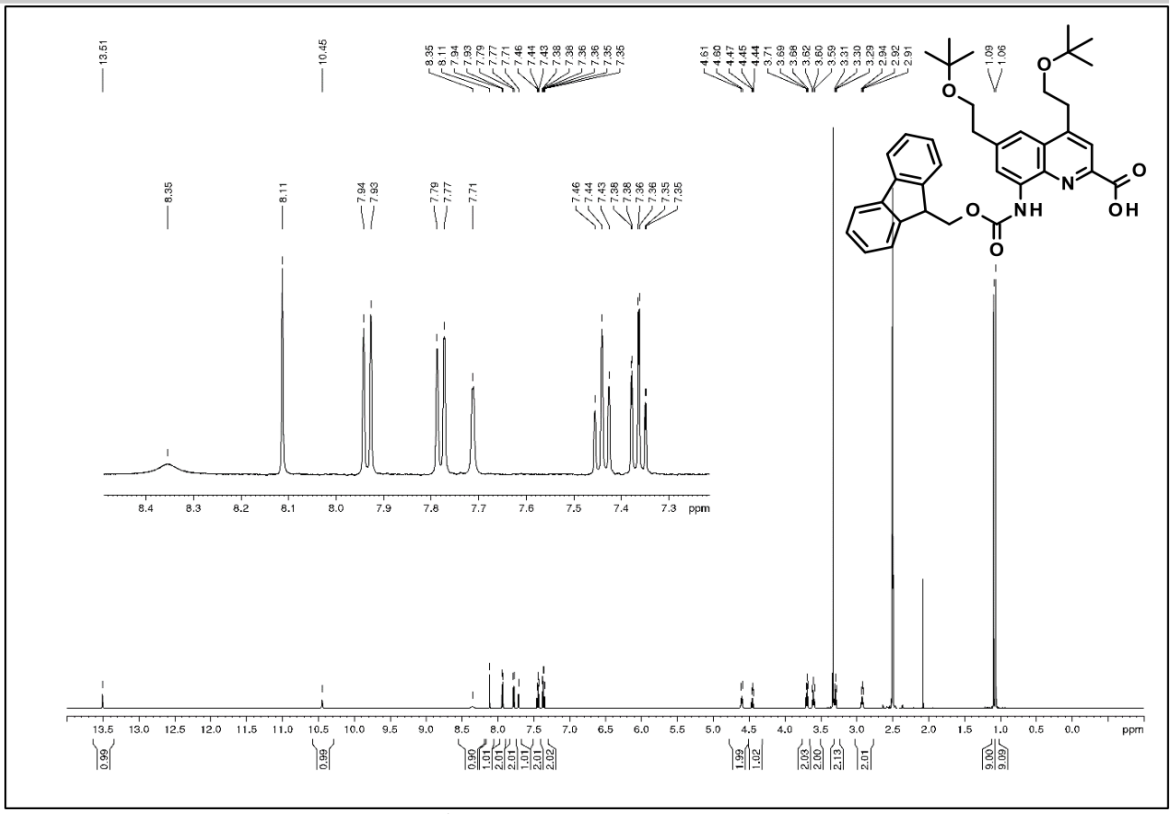

Figure S164. ^{1}H NMR (500 MHz, DMSO-d_6) of compound **28d**.

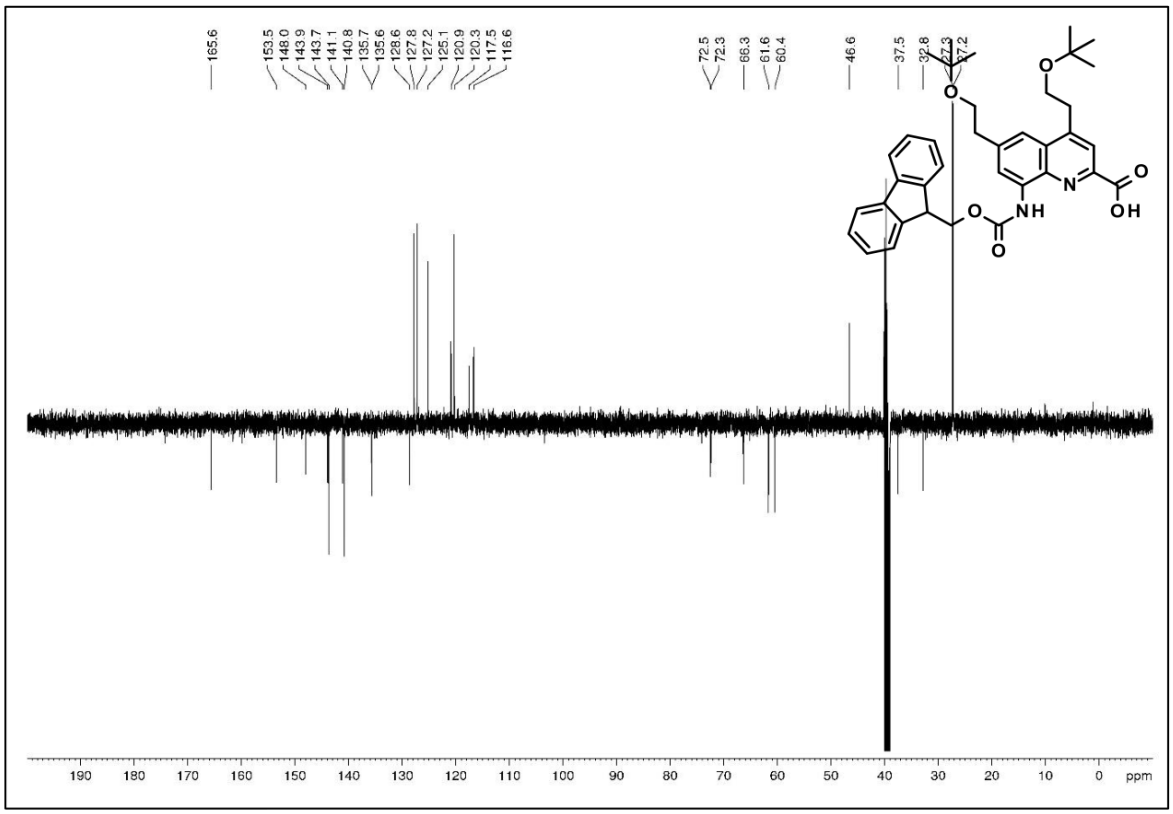

Figure S165. DEPT ^{13}C NMR (125 MHz, DMSO-d_6) of compound **28d**.

SUPPORTING INFORMATION

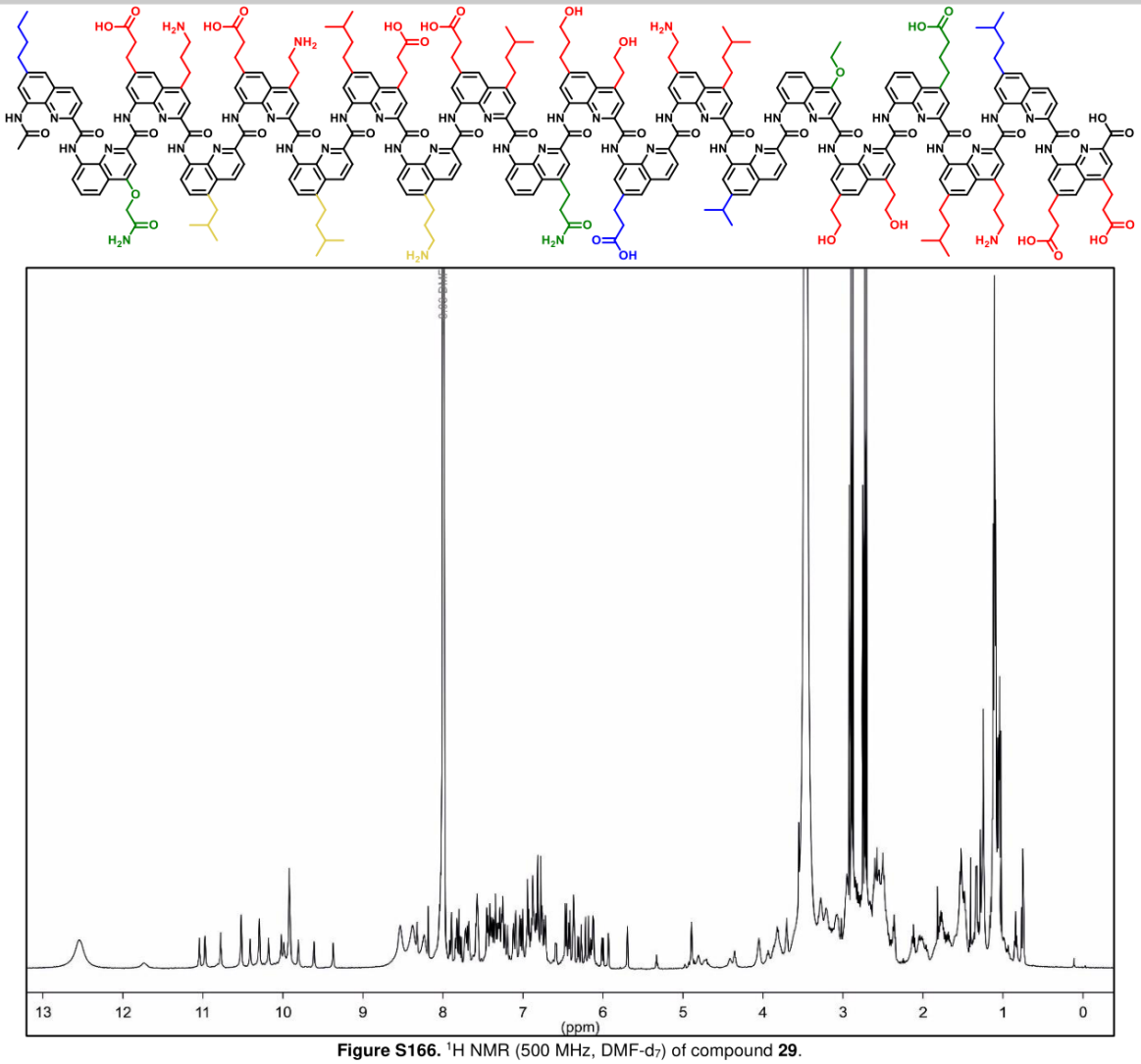

Figure S166. ^{1}H NMR (500 MHz, DMF-d_7) of compound **29**.

SUPPORTING INFORMATION

3.4 UV and MS spectra of newly synthesized compounds

A representative example of UV chromatogram and MS spectrum of final intermediate **7c** is shown below:

General conditions: LC-HRMS were determined on an Agilent 1290 Infinity II - Agilent 6545 LC-QTOF, ion source temperature 200°C, ESI +/-, ionization voltage: +/-4.5 kV. InfinityLab Poroshell 120 SB-C18, 2.1 mm, 1.9 µm column. Mass resolution: min. 10000.

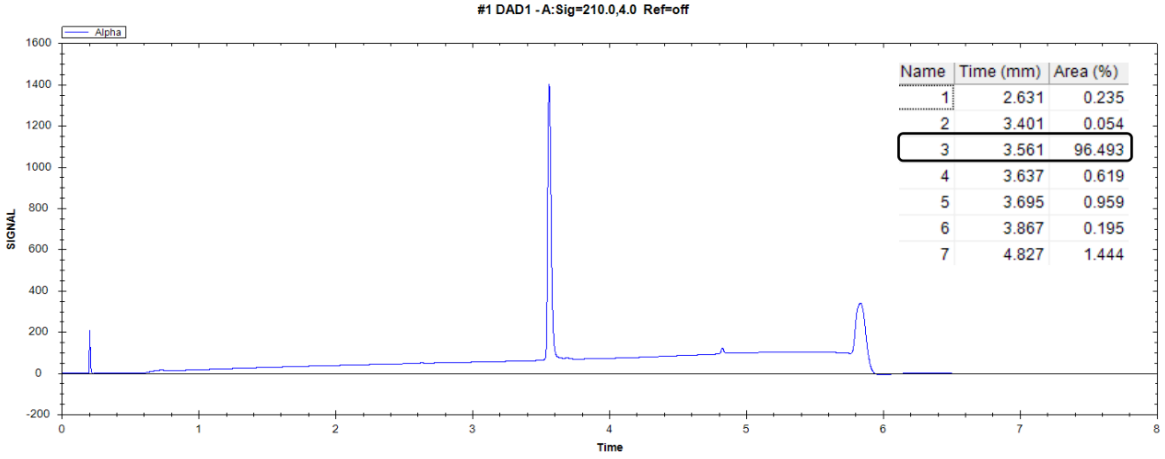

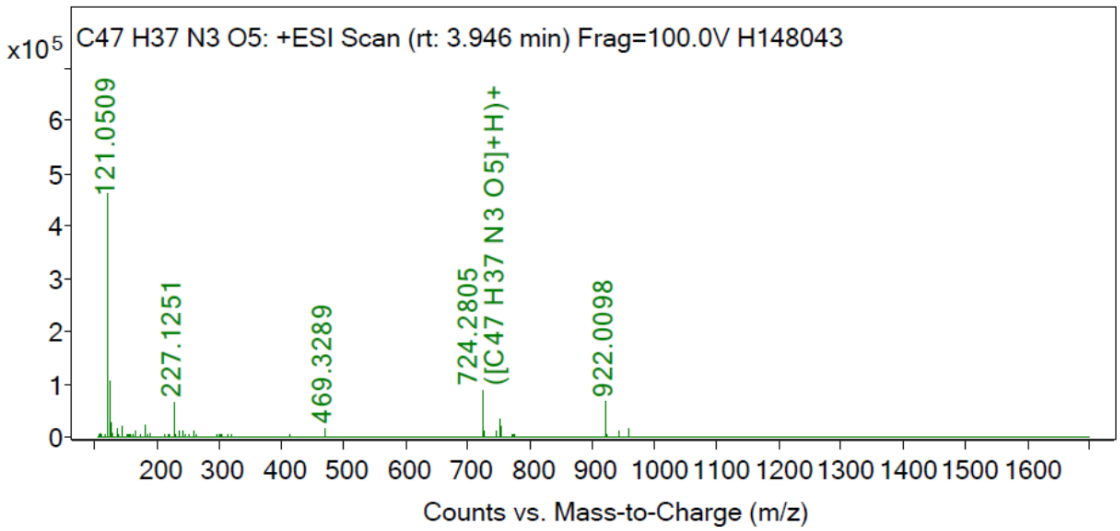

SUPPORTING INFORMATION

3.5 The cumulative yields of advanced intermediates and final building blocks

Quinoline precursor (side chain position)	Advanced intermediate	Cumulated yield (steps)	Final Fmoc-acid monomer	Cumulated yield (steps)	Yield limiting transformation
1 (4)	**6a**	93%(2)	**7a**	60% (3)	Fmoc installation
1 (4)	**6b**	75%(2)	**7b**	21%(3)	Fmoc installation
4 (4)	**6c**	35%(2)	**7c**	16%(3)	Heck coupling
4 (4)	**6d**	23%(2)	**7d**	12%(3)	Suzuki coupling
2 (5)	**9a**	47%(2)	**10a**	39% (3)	Suzuki coupling
2 (5)	**9b**	77%(2)	**10b**	59% (3)	Suzuki coupling/Fmoc installation
2 (5)	**9c**	46%(2)	**10c**	36%(3)	Reduction
2 (5)	**9d**	85%(2)	**10d**	78% (3)	Sonogashira coupling
2 (5)	**9e**	60%(2)	**10e**	43% (3)	Sonogashira coupling
3 (6)	**12a**	46%(2)	**13a**	30%(3)	Reduction/ Fmoc installation
3 (6)	**12b**	68%(2)	**13b**	44% (3)	Fmoc installation
3 (6)	**12c**	26%(2)	**13c**	6%(3)	Fmoc installation
3 (6)	**12d**	22%(2)	**13d**	12%(3)	Suzuki coupling
3 (6)	**12e**	47%(2)	**13e**	12%(3)	Fmoc installation
3 (4,6)	**16a**	51%(3)	**17a**	42% (4)	Sonogashira coupling
3 (4,6)	**16b**	31%(3)	**17b**	21% (4)	Suzuki coupling
3 (4,6)	**16c**	42%(3)	**17c**	34% (4)	Suzuki coupling
3 (4,6)	**16d**	26%(3)	**17d**	17% (4)	Suzuki coupling
3 (4,6)	**16e**	40%(3)	**17e**	34% (4)	Suzuki coupling

SUPPORTING INFORMATION

The cumulative yields of advanced intermediates and final building blocks (continued)

Quinoline precursor (side chain position)	Advanced intermediate	Cumulated yield (steps)	Final Fmoc-acid monomer	Cumulated yield (steps)	Yield limiting transformation
18 (4,6)	**20a**	36%(2)	**21a**	25% (3)	Suzuki coupling
18 (4,6)	**20b**	60%(2)	**21b**	36% (3)	Fmoc installation
18 (4,6)	**20c**	58%(2)	**21c**	35% (3)	Fmoc installation
18 (4,6)	**20d**	65%(2)	**21d**	40% (3)	Fmoc installation
18 (4,6)	**20e**	31%(2)	**21e**	25% (3)	Suzuki coupling
18 (4,6)	**22b**	25%(1)	**28d**	13%(2)	Suzuki coupling
23 (4,6)	**27a**	45%(2)	**28a**	31%(3)	Reduction
23 (4,6)	**27b**	80%(2)	**28b**	24%(3)	Fmoc installation
23 (4,6)	**27c**	51%(3)	**28c**	37%(4)	NO_2 reduction

SUPPORTING INFORMATION

3.6 Literature:

[1] Hu, X., Dawson, S. J., Mandal, P. K., de Hatten, X., Baptiste, B. and Huc, I. Optimizing side chains for crystal growth from water: a case study of aromatic amide foldamers. *Chem. Sci*. **2017**, 8, 3741-3749. https://doi.org/10.1039/C7SC00430C
[2] Zwillinger, M.; Reddy, P. S.; Wicher, B.; Mandal, P. K.; Csékei, M.; Fischer, L.; Kotschy, A.; Huc, I. Aromatic Foldamer Helices as α-Helix Extended Surface Mimetics. *Chem. Eur. J.* **2020**, *26* (72), 17366–17370. https://doi.org/10.1002/chem.202004064.
[3] Sőregi, P., Zwillinger, M., Vágó, L., Csékei, M., Kotschy, A. High density information storage through isotope ratio encoding. *Chem. Sci.* **2024**. https://doi.org/10.1039/D4SC03519D
[4] Baptiste, B., Douat-Casassus, C., Laxmi-Reddy, K., Godde, F., Huc, I., Solid Phase Synthesis of Aromatic Oligoamides: Application to Helical Water-Soluble Foldamer. *J. Org. Chem*. **2010**, *75*, 7175-7185. https://doi.org/10.1021/jo101360h
[5] Corvaglia, V., Sanchez, F., Menke, F. S., Douat, C., Huc, I. Optimization and Automation of Helical Aromatic Oligoamide Foldamer Solid-Phase Synthesis. *Chem. Eur. J.* 2023, 29, e202300898. https://doi.org/10.1002/chem.202300898

6.3. Publication: Optimisation and automation of of helical aromatic oligoamide foldamer solid-phase-synthesis

Authors: Valentina Corvaglia, Florian Sanchez, Friedericke S. Menke, Céline Douat and Ivan Huc.

Contributions: This project was planned by I. Huc. Foldamer synthesis performed by V. Corvaglia and C. Douat. Crystal structure of the ylide was obtained by F. S. Menke. Protocols for monomer recycling were established by D. Bindl and optimised by F. Sanchez. The mechanistic study of the formation of the ylide was established and characterised by I. Huc and F. Sanchez. The manuscript was written in collaboration with V. Corvaglia, F. Sanchez, C. Douat and I. Huc.

Publication: *Chem. Eur. J*. **2023**, 29, e202300898.

DOI: https://doi.org/10.1002/chem.202300898

Chemistry–A European Journal

Research Article
doi.org/10.1002/chem.202300898

Chemistry Europe
European Chemical Societies Publishing

www.chemeurj.org

Optimization and Automation of Helical Aromatic Oligoamide Foldamer Solid-Phase Synthesis

Valentina Corvaglia,[a] Florian Sanchez,[a] Friedericke S. Menke,[a] Céline Douat,[a] and Ivan Huc*[a]

Abstract: Helically folded oligoamides of 8-amino-2-quinolinecarboxylic acid composed of up to 41 units were prepared using optimized manual solid-phase synthesis (SPS). The high yield and purity of the final products places these SPS protocols among the most efficient known to date. Furthermore, analytical methods allowing for the clear identification and purity assessment of the products were validated, including ^{1}H NMR, a seldom used method for such large molecules. Adaption of the SPS protocols, in particular using in situ acid chloride activation under Appel's conditions, made it possible to efficiently implement SPS on a commercial peptide synthesizer, leading to a dramatic reduction of the laboratory work required to produce long sequences. Automation constitutes a breakthrough for the development of helical aromatic oligoamide foldamers.

Introduction

The advancement of efficient and reliable screening methodologies of peptides and peptide derivatives in the context of drug research such as, for example, display selection, has triggered a renewed interest for this class of compounds by the scientific community and pharmaceutical companies.[1] Concurrently, the offer in terms of peptide synthesis automation and parallelization has grown and new synthesizers have been launched on the market. Setting up a robust solid-phase peptide synthesis (SPPS) station is within the reach of many laboratories. In addition, recent achievements have unveiled the possibility to further accelerate the production of long peptides and entire proteins by relying on automated flow chemistry.[2] Along the same line, the level of perfection achieved in the solid-phase synthesis (SPS) of oligonucleotides using highly optimized variations of the phosphoramidite chemistry and fully automated synthesizers gives rapid and efficient access to all kinds of sequences.[3] The availability of synthetic oligonucleotides has enabled developments as diverse and important as PCR,[4] DNA-based nanotechnologies,[5] and therapeutic applications.[6]

In such a context of innovation, interest for efficient oligomer solid-phase synthetic methods has extended beyond peptides and nucleotides. For example, peptoids constitute a backbone with remarkable amenability to rapid SPS of long sequences (up to 36 units).[7] In the last decade, chemically diverse sequence-defined polymers produced by SPS have been designed and investigated for the purpose of information storage.[8] Conversely, foldamers are inherently oligomeric, and this field of research also requires its share of solid-phase synthetic methodologies (SPFS for solid-phase foldamer synthesis) to access to a variety of aliphatic[9] and aromatic[10] architectures and backbones in good purity and yield.

The efficiency of an SPS depends on multiple identified parameters that determine the yields of the many reaction steps carried out with no purification other than washing excess reagents away. However, not all these parameters are easy to control. The inherent efficacy of the chemical steps is of course central. For that reason, amide and phosphodiester formation, for which high yielding reactions are available, have been privileged. However, how these steps proceed also depends on the accessibility of the reactive functions on the resin to reagents in solution, which in turn depends on the conformations and possible aggregation of the sequences on the resin. Both aggregation and conformation may result into steric hindrance of coupling steps in a backbone-, length- and sequence-dependent manner. Optimizing the solvent, temperature, the nature of the resin and its swelling properties, or introducing specific removable chemical functions, may reduce on-resin aggregation or collapse of the growing sequences.[11] In practice, not many oligomer SPS show high conversion yields, i.e. good crude purity, beyond fifteen units. Poor purity may complicate final chromatographic purification though this may be partly alleviated by using capping reactions combined with capture and release approaches that prevent chain elongation after a failed coupling, and that may also confer distinct chromatographic retention behavior.[12]

[a] *Dr. V. Corvaglia, F. Sanchez, Dr. F. S. Menke, Dr. C. Douat, Prof. Dr. I. Huc*
Department of Pharmacy
Ludwig-Maximilians-Universität
Butenandtstr. 5–13, 81377 München (Germany)
E-mail: ivan.huc@cup.lmu.de
Homepage: https://huc.cup.uni-muenchen.de

Supporting information for this article is available on the WWW under https://doi.org/10.1002/chem.202300898

Chemistry–A European Journal | Research Article doi.org/10.1002/chem.202300898 | Chemistry Europe European Chemical Societies Publishing

Several classes of aromatic oligoamides (AOs) have been produced by SPS, meeting the particular challenge of the lower reactivity of aromatic amines[10] as compared to peptidic aliphatic amines.[9] Among these, helical AOs stand out as a class of foldamers with stable and predictable conformations that result in useful properties for the purpose of, for example, exomolecular recognition of proteins,[13] tertiary folding design,[14] endomolecular recognition,[15] charge transport,[16] or to template peptide conformations in hybrid sequences.[17] In this context, various types of aromatic amino acid monomers have been designed and combined to promote helical folding. A common building block is 8-amino-2-quinolinecarboxylic acid Q (Figure 1). Q monomers may be decorated with various side chains in position 4, 5, or 6 that diverge from the folded oligomers.[18] Q_n helical conformations are very stable in apolar, polar aprotic and protic solvents.[19] Until now, denaturation conditions of these helices have not been identified and unfolded conformations could be populated only by means of mechanical force or interactions with a surface.[20]

The SPS of Q_n oligomers thus required overcoming the low nucleophilicity of 8-amino-quinolines and also the steric hindrance associated with helical folding that will occur as soon as three units have been assembled. In earlier reports, we introduced Q_n microwave-assisted manual SPFS using acid chloride activation.[10a,21] Here, we report developments of this methodology including its optimization to produce long sequences (>40 units, ≈9.8 kDa, in 70% crude yield) and its adaptation to automation thanks to the utilization of an in situ acid chloride activation based on Appel's reaction.[22] We also show the high amenability of long sequences to RP-HPLC purification and to ^{1}H NMR spectroscopic and mass spectrometry analysis. Altogether, our results place Q_n synthesis among the most robust and efficient SPS of non-peptidic non-nucleotidic sequences. We speculate that such efficiency may in fact result not despite, but thanks to, on-resin helical folding. These developments pave the way to the easy and fast production of new AOs sequences for the applications mentioned above.[13–17]

Results and Discussion

Manual SPFS, analysis and purification of a 15 mer

The previously published method for manual SPFS of Q_n oligomers has demonstrated its efficiency for sequences having over ten units.[18b,23] In order to benchmark the synthesis of longer oligomers and potential analysis or purification problems, we first investigated the preparation of 15mer **1** composed of hydrophobic (L), cationic (O) and anionic (D) residues (Figure 1). Because of the inherent curvature of Q_n helices – 2.5 units per turn – the two L residues of **1** are displayed on the same side of the helix (Figure 1c). The charged residues are placed without any particular order and ensure good water solubility. Sequences **2**–**4** are 14mers derived from the sequence of **1** by a single deletion. They could thus potentially arise as impurities of **1** when a coupling or preceding deprotection step would not be high yielding. Specifically, **2** misses the terminal cationic O unit of **1**, **3** misses a central O unit, and **4** misses an L unit. These different types of deletion were expected to result in variable changes in the RP-HPLC retention times (t_R) and ^{1}H NMR spectra of the 14mers.

All four sequences were prepared individually via SPFS on a 15 μmol scale. Starting from low loading brominated Wang resin (0.41 mmol/g), the immobilization of the first Fmoc-O(Boc)-OH monomer was carried out in the presence of CsI and DIEA.[10a] After standard Fmoc deprotection (DMF/piperidine), Fmoc-D(O*t*Bu)-OH was converted to its acid chloride with 1-chloro-*N*,*N*,2-trimethyl-1-propenyl-amine (Ghosez's reagent) and coupled to the amine of the first residue under microwave irradiation.[10a,21a] The following units were next assembled using the same deprotection/coupling cycles (Scheme 1). During SPFS, mini-cleavages of the resin-bound growing sequences were performed to validate intermediates and monitor the efficiency of the syntheses (see Supporting Information for details). Three full deprotection/coupling cycles require 4 h. If we consider the time needed to activate the acids into acid chlorides prior to SPFS, a busy work day of 8 h is filled (four

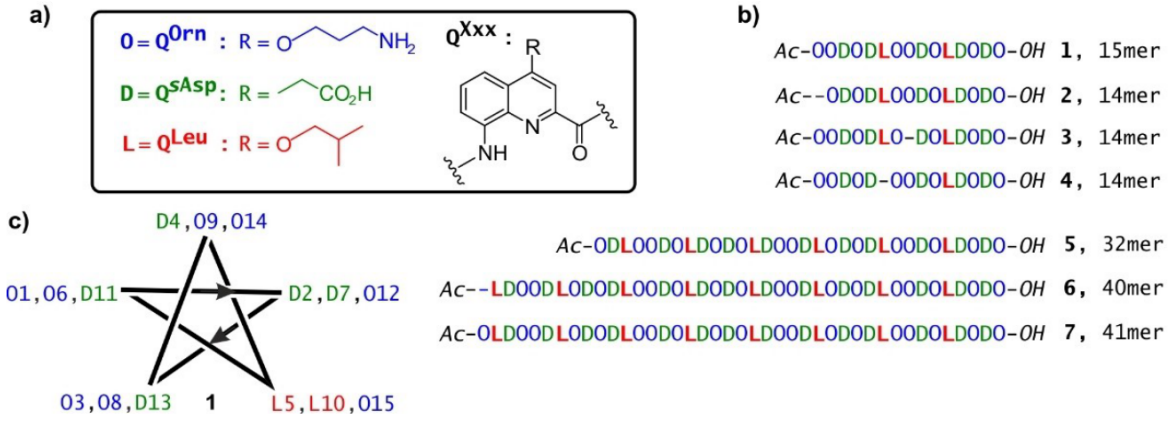

Figure 1. (a) Structures of quinoline monomers O, D and L (one letter code labels are inspired from those of α-amino acids). (b) Manually synthesized foldamer sequences. (c) Helical wheel projection of oligomer **1** showing the side-chain distribution along the 2.5 helix axis (5 aromatic units per two turns).

Chemistry–A European Journal | Research Article doi.org/10.1002/chem.202300898 | Chemistry Europe European Chemical Societies Publishing

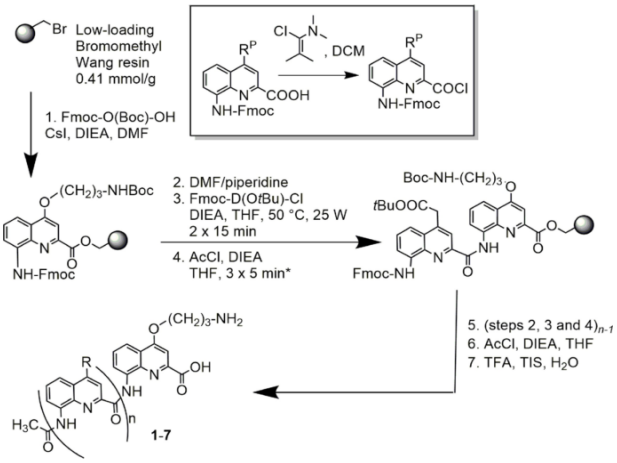

Scheme 1. SPFS protocols for oligomers **1**–**7**. R^P stands for protected R side-chain. *The acetylation capping step was introduced for sequences **5**–**7** only.

deprotection/coupling cycles are possible in a long work day of about 10 h). A 15mer such as **1** thus amounts to 40 h (5 work days), not counting the final deprotection and capping steps, and purification.

Foldamers **1**–**4** were finally N-acetylated prior to cleavage from the resin and side chain deprotection using a TFA/TIS/H_2O solvent mixture (95 : 2.5 : 2.5, v/v/v). Compounds **1**–**4** were then purified by RP-HPLC semi-preparative chromatography (isolated yields from 15–20 % and purity > 99 %). The purified chromatograms are shown in Figure 2a–d. The crude chromatogram of **1** is also shown in Figure 3a. Compounds were further characterized by ESI-MS and ^{1}H NMR (Figures 2f-g, S10, S11, S14, and S15). The chromatograms denote similar t_R values ascribable to the minor differences in sequence (Figure 2a–d). Nevertheless, upon optimizing RP-HPLC conditions with a shallow gradient, discrimination of the four different foldamers was achieved (Figure 2e). The retention times can be rationalized according to the hydrophilic/hydrophobic balance of the molecules. These chromatograms indicate that deleted products of a 15mer may be detected by RP-HPLC under optimized conditions but that preparative separation may become difficult. The mass spectra give clean charge envelopes that may allow for the detection of deleted sequences (Figure 2f). Differences were also clearly visible on ^{1}H NMR spectra where distinct chemical shifts of the amide NH signals were observed (Figure 2g). This level of discrimination for a single deletion contrasts with what may be expected with peptides of similar length.[24] If one deleted product was a contaminant of the 15mer, one could reasonably hope to detect it by NMR. In summary, the SPFS of a Q_{15} sequence proceeds smoothly and several reliable analytical methods of the final product purity are available. These results encouraged us to attempt the synthesis of even longer sequences.

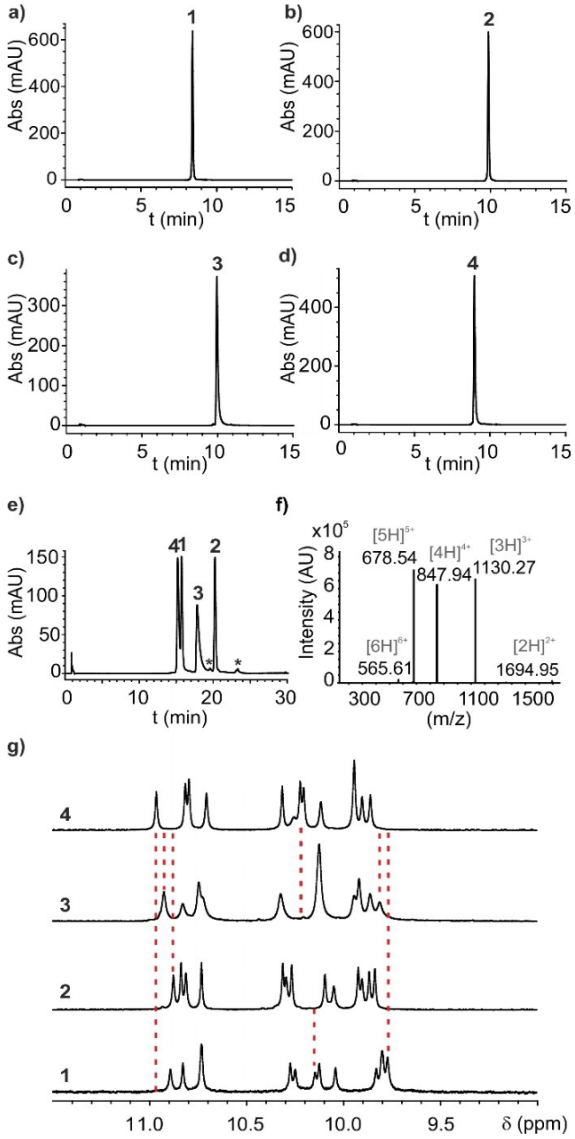

Figure 2. (a–d) RP-HPLC chromatograms of foldamers **1**–**4** using a linear gradient from 5 % B to 40 % B in 10 min; A: H_2O + 0.1 % TFA and B: CH_3CN + 0.1 % TFA. (e) RP-HPLC chromatogram of the co-injected foldamers **1**–**4** using a linear gradient from 5 % B to 20 % B in 23 min; A: H_2O, 0.1 % TFA and B: CH_3CN 0.1 % TFA. The stars show small impurities assigned to the solvents. (f) Representative example of multicharged species observed by ESI-MS of **1**. (g) NH amide region of the ^{1}H NMR spectra (700 MHz) of **1**–**4** (1 mM) in DMSO-d_6 at 60 °C. Red dashed lines indicate chemical shift (δ) differences between the NH amide resonances.

Manual SPFS, analysis and purification of a 41mer

In a second round of SPFS, oligoamides **5**–**7** were prepared (Figure 1). Sequence **5** is an extension of **2** to 32 units. Sequence **7** is an extension of **5** to 41 units. Sequence **6** is a 40mer missing the last unit of **7**. As for **1**–**4**, **5**–**7** have their hydrophobic L residues on the same face of the helix. Given the

Chemistry–A European Journal | Research Article
doi.org/10.1002/chem.202300898
Chemistry Europe
European Chemical Societies Publishing

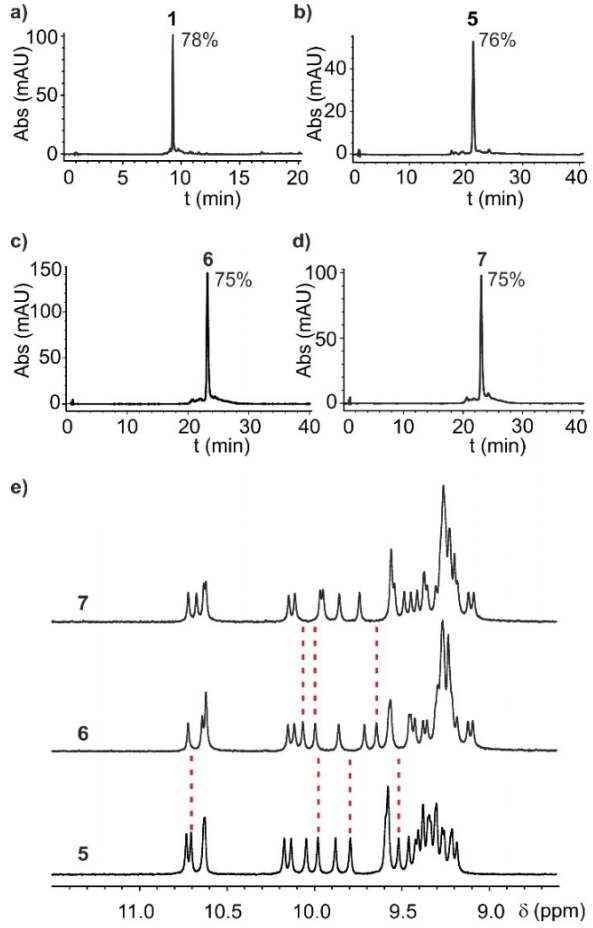

Figure 3. (a–d) RP-HPLC chromatograms of crude foldamers **1** introduced as a direct comparison, **5**, **6** and **7** showing the notable high purity obtained after **31**, **39** and **40** coupling cycles of SPFS (linear gradient from 20% B to 40% B in 35 min; A: H_2O + 0.1% TFA and B: CH_3CN + 0.1% TFA). (e) NH amide region of the ^{1}H NMR spectra (700 MHz) of **5**–**7** (1 mM) in DMSO-d_6 at 60 °C. Red dashed lines indicate the main chemical shift (δ) differences between the NH amide resonances.

similar t_R of **1**–**4** on RP-HPLC, it was expected that deleted products may be even more difficult to separate from the desired sequences in longer oligomers. Thus, a capping step was introduced after each coupling using acetyl chloride in the presence of DIEA in THF, at r.t. (3×5 min) as a modification of the SPFS procedure (step 4 in Scheme 1). Capping leads to truncated (instead of deleted) sequences that may be easier to separate, at least for the shorter ones. After TFA cleavage, the crude materials were analyzed by RP-HPLC (Figure 3b-3d). All chromatograms revealed one main product corresponding to the desired AO in high yield (over 70% after 40 SPS coupling cycles for **7**). The appearance of the crude chromatograms of **5**–**7** does not differ much from that of 15mer **1** (Figure 3a); thus demonstrating the robustness of the acid chloride-based SPFS methodology (Scheme 1). For comparison, Q_{41} is equivalent to an 82mer peptide in size. It appears that no drop in coupling and deprotection yields can be detected as elongation of the sequence is continued. This is all the more remarkable that the mass of foldamer exceeds the mass of resin at the end of the synthesis (for the 41mer, the mass of foldamer was three times bigger than the mass of resin). We hypothesize that on-resin helical folding during synthesis plays a favorable role. As shown in Figure 4a, the N-terminal amine function stacks on, and is sterically hindered by, the Q_n helix. However, this hindrance may also serve as a protection from further hindrance by other growing chains: the accessibility of the terminal amine would then not depend on the length of the neighboring chains. Furthermore, the fact that Q_n helices behave as rigid rods might favor their growth away from the resin and avoid the burial of a growing chain in the resin, which would result in a drop of coupling yield at some point (Figure 4b).

The purification of **5**–**7** was straightforward (isolated yields from 10–15% and purity >99% see Supporting Information). ESI-MS and ^{1}H NMR were again employed for the full characterization (Figures 3e, S12, S13, S16 and S17). As could be expected, even optimized RP-HPLC conditions did not allow for the separation of **6** and **7**. The chromatogram of a mixture of the two foldamers shows a single slightly broaden peak (Figure S9b). However, ^{1}H NMR spectroscopy allowed for the successful discrimination of these two compounds despite their minor difference in sequence (Figure 3e). Chemical shift values are different and ^{1}H NMR spectra would reveal the presence of **6** if it had been a significant inseparable impurity of **7**. The single set of sharp signals in the ^{1}H NMR spectrum of **7** is thus an excellent evidence of its high purity. ESI-MS also allows for efficient discrimination. By intentionally adding 10% of **6** to a solution of **7**, ESI-MS analysis reveal the presence of both foldamers. The absence of other ionized species in the mass spectra of **6** and **7** is also an indication of their purity (Figures S16b, S17).

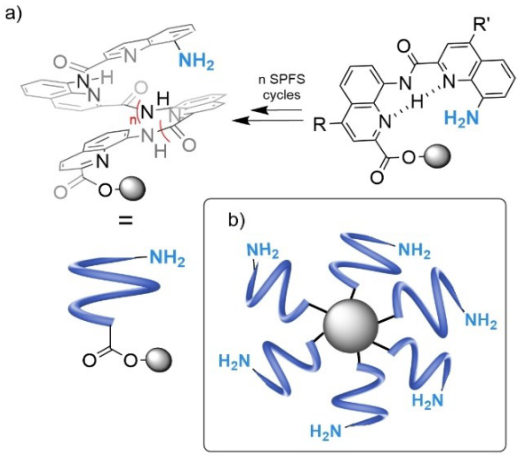

Figure 4. a) Schematic representation of a Q_n helix folding on a bead leaving the aromatic amine accessible for the next coupling. b) Cartoon depicting the hypothesis that on-bead foldamer sequences fold and grow away from the resin matrix.

Chemistry–A European Journal | Research Article doi.org/10.1002/chem.202300898 | Chemistry Europe European Chemical Societies Publishing

In summary, sequences as long as a 41mer may be synthesized without any apparent drop in coupling efficiency or any particular difficulty in analyzing and purifying the product. We have probably reached the limit of resolution of our RP-HPLC C_{18} column for differentiating large foldamers with high sequence similarity, but ^{1}H NMR and ESI-MS remain efficient at detecting minor differences. Even longer sequences are probably within reach of our SPFS methodology but such syntheses face a practical inconvenience: they become overly labor intensive and time consuming. The synthesis of **7** amounted to 112 h (14 work days) not counting the final steps and purification. Rather than focusing on longer sequences, we considered the prospect of automating the synthesis.

Automated SPFS

From the beginning, we considered that SPFS automation entailed accessing acid chloride monomers without resorting to the Ghosez's reagent. In our hands, this reagent required a high vacuum evaporation of all solvent and unreacted reagent before subsequent coupling that would be difficult to implement on a synthesizer. Without complete evaporation, the Ghosez's reagent competes with the acid chloride to cap the amine of the growing chain. This eventually generates amidines that were identified by mass spectrometry and ^{1}H NMR (Scheme 2 and Figure S24). Wilson *et al.*, who used Ghosez's reagent in substoichiometric amounts with respect to the acid to be activated for aromatic amide SPFS apparently did not observe such side reactions with their monomers.[10b] They also pointed to the fact that this reaction may not be problematic, if it occurs, with secondary amines because the by-product would then be an unstable quaternary amidinium that could degrade back to the amine in the presence of a nucleophile. Thus, in situ coupling with Ghosez's reagent may be more robust in the case of secondary amines.[10b,c]

We have previously used Appel's reaction to activate α-amino acids as acid chlorides in situ, and couple them to Q monomers.[21b] We therefore opted for this method which allows for the addition of the acid chloride mixed with reagents and by- products involved in its formation directly onto the amine. A second issue was to find a commercial synthesizer amenable to a use quite different from its initial purpose. Automated SPPS is well-documented and standardized,[25] but implementing SPFS required significant adaptation for our purpose. We needed the synthesizer to enable: *i)* the formation of the acid chloride in a pre-activation vessel (PV) different from the reaction vessel (RV) containing the resin-bound foldamer; *ii)* an accurate and fast heating of RVs; *iii*) working under an inert nitrogen atmosphere; *iv)* high versatility in terms of solvent compatibility, including some solvents not friendly to many plastics and seals such as THF; and *v)* the optional parallel synthesis of several sequences. The following protocols have been optimized for the PurePep Chorus peptide synthesizer from Gyros-Protein Technology. This synthesizer met all the above-mentioned criteria. Other synthesizers may also work. However, protocols would then have to be adapted accordingly. For example, Wilson *et al.* premixed monomers with Ghosez's reagent in the amino acid delivery tube, allowing some sort of in situ activation without requiring a preactivation vessel.[10b,c]

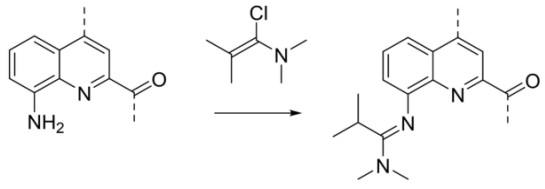

Scheme 2. Side reaction of 8-aminoquinolines with Ghosez's reagent producing an *N*,*N*-dimethyl-*N*′-(quinolin-8-yl)isobutyramidine.

An overview of the automated SPFS procedure is shown in Scheme 3. It entailed the programming of the synthesizer for the iteration of cycles consisting similar to those of manual SPFS (see Table S1 in the Supporting Information for detailed description): 1) Fmoc deprotection, 2) resin washings, 3) coupling, and 4) new round of washings. However, some changes were eventually implemented after several rounds of trials. We used low loading Cl-MPA ProTide resin (instead of the low loading Wang resin) because this resin has shown better purity of crude AOs during manual synthesis,[17a] and better AO recovery for sequences containing monomers bearing sulfonic acid side chains.[26] The Fmoc deprotection step was first tested using standard conditions (20 % piperidine in DMF).

However, we noticed the occasional presence of a side product in the RP-HPLC chromatogram of the crude AOs when using piperidine. This side product never occurred during manual synthesis. LC-MS analysis of the side product indicated +67 Da in mass with respect to the target mass. This corresponds to the addition of a piperidine molecule on the foldamer together with the loss of a water molecule. A possible side reaction may be the formation of a piperidinoaminidine that might arise from the activation of an amide into an imidoyl chloride by the in situ coupling reagents.[27] However, this hypothesis has not been ascertained. Nevertheless, the piperidine-derived adduct never formed when removing Fmoc protecting groups using 2 % DBU in NMP, so we opted for these conditions instead. Using DBU also proved more efficient than piperidine for monomers other than those discussed in this study and which will be described elsewhere.

Preactivation of the acid into the acid chloride was implemented in the PV by successive additions of the Fmoc-Q-OH monomer (3 equiv. relative to resin loading), Ph_3P (8 equiv.) and trichloroacetonitrile (TCAN, 9 equiv.) solutions in anhydrous THF and shaking the PV for 1 min before dispensing the acid chloride solution from the PV to the RV containing the resin pre-swollen with a solution of 2,4,6-collidine (9 equiv.) in anhydrous THF (Scheme 3). The acid chloride is formed in the absence of base using dry THF and reagents (moisture would lead to the production of HCl that would alter acid labile protecting groups of the side chains). Other solvents than THF can be used when needed. For example, NMP/THF (1 : 1 v/v) was used to solubilize Fmoc-O(Boc)-OH. Yet THF is preferable

Chemistry–A European Journal | Research Article doi.org/10.1002/chem.202300898 | Chemistry Europe European Chemical Societies Publishing

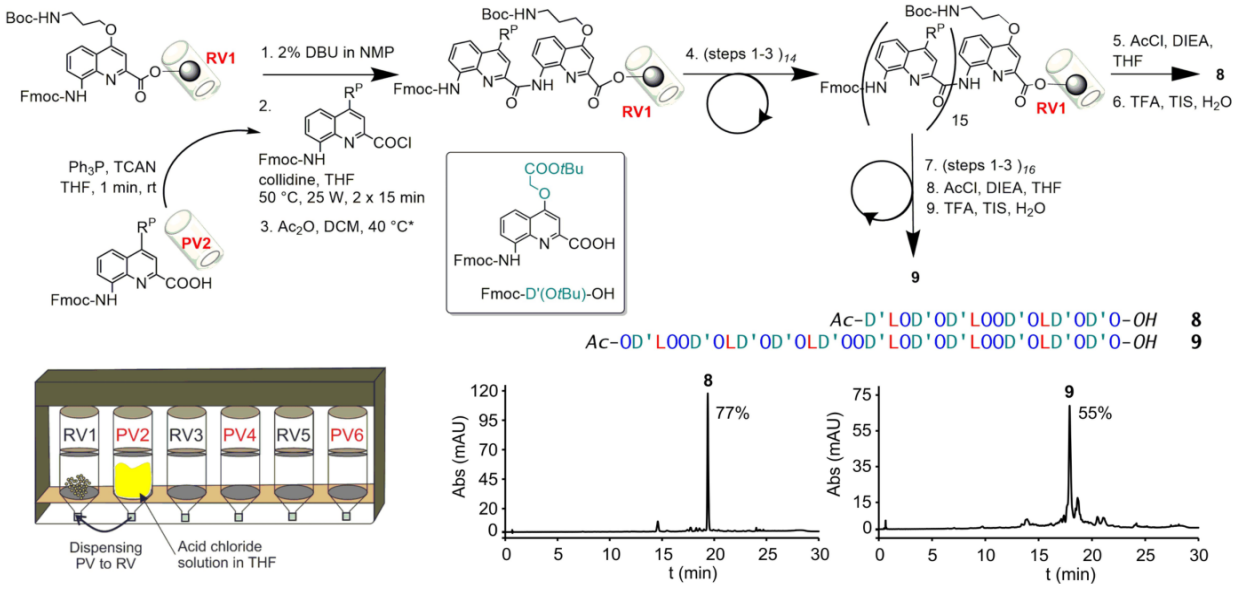

Scheme 3. SPFS protocols developed for the automation of the AO synthesis and exemplified for 16mer **8** and 32mer **9**. Bottom left: schematic representation of the Chorus synthesizer with RVs and PVs used during the coupling cycles. *The capping step was introduced after the 8th coupling. Bottom right: RP-HPLC chromatograms of foldamers **8** and **9** (linear gradient from 20% B to 40% B in 23 min; A: H_2O + 0.1% TFA and B: CH_3CN + 0.1% TFA).

for reasons that are detailed in the next section. The RV was next heated to 50 °C for 15 min before draining and resin washings with anhydrous THF. The coupling reaction was repeated once. Capping with acetic anhydride in DCM (50:50, v/v) at 40 °C for 10 min may be implemented prior to the next deprotection.[28]

The syntheses of 16mer **8** and of 32mer **9** are presented as representative examples of automated SPFS (Scheme 3). The sequence of **9** is identical to that of **5** but D units were replaced by the related D′ (Fmoc-D′(O*t*Bu)-OH as shown in Scheme 3). D′ is intensively used in our group and stocks are generally available. It is also easier and cheaper to produce than D. Sequence **8** corresponds to the sixteen C-terminal units of **9**. The syntheses were performed on a 15 μmol scale starting with the C-terminal Fmoc-O(Boc) preloaded on the MPA-Protide resin in 10 mL glass RVs (Scheme 3). This scale is the smallest for which we obtained good results. Scaling up the SPFS on the Chorus synthesizer can be implemented without hurdles. Three different RV sizes are available (10, 25, 40 mL) and allow to work at a scale up to 500 μmol. During the syntheses, a capping step was introduced after the 8th coupling. After final Fmoc deprotection and acetylation, **8** and **9** were cleaved from the resin and their purity was checked by RP-HPLC analysis. Sequence **8** was recovered in very good amount (50 mg of crude out of 59 mg expected, 85%). The RP-HPLC chromatogram showed one main peak indicating a crude purity of 77% (Scheme 3). Product identity was established by LC-MS analysis (Figure S18a). In terms of purity and amount recovered, these values are comparable to those obtained for the manual SPFS of **1**. The main difference between the two approaches is the significant reduction of work time. The automated SPFS of **8** required 2–3 h of work to prepare solutions followed by 19 h of instrument time, in comparison to 40 h of work (5 work days) required for the manual SPFS of **1**. Results were also satisfactory for the preparation of 32mer **9** whose identity was confirmed by LC-MS analysis (Figure S18b). The mass recovered was 83% of that expected. The RP-HPLC analysis showed a drop of crude purity with respect to manually synthesized **7** (55% versus 77%). This suggests that the couplings using the Appel reaction may not perform as perfectly as the activation with the Ghosez's reagent which may be understood given the complexity of the Appel reaction as discussed in the next section. Nevertheless, these yields compare favorably to the SPS of peptides of similar length (Q_{32} is equivalent to 64 α-amino acids, i.e. protein size).[29] The critical point is again the time saved. The preparation of **9** also required 2–3 h of work to set-up the Chorus synthesizer followed by 40 h of non-stop instrument time, to be compared to 88 h (11 work days) for the manual synthesis of **5**.

Monomer recycling

The automation of large AO SPFS plus the possibility to build up to three sequences in parallel makes the availability of monomers a limiting factor. Suitably protected Q monomers all require a multistep synthesis for their preparation. Even if these syntheses have been streamlined on a multigram scale, the monomers are valuable and used in excess (2×3 equiv.) during SPFS. We were therefore motivated to implement monomer recovery. The basic coupling reaction mixture that flows from the RV after coupling can be quenched by collecting it in a 5%

Chemistry–A European Journal | Research Article doi.org/10.1002/chem.202300898 | Chemistry Europe European Chemical Societies Publishing

aqueous citric acid solution. This can be easily implemented by inserting a collect step in the protocol which will dispense the coupling solution to the collect container. The citric acid serves to protonate the acid function of Fmoc-Q-OH, thus allowing its subsequent extraction in CH_2Cl_2, without damaging acid labile side chain protections. The extracted mixtures, however, may be more complicated than expected. RP-HPLC analysis allowed us to assess the presence of other substances than the Fmoc-Q-OH to be recycled. The most typical, and potentially most abundant species is a stable ylide. In the case of monomer L, this ylide was purified and characterized and its structure was confirmed by LC-MS, ^{1}H NMR, and x-ray crystallography (compound **10** in Scheme 4, Figure S19 and Table S3). Compound **10** results from the reaction of the acid chloride with (cyanomethylene)-triphenylphosphorane **11** ($Ph_3P{=}CH_2CN$).[30] This reaction

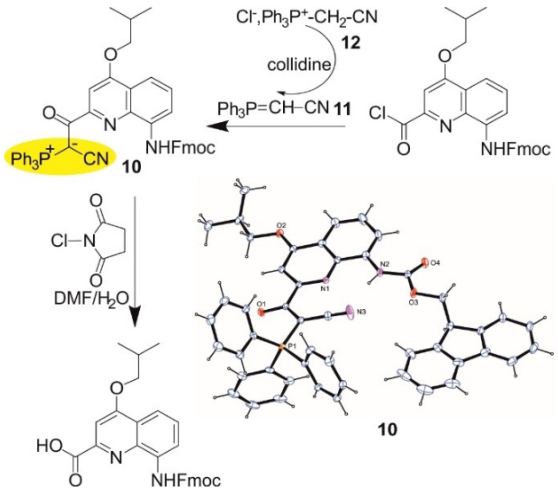

Scheme 4. Formation and crystal structure of ylide **10** produced during in situ acid chloride activation using TCAN, Ph_3P and Fmoc-L-OH monomer.

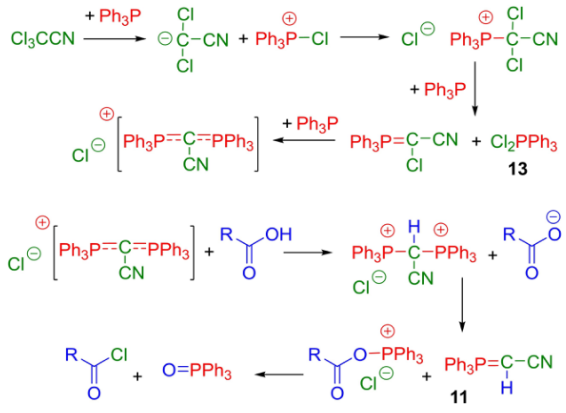

Scheme 5. Mechanism of the TCA/triphenylphosphine-mediated activation of an acid into an acid chloride explaining the formation of **11** as a by-product, adapted from Ref. [22a] where CCl_4 was used instead of TCAN. The colors of atoms belonging to the reagents are reflected in the formulas of the products.

could indeed be reproduced using commercial **11** (Figure S20). The presence of **11** in the reaction mixture is consistent with Appel's report that (chloromethylene)-triphenylphosphorane forms when using CCl_4 instead of TCAN (Eq. (57) in Ref. [22a]). The mechanism that leads to the formation of **11** is depicted in Scheme 5. The presence of **11** in the activation step thus threatens to reduce the amount of available acid chloride. However, when activation is performed in THF, we observe that (cyanomethyl)triphenylphosphonium chloride **12** (Scheme 4) immediately precipitates and remains in the PV after the acid chloride solution has been transferred to the RV. Collecting a sample of the precipitate allowed us to assign it to pure **12** (Figure S21). Subsequent washing of the PV with DMF flushes this precipitate away. A benefit of using THF for the activation step is thus to reduce the formation of ylides such as **10**. The proportion of ylide is for example higher for Fmoc-O(Boc)-OH which is activated in THF/NMP from which **12** does not precipitate.

Of note, the mechanism shown in Scheme 5 is typical of an acid chloride activation under neutral conditions: it does not generate HCl unlike many other typical reagents (e.g. $SOCl_2$, oxalyl chloride). However, this mechanism accounts for the formation of **11**, but not of the salt **12** which we isolated. A possible explanation for the presence of **12** may be the dichlorotriphenylphosphorane **13** that is generated during the activation. Compound **13** may also react with the carboxylic acid to produce the acid chloride, triphenylphosphine oxide and HCl. HCl would then be buffered by **11** to produce **12**. Another possible, less desirable, source of HCl is the reaction of the acid chloride with **11**. Indeed, when reacting Fmoc-L–Cl with **11**, **10** is produced along with **12**, showing the ability of **11** to act as a base and as a nucleophile (Figure S20). Of note, HCl is anyways produced during the subsequent coupling step, regardless of the pathway that produces the acid chloride, but the coupling is always performed in presence of a base.

Ylides such as by-product **10** are stable.[30] Yet we found that it is possible to chlorinate them with *N*-chlorosuccinimide (NCS) leading to their degradation into a carboxylic acid (Scheme 4), through a haloform-like reaction similar to the degradation of cyanosulfurylides recently developed as selective protecting group of Asp residue during SPPS.[31] Thus, **10** was exposed to increasing amounts of NCS in a DMF/H_2O mixture. The reaction was monitored by RP-HPLC analysis and proved to be almost complete after 2 days using up to 5 equivalents of NCS (Figure S22). In summary, excess Fmoc-protected monomers may be recycled after quenching the coupling reaction mixtures. In case significant amounts of cyanoketophosphoranes are present, these may be degraded back to the desired acid using NCS, before final purification.

Consequences for manual synthesis

The adaptation and optimization of the protocols for the automation of SPFS have led to developments that can also be useful in manual synthesis. For instance, the in situ activation via the Appel's reaction is much quicker to implement than the

Chemistry–A European Journal | Research Article doi.org/10.1002/chem.202300898 | Chemistry Europe European Chemical Societies Publishing

activation with Ghosez's reagent, allowing five deprotection/coupling cycles to be performed manually in 8–9 h. For this, we used the same reagents and the same stoichiometry with respect to Fmoc-Q-OH as for the automated synthesis. In manual synthesis, the acid activation mixture is typically transferred unfiltered to the resin. This requires a better solvent than pure THF and $CHCl_3$/THF (1 : 1, v/v) was typically used to dissolve all intermediates (including **12**). Acid chloride activation is then performed in a separate vial shaken by hand for a few seconds before being added to the resin suspended in THF containing collidine. Consequently, one has to anticipate the potential presence of ylide by-products when recovering the Fmoc-Q-OH after a manual coupling cycle. Other coupling cycle optimizations are currently being tested, including the reduction of the number of equivalents of Fmoc-Q-OH monomer and of activating reagents, or of the time necessary for complete Fmoc deprotection with 2% DBU in NMP. Progress will be reported in due course.

Conclusion

We have extended the manual SPS and the analysis and purification of helically folded aromatic oligoamides to sequences as long as a 41mer with excellent yields and purity. This places our SPS protocols among the most efficient known to date, giving access to sequences in the size range of an 80mer peptide. We speculate that this remarkable efficiency is in fact assisted by helical folding on the resin. This would contrast with the common observation in peptide synthesis that on-resin folding and aggregation result in decreasing coupling yields. Next, we have adapted and optimized the deprotection and coupling procedures to allow for the automation of the SPFS. A commercial peptide synthesizer was used to produce aromatic oligoamide sequences starting from Fmoc-acid monomers, that is, including their activation to acid chlorides in a preactivation vessel under a nitrogen atmosphere. Long AO sequences were produced with minimal laboratory work in good (32mer **9**) to high (16mer **8**) crude purity. The validation of the analytical techniques (RP-HPLC, NMR, and LC-ESI-MS) allowed for the identification and full characterization of the designed foldamers. This is of special importance for long and more complex structures, usually designed for biological or biomaterial applications, for which the final step of analysis and purification can be a limitation. These developments pave the way to the rapid access to new and longer sequences than before, and thus to quicker exploration of their properties. Automated SPFS of multiple sequences will also permit to investigate the ligation of long, pre-synthesized, fragments, as in protein synthesis, and to potentially explore the behavior of foldamers of 10 kDa and above.

Supporting Information

The data that support the findings of this study are available in the supplementary material of this article. Additional references cited within the Supporting Information.[32–35]

Deposition Number(s) 2243294 (for **10**) contain(s) the supplementary crystallographic data for this paper. These data are provided free of charge by the joint Cambridge Crystallographic Data Centre and Fachinformationszentrum Karlsruhe Access Structures service.

Acknowledgements

We are grateful to the Deutsche Forschungsgemeinschaft (DFG) for financial support via project HU1766/2-1 and CRC1309-C7 (project ID 325871075). We thank Dr. D. Bindl for helping with monomer recovery procedures, Dr. P. Mayer for assistance with crystallographic measurements and structure elucidation, and I. R. Alonso for the isolation and characterization of the *N*,*N*-dimethyl-*N*′-(quinolin-8-yl)isobutyramidine. Open Access funding enabled and organized by Projekt DEAL.

Conflict of Interests

The authors declare no conflict of interest.

Data Availability Statement

The data supporting these findings are available upon reasonable request from the authors. Deposition Number 2243294 (for **10**) contains the supplementary crystallographic data for this paper. These data are provided free of charge by the joint Cambridge Crystallographic Data Centre and Fachinformationszentrum Karlsruhe Access Structures service.

Keywords: aromatic oligoamides · automation · foldamers · in situ acid chloride activation · solid-phase synthesis

[1] a) L. Wang, N. Wang, W. Zhang, X. Cheng, Z. Yan, G. Shao, X. Wang, R. Wang, C. Fu, *Signal Transduct. Target. Ther.* **2022**, *7*, 48; b) C. Heinis, T. Rutherford, S. Freund, G. Winter, *Nat. Chem. Biol.* **2009**, *5*, 502–507; c) B. He, K. F. Tjhung, N. J. Bennett, Y. Chou, A. Rau, J. Huang, R. Derda, *Sci. Rep.* **2018**, *8*, 1214; d) J. Y. K. Wong, R. Mukherjee, J. Miao, O. Bilyk, V. Triana, M. Miskolzie, A. Henninot, J. J. Dwyer, S. Kharchenko, A. Iampolska, D. M. Volochnyuk, Y.-S. Lin, L.-M. Postovit, R. Derda, *Chem. Sci.* **2021**, *12*, 9694–9703; e) T. R. Oppewal, I. D. Jansen, J. Hekelaar, C. Mayer, *J. Am. Chem. Soc.* **2022**, *144*, 3644–3652; f) T. Passioura, T. Katoh, Y. Goto, H. Suga, *Annu. Rev. Biochem.* **2014**, *83*, 727–752; g) W. Liu, S. J. de Veer, Y.-H. Huang, T. Sengoku, C. Okada, K. Ogata, C. N. Zdenek, B. G. Fry, J. E. Swedberg, T. Passioura, D. J. Craik, H. Suga, *J. Am. Chem. Soc.* **2021**, *143*, 18481–18489.

[2] a) N. Hartrampf, A. Saebi, M. Poskus, Z. P. Gates, A. J. Callahan, A. E. Cowfer, S. Hanna, S. Antilla, C. K. Schissel, A. J. Quartararo, X. Ye, A. J. Mijalis, M. D. Simon, A. Loas, S. Liu, C. Jessen, T. E. Nielsen, B. L. Pentelute, *Science* **2020**, *368*, 980–987; b) H. Masui, S. Fuse, *Org. Process Res. Dev.* **2022**, *26*, 1751–1765; c) M. D. Simon, P. L. Heider, A. Adamo, A. A. Vinogradov, S. K. Mong, X. Li, T. Berger, R. L. Policarpo, C. Zhang, Y.

Chemistry–A European Journal | Research Article doi.org/10.1002/chem.202300898 | Chemistry Europe European Chemical Societies Publishing

Zou, X. Liao, A. M. Spokoyny, K. F. Jensen, B. L. Pentelute, *ChemBioChem* **2014**, *15*, 713–720.
[3] a) I. Sarac, C. Meier, *Chem. Eur. J.* **2015**, *21*, 16421–16426; b) D. A. Lashkari, S. P. Hunicke-Smith, R. M. Norgren, R. W. Davis, T. Brennan, *Proc. Natl. Acad. Sci. USA* **1995**, *92*, 7912–7915; c) S. Pitsch, P. A. Weiss, X. Wu, D. Ackermann, T. Honegger, *Helv. Chim. Acta* **1999**, *82*, 1753–1761; d) M. D. Matteucci, M. H. Caruthers, *J. Am. Chem. Soc.* **1981**, *103*, 3185–3191; e) S. Roy, M. Caruthers, *Molecules* **2013**, *18*, 14268–14284; f) A. F. Sandahl, T. J. D. Nguyen, R. A. Hansen, M. B. Johansen, T. Skrydstrup, K. V. Gothelf, *Nat. Commun.* **2021**, *12*, 2760.
[4] D. M. Hoover, J. Lubkowski, *Nucleic Acids Res.* **2002**, *30*, e43.
[5] N. C. Seeman, *Trends Biotechnol.* **1999**, *17*, 437–443.
[6] D. D. Ma, T. Rede, N. A. Naqvi, P. D. Cook, *Biotechnol. Annu. Rev.* **2000**, *5*, 155–196.
[7] H. Tran, S. L. Gael, M. D. Connolly, R. N. Zuckermann, *J. Visualization* **2011**, *57*, e3373.
[8] a) K. R. Strom, J. W. Szostak, *J. Org. Chem.* **2020**, *85*, 13929–13938; b) R. K. Roy, A. Meszynska, C. Laure, L. Charles, C. Verchin, J.-F. Lutz, *Nat. Commun.* **2015**, *6*, 7237.
[9] a) J. K. Murray, S. H. Gellman, *Org. Lett.* **2005**, *7*, 1517–1520; b) C. Douat-Casassus, K. Pulka, P. Claudon, G. Guichard, *Org. Lett.* **2012**, *14*, 3130–3133; c) A. Abdildinova, M. J. Kurth, Y.-D. Gong, *Asian J. Org. Chem.* **2021**, *10*, 2300–2317.
[10] a) B. Baptiste, C. Douat-Casassus, K. Laxmi-Reddy, F. Godde, I. Huc, *J. Org. Chem.* **2010**, *75*, 7175–7185; b) N. S. Murphy, P. Prabhakaran, V. Azzarito, J. P. Plante, M. J. Hardie, C. A. Kilner, S. L. Warriner, A. J. Wilson, *Chem. Eur. J.* **2013**, *19*, 5546–5550; c) K. Long, T. A. Edwards, A. J. Wilson, *Bioorg. Med. Chem.* **2013**, *21*, 4034–4040; d) H. M. König, R. Abbel, D. Schollmeyer, A. F. Kilbinger, *Org. Lett.* **2006**, *8*, 1819–1822; e) E. E. Baird, P. B. Dervan, *J. Am. Chem. Soc.* **1996**, *118*, 6141–6146.
[11] a) M. Badoux, A. F. M. Kilbinger, *Macromolecules* **2017**, *50*, 4188–4197; b) L. K. Mueller, A. C. Baumruck, H. Zhdanova, A. A. Tietze, *Front. Bioeng. Biotechnol.* **2020**, *8*, 162.
[12] V. Aucagne, I. E. Valverde, P. Marceau, M. Galibert, N. Dendane, A. F. Delmas, *Angew. Chem. Int. Ed.* **2012**, *51*, 11320–11324; *Angew. Chem.* **2012**, *124*, 11482–11486.
[13] a) K. Ziach, C. Chollet, V. Parissi, P. Prabhakaran, M. Marchivie, V. Corvaglia, P. P. Bose, K. Laxmi-Reddy, F. Godde, J.-M. Schmitter, S. Chaignepain, P. Pourquier, I. Huc, *Nat. Chem.* **2018**, *10*, 511–518; b) V. Corvaglia, D. Carbajo, P. Prabhakaran, K. Ziach, P. K. Mandal, V. D. Santos, C. Legeay, R. Vogel, V. Parissi, P. Pourquier, I. Huc, *Nucleic Acids Res.* **2019**, *47*, 5511–5521; c) J. Ahmed, T. C. Fitch, C. M. Donnelly, J. A. Joseph, T. D. Ball, M. M. Bassil, A. Son, C. Zhang, A. Ledreux, S. Horowitz, Y. Qin, D. Paredes, S. Kumar, *Nat. Commun.* **2022**, *13*, 2273; d) S. Kumar, M. Birol, D. E. Schlamadinger, S. P. Wojcik, E. Rhoades, A. D. Miranker, *Nat. Commun.* **2016**, *7*, 11412; e) D. Maity, S. Kumar, F. Curreli, A. K. Debnath, A. D. Hamilton, *Chem. Eur. J.* **2019**, *25*, 7265–7269.
[14] S. De, B. Chi, T. Granier, T. Qi, V. Maurizot, I. Huc, *Nat. Chem.* **2018**, *10*, 51–57.
[15] a) Y. Ferrand, I. Huc, *Acc. Chem. Res.* **2018**, *51*, 970–977; b) V. Koehler, A. Roy, I. Huc, Y. Ferrand, *Acc. Chem. Res.* **2022**, *55*, 1074–1085; c) T. A. Sobiech, Y. Zhong, B. Gong, *Org. Biomol. Chem.* **2022**, *20*, 6962–6978; d) T. A. Sobiech, Y. Zhong, D. P. Miller, J. K. McGrath, C. T. Scalzo, M. C. Redington, E. Zurek, B. Gong, *Angew. Chem. Int. Ed.* **2022**, *61*, e202213467; *Angew. Chem.* **2022**, *134*, e202213467; e) J.-L. Hou, X.-B. Shao, G.-J. Chen, Y.-X. Zhou, X.-K. Jiang, Z.-T. Li, *J. Am. Chem. Soc.* **2004**, *126*, 12386–12394; f) C. Li, S.-F. Ren, J.-L. Hou, H.-P. Yi, S.-Z. Zhu, X.-K. Jiang, Z.-T. Li, *Angew. Chem. Int. Ed.* **2005**, *44*, 5725–5729; *Angew. Chem.* **2005**, *117*, 5871–5875.
[16] X. Li, N. Markandeya, G. Jonusauskas, N. D. McClenaghan, V. Maurizot, S. A. Denisov, I. Huc, *J. Am. Chem. Soc.* **2016**, *138*, 13568–13578.
[17] a) S. Dengler, P. K. Mandal, L. Allmendinger, C. Douat, I. Huc, *Chem. Sci.* **2021**, *12*, 11004–11012; b) S. Dengler, C. Douat, I. Huc, *Angew. Chem. Int. Ed.* **2022**, *61*, e202211138; *Angew. Chem.* **2022**, *134*, e202211138.
[18] a) X. Hu, S. J. Dawson, P. K. Mandal, X. de Hatten, B. Baptiste, I. Huc, *Chem. Sci.* **2017**, *8*, 3741–3749; b) M. Zwillinger, P. S. Reddy, B. Wicher, P. K. Mandal, M. Csékei, L. Fischer, A. Kotschy, I. Huc, *Chem. Eur. J.* **2020**, *26*, 17366–17370.
[19] T. Qi, V. Maurizot, H. Noguchi, T. Charoenraks, B. Kauffmann, M. Takafuji, H. Ihara, I. Huc, *Chem. Commun.* **2012**, *48*, 6337–6339.
[20] a) F. Devaux, X. Li, D. Sluysmans, V. Maurizot, E. Bakalis, F. Zerbetto, I. Huc, A.-S. Duwez, *Chem* **2021**, *7*, 1333–1346; b) D. Meier, B. Schoof, J. Wang, X. Li, A. Walz, A. Huettig, H. Schlichting, F. Rosu, V. Gabelica, V. Maurizot, J. Reichert, A. C. Papageorgiou, I. Huc, J. V. Barth, *Chem. Commun.* **2022**, *58*, 8938–8941.
[21] a) S. J. Dawson, X. Hu, S. Claerhout, I. Huc, in *Methods Enzymol.*, Vol. 580 (Ed.: V. L. Pecoraro), Academic Press, Cambridge, Massachusetts, United States, **2016**, Ch. 13; b) X. Hu, S. J. Dawson, Y. Nagaoka, A. Tanatani, I. Huc, *J. Org. Chem.* **2016**, *81*, 1137–1150.
[22] a) R. Appel, *Angew. Chem. Int. Ed. Engl.* **1975**, *14*, 801–811; *Angew. Chem.* **1975**, *24*, 863–874; b) D. O. Jang, D. J. Park, J. Kim, *Tetrahedron Lett.* **1999**, *40*, 5323–5326; c) L. E. Barstow, V. J. Hruby, *J. Org. Chem.* **1971**, *36*, 1305–1306.
[23] a) P. S. Reddy, B. Langlois d'Estaintot, T. Granier, C. D. Mackereth, L. Fischer, I. Huc, *Chem. Eur. J.* **2019**, *25*, 11042–11047; b) F. S. Menke, B. Wicher, V. Maurizot, I. Huc, *Angew. Chem. Int. Ed.* **2023**, *62*, e202217325; *Angew. Chem.* **2023**, *135*, e202217325.
[24] For peptides of similar length, NMR spectra are poorly informative about compound identity or purity so much so that they are generally not requested for publication in organic chemistry journals.
[25] a) J. Tian, Y. Li, B. Ma, Z. Tan, S. Shang, *Front. Chem.* **2022**, *10*, 896098; b) F. Zieleniewski, D. N. Woolfson, J. Clayden, *Chem. Commun.* **2020**, *56*, 12049–12052; c) Y. Yu, A. Kononov, M. Delbianco, P. H. Seeberger, *Chem. Eur. J.* **2018**, *24*, 6075–6078; d) D. F. H. Winkler, in *Peptide Synthesis: Methods and Protocols*, Vol. 2103 (Eds.: W. M. Hussein, M. Skwarczynski, I. Toth), Springer US, New York, United States, **2020**.
[26] D. Bindl, P. K. Mandal, L. Allmendinger, I. Huc, *Angew. Chem. Int. Ed.* **2022**, *61*, e202116509; *Angew. Chem.* **2022**, *134*, e202116509.
[27] a) E. A. O'Brien, K. K. Sharma, J. Byerly-Duke, L. A. Camacho, III, B. VanVeller, *J. Am. Chem. Soc.* **2022**, *144*, 22397–22402; b) D. M. Szantai-Kis, C. R. Walters, T. M. Barrett, E. M. Hoang, E. J. Petersson, *Synlett* **2017**, *28*, 1789–1794.
[28] Ac_2O was preferred for the capping step. We avoided to introduce AcCl, which is highly reactive and potentially corrosive, in the synthesizer. Ac_2O had previously been shown to be efficient for this purpose (see Ref. [10a]).
[29] a) M. Cemazar, D. J. Craik, *J. Pept. Sci.* **2008**, *14*, 683–689; b) R. D. M. Silva, J. Franco Machado, K. Gonçalves, F. M. Lucas, S. Batista, R. Melo, T. S. Morais, J. D. G. Correia, *Molecules* **2021**, *26*, 7349.
[30] H. H. Wasserman, W.-B. Ho, *J. Org. Chem.* **1994**, *59*, 4364–4366.
[31] K. Neumann, J. Farnung, S. Baldauf, J. W. Bode, *Nat. Commun.* **2020**, *11*, 982.
[32] Bruker (**2012**). SAINT. Bruker AXS Inc., Madison, Wisconsin, USA.
[33] G. M. Sheldrick (**1996**). SADABS. University of Göttingen, Germany.
[34] G. M. Sheldrick, *Acta Crystallogr. Sect. A* **2015**, *71*, 3–8.
[35] A. L. Spek, *Acta Crystallogr. Sect. C* **2015**, *71*, 9–18.

Manuscript received: March 21, 2023
Accepted manuscript online: April 6, 2023
Version of record online: ■■, ■■

RESEARCH ARTICLE

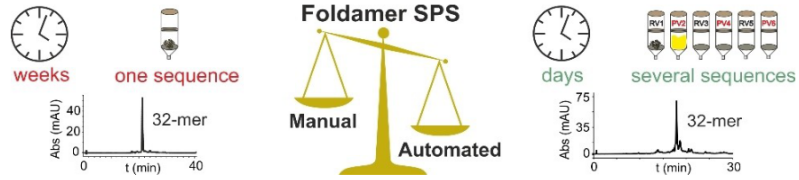

*Dr. V. Corvaglia, F. Sanchez, Dr. F. S. Menke, Dr. C. Douat, Prof. Dr. I. Huc**

1 – 10

Optimization and Automation of Helical Aromatic Oligoamide Foldamer Solid-Phase Synthesis

On-resin folding during solid-phase synthesis is not always an impediment! Under optimized conditions, helices of aromatic oligoamide foldamers are produced in high yield even when their length reaches tens of units. Automation of synthesis on a commercial peptide synthesizer is a game changer for the development of these compounds.

6.4. Supporting information: Optimisation and automation of of helical aromatic oligoamide foldamer solid-phase-synthesis

Chemistry–A European Journal

Supporting Information

Optimization and Automation of Helical Aromatic Oligoamide Foldamer Solid-Phase Synthesis

Valentina Corvaglia, Florian Sanchez, Friedericke S. Menke, Céline Douat, and Ivan Huc*

Content

1. Materials and Methods 2
1.1. Methods for RP-HPLC analysis 2
1.2. Methods for NMR analysis 2
1.3. Methods for LC-ESI-MS analysis 2
2. Experimental section 3
2.1. Manual microwave-assisted SPFS of foldamers 1-4 3
2.2. Manual microwave-assisted SPFS of foldamers 5-7 5
2.3. Automation of the SPFS of foldamers 8-9 6
2.4. Setting up the Chorus PurePep ® synthesizer for SPFS 7
2.5. Synthesis of Ylide 10 in solution 11
2.6. Regeneration of Fmoc-L-OH from 10 11
3. Characterization of foldamers 11
3.1. HPLC chromatograms of crude foldamers 11
3.2. HPLC chromatograms of pure foldamers 13
3.3. ^{1}H NMR spectra of pure foldamers 15
3.4. Mass spectrometry analysis of pure foldamers 19
3.5. Mass spectrometry analysis of crude foldamers 8-9 23
4. Synthesis and Characterization of ylide 10 24
5. Crystal structure of isolated ylide 10 27
6. Characterization of the *N*,*N*-dimethyl-*N'*-(quinolin-8-yl)isobutyramidine 29

1. Materials and Methods

Chemicals and reagents were used as commercially supplied without any further purification unless otherwise stated. Low loading Wang resin (0.41 mmol/g) was purchased from Novabiochem. Ghosez reagent (1-chloro-*N*,*N*,2-trimethyl-1 propenylamine) was purchased from Sigma Aldrich. *N,N*-diisopropylethylamine (DIPEA) was distilled over calcium hydride. Reactions requiring anhydrous conditions were performed under nitrogen. Quinoline monomers (O), (D, D'), and (L) were synthesized following procedures reported previously by our group.[1]

Analytical grade organic solvents were used for solid phase synthesis. Anhydrous THF and CH_2Cl_2 for solid phase synthesis were dispensed from an MBRAUN SPS-800 solvent purification system. Peptide synthesis-grade DMF was purchased from Carlo Erba and NMP from IRIS Biotech. HPLC grade acetonitrile and MilliQ water were used for RP-HPLC analyses and purification. RP-HPLC analyses were performed at 1.0 mL.min^{-1} by using a Macherey–Nagel Nucleodur C18 HTec column (4 x 100 mm, 5 µm). The mobile phase was composed of 0.1% (v/v) TFA/H_2O (solvent A) and 0.1% TFA/CH_3CN (solvent B). Monitoring was performed by UV detection at 214, 254 and 300 nm with a diode array detector. Semi-preparative RP-HPLC purifications of oligomers were performed at 5 mL.min^{-1} by using a Macherey-Nagel Nucleodur C18 HTEC column (10 x 125 mm, 5 µm). The mobile phase was the same as for the analytic inJections. Monitoring was performed by UV detection at 300 nm.

NMR spectra were recorded on Avance III NMR spectrometer (Bruker Biospin) with a vertical 16.45 T narrowbore/ultrashield magnet operating at 700 MHz for ^1H observation by means of a 5-mm TXI $^1H/^{13}C/^{15}N$ probe with single axis Z-gradient capabilities. Chemical shifts are reported in ppm and are calibrated against residual solvent signal of DMSO-d_6 (δ 2.50). Data processing was performed with Bruker TOPSPIN 2.1 software.

LC-ESI-MS spectra were recorded on Agilent Technologies 6230 Time of Flight LC/MS for foldamers **1**-**7.** The analyses were performed at 0.4 mL.min^{-1} by using a Macherey–Nagel Nucleoshell C18 RP 18plus column (2 x 50 mm, 2.7 µm). 0.1% formic acid was added to the aqueous mobile phase (solvent A) and acetonitrile (solvent B). The column eluent was monitored by UV detection at 214, 254, and 300 nm with a diode array detector. LC-ESI-MS spectra of foldamers **8** and **9** were recorded on a Bruker microTOF II in positive ionization mode. The HPLC line was an Ultimate 3000 RP-HPLC System (ThermoFisher Scientific) equipped with a Nucleodur C18 Gravity column (2 x 50 mm, 1.8 µm, Macherey-Nagel) at a flow rate of 0.33 ml.min^{-1} with the same set of solvents and UV detection mode to the previous analyses.

1.1. Methods for RP-HPLC analysis

Solutions of foldamers **1**-**9** (100 µM) were prepared in a mixture of 0.1% (v/v) TFA/H_2O and 0.1% TFA/CH_3CN. HPLC chromatograms of crude and pure oligomers were recorded at r.t.

1.2. Methods for NMR analysis

Solutions of foldamers **1-7** (1 mM) were prepared in DMSO-d_6 (99.9%). ^1H NMR spectra were recorded at 333 K using a water suppression sequence (watergate).

1.3. Methods for LC-ESI-MS analysis

LC-ESI-MS experiments were performed in positive ion mode. Solutions of oligomers **1**-**9** were prepared in a mixture of 0.1% (v/v) formic acid in H_2O (solvent A) and 0.1% formic acid in CH_3CN (solvent B). Foldamers **1**-**4** were analyzed by using a flow rate of 0.4 ml.min^{-1} and a gradient from 10% B to 100% B in 5 min.

Foldamers **5**-**7** were analyzed by using a flow rate of 0.4 ml.min^{-1} and a gradient from 20% B to 100% B in 5 min.

Foldamers **8** and **9** were analyzed by using a flow rate of 0.33 ml.min^{-1} and a gradient from 20% B to 100% B in 8 min.

2. Experimental section

2.1. Manual microwave-assisted SPFS of foldamers 1-4

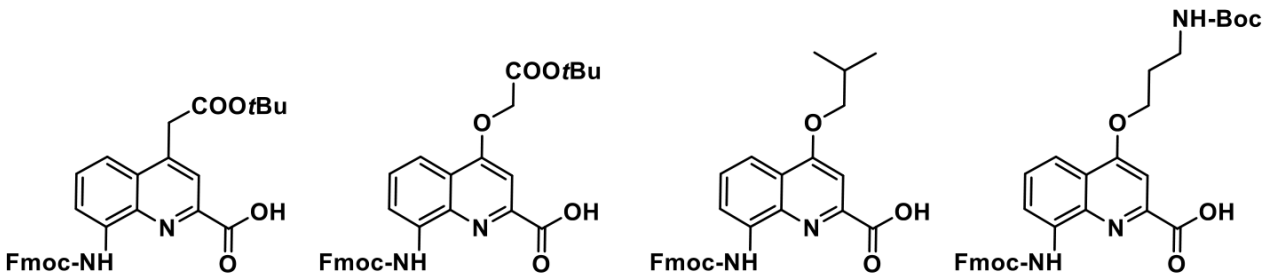

Fmoc-D(O*t*Bu)-OH Fmoc-D'(O*t*Bu)-OH Fmoc-L-OH Fmoc-O(Boc)-OH

Bromination of low loading Wang resin: Low loading Wang resin (150 mg, 0.0615 mmol) was swollen in 2 mL anhydrous DMF for 1 h under N_2. PPh_3 (81 mg, 0.3075 mmol, 5.0 equiv.) and CBr_4 (103 mg, 0.3075 mmol, 5 equiv.) were then added in that order and the resin was stirred overnight under N_2 at room temperature. The resin was filtered off, and washed with anhydrous DMF (3 x 3 mL), DCM (3 x 3 mL) and isopropanol (3 x 3 mL, sequence repeated three times) and then dried under high vacuum.

Loading of first monomer unit: Low loading bromo-Wang resin (150 mg, 0.0615 mmol) was swollen in anhydrous DMF (2 mL) for 1 h under N_2. Fmoc-O(Boc)-OH (178 mg, 0.1845 mmol, 3.0 equiv.) and CsI (48 mg, 0.1845 mmol, 3.0 equiv.) were then added, followed by DIEA (64 µL, 0.369 mmol, 6.0 equiv.). The reaction vessel was then placed under microwave irradiation (50 W, ramp to 50 ºC over 5 min, then hold at 50 ºC for 5 min). The resin was washed with anhydrous DMF (3 x 3 mL) and the process was repeated once. The resin was then washed thoroughly with DMF (6 x 3 mL).

General procedure for Fmoc deprotection: To Fmoc- O(Boc)-Wang resin was added a 20% solution of piperidine in DMF (4 mL) and the resin was stirred for 3 min at room temperature. The resin was washed with DMF (3 x 3 mL) and the deprotection step was repeated once for 7 min. After filtration, the resin was then washed thoroughly with DMF (3 x 3 mL) and anhydrous THF (3 x 3 mL) prior to coupling reaction.

General procedure for acid chloride activation exemplified by preparation of Fmoc-D(O*t*Bu)-Cl: Fmoc-D(O*t*Bu)-OH (200 mg, 0.369 mmol) was dissolved in anhydrous DCM (3 mL) under N_2, and 1-chloro-*N,N*,2-trimethyl-1-propenylamine (100 µL, 0.718 mmol) was added. The mixture was stirred for 1 h before solvent removal and drying under high vacuum.

General procedure of Fmoc-Q-Cl coupling on Wang resin-bound oligoquinoline, exemplified with Fmoc-D(O*t*Bu)-Cl: To a H-$(Q)_n$-Wang resin (150 mg, 0.0615 mmol) swollen in anhydrous THF (1.5 mL), was added DIEA (64 µL, 0.369 mmol, 6.0 equiv.). Next, freshly prepared Fmoc-D(O*t*Bu)-Cl was dissolved in anhydrous THF (3 mL) and 1.5 mL of this solution (0.184 mmol, 3 equiv.) was added to the resin. The reaction vessel was then placed under microwave irradiation (50 W, ramp to 50° C over 5 min, then hold at 50 °C for

15 min). The resin was filtered off and washed with anhydrous THF (3 x 3 mL) and the coupling was repeated once. The resin was filtered off before and washed thoroughly with DMF (6 x 3 mL).
The same deprotection/coupling cycles were performed until 8-mer **O-D-O-L-D-O-D-O-Wang**. This sequence is common for the SPFS of all the oligomers. The resin was then divided into several batches to prepare foldamers **1**-**7**.
General procedure for resin cleavage and side chain deprotection: The resin-bound foldamer was washed with DMF (3 x 3 mL), DCM (3 x 3 mL) before to be dried under desiccator. The resin was then suspended in a solution of TFA/TIS/H_2O (95:2.5:2.5, v/v/v, 4-5 ml) and next was shaken for 2 h at room temperature. The resin was then filtered off and washed once with the TFA solution. The combined filtrate was evaporated under reduced pressure. The resulting oily solid was precipitated with cold Et_2O, triturated, washed with Et_2O, centrifuged and lyophilized to obtain the crude foldamer.

Compound 1: Foldamer **1** was purified by RP-HPLC semi-preparative chromatography using a linear gradient from 5% B to 40% B in 20 min (C_{18} column; A: H_2O + 0.1% TFA and B: CH_3CN + 0.1% TFA; HPLC purity >99%). **^{1}H NMR** (700 MHz, DMSO-d_6): **amide NHs** δ 10.90 (s, 1H), 10.84 (s, 1H), 10.74 (s, 2H), 10.27 (d, *J* = 17.8 Hz, 2H), 10.14 (d, *J* = 15.6 Hz, 2H), 10.05 (s, 1H), 9.82 – 9.77 (m, 5H); **aromatic CHs** δ 8.20 (s), 7.95 (t, *J* = 7.1 Hz), 7.82 (d, *J* = 6.8 Hz), 7.62 – 7.46 (m), 7.45 – 7.31 (m), 7.29 – 7.09 (m), 7.05 (t, *J* = 6.9 Hz), 7.02 – 6.89 (m), 6.85 (d, *J* = 6.5 Hz), 6.81 – 6.78 (m), 6.75 (d, *J* = 6.5 Hz), 6.71 (s), 6.67 (s), 6.56 (s), 6.44 (s), 6.34 (s), 6.28 (s), 6.23 (s), 6.18 (d, *J* = 5.8 Hz), 5.88 (s), 5.66 (s), 5.54 (d, *J* = 13.9 Hz), 5.41 (s); **aliphatic CHs** δ 4.47 – 3.73 (m), 3.05 – 2.96 (m), 2.32 – 1.96 (m), 1.91 (s), 1.65 – 1.47 (m), 1.31 – 1.19 (m), 1.15 (d, *J* = 6.6 Hz). **HRMS** (ESI$^+$) m/z calcd. (most abundant mass peak) for $C_{194}H_{181}N_{38}O_{37}$: 726.8684 $(M+5H)^{5+}$; found: 726.9652.

Compound 2: Foldamer **2** was purified by RP-HPLC semi-preparative chromatography using a linear gradient from 5% B to 40% B in 20 min (C_{18} column; A: H_2O + 0.1% TFA and B: CH_3CN + 0.1% TFA; HPLC purity >99%). **^{1}H NMR** (700 MHz, DMSO-d_6): **amide NHs** δ 10.89 (s, 1H), 10.83 (d, *J* = 17.8 Hz, 2H), 10.74 (s, 1H), 10.31 (d, *J* = 12.4 Hz, 2H), 10.27 (s, 1H), 10.10 (s, 1H), 10.06 (s, 1H), 9.92 (d, *J* = 14.4 Hz, 2H), 9.88 (s, 1H), 9.85 (s, 1H); **aromatic CHs** δ 8.30 (s), 7.96 (d, *J* = 7.0 Hz), 7.82 (d, *J* = 6.9 Hz), 7.63 – 7.43 (m), 7.41 – 7.33 (m), 7.29 – 7.20 (m), 7.20 (d, *J* = 7.5 Hz), 7.18 – 7.13 (m), 7.12 (dd, *J* = 13.3, 6.0 Hz), 7.05 (dt, *J* = 17.9, 8.7 Hz), 7.03 – 6.94 (m), 6.94 – 6.85 (m), 6.81 (d, *J* = 6.5 Hz), 6.75 (t, *J* = 6.1 Hz), 6.70 (s), 6.57 (s), 6.45 (s), 6.36 (d, *J* = 9.5 Hz), 6.18 (d, *J* = 6.1 Hz), 5.89 (s), 5.65 – 5.57 (m), 5.56 (s); **aliphatic CHs** δ 4.24 – 3.80 (m), 3.26 – 3.13 (m), 3.09 – 2.90 (m), 2.36 – 2.11 (m), 2.09 – 2.0 (m), 1.30 – 1.20 (m). **HRMS** (ESI$^+$) m/z calcd. (most abundant mass peaks) for $C_{181}H_{168}N_{35}O_{35}$: 678.4490 $(M+5H)^{5+}$; for $C_{181}H_{167}N_{35}O_{35}$: 848.0602 $(M+4H)^{4+}$; for $C_{181}H_{166}N_{35}O_{35}$: 1130.0768 $(M+3H)^{3+}$; found: 678.7491; 848.4468; 1130.2835.

Compound 3: Foldamer **3** was purified by RP-HPLC semi-preparative chromatography using a linear gradient from 5% B to 40% B in 20 min (C_{18} column; A: H_2O + 0.1% TFA and B: CH_3CN + 0.1% TFA; HPLC purity >99%). **^{1}H NMR** (700 MHz, DMSO-d_6): **amide NHs** δ 10.93 (s, 1H), 10.84 (s, 1H), 10.75 (s, 2H), 10.33 (s, 1H), 10.13 (s, 4H), 9.95 (s, 1H), 9.93 (s, 1H), 9.87 (s, 1H), 9.82 (s, 1H); **aromatic CHs** δ 8.21 (s), 7.97 (s), 7.82 – 7.79 (m), 7.60 – 6.65 (m), 6.44 (s), 6.39 (s), 6.33 (s), 6.23 – 6.16 (m, 5H), 5.91 (s), 5.76 (s), 5.65 (d, *J* = 17.3 Hz), 5.45 (s); **aliphatic CHs** δ 4.35 – 3.94 (m), 3.11 – 2.90 (m), 2.37 – 1.94 (m), 1.31 – 1.19 (m). **HRMS** (ESI$^+$) m/z calcd. (most abundant mass peaks) for $C_{181}H_{168}N_{35}O_{35}$: 678.4490 $(M+5H)^{5+}$; for $C_{181}H_{167}N_{35}O_{35}$: 847.8090 $(M+4H)^{4+}$; for $C_{181}H_{166}N_{35}O_{35}$: 1130.0768 $(M+3H)^{3+}$; found: 678.5468; 847.9452; 1130.2755.

Compound 4: Foldamer **4** was purified by RP-HPLC semi-preparative chromatography using a linear gradient from 5% B to 40% B in 20 min (C_{18} column; A: H_2O + 0.1% TFA and B: CH_3CN + 0.1% TFA; HPLC purity

>99%). **^{1}H NMR** (700 MHz, DMSO-d_6): **amide NHs** δ 10.97 (s, 1H), 10.81 (d, *J* = 13.3 Hz, 2H), 10.72 (s, 1H), 10.32 (s, 1H), 10.27 (s, 1H), 10.22 (d, *J* = 12.5 Hz, 2H), 10.12 (s, 1H), 9.95 (s, 2H), 9.91 (s, 1H), 9.87 (s, 1H); **aromatic CHs** δ 8.21 (s), 7.97 (d, *J* = 6.9 Hz), 7.82 (d, *J* = 6.9 Hz), 7.65 – 7.45 (m), 7.44 – 7.33 (m), 7.29 (t, *J* = 7.4 Hz), 7.26 – 7.19 (m), 7.14 – 7.05 (m), 7.02 – 6.88 (m), 6.80 (d, *J* = 6.4 Hz), 6.76 (s), 6.69 (d, *J* = 8.2 Hz), 6.43 (s), 6.35 (d, *J* = 14.9 Hz), 6.20 (d, *J* = 6.8 Hz), 6.15 (s), 5.92 (s), 5.78 (s), 5.67 (s), 5.59 (s), 5.49 (s); **aliphatic CHs** δ 4.35 – 3.77 (m), 3.26 – 3.16 (m), 3.09 – 2.90 (m), 2.38 – 2.21 (m), 2.19 – 2.10 (m), 2.07 – 1.97 (m), 1.28 (t, *J* = 6.8 Hz, 14H), 1.25 – 1.21 (m). **HRMS** (ESI$^+$) m/z calcd. (most abundant mass peaks) for $C_{180}H_{167}N_{36}O_{35}$: 678.6480 $(M+5H)^{5+}$; for $C_{180}H_{166}N_{36}O_{35}$: 848.0582 $(M+4H)^{4+}$; for $C_{180}H_{165}N_{36}O_{35}$: 1130.4085 $(M+3H)^{3+}$; found: 678.7487; 847.9458; 1130.6132.

2.2. Manual microwave-assisted SPFS of foldamers 5-7

The SPFS of oligomers **5**-**7** was performed as described before.[10a] The only difference was the introduction of a capping step after each quinoline monomer coupling. Resin-bound foldamer (35 mg, 0.0143 mmol) was suspended in anhydrous THF (1 mL), to which was added DIEA (30 µL, 0.1722 mmol, 12.0 equiv.) followed by Ac-Cl (6 µL, 0.0861 mmol, 6.0 equiv.). The resin was shaken at r.t. for 5 min, washed with anhydrous THF (3 x 3 mL), and the capping step was repeated twice. The resin was then washed thoroughly with THF (6 x 3 mL) and DMF (6 x 3 mL).

Compound 5: Foldamer **5** was purified by RP-HPLC semi-preparative chromatography using a linear gradient from 20% B to 40% B in 35 min (C_{18} column; A: H_2O + 0.1% TFA and B: CH_3CN + 0.1% TFA; HPLC purity >99%). **^{1}H NMR** (700 MHz, DMSO-d_6): **amide NHs** δ 10.64 (s, 1H), 10.61 (s, 1H), 10.53 (s, 2H), 10.08 (s, 1H), 10.04 (s, 1H), 9.95 (s, 1H), 9.88 (s, 1H), 9.78 (s, 1H), 9.70 (s, 1H), 9.51 – 9.46 (m, 4H), 9.42 (s, 1H), 9.37 (s, 1H), 9.34 – 9.07 (m, 15H); **aromatic CHs** δ 8.01 (s), 7.78 (d, *J* = 6.3 Hz), 7.65 (d, *J* = 6.4 Hz), 7.44 – 7.26 (m), 7.23 – 7.19 (m), 7.17 – 7.12 (m), 7.13 – 7.04 (m), 7.06 – 6.98 (m), 6.98 – 6.88 (m), 6.83 (t, *J* = 6.9 Hz), 6.79 (t, *J* = 6.3 Hz), 6.77 – 6.70 (m), 6.67 (m, *J* = 4.8 Hz), 6.61 – 6.45 (m), 6.42 – 6.29 (m), 6.23 (s), 6.07 (s), 5.96 (d, *J* = 6.9 Hz), 5.83 (d, *J* = 12.6 H), 5.79 (s), 5.74 (s), 5.71 (s), 5.67 (s), 5.49 (s), 5.47 (s), 5.40 (s), 5.33 (s), 5.30 (s), 5.26 (s), 5.24 – 5.20 (m), 5.17 (s), 5.16 – 5.11 (m), 5.09 (d, *J* = 7.1 Hz); **aliphatic CHs** δ 4.13 – 3.31 (m), 2.18 – 1.88 (m, 1H), 1.60 – 1.55 (m), 1.50 – 1.46 (m), 1.34 (d, *J* = 4.5 Hz), 1.19 – 1.14 (m), 1.09 (q), 1.00 – 0.89 (m, 31H). **HRMS** (ESI$^+$) m/z calcd. (most abundant mass peaks) for $C_{413}H_{379}N_{79}O_{77}$: 959.9783 $(M+8H)^{8+}$; for $C_{413}H_{378}N_{79}O_{77}$: 1096.9741 $(M+7H)^{7+}$; found: 959.9868; 1096.9943.

Compound 6: Foldamer **6** was purified by RP-HPLC semi-preparative chromatography using a linear gradient from 20% B to 40% B in 35 min (C_{18} column; A: H_2O + 0.1% TFA and B: CH_3CN + 0.1% TFA; HPLC purity >99%). **^{1}H NMR** (700 MHz, DMSO-d_6): **amide NHs** δ 10.73 (s, 1H), 10.64 (d, *J* = 15.1 Hz, 3H), 10.16 (s, 1H), 10.12 (s, 1H), 10.07 (s, 1H), 10.00 (s, 1H), 9.87 (s, 1H), 9.72 (s, 1H), 9.65 (s, 1H), 9.57 (s, 3H), 9.47 – 9.42 (m, 3H), 9.38 (d, *J* = 16.3 Hz, 2H), 9.33 – 9.18 (m, 18H), 9.13 (s, 1H), 9.10 (s, 1H); **aromatic CHs** δ 8.09 (s), 7.87 (d, *J* = 6.1 Hz), 7.74 (d, *J* = 6.4 Hz), 7.58 (d, *J* = 5.8 Hz), 7.52 – 7.38 (m), 7.36 – 7.28 (m), 7.27 – 7.16 (m), 7.16 – 7.06 (m), 7.06 – 6.97 (m), 6.96 – 6.87 (m), 6.86 – 6.31 (m), 6.16 (s), 6.11 (s), 6.05 (s), 5.98 (s), 5.91 (d, *J* = 7.0 Hz), 5.86 (d, *J* = 11.7 Hz), 5.79 (d, *J* = 9.4 Hz), 5.75 (d, *J* = 3.8 Hz), 5.68 (s), 5.57 (s), 5.49 (d, *J* = 6.8 Hz), 5.39 (d, *J* = 7.5 Hz), 5.32 (s), 5.28 (s), 5.25 (d, *J* = 10.6 Hz), 5.23 – 5.15 (m), 5.11 (s); **aliphatic CHs** δ 4.10 – 3.43 (m), 2.28 – 1.97 (m), 1.68 (m), 1.61 – 1.56 (m), 1.53 – 1.47 (m), 1.29 – 1.24 (m), 1.20 – 1.15 (m), 1.13 – 1.08 (m), 1.07 – 0.93 (m). **HRMS** (ESI$^+$) m/z calcd. (most abundant mass peaks) for $C_{516}H_{471}N_{98}O_{96}$: 1064.3901 $(M+9H)^{9+}$; for $C_{516}H_{470}N_{98}O_{96}$: 1197.3129 $(M+8H)^{8+}$; found: 1064.3789; 1197.3117.

Compound 7: Foldamer **7** was purified by RP-HPLC semi-preparative chromatography using a linear gradient from 20% B to 40% B in 35 min (C_{18} column; A: H_2O + 0.1% TFA and B: CH_3CN + 0.1% TFA; HPLC purity >99%). **^{1}H NMR** (700 MHz, DMSO-d_6): **amide NHs** δ 10.72 (s, 1H), 10.67 (s, 1H), 10.63 (d, *J* = 9.1 Hz, 2H), 10.15 (s, 1H), 10.11 (s, 1H), 9.96 (d, *J* = 11.6 Hz, 2H), 9.86 (s, 1H), 9.74 (s, 1H), 9.58 – 9.52 (m, 4H), 9.49 (s, 1H), 9.45 (s, 1H), 9.41 (s, 1H), 9.36 (d, *J* = 13.2 Hz, 3H), 9.31 – 9.16 (m, 18H), 9.12 (s, 1H), 9.09 (s, 1H); **aromatic CHs** δ 8.07 (s), 7.86 (d, *J* = 6.3 Hz), 7.73 (d, *J* = 6.3 Hz), 7.61 (d, *J* = 5.8 Hz), 7.55 – 7.35 (m), 7.34 – 7.26 (m), 7.23 (t, *J* = 8.2 Hz), 7.19 – 6.95 (m), 6.93 – 6.72 (m), 6.70 – 6.56 (m), 6.54 – 6.30 (m), 6.21 (s), 6.15 (s), 6.04 (s), 6.01 (s), 5.95 (s), 5.89 (d, *J* = 6.9 Hz), 5.85 (d, *J* = 14.3 Hz), 5.80 – 5.75 (m), 5.73 (s), 5.60 (s), 5.56 (s), 5.48 (s), 5.38 (s), 5.31 (s), 5.27 (s), 5.25 (s), 5.23 (s), 5.21 – 5.14 (m), 5.10 (s); **aliphatic CHs** δ 4.17 (s), 4.12 (s), 4.0 – 3.75 (m, 1H), 3.73 – 3.42 (m), 2.25 – 1.95 (m), 1.69 – 1.65 (m), 1.59 – 1.55 (m), 1.29 – 1.24 (m), 1.23 – 1.14 (m), 1.13 – 1.08 (m), 1.10 – 1.06 (m), 1.06 – 0.96 (m), 0.98 – 0.93 (m). **HRMS** (ESI$^+$) m/z calcd. (most abundant mass peaks) for $C_{529}H_{484}N_{101}O_{98}$: 1091.4013 $(M+9H)^{9+}$; for $C_{529}H_{483}N_{101}O_{98}$: 1227.7005 $(M+8H)^{8+}$; found: 1091.3884; 1227.6965.

2.3. Automation of the SPFS of foldamers 8-9

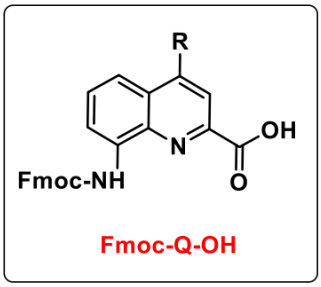

Construction of the library of Fmoc-Q-OH

In order to automate the SPFS of aromatic oligoamides on Chorus PurePep synthesizer, the first step was to build a library of aromatic monomers and to assign them a specific and unique location of amino acid bottle line. To do so an excel file was generated and each aromatic building block was named in a similar manner to the one or three letters code used for α-amino acid residues (Figure S1).

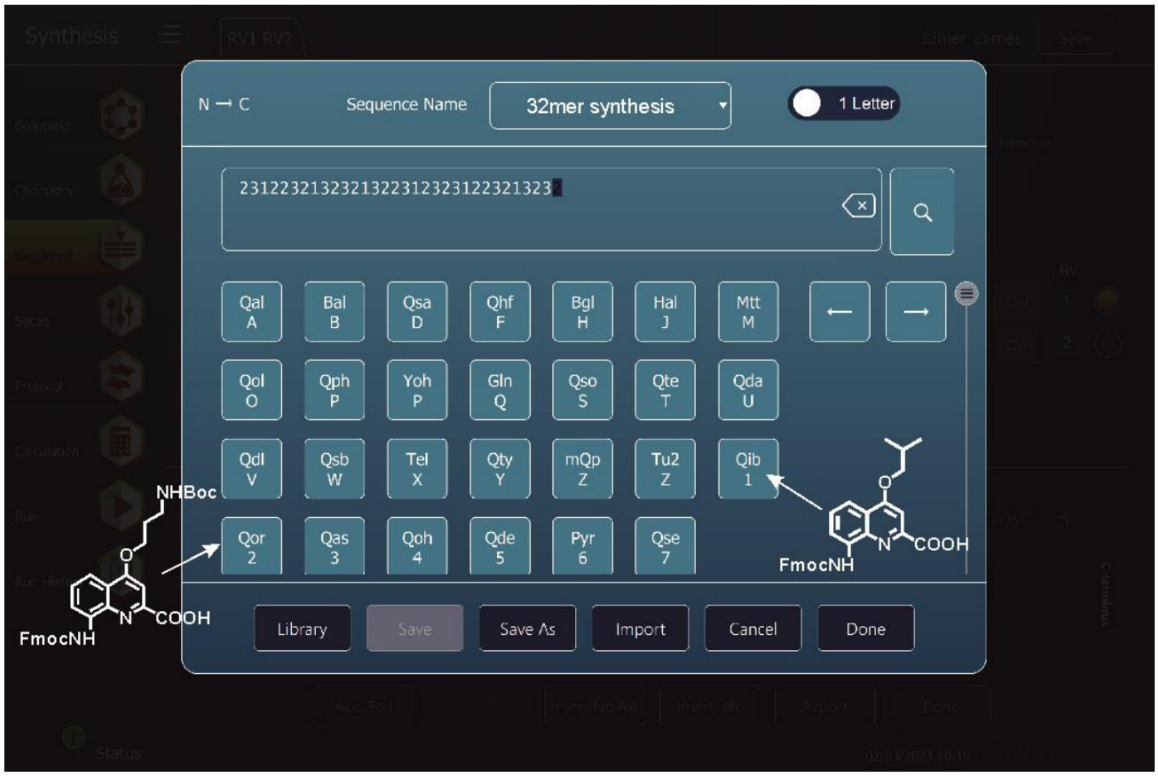

Figure S1. Illustration of the sequence building and the library of aromatic monomers with their one and three letter code, respectively.

2.4. Setting up the Chorus PurePep ® synthesizer for SPFS

Solvent lines and solvent distribution

Each bottle is always filled-up with the same solvent or reagent solution so that there will never be any contamination.
The two first solvent lines are meant for top and timed delivery. Peptide grade DMF was assigned in position 1 because it is the most used solvent for resin and system washings.
Anhydrous THF is in solvent line 2, 2% DBU in NMP in solvent 3 and when capping is required the line 4 is filled up with AC_2O in DCM (50/50, v/v).
For metered delivery, we use the solvent lines 5-7. Solvent line 5 for PPh_3 in anhydrous THF, line 6 TCAN in anhydrous THF and line 7 for 2,4,6-collidine in anhydrous THF.
If solvent line 1 and 2 deliver the solvent from the top of the RV, all the remaining lines perform solution dispensing from the bottom of the RV. The set-up of solvent is recapitulated in following table S1.

Table S1. Description of solvent set-up for SPFS

Solvent line	Solvent
1	DMF
2	Anhydrous THF
3	2% DBU in NMP
4	Ac_2O in DCM (50:50, v/v)
5	PPh_3 in anhydrous THF
6	TCAN in anhydrous THF
7	Collidine in anhydrous THF
8	DCM

The implementation of the coupling protocol for quinoline-type monomers on solid support follows the same series of steps for protocols earlier developed by Protein Technologies for SPPS. In other words, a coupling cycle in SPFS is composed of three main tasks: Deprotection, washings and coupling. A cycle begins always with the Fmoc-deprotection and ends with resin washings.

In the context of aromatic oligoamides, the deprotection is performed twice for 10 min with 2% DBU in NMP (step 1 in table S2). At the contrary to what has been reported for Fmoc deprotection in peptide chemistry, we have never observed any difficulty in removing the Fmoc protecting group on quinoline monomers. This deprotection step has not yet been optimized. However, because we favour high purity of the crude material with respect of synthesis time, we have not yet spent efforts in optimizing this specific step. If performed, it will be reported in due course.

Once the deprotection steps are completed, the resin is filtered off and washed (see steps 2 and 3 in table S2). The extensive washings with THF are meant for preparing the resin to the coupling in anhydrous THF. For the same reason although empty, the PV is rinsed twice with anhydrous THF (see line 4, PV box crossed) for pre-conditioning before the in situ activation process in this vessel.

Next, start the coupling phase. At first, like performed manually, the solution of collidine in anhydrous THF is added to the RV. The solution of aromatic monomer is then delivered to the PV and subsequently, PPh_3 solution in THF and at last TCAN solution in THF (steps 6-8 in table S2). The PV is then shaken for one minute and N_2 bubbling is performed for Fmoc-Q-Cl solution homogenisation. Because, we performed the acid chloride activation in pure THF, an eye-visible precipitate forms spontaneously upon TCAN addition. This precipitate has been characterized and does correspond to the phosphonium salt: Cl^-,$^+PPh_3$-CH_2CN. It is washed away at the end of the cycle by rinsing the PV with DMF (see step 25 in table S2).

After one minute of activation, the freshly made acid chloride solution is transferred to the RV by using the "*PV to RV operation*" (row 9 in table S2).

The coupling then takes place in the RV by heating it at 50 °C for 15 min. The monitoring of the temperature shows a fast ramping time and a stable target temperature over the course of the coupling step. At the end of the coupling cycle, the resin is filtered off and the steps 3 to 11 are repeated once.

Final washings of the RV and PV with DMF allow the resin to be placed in the conditions of the next cycle.

If a capping step is required, it is performed after the coupling steps (see steps 22 and 23 in table S2).

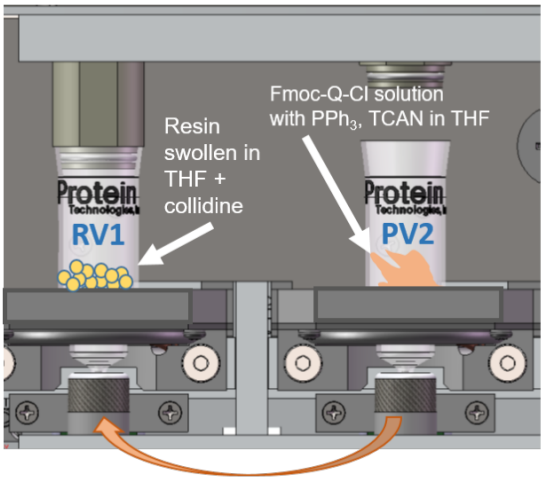

Figure S2. Cartoon illustrating the formation of the Fmoc-Q-Cl in the pre-activation vessel (PV) followed by the step called PV to RV.

Table S2. General protocol developed for SPFS automation on Chorus PurePep ® synthesizer

Step	operation	Solvent	Vol(mL)	Mix Time(HH:MM:SS)	Drain	PV	Reps	N_2	Shake/ RPM	Heat (depro*)
1	Bottom Delivery	DBU/NMP	3.00	00:10:00	✓		2	✓	250	
2	Top Delivery	DMF	3.00	00:00:15	✓		1	✓		
3	Top Delivery	THF	3.00	00:00:20	✓		3	✓		
4	Top Delivery	THF	2.00	00:00:10	✓		2	✓		
5	Bottom Delivery	Coll	0.50	00:00:01			1			
6	AA Building Block	None	1.00	00:00:01		✓	1	✓		
7	Bottom Delivery	PPh_3	1.00	00:00:01		✓	1	✓		
8	Bottom Delivery	TCAN	0.50	00:01:00		✓	1	✓	150	
9	PV to RV	None					1			
10	Mix	None		00:15:00	✓		1		250	✓ 50°C
11	Drain	None					1			
Repeat steps 3 to 11 one time										
21	Top Delivery	DMF	3.00	00:00:15	✓		3	✓		
22	Bottom Delivery	DCM	3.00	00:00:10	✓		3	✓		
23	Bottom Delivery	Ac_2O	3.00	00:00:10	✓		1	✓		✓ 40°C
24	Top Delivery	DMF	3.00	00:00:15	✓		3	✓		
25	Top Delivery	DMF	2.00	00:00:10	✓		2	✓		

*When a capping step is included in the protocol to heat it at a different temperature to the coupling one, the deprotection box is selected, thus offering the possibility to apply two different temperatures per coupling cycle. The steps 22 & 23 were introduced after the 8th coupling; i.e. the eight first coupling cycles were done with no capping.

Figure S3. Views of the protocol sub-window where the protocol for a given cycle is selected and the target temperatures for coupling and capping are saved.

2.5. Synthesis of Ylide 10 in solution

Fmoc-L-Cl: In a 25 mL flask, Fmoc-L-OH (24.2 mg, 0.05 mmol, 1.0 equiv) was suspended in 2 mL of dry DCM. Oxalyl chloride (5 μL, 0.06 mmol, 1.2 equiv.) was then added. The reaction mixture instantly became homogenous and turned yellow. After 1 h, solvent and excess of oxalyl chloride were removed under high vacuum.

Ylide 10: In a NMR tube (5 mm diameter), freshly formed Fmoc-L-Cl was dissolved in 0.5 mL of $CDCl_3$, previously passed through activated alumina. Commercially available (Cyanomethylene)-triphenylphosphorane **11** (15.1 mg, 0.05 mmol, 1 equiv.) was then added to the reaction mixture. After 15 min, a ^{31}P NMR spectrum of the mixture was recorded at 298 K and showed the formation of ylide **10** (see Figure S20d).

2.6. Regeneration of Fmoc-L-OH from 10

In a 10 mL flask, **10** (38.5 mg, 0.05 mmol, 1.0 equiv.) was dissolved in a mixture of 2 mL 1:1 DMF/H_2O. N-chlorosuccinimide (NCS) (67.5 mg, 0.25 mmol, 5 equiv.) was then added. The reaction was then monitored by RP-HPLC until complete disappearance of the starting material (see Figure S22).

3. Characterization of foldamers

3.1. HPLC chromatograms of crude foldamers

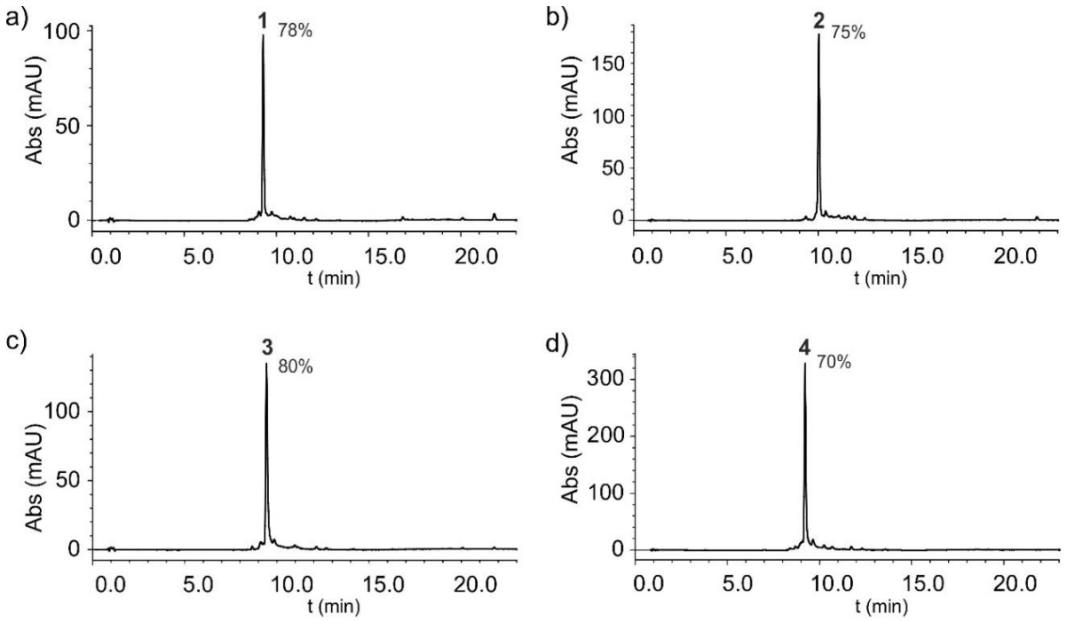

Figure S4. RP-HPLC chromatograms of crude foldamers **1** (a), **2** (b), **3** (c), and **4** (d) using a linear gradient from 5% B to 40% B in 10 min; A: H_2O + 0.1% TFA and B: CH_3CN + 0.1% TFA; UV detection at λ = 300 nm.

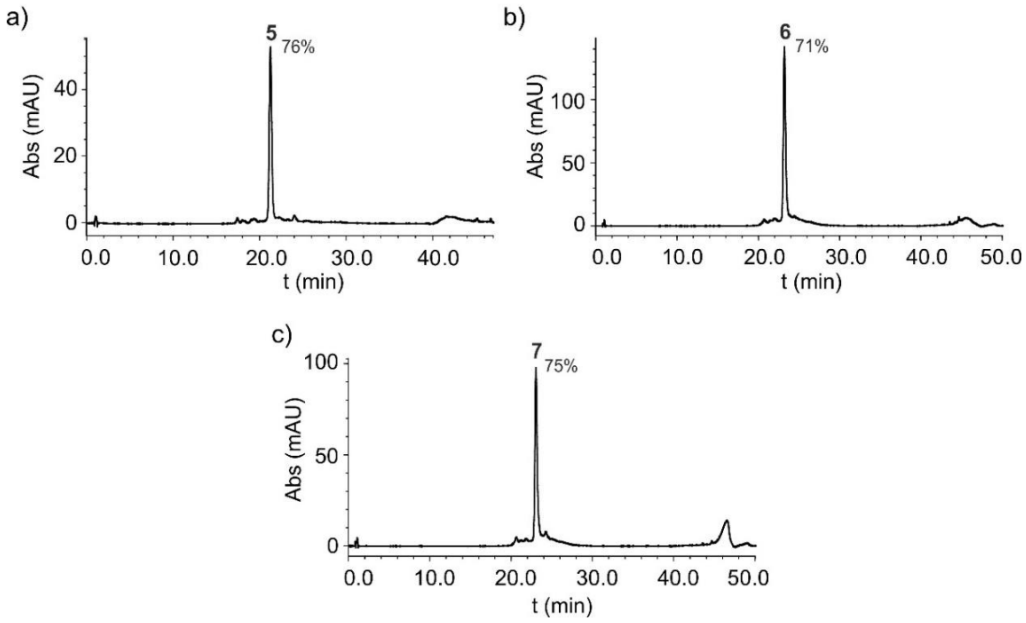

Figure S5. RP-HPLC chromatograms of crude foldamers **5** (a), **6** (b), and **7** (c) using a linear gradient from 20% B to 40% B in 35 min; A: H_2O + 0.1% TFA and B: CH_3CN + 0.1% TFA; UV detection at λ = 300 nm.

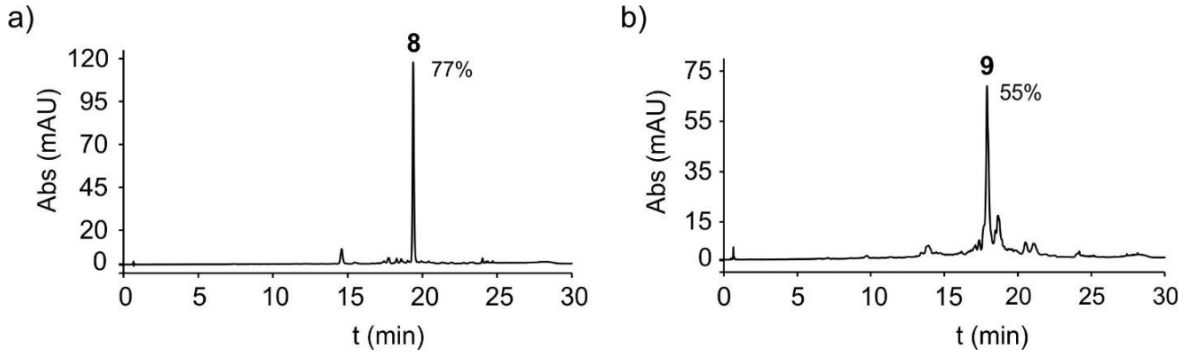

Figure S6. RP-HPLC chromatograms of crude foldamers **8** (a), and **9** (d) using a linear gradient from 20% B to 40% B in 23 min; A: H_2O + 0.1% TFA and B: CH_3CN + 0.1% TFA; UV detection at λ = 300 nm.

3.2. HPLC chromatograms of pure foldamers

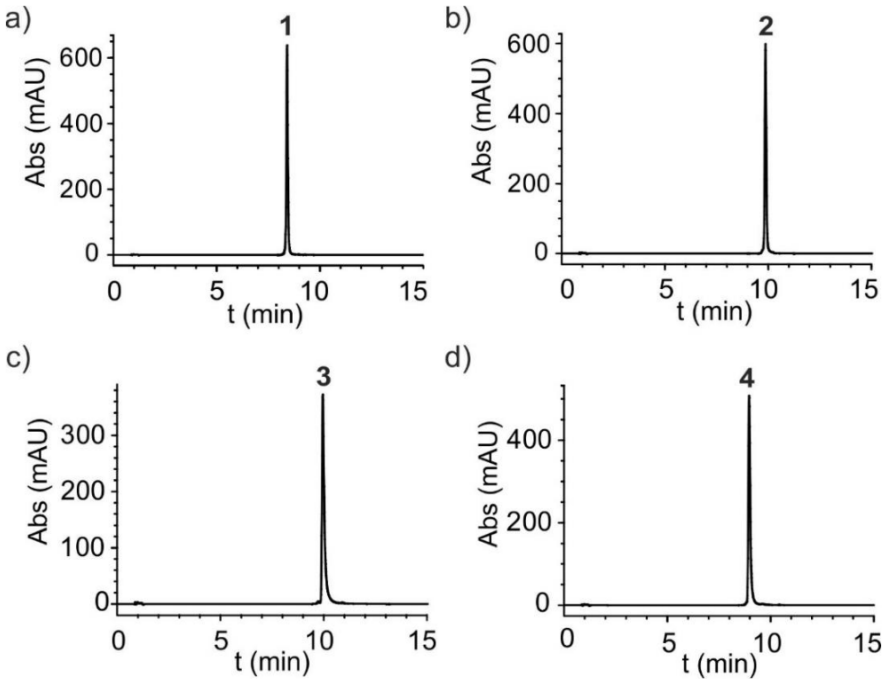

Figure S7. RP-HPLC chromatograms of pure foldamers **1** (a), **2** (b), **3** (c), and **4** (d) using a linear gradient from 5% B to 40% B in 10 min; A: H_2O + 0.1% TFA and B: CH_3CN + 0.1% TFA; UV detection at λ = 300 nm.

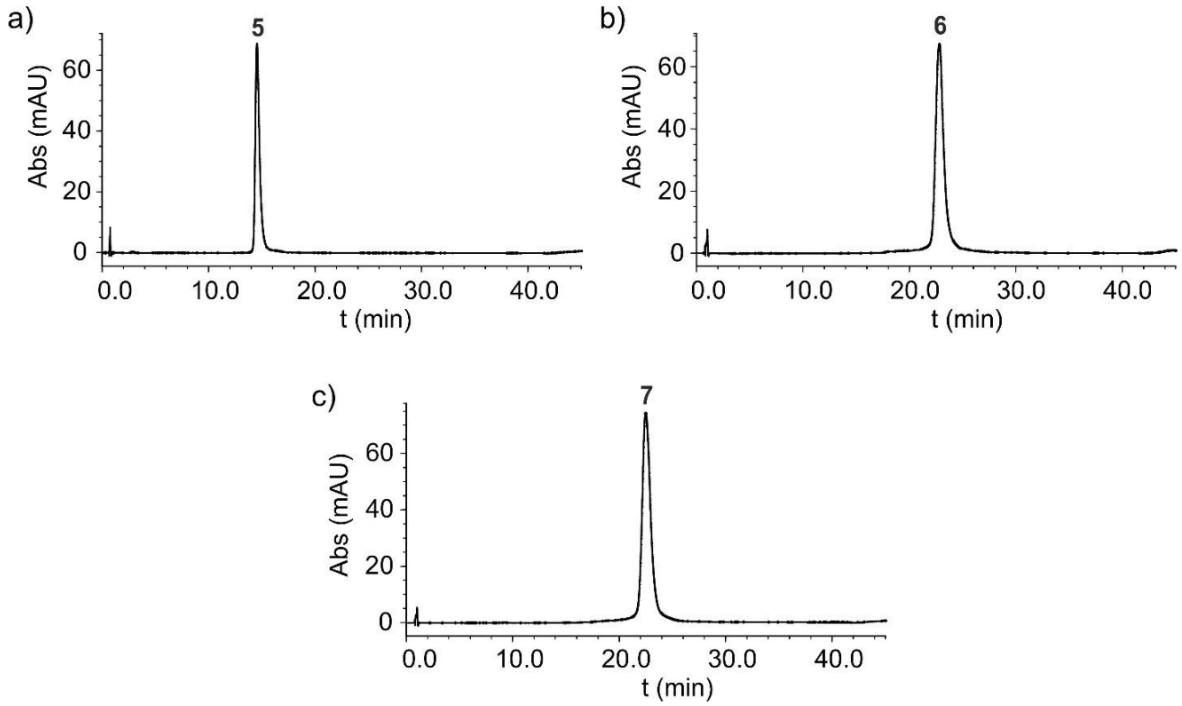

Figure S8. RP-HPLC chromatograms of pure foldamers **5** (a), **6** (b), and **7** (c) using a linear gradient from 20% B to 40% B in 35 min; A: H_2O + 0.1% TFA and B: CH_3CN + 0.1% TFA; UV detection at λ = 300 nm.

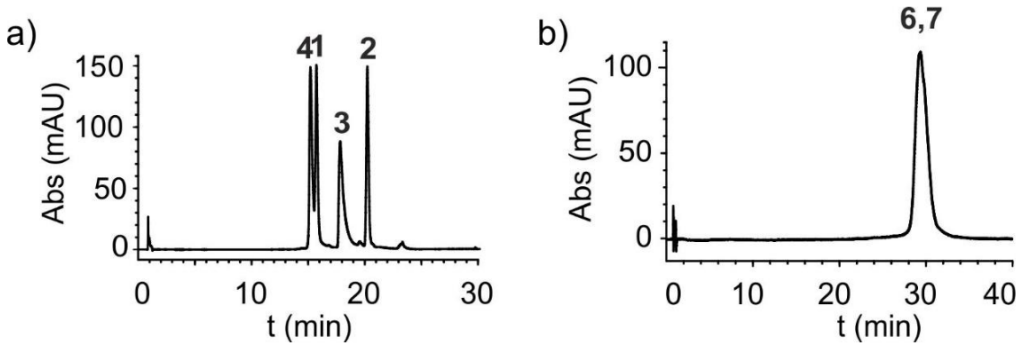

Figure S9. RP-HPLC chromatograms of the co-inJection of foldamers **1**, **2**, **3**, and **4** (a) using a linear gradient from 5% B to 20% B in 23 min; A: H_2O + 0.1% TFA and B: CH_3CN + 0.1% TFA, and foldamers **6** and **7** (b) using a linear gradient from 20% B to 40% B in 35 min; A: H_2O + 0.1% TFA and B: CH_3CN + 0.1% TFA; UV detection at λ = 300 nm.

3.3. ^{1}H NMR spectra of pure foldamers

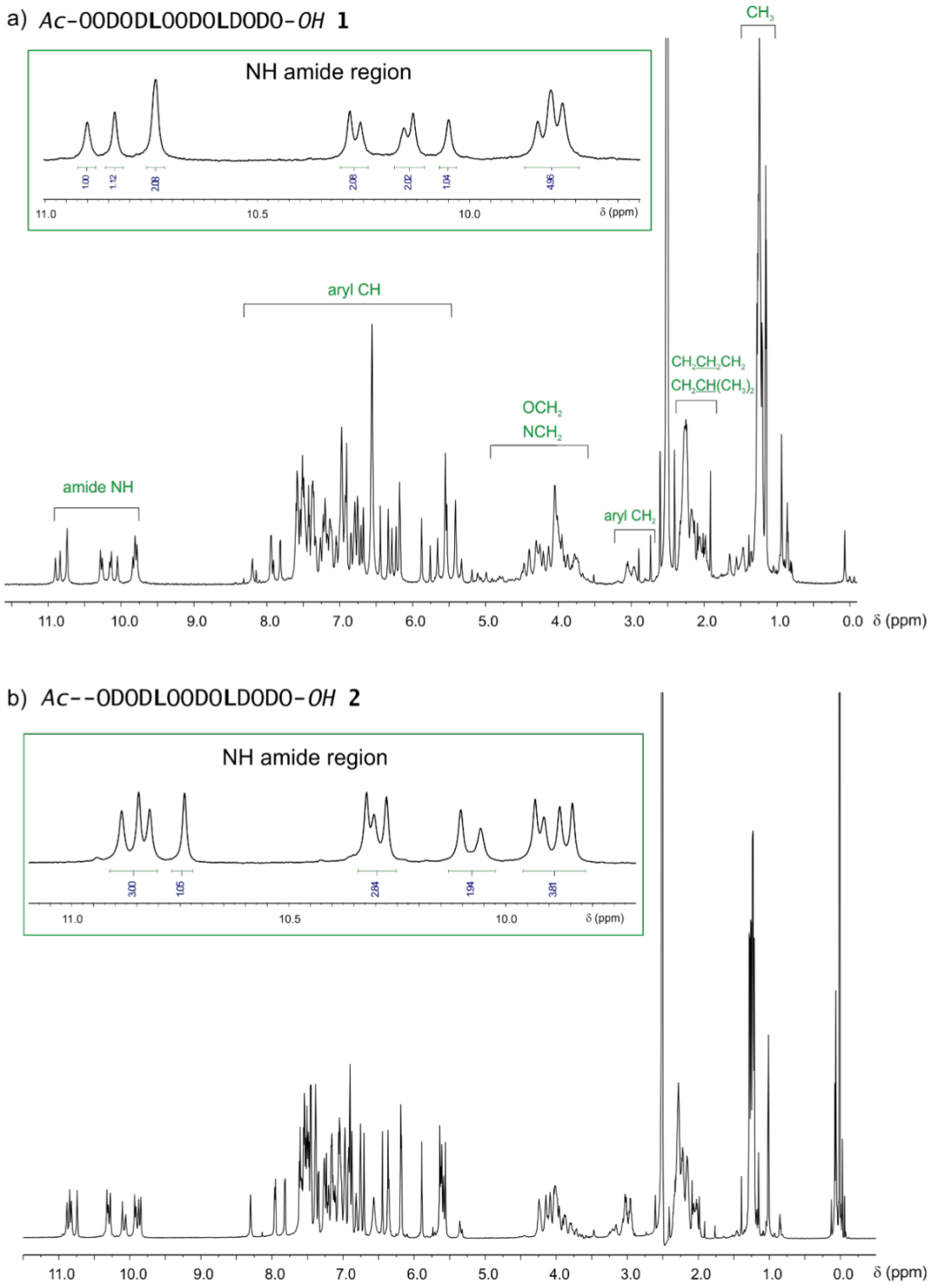

Figure S10. ^{1}H NMR spectra (700 MHz) at 333 K of foldamers **1** (a), and **2** (b), (1 mM) in DMSO-d_6.

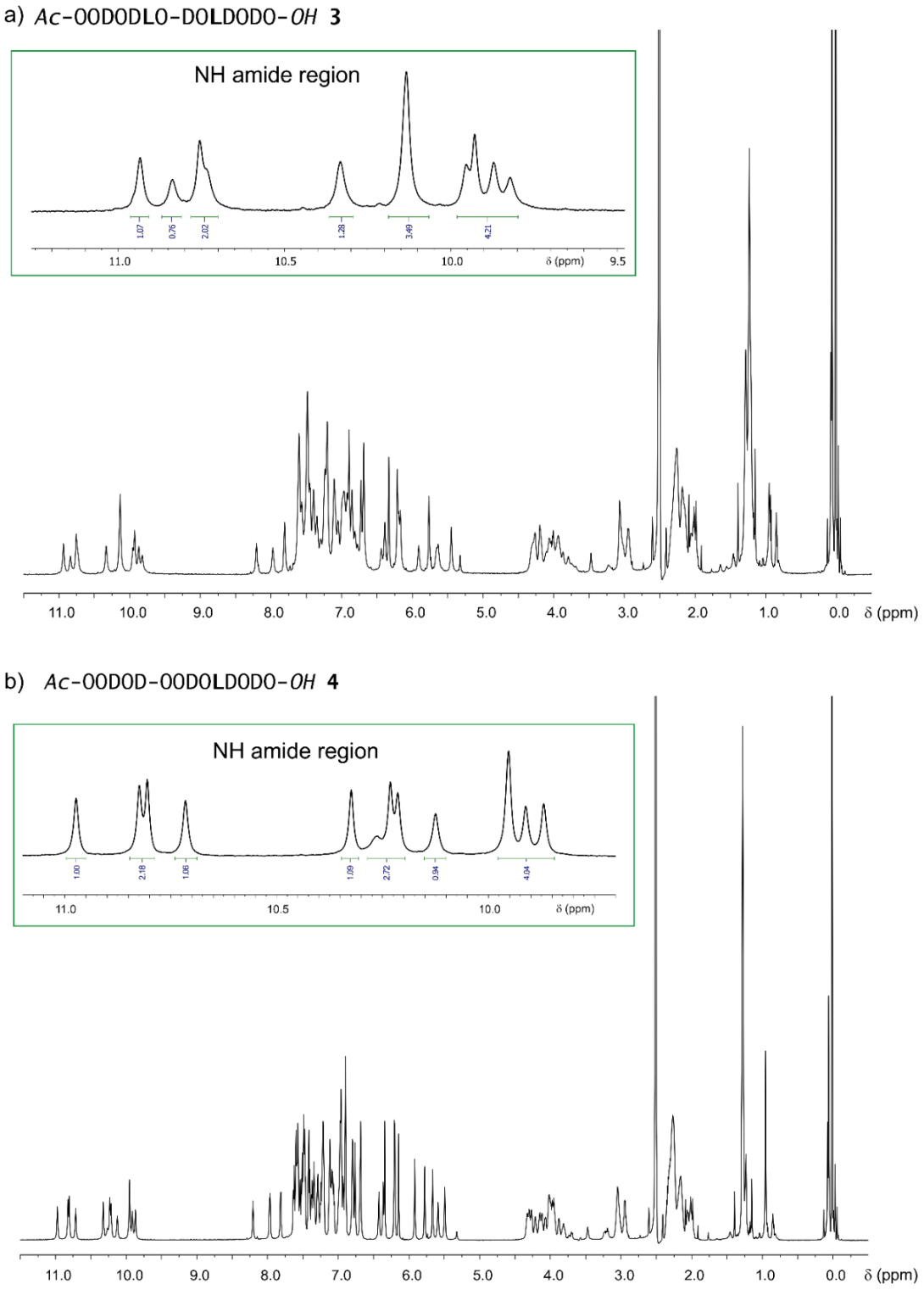

Figure S11. ^{1}H NMR spectra (700 MHz) at 333 K of foldamers **3** (a), and **4** (b), (1 mM) in DMSO-d_6.

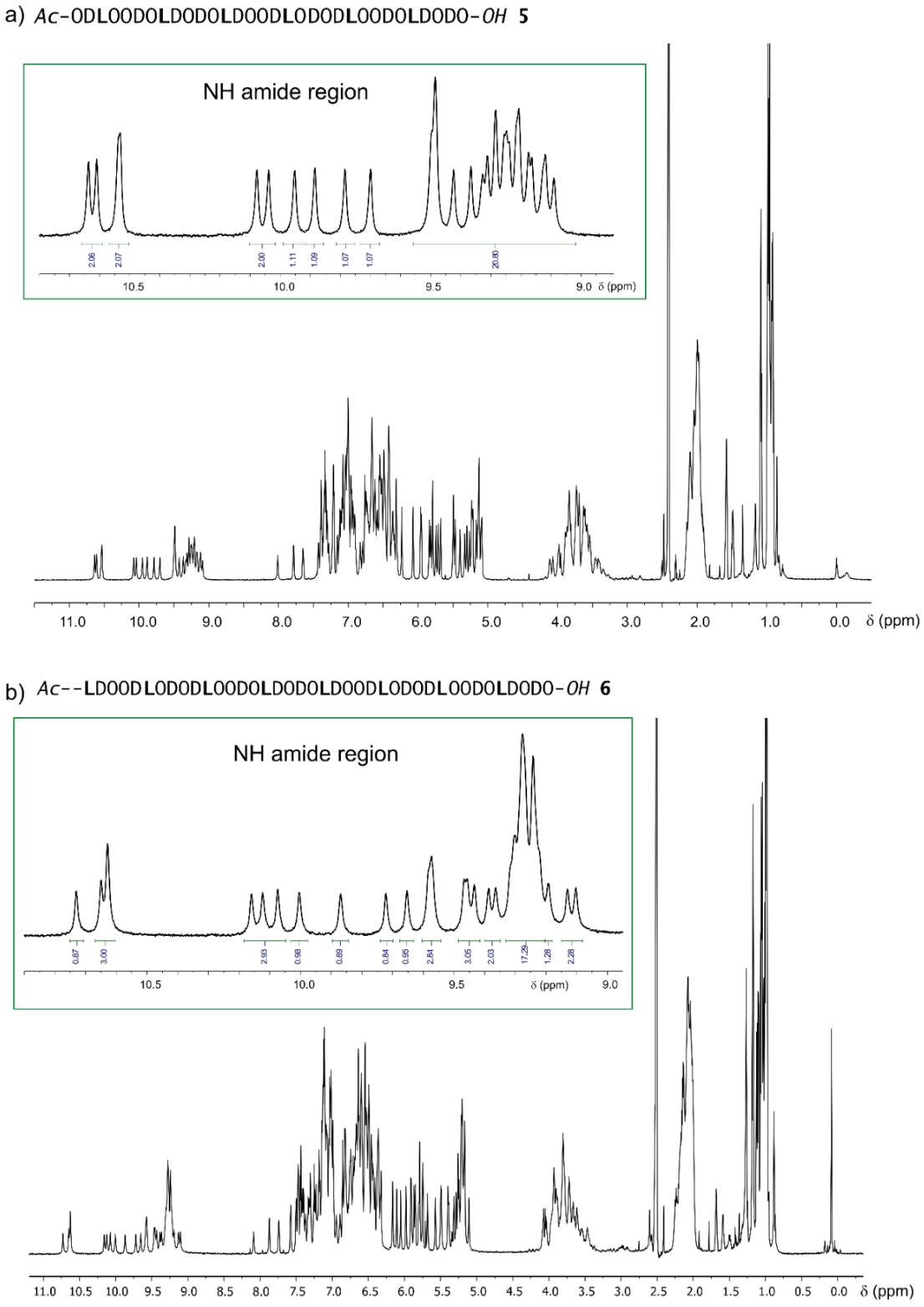

Figure S12. ^{1}H NMR spectra (700 MHz) at 333 K of oligomers **5** (a), and **6** (b), (1 mM) in DMSO-d_6.

Ac-OLDOODLODODLOODOLDODOLDOODLODODLOODOLDODO-*OH* **7**

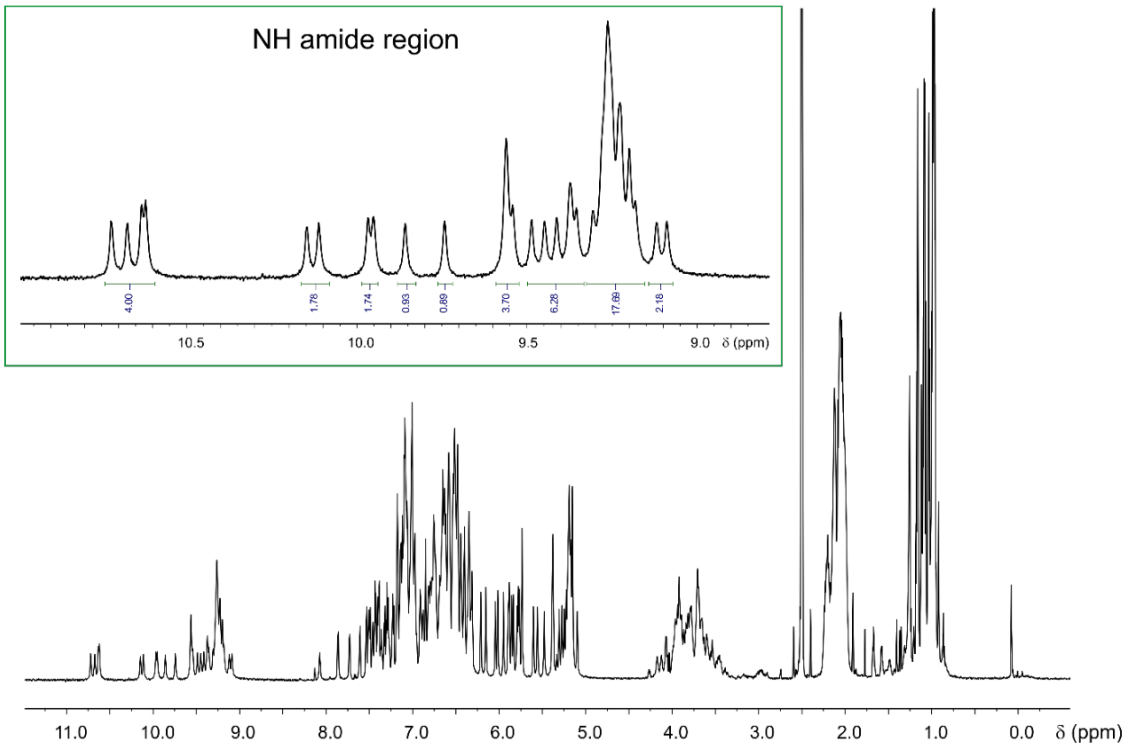

Figure S13. ^{1}H NMR spectrum (700 MHz) at 333 K of oligomer **7**, (1 mM) in DMSO-d_6.

3.4. Mass spectrometry analysis of pure foldamers

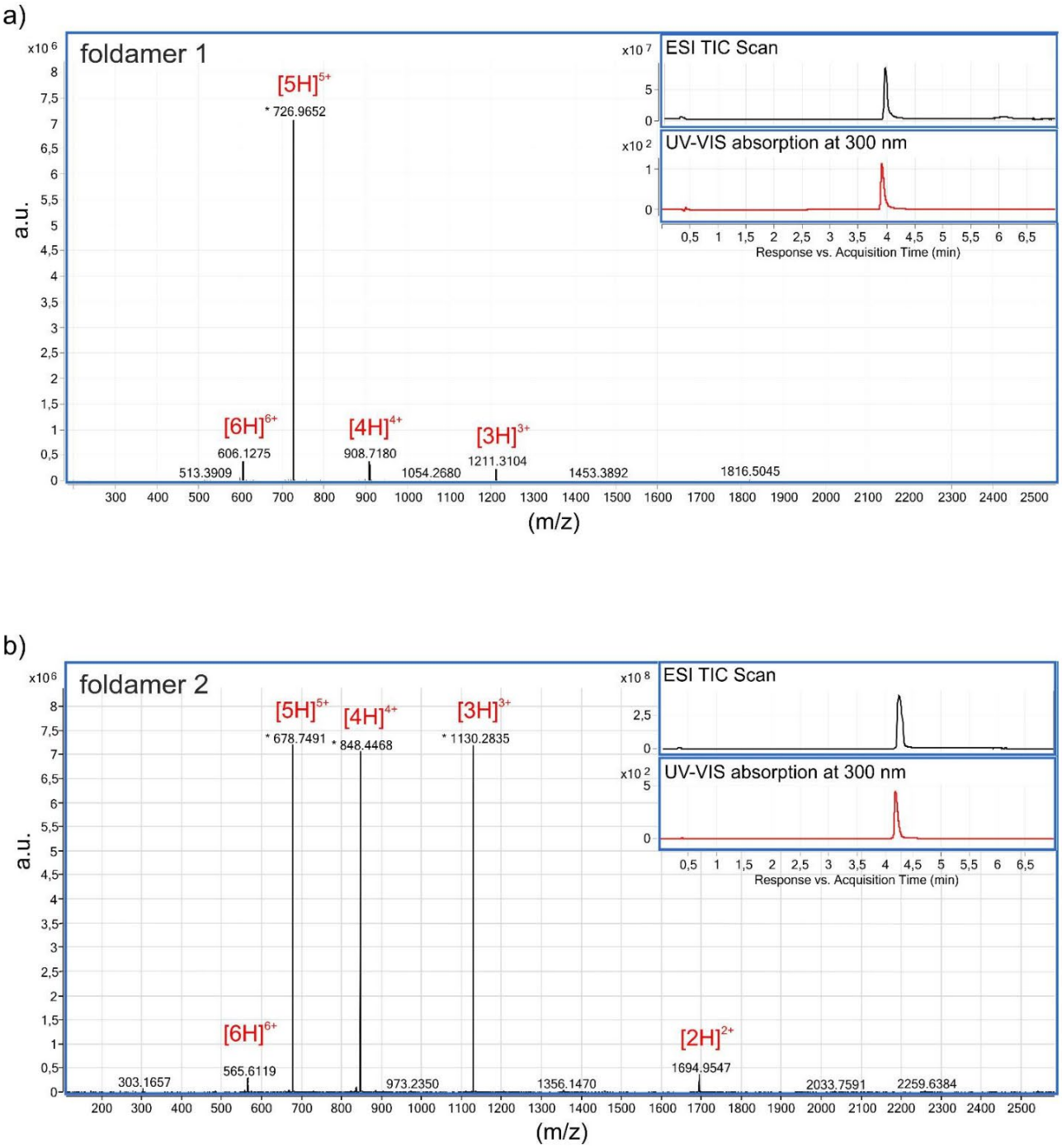

Figure S14. Multicharged species observed by LC-ESI-MS of foldamers **1** (a), and **2** (b).

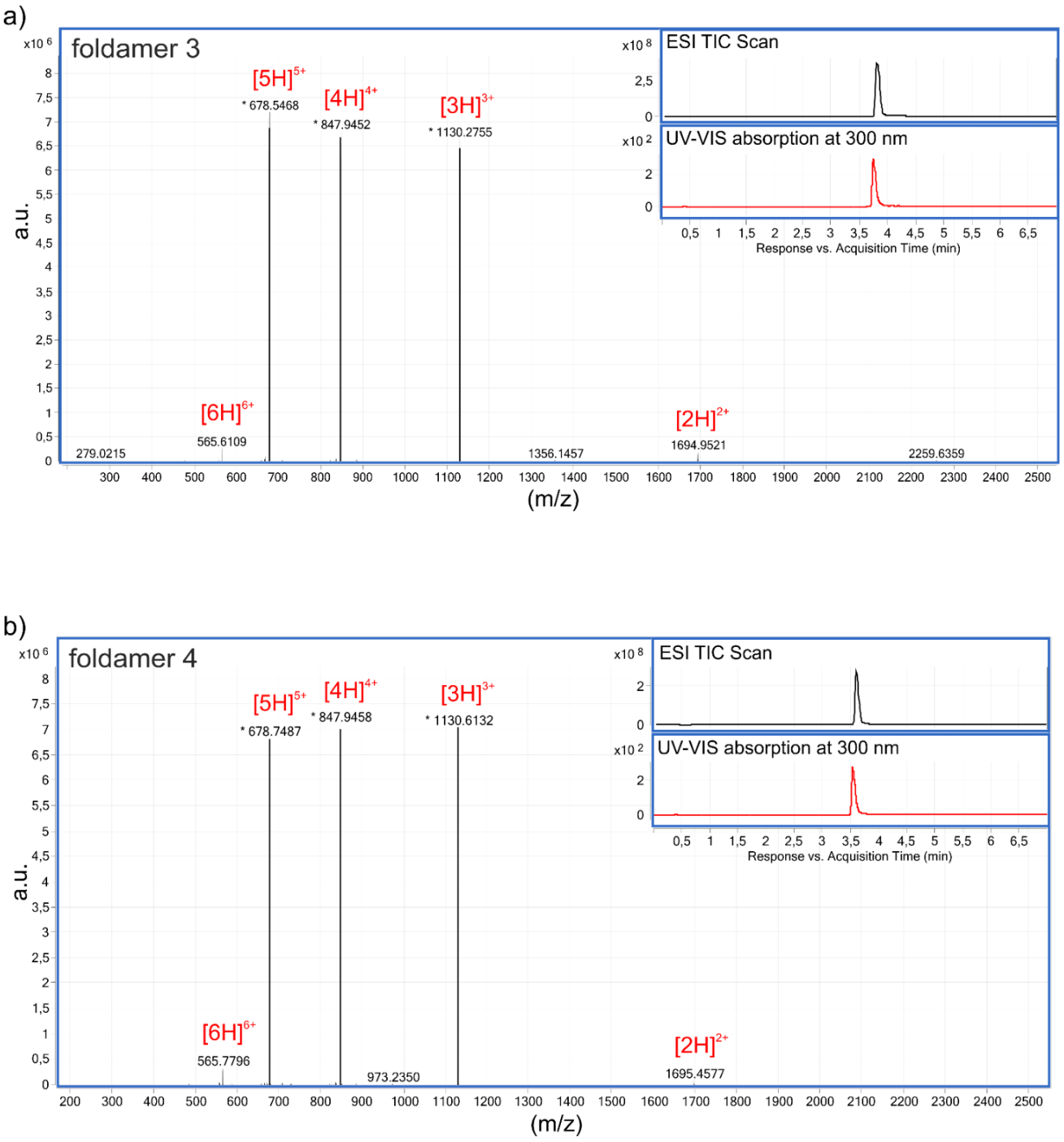

Figure S15. Multicharged species observed by LC-ESI-MS of foldamers **3** (a), and **4** (b).

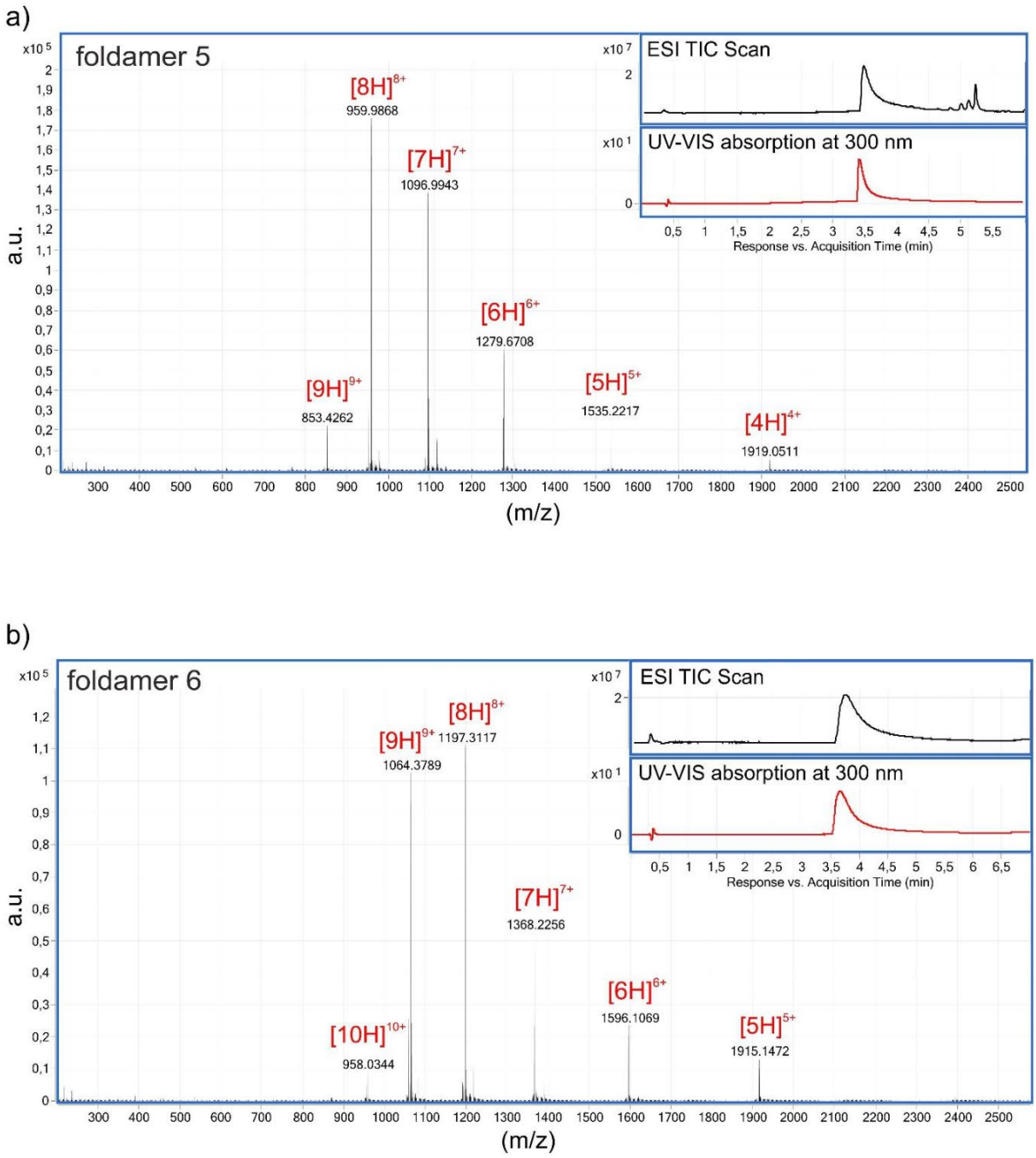

Figure S16. Multicharged species observed by LC-ESI-MS of foldamers **5** (a), and **6** (b).

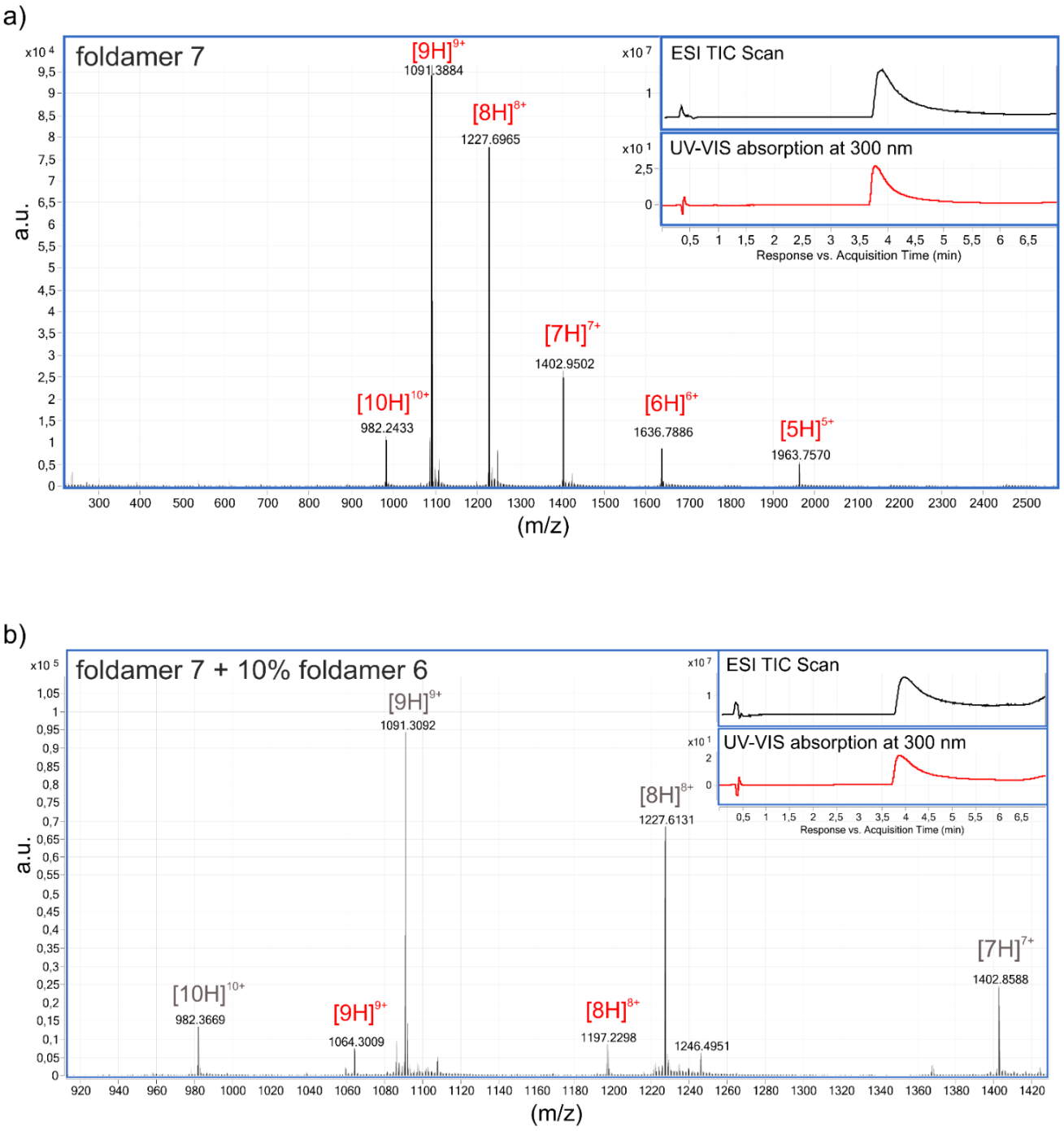

Figure S17. Multicharged species observed by LC-ESI-MS of foldamer **7** (a), and a mixture of **6** (10%) and **7** (b). Red and grey multicharged species correspond to foldamers **6** and **7**, respectively.

3.5. Mass spectrometry analysis of crude foldamers 8-9

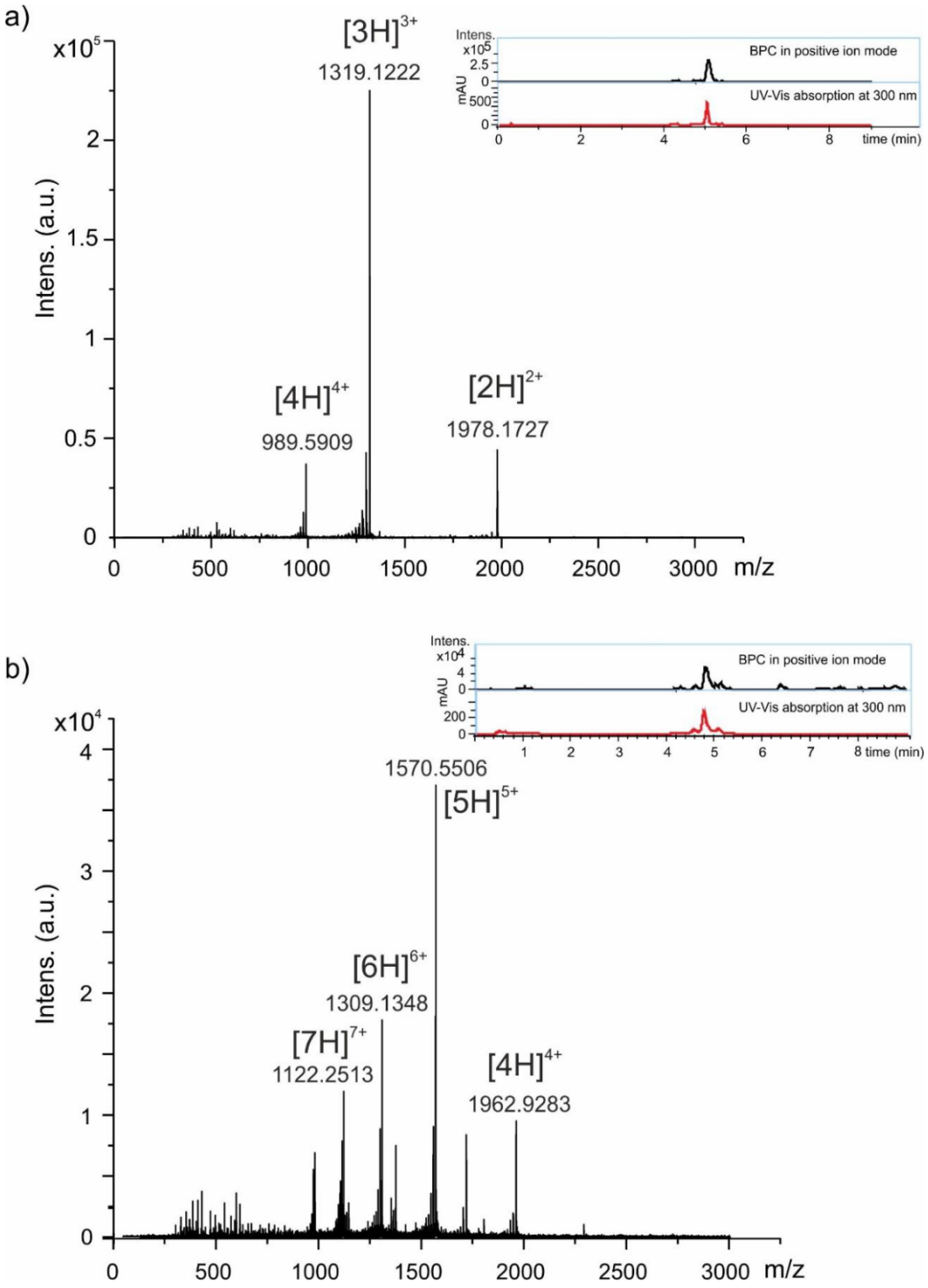

Figure S18. Multicharged species observed by LC-ESI-MS of crude foldamers **8** (a), and **9** (b).

4. Synthesis and Characterization of ylide 10

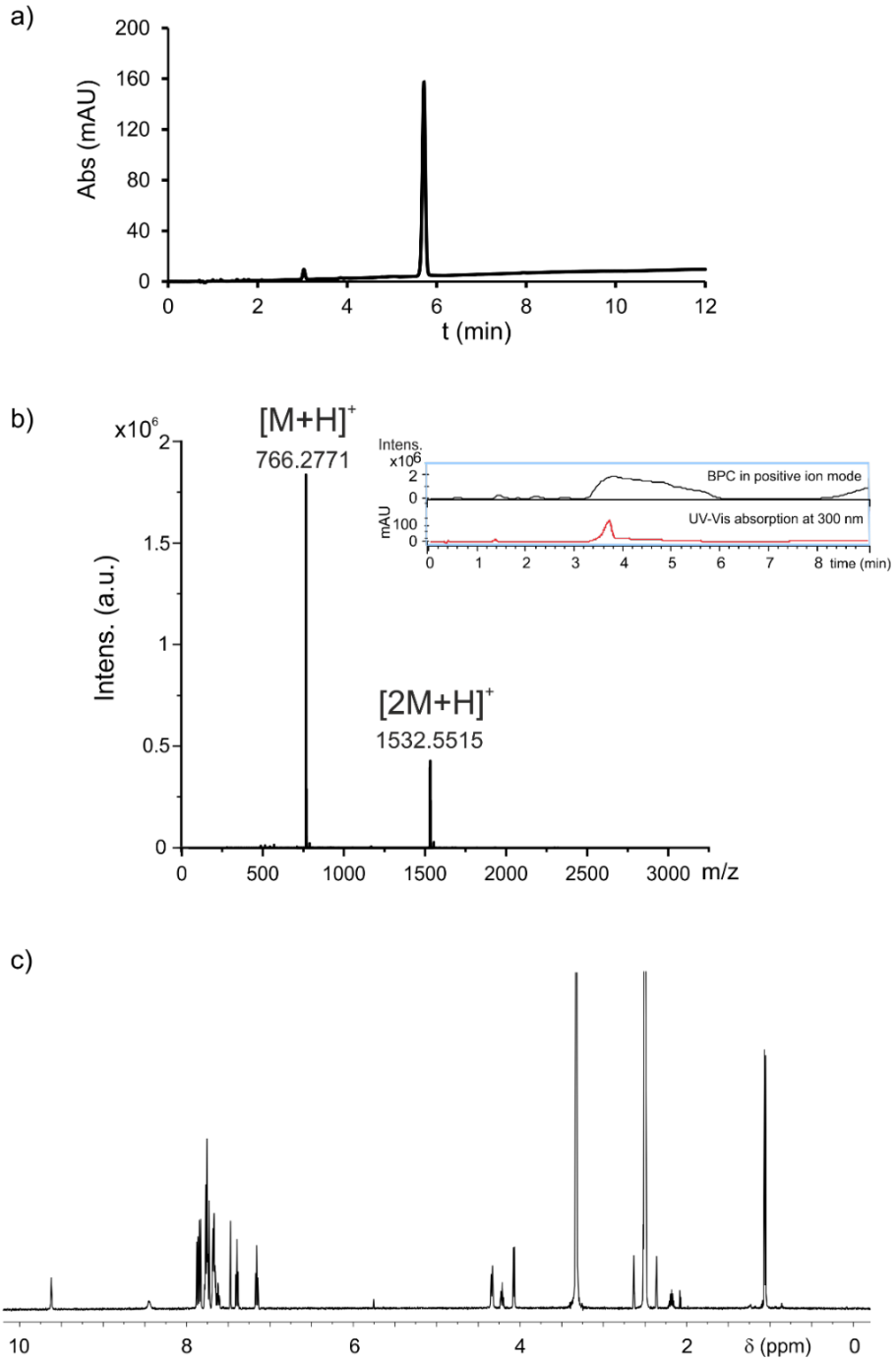

Figure S19. (a) RP-HPLC chromatogram (linear gradient from 80% B to 100% B in 10 min; A: H_2O + 0.1% TFA and B: CH_3CN + 0.1% TFA; UV detection at λ = 300 nm), (b) multicharged species observed by LC-ESI-MS, and (c) ^{1}H NMR spectrum (500 MHz at 298 K in DMSO-d_6) of ylide **10**. **^{1}H NMR**: δ 9.62 (s, 1H), 8.45 (s, 1H), 7.85 (dd, *J* = 15.7, 7.8 Hz, 5H), 7.80 – 7.71 (m, 9H), 7.71 – 7.59 (m, 7H), 7.47 (s, 1H), 7.40 (t, *J* = 7.5 Hz, 2H), 7.16 (td, *J* = 7.5, 1.1 Hz, 2H), 4.34 (d, *J* = 7.8 Hz, 2H), 4.21 (t, *J* = 7.6 Hz, 1H), 4.07 (d, *J* = 6.5 Hz, 2H), 2.18 (dt, *J* = 13.3, 6.7 Hz, 1H), 1.06 (d, *J* = 6.7 Hz, 6H).

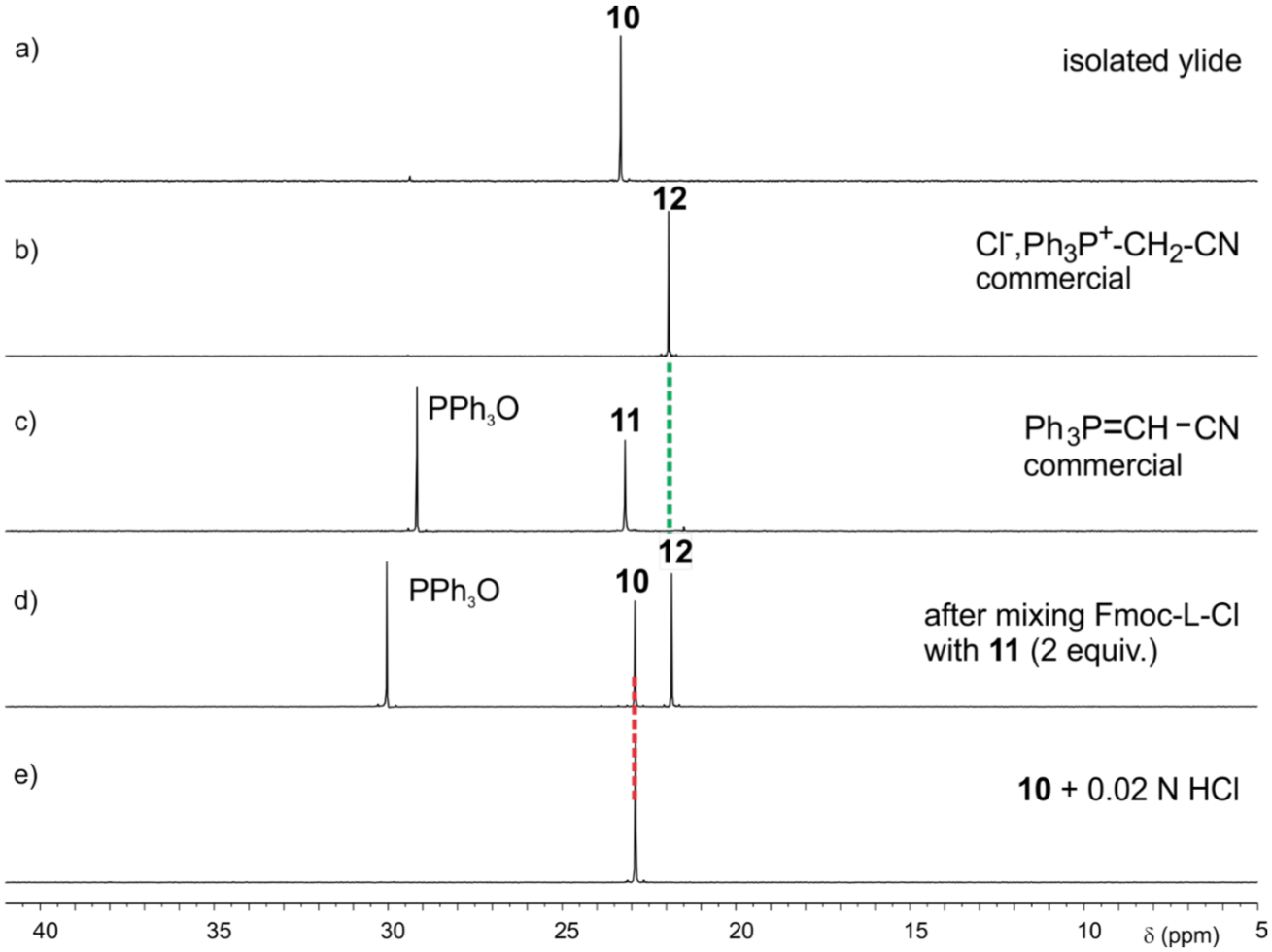

Figure S20. ^{31}P NMR spectra (162 MHz at 298K in $CDCl_3$) showing the formation of ylide **10** using commercial (cyanomethylene)-triphenylphosphorane **11**.

To confirm that **11** formed during the coupling step, thus leading to the formation of ylide **10** (a), the latter was synthesized on purpose. The acyl chloride of the monomer Fmoc-L-OH (Fmoc-L-Cl) was first synthesized in the presence of oxalyl chloride. After isolation, it was mixed with commercial phosphorane **11** (2 equiv.) (c). The ^{31}P NMR of the mixture was next recorded in $CDCl_3$ (d) (see section 2.5). Since no base was introduced during this reaction, the phosphonium salt **12** quickly formed and its identity (d) was further confirmed by overlaying the ^{31}P NMR spectrum of the mixture (d) with the one of the commercial compound (b). The formation of ylide **10** was then proven by ^{31}P NMR. Due to the acidic environment in the mixture, a visible difference in the chemical shift value was observed (spectra in a, and d). A fast addition of 0.02 N HCl solution in the NMR tube of the isolated ylide **10** showed the good alignment of the signals at 23 ppm (spectra in a, and e).

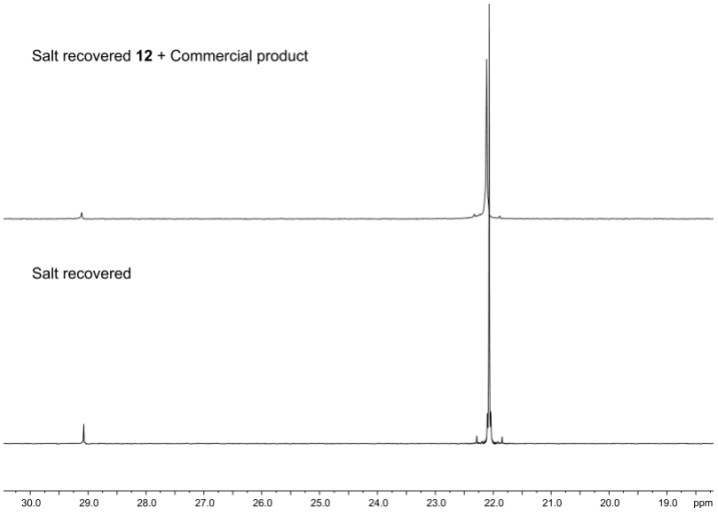

Figure S21. ^{31}P NMR spectra (162 MHz at 298K in $CDCl_3$) of the phosphonium salt **12** isolated as a precipitate during in situ acid chloride activation with TCAN/PPh_3 (bottom) and of a mixture of that salt and a genune commercial sample of **12** (top).

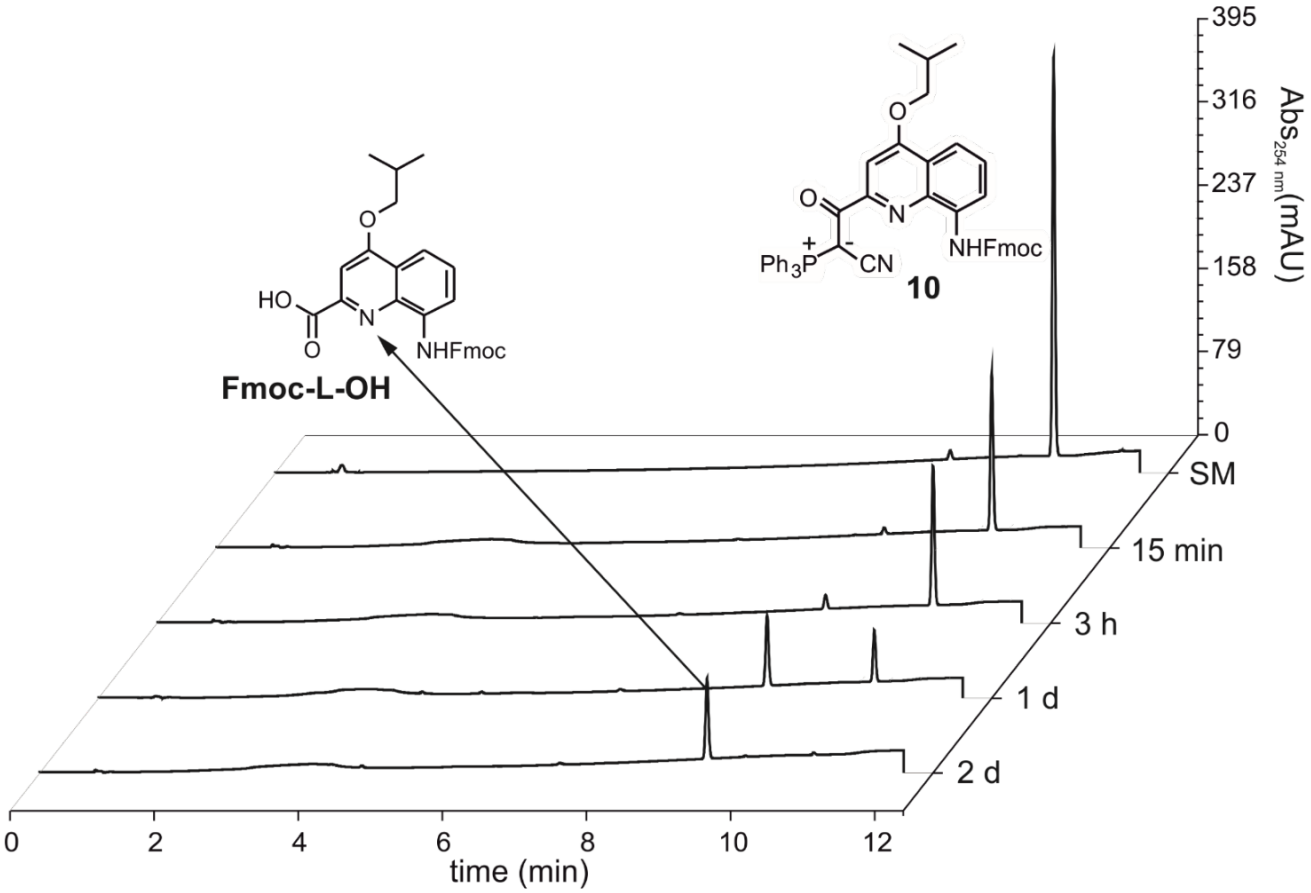

Figure S22. RP-HPLC monitoring of the degradation of ylide **10** into **Fmoc-L-OH** in the presence of NCS (linear gradient from 30% B to 100% B in 10 min; A: H_2O + 0.1% TFA and B: CH_3CN + 0.1% TFA; UV detection at λ = 300 nm).

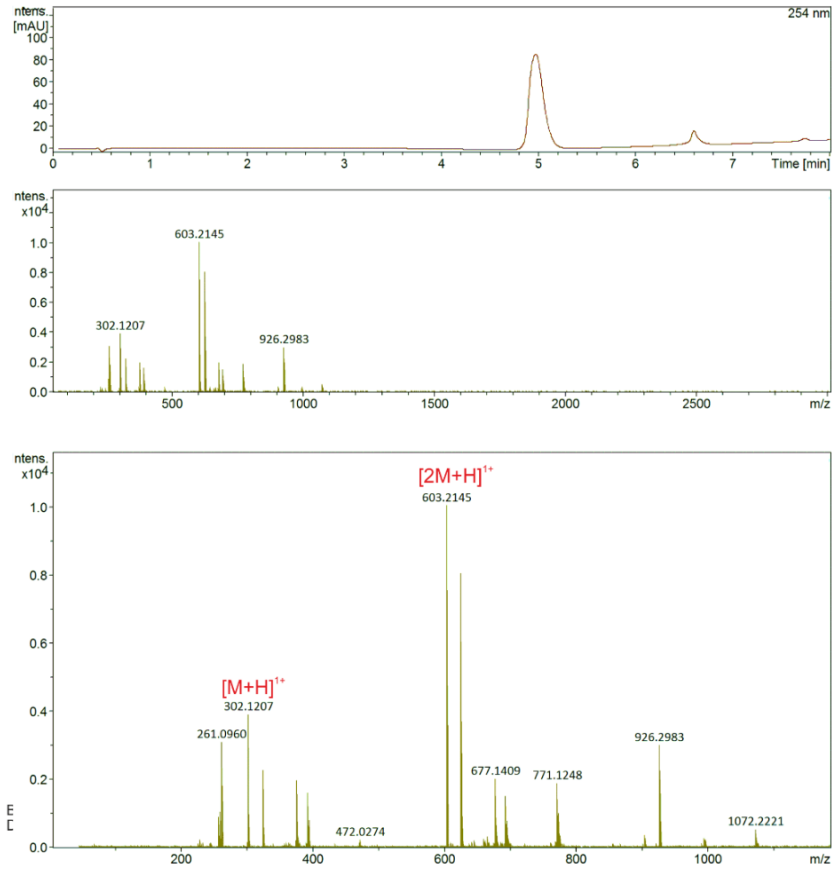

Figure S23. LC-ESI-MS analysis of the recovered precipitate from the RV after acid chloride formation.

5. Crystal structure of isolated ylide 10

The X-ray intensity data of compound **10** were measured on a Bruker D8 Venture TXS system equipped with a multilayer mirror monochromator and a Mo Kα rotating anode X-ray tube (λ = 0.71073 Å). The frames were integrated with the Bruker SAINT software package.[32] Data were corrected for absorption effects using the Multi-Scan method (SADABS).[33] The structure was solved and refined using the Bruker SHELXTL Software Package.[34] All C-bound hydrogen atoms have been calculated in ideal geometry riding on their parent atoms, the N-bound hydrogen atom has been refined freely. The PLATON SQUEEZE[35] program has been applied in order to squeeze-out solvent contents which could not be modelled properly. The voids contain 60 electrons, which would fit to CH_2Cl_2 (42 electrons) and CH_3OH (18 electrons).

Table S3. Crystallographic data of **10**

	10
net formula	$C_{49}H_{40}N_3O_4P$
M_r/g mol^{-1}	765.81
crystal size/mm	0.080 × 0.060 × 0.040
T/K	102.(2)
radiation	MoKα
diffractometer	'Bruker D8 Venture TXS'
crystal system	monoclinic
space group	'P 1 21/c 1'
a/Å	14.3498(6)
b/Å	9.0342(3)
c/Å	34.3552(14)
α/°	90
β/°	98.325(2)
γ/°	90
V/Å^3	4406.8(3)
Z	4
calc. density/g cm^{-3}	1.154
μ/mm^{-1}	0.108
absorption correction	Multi-Scan
transmission factor range	0.94–1.00
refls. measured	75978
R_{int}	0.0733
mean σ(*I*)/*I*	0.0369
θ range	2.553–25.345
observed refls.	6985
x, y (weighting scheme)	0.0457, 15.3618
hydrogen refinement	mixed
refls in refinement	8048
parameters	520
restraints	0
$R(F_{obs})$	0.0915
$R_w(F^2)$	0.2192
S	1.263
shift/error$_{max}$	0.001
max electron density/e Å^{-3}	0.744
min electron density/e Å^{-3}	−0.363
CCDC#	2243294

6. Characterization of the *N,N*-dimethyl-*N'*-(quinolin-8-yl)isobutyramidine

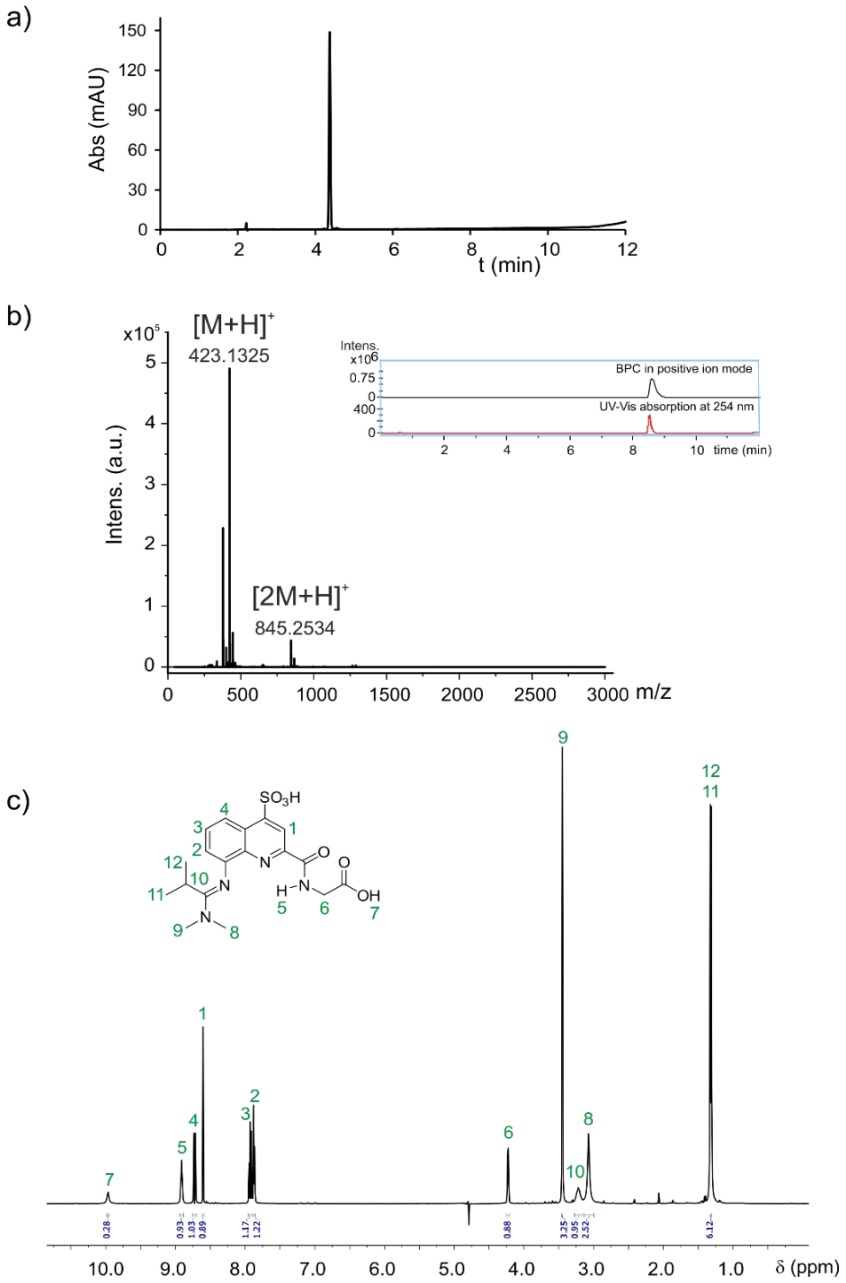

Figure 24. Characterization of the *N,N*-dimethyl-*N'*-(quinolin-8-yl)isobutyramidine isolated from the side reaction of 8-aminoquinoline bearing sulfonic acid side chain with Ghosez's reagent**.** (a) RP-HPLC chromatogram (linear gradient from 0% B to 50% B in 10 min; A: H_2O + 0.1% TFA and B: CH_3CN + 0.1% TFA; UV detection at λ = 254 nm), (b) multicharged species observed by LC-ESI-MS, and (c) ^{1}H NMR spectrum (500 MHz at 298 K in H_2O/D_2O 9:1 with water suppression). **^{1}H NMR**: δ 9.97 (s_{br}, 1H), 8.91 (t, *J* = 5.7 Hz, 1H), 8.72 (d_{br}, *J* = 9.2 Hz, 1H), 8.60 (s, 1H), 7.93 (t_{br}, *J* = 7.9 Hz, 1H), 7.87 (d_{br}, *J* = 7.1 Hz, 1H), 4.23 (d, *J* = 5.5 Hz, 2H (reduced integration due to water suppression)), 3.45 (s, 3H), 3.25 – 3.16 ($sept_{br}$, 1H), 3.07 (s, 3H), 1.32 (d, *J* = 7.5 Hz, 6H). Assignment of CH_3 (8) and CH_3 (9) has been performed based on ^{1}H NOESY spectrum. **HRMS** (ESI^+) m/z calcd. (most abundant mass peak) for $C_{18}H_{23}N_4O_6S$: 423.1333 $(M+H)^+$; found: 423.1325.

7. Decoding aromatic helix recognition: α-helices vs. β-sheets

Manuscript to be submitted.

Authors: **Florian Sanchez, **Vasilii Morozov, **Johan Nilvebrant, Lingfei Wang, Johannes Sigl, Vadzim Haiduk, Lisa Gourdon-Grünewaldt, Céline Douat, Per-Åke Nygren, Ivan Huc.

*Equal contributors

**The author list has not yet been discussed with all authors and may differ in the final manuscript

Contributions: This project is a joint collaboration between two groups. It was planned by I. Huc and P-Å. Nygren. Oligomers syntheses were performed by F.Sanchez, L. Wang and C. Douat. Phage display selection and clone identification were performed by J. Nivelbrant. Proteins expressions were performed by V. Morozov, F. Sanchez, V. Haiduk (supervised by L. Gourdon-Grünewaldt) and J. Sigl. Crystal growth and analyses was done by V. Morozov. Binding affinity experiments were performed by C. Douat and L. Gourdon-Grünewaldt. Project was co-supervised by C. Douat and I. Huc The manuscript was written in collaboration with F. Sanchez, C. Douat and I. Huc.

7.1. Introduction

Proteins are remarkable for their ability to bind other proteins, nucleic acids, or small molecules with high specificity. This specificity is the basis of many biological processes and motivates efforts in synthetic biology to engineer precise protein assemblies of particular geometry and/or function. Artificial assemblies are increasingly generated through engineered protein-protein interfaces, *de novo* design, or the use of synthetic molecules such as molecular glues and proteolysis-targeting chimeras (PROTACs).[1-5] However, the precise co-assembly of proteins with synthetic molecular objects remains limited by the lack of supramolecular synthons capable of providing large, well-defined, and versatile binding interfaces. Here, we present a rare case where structurally unrelated proteins, one is a three α-helices bundle, the other is β-sheet based, converge on the same abiotic target, stereoisomer, and even the same epitope, demonstrating a surprising versatility in molecular recognition.

Recently, our group described a hybrid supramolecular synthon. The complex consists of a synthetic aromatic oligoamide foldamer, referred now as AOF (**Figure 1c**), and a small affitin protein (~ 7 kDa and 66 residues). AOFs adopt stable and predictable helical conformations[6] and can be synthesised at sizes comparable to small proteins thanks to automated solid-phase synthesis.[7] Their surface can be readily functionalised with biogenic side chains resembling those of natural amino acids.[8] These features make AOFs promising candidates for engaging in extended protein surface recognition. Concurrently, affitins are small engineered proteins derived from Sac7d.[9] Their protein scaffold consists of a β-sheet packed against a short α-helix and is advantageously cysteine-free. They typically exhibit remarkable stability against temperature and pH variation.[10] The affitin clone, referred here as C10 (**Figure 1a**), was identified through ribosome display selection against an AOF of similar size, enabling the discovery of a foldamer-protein interface that is stable, well-defined yet dynamic, according to structural NMR analysis. Thanks to solid state and solution structures, we were able to characterise the binding interface between C10 and the AOF, which is essentially due to hydrophobic aromatic cross-section of the AOF sitting on the β-sheet of the protein.

Using this structural information, we sought to use the same dodecaamide AOF candidate to discover new protein binders with a different scaffold. We opted for the selection of affibodies, which are small, engineered affinity proteins (~ 6.5 kDa and 58 residues) also referred as Z-proteins derived from the B-domain of *Staphylococcus Aureus* protein A.[11] They consist of a three α-helix bundle and are cysteine-free. Phage display selection was performed against the same biotinylated AOF and yielded the identification of an affibody clone, named G02 (**Figure**

1b). Further experiments confirmed the selective binding of G02 for the *P*-helix of the AOF, which was characterised in solution (via CD and BLI) and in the solid state.

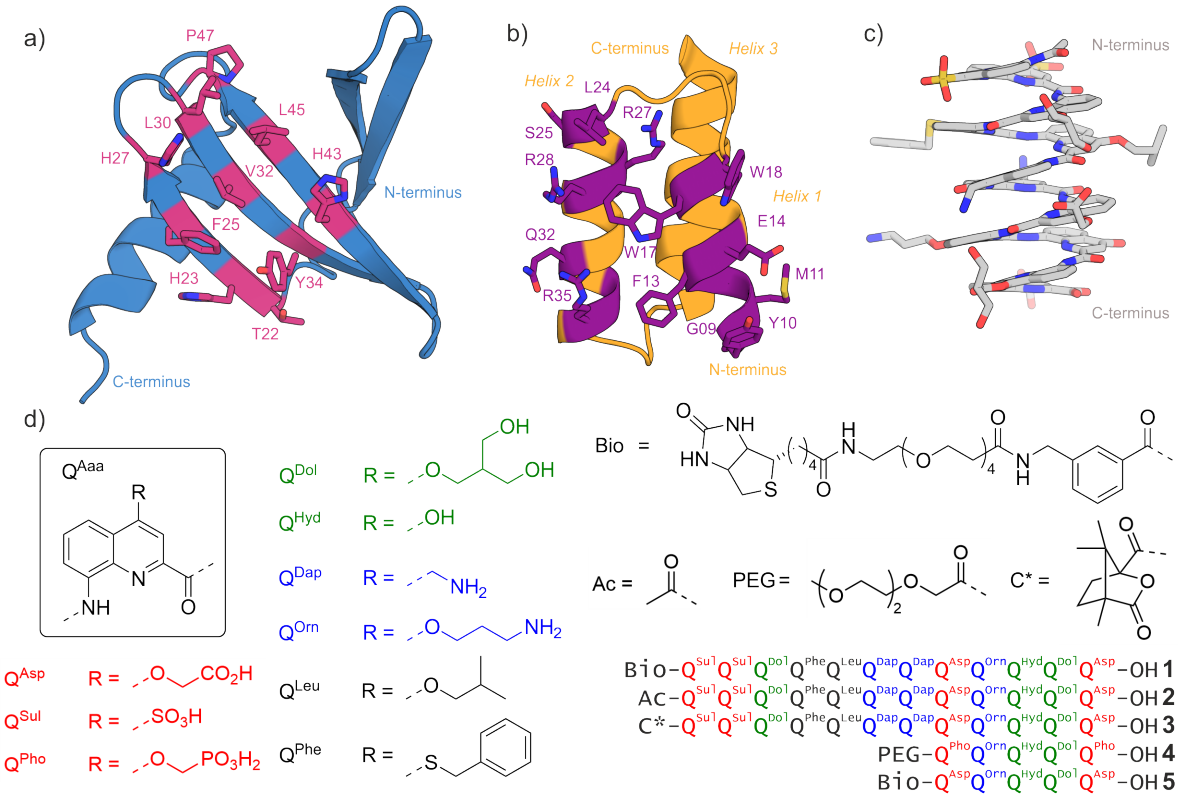

Figure 1. (a) Crystal structure of the nanofitin C10 previously selected against AOF **1** with highlighted randomised ten residues in pink (PDB#9QDO). (b) Crystal structure of affibody clone selected G02 with randomised thirteen residues depicted in purple. (c) Crystal structure of AOF **2** shown from the side, right-handed AOF is represented. The crystal contains the left-handed AOF as well. Bond order and hydrogen atoms are omitted for clarity. (d) Monomer building-blocks for AOFs synthesised **1-5**. Residues are coloured according to the chemical functions of their side chains, red for anionic, green for polar neutral, blue for cationic and black for hydrophobic.

7.2. Results and discussion

7.2.1. Phage display selection, characterisation of the selected clone and structural comparison with C10

A dodecaamide biotinylated, AOF **1** (**Figure 1d**), was synthesised on solid support and comprise eight distinct side chains representing anionic, cationic, hydrophobic, and polar uncharged functionalities. These side chains were strategically distributed across the different faces of the AOF to ensure a chemically diverse environment.[12] AOF **1** was subsequently employed as a target in phage display selections against a large affibody clone library.

Using phage display, a large library of affibody clones was subjected to multiple rounds of selection against the immobilised AOF **1** on streptavidin beads. Following the enrichment of specific binders, individual clones were screened, sequenced, and characterised, ultimately leading to the discovery of the affibody clone G02. It was then recombinantly expressed and its thermal stability was assessed via circular dichroism (CD) spectroscopy with a melting temperature, T_m of about 60 °C, whereas C10 showed no melting transition between 5 °C and 95 °C (**Figure 2**).

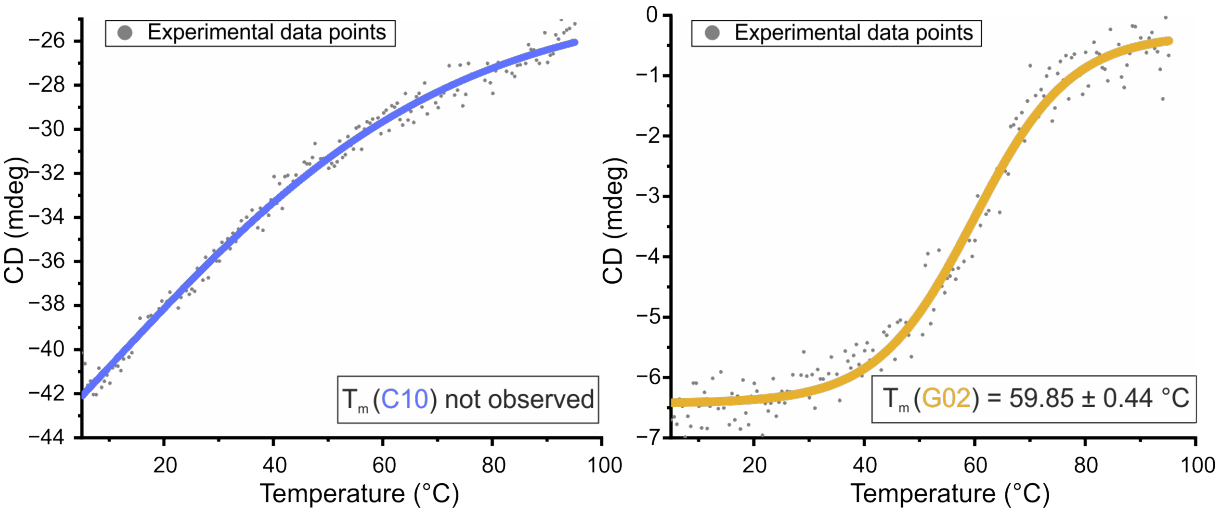

Figure 2. Circular Dichroism (CD) spectra of C10 in blue on the left measured at 30 µM in PBS and G02 in orange on the right at 5 µM in PBS both measured at 222 nm with heating from 5°C to 95°C. Lines are for guiding the eye only, they do not represent a fit.

The biotinylated AOF **1** exists as a mixture of right-handed (*P*) and left-handed (*M*) conformers. The stereocenter in the biotin moiety in AOF **1** renders these conformers diastereomers, in contrast to enantiomers as in AOF **2**. As the initial phage display selection was conducted using the racemic AOF **1**, determination of the preferential helix-handedness for the interaction with G02 was investigated. We recently described the possibility to isolate the *P*- and *M*-helices of AOF **1** by chiral HPLC in reverse phase.[12] Bio-layer interferometry (BLI) experiments revealed that the *P*-helix of AOF **1** binds to the affibody clone G02 with an apparent dissociation constant (K_D) of 270 nM (**Figure 3a**). Concurrently, in the same range of concentration screened, no binding could be detected for the *M*-helix.

Based on the structural insight in solution obtained by NMR spectroscopy of affitin C10 in complex with chiral AOF **3**, a C-terminal pentamer variant **4** was synthesised to further characterise the interaction with affibody G02. Due to their conformational flexibility, such short AOFs can adopt a preferred helical handedness upon binding to their protein target, allowing this bias to be detected by CD spectroscopy at wavelengths where the AOF absorbs while the protein does not. At 40 µM, pentamer **4** showed a positive CD band induction upon interaction with G02 after 1 hour (**Figure 3b**), consistent with observations made for the C10-AOF

complex, which led us to assume a similar binding epitope for both protein scaffold and presumably the same mode of interaction via the AOF aromatic cross-section. A biotinylated version of this pentamer (**5**) was then synthesised and showed a K_D value comparable to that of biotinylated *P*-Q_{12} **1** in BLI binding assays with G02.

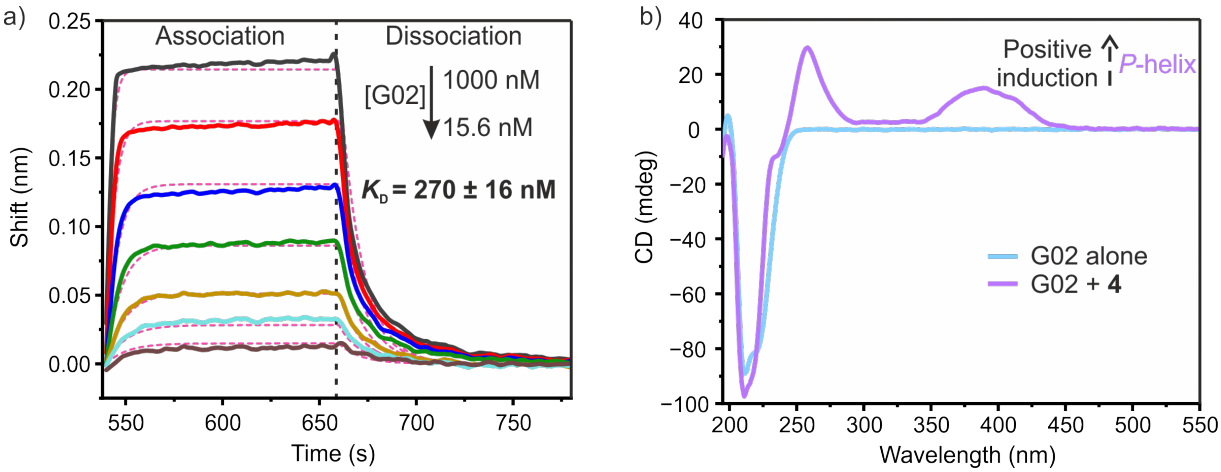

Figure 3. a) BLI sensorgrams of AOF *P*-**1** used as ligand against affibody clone G02 (analyte) in a serial dilution from 1000 nM to 15.6 nM recorded in PBS+0.05% Tween 20 + 0.5% BSA buffer at 25 °C. b) CD spectra of affibody G02 alone in blue recorded at 40 μM in TBS buffer from 190 nm to 550 nm. In purple is the CD spectra of G02 with AOF **4** (1:1) after 1 hour of incubation at room temperature in the same buffer. Positive bands can be seen in a region where the protein is CD silent (300 – 450 nm), confirming the bias of **4** towards the *P*-helix upon interaction with affibody clone G02.

7.2.2. X-ray crystal structure and characterisation of the binding

Initial crystallisation trials with G02 and AOF **1** did not produce crystals of sufficient quality, likely due to solubility differences between the highly soluble affibody and the AOF. Crystallisation attempts were then conducted using an antiparallel coiled-coil construct of G02. Incorporating a coiled-coil based on the talin dimerisation domain[13] (PDB#2QDQ), was intended to enhance symmetry and facilitate crystal packing. Unlike with C10 coiled-coil dimer, co-crystallisation attempts with pentamer **4** remained unsuccessful. To improve aqueous solubility, AOF **4** was extended by one Q^{Pho} unit at the N-terminus, which led to the solid phase synthesis of hexamer **6**. Using **6**, high-quality crystals were obtained, enabling the determination of the complex structure between G02CCDi and the AOF (**Figure 4**). The structure revealed that the randomised aromatic residues (W17, W18 and F13) of the affibody interact with the C-terminal cross-section of the foldamer. Moreover, several salt bridges were observed, notably involving residues E14, R27, and R35.

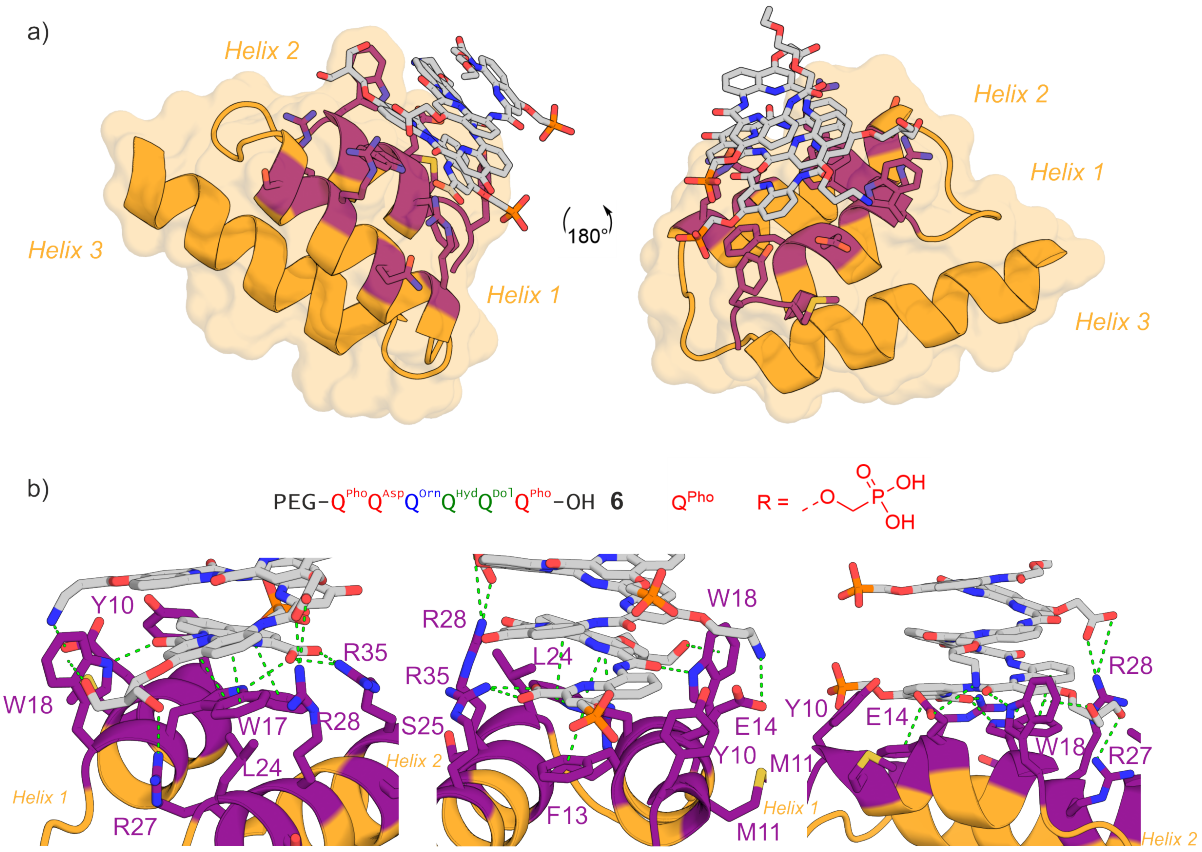

Figure 4. (a) X-ray structure of affibody coiled-coil dimer fusion G02CCDi in complex with foldamer **6**. Residues randomised are shown in purple. (b) Different views of the interaction of the foldamer with the protein. Contacts are marked with dashed green lines while residues of the protein are labelled in purple.

7.2.3. Structural comparison with affitin C10

An interesting aspect of this study is that the AOF candidate, when used as a selection target in another campaign with a very different protein scaffold, yielded a β-sheet protein binder that engages the foldamer in a binding mode strikingly similar to that of the identified α-helix-based affibody clone G02, illustrated in **Figure 5**. Despite relying on distinct structural scaffolds, both proteins recognise the same molecular features of the foldamer, highlighting a potential convergence in binding interface architecture across unrelated protein folds.

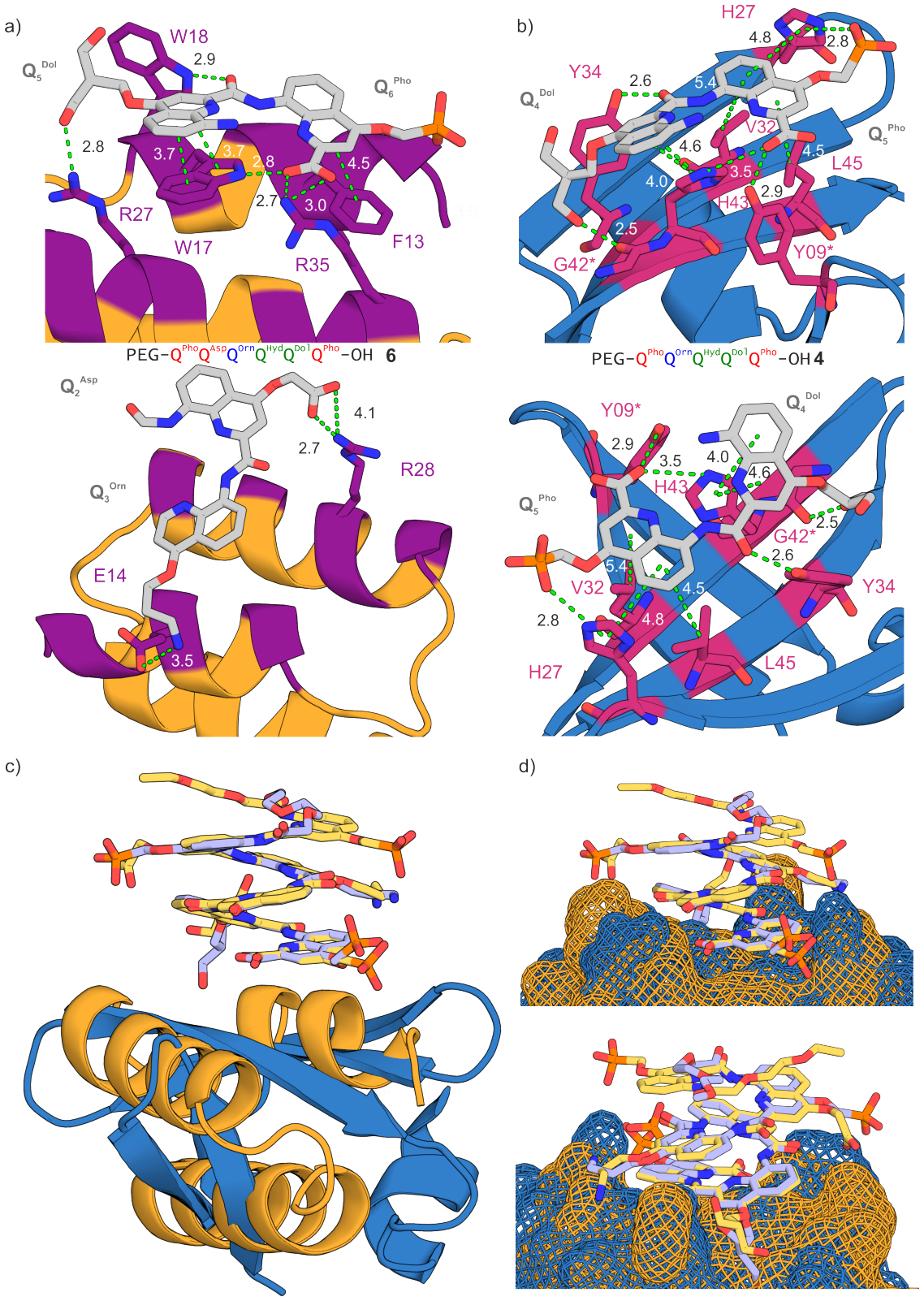

Figure 5. (a). Representation of Q_6^{Pho} and Q_5^{Dol} units of **6** in contact with residues of G02CCDi above and Q_4^{Orn} and Q_2^{Asp} units below. Interactions are shown as green dashed lines with distances in Å. (b). Representation of different views of Q_5^{Pho} and Q_4^{Dol} of **4** in interaction with residues of C10CCDi (PDB#9QDO). Residues marked with * are conserved residues of Sac7d. (c) Overlay of both foldamers-proteins structures. G02 is coloured in orange and C10 in blue, similar colour code is used for the two foldamers. (d) Highlight of the flat surface of both proteins in interaction with the foldamer binder.

7.2.4. Ala-scan mutagenesis of affibody clone G02

An Ala-scan mutagenesis was conducted on the thirteen randomised residues of the selected affibody clone G02. Thirteen individual mutants were expressed and evaluated via BLI using biotinylated **5** as the binding partner (**section 7.5.3.5.**). The analyses identified four residues as critical for interaction, including all aromatic positions (F13, W17, W18), as well as R35. Mutations at these positions significantly impaired binding affinity. In contrast, substitutions at the remaining positions (G9A, L24A, R28A, Q32A, S25A, E14A, and R27A) had minimal impact on binding. Notably, the Y10A mutant could not be expressed and was therefore excluded from functional analysis. These findings are consistent with the crystallographic data obtained for the G02CCDi-**6** complex.

7.2.5. Foldamer mutagenesis study and binding affinity

In a similar manner to the Ala-scan for proteins, we performed a Q-Glycine-scan of the AOF. Each quinoline unit of the pentamer **5** was iteratively replaced by a Q^{Gly} (no substitution on position 4 of the quinoline ring) to assess the contribution of the side chains to the binding with the clone G02 and C10 respectively. Five new biotinylated AOF sequences (**7**-**11**) were synthesised. Overall, scanning the side chains did not result in any complete loss of binding, which corroborates with the aromatic cross-section binding of the AOFs **1**, **4** and **6** to the two protein scaffolds. However, a threefold reduction in affinity was observed for G02 upon removal of the propanediol side chain at position Q4 and the aspartate-mimicking side chain at position Q1. Similarly, removal of the propanediol side chain resulted in a threefold decrease in binding to C10 (**Table 1**).

Table 1. Determined K_D values (in nM) by BLI of Q^{Gly} mutant against either C10 (on the right) or G02 (on the left).

	C10 K_D (nM)	Q^{Gly} R = 	G02 K_D (nM)
5	118 ± 15	Bio-$Q^{Asp}Q^{Orn}Q^{Hyd}Q^{Dol}Q^{Asp}$-OH	234 ± 28
7	231 ± 38	Bio-$Q^{Asp}Q^{Orn}Q^{Hyd}Q^{Dol}Q^{Gly}$-OH	230 ± 22
8	369 ± 52	Bio-$Q^{Asp}Q^{Orn}Q^{Hyd}Q^{Gly}Q^{Asp}$-OH	630 ± 37
9	198 ± 26	Bio-$Q^{Asp}Q^{Orn}Q^{Gly}Q^{Dol}Q^{Asp}$-OH	299 ± 40
10	221 ± 43	Bio-$Q^{Asp}Q^{Gly}Q^{Hyd}Q^{Dol}Q^{Asp}$-OH	377 ± 33
11	131 ± 19	Bio-$Q^{Gly}Q^{Orn}Q^{Hyd}Q^{Dol}Q^{Asp}$-OH	608 ± 131

Based on the observed binding affinities and structural insights, targeted mutations of the foldamer side chains were introduced with the aim of either enhancing or diminishing binding affinity for each protein. Our design strategy sought to create foldamer variants capable of discriminating between the two proteins, ideally resulting in selective binding to one while minimising interaction with the other protein. To explore these designs, a small library of

biotinylated AOFs were synthesised, and their binding affinities for the two protein scaffolds were determined using BLI.

Initially single mutations were introduced on the AOF, six new sequences were synthesised (**12-17**) and their binding affinity towards both proteins were assessed by BLI. **Table 2** summarises the sequences as well as the K_D measured. Although the Q^{Gly}-scan on the fifth position showed that this side chain was not critical for the binding to G02, it resulted in a loss of a factor two for C10, presumably due to a contact of the first anionic side chain with a neighbouring histidine (**Figure 6**). Guided by the crystal structures of G02 and C10 in complex with their respective AOF, featuring a phosphonate side chain in position 5, the aspartate unit was replaced with a phosphonate one, leading to the synthesis of **12**. This mutation resulted in a twofold improvement in binding affinity for C10. In the case of G02, the binding affinity was reduced by approximately fourfold, which is a result that may seem unexpected given the crystal structure obtained with the same unit positioned identically. However, it is important to consider the significant differences in concentration between crystallisation assays and BLI measurements, which can influence observed binding behaviour. In this context, the reduced affinity could plausibly be attributed to the presence of Y10 and the adjacent -CH_2 group near Q_6^{Pho}, which may introduce steric hindrance or alter local interactions unfavourably.

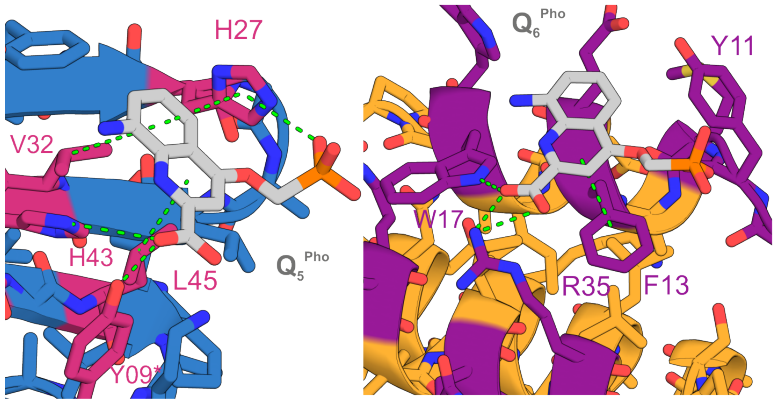

Figure 6. Comparison of interaction on the last unit Q_5^{Pho} for C10 on the left in blue and Q_6^{Pho} for G02 on the right in orange. Interactions are represented by dashed green lines.

Similarly, the side chain of Q_1 was replaced with a phosphonate group (**13**). The Q^{Gly}-scan binding affinity data at this position indicated that the loss of the anionic side chain reduces by a factor of three the binding to G02, likely due to the charged reinforced hydrogen bond formed between the aspartate side chain and the arginine R28 (**Figure 7**). In contrast, both the Q^{Gly}-scan and the crystal structure suggest no significant interaction between the side chain at the first position and C10, but the mutation resulted in a slight improved binding affinity for C10. Exchanging this side chain for G02 did not alter the binding affinity, suggesting that the interaction with R28 is likely unaffected by the chemical nature of the side chain, whether it is

a carboxylate or a phosphonate. This observation supports the idea that, in this context, both substituents provide sufficiently similar charge and geometry to maintain the interaction.

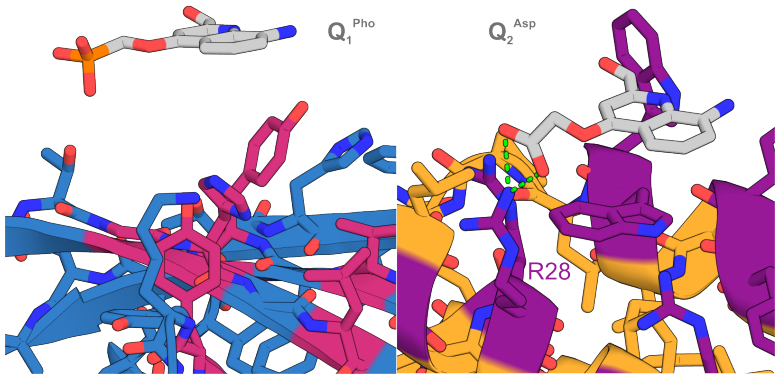

Figure 7. Comparison of interaction on last unit Q_1^{Pho} for C10 on the left in blue and on Q_2^{Asp} for G02 on the right in orange. Interactions are represented by dashed green lines.

Mutation of the propanediol side chain at the position 4 of the AOF (**14**) resulted in the most pronounced loss of binding affinity for both proteins. However, the role of this side chain in the binding is not immediately apparent from either crystal structure. This long, bulky, hydrophobic, and polar moiety appears to occupy a hydrophobic cleft in both proteins in a similar manner (**Figure 8**). To further enhance its hydrophobicity, the side chain was replaced with a leucine-like side chain, which resulted only in a modest change in C10 binding affinity. A similar modest change was observed for G02, though in this case with a slight decrease in binding affinity, which could be likely attributable to the loss of interaction with R27.

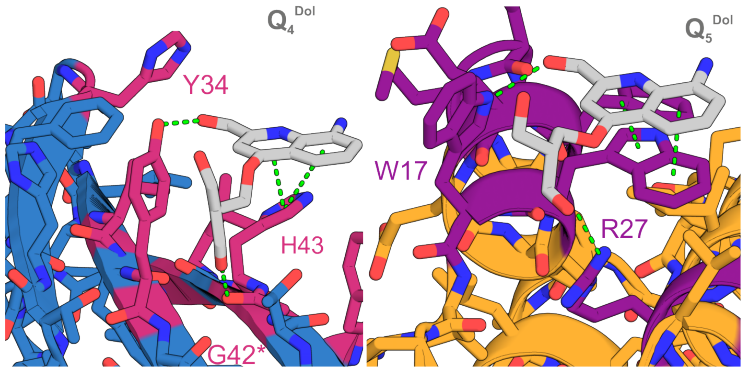

Figure 8. Comparison of interaction on fourth unit Q_4^{Dol} for C10 on the left in blue and on Q_5^{Dol} for G02 on the right in orange. Interactions are represented by dashed green lines.

In both cases, the hydroxyl side chain appeared to have no significant impact on binding. Neither protein possesses residues in the vicinity capable of interacting with an alternative side chain (**Figure 9**). Accordingly, substitution with an aspartate-like group (**15**) provided no appreciable change in C10 binding affinity. The mutation from a hydroxyl to a carboxylate side chain at this position enhanced the binding affinity by nearly twofold. A plausible explanation

lies in the proximity of R35, which, although observed in the crystal structure to interact with the carboxylate of Q_6^{Pho}, may not always maintain this contact in solution. In such a scenario, the presence of the aspartate side chain could help retain partial interaction with R35, thereby preventing its complete dissociation from the AOF and contributing to the improved affinity.

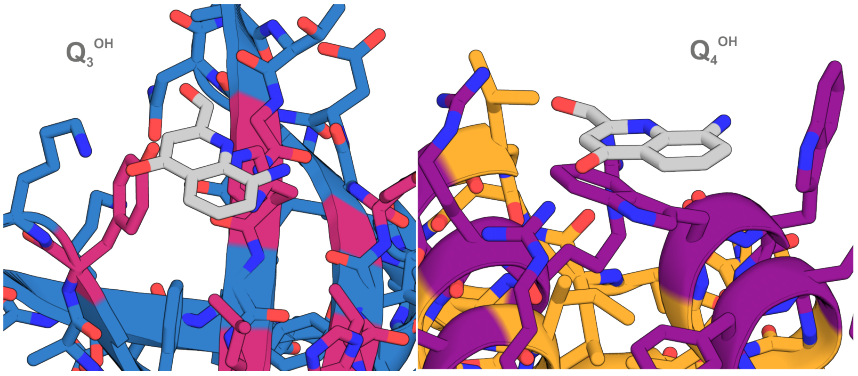

Figure 9. Comparison of interaction on third unit Q_3^{OH} for C10 on the left in blue and on Q_4^{OH} for G02 on the right in orange.

Q^{Gly}-scan analysis indicated that the Q^{Orn} side chain contributes to the binding with G02, a result supported by the crystal structure, which reveals a charged reinforced hydrogen bond with E14. This trend was not reproduced in the Ala-scan. Structural inspection of the surrounding region shows the essential residue W18 for the binding to G02 in proximity of Q^{Orn}, while in C10, the nearby F25 could also be within reach (**Figure 10**). To exploit these potential aromatic contacts, the cationic side chain was replaced with a tyrosine-like side chain (**16**). However, BLI measurements showed no improvement in C10 binding affinity, the same mutation led to an almost fourfold decrease in affinity towards G02. This contrast suggests that the mutation may serve as a useful tool for discriminating binding behaviour between the two protein targets.

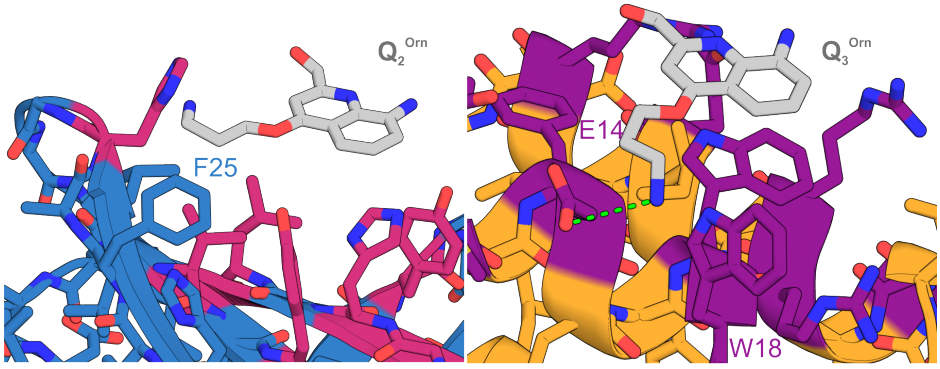

Figure 10. Comparison of interaction on second unit Q_2^{Orn} for C10 on the left in blue and on Q_3^{Orn} for G02 on the right in orange. Interactions are represented by dashed green lines.

In an effort to identify another diverging mutation, we substituted the anionic side chain at the C-terminus, which is engaged in binding with C10 but not with G02. In the context of C10, the

phosphonate group forms a charge-reinforced hydrogen bond with the adjacent H27 (**Figure 6**). This residue was replaced with a positively charged diaminopropionic acid (Dap) moiety (**17**), a change anticipated to introduce electrostatic repulsion and reduce binding affinity. Consistent with this prediction, binding to C10 decreased approximately fourfold. Affinity towards G02 was also affected, though to a lesser extent, with only a modest decrease observed. These results suggest that this mutation may serve as another useful discriminator between the two protein targets, offering a potential strategy for selective binding modulation.

Table 2. Determined K_D values (in nM) by BLI of pentamers mutant against either C10 (on the right) or G02 (on the left).

	C10 K_D (nM)		G02 K_D (nM)
12	48.2 ± 0.4	Bio-Q^{Asp}Q^{Orn}Q^{Hyd}Q^{Dol}Q^{Pho}-OH	922 ± 17
13	64.9 ± 0.6	Bio-Q^{Pho}Q^{Orn}Q^{Hyd}Q^{Dol}Q^{Asp}-OH	286 ± 1.7
14	87.3 ± 0.8	Bio-Q^{Asp}Q^{Orn}Q^{Hyd}Q^{Leu}Q^{Asp}-OH	302 ± 2.9
15	140 ± 1.1	Bio-Q^{Asp}Q^{Orn}Q^{Asp}Q^{Dol}Q^{Asp}-OH	113 ± 0.7
16	143 ± 7.0	Bio-Q^{Asp}Q^{Tyr}Q^{Hyd}Q^{Dol}Q^{Asp}-OH	911 ± 49
17	426 ± 3.4	Bio-Q^{Asp}Q^{Orn}Q^{Hyd}Q^{Dol}Q^{Dap}-OH	352 ± 1.8

Building on these results, we initiated the design of new pentamers incorporating multiple side chain mutations to investigate whether the effects observed with individual substitutions are reproducible or potentially additive, which is an outcome not typically seen with peptides. Ultimately, our goal is to determine whether, based on our crystal structures and molecular design strategies, it is possible to discriminate interactions between these proteins and a specific pentamer sequence. Several pentamers have already been synthesised, and additional candidates are currently being prepared. Their binding affinities will be systematically measured against G02 and C10 in order to assess the selectivity and robustness of scaffold-sequence recognition.

7.3. Conclusion and perspectives

In conclusion, our study described the discovery of a AOF with the ability to bind two different scaffolds based on either β-sheet (C10) or α-helices (G02) coming from different display selection methods (mRNA and phage). Thanks to solution study on C10, we were able to truncate the AOF to its binding epitope. We discovered that the AOF binds both proteins in an enantioselective manner, with its *P*-handedness, thanks to CD measurements using AOF **4**, achiral and dynamic pentamer. Crystals of high quality from G02CCDi-**6** complex were obtained and diffracted up to 2.7 Å. Thorough structural investigations of both protein surfaces revealed striking similarities in the binding mode with the AOF. The hydrophobic cross-section

of the AOF plays a major role in the interaction towards C10 via the hydrophobic patch made of V32 and L45, while G02 possess two aromatic residues F13 and W17 which stacks perfectly with the two last **Q** units of the AOF. Ala-scan of G02 demonstrated the necessity for the binding of the presence of the aromatic residues F13, W17 and W18, on the first helix of the bundle, but also of R35, located on the second helix.

In an attempt to potentially find a diverging design, we performed a Gly-scan of the AOF, which essentially is the same concept as an Ala-scan but on the AOF, by replacing iteratively each side chain by a hydrogen atom and measuring the resulting binding affinity with each protein. These experiments confirmed the structural data already obtained, that is the cross-section is the hotspot for the interaction while the side chains are moderately important for the binding. Still, removal of Dol side chain on Q_4 decreased the binding affinity threefold for C10 and G02 respectively. Interestingly, removal of Orn side chain in Q_3 induced the same effect on G02.

Guided by these findings and the insights from two crystal structures, we synthesised several new series of AOF variants, each bearing a single mutation in their sequence. The aim was to design AOFs capable of discriminating between C10 and G02 by selectively enhancing or reducing binding affinity toward one protein over the other. This approach led to the identification of several side chains that bias binding in a protein-specific manner. For instance, replacing the C-terminal Q^{Asp} with Q^{Pho} proved highly detrimental for G02, resulting in a fourfold decrease in binding affinity, while simultaneously benefiting C10. Similarly, substituting Q^{Orn} with Q^{Tyr} had no measurable impact on C10 binding but significantly impaired interaction with G02, again with a fourfold reduction in affinity. The only mutation that led to a substantial loss of binding for C10 was the replacement of the C-terminal Q^{Asp} with a positively charged Q^{Dap} side chain, which had only a modest effect on G02 binding.

Building on these results, a new series of targeted mutations has been planned, leading to the synthesis of additional pentamer sequences. Their binding affinities will be evaluated and reported in due course. These efforts represent a promising step toward the rational design of AOFs with tailored selectivity.

7.4. Supporting information: chemical synthesis

7.4.1. Materials

All chemicals were purchased from commercial suppliers (*Sigma-Aldrich*, *Fisher Scientific*, *IRIS Biotech*, *ABCR*) and used without further purification unless stated otherwise. Low loading (LL)-Wang resin was purchased from *Merck-Novabiochem.* Solvents were purchased from *Fisher Scientific* (cyclohexane, ethyl acetate, dichloromethane (DCM), methanol, tetrahydrofurane (THF) and acetone, analytical grade), *IRIS Biotech* (*N*-methyl-2-pyrrolidinone (NMP)) or *Carlo Erba* (*N*,*N*-dimethylformamide (DMF), peptide grade) and used without further purification. Anhydrous DCM and THF were obtained from a SPS-800 Solvent Purification System (*MBraun*). *N,N*-diisopropylethylamine (DIPEA), NEt_3 and $CHCl_3$ were freshly distilled over CaH_2 prior to use. HPLC grade acetonitrile (MeCN, *Fisher Scientific*) and ultra-pure water (Omnia xs^{touch} Blueline, Stakpure system) were used for RP-HPLC analyses and purification. LCMS grade MeCN (*Fisher Scientific*) was used for LCMS analyses.

7.4.2. General methods for HPLC analysis and purification, LCMS and NMR analyses

RP-HPLC analyses were performed on an Ultimate 3000 HPLC system (*Thermo Fischer Scientific*) equipped with an UV diode array detector, monitoring absorbance at 254 nm and 300 nm if not stated otherwise, using a Nucleodur C18 Htec (4.6 × 100 mm, 5 µm, *Macherey-Nagel*). For acidic RP-HPLC analyses, 0.1% trifluoroacetic acid (TFA) in water (solvent A) and 0.1% TFA in acetonitrile (solvent B) were used as the mobile phase at a flow rate of 1 mL/min. All the RP-HPLC analyses were run at 50 °C. For basic RP-HPLC analyses, the mobile phase was composed of 12.5 mM TEAA in water at pH 8.5 (A) and 12.5 mM TEAA in water: acetonitrile mixture (1:2, v/v) at pH = 8.5 at a flow rate of 1mL/min.

Semi-preparative RP-HPLC was performed on an Ultimate 3000 HPLC system, using a Nucleodur C18 Gravity column (10 × 250 mm, 5 µm, *Macherey-Nagel*) at a flow rate of 5 ml/min. The same solvent composition to the analytical conditions was used either in acidic or basic mode.

LC-MS analyses were recorded on an Ultimate 3000 HPLC system, coupled to a micrOTOF II mass spectrometer (*Bruker Daltonics*) with electron spray ionization (ESI). The LC column used was a Nucleodur Gravity Ec column (2 × 50 mm, 1.8 mM, *Macherey-Nagel*). All LC analyses were run at 50 °C. The MS spectrometer was calibrated, prior to analysis, in positive

and negative mode by direct infusion of an ESI-Low Concentration Tuning Mix (*Agilent Technologies*).

^{1}H-NMR spectra were recorded on Avance III HD 500 MHz BioSpin spectrometer (*Bruker*). All chemical shifts are reported in ppm and calibrated against residual solvents signals of CD_3CN (δ = 1.94 ppm) and DMSO-d_6 (δ = 2.50 ppm). NMRs recorded in CD_3CN/H_2O (1:1; vol/vol) were performed with water suppression with excitation sculpting using the zgesgp pulse sequence from the Bruker pulse sequence library. Signal multiplicities are reported as *s*, singlet; *d*, doublet; *t*, triplet; *q*, quartet; *dd,* doublet of doublet; and *m*, multiplet. Coupling constants (*J*) are reported in Hz. Data were processed on MestReNova v.12.0.

7.4.3. Generalities on solid phase foldamer synthesis (SPFS)

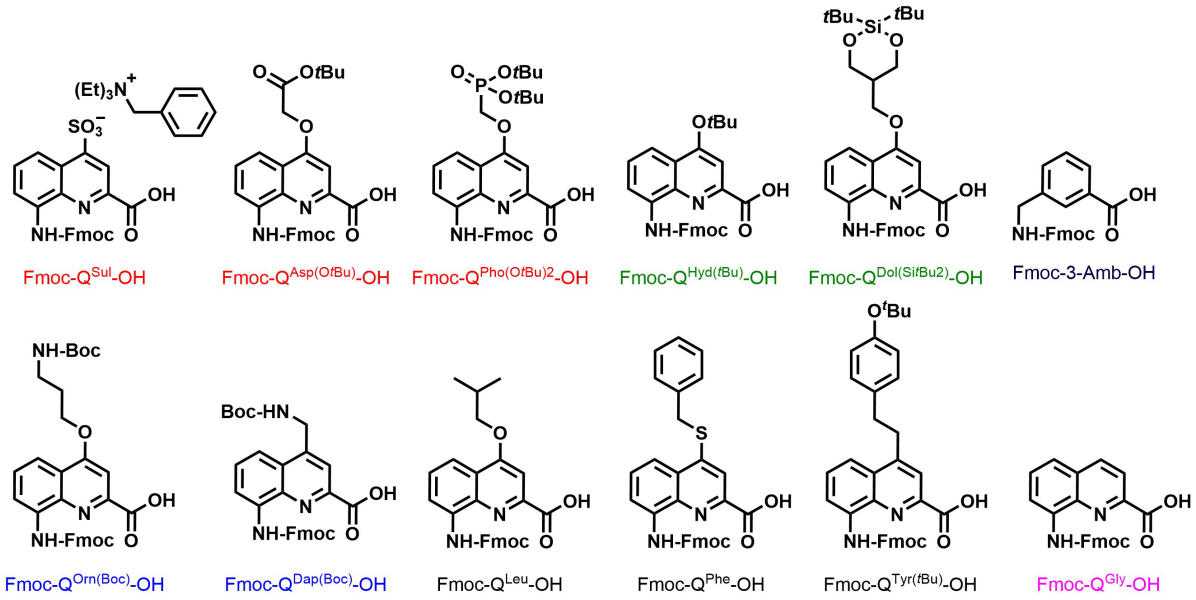

All protected Fmoc-Q$^{Xxx(PG)}$-OH and Fmoc-3-Amb-OH monomers (shown above) used for the solid phase synthesis of the oligomers were prepared following reported synthetic protocols. [14-20]

SPFS was performed following recently reported conditions using a PurePep® Chorus peptide synthesiser (*Gyros-Protein Technologies*) for the different sequences.[7] Generally, all monomers were activated as their respective acid chlorides, by applying *in situ* Appel's conditions in the presence of PPh_3, trichloroacetonitrile (TCAN), and 2,4,6-collidine as base. For the synthesis of **7** a special activation procedure was developed to avoid the deprotection of the acid sensitive *t*Bu protection on the phosphonate side chain (see procedure below).

The synthesis of compounds **1**, and **2** have been recently described, alongside optimized Fmoc deprotection conditions. Oligomer **3** was synthesized following the same procedures on Cl-MPA protide resin.[12]

Additionally, we have recently developed a new loading procedure on Wang resins using DIC/OxymaPure conditions (see below).

- *Loading of the first quinoline unit on Wang resin*

Loading of Fmoc-$Q^{Asp(OtBu)}$-OH to the Wang Resin (0.43 mmol.g^{-1}). 117 mg of resin (0.1 mmol) was dispensed in a 5 mL syringe equipped with a filter and swollen in 3 mL of dry DCM for 30 min. Fmoc-$Q^{Asp(OtBu)}$-OH (0.2 mmol, 2 equiv.) was dissolved in 1 mL of DCM. OxymaPure (2 equiv.) was dissolved in 1 mL of DMF and added to the monomer solution. Subsequently, the mixture was poured to the freshly filtered resin. In a separate vial, DMAP (0.1 equiv.) was dissolved in a minimum volume of DCM (0.5 mL). DIC (2 equiv.) was added to the suspended resin directly followed by the solution of DMAP. The resin was next gently shaken overnight at room temperature. After resin filtration and washings with DCM, a capping step was performed using acetic anhydride Ac_2O in DCM (1:1, v/v, 4 mL) for 1 h. The resin was lastly washed thoroughly with DCM. Loading determination by UV gave a loading yield of 50% (0.215 mmol.g^{-1}, 21.5 µmol).

- *General procedure for Fmoc deprotection*

First, the resin was washed three times with a solution of DCM:NMP (80:20; v/v), before adding a solution of 2% DBU in NMP. The Fmoc deprotection was performed for 2 × 3 min. After deprotection, the resin was washed two times with 20% NMP in DCM and then three times with dry THF.

- *In situ activation and aromatic monomer couplings*

The aromatic monomers were coupled on Wang resin-bound oligoquinoline with *in situ* activation using an excess of three equivalents of monomer relative to the resin loading. Each coupling was performed twice at 50°C for 15 min.[12]

- *Coupling of the Biotin-PEG_4-COOH linker*

The Biotin-PEG_4-COOH linker (1.5 equiv. relative to resin loading) was coupled manually on the resin-bound H-Amb-foldamer by applying peptide coupling conditions with the use of BOP (1.5 equiv.) and DIPEA (3 equiv.) in dry DMF overnight at room temperature.

- *TBAF deprotection of the di-tert-butyl silylether protection group of Q^{Dol}*

Prior to TFA cleavage, the silyl protecting group on the diol side chain was removed using tetrabutylammonium fluoride (TBAF, 1 M in THF). The resin was suspended in dry THF and TBAF (8 equiv. per Q^{Dol}) was added. The deprotection took place under microwave irradiation (50 W, ramp to 50 °C for 5 min, hold at 50°C for 15 min) and this step was repeated once. The resin was then thoroughly washed with THF, and DCM prior to TFA cleavage.

➢ *TFA cleavage of the oligomers from the Wang resin*

Cleavage of the oligomer from the Wang resin was performed using a mixture of TFA, tri-isopropyl silane (TIS) and H_2O (95: 2.5: 2.5; v/v/v), for 3 h at room temperature. The crude oligomer was precipitated with diethylether (Et_2O), redissolved in water/MeCN and lyophilised.

7.4.4. Syntheses of oligomers

7.4.4.1. Synthesis of 3

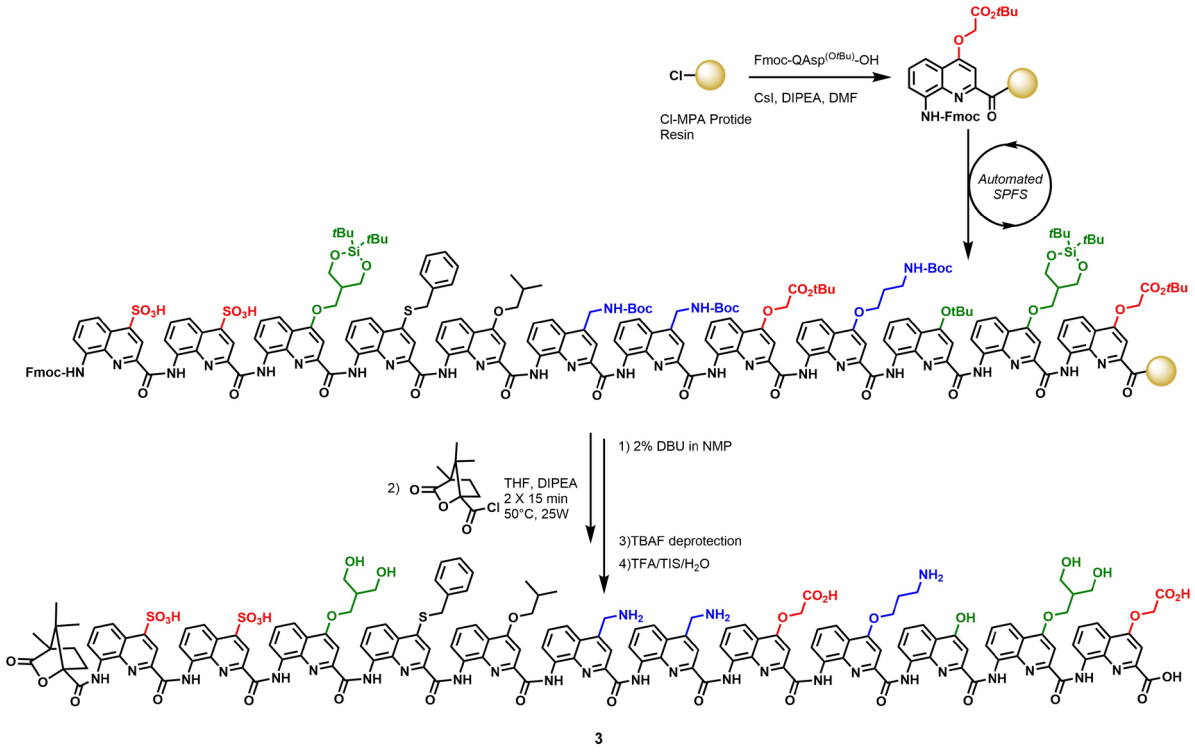

3

Compound 3: Oligomer **3** was synthesised on Cl-MPA Protide resin (0.17 mmol.g^{-1}, 28 µmol scale after first monomer loading using CsI and DIPEA.[21] The N-terminal camphanyl moiety was introduced according to recently published procedures.[12] After TBAF deprotection of the silyl ether, TFA cleavage and purification by preparative RP-HPLC, compound **1** was obtained as a yellow powder in 17% yield (5.2 mg, 5.0 µmol).

^{1}H-NMR (500 MHz, DMSO- *d*$_6$): δ = 10.94 (m, 2H), 10.71 (s, 1H), 10.59– 10.43 (m, 3H), 10.32 (s, 1H), 10.04 (m, 2H), 9.73 (s, 1H), 9.05 (s, 1H), 8.32 (d, *J* = 8.1 Hz, 1H), 8.23 (d, *J* = 8.2 Hz, 1H), 8.14 (s, 1H), 8.01 (d, *J* = 7.2 Hz, 1H), 7.93 (d, J = 7.2 Hz, 1H), 7-82– 6.63 (m, 41H), 6.36 (s, 1H), 6.33 (s, 1H), 6.16 (s, 1H), 6.12 (s, 1H), 5.97 (s, 1H), 5.91 (s, 1H), 5.88 (s, 1H), 5.56 (s, 1H), 4.85 – 3.91 (m, 19 H), 3.87 – 3.55 (m, 14H), 3.50 (s, 2H), 2.35 (bp, 5H), 2.27 (m, 1H), 2.12 (m, 1H), 1.98 (m, 1H), 1.57 (m, 2H), 1.46 (m, 1H), 0.39 (d, *J* = 8.4 Hz, 6H), -0.12 (s, 3H).

HRMS (ESI⁺): *m/z* calculated for $C_{158}H_{133}N_{27}O_{37}S_3$ 1033.2842 $[M+3H]^{3+}$; found 1033.2800 $[M+3H]^{3+}$.

7.4.4.2. Synthesis of 4

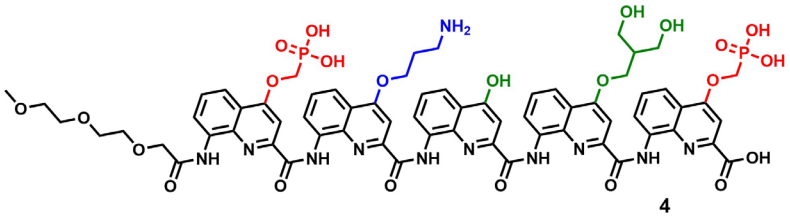

Compound 4: Oligomer **4** was synthesised on LL-Wang resin (30 µmol scale) using the automated SPFS procedure. Coupling of the final aromatic monomer, Fmoc-$Q^{Pho(OtBu)2}$-OH, was carried out using a distinct protocol due to its acid sensitivity. The collidine solution in dry THF (9 equiv. relative to the resin loading) was first dispensed in the pre-activation vessel (PV), followed by the addition of Fmoc-$Q^{Pho(OtBu)2}$-OH (3 equiv.), PPh_3 (8 equiv.) and lastly the TCAN (9 equiv.) solution. Acid chloride activation was performed for 1 min in the PV.[7] The solution was then dispensed to the RV containing the resin-bound amine tetramer (PV to RV step). Coupling was performed under heat induction at 50 °C for 15 min. After resin filtration and washing twice with dry THF, the same procedure was repeated once.

After TBAF deprotection of the silyl ether, TFA cleavage, lyophilisation and purification by preparative RP-HPLC in acidic conditions, compound **4** was obtained as a yellow powder in 39% yield (16.7 mg, 11.6 µmol).

^{1}H-NMR (500 MHz, DMSO-d_6): δ = 11.57 (s, 3H), 11.41 (s, 1H), 9.58 (s, 1H), 8.57 – 8.20 (m, 2H), 8.17 – 7.50 (m, 16H), 7.42 (t, *J* = 7.9 Hz, 1H), 7.37 – 7.14 (m, 4H), 6.85 – 6.47 (m, 3H), 4.75 – 4.24 (m, 5H), 4.14 (s, 3H), 4.05 (s, 1H), 2.70 (s, 10H).

HRMS (ESI⁺): *m/z* calculated for $C_{66}H_{65}N_{11}O_{23}P_2$ 1442.3803 $[M+H]^+$; found 1442.3383 $[M+H]^+$.

7.4.4.3. Synthesis of 5

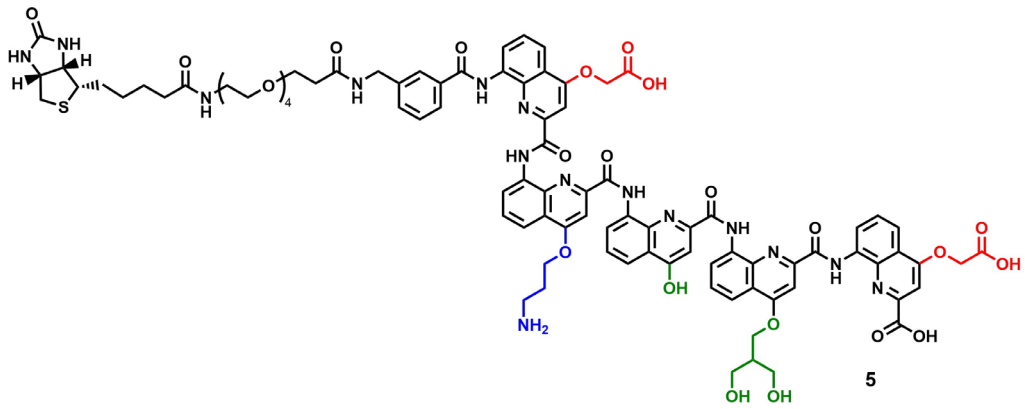

Compound 5: Oligomer **5** was synthesised on LL-Wang resin (20 µmol scale) using the automated conditions. Biotin linker was added using the conditions mentioned before. After TBAF deprotection of the silyl ether, TFA cleavage, lyophilisation and purification by preparative RP-HPLC, compound **5** was obtained as a yellow powder in 39% yield (14.2 mg, 7.82 µmol).

^{1}H-NMR (500 MHz, CD_3CN/H_2O (1:1, v/v)): δ = 11.26 – 11.15 (m, 2H), 11.05 (s, 1H), 10.99 (s, 1H), 9.46 (s, 1H), 8.02 – 7.93 (m, 2H), 7.88 (d, *J* = 9.0 Hz, 1H), 7.75 (d, *J* = 9.1 Hz, 3H), 7.59 – 7.66 (m, 1H), 7.54 – 7.37 (m, 3H), 7.31 (t, *J* = 8.3 Hz, 1H), 7.22 (t, *J* = 8.5 Hz, 1H), 7.11 (t, *J* = 8.3 Hz, 1H), 7.03 (s, 1H), 6.94 – 6.87 (m, 4H), 6.85 (s, 1H), 6.48 (t, *J* = 8.1 Hz, 1H), 6.42 (s, 1H), 6.16 (s, 1H), 6.02 (s, 2H), 5.01 (d, *J* = 15.6 Hz, 1H), 4.94 (d, *J* = 15.3 Hz, 1H), 3.82 (d, *J* = 6.8 Hz, 1H), 3.56 – 3.48 (m, 1H), 3.49 -3.21 (m, 18H), 3.13 (q, *J* = 5.6 Hz, 3H), 3.09 – 2.97 (m, 2H), 2.74 (dd, *J* = 5.0, 2.3 Hz, 1H), 2.55 (dd, *J* = 13.1, 3.5 Hz, 2H), 2.45 – 2.36 (m, 4H), 2.29 - 2.19 (m 4H), 2.03 – 1.96 (m, 2H), 1.54 – 1.44 (m, 1H), 1.42 – 1.34 (m, 5H), 1.22 – 1.10 (m, 5H).

HRMS (ESI$^+$): *m/z* calculated for $C_{90}H_{94}N_{15}O_{25}S_1$1816.6261 $[M+H]^+$; found 1816.6172 $[M+H]^+$.

7.4.4.4. Synthesis of 6

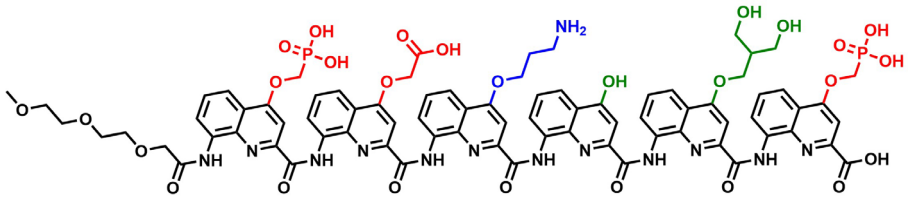

6

Compound 6: Oligomer **6** was synthesised on LL-Wang resin (15 µmol scale) using the automated SPFS procedure. Coupling of the final aromatic monomer, Fmoc-Q$^{Pho(OtBu)2}$-OH, was carried out using a distinct protocol due to its acid sensitivity. The collidine solution in dry THF (9 equiv. relative to the resin loading) was first dispensed in the pre-activation vessel (PV), followed by the addition of Fmoc-Q$^{Pho(OtBu)2}$-OH (3 equiv.), PPh_3 (8 equiv.) and lastly the TCAN (9 equiv.) solution. Acid chloride activation was performed for 1 min in the PV.[7] The solution was then dispensed to the RV containing the resin-bound amine tetramer (PV to RV step). Coupling was performed under heat induction at 50 °C for 15 min. After resin filtration and washing twice with dry THF, the same procedure was repeated once.

After TBAF deprotection of the silyl ether, TFA cleavage, lyophilisation and purification by preparative RP-HPLC in acidic conditions, compound **6** was obtained as a yellow powder in 24% yield (6.0 mg, 3.56 µmol).

^{1}H-NMR (500 MHz, 12.5 mM NH_4OAc pH = 8.5/D_2O (9:1, v/v)): δ = 11.20 (s, 1H), 11.08 (s, 1H), 10.93 (s, 1H), 10.86 (s, 1H), 10.62 (s, 1H), 9.31 (s, 1H), 7.98 (d, *J* = 8.9 Hz, 1H), 7.77 (d, *J* = 8.8 Hz, 1H), 7.72 (d, *J* = 9.0 Hz, 1H), 7.65 (d, *J* = 9.0 Hz, 2H), 7.58 – 7.46 (m, 4H), 7.43 – 7.36 (m, 1H), 7.34 – 7.23 (m, 2H), 7.20 – 6.98 (m, 2H), 6.90 (s, 1H), 6.87 (s, 1H), 6.42 (s, 1H), 5.97 (s, 1H), 5.72 (s, 1H), 4.33 – 4.21 (m, 1H), 4.19 – 4.12 (m, 1H), 3.98 – 3.91 (m, 5H), 3.83 (t, *J* = 10.9 Hz, 1H), 3.65 (s, 1H), 3.58 (s, 1H), 3.45 (q, *J* = 8.6 Hz, 2H), 3.22 – 3.10 (m, 3H), 2.75 – 2.65 (m, 1H), 2.60 (s, 4H), 2.56 – 2.47(m, 5H), 2.46 – 2.20 (m, 2H), 2.13 (s, 1H), 1.40 (s, 1H).

HRMS (ESI$^-$): *m/z* calculated for $C_{78}H_{73}N_{13}O_{27}P_2$ 1684.4141 $[M-H]^-$; found 1741.6471 $[M-H]^-$.

7.4.4.5. Synthesis of 7

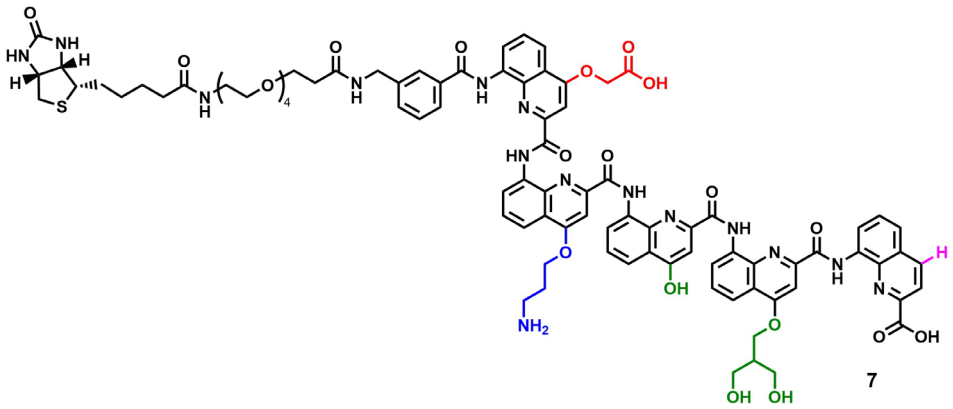

7

Compound 7: Oligomer **7** was synthesised on LL-Wang resin (20 μmol scale) using the automated conditions. Biotin linker was added using the conditions mentioned before. After TFA cleavage, lyophilisation and purification by preparative RP-HPLC, compound **7** was obtained as a yellow powder in 15% yield (5.0 mg, 2.9 μmol).

^{1}H-NMR (500 MHz, CD_3CN/H_2O (1:1, v/v)): δ = 11.71 (s, 1H), 11.56 (s, 2H), 11.34 (s, 1H), 9.76 (s, 1H), 8.41 (s, 1H), 8.33 (d, *J* = 15.2 Hz, 1H), 8.06 (d, *J* = 9.5 Hz, 1H), 8.01 – 7.86 (m, 5H), 7.72 (d, *J* = 8.5 Hz, 2H), 7.68 – 7.53 (m, 4H), 7.48 (s, 1H), 7.40 (t, *J* = 8.6 Hz, 1H), 7.29 – 7.00 (m, 8H), 6.67 (s, 3H), 6.61 (s, 1H), 6.48 – 6.37 (m, 1H), 4.97 (d, *J* = 14.6 Hz, 1H), 4.84 (d, *J* = 13.9 Hz, 1H), 3.55 (s, 2H), 3.47 – 3.29 (m, 15H), 2.49 (s, 3H), 2.37 (s, 2H), 2.26 (s, 2H), 1.48 (s, 6H), 1.28 – 1.11 (m, 13H), 0.83 – 0.78 (m, 2H).

HRMS (ESI$^-$): *m/z* calculated for $C_{68}H_{91}N_{15}O_{22}S$ 1741.6141 $[M-H]^-$; found 1741.6471 $[M-H]^-$.

7.4.4.6. Synthesis of 8

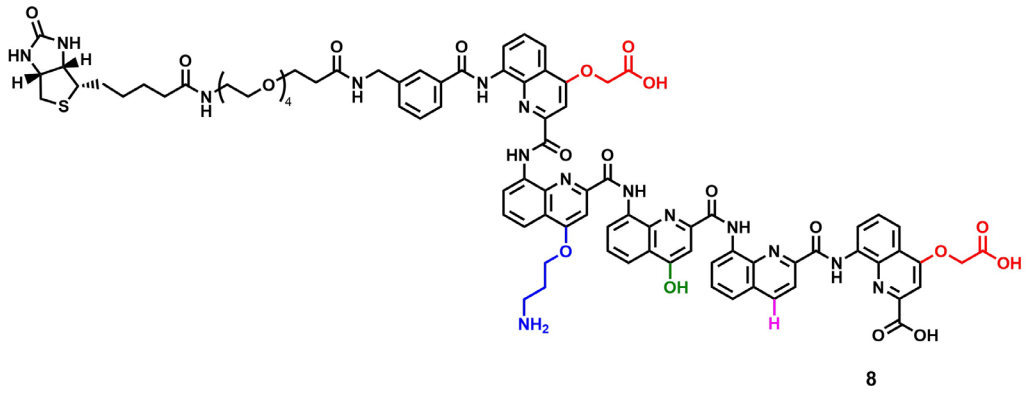

8

Compound 8: Oligomer **8** was synthesised on LL-Wang resin (20 μmol scale) using the automated conditions. Biotin linker was added using the conditions mentioned before. After TFA cleavage, lyophilisation and purification by preparative RP-HPLC, compound **8** was obtained as a yellow powder in 17% yield (5.7 mg, 3.3 μmol).

^{1}H-NMR (500 MHz, CD_3CN/H_2O (1:1, v/v)): δ = 11.60 (s, 1H), 11.55 (s, 2H), 11.41 (s, 1H), 11.30 (s, 1H), 9.74 (s, 1H), 8.44 (s, 1H), 8.29 (s, 1H), 8.11 (s, 1H), 8.05 (d, J = 9.5 Hz, 1H), 7.96 (d, J = 9.3 Hz, 1H), 7.90 (d, J = 9.5 Hz, 1H), 7.85 – 7.69 (m, 2H), 7.63 (d, J = 8.1 Hz, 2H), 7.45 – 7.36 (m, 1H), 7.29 (t, J = 8.3 Hz, 1H), 7.22 (d, J = 14.5 Hz, 2H), 7.10 (s, 1H), 7.08 – 7.00 (m, 2H), 6.63 (s, 2H), 6.34 (s, 1H), 5.02 (d, J = 14.8 Hz, 1H), 4.90 (d, J = 14.5 Hz, 1H), 3.56 (s, 1H), 3.47 – 3.33 (m, 6H), 2.48 (s, 3H), 2.35 (s, 2H), 2.28 (t, J = 6.4 Hz, 1H), 2.17 (s, 4H), 1.61 – 1.29 (m, 10H), 1.26 – 1.18 (m, 1H).

HRMS (ESI$^+$): *m/z* calculated for $C_{86}H_{85}N_{15}O_{22}S$ 1713.5817 $[M+H]^+$; found 1713.5721 $[M+H]^+$.

7.4.4.7. Synthesis of 9

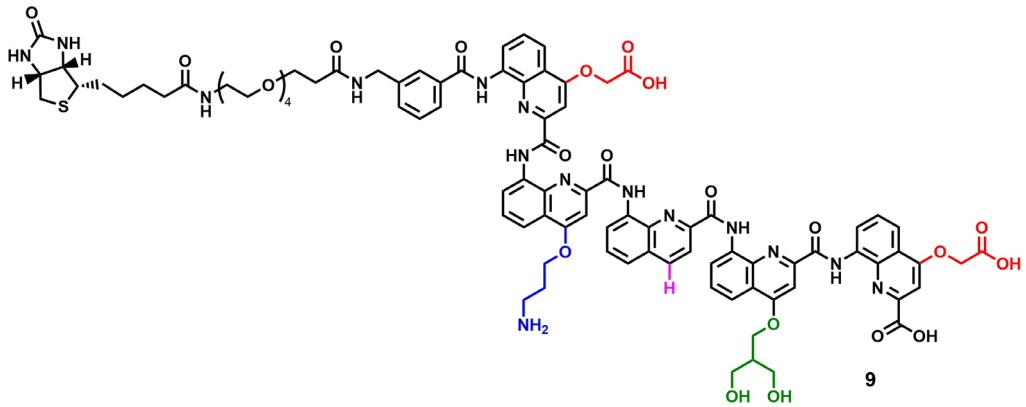

9

Compound 9: Oligomer **9** was synthesised on LL-Wang resin (20 μmol scale) using the automated conditions. Biotin linker was added using the conditions mentioned before. After

TFA cleavage, lyophilisation and purification by preparative RP-HPLC, compound **9** was obtained as a yellow powder in 19% yield (6.8 mg, 3.8 µmol).

^{1}H-NMR (500 MHz, CD_3CN/H_2O (1:1, v/v)): δ =11.24 (s, 2H), 11.04 (s, 1H), 9.53 (s, 1H), 8.04 (d, *J* = 9.3 Hz, 2H), 7.91 (d, *J* = 9.0 Hz, 1H), 7.82 – 7.73 (m, 5H), 7.70 – 7.48 (m, 9H), 7.44 (s, 1H), 7.27 (t, *J* = 8.2 Hz, 3H), 7.18 (d, *J* = 9.4 Hz, 1H), 7.06 (s, 2H), 6.96 – 6.86 (m, 4H), 6.52 (s, 1H), 6.10 (s, 1H), 6.03 (s, 1H), 4.94 (d, *J* = 15.2 Hz, 1H), 4.86 (d, *J* = 15.1 Hz, 1H), 3.81 (s, 1H), 3.62 (s, 1H), 3.57 – 3.48 (m, 2H), 3.46 – 3.30 (m, 9H), 3.19 – 3.10 (m, 1H), 3.09 – 2.94 (m, 1H), 2.76 – 2.69 (m, 1H), 2.54 (dd, *J* = 13.0, 3.2 Hz, 1H), 2.41 (s, 4H), 2.27 – 2.22 (m, 6H), 1.99 (s, 1H), 1.70 – 1.64 (m, 1H), 1.55 – 1.28 (m, 1H), 1.24 – 1.10 (m, 2H).

HRMS (ESI$^+$): *m/z* calculated for $C_{90}H_{93}N_{15}O_{24}S$ 1801.6342 $[M+H]^+$; found 1801.6102 $[M+H]^+$.

7.4.4.8. Synthesis of 10

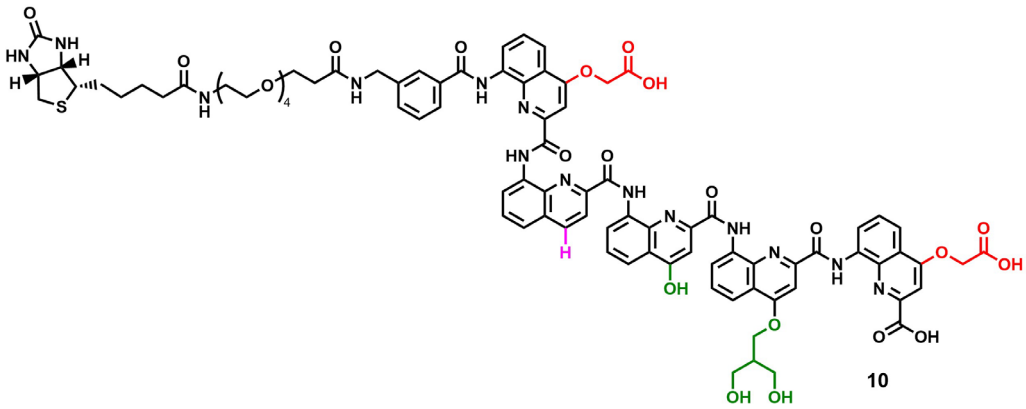

10

Compound 10: Oligomer **10** was synthesised on LL-Wang resin (20 µmol scale) using the automated conditions. Biotin linker was added using the conditions mentioned before. After TFA cleavage, lyophilisation and purification by preparative RP-HPLC, compound **10** was obtained as a yellow powder in 14% yield (4.8 mg, 2.8 µmol).

^{1}H-NMR (500 MHz, CD_3CN/H_2O (1:1, v/v)): δ = 11.64 (s, 2H), 11.50 (s, 2H), 8.81 (s, 1H), 8.55 (d, *J* = 9.3 Hz, 1H), 8.33 (s, 2H), 8.05 – 7.90 (m, 5H), 7.83 (s, 1H), 7.80 – 7.62 (m, 10H), 7.57 – 7.43 (m, 3H), 7.41 – 7.14 (m, 5H), 7.11 – 6.96 (m, 1H), 6.58 (s, 1H), 6.34 (s, 1H), 4.94 (d, *J* = 14.2 Hz, 1H), 4.84 (t, *J* = 15.7 Hz, 1H), 3.63 – 3.51 (m, 2H), 3.50 – 3.31 (m, 11H), 3.16 (s, 1H), 2.88 (s, 1H), 2.40 – 2.24 (m, 4H), 1.47 (s, 2H), 1.35 (s, 3H), 1.22 – 1.09 (m, 3H).

HRMS (ESI$^+$): *m/z* calculated for $C_{87}H_{86}N_{14}O_{24}S$ 1744.5763 $[M+H]^+$; found 1743.5733 $[M+H]^+$.

7.4.4.9. Synthesis of 11

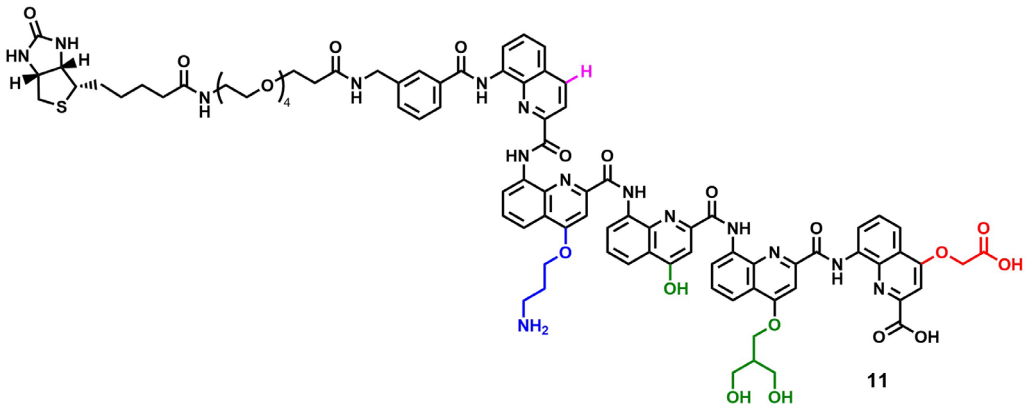

Compound 11: Oligomer **11** was synthesised on LL-Wang resin (20 μmol scale) using the automated conditions. Biotin linker was added using the conditions mentioned before. After TFA cleavage, lyophilisation and purification by preparative RP-HPLC, compound **11** was obtained as a yellow powder in 13% yield (4.6 mg, 2.6 μmol).

^{1}H-NMR (500 MHz, CD_3CN/H_2O (1:1, v/v)): δ = 11.35 (s, 2H), 11.23 (s, 1H), 11.14 (s, 1H), 9.61 (s, 1H), 8.48 (d, *J* = 9.1 Hz, 1H), 8.08 (s, 1H), 7.96 – 7.80 (m, 4H), 7.80 – 7.68 (m, 6H), 7.68 – 7.58 (m, 3H), 7.59 – 7.46 (m, 4H), 7.41 (t, *J* = 8.3 Hz, 1H), 7.32 (s, 1H), 7.13 – 6.91 (m, 5H), 6.59 (s, 1H), 6.50 (s, 1H), 6.15 – 5.93 (m, 1H), 3.59 – 3.46 (m, 2H), 3.46 – 3.30 (m, 23H), 2.45 (s, 3H), 2.32 (s, 3H), 2.25 (t, *J* = 6.3 Hz, 2H), 2.17 (s, 3H), 1.72 – 1.65 (m, 1H), 1.54 – 1.44 (m, 1H), 1.43 – 1.33 (m, 1H), 1.24 – 1.19 (m, 2H).

HRMS (ESI$^+$): *m/z* calculated for $C_{88}H_{91}N_{15}O_{22}S$ 1743.6287 $[M+H]^+$; found 1743.6409 $[M+H]^+$.

7.4.4.10. Synthesis of 12

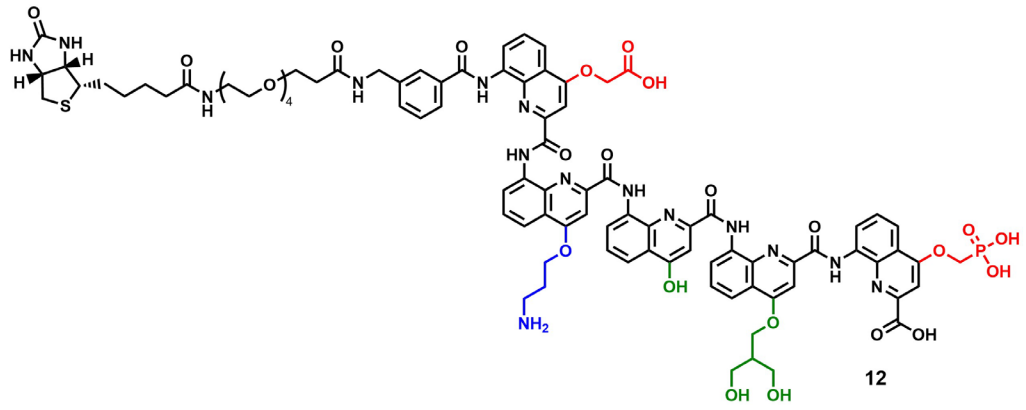

Compound 12: Oligomer **12** was synthesised on LL-Wang resin (20 μmol scale) using the automated conditions and sensitive activation conditions. Biotin linker was added using the conditions mentioned before. After TFA cleavage, lyophilisation and purification by preparative RP-HPLC, compound **12** was obtained as a yellow powder in 21% yield (7.7 mg, 4.2 μmol).

^{1}H-NMR (500 MHz, CD_3CN/H_2O (1:1, v/v)): δ = 11.60 – 11.30 (m, 2H), 11.17 (s, 1H), 9.68 (s, 2H), 8.26 (s, 1H), 8.15 (s, 1H), 8.02 (d, *J* = 9.1 Hz, 1H), 7.95 – 7.62 (m, 2H), 7.60 (s, 1H), 7.51 (s, 2H), 7.38 (t, *J* = 8.8 Hz, 2H), 7.27 (s, 1H), 7.17 (s, 1H), 7.13 – 6.88 (m, 7H), 6.63 (s, 1H), 6.55 (s, 1H), 6.42 (s, 1H), 6.32 (s, 1H), 6.04 (s, 1H), 5.99 (s, 1H), 4.95 (d, *J* = 14.9 Hz, 1H), 4.82 (d, *J* = 13.9 Hz, 1H), 3.86 (s, 1H), 3.54 – 3.49 (m, 4H), 3.45 – 3.25 (m, 20H), 3.15 – 2.95 (m, 11H), 2.72 (dd, *J* = 13.5, 4.9 Hz, 1H), 2.57 – 2.51 (m, 1H), 2.46 (s, 4H), 2.34 (s, 3H), 2.23 (t, *J* = 6.4 Hz, 3H), 1.48 (s, 1H), 1.40 – 1.33 (m, 6H), 1.26 – 1.13(m, 18H).

HRMS (ESI$^-$): *m/z* calculated for $C_{89}H_{94}N_{15}O_{26}PS$ 1851.5910 $[M-H]^-$; found 1851.5406 $[M-H]^-$.

7.4.4.11. Synthesis of 13

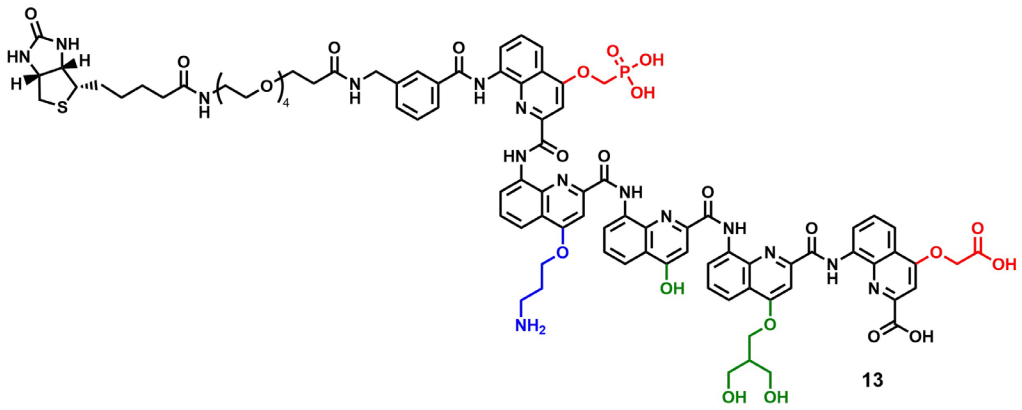

Compound 13: Oligomer **13** was synthesised on LL-Wang resin (20 µmol scale) using the automated conditions and sensitive activation conditions. Biotin linker was added using the conditions mentioned before. After TFA cleavage, lyophilisation and purification by preparative RP-HPLC, compound **13** was obtained as a yellow powder in 19% yield (7.1 mg, 3.8 µmol).

^{1}H-NMR (500 MHz, DMSO-d_6): δ = 12.13 (s, 1H), 11.64 (s, 1H), 11.57 – 11.47 (m, 2H), 11.32 (s, 1H), 9.64 (s, 1H), 8.52 – 8.35 (m, 2H), 8.15 – 7.86 (m, 11H), 7.86 – 7.76(m, 3H), 7.75 – 7.65 (m, 2H), 7.57 – 7.50 (m, 1H), 7.47 – 7.38 (m, 2H), 7.25 – 6.94 (m, 7H), 6.82 – 6.62 (m, 4H), 6.46 – 6.33 (m, 2H), 4.91 – 4.75 (m, 3H), 4.74 – 4.54 (m, 1H), 4.35 – 4.19 (m, 3H), 3.86 – 3.69 (m, 6H), 2.95 – 2.84 (m, 1H), 2.24 – 2.14 (m, 1H), 2.09 – 1.95 (m, 2H), 1.61 – 1.31 (m, 5H), 1.31 – 1.13 (m, 7H), 0.85 (t, J = 6.8 Hz, 1H).

HRMS (ESI$^-$): *m/z* calculated for $C_{89}H_{94}N_{15}O_{26}PS$ 1851.5910 $[M-H]^-$; found 1851.5664 $[M-H]^-$.

7.4.4.12. Synthesis of 14

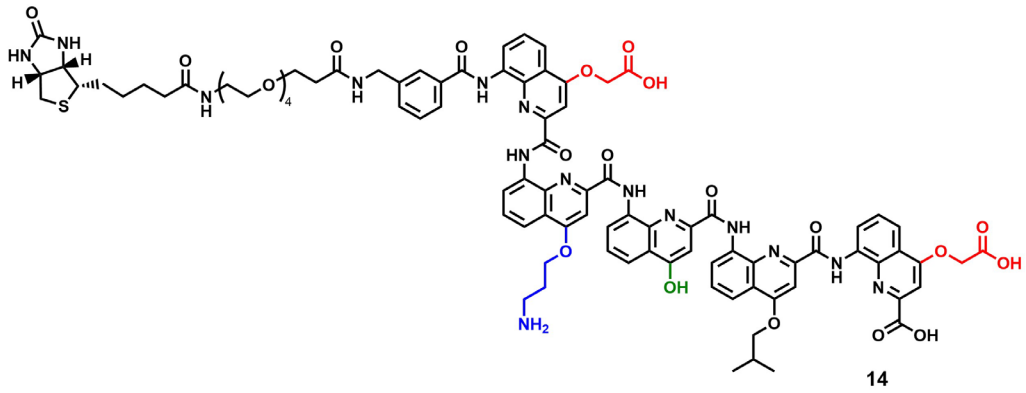

14

Compound 14: Oligomer **14** was synthesised on LL-Wang resin (20 µmol scale) using the automated conditions. Biotin linker was added using the conditions mentioned before. After TFA cleavage, lyophilisation and purification by preparative RP-HPLC, compound **14** was obtained as a yellow powder in 18% yield (6.2 mg, 3.5 µmol).

^{1}H-NMR (500 MHz, CD_3CN/H_2O (1:1, v/v)): δ = 11.49 (s, 1H), 11.37 (s, 1H), 11.28 (s, 1H), 11.18 (s, 1H), 9.62 (s, 1H), 8.25 – 8.17 (m, 2H), 8.00 (d, *J* = 8.9 Hz, 1H), 7.88 – 7.67 (m, 5H), 7.66 – 7.57 (m, 2H), 7.56 – 7.50 (m, 2H), 7.38 (t, *J* = 8.3 Hz, 1H), 7.22 (t, *J* = 8.2 Hz, 2H), 7.15 (s, 1H), 7.11 – 6.90 (m, 6H), 6.61 – 6.53 (m, 2H), 6.39 (s, 1H), 6.24 (s, 1H), 6.05 (s, 1H), 5.99 (s, 1H), 5.01 (d, *J* = 15.1 Hz, 1H), 4.89 (d, *J* = 14.7 Hz, 1H), 3.75 – 3.63 (m, 1H), 3.57 (t, *J* = 7.0 Hz, 1H), 3.45 – 3.32 (m, 12H), 3.20 – 3.13 (m, 2H), 3.10 – 3.00 (m, 1H), 2.77 (d, *J* = 5.0 Hz, 1H), 2.57 (d, *J* = 13.1 Hz, 1H), 2.51 – 2.39 (m, 3H), 2.29 (t, *J* = 6.2 Hz, 2H), 2.06- 1.98 (m, 2H), 1.57 – 1.32 (m, 2H), 1.31 – 1.03 (m, 13H).

HRMS (ESI$^-$): *m/z* calculated for $C_{90}H_{93}N_{15}O_{23}S$ 1783.6247 $[M-H]^-$; found 1783.5786 $[M-H]^-$.

7.4.4.13. Synthesis of 15

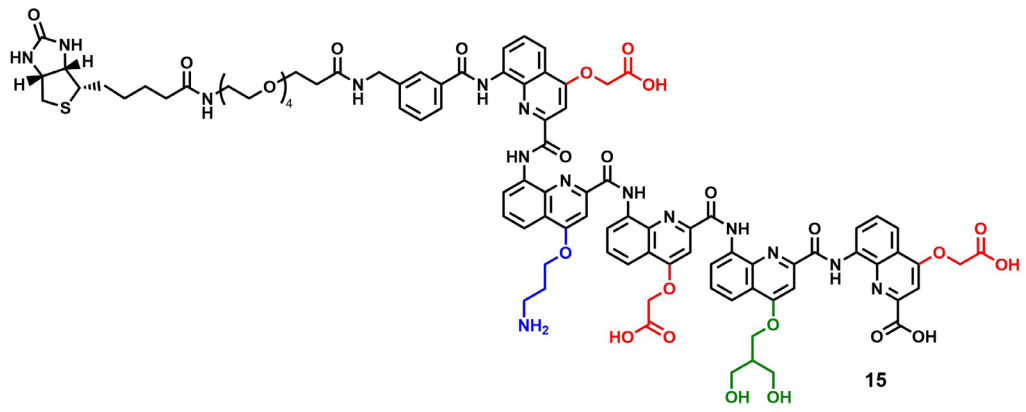

15

Compound 15: Oligomer **15** was synthesised on LL-Wang resin (20 µmol scale) using the automated conditions. Biotin linker was added using the conditions mentioned before. After

TFA cleavage, lyophilisation and purification by preparative RP-HPLC, compound **15** was obtained as a yellow powder in 17% yield (3.3 mg, 3.4 μmol).

^{1}H-NMR (500 MHz, DMSO-d_6): δ =11.56 (s, 1H), 11.50 (s, 2H), 9.73 (s, 1H), 8.53 – 8.35 (m, 4H), 8.06 – 8.01 (m, 2H), 7.98 – 7.85 (m, 6H), 7.83 – 7.73 (m, 4H), 7.54 (t, *J* = 8.1 Hz, 1H), 7.42 (t, *J* = 8.0 Hz, 1H), 7.25 (s, 2H), 7.21 – 7.14 (m, 4H), 7.03 (d, *J* = 7.7 Hz, 1H), 6.79 – 6.65 (m, 3H), 6.53 (s, 2H), 6.41 (s, 1H), 5.32 – 5.27 (m, 3H), 4.89 – 4.57 (m, 6H), 4.35 – 4.18 (m, 2H), 3.93 (s, 1H), 3.84 – 3.72 (m, 6H), 3.53 – 3.48 (m, 6H), 3.46 – 3.39 (m, 9H), 1.53 – 1.38 (m, 5H), 1.28 – 1.21 (m, 3H), 1.17 (t, *J* = 7.3 Hz, 1H).

HRMS (ESI$^-$): *m/z* calculated for $C_{92}H_{95}N_{15}O_{27}S$ 1873.6200 [M-H]$^-$; found 1873.6046 [M-H]$^-$.

7.4.4.14. Synthesis of 16

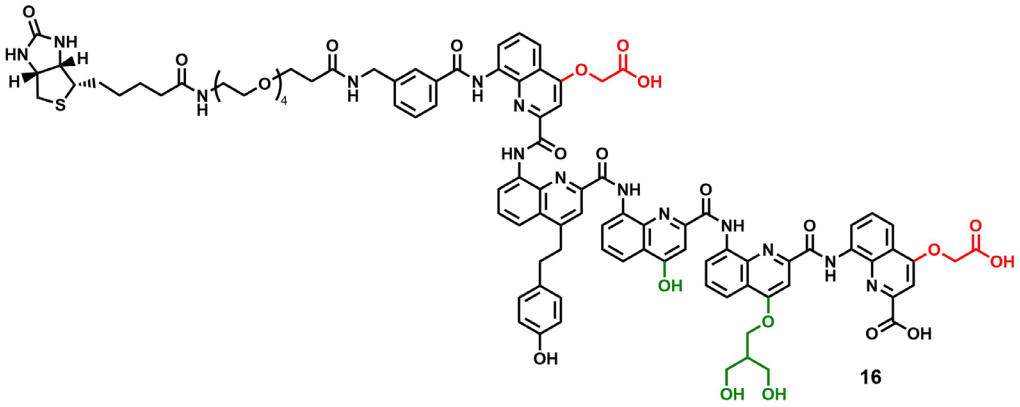

Compound 16: Oligomer **16** was synthesised on LL-Wang resin (20 μmol scale) using the automated conditions. Biotin linker was added using the conditions mentioned before. After TFA cleavage, lyophilisation and purification by preparative RP-HPLC, compound **17** was obtained as a yellow powder in 16% yield (5.9 mg, 3.2 μmol).

^{1}H-NMR (500 MHz, CD_3CN/H_2O (1:1, v/v)): δ = 11.63 (s, 2H), 11.38 (s, 1H), 11.22 (s, 1H), 9.76 (s, 1H), 8.44 (s, 1H), 8.24 (s, 1H), 8.04 (d, *J* = 8.9 Hz, 1H), 7.95 (d, *J* = 9.6 Hz, 3H), 7.87 (d, *J* = 8.2 Hz, 1H), 7.79 – 7.67 (m, 4H), 7.57 – 7.50 (m, 1H), 7.43 – 7.35 (m, 2H), 7.27 (d, *J* = 8.4 Hz, 1H), 7.25 – 7.18 (m, 4H), 7.14 (s, 1H), 7.02 (d, *J* = 8.5 Hz, 1H), 6.87 (d, *J* = 8.5 Hz, 1H), 6.79 (d, *J* = 8.8 Hz, 3H), 6.69 (s, 1H), 6.62 (s, 1H), 6.32 (s, 1H), 6.21 (t, *J* = 8.1 Hz, 1H), 6.02 (s, 1H), 4.98 (d, *J* = 14.7 Hz, 1H), 4.85 (d, *J* = 14.1 Hz, 1H), 3.51 (s, 2H), 3.48 – 3.42 (m, 6H), 3.37 (t, *J* = 5.5 Hz, 1H), 3.23 – 3.14 (m, 2H), 3.10 – 3.02 (m, 10H), 2.57 – 2.51 (m, 1H), 2.43 – 2.34 (m, 5H), 1.49 – 1.45 (s, 2H), 1.42 – 1.34 (m, 1H), 1.26 – 1.13 (m, 23H).

HRMS (ESI$^-$): *m/z* calculated for $C_{95}H_{94}N_{14}O_{25}S$ 1862.6193 [M-H]$^-$; found 1862.6049 [M-H]$^-$.

7.4.4.15. Synthesis of 17

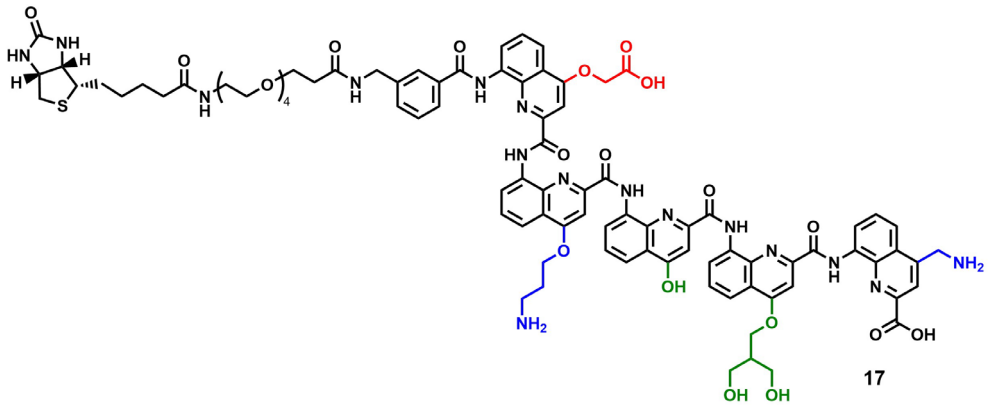

Compound 17: Oligomer **17** was synthesised on LL-Wang resin (20 µmol scale) using the automated conditions. Biotin linker was added using the conditions mentioned before. After TFA cleavage, lyophilisation and purification by preparative RP-HPLC, compound **17** was obtained as a yellow powder in 18% yield (6.4 mg, 3.6 µmol)

^{1}H-NMR (500 MHz, DMSO-d_6): δ = 13.59 (s, 1H), 12.34 (s, 1H), 11.69 (s, 1H), 11.65 – 11.51 (m, 1H), 11.44 (s, 1H), 11.34 (s, 1H), 9.63 (s, 1H), 8.65 – 8.43 (m, 2H), 8.35 – 8.20 (m, 2H), 8.08 – 7.77 (m, 8H), 7.69 (d, *J* = 8.2 Hz, 1H), 7.56 (t, *J* = 7.9 Hz, 1H), 7.44 (t, *J* = 8.1 Hz, 1H), 7.28 (s, 1H), 7.24 (s, 1H), 7.20 – 7.12 (m, 2H), 7.11 – 7.06 (m, 2H), 7.01 (d, *J* = 7.5 Hz, 1H), 6.78 – 6.64 (m, 5H), 6.41 – 6.34 (m, 1H), 5.35 – 5.23 (m, 3H), 4.86 – 4.76 (m, 2H), 4.75 – 4.69 (m, 1H), 4.67 – 4.69 (m, 2H), 4.33 – 4.19 (m, 4H), 4.14 – 4.07 (m, 1H), 3.85 – 3.72 (m, 4H), 3.69 – 3.61 (m, 1H), 3.56 – 3.48 (m, 7H), 3.17 – 3.12 (m, 1H), 2.25 – 2.16 (m, 1H), 2.08 – 1.96 (m, 3H), 1.53 – 1.40 (m, 7H), 1.30 – 1.15 (m, 13H), 0.85 (t, *J* = 6.8 Hz, 2H).

HRMS (ESI$^-$): *m/z* calculated for $C_{89}H_{94}N_{16}O_{22}S$ 1770.6407 $[M-H]^-$; found 1770.6153 $[M-H]^-$.

7.4.5. Characterisation data

7.4.5.1. Compound 3

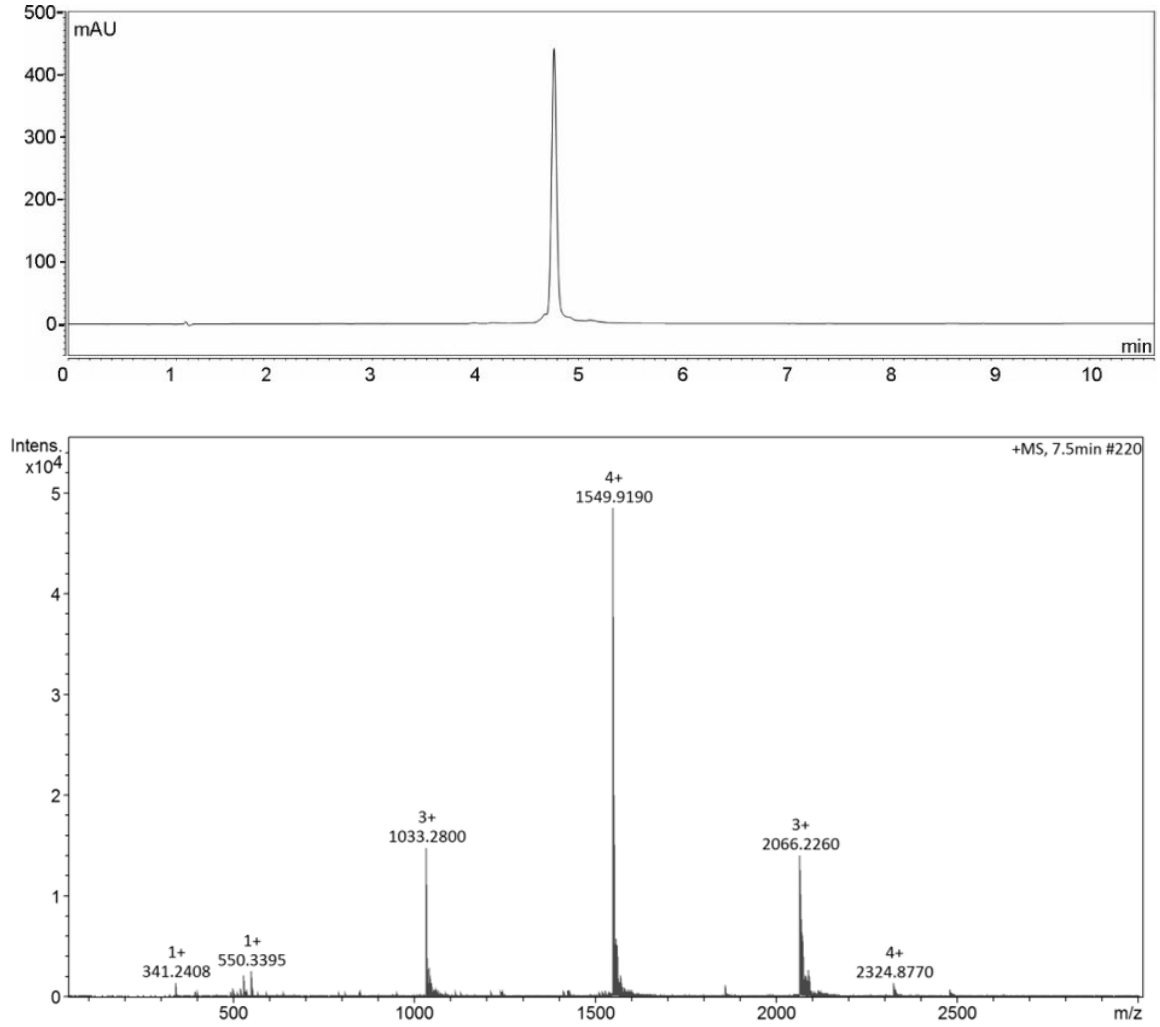

RP-HPLC chromatogram and ESI-MS spectrum of compound **3**.

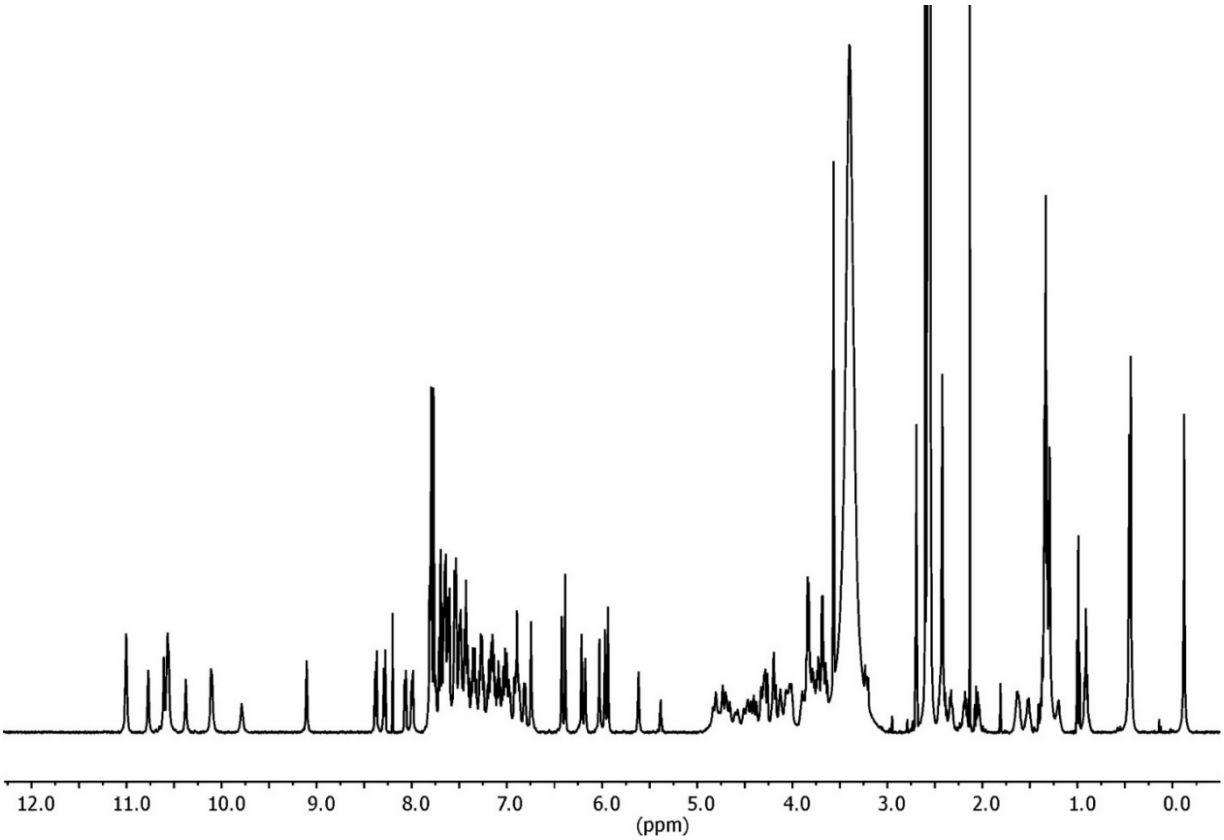

^{1}H-NMR spectrum (500 MHz, DMSO-d_6, 25 °C) of **3**.

7.4.5.2. Compound 4

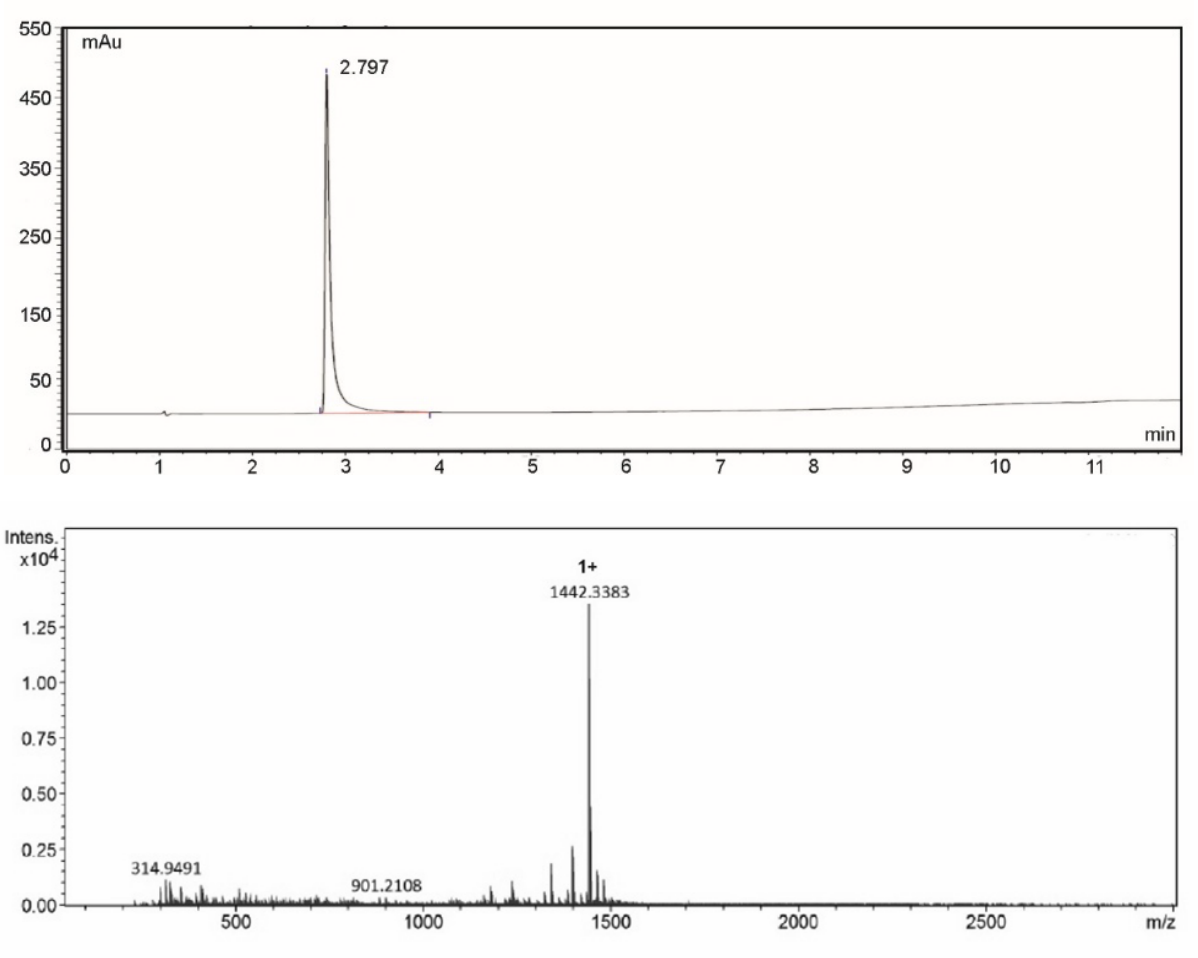

RP-HPLC chromatogram and ESI-MS spectrum of compound **4**.

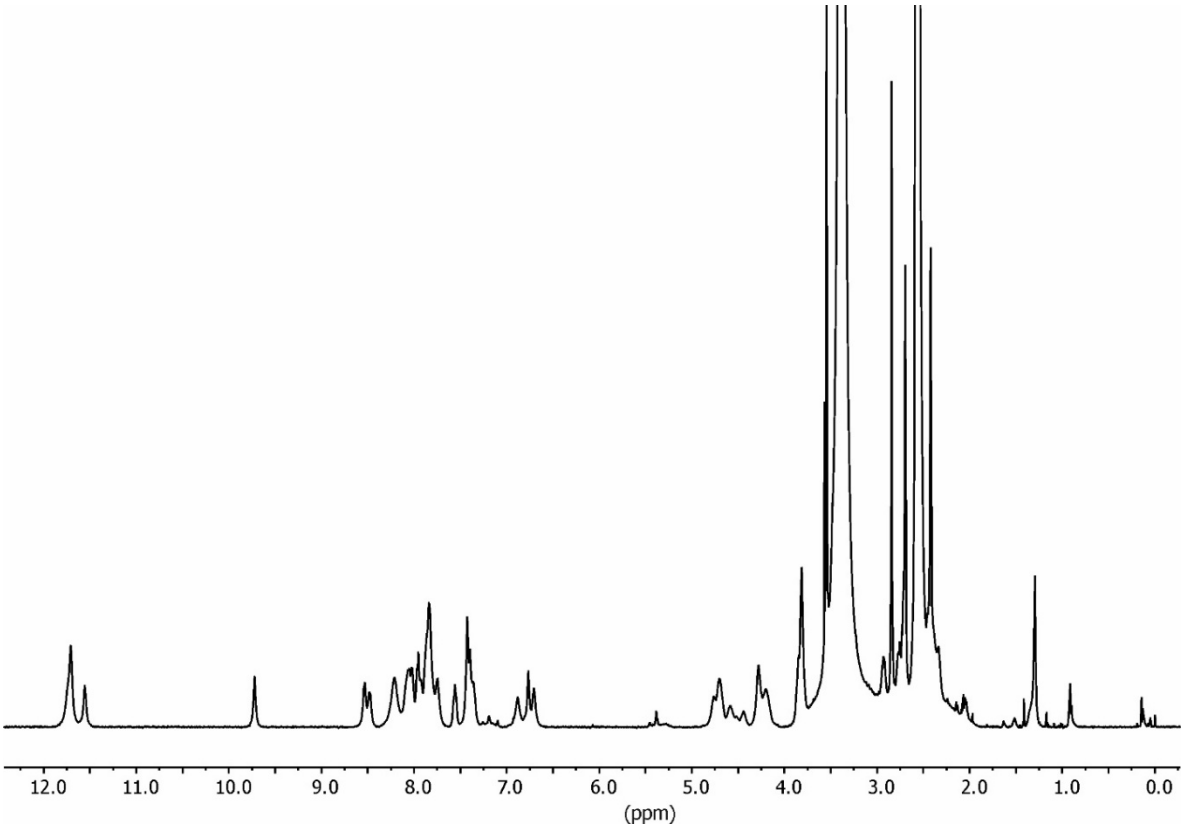

^{1}H-NMR spectrum (500 MHz, DMSO-d_6, 25 °C) of **4** after anion exchange.

7.4.5.3. Compound 5

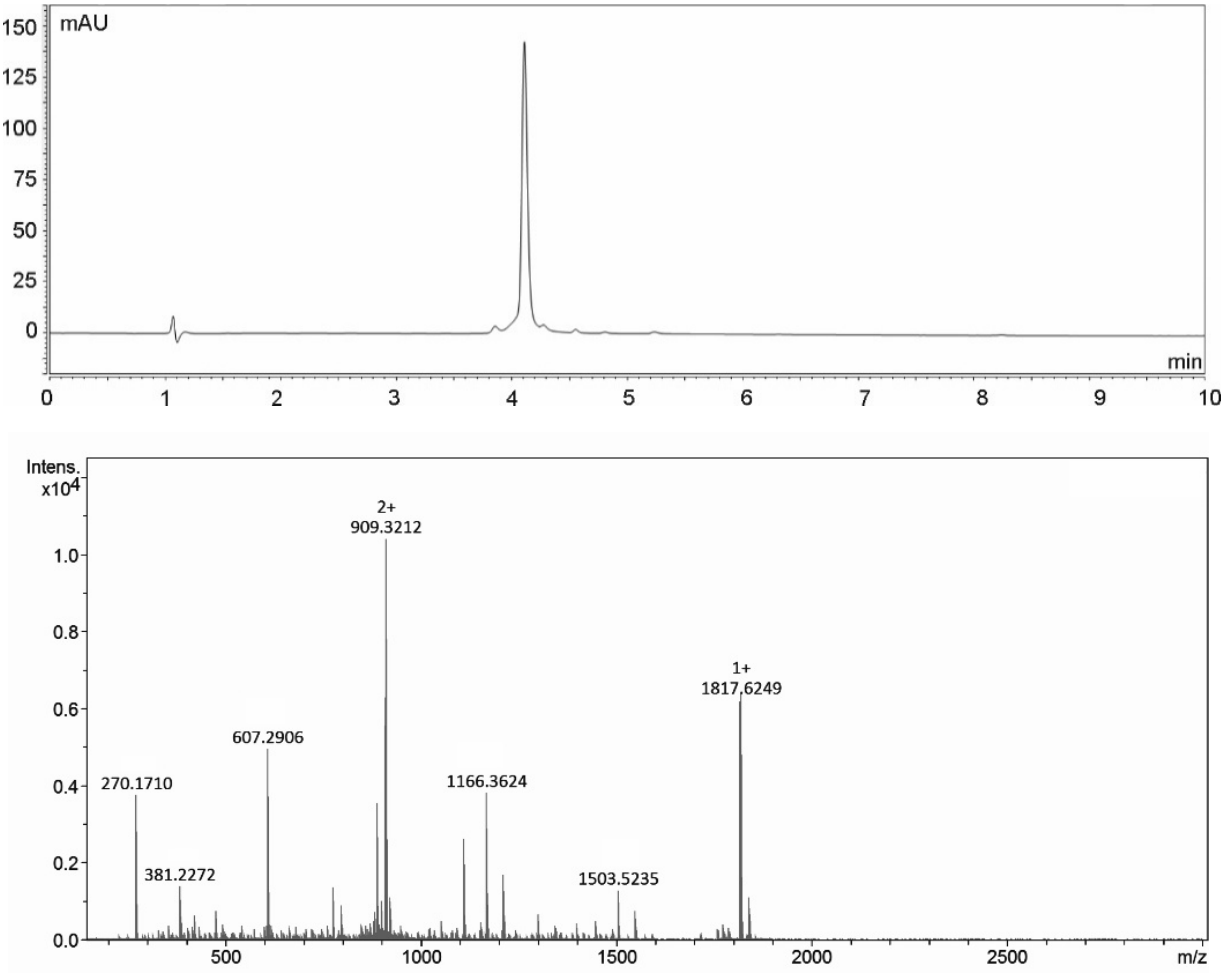

RP-HPLC chromatogram and ESI-MS spectrum of compound **5**.

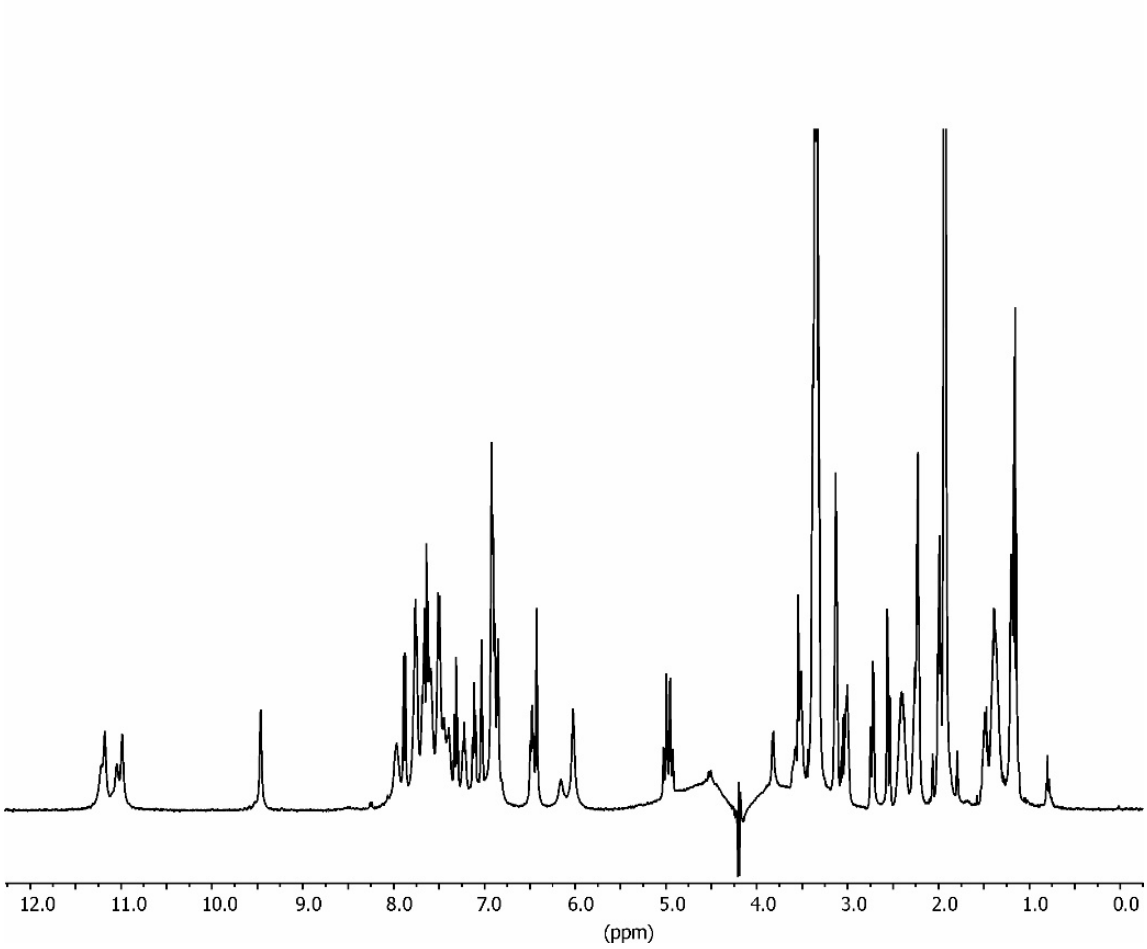

^{1}H-NMR spectrum (500 MHz, CD_3CN/H_2O, 25 °C) of **5**.

7.4.5.4. Compound 6

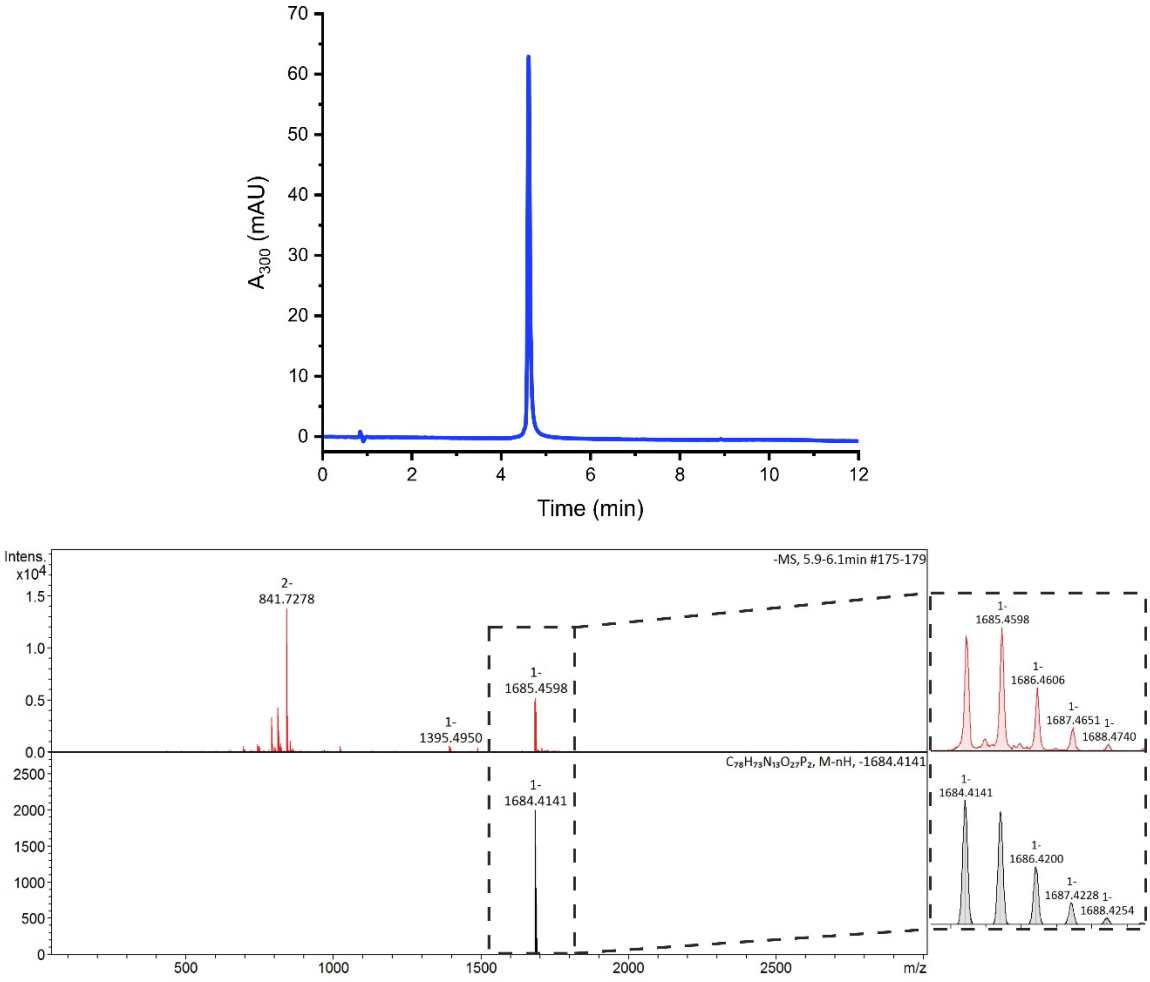

RP-HPLC chromatogram and ESI-MS spectrum of compound **6**.

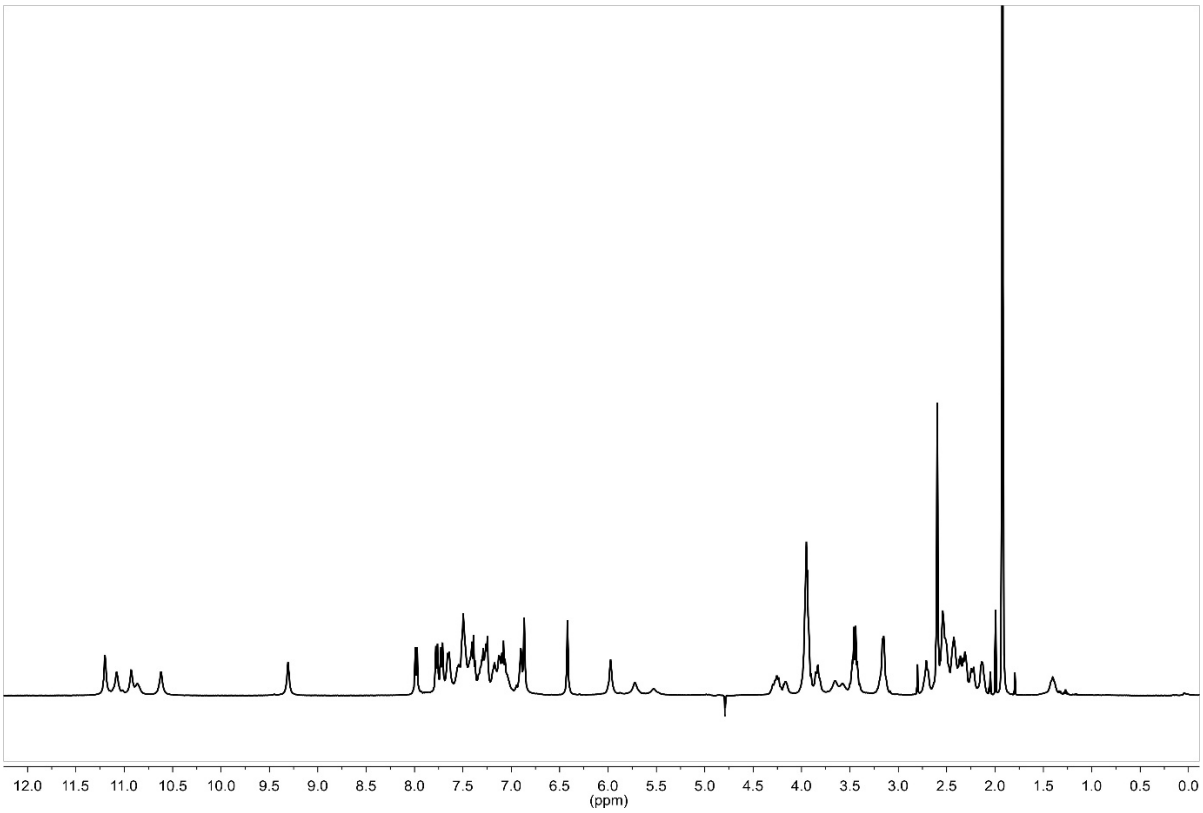

^{1}H-NMR spectrum (500 MHz, 12.5 mM NH_4OAc pH = 8.5/D_2O, 25 °C) of **6**.

7.4.5.5. Compound 7

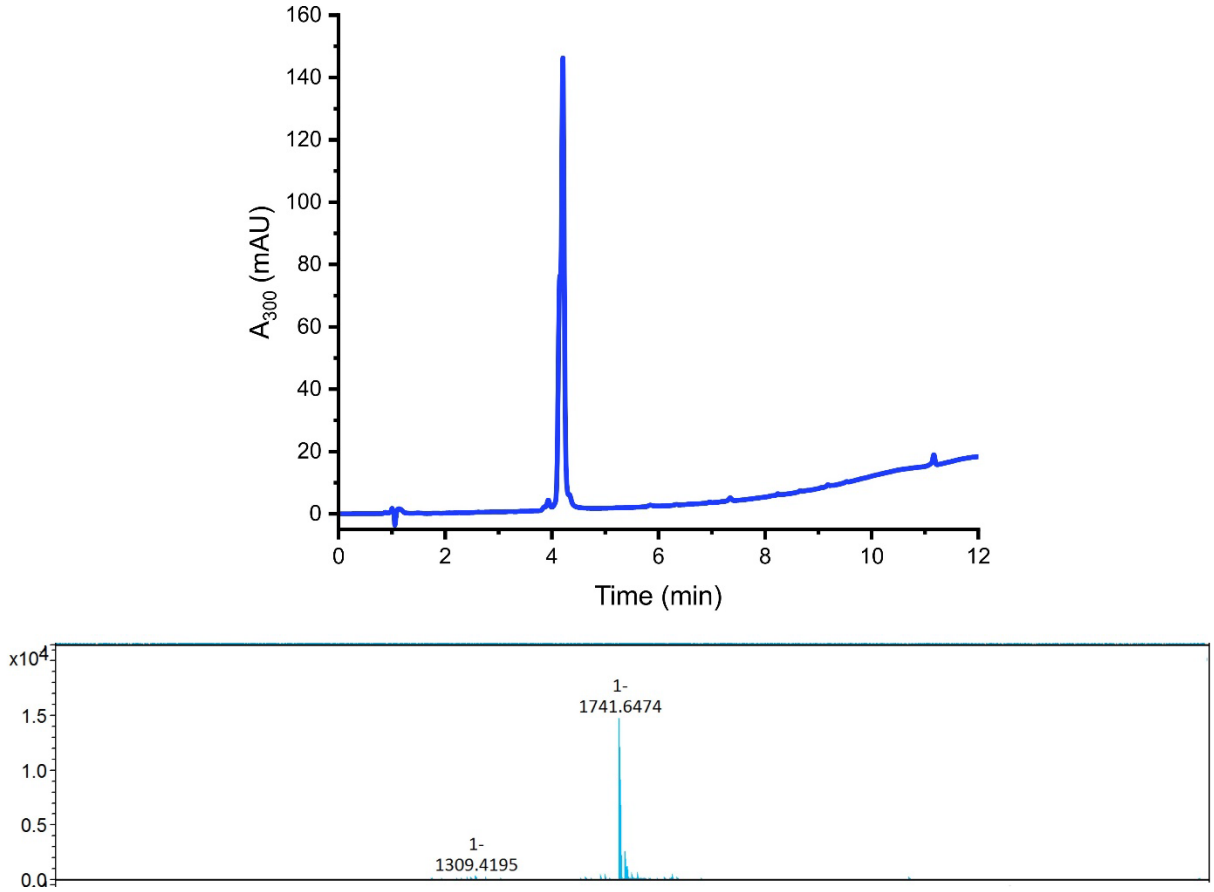

RP-HPLC chromatogram and ESI-MS spectrum of compound **7**.

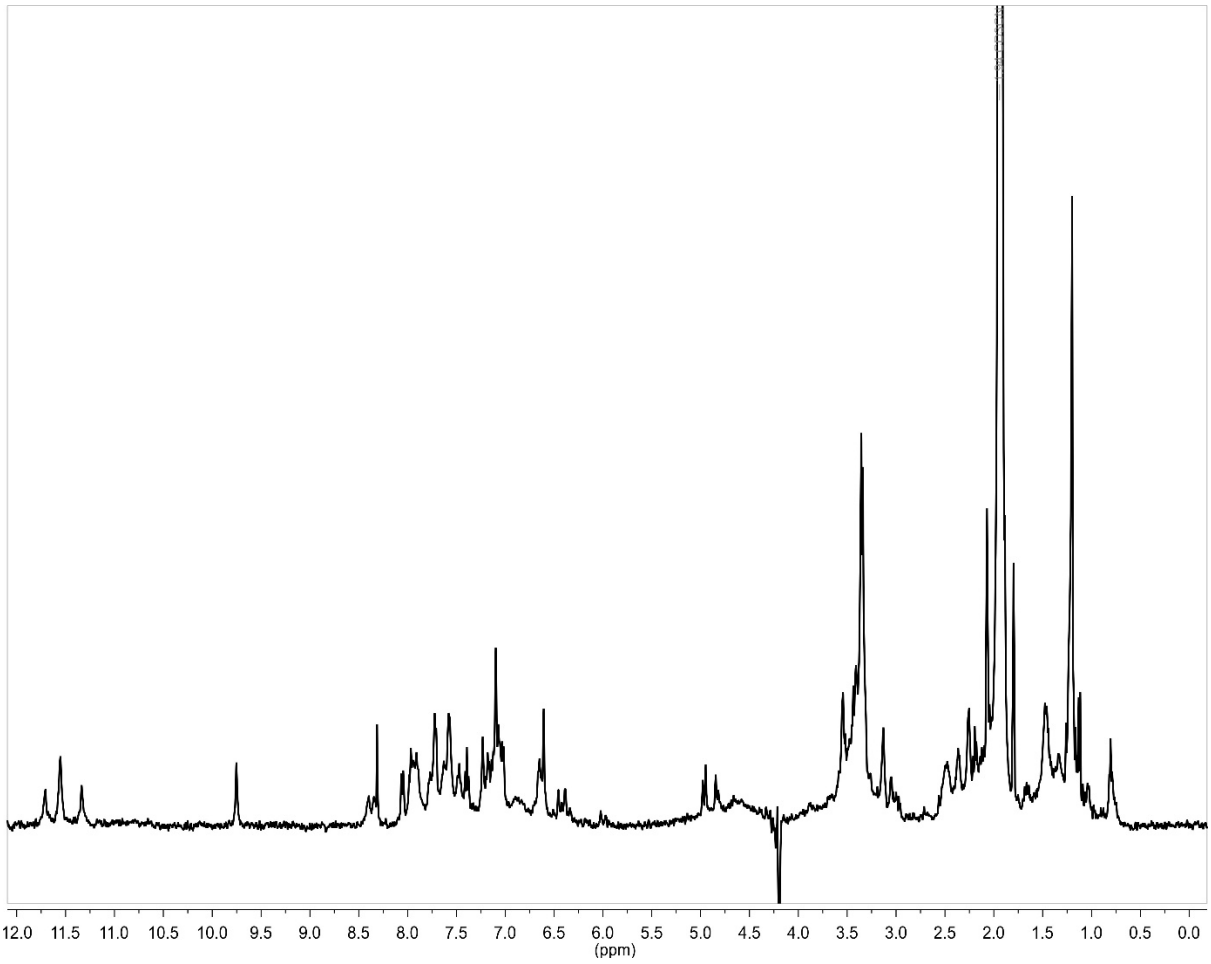

^{1}H-NMR spectrum (500 MHz, CD_3CN/H_2O, 25 °C) of **7**.

7.4.5.6. Compound 8

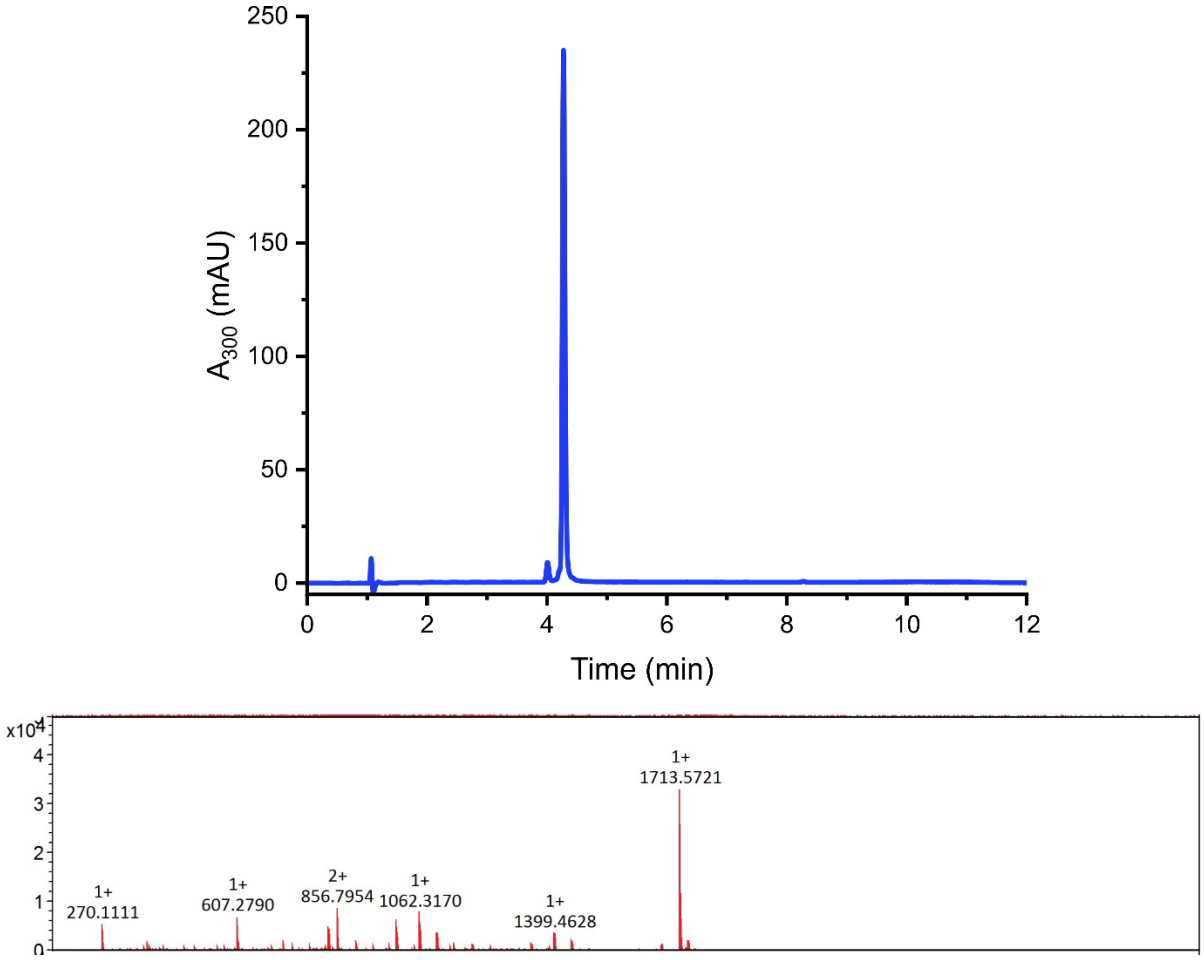

RP-HPLC chromatogram and ESI-MS spectrum of compound **8**.

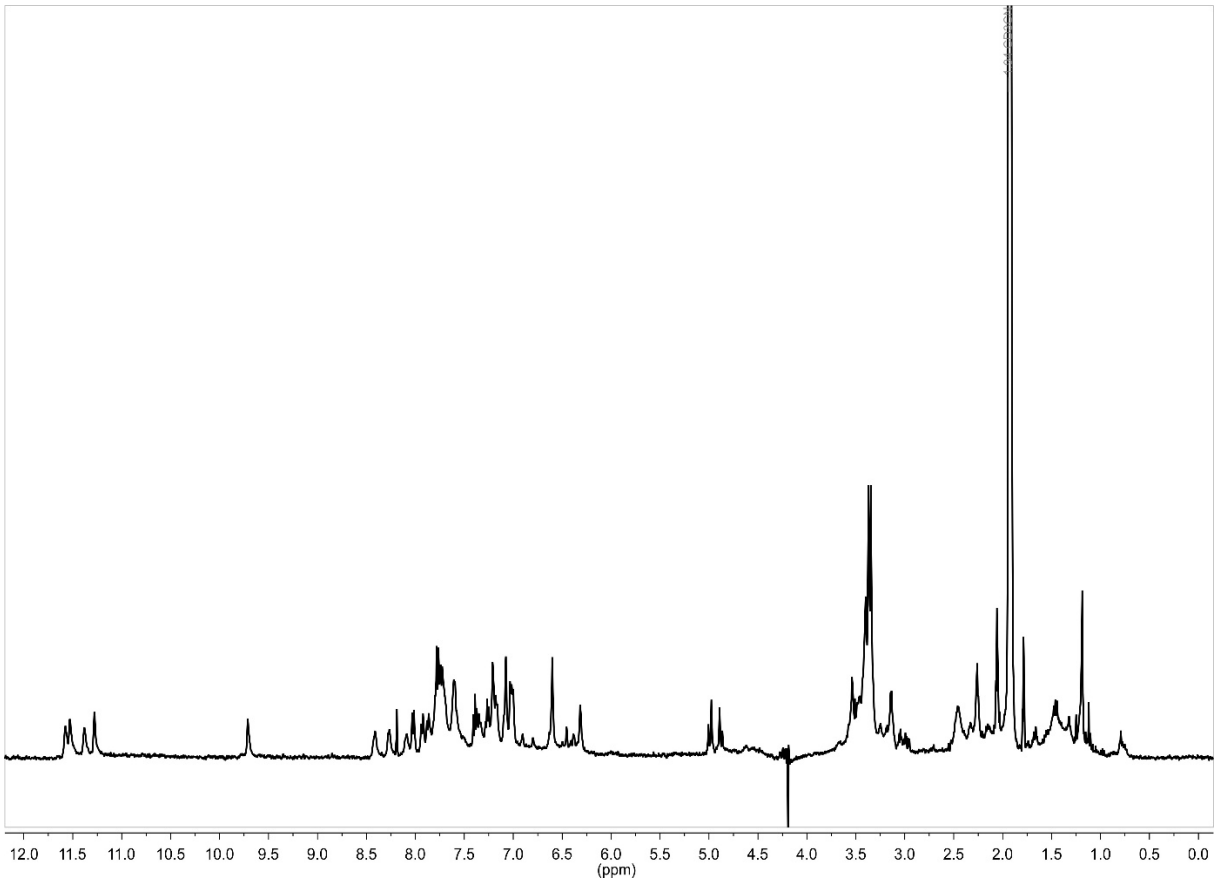

^{1}H-NMR spectrum (500 MHz, CD_3CN/H_2O, 25 °C) of **8**.

7.4.5.7. Compound 9

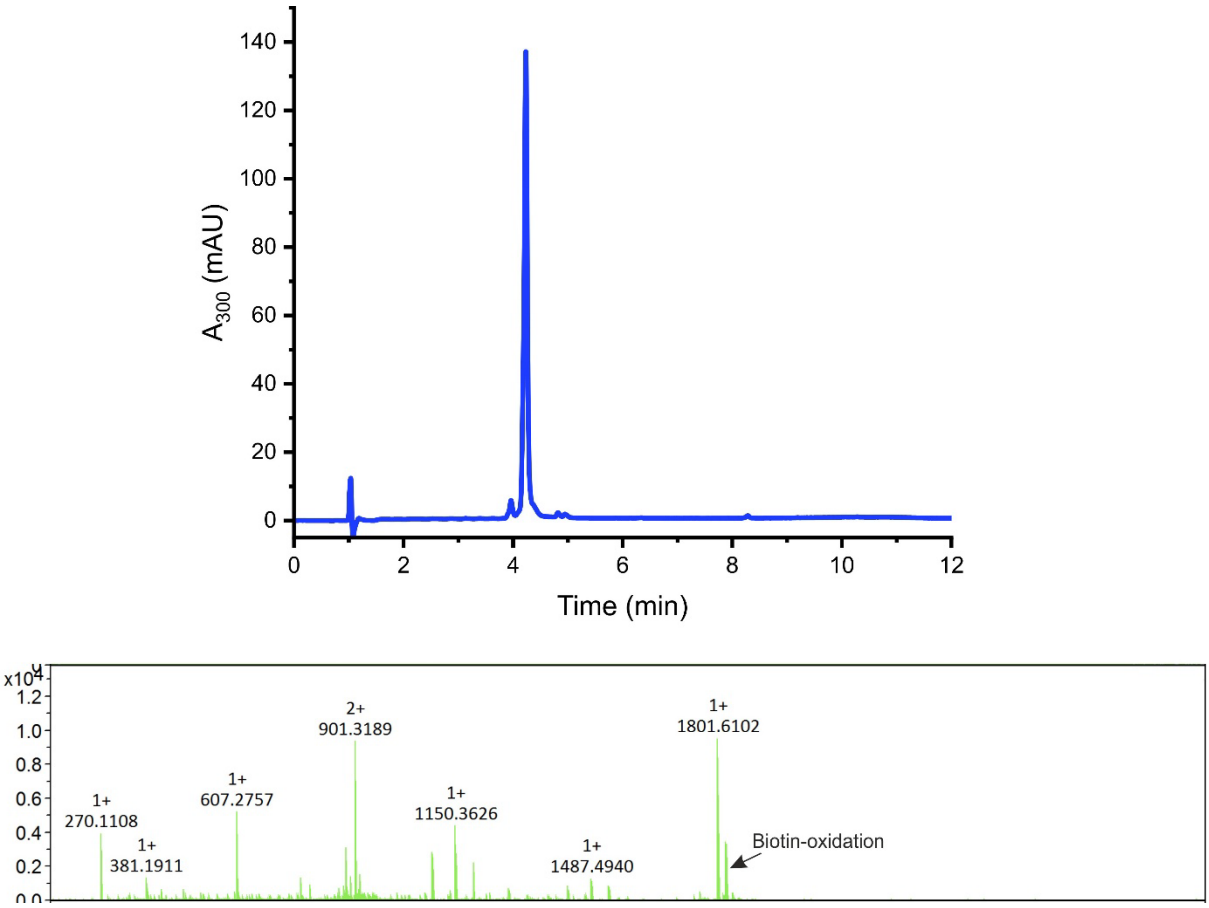

RP-HPLC chromatogram and ESI-MS spectrum of compound **9**.

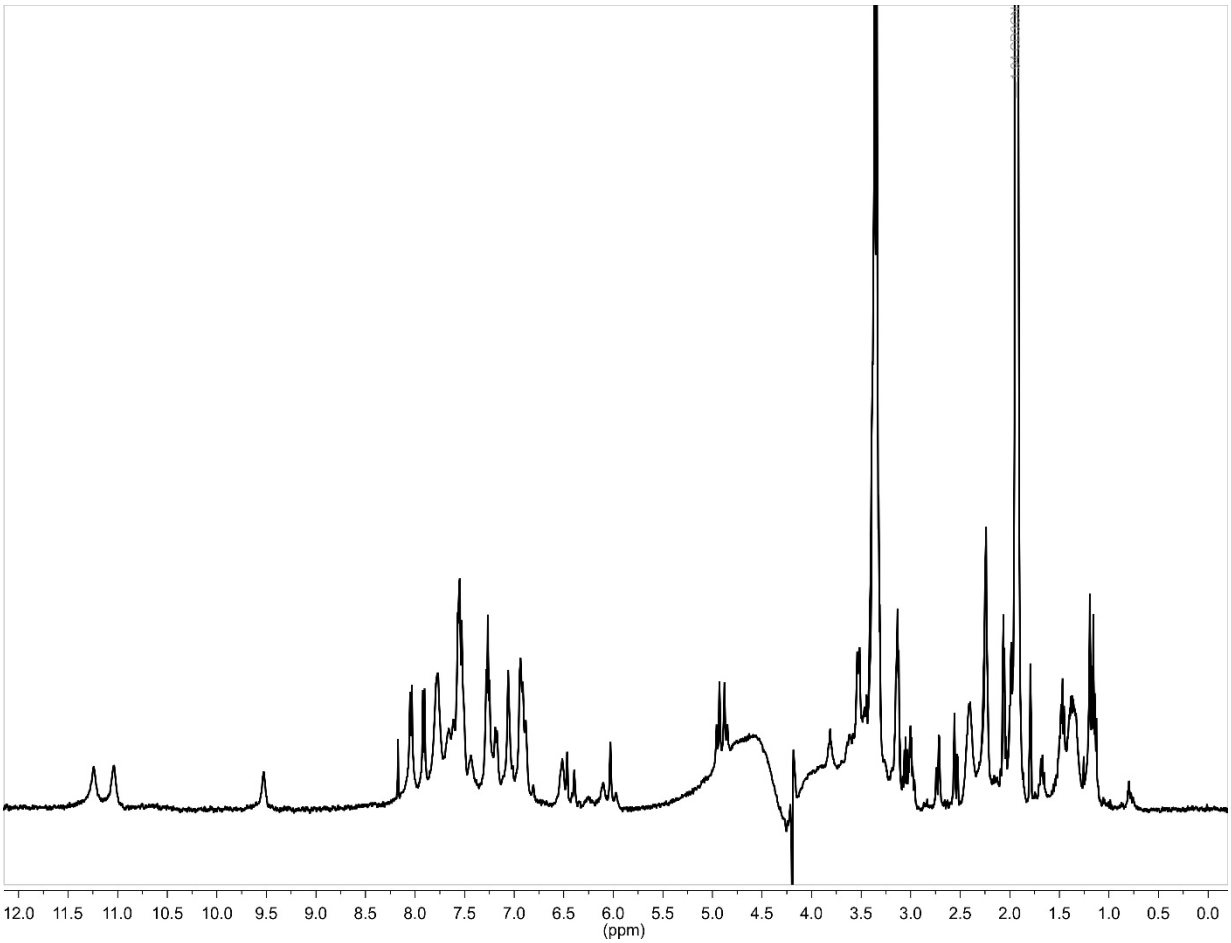

^{1}H-NMR spectrum (500 MHz, CD_3CN/H_2O, 25 °C) of **9**.

7.4.5.8. Compound 10

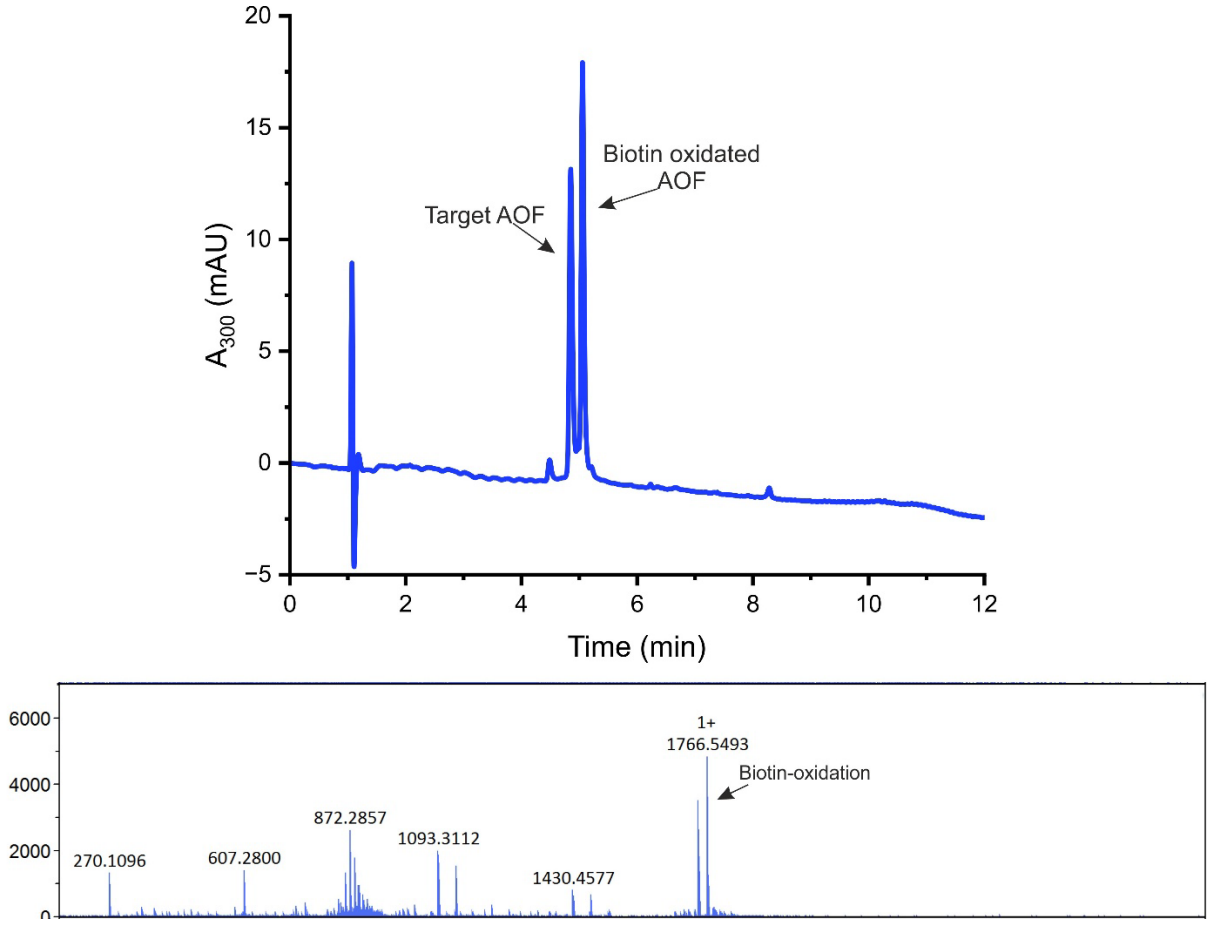

RP-HPLC chromatogram and ESI-MS spectrum of compound **10**.

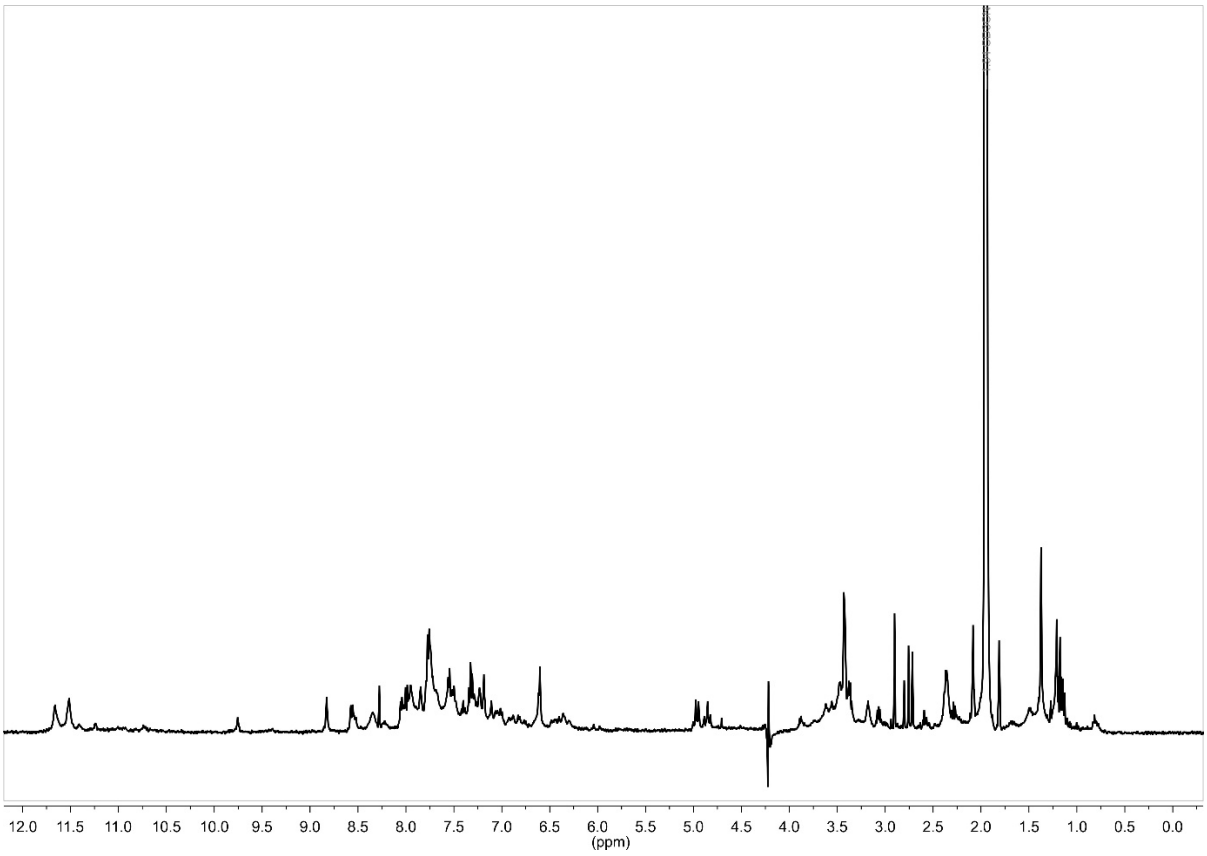

^{1}H-NMR spectrum (500 MHz, CD_3CN/H_2O, 25 °C) of **10**.

7.4.5.9. Compound 11

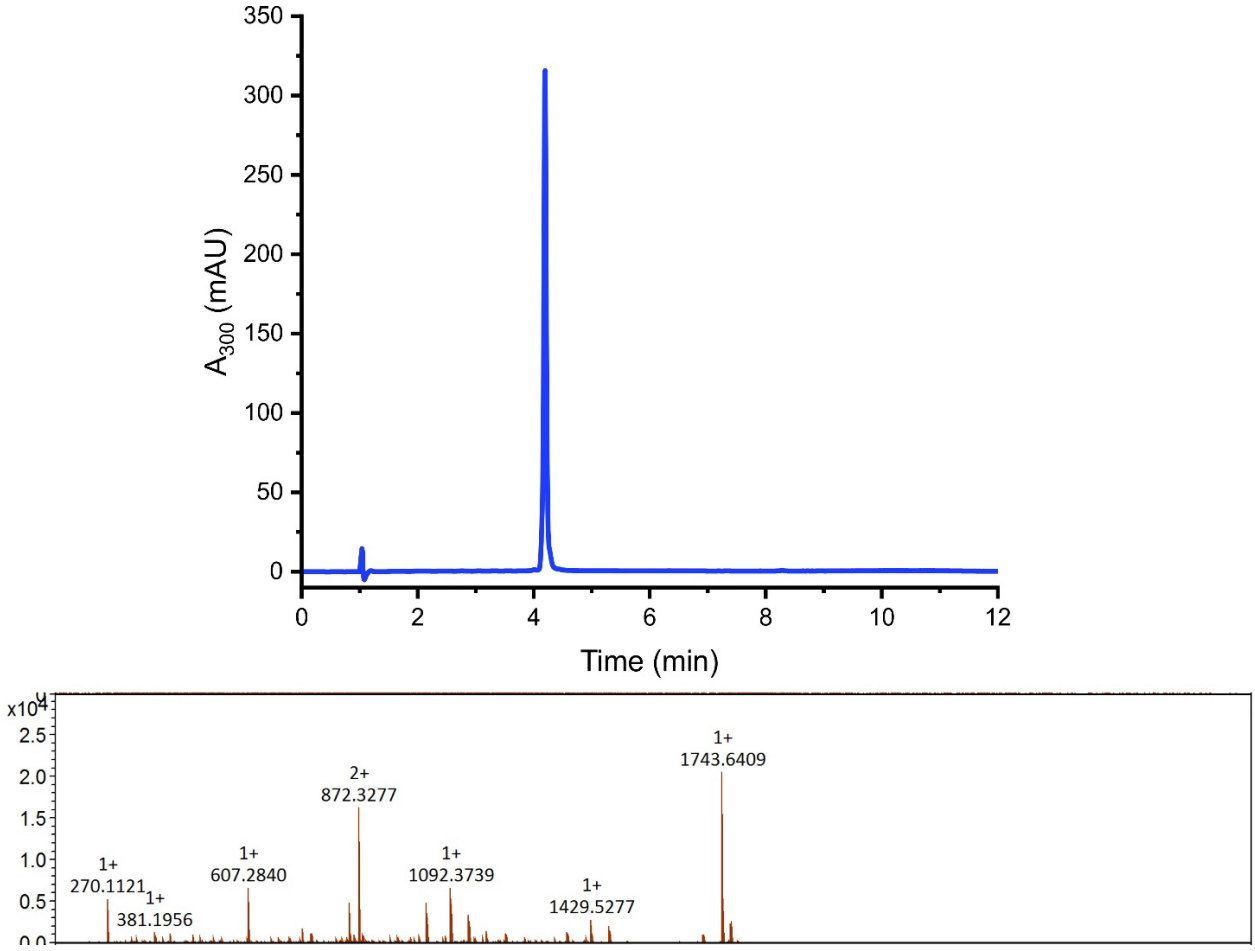

RP-HPLC chromatogram and ESI-MS spectrum of compound **11**.

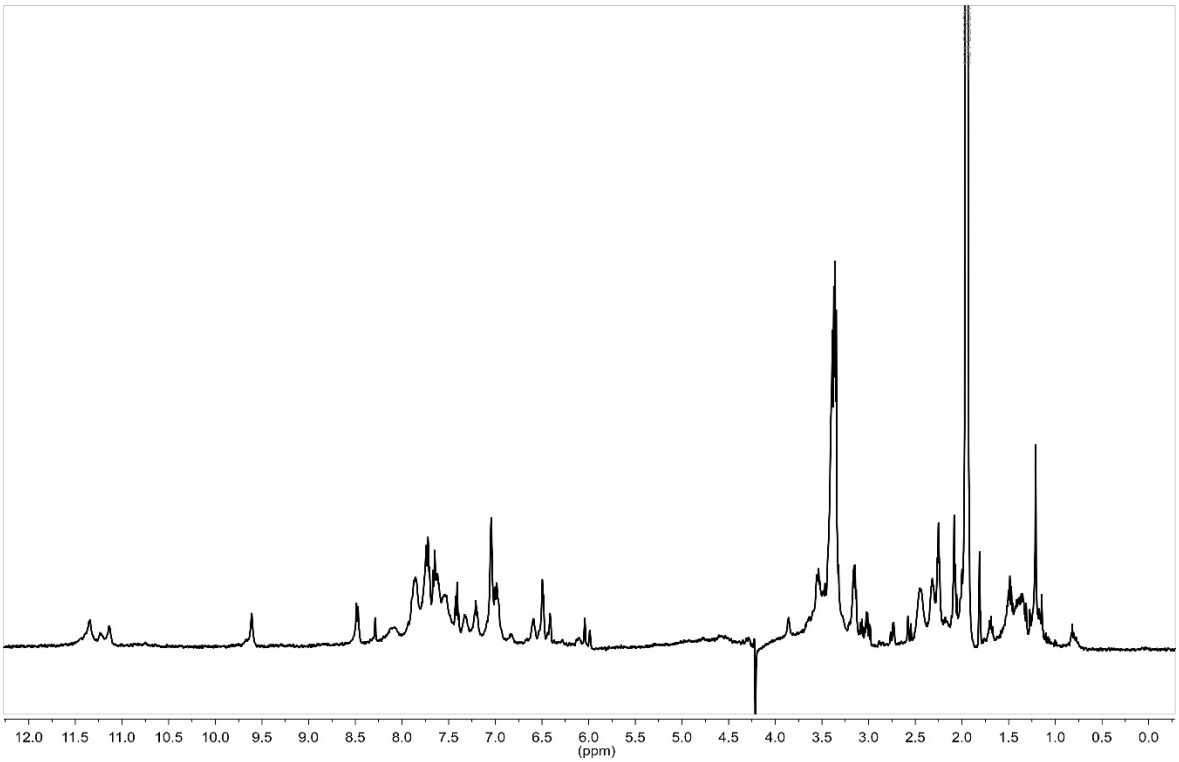

^{1}H-NMR spectrum (500 MHz, CD_3CN/H_2O, 25 °C) of **11**.

7.4.5.10. Compound 12

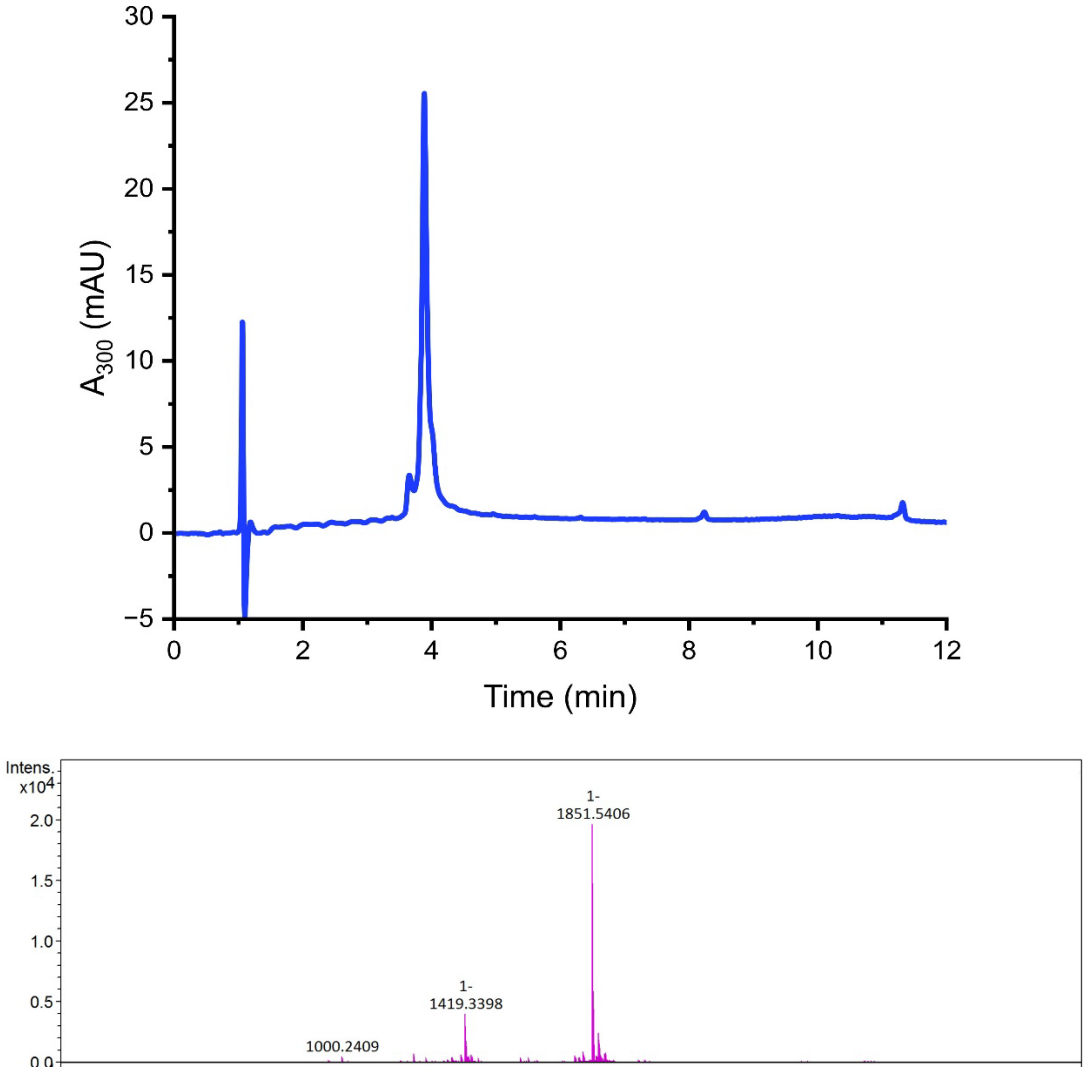

RP-HPLC chromatogram and ESI-MS spectrum of compound **12**.

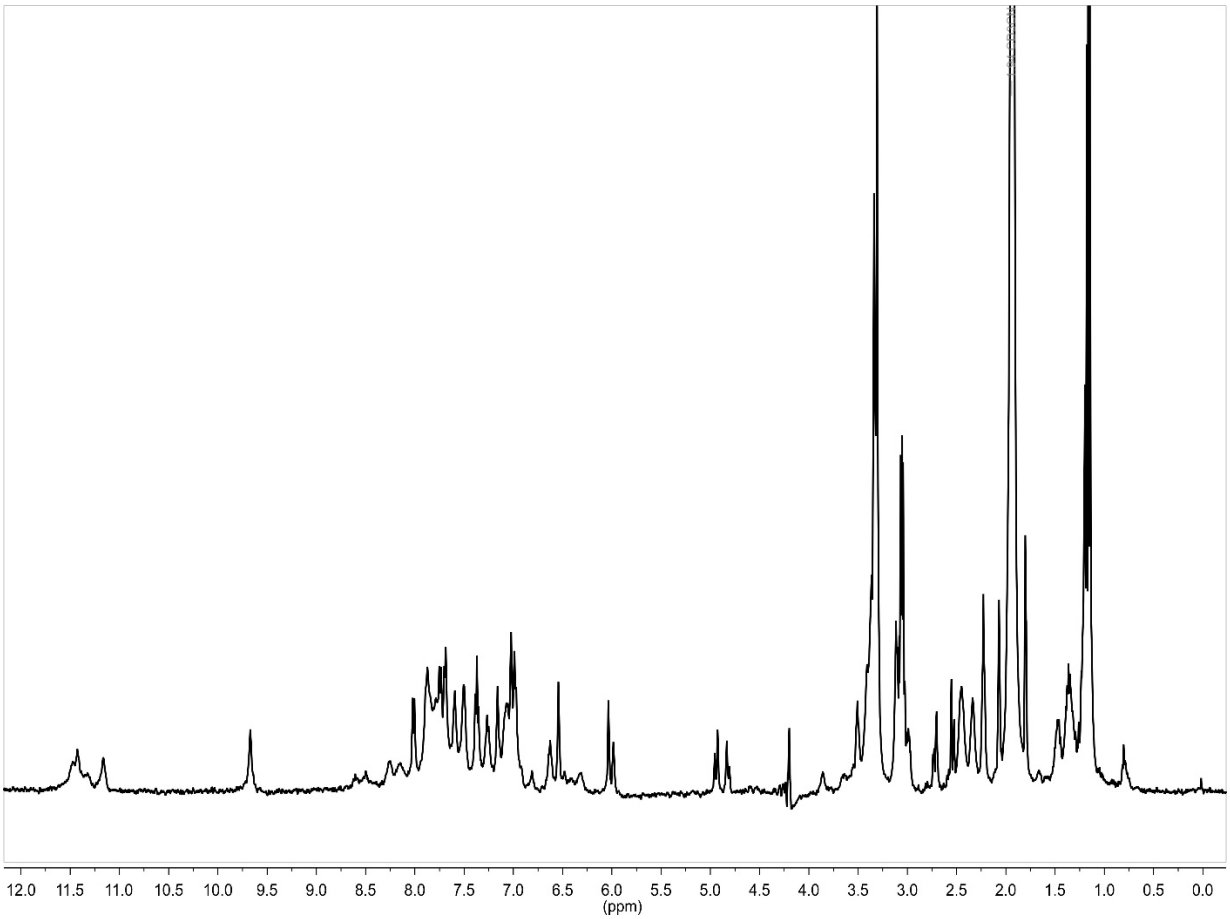

^{1}H-NMR spectrum (500 MHz, CD_3CN/H_2O, 25 °C) of **12**.

7.4.5.11. Compound 13

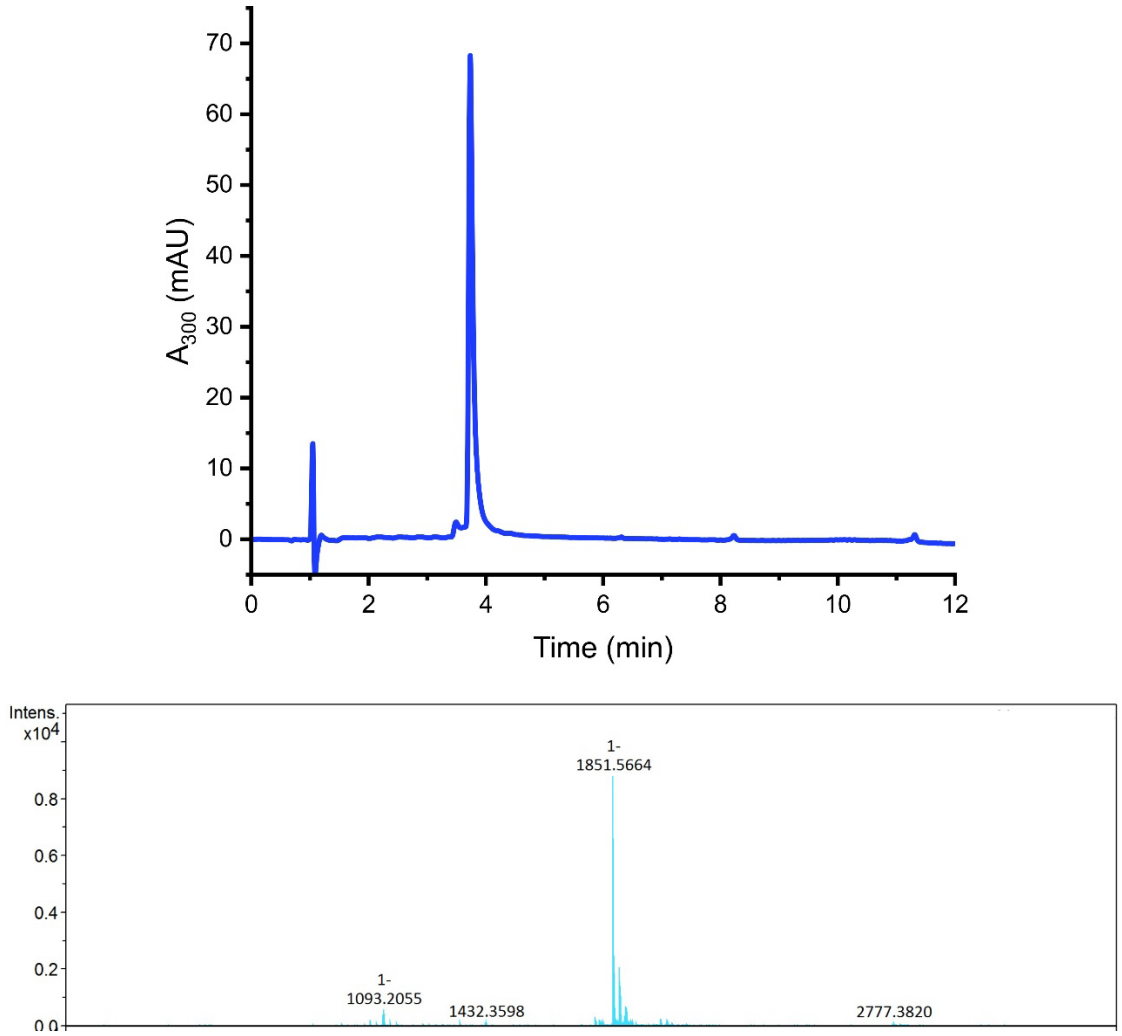

RP-HPLC chromatogram and ESI-MS spectrum of compound **13**.

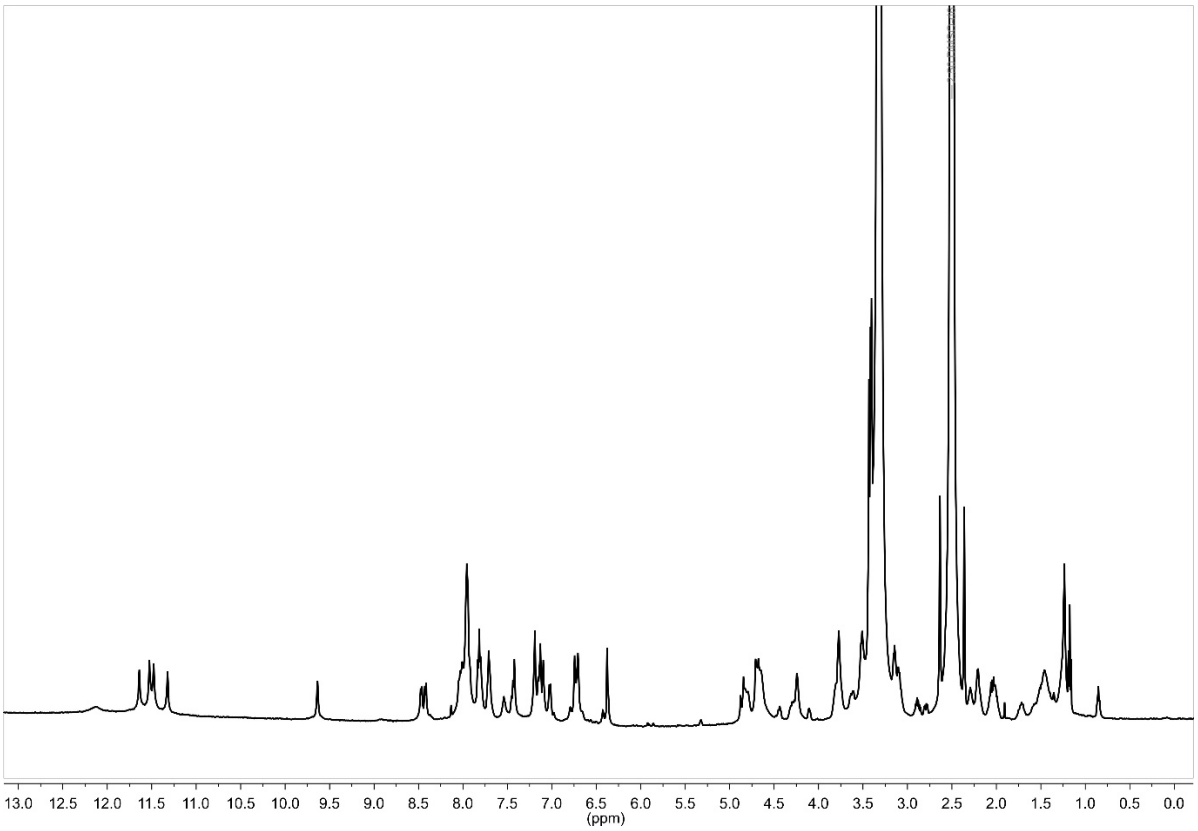

^{1}H-NMR spectrum (500 MHz, DMSO-d_6, 25 °C) of **13**.

7.4.5.12. Compound 14

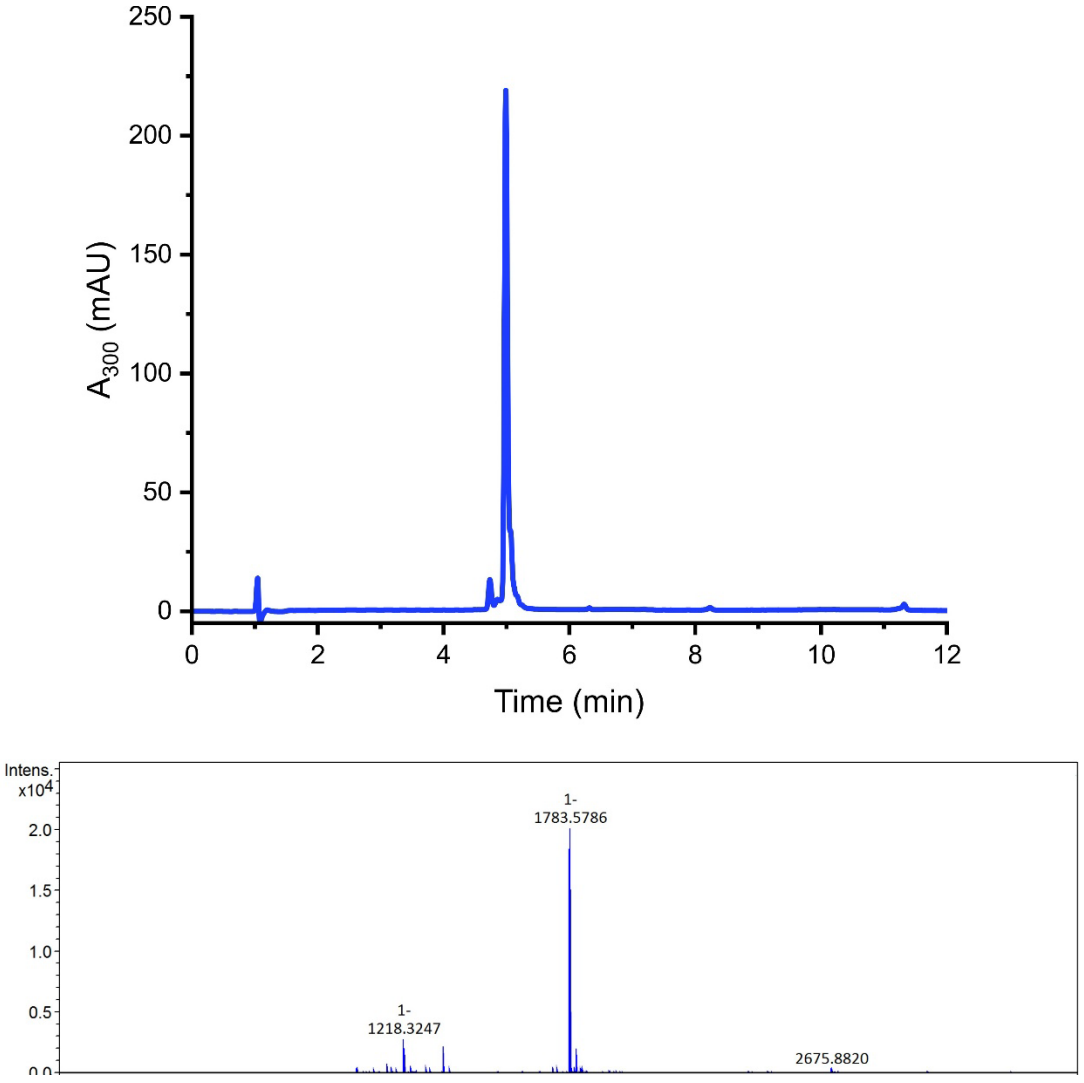

RP-HPLC chromatogram and ESI-MS spectrum of compound **14**.

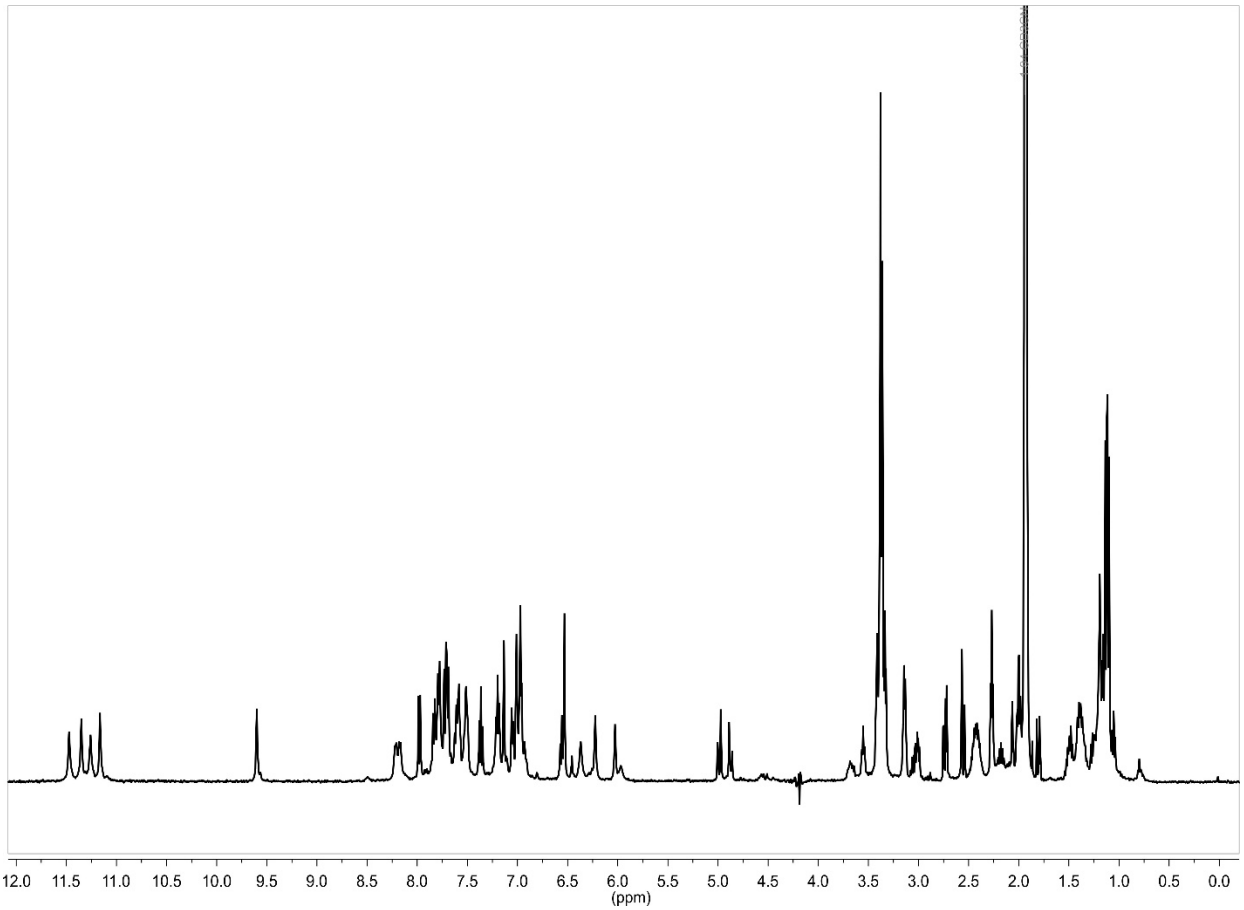

^{1}H-NMR spectrum (500 MHz, CD_3CN/H_2O, 25 °C) of **14**.

7.4.5.13. Compound 15

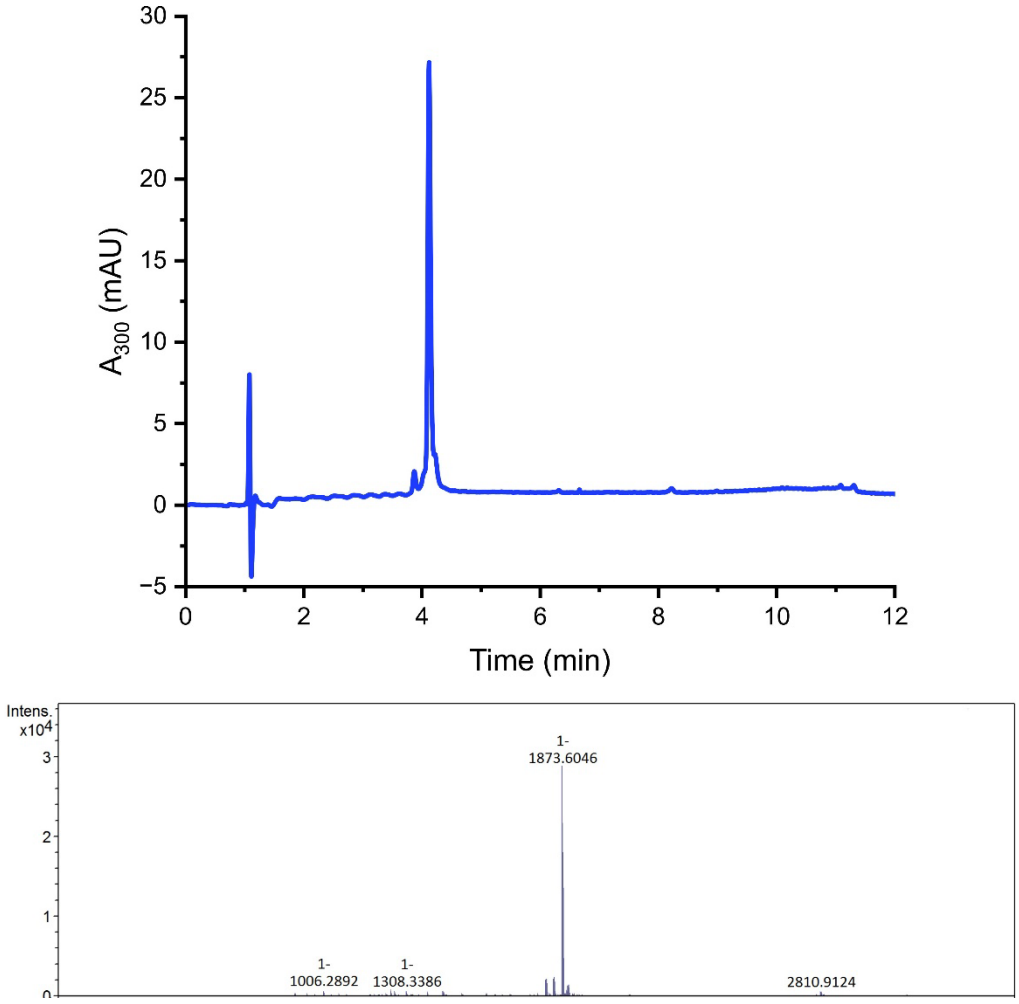

RP-HPLC chromatogram and ESI-MS spectrum of compound **15**.

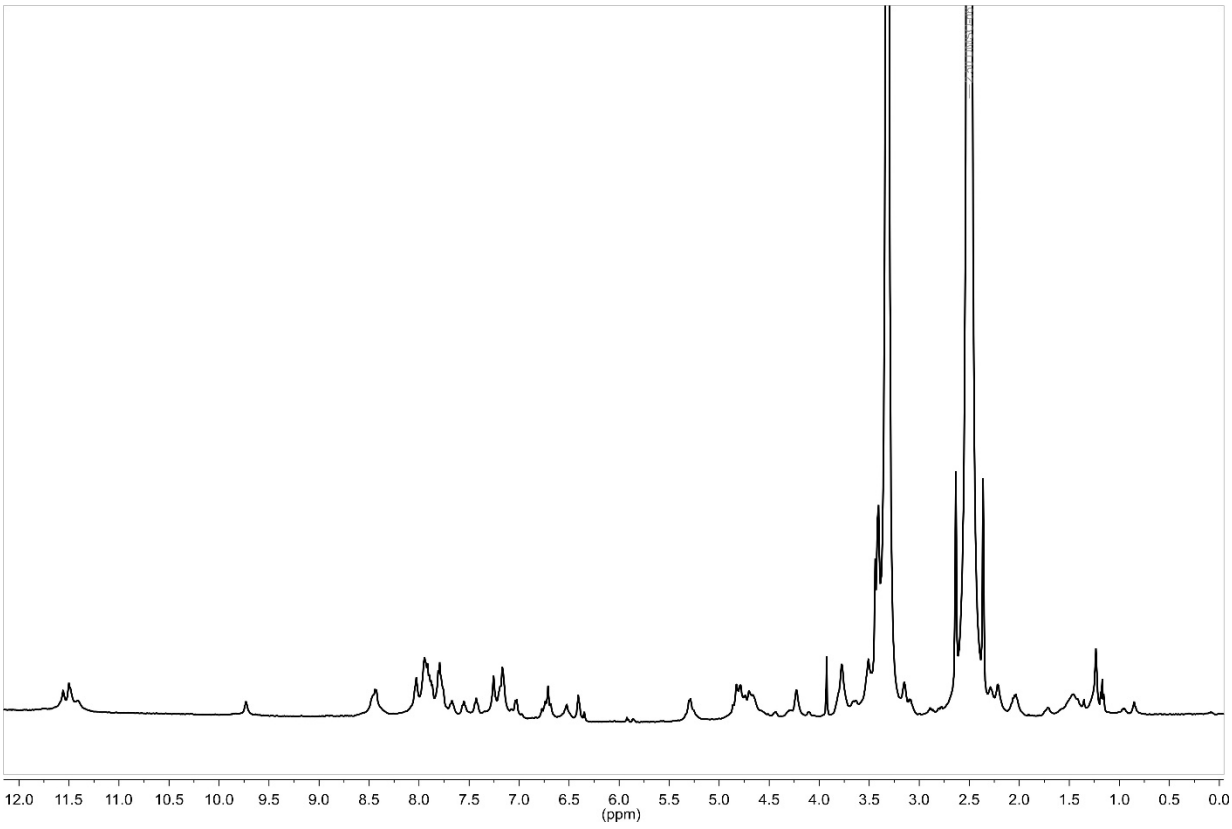

^{1}H-NMR spectrum (500 MHz, DMSO-d_6, 25 °C) of **15**.

7.4.5.14. Compound 16

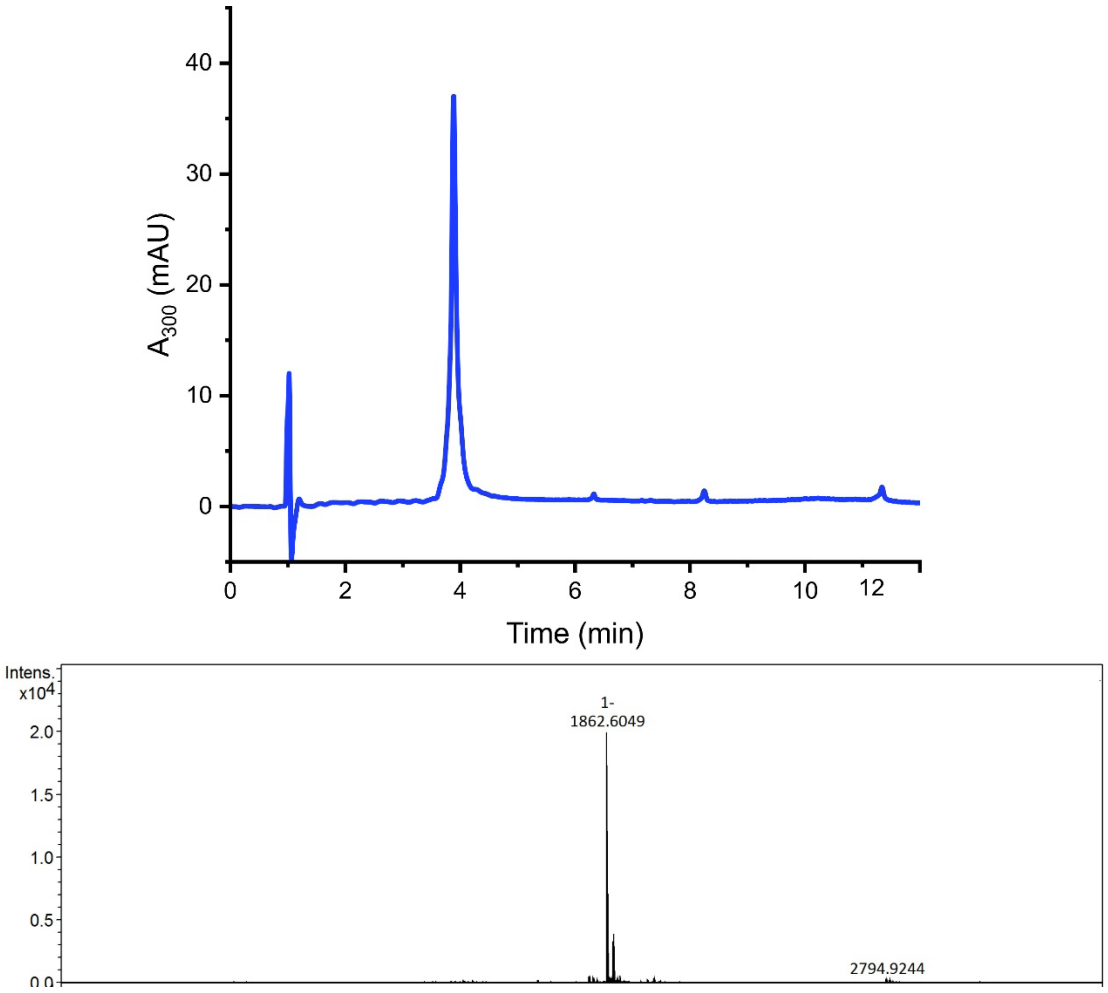

RP-HPLC chromatogram and ESI-MS spectrum of compound **16**.

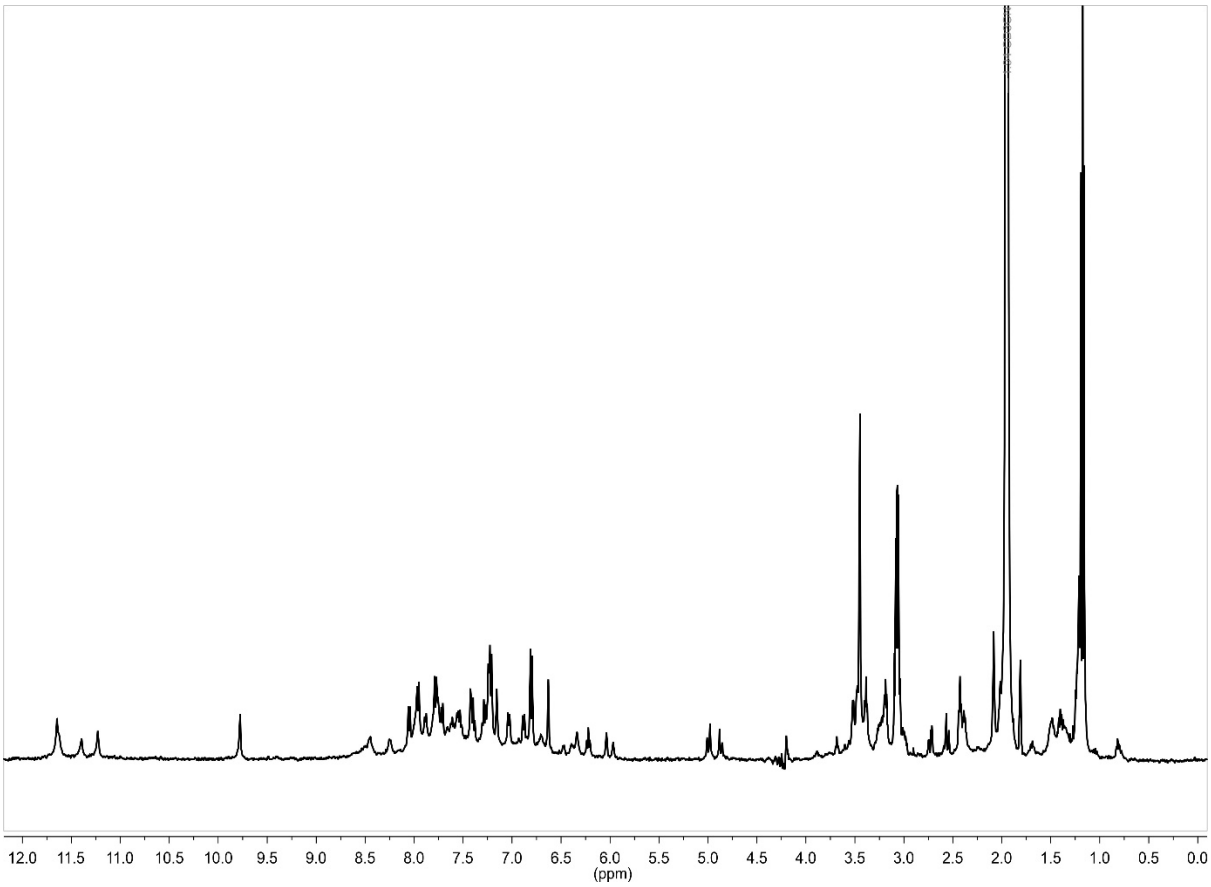

^{1}H-NMR spectrum (500 MHz, CD_3CN/H_2O, 25 °C) of **16**.

7.4.5.15. Compound 17

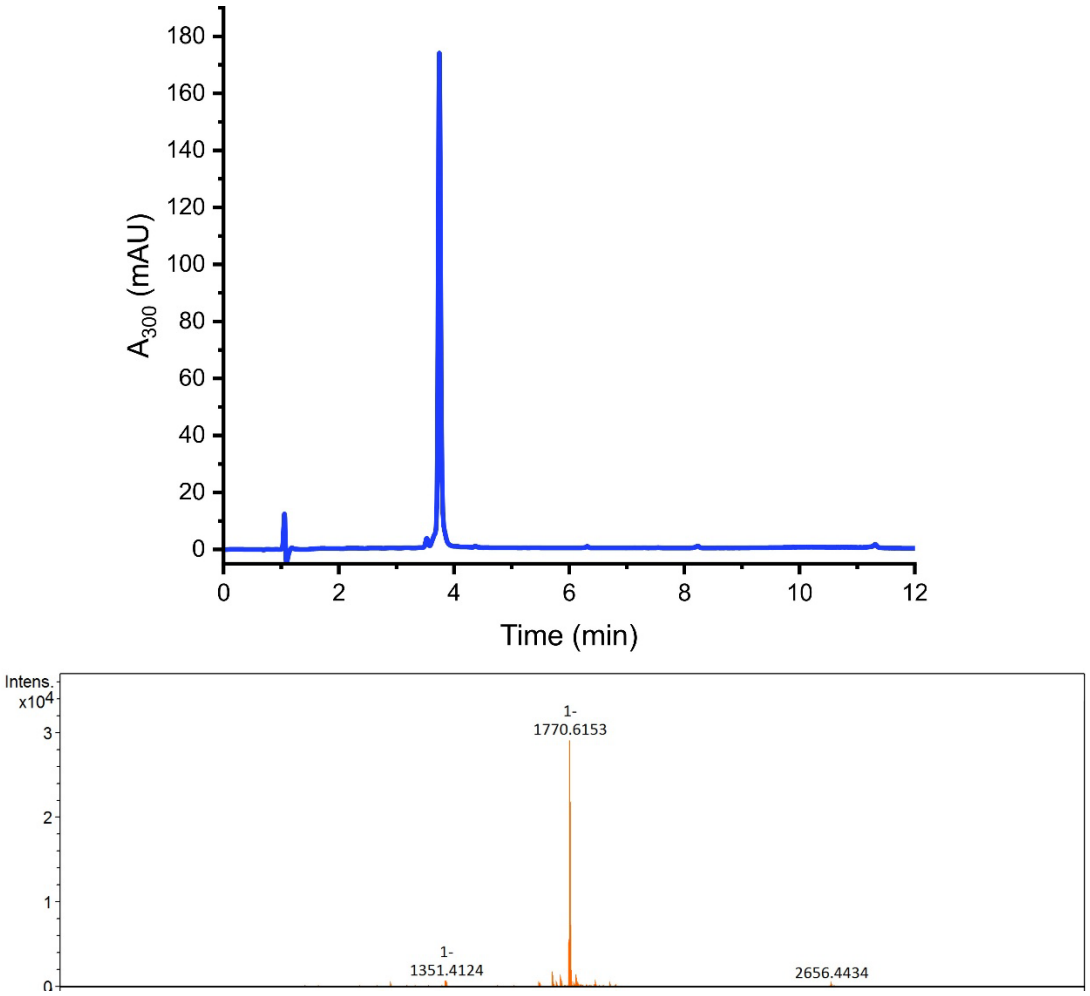

RP-HPLC chromatogram and ESI-MS spectrum of compound **17**.

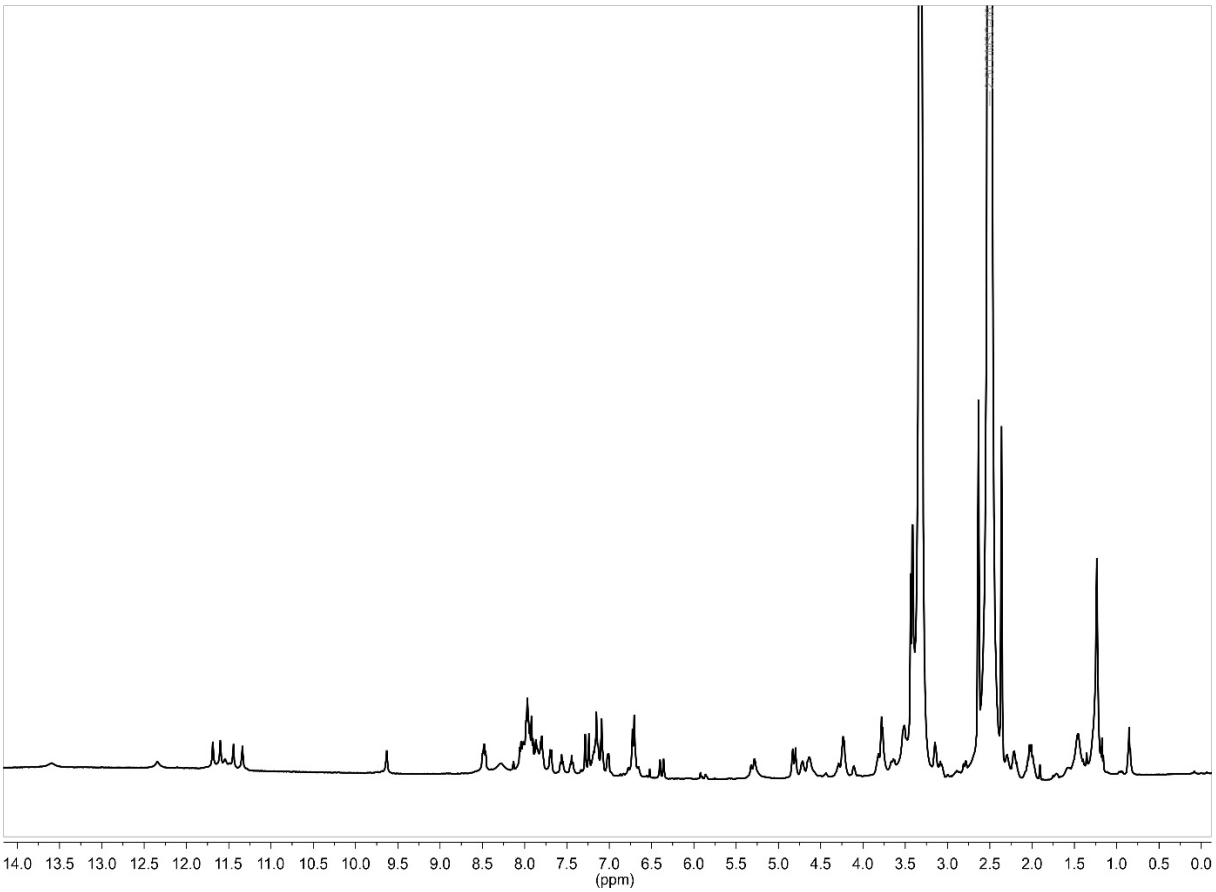

^{1}H-NMR spectrum (500 MHz, DMSO-d_6, 25 °C) of **17**.

7.5. Supporting information: biochemistry, biophysical measurements, and binding analyses

7.5.1. Material and general methods

All chemicals were purchased from commercial suppliers (*Fischer Scientific*, *Thermo Fischer Scientific*, *Sigma Aldrich* / *Merck*) in bio-grade quality and used without further purification. Tris-buffered saline (50 mM tris, 300 mM NaCl; TBS) and phosphate-buffered saline (137 mM NaCl, 2.7 mM KCl, 10 mM Na_2HPO_4, 1.8 mM KH_2PO_4; PBS) were freshly prepared from the respective compounds dissolved in ultra-pure water (dispensed from OmniaPure xs^{basic}, *Stakpure*), and pH was adjusted using a SevenCompact pH-meter (*Mettler Toledo*). Sterilisation of buffers and stock solutions was achieved by vacuum filtration or syringe filtration through 0.2 µm polyvinylidene fluoride (PVDF) membranes. Concentration of protein solutions and foldamer solutions were determined by measuring absorbance at the respective absorption maxima (280 nm for proteins, 375 nm for foldamers) on a NanoDrop™ OneC photo spectrometer (*ThermoFischer Scientific*) and calculation via extinction coefficients. OD_{600} of bacterial cultures were monitored on the same device using 1 cm disposable cuvettes. Centrifugal concentrator units Pierce™ (*ThermoFischer Scientific*) with suitable molecular weight cut-offs were used to concentrate protein solutions. For buffer exchange Slide-A-Lyzer™ (*ThermoFischer Scientific*) dialysis cassettes were used.

All work with bacteria was performed under antiseptic conditions next to a Bunsen burner flame. Pipette tips and liquid containers were sterilised by autoclaving at 121 °C. Transformation medium SOC (Super Optimal broth with Catabolite repression) was purchased pre-prepared (*Sigma Adlrich*), LB medium for bacterial growth cultures was prepared from solid LB broth (*CarlRoth*) and ultra-pure water and sterilised by autoclaving at 121 °C. Ampicillin and Kanamycin were used as 1000 x stock solutions in respective dilution. Competent *E. coli* BL21(DE3) cells were purchased as cryo-stocks (*New England BioLabs*, *ThermoFischer Scientific*), stored at -80 °C and handled on ice during usage.

Plasmids were purchased as lyophilised solids (*Genescript*) and dissolved in autoclaved water to a final concentration of 200 ng/µL. Bacterial colony selection on LB-agarose culture plates, containing 50 µg/mL of antibiotic were conducted overnight at 37 °C. Cryo-stocks of selected colonies were produced by small culture growth overnight and liquid nitrogen flash freezing 600 µL of the growth media mixed 1:1 with 60% v/v sterile glycerol solution. IPTG for expression induction was used as 1 M sterile filtered stock solution in respective dilution. Pelleting of expression cultures was achieved by centrifugation in an Avanti JXN-26 (*Beckman Coulter*) centrifuge. Cell lysis was performed on an UP200St (*Hielscher*) ultrasonic homogeniser.

HisPur™ Ni-NTA resin (*ThermoFischer Scientific*) was used for affinity chromatography of His-tagged proteins.

SDS-PAGE gels were casted using commercially available SureCast™ (*ThermoFischer Scientific*) stacking and resolving buffers, aqueous acrylamide solution (40 vol%), APS and TMED, according to the manufacturer's composition guide for the desired volume-percentage of acrylamide. Protein samples were mixed with 4× sample loading buffer (0.2 M Tris-HCl, 8% v/v SDS, 6 mM bromophenol blue, 4.3 M glycerol) and heated to 95 °C for 10 min prior to loading. Protein marker color prestained protein standard broad range 10-250 kDa (*New England BioLabs*) was loaded in the marker lane (3 µL). Electrophoresis was performed with 1x SDS running buffer in a Mini-PROTEAN® Tetra Cell (*BioRad*) at 125 W/0.03 A, delivered by a PowerPac HC (*BioRad*) power supply. Separated proteins were stained with Brilliant Blue R Concentrate (*Sigma-Aldrich*) for 15 min under shaking and SDS-PAGE gels were subsequently destained in a H_2O/AcOH/MeOH (6:3:1) solution.

Protein purification by FPLC-SEC was performed on a modular Azura system (*Knauer*) with a MWD 2.1L UV-detector, equipped with HiLoad 16/600 Superdex 75 and 200 pg SEC gel filtration columns (*Cytiva*) or on an Äkta Go system (*Cytiva*) with a UV on 9L Cpl, equipped with a HiLoad 26/600 Superdex 200 pg SEC gel filtration column (*Cytiva*). Chromatographic monitoring was performed at λ = 280 nm. Data was processed in OriginPro V.2019b (*OriginLab*).

The CD spectra were recorded on a *Jasco* J-1500 spectrometer with 1 mm quartz cuvette; the following parameters were used: scan speed: 100 nm/min; accumulation: 2; response time: 1.0 s; bandwidth: 1; temperature: 25 °C; data pitch: 1 nm, baseline corrected. The spectra were smoothed with a Savitzky-Golay filtering. Variable temperature spectra were recorded in 10 °C intervals, heating/cooling with a 5 °C/min ramp rate, conducted in duplicate at each temperature and averaged. Variable temperature single wavelength CD were recorded in 0.5 °C intervals, heating/cooling in 0.5 °C steps with 5 °C/min ramp rate and a 2 second delay for data acquisition at each point.

BLI experiments were performed on an Octet R8 instrument (*Sartorius*) according to manufacturers' recommendations. In all cases, Streptavidin (SA) Octet biosensors were soaked for 15 min in PBS prior to the assays. Before loading, a baseline was recorded in PBS+0.05% Tween 20 (PBS-T) for 60 seconds.

For single concentration binding assays, the SA biosensors were loaded with the biotinylated oligomers (1.5-2.5 µg/mL in PBS-T) for 30 s, followed by a washing and base line step in PBS-T and PBS-T/0.5% BSA for 30 s and 120 s respectively.

For kinetic assays, the SA biosensors were loaded with the biotinylated oligomers (1.5-2.5 µg/mL in PBS-T) for 30 s, followed by a washing and base line step in PBS-T and PBS-T/0.5% BSA for 30 s and 120 s respectively. The association was recorded against 2x serial column

dilutions of the proteins (concentration ranges are indicated at the respective figures) in PBS-T/0.5% BSA. Dissociation was recorded in the same wells used for the baseline. Biosensors without an immobilised foldamer were used to ensure no unspecific binding of the protein towards the SA sensors occurred. All experiments were conducted at 25 °C. Data were processed in Octet Analysis Studio V.13 and K_D values, when applicable, were calculated from group fitting the kinetic curves of association and dissociation to a 1:1 binding model.

7.5.2. Expression and purification of proteins

- *Standard recombinant protein expression*

All variants of G02 and C10 were expressed using either the pMAL-c5E or pET-28a(+) vector systems, encoding for the target sequence N-terminally fused to a HRV 3C cleavable MBP-10×His or 6×His tag respectively. Plasmids were transformed into competent *E. coli* BL21(DE3) cells by mixing 1 µL of plasmid stock solution with one tube of bacteria stock (50 µL), incubation on ice for 10 min and subsequent heat-shock at 42 °C for 30 s. The transformed cells were cooled on ice for 5 minutes, mixed with 600 mL S.O.C. medium and incubated at 37 °C for 1 h under shaking (600 rpm). The mixture was spread on LB-Amp (for pMAL-c5E) or LB-Kan (for pET-28a(+)) agarose plates and incubated over-night at 37 °C. Subsequently, starter cultures were grown from single colonies in 10-50 mL LB medium containing the respective antibiotic (Amp: 100 µg/mL; Kan: 50 µg/mL) at 37 °C overnight. Starter cultures showing visible growth were used for inoculation (1:100 Vol%) of 100 mL-4 L LB-Amp/Kan medium and cells were grown at 37 °C under shaking (200 rpm) until an OD600 of ~ 0.6 was reached. For pET-28a(+) constructs, expression was induced by adding IPTG (1 mM final concentration) and continued for 3 h at 37 °C. For pMAL-c5E constructs the temperature was lowered to 22 °C for 1.5 h and protein expression was induced by adding IPTG (1 mM final concentration) and continued for 18 h. After the expression cells were harvested by centrifugation at 8000 × g for 15 – 20 min at 4 °C. The supernatant was discarded, and cell pellets were either frozen at −20 °C or used directly in the next step.

- *Small-scale protein purification*

The cells were harvested at 4000 rpm at 4 °C for 40 min and stored at -20 °C. The cells were then disrupted by chemical lysis (20 mM sodium phosphate, 300 mM NaCl, pH 7.4 supplemented with 1 × BugBuster® Protein Extraction Reagent 1X, Merck). Suspensions were gently agitated for 15 min on ice and clarified by centrifugation (15 000 ×g, 20 min, 4 °C). The supernatant was treated with DNase I (20 µg/mL, 10 min, on ice) immediately prior to immobilised-metal affinity chromatography. All centrifugation steps were performed at 800 ×g

for 1 min at 4 °C unless otherwise stated. Ni-NTA spin columns (NEBExpress®, #S1427) were equilibrated with 250 µL lysis/binding buffer after removal of the storage solution. Clarified lysate (≤ 500 µL per load) was applied, the resin was gently tapped to mix and allowed to bind for 2 min on ice, and the flow-through was collected. The loading procedure was repeated until all lysates had been processed. Columns were washed three times with 250 µL wash buffer (20 mM sodium phosphate, 300 mM NaCl, 5 mM imidazole, pH 7.4). Bound proteins were eluted twice with 200 µL elution buffer (20 mM sodium phosphate, 300 mM NaCl, 500 mM imidazole, pH 7.4). Eluate fractions were exchanged into PBS by four successive cycles of dilution to the 6 mL capacity of a 3 kDa-MWCO PES centrifugal concentrator (Pierce™) followed by centrifugation (4 000 rpm, 8 °C) to ~1 mL. The final solution was concentrated to ~500 µL stabilised by adding 1 vol. of 50 % (v/v) glycerol to 9 vol. of protein solution, flash-frozen in liquid N_2 and stored at –80 °C. The protein concentration was determined by measuring the UV_{280}. The mutants were analysed by 15 % SDS-PAGE and characterized by LCMS. Finally, the protein mutants were concentrated, frozen in liquid nitrogen and stored at -80 °C prior to all analysis.

- *Large-scale protein purification*

Harvested or frozen cell pellets were re-suspended in lysis buffer (TBS, 25 mM imidazole, pH = 7.4). Cells were sonicated in 4-5 rounds of 3 min each on ice (Frequency = 90%; Amplitude = 100%, Power = max) with 10 minutes breaks between rounds to prevent sample overheating. The resulting suspension was centrifuged at 45000 × g for 45 min at 4 °C and the supernatant was incubated with Ni-NTA resin (5 mL suspension per 1 L of expression) at 4°C for 30 min to 1 h. The incubated resin was loaded onto a gravity-flow column, washed with 10 CVs of lysis buffer, 3 CVs of wash buffer (TBS, 50 mM imidazole, pH = 7.4) and the target fusion protein was lastly eluted with elution buffer (TBS, 300 mM imidazole, pH = 7.4). The UV_{280} was monitored using a Nanodrop photo spectrometer to track protein elution and assist with sample collection during the washing and elution steps. The elution fractions were combined, HRV 3C protease (1 u/100 µg) was added and the mixture was dialysed against lysis buffer (TBS, 25 mM imidazole, pH = 7.4) overnight. The cleavage mixture was incubated with Ni-NTA resin for 30 min at 4 °C and subsequently loaded on a gravity-flow column and the flow-through, containing the cleaved target protein was collected and concentrated for SEC purification in TBS. Fractions containing the target protein were pooled, concentrated and either used directly in subsequent experiments or aliquoted and stored at -80 °C.

7.5.3. Protein expressions and characterisation

7.5.3.1. Expression of G02CCDi

G02CCDi was always recombinantly expressed using the large scale protein expression and purification methods explained above.

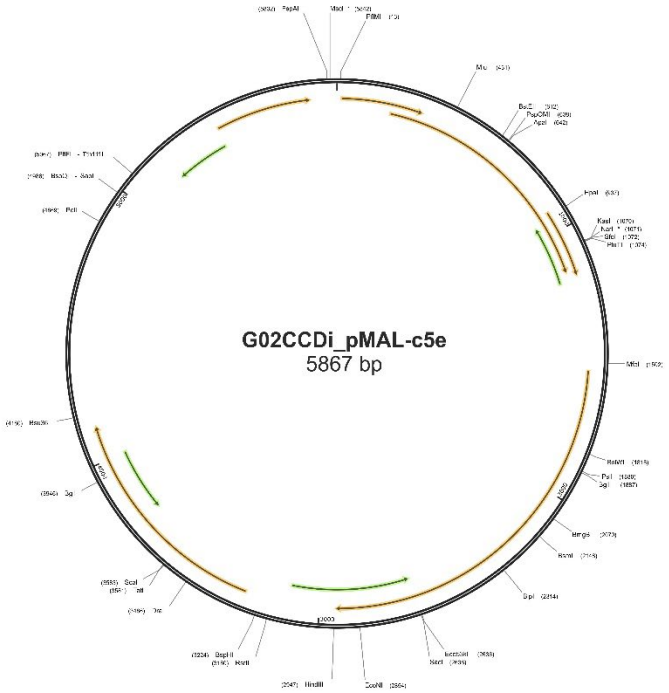

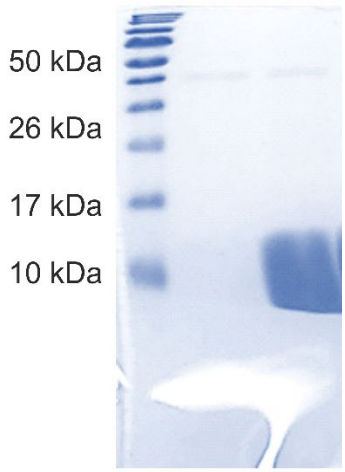

MKIEEGKLVIWINGDKGYNGLAEVGKKFEKDTGIKVTVEHPDKLEEKFPQVAATGDGPD
IIFWAHDRFGGYAQSGLLAEITPDKAFQDKLYPFTWDAVRYNGKLIAYPIAVEALSLIY
NKDLLPNPPKTWEEIPALDKELKAKGKSALMFNLQEPYFTWPLIAADGGYAFKYENGKY
DIKDVGVDNAGAKAGLTFLVDLIKNKHMNADTDYSIAEAAFNKGETAMTINGPWAWSNI
DTSKVNYGVTVLPTFKGQPSKPFVGVLSAGINAASPNKELAKEFLENYLLTDEGLEAVN
KDKPLGAVALKSYEEELVKDPRIAATMENAQKGEIMPNIPQMSAFWYAVRTAVINAASG
RQTVDEALKDAQTNSSSHHHHHHHHHHLEVLFQGPVDNKFNKERSYAFEEIWKLPNLNY
HQHKAFISSLRDDPSQSANLLIEAKILNIAQEIAAIKQEIAAIKKEIAAIKWEIAAIKQ

On the left, expression vector used for the expression of G02CCDi. The coiled-coil fusion of G02 is highlighted in green, the cleavage site for HRV-3C is coloured in red, the polyhistidine tag in blue while the MBP tag is coloured in pink. On the right, purity of G02CCDi after expression and purification on 15% SDS-PAGE.

7.5.3.2. Expression of G02-His6

G02-His6 was mostly recombinantly expressed using the small scale protein expression and purification methods explained above.

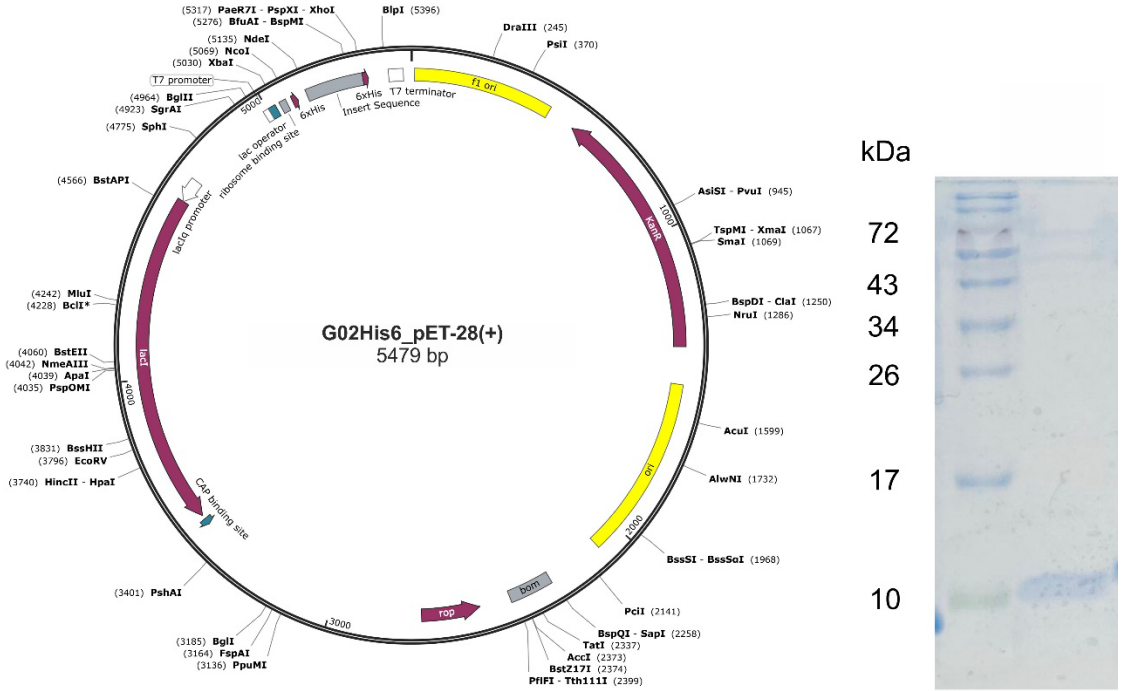

MGSSHHHHHHLEVLFQGPHMVDNKFNKEGYMAFEEIWWL
PNLNLSQRRAFIQSLRDDPSQSANLLAEAKKLNDAQAPK

On the left, expression vector used for the expression of G02His6. The sequence of G02 is highlighted in green, the cleavage site for HRV-3C is coloured in red and the polyhistidine tag. On the right, purity of G02His6 after expression and purification on 15% SDS-PAGE.

7.5.3.3. Expression of C10-His6

C10His6 was always recombinantly expressed using the small scale protein expression and purification methods explained above.

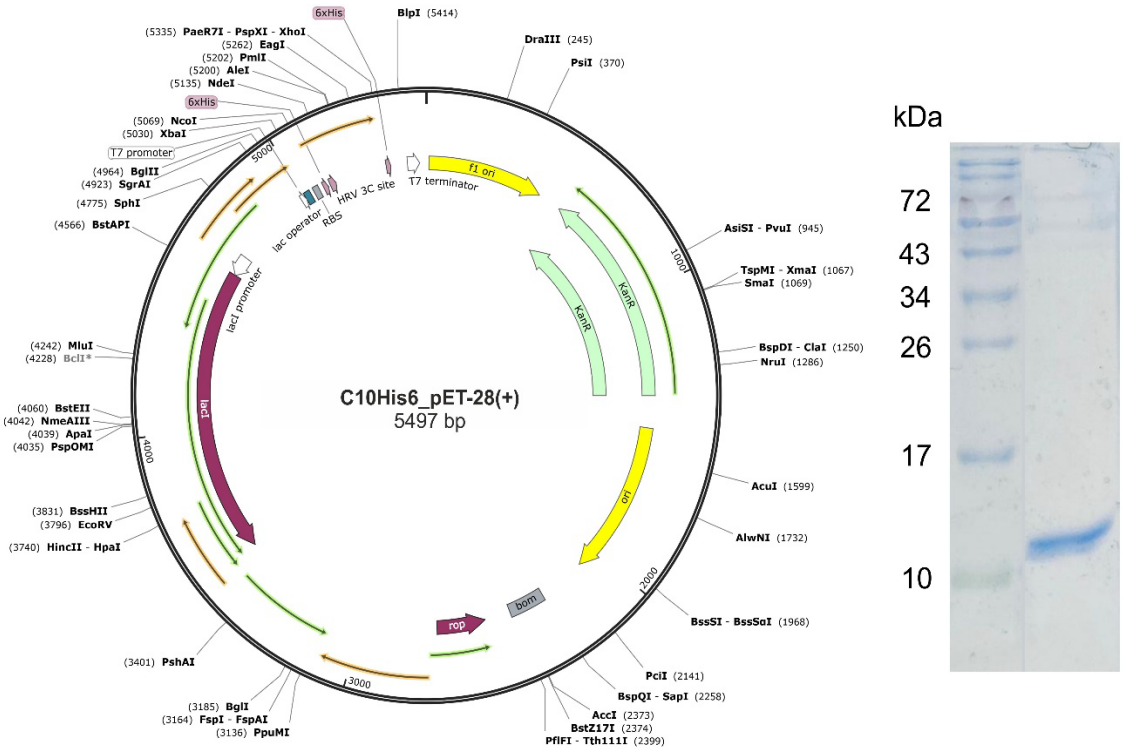

On the left, expression vector used for the expression of C10His6. The sequence of C10 is highlighted in green, the cleavage site for HRV-3C is coloured in red and the polyhistidine tag. On the right, purity of C10His6 after expression and purification on 15% SDS-PAGE.

7.5.3.4. Expression of G02 Ala-scan variants

The wild type G02 sequence is the following (the tag and cleavage site are in italics; the sequence numbering starts after the cleavage site):

*MGSSHHHHHHSSGLEVLFQ*GPHM**VDNKFNKEGYMAFEEIWWLPNLNLSQRRAFIQSLRD DPSQSANLLAEAKKLNDAQAPK**

The following mutants were considered: G9A, Y10A, M11A, F13A, E14A, W17A, W18A, L24A, S25A, R27A, R28A, Q32A, R35A.

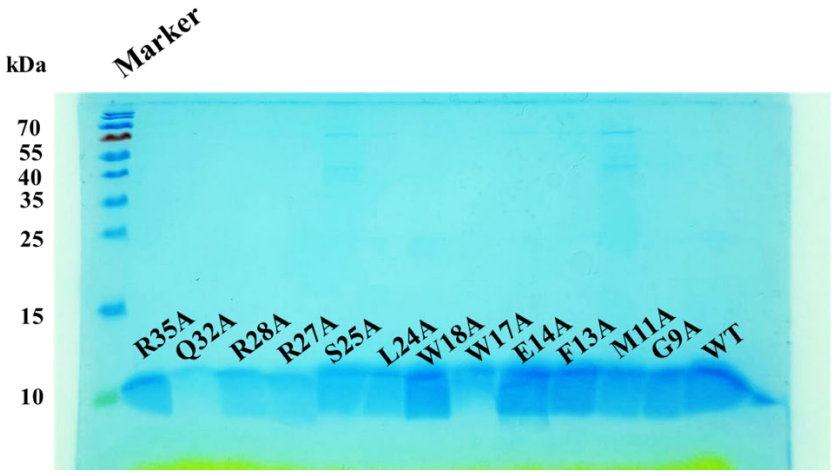

SDS-PAGE gel on 15% acrylamide of all Ala-mutant of G02 and G02WT.

➢ *LC-MS of G02-Ala scan variants:*

- **G09A :**

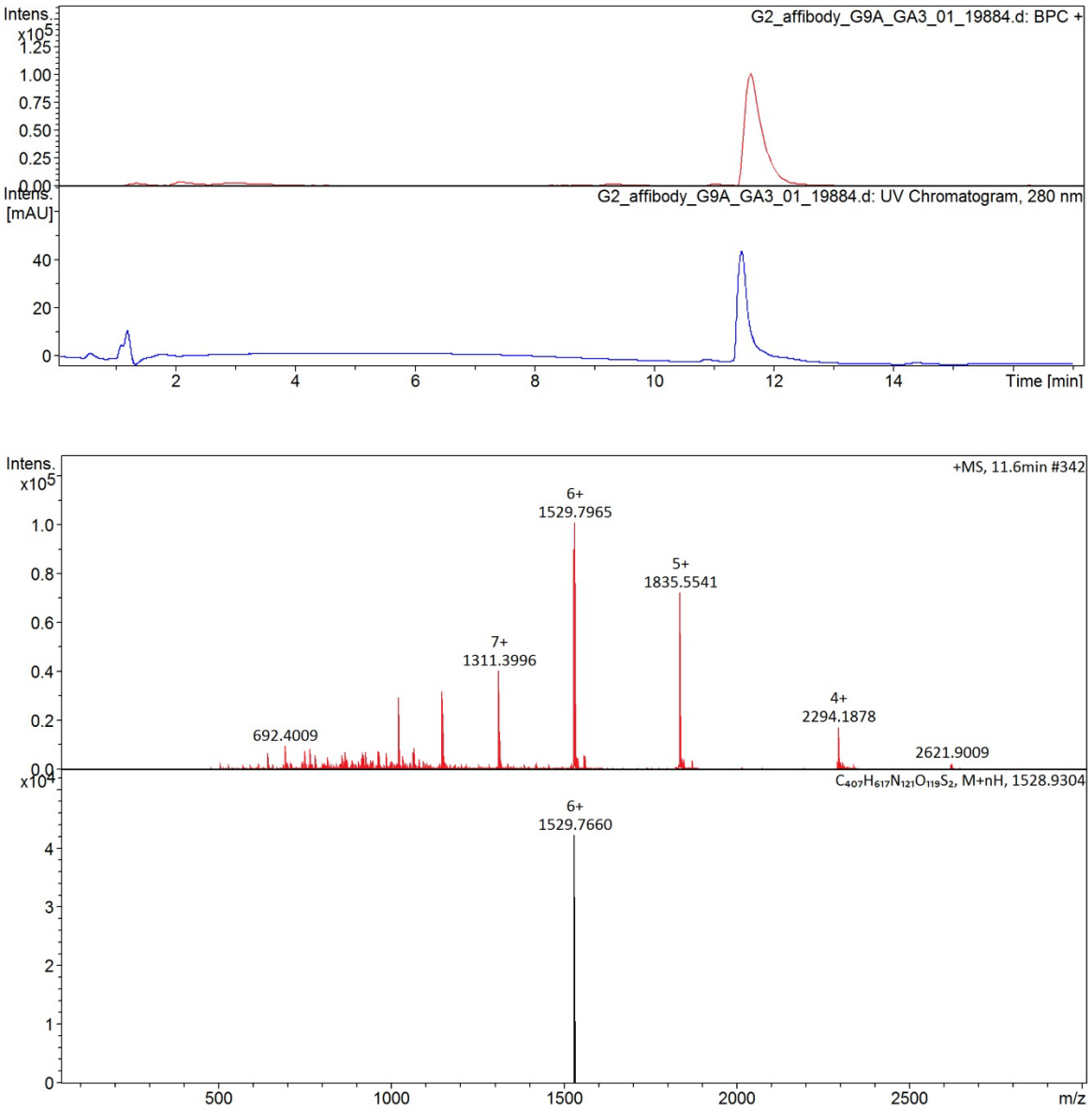

LC chromatogram measured at 280nm of G02-Ala scan variant G09A at the top with MS measured in the middle. Simulated pattern calculated is shown in black at the bottom.

- **M11A :**

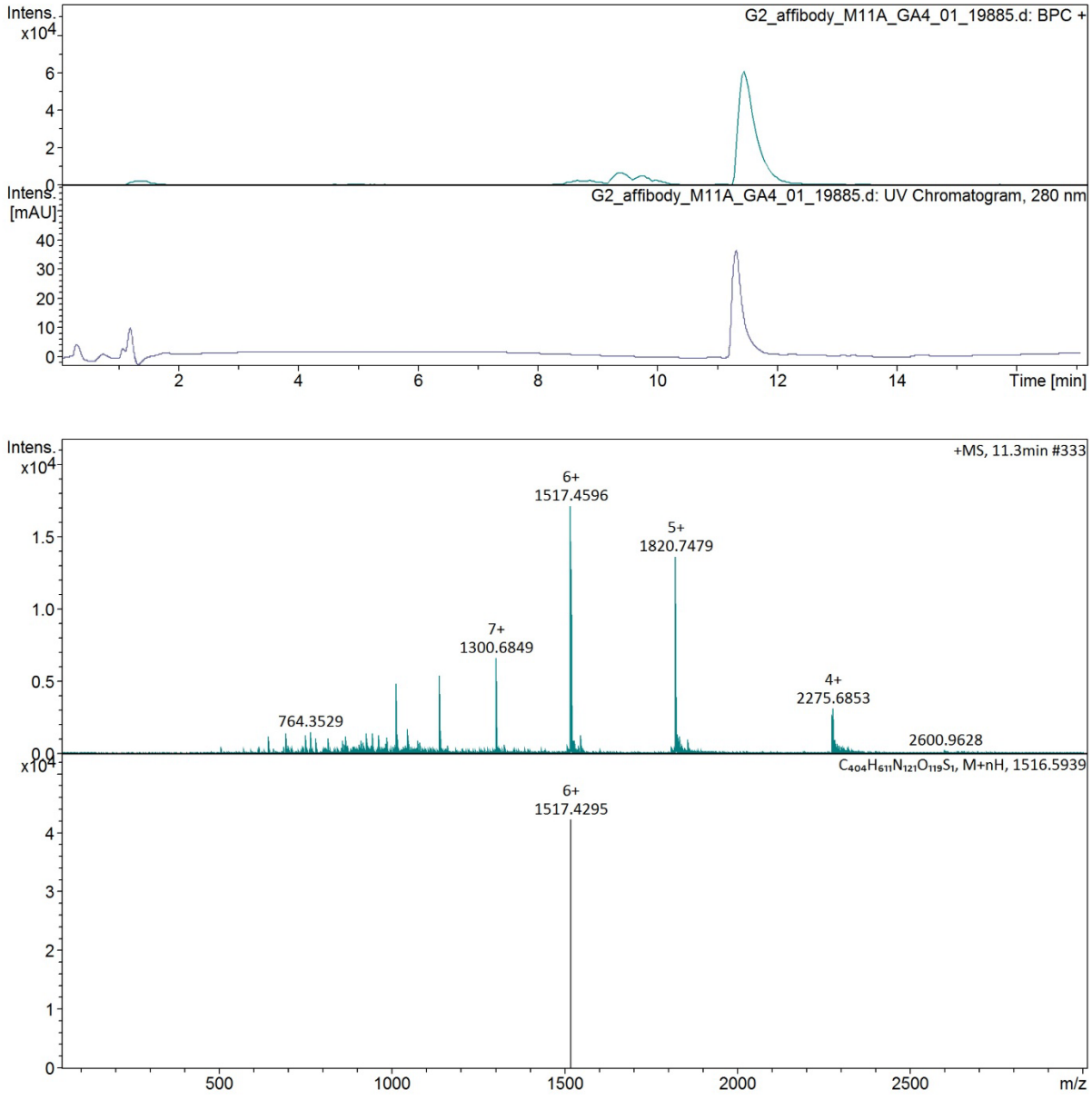

LC chromatogram measured at 280nm of G02-Ala scan variant M11A at the top with MS measured in the middle. Simulated pattern calculated is shown in black at the bottom.

- **F13A :**

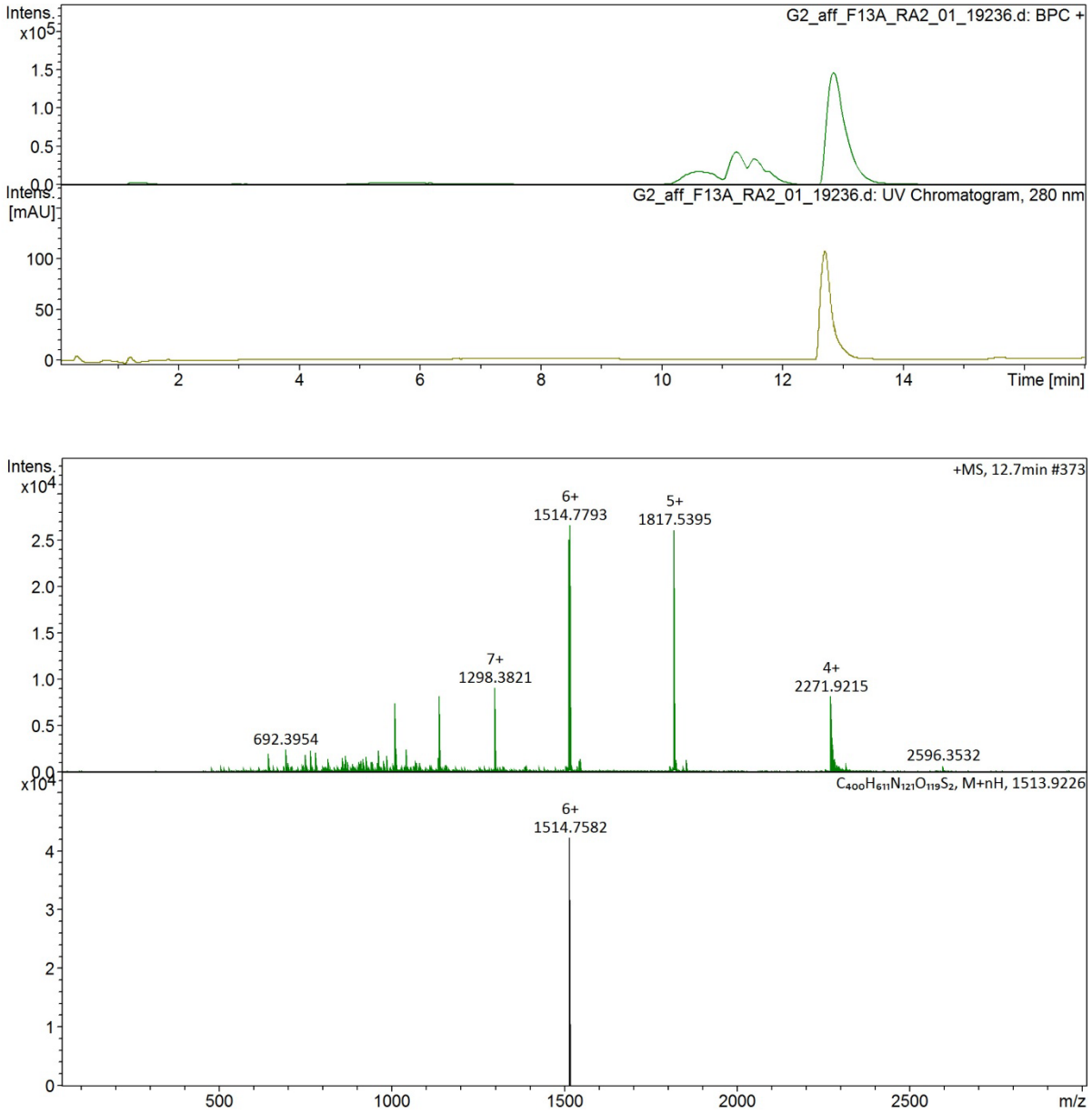

LC chromatogram measured at 280nm of G02-Ala scan variant F13A at the top with MS measured in the middle. Simulated pattern calculated is shown in black at the bottom.

- **E14A :**

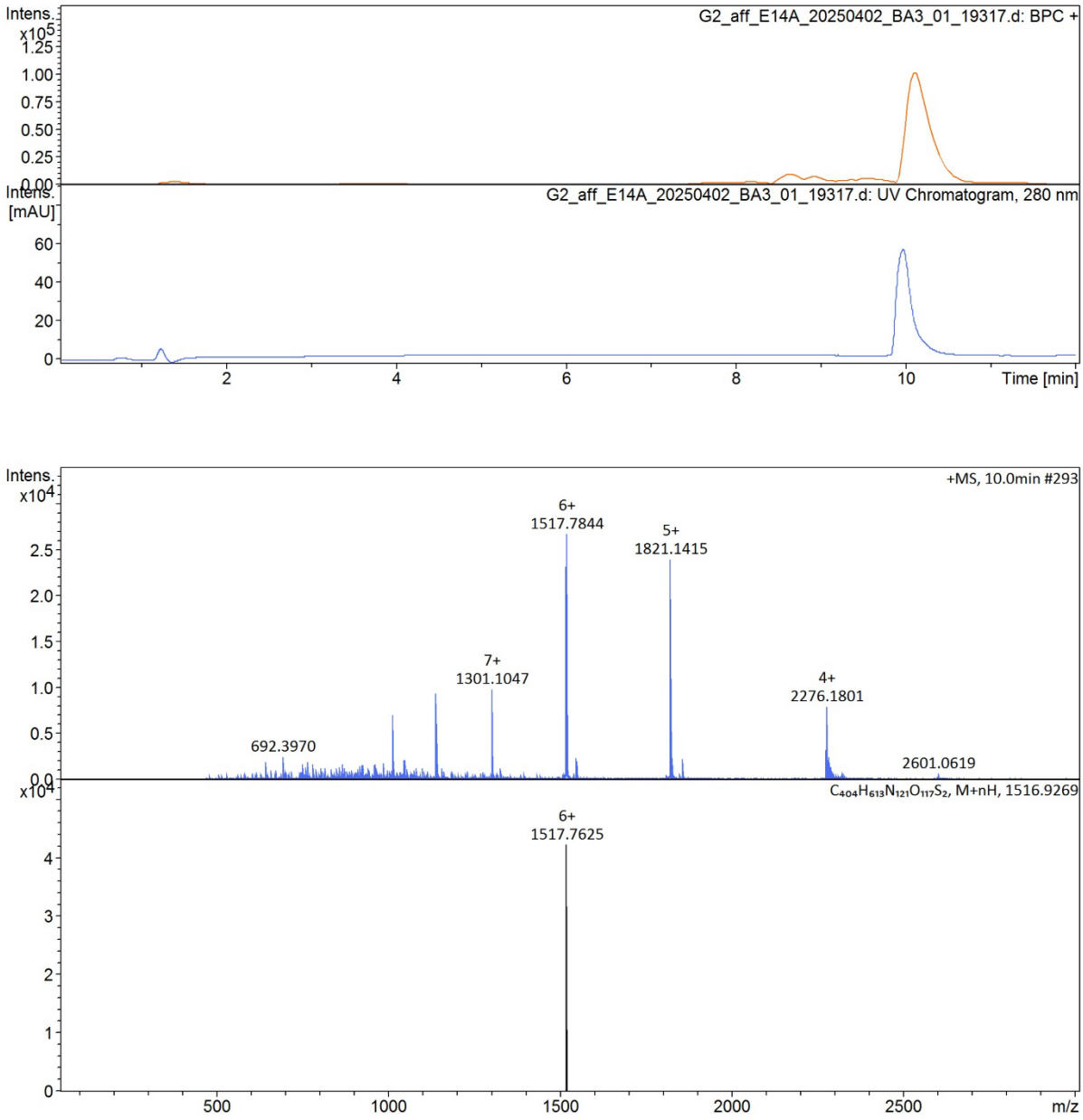

LC chromatogram measured at 280nm of G02-Ala scan variant E14A at the top with MS measured in the middle. Simulated pattern calculated is shown in black at the bottom.

- **W17A :**

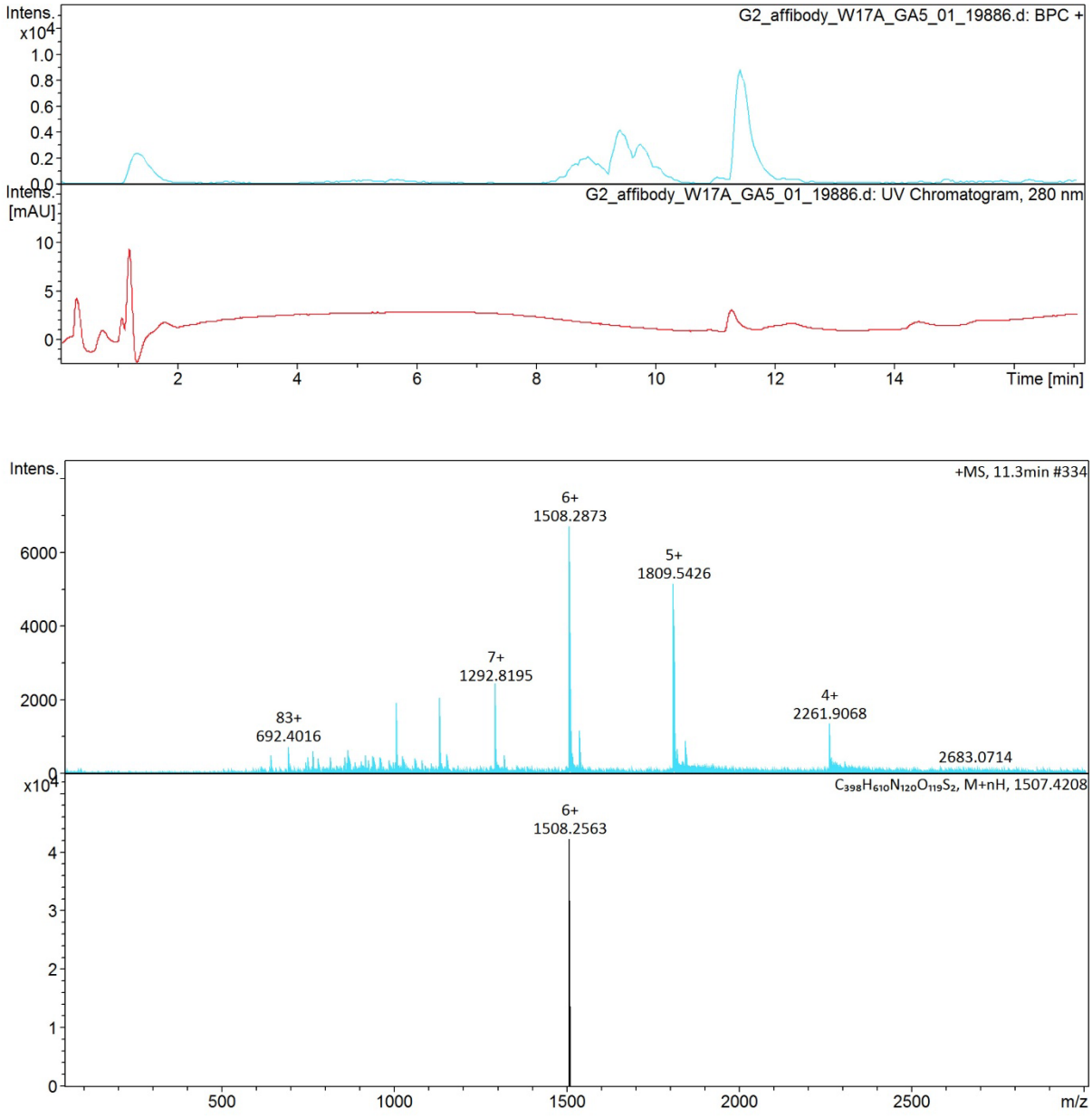

LC chromatogram measured at 280nm of G02-Ala scan variant W17A at the top with MS measured in the middle. Simulated pattern calculated is shown in black at the bottom.

- **W18A :**

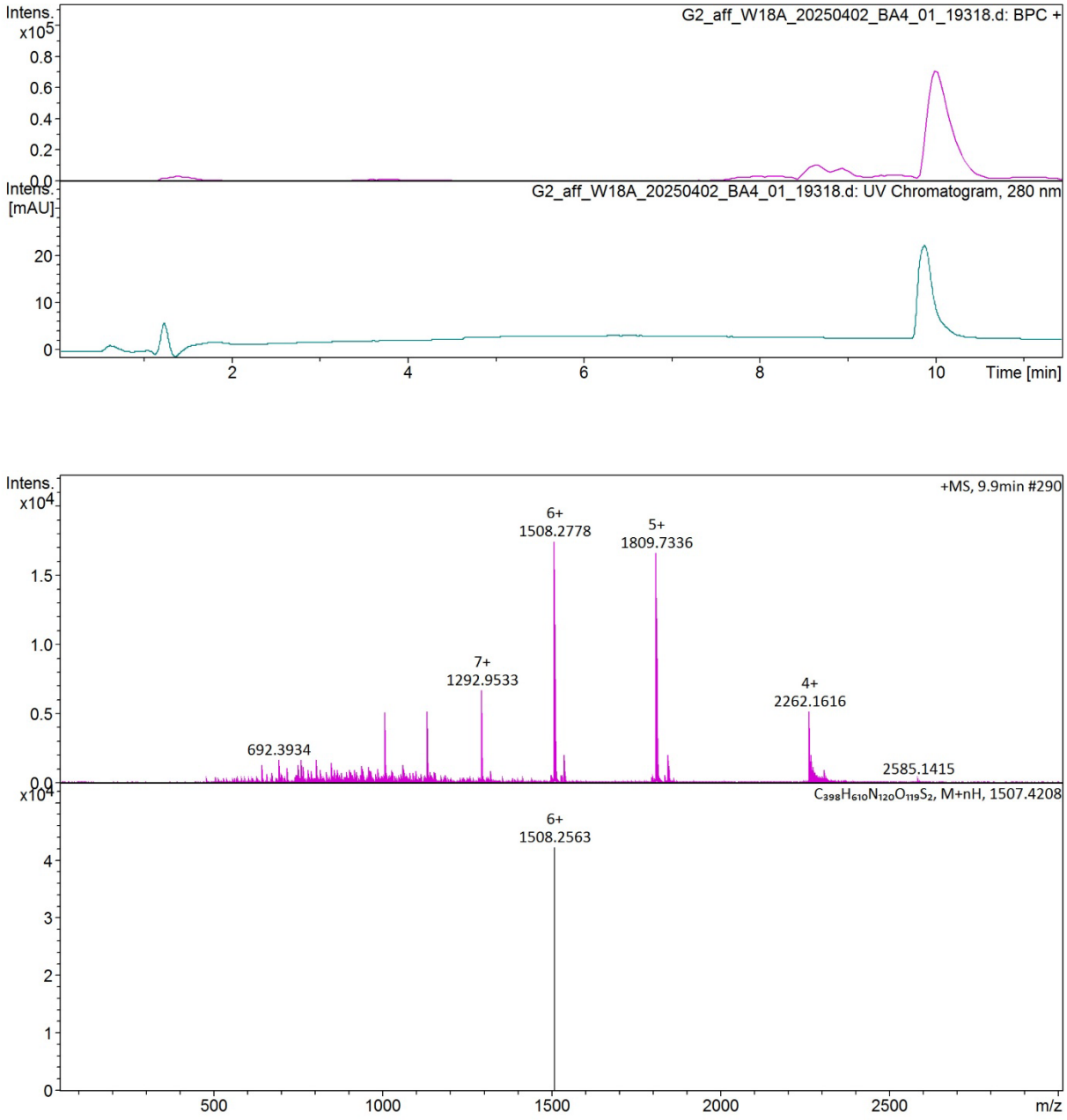

LC chromatogram measured at 280nm of G02-Ala scan variant W18A at the top with MS measured in the middle. Simulated pattern calculated is shown in black at the bottom.

- **L24A :**

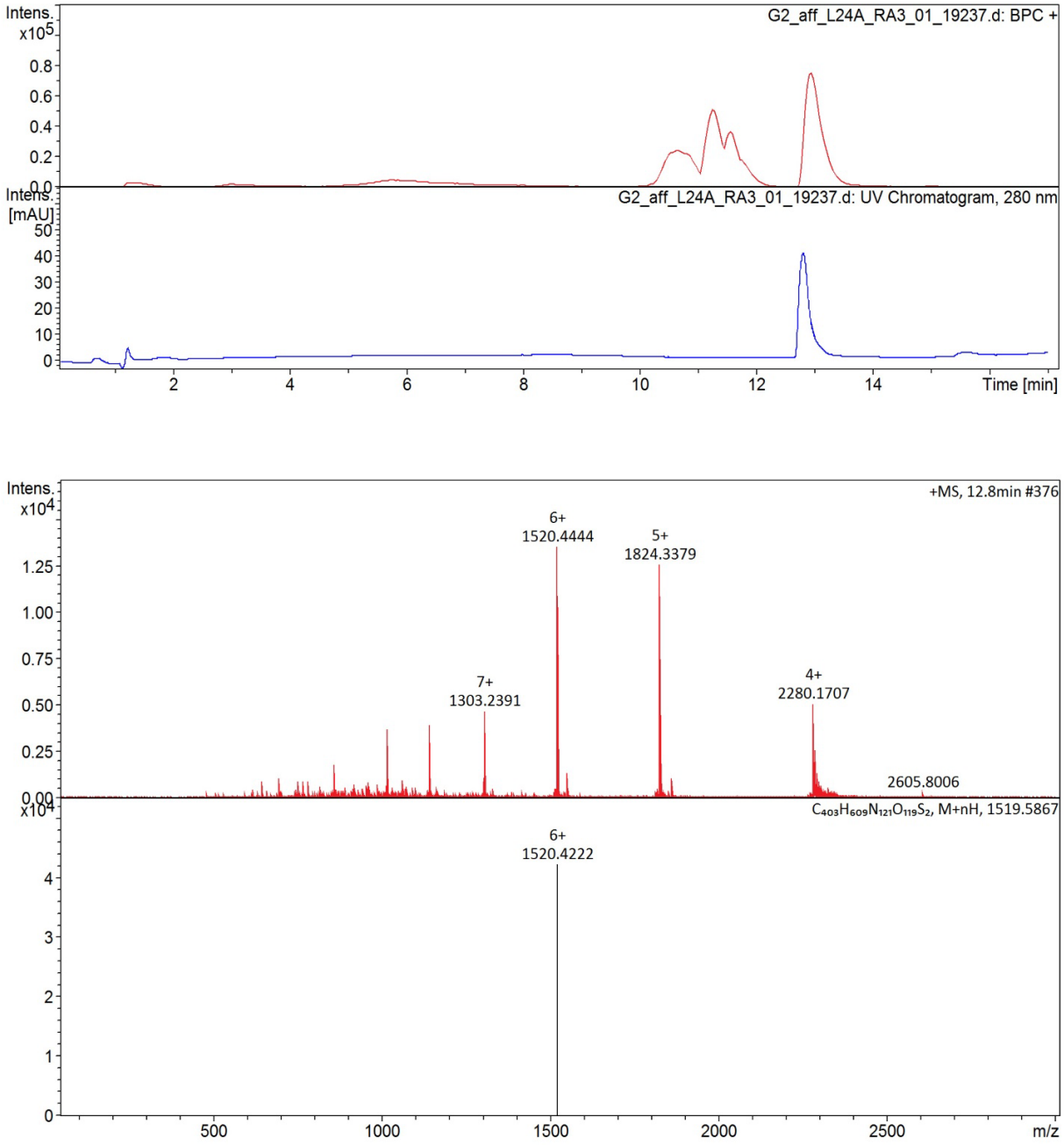

LC chromatogram measured at 280nm of G02-Ala scan variant L24A at the top with MS measured in the middle. Simulated pattern calculated is shown in black at the bottom.

- **S25A :**

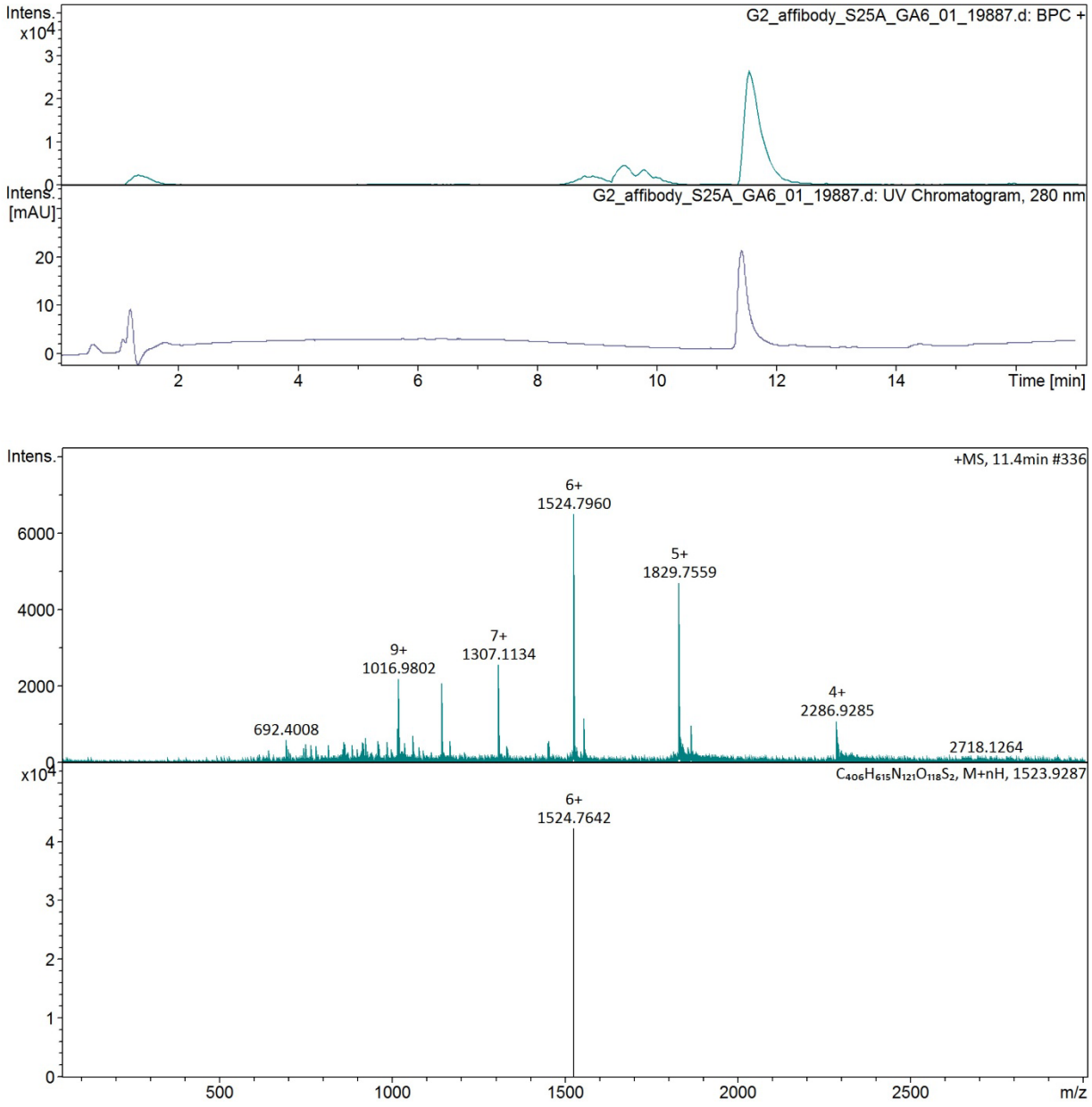

LC chromatogram measured at 280nm of G02-Ala scan variant S25A at the top with MS measured in the middle. Simulated pattern calculated is shown in black at the bottom.

- **R27A :**

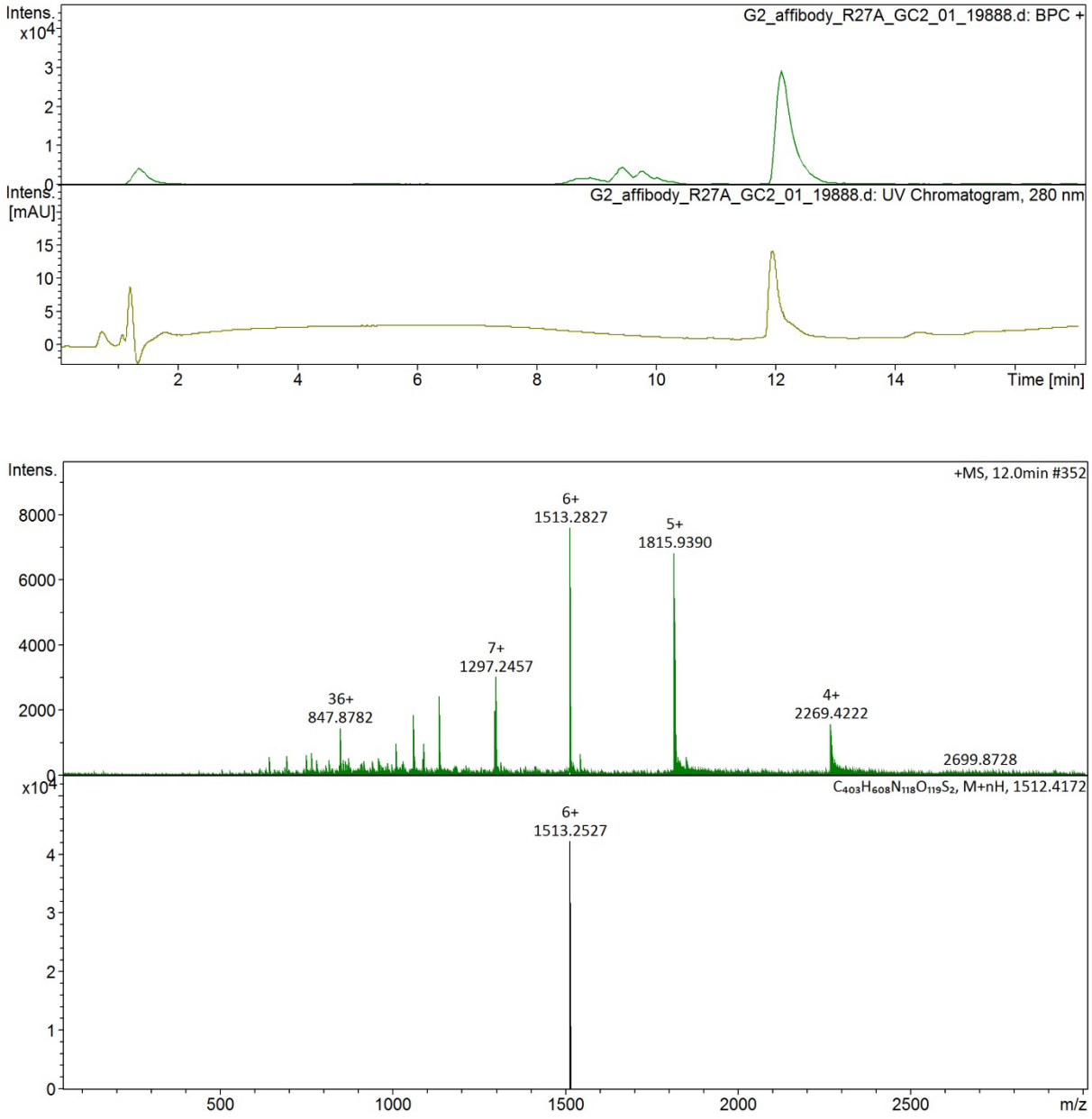

LC chromatogram measured at 280nm of G02-Ala scan variant R27A at the top with MS measured in the middle. Simulated pattern calculated is shown in black at the bottom.

- **R28A :**

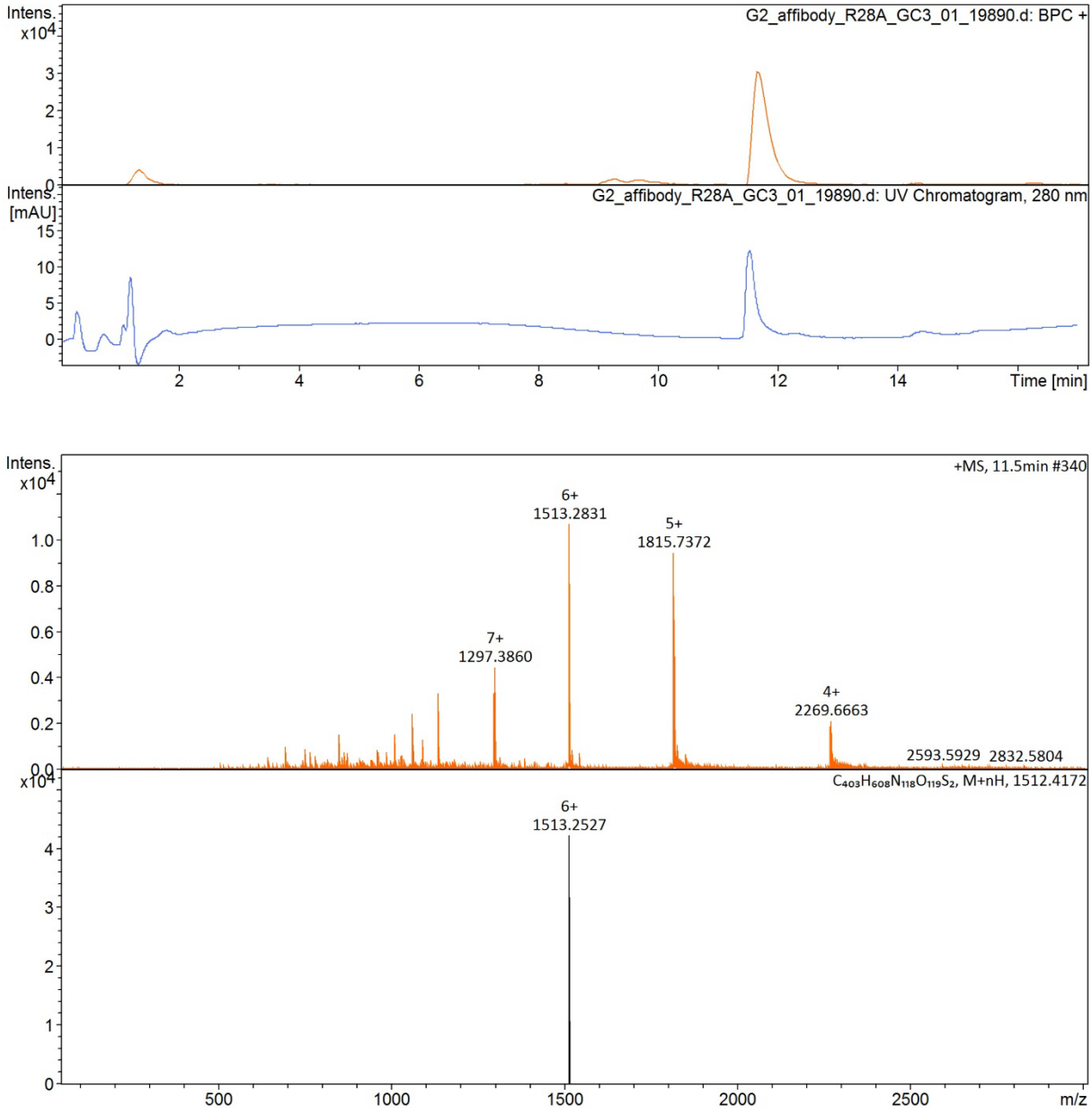

LC chromatogram measured at 280nm of G02-Ala scan variant R28A at the top with MS measured in the middle. Simulated pattern calculated is shown in black at the bottom.

- **Q32A :**

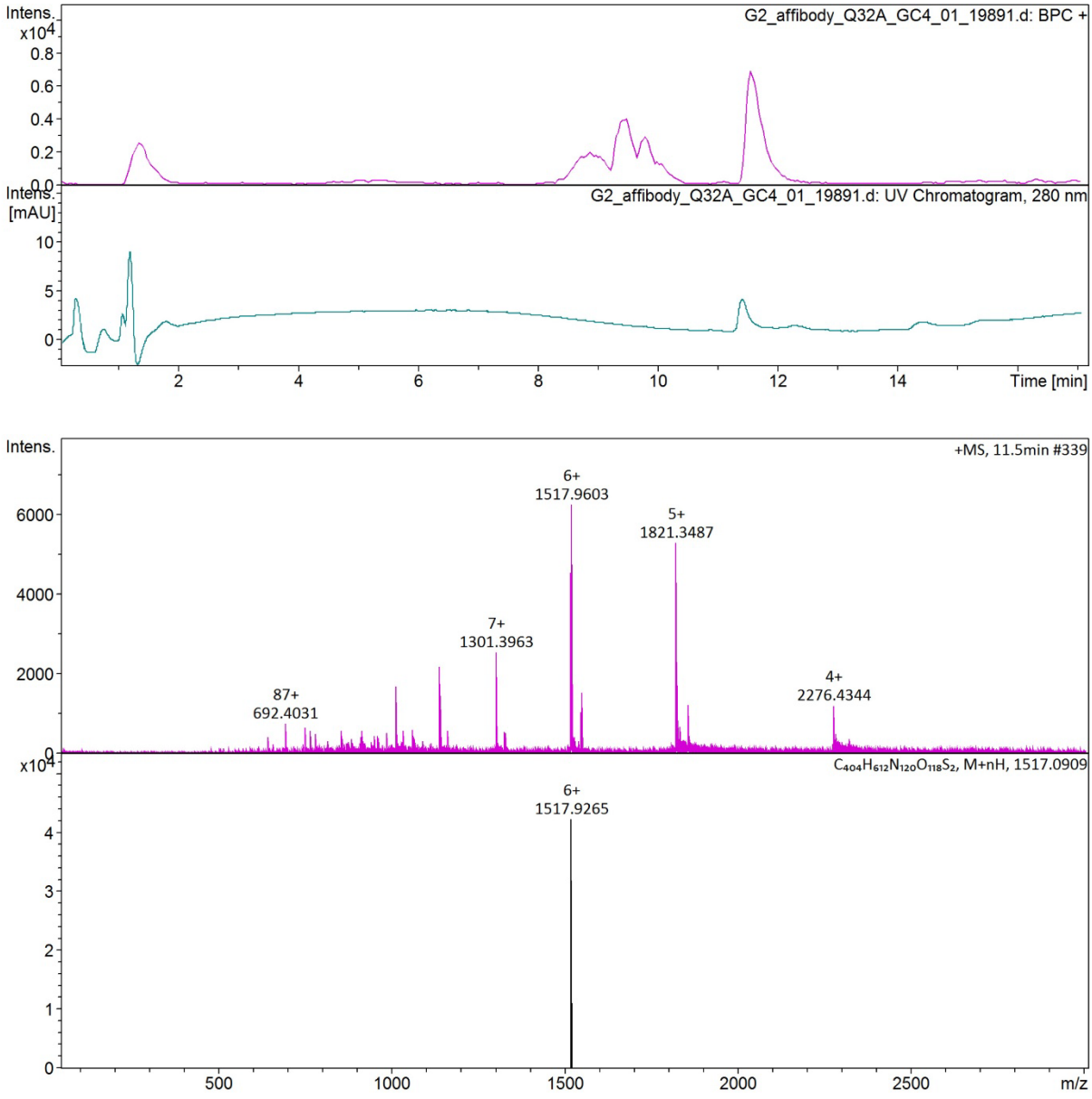

LC chromatogram measured at 280nm of G02-Ala scan variant Q32A at the top with MS measured in the middle. Simulated pattern calculated is shown in black at the bottom.

- **R35A :**

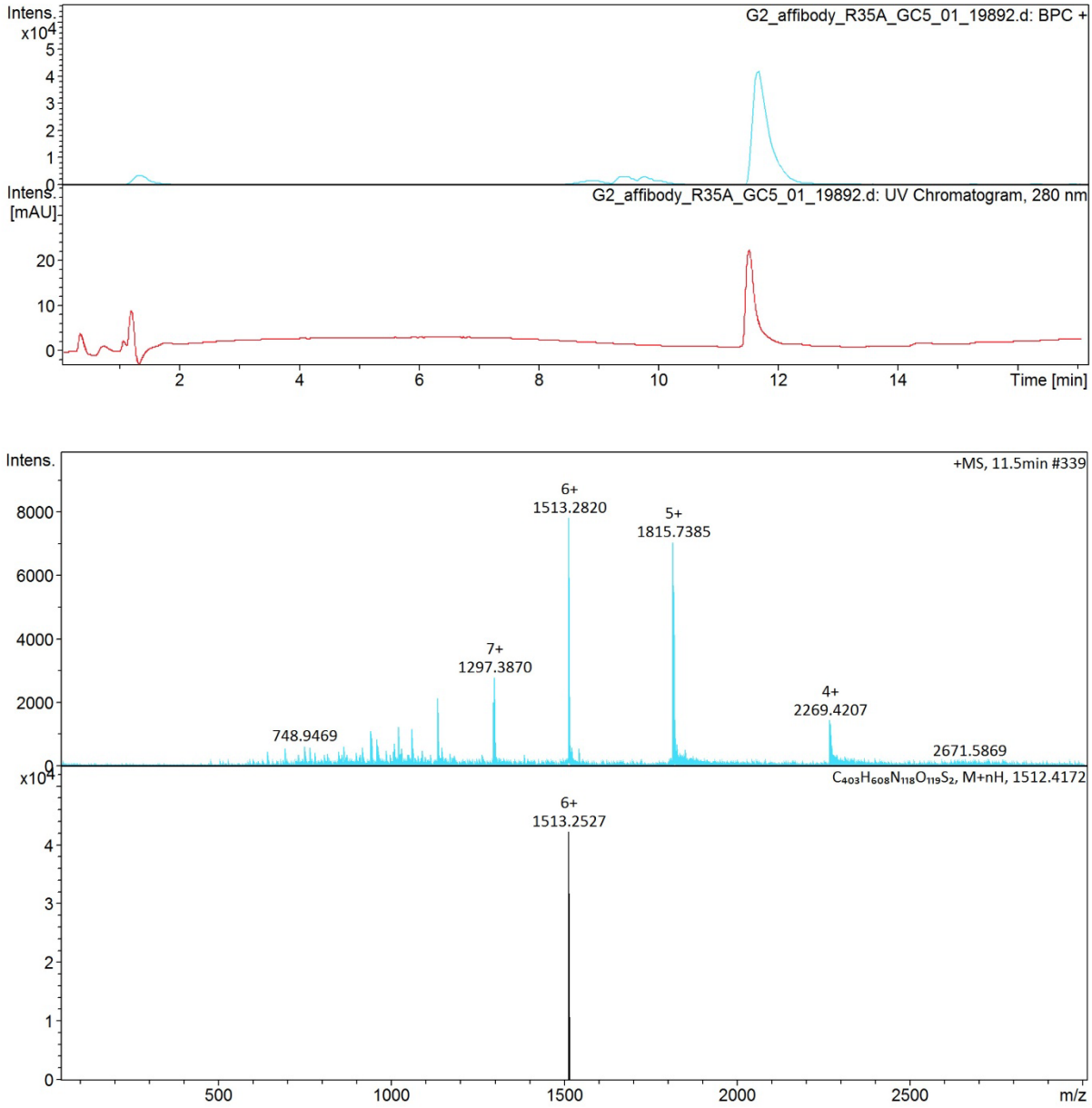

LC chromatogram measured at 280nm of G02-Ala scan variant R35A at the top with MS measured in the middle. Simulated pattern calculated is shown in black at the bottom.

➢ *CD of G02-Ala scan variants:*

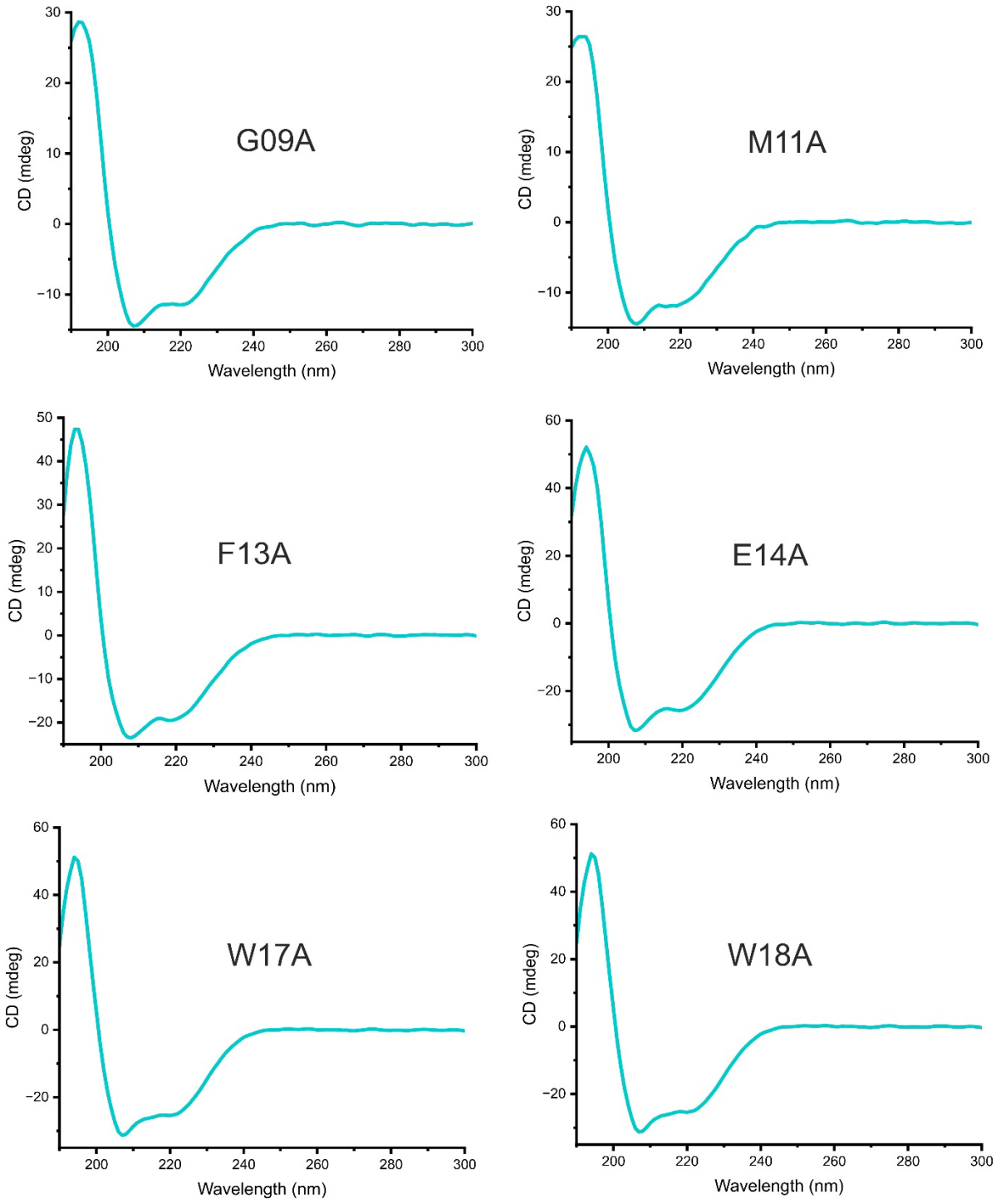

Measured CDs of G02 Ala mutants G09A, M11A, F13A, E14A, W17A and W18A all in PBS at pH = 7.4 in a 1 mm cuvette at 25 °C.

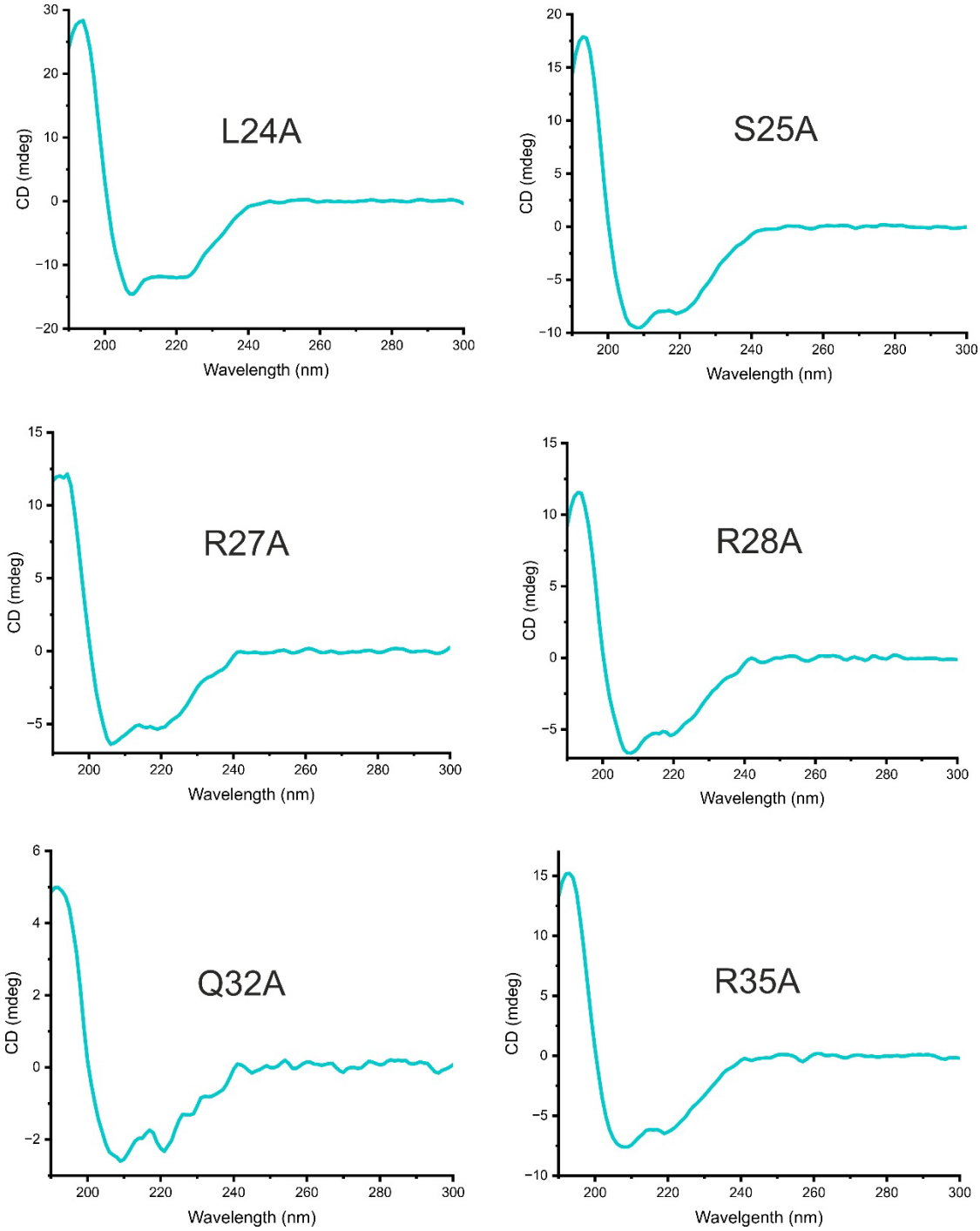

Measured CDs of G02 Ala mutants L24A, S25A, R27A, R28A, Q32A and R35A all in PBS at pH = 7.4 in a 1 mm cuvette at 25 °C.

7.5.3.5. BLI experiments data

- *BLI of P-Q_{12} and Q_5 against G02:*

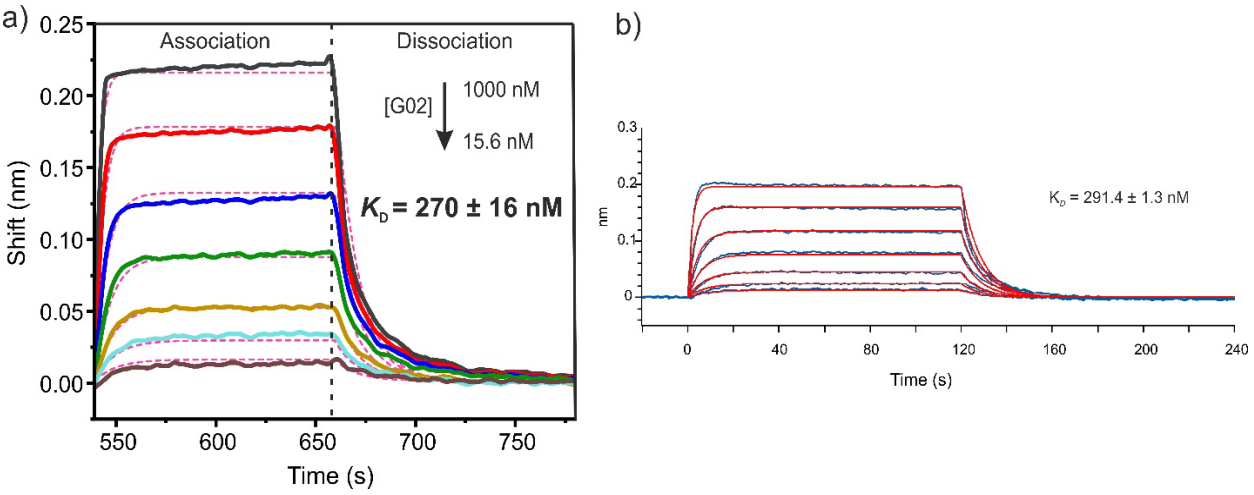

a) BLI sensorgrams of AOF *P*-**1** used as ligand against affibody clone G02 (analyte) in a serial dilution from 1000 nM to 15.6 nM recorded in PBS+0.05% Tween 20 + 0.5% BSA buffer at 25 °C. b) BLI sensorgrams of AOF **5** used as ligand against affibody clone G02 (analyte) in a serial dilution from 1000 nM to 15.6 nM recorded in PBS+0.05% Tween 20 + 0.5% BSA buffer at 25 °C.

➢ *BLI of Ala scans variants of G02 against AOF **5**:*

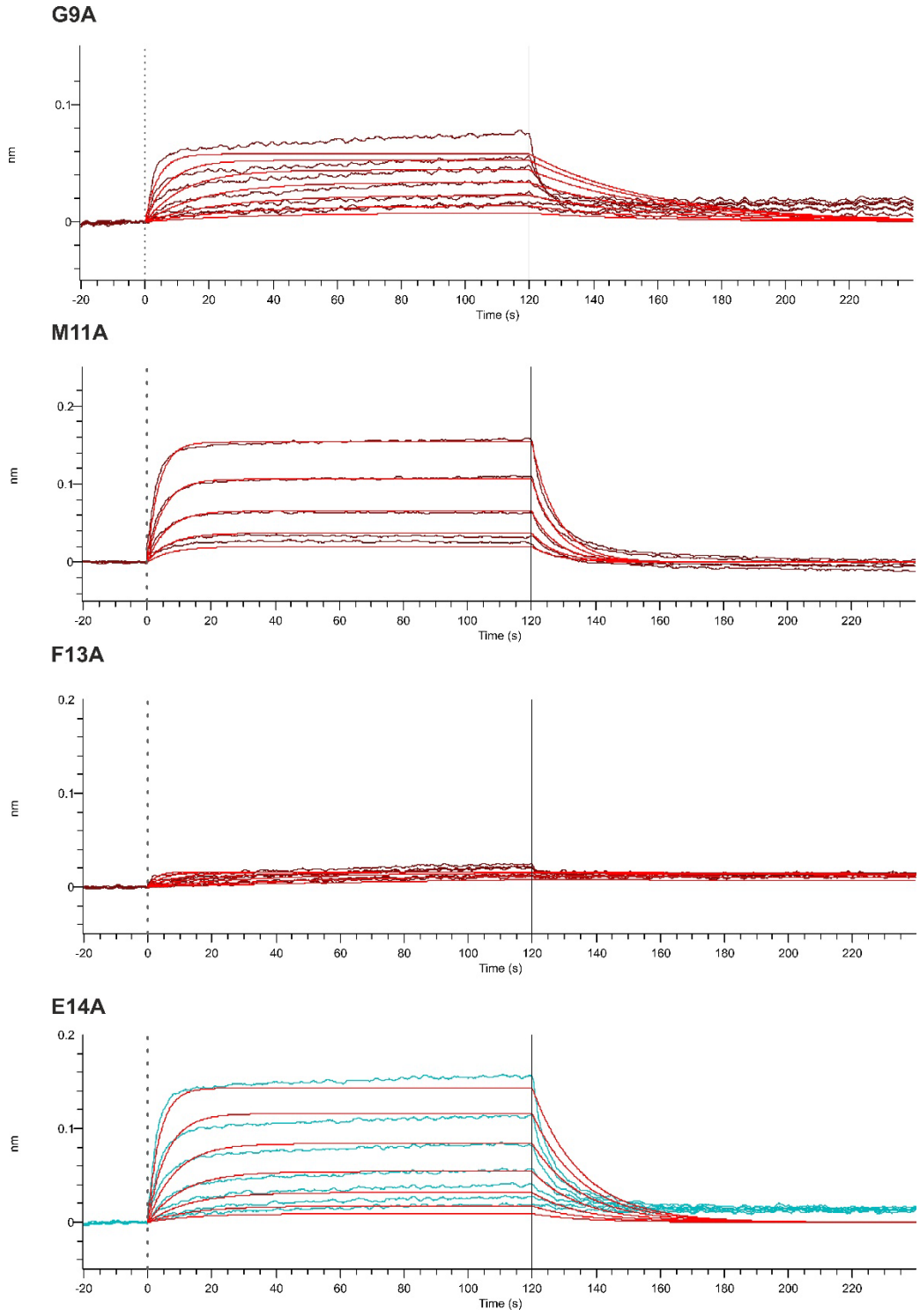

BLI sensorgrams of all G02 mutants used as analyte against AOF **5** (immobilised) in a serial dilution from 1000 nM to 15.6 nM. All experiences were recorded in PBS+0.05% Tween 20 + 0.5% BSA buffer at 25 °C.

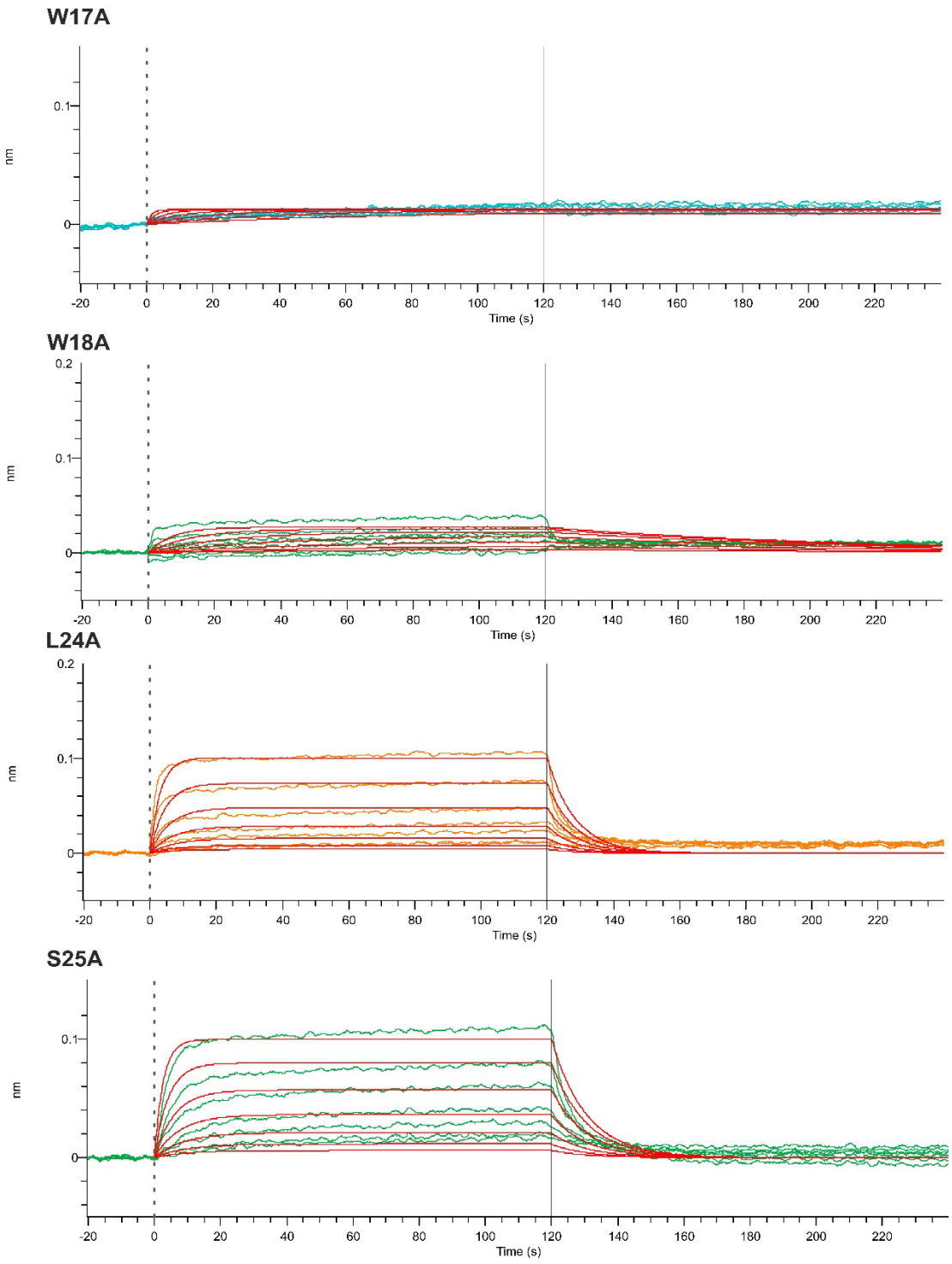

BLI sensorgrams of all G02 mutants used as analyte against AOF **5** (immobilised) in a serial dilution from 1000 nM to 15.6 nM. All experiences were recorded in PBS+0.05% Tween 20 + 0.5% BSA buffer at 25 °C.

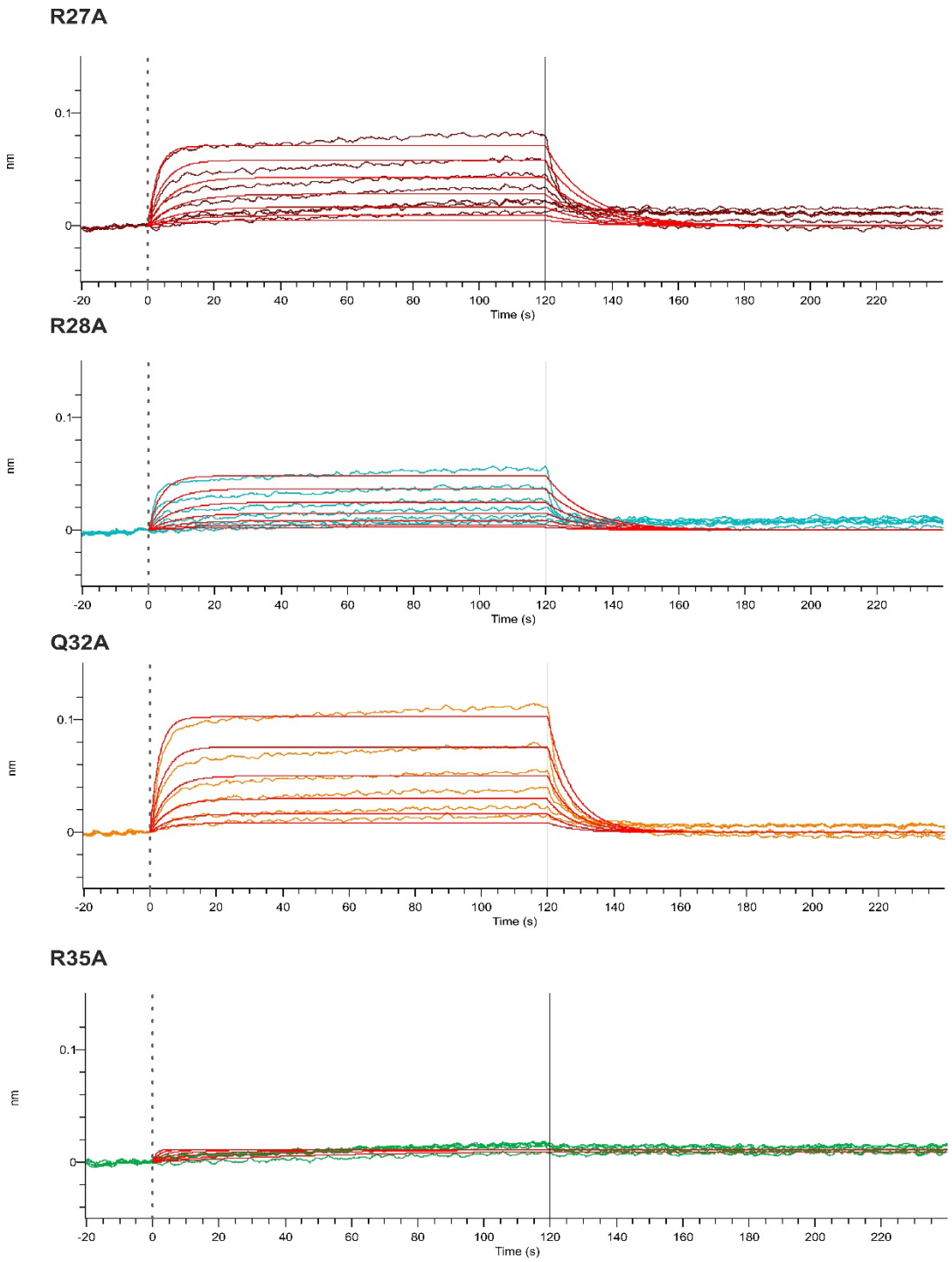

BLI sensorgrams of all G02 mutants used as analyte against AOF **5** (immobilised) in a serial dilution from 1000 nM to 15.6 nM. All experiences were recorded in PBS+0.05% Tween 20 + 0.5% BSA buffer at 25 °C.

➢ *BLI of Q^{Gly} scan against G02:*

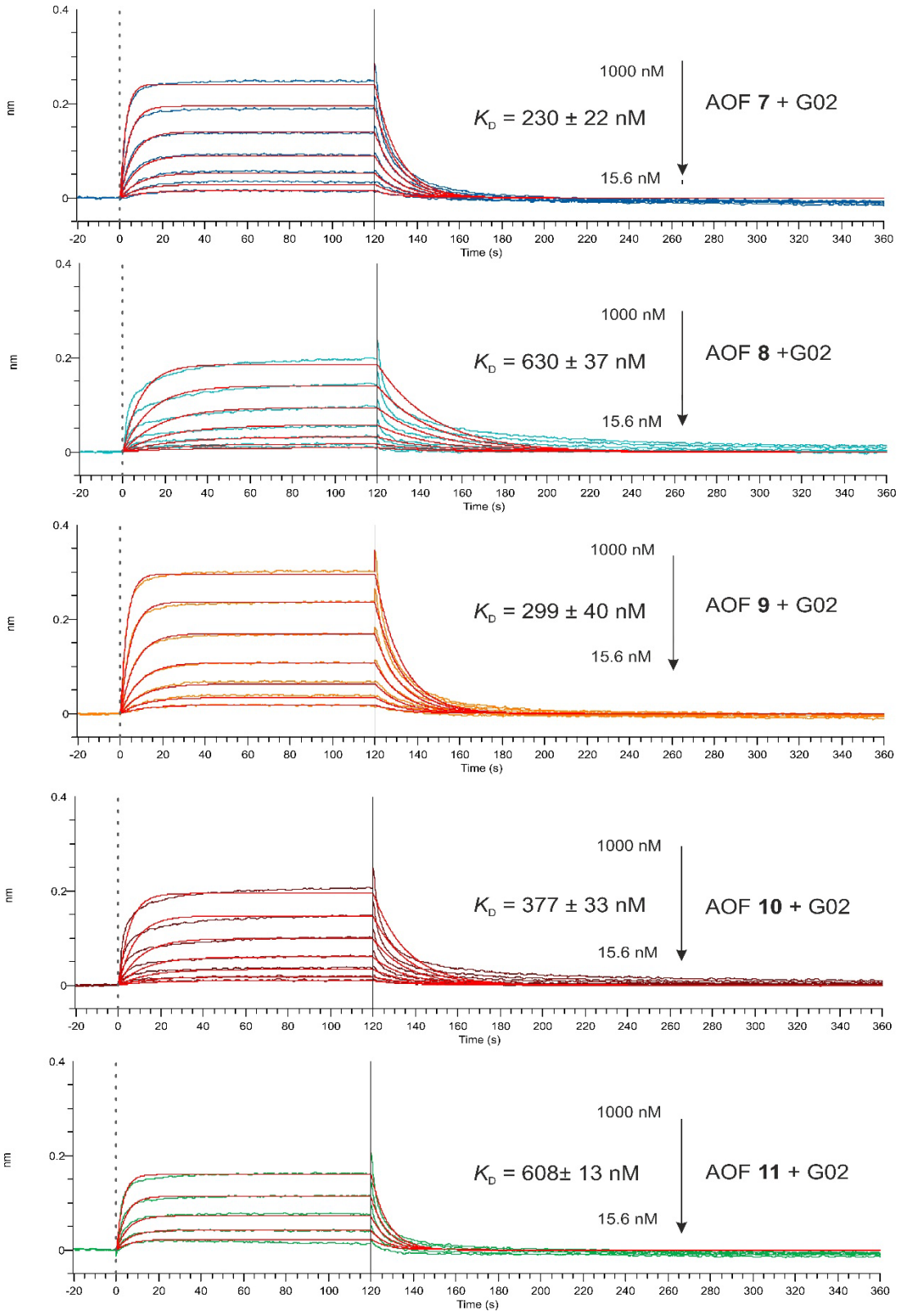

BLI sensorgrams of AOF **7** to **11** used as ligand against nanofitin G02 (analyte) in a serial dilution from 1000 nM to 15.6 nM recorded in PBS+0.05% Tween 20 + 0.5% BSA buffer at 25 °C

➢ *BLI of Q^{Gly} scan against C10:*

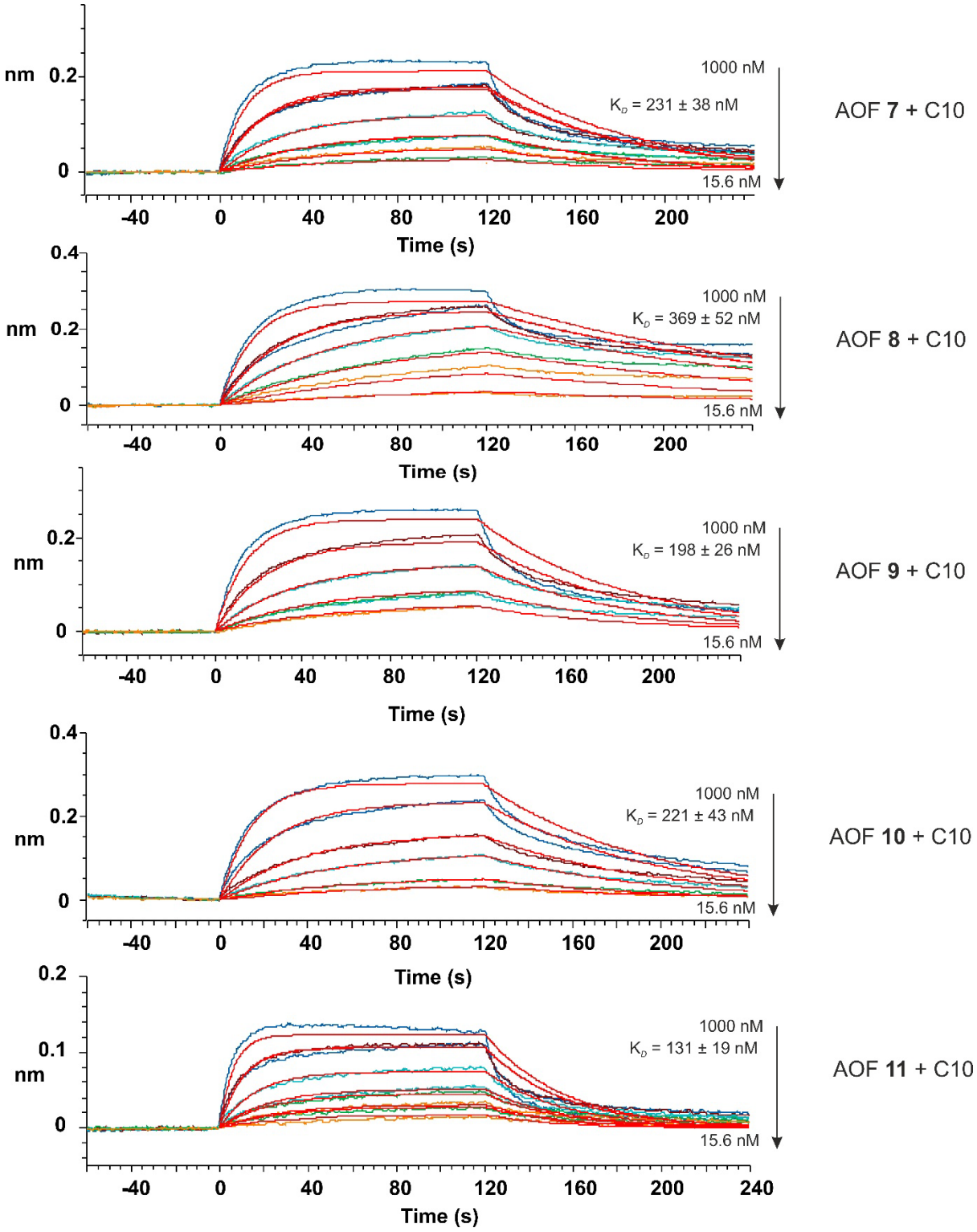

BLI sensorgrams of AOF **7** to **11** used as ligand against nanofitin C10 (analyte) in a serial dilution from 1000 nM to 15.6 nM recorded in PBS+0.05% Tween 20 + 0.5% BSA buffer at 25 °C

➢ *BLI of single mutation pentamers against G02:*

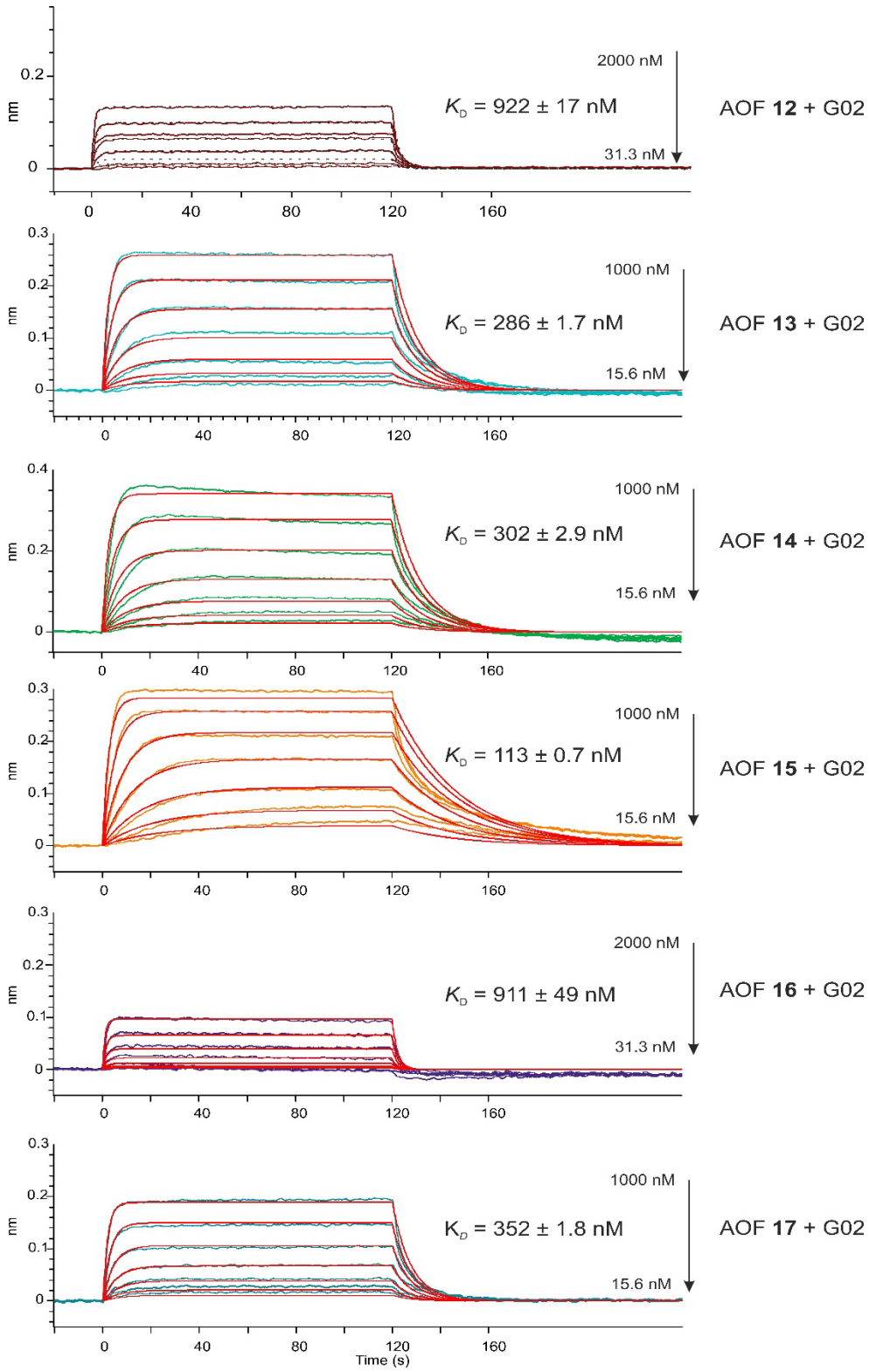

BLI sensorgrams of AOF **12** to **17** used as ligand against affibody clone G02 (analyte) in a serial dilution from 1000 nM to 15.6 nM for AOF **13-15** and **17** and from 2000 nM to 31.3 nM for AOFs **12** and **16**. All experiences were recorded in PBS+0.05% Tween 20 + 0.5% BSA buffer at 25 °C

➢ *BLI of single mutation pentamers against C10:*

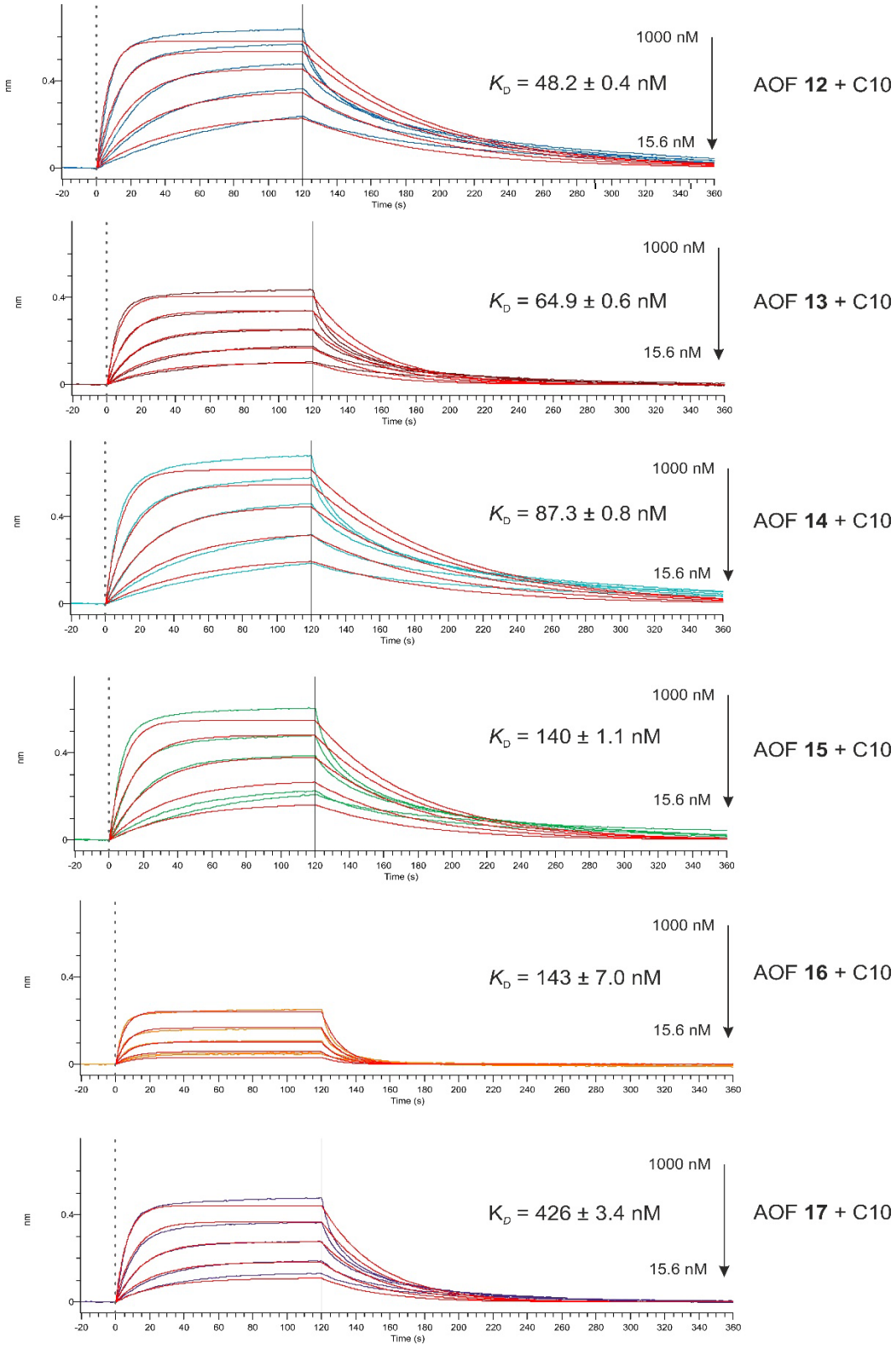

BLI sensorgrams of AOF **12** to **17** used as ligand against affibody clone C10 (analyte) in a serial dilution from 1000 nM to 15.6 nM. All experiences were recorded in PBS+0.05% Tween 20 + 0.5% BSA buffer at 25 °C

7.6. Crystallography

Initial broad screening of crystallisation conditions was performed at the Crystallization Facility of the Max Planck Institute for Biochemistry (Martinsried, Germany). Experiments were conducted in small volumes (100 nL) using sitting-drop vapor diffusion setups. Subsequent optimisation of promising conditions was carried out using hanging-drop vapor diffusion experiments (0.5-1 µL) at 4 °C. Crystals of the G02 coiled-coil dimer with **6** were obtained using 18% MPEG 5000 and 100 mM HEPES pH 7.0 as the precipitant. These crystals diffracted up to 2.7 Å and consistently indexed in the orthorhombic space group F222 with unit cell dimensions a = 91.373 Å, b = 111.367 Å and c = 144.359 Å.

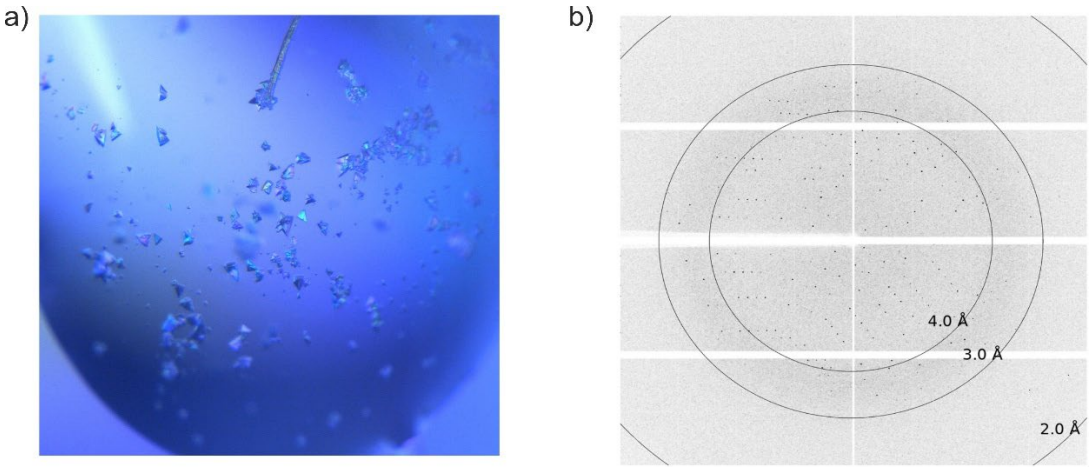

a) Crystals of complex G02CCDi and **6** observed under crossed polarising microscope grown in 18% MPEG 500 and 100mM HEPES pH = 7.0 at 4 °C. b) Diffraction pattern image during characterisation of the crystals.

7.7. References

[1] Y. Hsia, J. B. Bale, S. Gonen, D. Shi, W. Sheffler, K. K. Fong, U. Nattermann, C. Xu, P.-S. Huang, R. Ravichandran, S. Yi, T. N. Davis, T. Gonen, N. P. King, D. Baker, *Nature* **2016**, *535*, 136-139.

[2] Z. Liu, M. Hu, Y. Yang, C. Du, H. Zhou, C. Liu, Y. Chen, L. Fan, H. Ma, Y. Gong, Y. Xie, *Molecular Biomedicine* **2022**, *3*, 46.

[3] L. Regan, W. F. DeGrado, *Science* **1988**, *241*, 976-978.

[4] L. Soini, S. Leysen, J. Davis, C. Ottmann, *Current Opinion in Chemical Biology* **2022**, *69*, 102169.

[5] A. R. Thomson, C. W. Wood, A. J. Burton, G. J. Bartlett, R. B. Sessions, R. L. Brady, D. N. Woolfson, *Science* **2014**, *346*, 485-488.

[6] S. Wang, J. Sigl, L. Allmendinger, V. Maurizot, I. Huc, *Chemical Science* **2025**, *16*, 1136-1146.

[7] V. Corvaglia, F. Sanchez, F. S. Menke, C. Douat, I. Huc, *Chemistry – A European Journal* **2023**, *29*, e202300898.

[8] M. Zwillinger, P. Sőregi, F. Sanchez, C. Douat, M. Csékei, I. Huc, A. Kotschy, *The Journal of Organic Chemistry* **2025**, *90*, 3043-3052.

[9] B. Mouratou, F. Schaeffer, I. Guilvout, D. Tello-Manigne, A. P. Pugsley, P. M. Alzari, F. Pecorari, *Proceedings of the National Academy of Sciences* **2007**, *104*, 17983-17988.

[10] H. Robinson, Y.-G. Gao, B. S. McCrary, S. P. Edmondson, J. W. Shriver, A. H. J. Wang, *Nature* **1998**, *392*, 202-205.

[11] M. Högbom, M. Eklund, P.-Å. Nygren, P. Nordlund, *Proceedings of the National Academy of Sciences* **2003**, *100*, 3191-3196.

[12] S. Kwon, V. Morozov, L. Wang, P. K. Mandal, S. Chaignepain, C. Douat, I. Huc, *Organic & Biomolecular Chemistry* **2024**, *22*, 9342-9347.

[13] A. R. Gingras, N. Bate, B. T. Goult, L. Hazelwood, I. Canestrelli, J. G. Grossmann, H. Liu, N. S. M. Putz, G. C. K. Roberts, N. Volkmann, D. Hanein, I. L. Barsukov, D. R. Critchley, *The EMBO Journal* **2008**, *27*, 458-469-469.

[14] X. Hu, S. J. Dawson, P. K. Mandal, X. de Hatten, B. Baptiste, I. Huc, *Chemical Science* **2017**, *8*, 3741-3749.

[15] B. Baptiste, C. Douat-Casassus, K. Laxmi-Reddy, F. Godde, I. Huc, *The Journal of Organic Chemistry* **2010**, *75*, 7175-7185.

[16] M. Vallade, P. Sai Reddy, L. Fischer, I. Huc, *European Journal of Organic Chemistry* **2018**, *2018*, 5489-5498.

[17] B. Teng, J. Atcher, L. Allmendinger, C. Douat, Y. Ferrand, I. Huc, *Organic & Biomolecular Chemistry* **2023**, *21*, 3525-3530.

[18] D. Mazzier, S. De, B. Wicher, V. Maurizot, I. Huc, *Angewandte Chemie International Edition* **2020**, *59*, 1606-1610.

[19] T. Christos, J. D. Simon, H. Ivan, *Comptes Rendus. Chimie* **2016**, *19*, 132-142.

[20] D. Bindl, E. Heinemann, P. K. Mandal, I. Huc, *Chemical Communications* **2021**, *57*, 5662-5665.

[21] S. Dengler, P. K. Mandal, L. Allmendinger, C. Douat, I. Huc, *Chemical Science* **2021**, *12*, 11004-11012.

8. Targeting the NEMO-di-ubiquitin complex by mimicking the interaction of the coiled-coil NEMO with AOFs

Authors: Florian Sanchez, Petra Sőregi, Márton Zwillinger, Johannes Sigl, Céline Douat, Lucile Fischer, Márton Csékei, András Kotschy and Ivan Huc.

Contributions: This project is a joint collaboration between two groups. It was planned by I. Huc and A. Kotschy. Monomer syntheses were performed by F. Sanchez, P. Sőregi and M. Zwillinger. Oligomers syntheses were performed by F. Sanchez and C. Douat. Proteins expressions and ligations were performed by F. Sanchez. Crystal growth and analyses were done by F. Sanchez and J. Sigl. NMR elucidations were performed by L. Fischer. This project was supervised by L. Fischer, C. Douat and I. Huc. This chapter was written in collaboration with F. Sanchez, C. Douat and I. Huc.

8.1. Introduction

The transcription factor NF-κB (also known as nuclear factor kappa enhancer binding protein) plays a central role in immune and inflammatory responses, cell survival, and development. Its activation depends on the IκB kinase (IKK) complex, composed of the catalytic subunits IKKα and IKKβ together with the regulatory protein NEMO (NF-κB essential modulator). Although NEMO lacks intrinsic enzymatic activity, it functions as a molecular hub that recruits kinase subunits to upstream signalling complexes and bridges interactions with ubiquitin chains, thereby enabling efficient pathway activation (**Figure 1**).[1] In this sense, any mutation of NEMO would disrupt the IκB complex which in turn could block NF-κB signalling and lead to immunodeficiency or cancer.[2-3][4] Ubiquitin itself has roles beyond proteasomal degradation: Lys63-linked and linear di-ubiquitin chains form higher-order signalling platforms that assemble kinases in proximity and thus promote NF-κB activation.

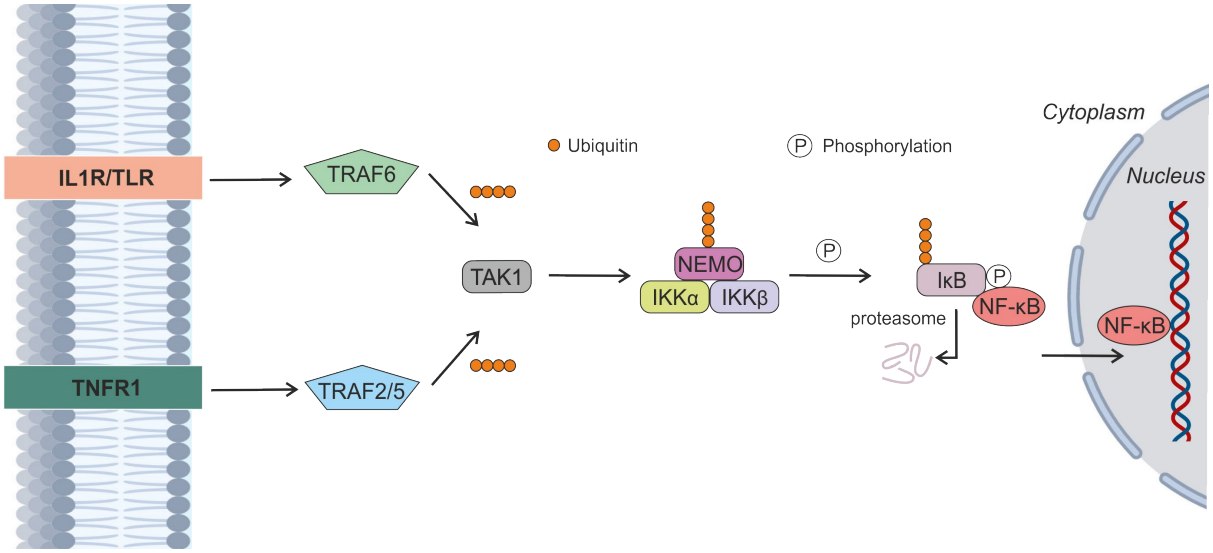

Figure 1. NF-κB signalling pathway mediated by ubiquitination. In the canonical NF-κB pathway, stimulation of TNF receptors (TNFRs), IL-1 receptor (IL-1R), or Toll-like receptors (TLRs) by their respective ligands triggers the activation of TNFR-associated factor (TRAF) proteins. This, in turn, stimulates TGFβ-activated kinase 1 (TAK1), which phosphorylates and activates IKKβ. Activated IKKβ phosphorylates IκB, tagging it for ubiquitination and subsequent proteasomal degradation. Once IκB is degraded, NF-κB is released and translocates into the nucleus, where it drives the transcription of genes which orchestrate inflammation, immune responses, and cell survival.

Structural studies have clarified how NEMO recognises these ubiquitin-based signals. In 2009 Lo *et al.* first demonstrated that NEMO binds di-ubiquitin, showing that linkage type governs binding affinity and selectivity.[5] Yoshikawa *et al.* further resolved the X-ray crystal structure of the CC2-LZ region of NEMO in complex with Lys63-linked di-ubiquitin at 2.7 Å resolution, showing that the interaction occurs mainly through the Ile44 hydrophobic patch of ubiquitin.[6] This relatively limited interface explains in part the modest affinity of NEMO for Lys63-linked chains, with dissociation constants K_D typically in the range of 100 μM.

Rahighi *et al.* provided the most detailed structural explanation of the selectivity of NEMO for ubiquitin. They showed that the UBAN domain (Ubiquitin Binding in ABIN and NEMO) binds the linear di-ubiquitin with micromolar affinity (K_D = 1.6 µM).[7] Crystallographic data revealed a parallel coiled-coil dimer of NEMO forming two symmetric grooves, each engaging a linear di-ubiquitin molecule. Critical residues within the UBAN domain include Glu291, Phe305, and Leu312, which are establishing contacts with the Ile44 hydrophobic patch and the extended linkage of the ubiquitins. Mutations at these sites abolish binding and impair NF-κB activation, firmly positioning linear di-ubiquitin recognition by the UBAN domain as a decisive molecular event in NF-κB signalling.

8.2. Structural information on coiled-coil NEMO and linear di-ubiquitin

NEMO is a dimeric protein of 419 amino acids which features two coiled-coil domains, a leucine zipper, and a zinc finger domain. Several studies have identified the coiled-coil domain and leucine zipper region, also known as the CoZi region, as the portion of NEMO required for ubiquitin chain binding.[8-10] Embedded within this region is the UBAN motif, a conserved domain shared with other ubiquitin-binding proteins and central to NEMO's ubiquitin recognition (**Figure 2**).[11]

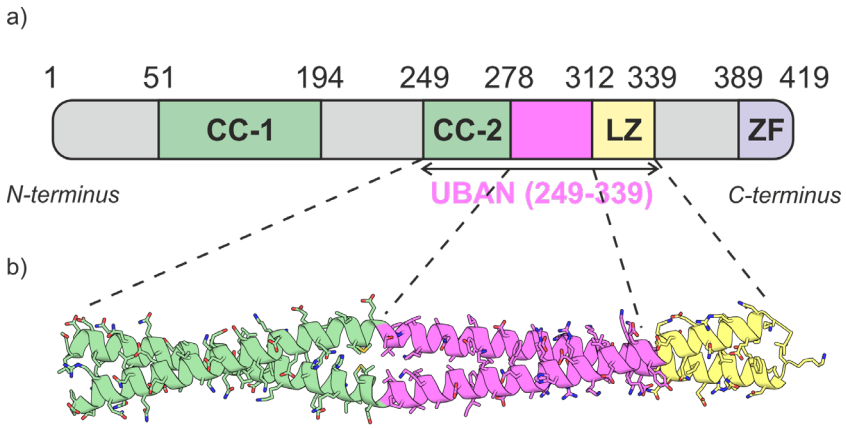

Figure 2. a) Schematic domain organisation of NEMO with the different part highlighted in green as CC for coiled-coil, UBAN in purple for the ubiquitin binding domain, LZ in yellow for the leucine zipper domain and ZF in blue for the zinc finger domain. b) Isolated X-ray crystal structure of the CoZi domain of NEMO (PDB#2ZVN), the different domains are highlighted in the same colours as the schematic representation above.

The linear di-ubiquitin (or diUb for the rest of this chapter) is also called Met1-linked diubiquitin. Each ubiquitin is composed of 76 amino acids (~ 8.5 kDa); they possess a β-sheet region, a very small 3_{10}-helix region and a α-helix. The linear diUb is formed when the C-terminal glycine (Gly76) of one ubiquitin is covalently linked to the amino group of the first methionine (Met1) of another ubiquitin (**Figure 3**). This head-to-tail connection creates a linear topology that

distinguishes it from Lys48- or Lys63-linked chains and makes it a key signalling scaffold in NF-κB activation.

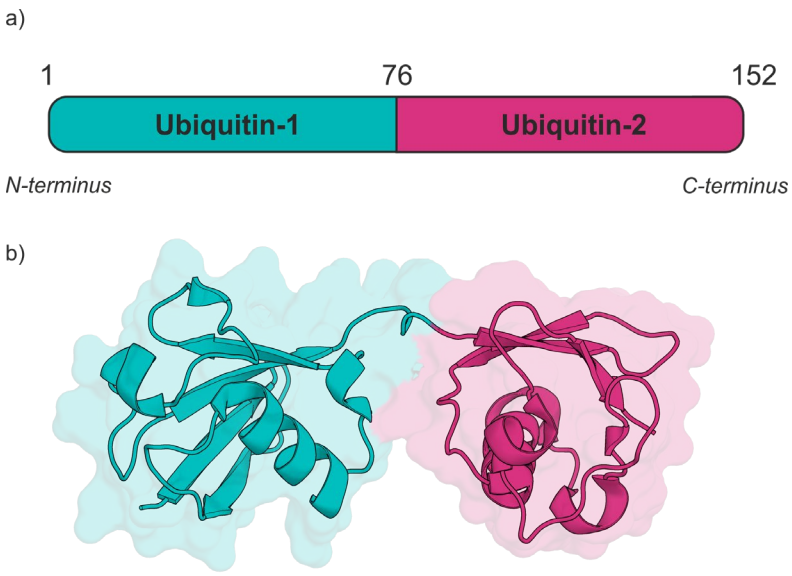

Figure 3. a) Schematic domain organisation of linear diUb with each ubiquitin showed as either teal or pink. b) Isolated X-ray crystal structure of the linear diUb (PDB#2ZVN), the ubiquitins are coloured in a same manner as the schematic representation above.

8.3. Design and strategy for the mimicry

Linear diUb was selected as the target protein for our study because ubiquitin, and by extension diubiquitin, is a very well-characterised protein. It possesses remarkable features such as high thermostability, resistance to proteolysis, outstanding folding properties, stability across a broad pH range and can be recombinantly expressed with consistent high yields.[12] [13] Its relatively small size (76 amino acids per ubiquitin unit) makes it particularly amenable to structural studies such as ^{15}N-HSQC NMR. Moreover, the wide library of structural insights already available for ubiquitin provided an ideal framework to test our ability to design single helix AOFs, which could reproduce the spatial orientation of the α-residues of a coiled-coil domain interacting with the surface of the partner protein.

8.3.1. Protein construct choice Ub(H68C)

To initiate our investigation into the mimicry of the coiled-coil domain of NEMO protein with AOFs, we focused our approach on the crystal structure of NEMO in complex with linear diUb, published in 2009 (**Figure 4a**).[14] In this study, the two ubiquitin moieties are distinguished as distal (N-terminal) and proximal (C-terminal). Importantly, these subunits contribute unequally to the interaction with the UBAN region of NEMO. The Ub distal is positioned in close proximity

to one helix of NEMO and establishes a greater number of contacts compared to the Ub proximal (**Figure 4b**). Its binding is mediated by the canonical hydrophobic pocket centred on Ile44, complemented by charge-reinforced hydrogen bonds involving Arg42, Arg72, and Arg74 (**Figure 4c**). By contrast, the $Ub_{proximal}$ makes fewer contacts and is predominantly engaged in polar interactions, primarily involving the region around Thr89 (Figure 4b). This asymmetry in binding highlights the critical role of Ub_{distal} in stabilising the complex and provides a rational starting point for our design strategy.

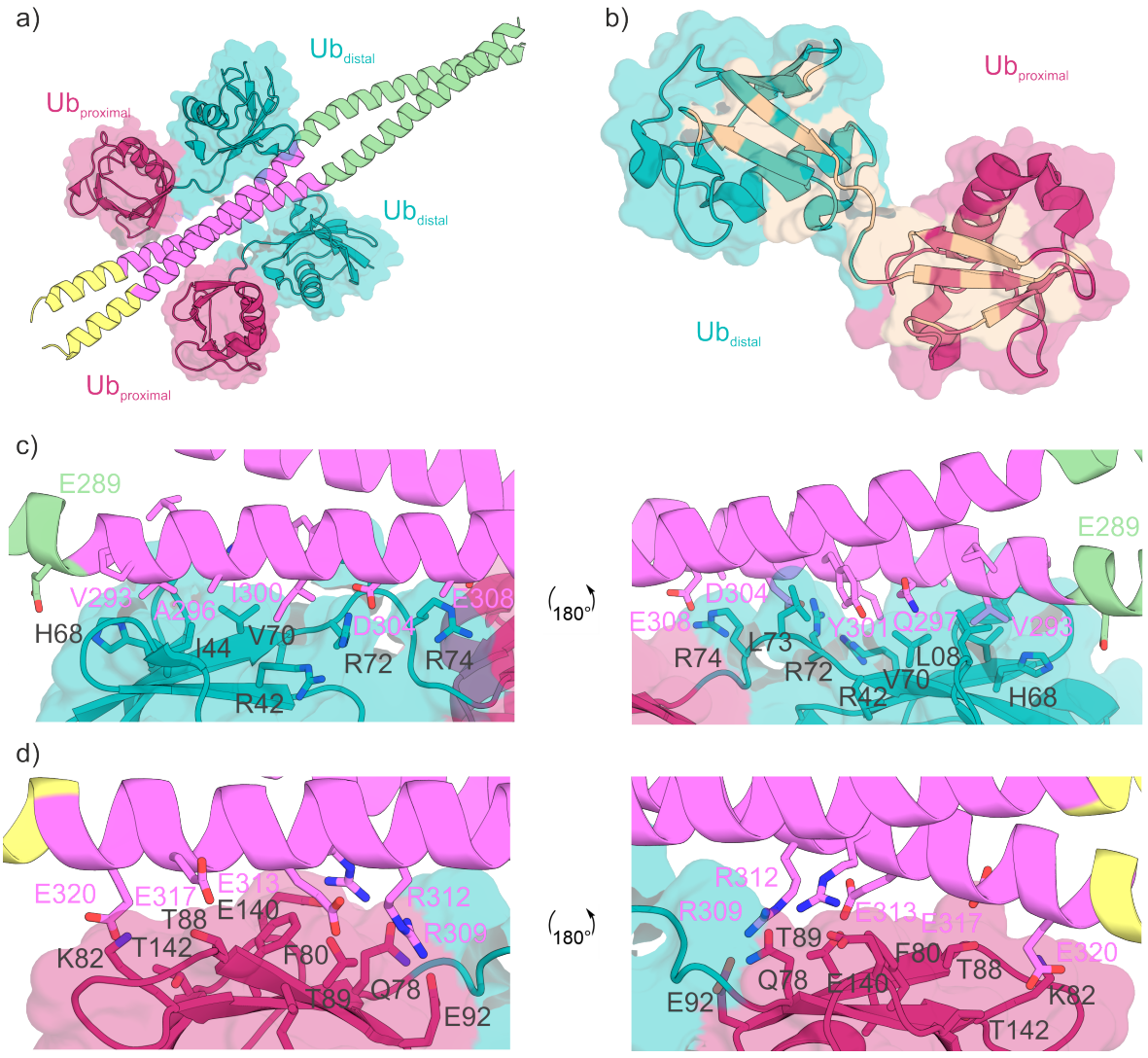

Figure 4. a) X-ray crystal structure of $NEMO_{CoZi}$ in interaction with two linear diUb (PDB#2ZVN). The yellow region of NEMO correspond to the leucine zipper region, the pink one to the UBAN motif while the green one is the coiled-coil domain (same colour scheme as Figure 2. b) Highlights of the contacts made by both Ub_{distal} and $Ub_{proximal}$ in light orange. c) Representation of the residues involved in the binding of $NEMO_{CoZi}$ and the Ub_{distal} (in teal). Residues labelled in black belong to the Ub_{distal} while the residues in purple/green belong to $NEMO_{CoZi}$. b) Representation of the residues involved in the binding of $NEMO_{CoZi}$ and the $Ub_{proximal}$ (in red). Residues labelled in black belong to the $Ub_{proximal}$ while the residues in purple/green belong to $NEMO_{CoZi}$.

Based on these preliminary results, we chose to concentrate our initial designs exclusively on the Ub_{distal}. As previously reported, the binding affinity of linear diUb for the UBAN domain of NEMO has been evaluated at 1.6 µM. To enhance our chances of obtaining structural information on the mode of interaction between the AOFs designed and diUb, we opted for a chemical ligation strategy based on disulphide bridge formation. This approach drives the foldamer into surface proximity with the protein, so that we can circumvent the original average binding affinity. To implement this, we needed to identify a surface-exposed residue of the Ub suitable for mutation to cysteine, which is close enough to maintain the interaction, yet not essential for the binding to NEMO according to the structural data. After examining the surface of Ub, we selected His68 for substitution with Cys68, enabling the formation of a covalent linkage with our AOF candidates.

8.3.2. AOF designs for mimicry

The designs developed in this study are based on the X-ray crystal structure described above, in which we attempted to dock an AOF backbone onto the UBAN region of NEMO at the interface with Ub_{distal}. Our strategy was to mimic key side-chain interactions contributed by Val293, Gln297, Ile300, and Tyr301 of NEMO, which are central to the stabilisation of the complex. This guided the construction of single helix AOF candidates ranging in size from 10 to 13 residues potentially able to mimic the spatial arrangement of the α-residues in a coiled-coil domain as we recently determined.[15] During the docking procedure, using Discovery Studio Visualizer (version 17.2.0), we explored different ways of positioning the quinoline rings: either by aligning their first exocyclic carbon atom or directly the aromatic carbon atom, and by varying the substitution sites at positions 4, 5, and 6 (as explained in the previous chapters). These substituents were tethered to different atomic positions of the NEMO side chains, Cα, Cβ, or nitrogen, depending on the targeted residue (**Figure 5**). To account for conformational variability, both *P*- and *M*-helical models of AOFs were considered. After superimposition of the AOF and the residues of NEMO we were able to generate diverse series of candidates assembled from our newly established monomer library with substitutions at positions 4, 5, or 6.[16]

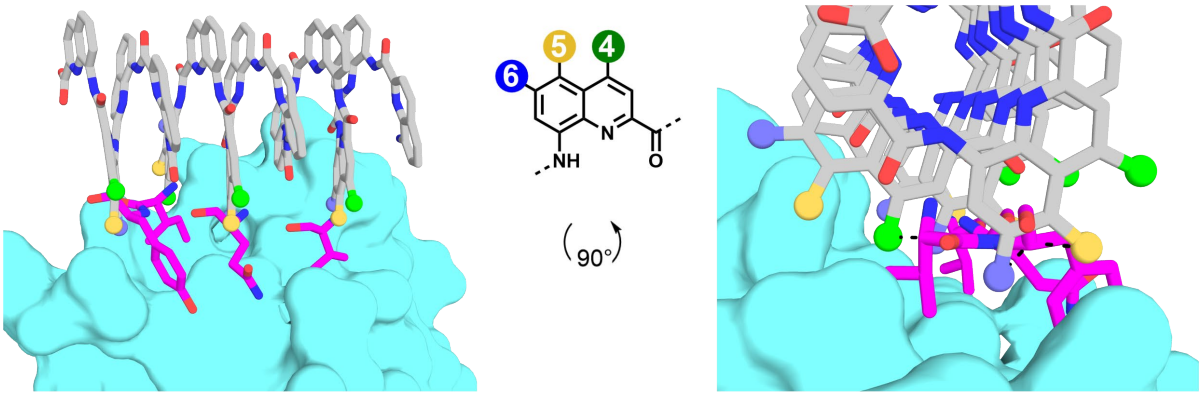

Figure 5. AOF backbone model docked onto the residues of NEMO represented in pink. The exocyclic carbons of the quinoline rings of the AOF are coloured in accordance with the position on the ring: 4 as green spheres, 5 as golden spheres and 6 as blue spheres. The Ub surface is represented in teal. The residues of NEMO are shown in pink. On the right, black dashed lines represent the possible tethering position between exocyclic carbons of the quinoline ring and the Cα of Tyr300 or Ile301.

In parallel, we incorporated additional design constraints to ensure the structural and functional viability of the candidates. One important consideration was the control of AOF handedness, achieved by incorporating a chiral **B** unit described in **section 2.4.1.** previously. Another was the prevention of steric clashes between the docked AOFs and the Ub surface after superimposition, which was carefully monitored during the modelling process. To evaluate the stability of the AOF/Ub complexes, energy minimisation followed by short molecular dynamics simulations were carried out in Maestro (version 11.5 from Schrödinger Inc.). AOF candidates that remained stably associated with the protein were selected for further analysis, whereas those that dissociated within the first nanoseconds of simulation were excluded from subsequent design iterations.

8.4. Results and discussion

8.4.1. Syntheses of AOF candidates

Several series of AOF models were generated with side chains designed to mimic the key residues and enable interactions with Ub. From these, three representative candidates were selected for initial binding studies. The candidates were chosen to maximise structural diversity: two were designed as *P*-helices, while the third adopted an *M*-helical conformation. Within the pair of *P*-helical AOFs, the primary distinction lay in the substitution pattern of the quinoline rings. Each of the three designs incorporated four quinolines functionalised with proteinogenic side chains, while the remaining rings were predicted by modelling to be solvent-exposed and were therefore substituted with solubilising aspartate-like or sulfonic acid side chains. During modelling of the *P*-helical AOFs, steric clashes were observed, predominantly involving a single quinoline unit with the surface of Ub around the region of Ala46, Gly47 and

Lys48. To resolve this, one **Q** ring was replaced with a **P** ring, a modification that preserved the overall fold and architecture of the foldamer while eliminating steric hindrance. All AOF candidates were synthesised using a PurePep Chorus peptide synthesiser, following optimised SPFS protocols described in **section 5** (**Figure 6a**)[17]. The crude RP-HPLC chromatogram of the SPFS of **AOF-1** (**Figure 6b**) shows the efficiency (purity > 95 %) of the synthesis for this average size of AOFs.

As mentioned before, we opted for chemical ligation through disulphide bridge formation to generate the AOF-Ub(H68C) covalent adducts. The methodology for introducing an activated disulphide linker onto AOFs on solid support has been previously established (**Figure 6a**) and has also been successfully utilised to attach a high affinity ligand on a designed AOF to interact with a target protein.[18-19] In this approach, the terminal amine of the last **Q** unit is converted into an isocyanate using triphosgene under microwave-assisted conditions. It then subsequently reacts with a linker amine to form a urea bond. The linkers employed are typically polyethylene glycol-based or ethylene diamine based for the shorter version, with variations in length designed to probe their effect on binding. Linker length is a critical parameter: a short linker is expected to restrict the foldamer more tightly to the protein surface, thereby favouring more defined interactions, whereas a longer linker provides greater conformational flexibility, allowing the foldamer to explore a wider surface area around the anchoring point on the protein and therefore increasing the likelihood of forming productive contacts. The first designs were all synthesised with a short linker (**SL**), only a latter AOF with a design based on **AOF-1** was synthesised with a long linker (**LL**). The crude RP-HPLC chromatogram of **AOF-1SL** shows a purity over 75 % after SPFS (**Figure 6c**); purification using semi-preparative RP-HPLC delivered the final AOF candidate in fairly good yield (14.8 mg, 4.71 µmol, 31.4 %) and in high purity (>98%).

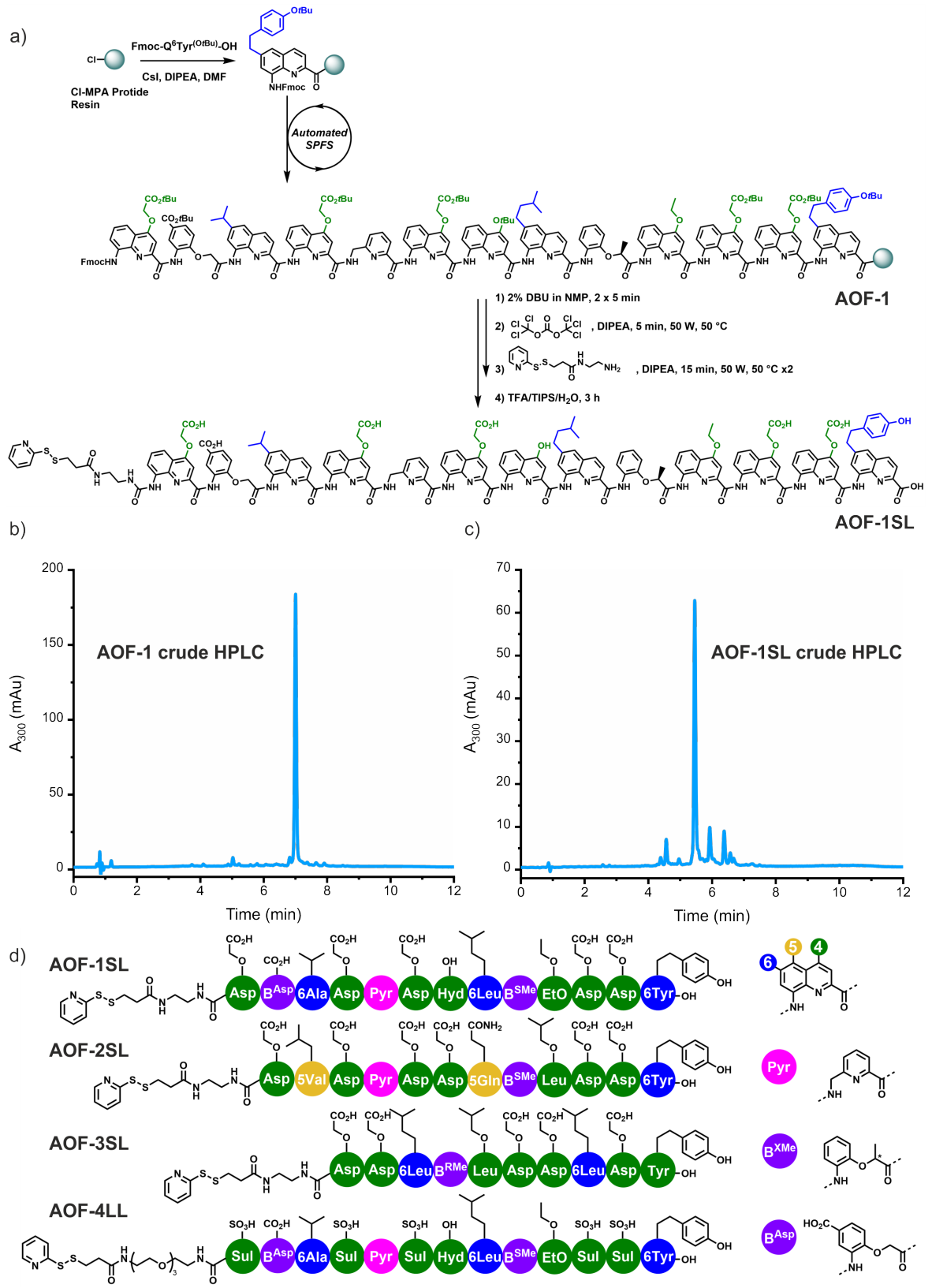

Figure 6. a) Description of automated SPFS of AOF-1 followed by linker installation protocol of **AOF-1SL**. b) RP-HPLC chromatogram of crude **AOF-1**, gradient used: 30% to 100% H_2O + 0.1 % TFA/MeCN + 0.1 % TFA, C_{18} column. c) RP-HPLC chromatogram of crude **AOF-1SL** after linker installation, same gradient used. d) Schematic representation in spheres of four AOF candidates synthesised. Green spheres represent **Q** monomers substituted in position 4 of the quinoline ring, golden sphere in position 5 and blue sphere in position 6. Pink and purple spheres represent **P** and **B** units respectively.

8.4.2. Protein overexpression and purification

Ub(H68C) was overexpressed using a pET-9a vector encoding the H68C-mutated ubiquitin sequence, fused at the N-terminus to a polyhistidine (His_6) tag and a *Tobacco Etch Virus* (TEV) protease cleavage site to enable affinity purification (**Figure 7**). The plasmid was transformed into *E.coli* competent cells, and successfully transformed colonies were selected on kanamycin-containing LB (lysogeny broth) agar plates thanks to the kanamycin resistance gene (KanR). Positive colonies were then utilised for large-scale culture, and protein expression was induced with isopropyl-β-D-thio galactopyranoside (IPTG).

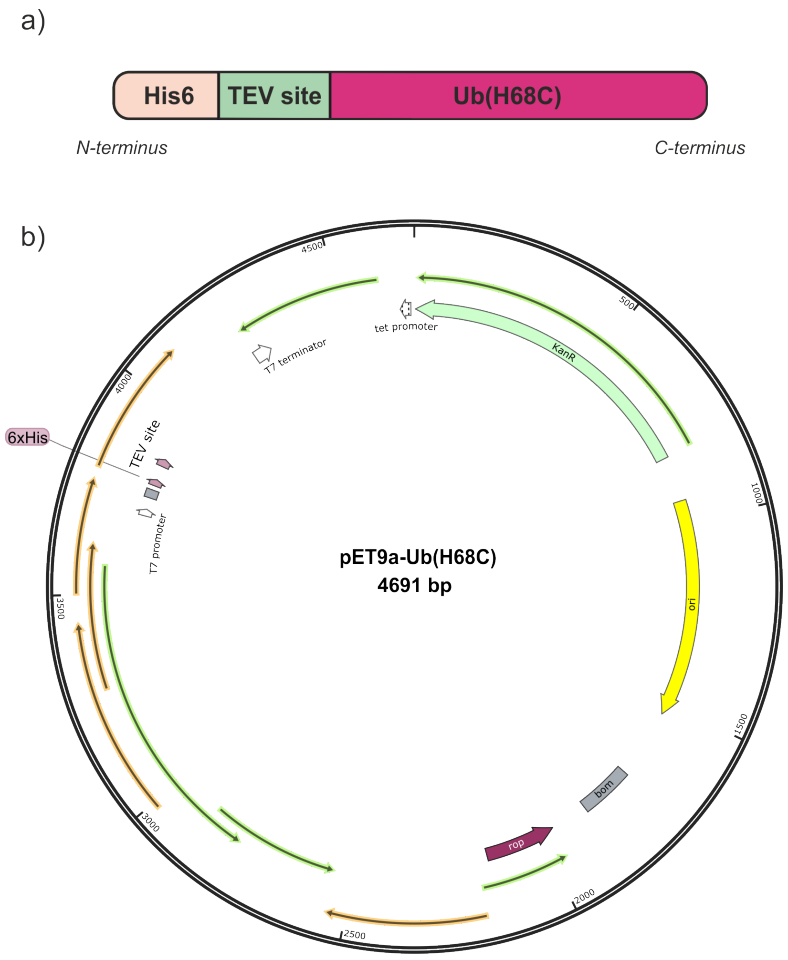

Figure 7. Plasmid map of pET9a utilised for protein expression of Ub(H68C) in *E.coli* coupled to a His_6 affinity tag and a TEV protease cleavage site with the kanamycin resistance gene KanR.

Following expression, the cells were harvested, lysed by sonication, and centrifuged to get rid of cell debris. His_6-Ub(H68C) protein was then isolated from the supernatant using immobilised metal affinity chromatography (IMAC) on nitriloacetic acid Ni-NTA agarose resin. In this system, the histidine side chains of the tag coordinate strongly to the nickel ions chelated by nitrilotriacetic acid, allowing for selective retention of the tagged Ub(H68C). While other bacterial proteins containing surface-exposed histidines may also bind, their interaction is

weaker and can be removed by washing steps. The target protein is then efficiently eluted by increasing the concentration of imidazole, which competes with histidine residues for nickel coordination sites (**Figure 8a**).

The His_6-tag was then removed by cleavage with TEV protease, and the resulting mixture was passed again over Ni-NTA resin to separate the cleaved Ub(H68C) from the free tag and protease. Finally, the protein was purified by size-exclusion chromatography (SEC), before being utilised for adduct formation (**Figure 8b**).

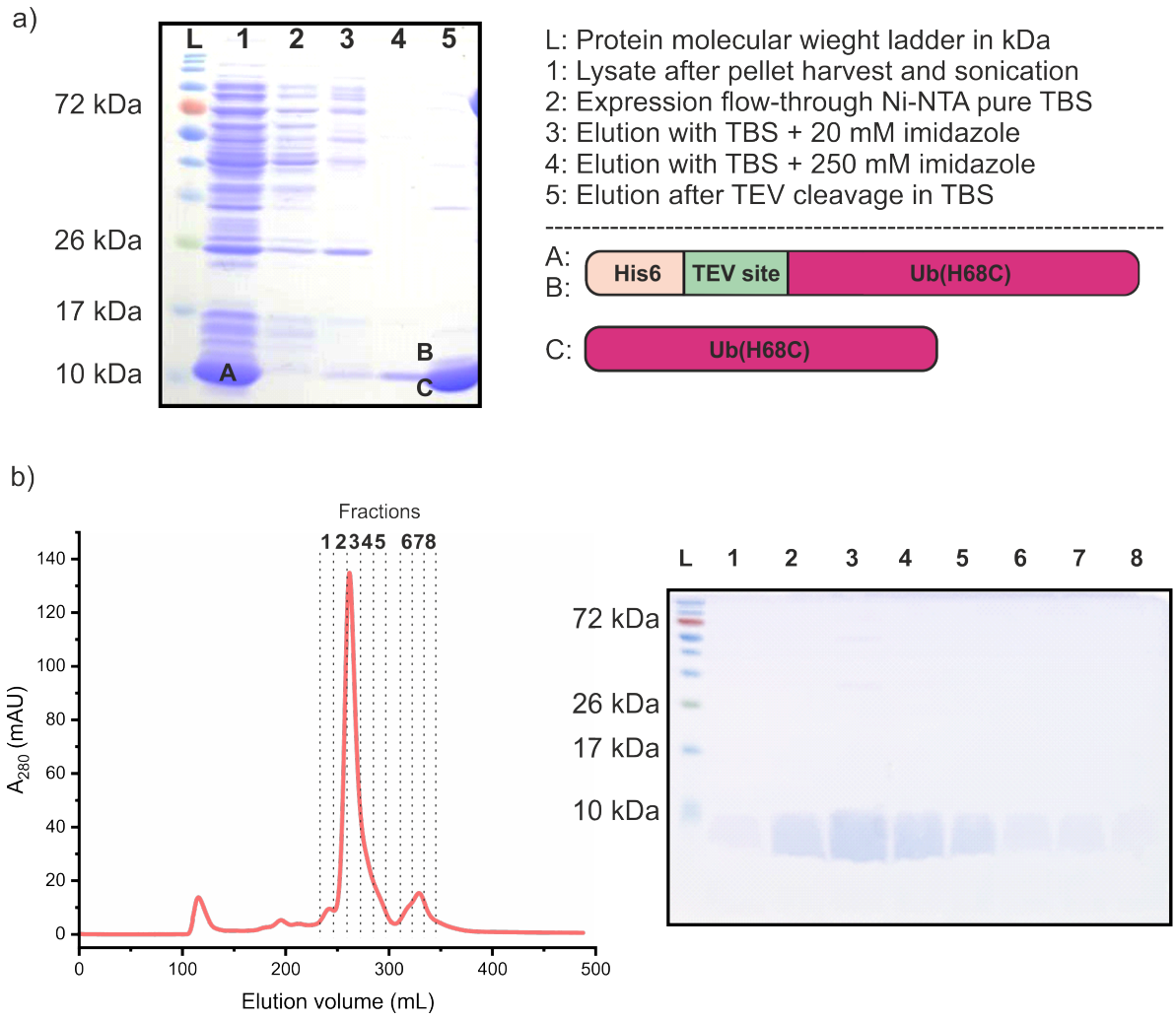

Figure 8. a) SDS-PAGE gel (15% acrylamide) of the expression and cleavage of His_6-Ub(H68C). b) SEC-FPLC chromatogram of Ub(H68C) purification on the left with SDS-PAGE gel (15% acrylamide) of the fractions on the left.

8.4.3. Ligation chemistry and adduct formation

Ligation chemistry through disulphide bridge formation is a well-established and straightforward approach for covalently attaching synthetic ligands to proteins. This method enables the conjugation of a ligand with a protein, by exploiting the thiol-disulphide exchange

with cysteine residues, in aqueous conditions without compromising the integrity of the protein. This approach is therefore well-suited for designing and evaluating protein-AOFs adducts interaction.

In order to perform the ligation with the AOF candidate, the protein was first placed in reducing environment to ensure its monomeric state. With its free cysteine on its surface, Ub(H68C) could in principle dimerise which would impair the adduct formation. Dithiothreitol, DTT (10 mM), was therefore added to the protein solution. It was removed prior to ligation utilising small size exclusion chromatography column (NAP™). The AOF was then dissolved in the protein buffer and was added in a slight excess (1.1 equiv.) to the protein solution (**Figure 9a**). Adding an excess of the AOF allows for easier purification after ligation. Ub(H68C) and Ub(H68C)-AOF adducts possess a very minor molecular weight difference making the SEC purification very challenging, but the difference of molecular weight between the AOF and the covalent adduct is way bigger making the purification by SEC possible. The ligation reaction was complete after 2 hours at room temperature under gentle shaking. After sample concentration, the adduct was purified with SEC (**Figure 9b**), the fractions were collected and concentrated for further crystallisation assays and NMR structure elucidation.

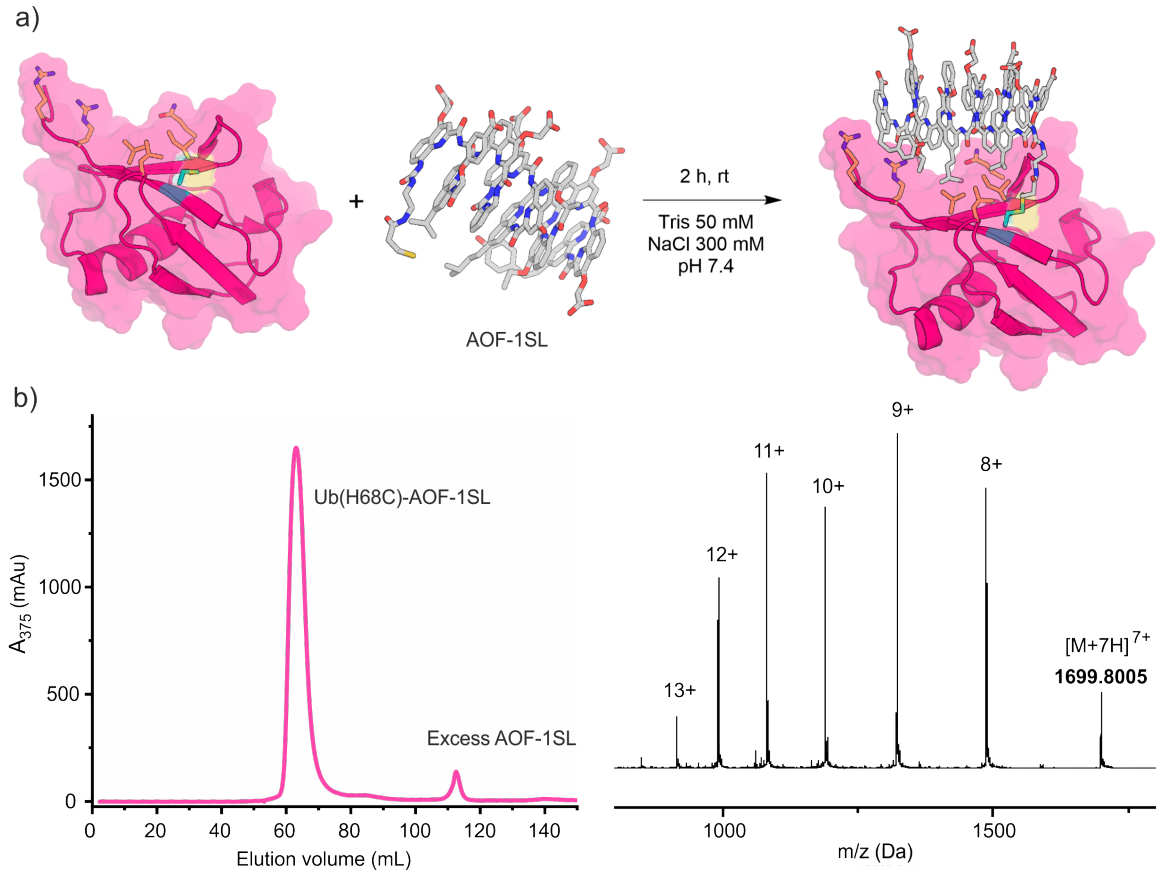

Figure 9. a) Schematic representation of the ligation between Ub(H68C) and **AOF-1SL**. The end structure is a minimised model of the adduct. The ligation site is highlighted in gold and teal. b) SEC chromatogram of the purification of adduct Ub(H68)-AOF-1SL on the left. Mass distribution of the adduct showing charge state.

8.4.4. Structural elucidation of adducts via NMR analysis

To investigate whether our AOF candidates interact with the targeted ubiquitin residues, we conducted NMR analyses of the protein-ligand adducts. Specifically, ^{15}N-HSQC NMR was employed to assess whether the amide protons of the protein residues were influenced by the presence of the AOF. Ubiquitin was expressed in isotopically enriched media containing $^{15}NH_4Cl$ and D-Glucose-$^{13}C_6$**,** yielding labelled [^{15}N]-Ub(H68C) and [^{13}C,^{15}N]-Ub(H68C)**.** NMR spectra of the mono- and di-labelled ubiquitin variants were recorded to map the amide proton resonances of Ub(H68C)**.** Subsequently, ligation of the AOF candidates to both mono- and di-labelled ubiquitin was performed, followed by 2D and 3D NMR analyses.

By interpreting the HSQC spectra and identifying the corresponding proton amide signals, we were able to calculate chemical shift perturbation (CSP) values, providing insights into which ubiquitin residues were affected by the ligated AOF. This analysis was carried out for the **AOF-1SL**, **AOF-2SL**, and **AOF-3SL** candidates. The characterisation of the adduct formed with **AOF-1SL** provided valuable information regarding its interactions with Ub(H68C)**. Figure 10a** displays the CSP representation of the amides of the adduct. The data clearly demonstrate perturbations in the chemical environment of the amide protons in the presence of the AOF. Detailed analysis revealed two key regions of perturbation on the surface of ubiquitin. The first, as expected, corresponds to the anchoring site of the AOF, which significantly affects nearby residues. The second region, a hydrophobic pocket originally targeted on the protein's surface, also exhibited considerable perturbation upon AOF binding. These findings are promising and offer valuable insights for the design of future Ub(H68C)-AOF interactions.

However, in the case of the adduct formed with **AOF-2SL**, most amide resonances are still present, although some are strongly perturbed, particularly at the anchoring site, as expected (**Figure 10b**). The amides in the hydrophobic pockets surrounding Ile44 and Leu73 are completely broadened and disappear, consistent with intermediate exchange of these protons. While we would like to attribute this effect to close contacts with the AOF side chains which we designed, we can only rule that the presence of the AOF strongly perturbs these regions.

The adduct formed with **AOF-3SL** exhibits an even more pronounced broadening of the backbone amide signals (**Figure 10c**). Only a few amide resonances remain detectable and could be used for CSP calculations. Leu43 appears to be strongly affected by the presence of the AOF, suggesting that this hydrophobic pocket could represent a promising target site.

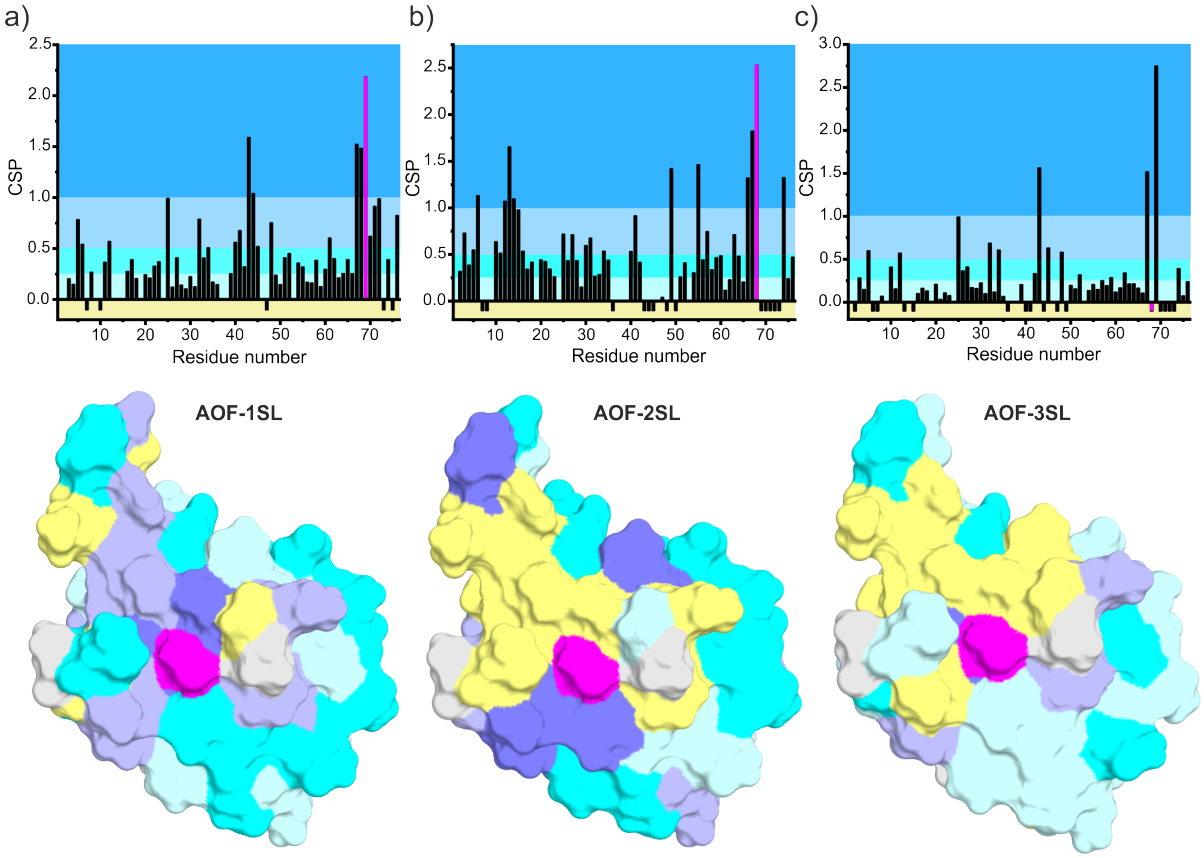

Figure 10. a) CSP representation of [^{15}N]-Ub(H68C)-AOF-1SL backbone amide ^{1}H-^{15}N HSQC. The darker the blue, the more affected is the amide signal. The negative, yellow, corresponds to loss of amide signal from protein alone to adduct. The ladder in pink shows the anchoring point of the AOF, Cys68. CSPs were calculated as the root-mean-square deviation $((\Delta\delta_H/0.14)^2 + (\Delta\delta_N)^2)^{0.5}$. At the bottom the protein surface of Ub(H68C) is coloured according to the CSP values of the table above. Grey areas correspond to missing signal for the protein alone. b) CSP representation of [^{15}N]-Ub(H68C)-AOF-2SL backbone amide ^{1}H-^{15}N HSQC. c) CSP representation of [^{15}N]-Ub(H68C)-AOF-3SL backbone amide ^{1}H-^{15}N HSQC.

8.4.5. Structural elucidation of covalent adducts via crystallisation assays

Structural elucidation via crystallisation assay could lead to a big step in the understanding of the interaction of our AOF candidates with the protein. Each produced adduct was subjected to a series of crystallisation broad screening utilising vapour-diffusion methods, against several commercial and in-house 96-conditions sets.

Despite obtaining several crystallisation hits, none yielded crystals of sufficient quality for structural analysis, as diffraction was poor or absent. The initial strategy, which relied on a short linker to tether the AOFs to the Ub(H68C) was therefore revised. **AOF-1SL** design was then changed into **AOF-4LL**: in this new design the linker was elongated with a PEG_4 spacer, and the solvent-exposed Asp-type side chain replaced by sulfonic acid moieties (**Figure 6d**). These modifications were motivated by prior successes within our group, where Q^{Sul}

monomers (SO_3H side chain in position 4) had been associated with improved crystallisation outcomes.

Using the new protein-adduct Ub(H68C)-**AOF-4LL** in broad screening crystallisation assays, it was possible to obtain numerous hits. Optimisation with larger drop-size and hanging drop crystallisation growth method allowed for the obtention of very reproducible single crystals of the adducts. Crystals were obtained at 4 °C in a mixture of 0.5 μL of the adduct solution at 15 mg/mL with 0.5 μL of reservoir solution (1 M sodium tri-citrate, 100 mM Tris pH = 8.5) hanging over a well solution of 500 μL. These crystals diffracted up to 3.0 Å and consistently indexed in the orthorhombic space group P222 with unit cell dimensions a = 80.5572 Å, b = 101.143 Å and c = 90.236 Å (**Figure 11**).

Data assessment and asymmetric unit (ASU) composition and estimation utilising solvent content and the Matthews coefficient in PHENIX Xtriage[20] suggested a large asymmetric unit of ~77 kDa, most likely corresponding to six copies of the conjugate. Efforts to solve the structure by molecular replacement in PHASER[21] using many combinations of ubiquitin and AOF structures as search models were not successful. Presumably, the large number of copies in the ASU, as well as the high scattering contribution of the AOF complicate structure solution attempts.

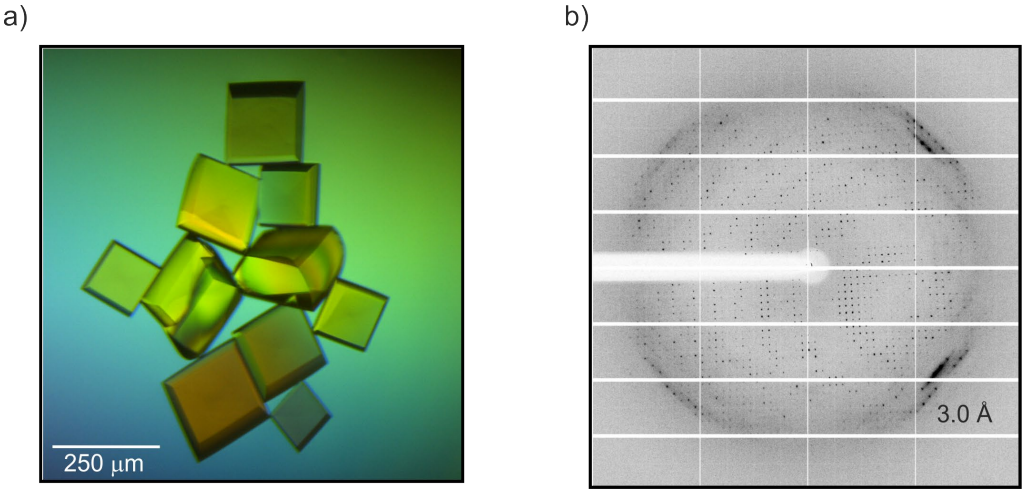

Figure 11. a) Crystals of adduct Ub(H68C)-AOF-4LL observed under crossed polarising microscope grown in 1 M sodium tri-citrate, 100 mM Tris pH = 8.5 at 15 mg/mL at 4 °C. b) Diffraction pattern image during characterisation of the crystals.

8.5. Conclusion and perspectives

To conclude on this project, starting from a natural complex, we were able to model and design AOF candidates for the mimicry of coiled-coil NEMO. From our designs, we successfully demonstrated the efficiency of our automatic synthesiser system in producing the AOF desired

candidates for the mimicry. Furthermore, we achieved chemical ligations with all our AOFs and the mutated ubiquitin in order to obtain our final stable protein-AOFs adducts.

Solution studies using NMR analyses on both the protein and the corresponding adducts provided valuable insights and encouraging evidence for the interaction of AOFs with the targeted site of the protein. Intensive efforts were dedicated to crystallisation with the aim to gain structural understanding on the positioning of the AOFs on the protein surface. Although our initial attempts were unsuccessful, optimisation of the length of the linker for tethering the AOF to the Ub(H68C) led us to the synthesis of new AOF candidate **AOF-4LL**, based on the previously characterised **AOF-1SL**. The crystallogenesis attempts of this adduct yielded reproducible, high-quality crystals diffracting up to 3.0 Å but structural elucidation was also unsuccessful. Additional optimisations of crystallisation conditions, temperature, and concentrations did not improve the resolution so that the crystal structure of the adduct could be elucidated.

At this stage, further exploration of the adduct Ub(H68C)-**AOF-4LL** remains still promising. Phasing using the anomalous signal of the numerous sulphur atoms by single-wavelength anomalous diffraction (SAD) may be considered in the future. Presently, we are interested in investigating the original target, the linear di-ubiquitin, with longer AOF candidates, involving new building blocks, to challenge our capacity to synthesise diverse and long oligomers on our automated system. Collaboration with a dedicated group on molecular dynamics (Dr. Zhiwei Liu, Rowan University, USA) led to the designs of new AOFs (**Figure 12**). **AOF-5LL** was synthesised and chemical ligation with linear diUb(H68C) was successful. Broad screening crystallisation is undergoing and will hopefully bring the first structural milestone for the mimicry of the projection of the spatial side-chain arrangement found in the coiled-coil NEMO.

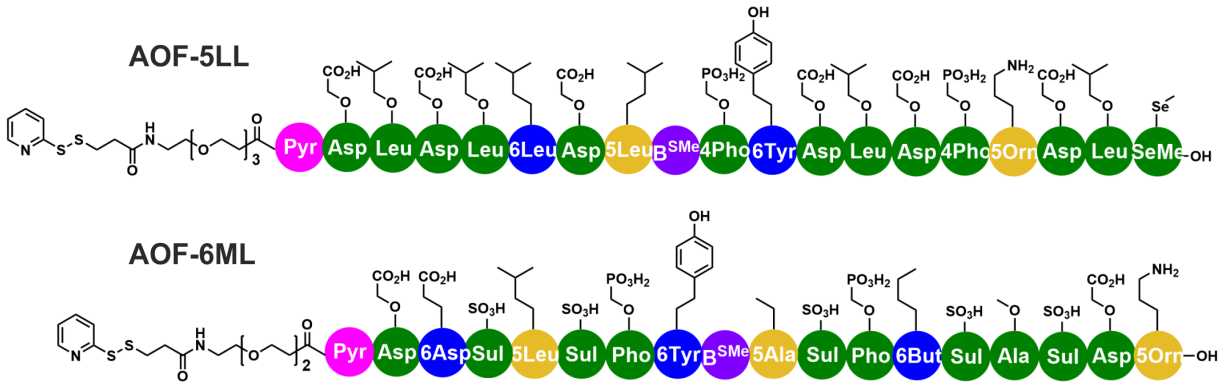

Figure 12. AOF candidate for the ligation with linear diUb(H68C). **AOF-5LL** possess a long linker with a total of 19 units while **AOF-6ML**, possess a medium linker with a total of 18 units. New designs incorporate a N-terminal **P** unit so the triphosgene activation of the aromatic amine for linker installation can be avoided and replaced by simple peptide coupling on the aliphatic amine of the **P** unit.

8.6. Experimental part : chemical synthesis

8.6.1. Materials

All chemicals were purchased from commercial suppliers (*Sigma-Aldrich*, *Fisher Scientific*, *IRIS Biotech*, *ABCR*) and used without further purification unless stated otherwise. Low loading (LL)-Wang and Cl-MPA Protide resins were purchased from *Merck-Novabiochem.* Solvents were purchased from *Fisher Scientific*, *IRIS Biotech* (*N*-methyl-2-pyrrolidinone (NMP)) or *Carlo Erba* (*N*,*N*-dimethylformamide (DMF), peptide grade) and used without further purification. Anhydrous DCM and THF were obtained from a SPS-800 Solvent Purification System (*MBraun*). *N,N*-diisopropylethylamine (DIPEA), NEt_3 were freshly distilled over CaH_2 prior to use. HPLC grade acetonitrile (MeCN, *Fisher Scientific*) and ultra-pure water (Omnia xs^{touch} Blueline, Stakpure system) were used for RP-HPLC analyses and purification. LCMS grade MeCN (*Fisher Scientific*) was used for LCMS analyses.

8.6.2. General methods for HPLC analysis and purification, LCMS and NMR analyses

RP-HPLC analyses were performed on an Ultimate 3000 HPLC system (*Thermo Fischer Scientific*) equipped with an UV diode array detector, monitoring absorbance at 254 nm and 300 nm if not stated otherwise, using a Nucleodur C18 Htec (4.6 × 100 mm, 5 µm, *Macherey-Nagel*). For acidic RP-HPLC analyses, 0.1% trifluoroacetic acid (TFA) in water (solvent A) and 0.1% TFA in acetonitrile (solvent B) were used as the mobile phase at a flow rate of 1 mL/min. All the RP-HPLC analyses were run at 50 °C. For basic RP-HPLC analyses, the mobile phase was composed of 12.5 mM TEAA in water at pH 8.5 (A) and 12.5 mM TEAA in water: acetonitrile mixture (1:2, v/v) at pH = 8.5 at a flow rate of 1mL/min.

Semi-preparative RP-HPLC was performed on an Ultimate 3000 HPLC system, using a Nucleodur C18 Gravity column (10 × 250 mm, 5 µm, *Macherey-Nagel*) at a flow rate of 5 ml/min. The same solvent composition to the analytical conditions was used either in acidic or basic mode.

LC-MS analyses were recorded on an Ultimate 3000 HPLC system, coupled to a micrOTOF II mass spectrometer (*Bruker Daltonics*) with electron spray ionization (ESI). The LC column used was a Nucleodur Gravity Ec column (2 × 50 mm, 1.8 mM, *Macherey-Nagel*). All LC analyses were run at 50 °C. The MS spectrometer was calibrated, prior to analysis, in positive and negative mode by direct infusion of an ESI-Low Concentration Tuning Mix (*Agilent Technologies*).

^{1}H-NMR spectra were recorded on Avance III HD 500 MHz BioSpin spectrometer (*Bruker*). All chemical shifts are reported in ppm and calibrated against residual solvents signals of CD_3CN (δ = 1.94 ppm) and DMF-d_7 (δ = 8.03 ppm). **AOF-4LL** was recorded CD_3CN/H_2O (1:1; vol/vol) with water suppression with excitation sculpting using the zgesgp pulse sequence from the Bruker pulse sequence library. Signal multiplicities are reported as *s*, singlet; *d*, doublet; *t*, triplet; *hept*, heptet; *dd,* doublet of doublet; and *m*, multiplet. Coupling constants (*J*) are reported in Hz. Data were processed on MestReNova v.12.0.

15N-HSQCs were recorded on an Avance NEO NMR spectrometer (Bruker BioSpin) with a vertical 16.45 T narrow-bore / ultrashield magnet operating at 700 MHz for 1H observation by means of a 5-mm TXI 1H / 13C / 15N probe with Z gradient capabilities.

8.6.3. Generalities on solid phase foldamer synthesis (SPFS)

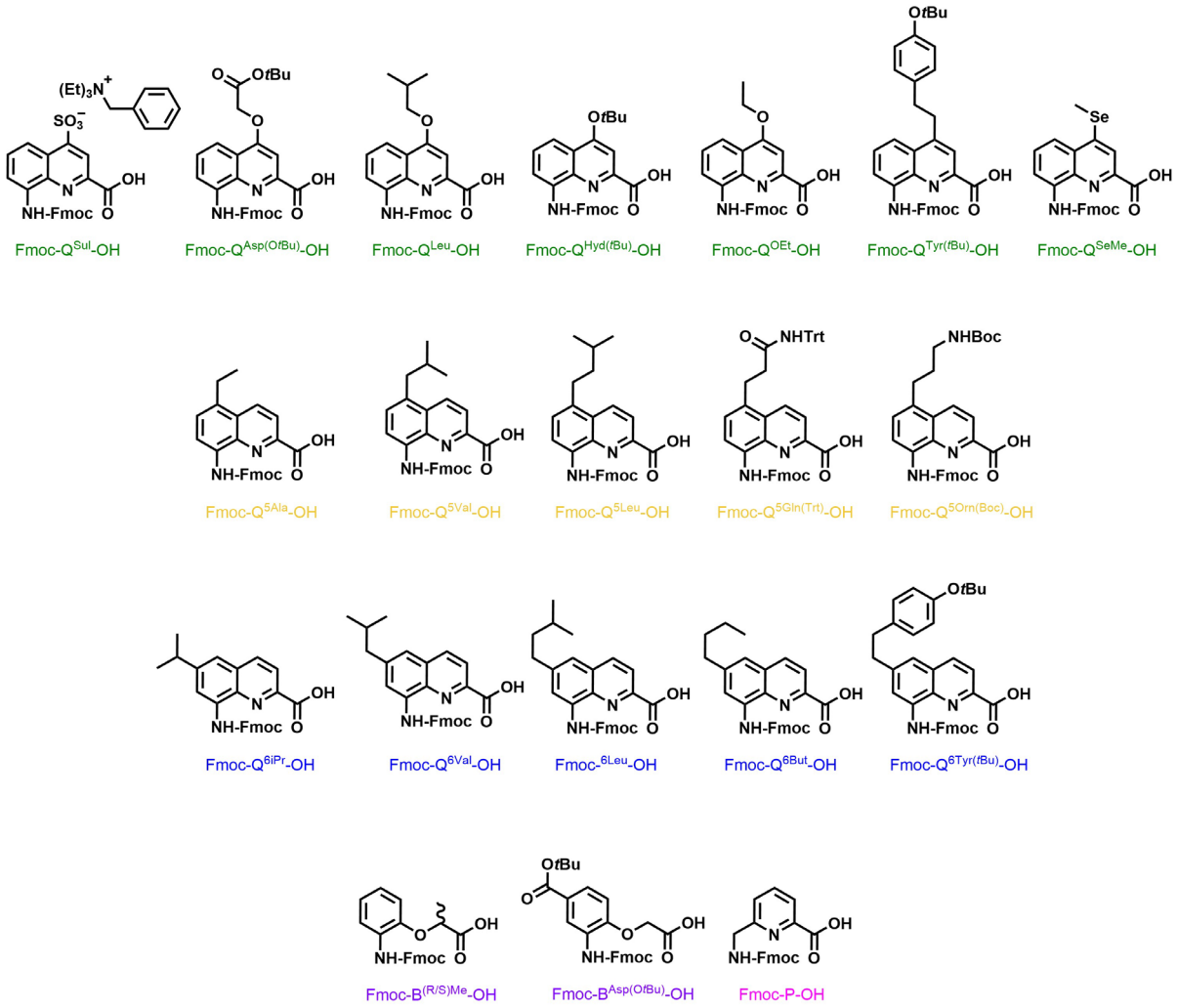

All protected Fmoc-Q$^{Xxx(PG)}$-OH and Fmoc-3-Amb-OH monomers (shown above) used for the solid phase synthesis of the oligomers were prepared following reported synthetic protocols. [16, 19, 22-27]

SPFS was performed following recently reported conditions using a PurePep® Chorus peptide synthesiser (*Gyros-Protein Technologies*) for the different sequences.[17] Generally, all monomers were activated as their respective acid chlorides, by applying *in situ* Appel's conditions in the presence of PPh_3, trichloroacetonitrile (TCAN), and 2,4,6-collidine as base. For the synthesis of **7** a special activation procedure was developed to avoid the deprotection of the acid sensitive *t*Bu protection on the phosphonate side chain (see procedure below).

- *Loading of the first quinoline unit on Cl-MPA Protide resin*

Loading of Fmoc-Q^{Xxx}-OH to the Cl-MPA Protide resin was performed using CsI and DIPEA as previously described.[28]

- *General procedure for Fmoc deprotection*

First, the resin was washed three times with a solution of DCM:NMP (80:20; v/v), before adding a solution of 2% DBU in NMP. The Fmoc deprotection was performed for 2 × 3 min. After deprotection, the resin was washed two times with 20% NMP in DCM and then three times with dry THF.

- *In situ activation and aromatic monomer couplings*

The aromatic monomers were coupled on Wang resin-bound oligoquinoline with *in situ* activation using an excess of three equivalents of monomer relative to the resin loading. Each coupling was performed twice at 50 °C for 15 min.[28]

- *Coupling of the activated disulphide linker via urea bond formation*

For urea bond formation, before coupling of **SL** or **LL** (**AOF-1SL**, **AOF-2SL**, **AOF-3SL** and **AOF-4LL**), the protected NHBoc amine is deprotected with DCM/TFA (1:1, v/v) for 1h at room temperature. The solution is evaporated and put on high vacuum overnight. On resin, Fmoc is deprotected with the classic conditions. Resin is washed thoroughly with dry THF and 1.5 mL of dry THF is added to the resin with 10 equiv. of freshly distilled DIPEA. 5 equiv. of triphosgene are dissolved in 1.5 mL of dry THF, the solution is added onto the resin and put under microwave for 5 min at 50 °C. Mixture is then filtered off and washed thoroughly with 5 x 5 mL dry THF. Resin is then suspended again with 1.5 mL of dry THF. On the side, the linker is dissolved in 1.5 mL of dry THF as well and 10 equiv. of DIPEA is added to it. The solution is then poured on the resin and coupling is performed twice at 50 °C for 15 min like a regular monomer coupling.

- *Coupling of the activated disulphide linker via classical peptide coupling*

The linker (1.5 equiv. relative to resin loading) is coupled manually on the resin-bound H-P-AOF (**AOF-5LL**) by applying peptide coupling conditions with the use of BOP (1.5 equiv.) and DIPEA (3 equiv.) in dry DMF overnight at room temperature.

- *TFA cleavage of the oligomers from the Wang resin*

Cleavage of the oligomer from the Wang resin was performed using a mixture of TFA, tri-isopropyl silane (TIS) and H_2O (95: 2.5: 2.5; v/v/v), for 3 h at room temperature. The crude oligomer was precipitated with diethylether (Et_2O), redissolved in water/MeCN and lyophilised.

8.6.4. AOFs syntheses and characterisation

8.6.4.1. Synthesis of AOF-1SL

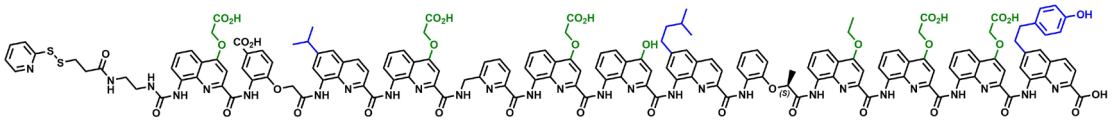

AOF-1SL: Oligomer **AOF-1SL** was synthesized on Cl-MPA resin (0.17mmol.g^{-1}, 100µmol scale) according to the standard method. Loading of the first monomer: 0.11mmol.g^{-1} (65%). The linker was added on half the resin using standard triphosgene activation conditions. After purification by semi-prep HPLC (C8, 30-70, 50°C, A: H_2O + 0.1% TFA, B: MeCN + 0.1% TFA), the title compound was obtained as a yellow powder (14.20mg, 4.28µmol, 13.2%)

^{1}H NMR (500 MHz, DMF-d_7): δ = 13.81 (s, 6H), 13.04 (s, 1H), 12.34 (s, 1H), 12.22 (s, 1H), 11.67 (s, 1H), 11.20 (s, 1H), 10.91 (s, 1H), 10.65 (s, 1H), 10.47 (s, 1H), 10.37 (s, 1H), 9.95 (s, 1H), 9.80 (s, 1H), 9.54 (s, 1H), 9.44 (s, 1H), 8.67 (d, *J* = 6.9 Hz, 3H), 8.61 – 8.58 (m, 1H), 8.46 – 8.44 (m, 1H), 8.22 (s, 1H), 8.13 (s, 1H), 7.96 – 7.86 (m, 4H), 7.86 – 7.79 (m, 2H), 7.79 – 7.74 (m, 2H), 7.71 – 7.63 (m, 5H), 7.61 – 7.43 (m, 11H), 7.42 – 7.37 (m, 2H), 7.33 (t, *J* = 7.8 Hz, 1H), 7.26 – 7.21 (m, 2H), 7.21 – 7.14 (m, 6H), 7.14 – 7.04 (m, 4H), 7.01 – 6.93 (m, 2H), 6.87 – 6.83 (m, 2H), 6.82 – 6.78 (m, 3H), 6.75 (dd, *J* = 7.9, 1.5 Hz, 1H), 6.70 (t, *J* = 7.8 Hz, 1H), 6.57 – 6.51 (m, 2H), 6.46 (s, 1H), 6.41 – 6.38 (m, 2H), 6.34 (d, *J* = 8.1 Hz, 1H), 6.31 (s, 1H), 6.28 – 6.23 (m, 1H), 6.08 (d, *J* = 7.8 Hz, 1H), 5.88 (s, 1H), 5.73 (t, *J* = 7.3 Hz, 1H), 5.19 – 5.08 (m, 2H), 5.06 – 4.93 (m, 2H), 4.85 (d, *J* = 15.9 Hz, 1H), 4.81 – 4.72 (m, 2H), 4.68 (d, *J* = 15.9 Hz, 1H), 4.56 – 4.45 (m, 3H), 4.34 – 4.15 (m, 3H), 3.88 (dd, *J* = 16.9, 4.5 Hz, 1H), 3.30 – 3.23 (m, 1H), 3.11 – 2.97 (m, 5H), 2.62 – 2.60 (m, 1H), 2.51 (t, *J* = 7.1 Hz, 2H), 2.19 – 2.11 (m, 1H), 2.07 – 2.01 (m, 1H), 1.86 (hept, *J* = 6.6 Hz, 1H), 1.67 – 1.53 (m, 4H), 1.37 – 1.24 (m, 14H), 1.15 – 1.08 (m, 7H), 0.90 – 0.84 (m, 1H), 0.15 – 0.12 (m, 1H), -0.25 (d, *J* = 6.5 Hz, 3H).

HRMS: (ESI$^+$) *m/z* calculated for $C_{165}H_{137}N_{27}O_{38}S_2$: 1578.9552 $[M+2H]^{2+}$; found: 1578.9683 $[M+2H]^{2+}$.

8.6.4.2. Synthesis of AOF-2SL

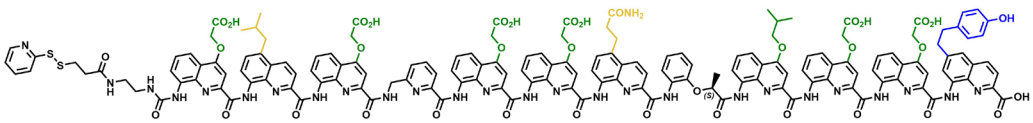

AOF-2SL: Oligomer **AOF-2SL** was synthesized on Cl-MPA resin (0.17mmol.g^{-1}, 100µmol scale) according to the standard method. Loading of the first monomer: 0.11mmol.g^{-1} (65%). The linker was added on half the resin using standard triphosgene activation conditions. After

purification by semi-prep HPLC (C8, 30-70, 50°C, A: H_2O + 0.1% TFA, B: MeCN + 0.1% TFA), the title compound was obtained as a yellow powder (14.20mg, 4.28µmol, 13.2%)

^{1}H NMR (500 MHz, DMF-d_7): δ = 14.20 – 13.53 (m, 7H), 11.69 (s, 1H), 11.25 (s, 1H), 11.14 – 11.07 (m, 2H), 10.85 (s, 1H), 10.50 (s, 1H), 10.44 (s, 1H), 10.08 (s, 1H), 9.41 (s, 1H), 8.79 (s, 1H), 8.63 – 8.54 (m, 2H), 8.42 – 8.39 (m, 1H), 8.36 (d, *J* = 8.6 Hz, 1H), 8.18 – 8.15 (m, 2H), 8.07 (s, 1H), 7.94 (d, *J* = 8.3 Hz, 1H), 7.93 – 7.88 (m, 2H), 7.88 – 7.83 (m, 2H), 7.80 – 7.74 (m, 2H), 7.72 – 7.60 (m, 7H), 7.60 – 7.54 (m, 2H), 7.53 – 7.48 (m, 2H), 7.48 – 7.41 (m, 3H), 7.40 – 7.36 (m, 2H), 7.34 (s, 1H), 7.32 (s, 1H), 7.26 (t, *J* = 7.8 Hz, 1H), 7.23 – 7.14 (m, 9H), 7.14 – 7.02 (m, 8H), 6.86 – 6.81 (m, 3H), 6.66 – 6.57 (m, 3H), 6.54 (d, *J* = 8.4 Hz, 1H), 6.42 – 6.38 (m, 1H), 6.30 (s, 1H), 6.17 (t, *J* = 7.3 Hz, 1H), 6.06 (s, 1H), 6.02 (d, *J* = 7.9 Hz, 1H), 5.96 (s, 1H), 5.69 (t, *J* = 7.5 Hz, 1H), 5.27 – 5.10 (m, 4H), 5.04 (s, 2H), 4.90 – 4.74 (m, 3H), 4.65 (d, *J* = 15.9 Hz, 1H), 4.62 – 4.53 (m, 2H), 4.01 (p, *J* = 7.6 Hz, 2H), 3.81 – 3.32 (m, 4H), 3.11 – 2.97 (m, 3H), 2.89 – 2.80 (m, 4H), 2.67 – 2.60 (m, 1H), 2.59 (s, 4H), 2.54 – 2.45 (m, 1H), 2.39 – 2.24 (m, 3H), 2.06 – 1.95 (m, 2H), 1.35 – 1.26 (m, 7H), 1.25 – 1.18 (m, 7H), 1.06 (d, *J* = 6.4 Hz, 3H), 1.00 (d, *J* = 6.4 Hz, 3H), 0.88 (t, *J* = 6.8 Hz, 1H), -0.32 (d, *J* = 6.5 Hz, 3H).

HRMS: (ESI$^-$) *m/z* calculated for $C_{158}H_{131}N_{27}O_{37}S_2$: 1530.9275 $[M-2H]^{2-}$; found: 1530.9409 $[M-2H]^{2-}$.

8.6.4.3. Synthesis of AOF-3SL

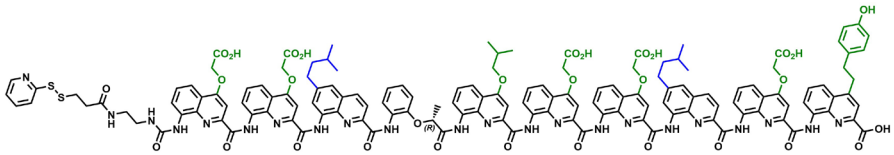

AOF-3SL: Oligomer **AOF-3SL** was synthesized on Cl-MPA resin (0.17mmol.g^{-1}, 100µmol scale) according to the standard method. Loading of the first monomer: 0.11mmol.g^{-1} (65%). The linker was added on half the resin using standard triphosgene activation conditions. After purification by semi-prep HPLC (C18, 30-100, 50°C, A: H_2O + 0.1% TFA, B: MeCN + 0.1% TFA), the title compound was obtained as a yellow powder (14.20mg, 4.28µmol, 13.2%)

^{1}H NMR (500 MHz, DMF-d_7): δ = 14.09 – 13.63 (m, 6H), 12.14 (s, 1H), 11.38 – 11.26 (m, 3H), 11.23 (s, 1H), 10.82 – 10.72 (m, 2H), 10.29 (s, 1H), 9.38 (s, 1H), 8.96 (s, 1H), 8.71 – 8.67 (m, 1H), 8.62 – 8.57 (m, 1H), 8.48 – 8.45 (m, 1H), 8.42 – 8.39 (m, 1H), 8.35 (s, 1H), 8.26 (s, 1H), 8.22 (s, 1H), 8.15 – 8.12 (m, 1H), 7.87 – 7.82 (m, 2H), 7.80 – 7.74 (m, 3H), 7.74 – 7.70 (m, 2H), 7.69 – 7.67 (m, 1H), 7.67 – 7.63 (m, 2H), 7.63 – 7.60 (m, 1H), 7.56 (d, *J* = 8.4 Hz, 1H), 7.52 – 7.45 (m, 2H), 7.41 – 7.37 (m, 1H), 7.36 – 7.28 (m, 3H), 7.28 – 7.24 (m, 3H), 7.19 – 7.17 (m, 1H), 7.15 – 7.11 (m, 3H), 7.04 – 6.97 (m, 3H), 6.94 (dd, *J* = 8.0, 1.6 Hz, 1H), 6.91 (s, 1H), 6.78 – 6.74 (m, 2H), 6.72 – 6.65 (m, 2H), 6.63 (s, 1H), 6.53 (d, *J* = 8.2 Hz, 1H), 6.49 (s, 1H),

6.25 – 6.19 (m, 1H), 6.07 – 6.02 (m, 1H), 5.87 (s, 1H), 5.67 (t, *J* = 7.6 Hz, 1H), 5.44 – 5.31 (m, 4H), 5.09 (d, *J* = 16.2 Hz, 1H), 4.98 (d, *J* = 16.1 Hz, 1H), 4.86 (dd, *J* = 15.8, 2.6 Hz, 2H), 4.67 (dd, *J* = 18.0, 15.7 Hz, 2H), 4.00 – 3.92 (m, 2H), 3.07 – 2.98 (m, 3H), 2.63 – 2.57 (m, 1H), 2.42 – 2.28 (m, 3H), 2.18 – 2.11 (m, 1H), 2.07 – 2.01 (m, 1H), 1.87 – 1.60 (m, 5H), 1.37 – 1.23 (m, 12H), 1.14 – 1.06 (m, 12H), 0.91 – 0.85 (m, 1H), -0.17 (d, *J* = 6.5 Hz, 3H).

HRMS: (ESI$^+$) *m/z* calculated for $C_{142}H_{124}N_{22}O_{31}S_2$: 1349.9210 $[M+2H]^{2+}$; found: 1349.9567 $[M+2H]^{2+}$.

8.6.4.4. Synthesis of AOF-4LL

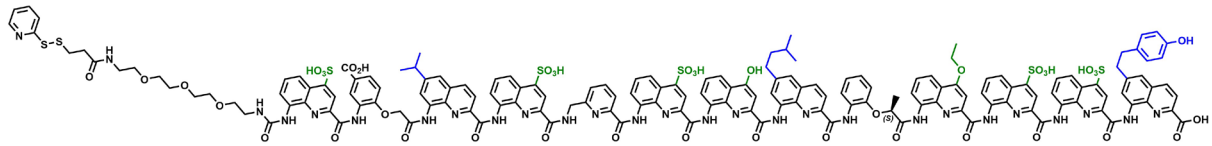

AOF-4LL: Oligomer **AOF-4LL** was synthesized on Cl-MPA resin (0.17mmol.g^{-1}, 100µmol scale) according to the standard method. Loading of the first monomer: 0.11mmol.g^{-1} (65%). The linker was added on half the resin using standard triphosgene activation conditions. After purification by semi-prep HPLC (C18, 0-100, 50°C, A: 12.5 mM TEAA in H_2O pH = 8.5, B: 12.5 mM TEAA in H_2O:MeCN mixture (1:2, v/v) pH = 8.5), the title compound was obtained as a yellow powder (14.20mg, 4.28µmol, 13.2%)

^{1}H NMR (500 MHz, CD_3CN/H_2O 1:1): δ= 11.46 (s, 1H), 11.03 (s, 1H), 10.59 (s, 1H), 10.52 (s, 1H), 10.32 (s, 1H), 9.98 (s, 1H), 9.89 (s, 1H), 9.76 (s, 1H), 9.39 (s, 1H), 8.77 (s, 1H), 8.61 – 8.42 (m, 3H), 8.12 – 8.00 (m, 3H), 7.96 (s, 1H), 7.89 (t, J = 10.3 Hz, 2H), 7.82 – 7.73 (m, 2H), 7.72 (s, 1H), 7.65 (d, J = 8.6 Hz, 1H), 7.61 (s, 1H), 7.57 – 7.46 (m, 3H), 7.46 – 7.30 (m, 5H), 7.29 – 7.21 (m, 2H), 7.20 – 7.11 (m, 4H), 7.11 – 6.98 (m, 5H), 6.94 (d, J = 9.4 Hz, 2H), 6.89 – 6.79 (m, 2H), 6.74 – 6.65 m, 4H), 6.57 (d, J = 9.1 Hz, 1H), 6.43 – 6.32 (m, 1H), 6.30 (d, J = 8.0 Hz, 1H), 6.25 – 6.15 (m, 2H), 6.09 – 5.93 (m, 2H), 5.85 (s, 1H), 2.96 – 2.79 (m, 2H), 2.74 – 2.57 (m, 3H), 2.45 (s, 3H), 2.31 – 2.20 (m, 3H), 1.57 – 1.37 (m, 3H), 1.21 – 1.10 (m, 7H), 1.06 – 0.96 (m, 7H), -0.50 (d, J = 6.8 Hz, 3H).

HRMS: (ESI$^-$) *m/z* calculated for $C_{160}H_{137}N_{27}O_{41}S_7$: 1104.9101 $[M-3H]^{3-}$; found: 1104.9136 $[M-3H]^{3-}$.

8.6.4.5. Synthesis of AOF-5LL

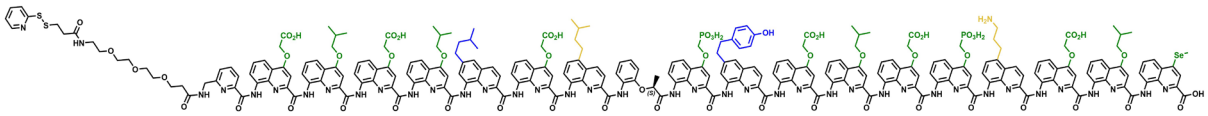

AOF-5LL: Oligomer **AOF-5LL** was synthesized on Cl-MPA resin (0.17mmol.g^{-1}, 100µmol scale) according to the standard method. Loading of the first monomer: 0.11mmol.g^{-1} (65%). The linker was added on half the resin using standard triphosgene activation conditions. After purification by semi-prep HPLC (C8, 30-70, 50°C, A: H_2O + 0.1% TFA, B: MeCN + 0.1% TFA), the title compound was obtained as a yellow powder (14.20mg, 4.28µmol, 13.2%)

^{1}H NMR (500 MHz, DMF-d_7): δ = 11.21 (s, 1H), 11.04 (s, 2H), 10.78 (s, 2H), 10.68 (s, 1H), 10.51 – 10.28 (m, 3H), 10.11 (s, 2H), 9.37 (s, 1H), 8.56 – 8.25 (m, 6H), 7.94 – 7.50 (m, 6H), 7.50 – 7.25 (m, 2H), 7.24 – 7.06 (m, 4H), 7.06 – 6.88 (m, 4H), 6.77 (s, 2H), 6.56 – 6.34 (m, 2H), 6.25 (s, 1H), 6.12 – 5.96 (m, 2H), 5.89 – 5.68 (m, 2H), 5.47 (s, 1H), 5.39 – 5.27 (m, 1H), 5.19 – 5.02 (m, 1H), 4.95 – 4.64(m, 2H), 4.45 (d, J = 14.3 Hz, 1H), 4.28 – 3.38 (m, 44H), 3.34 – 3.13 (m, 13H), 3.08 – 2.97 (m, 2H), 2.53 (t, J = 7.1 Hz, 1H), 2.3 – 2.31 (m, 4H), 1.90 (s, 2H), 1.67 (s, 6H), 1.56 (s, 1H), 1.46 – 1.05 (m, 21H), 0.88 (t, J = 6.7 Hz, 1H), -0.89 (s, 3H).

HRMS: (ESI$^-$) *m/z* calculated for $C_{255}H_{230}N_{40}O_{57}P_2S_2Se$: 1656.1425 $[M-3H]^{3-}$; found: 1656.1703 $[M-3H]^{3-}$.

8.6.5. Characterisation data

8.6.5.1. AOF-1SL

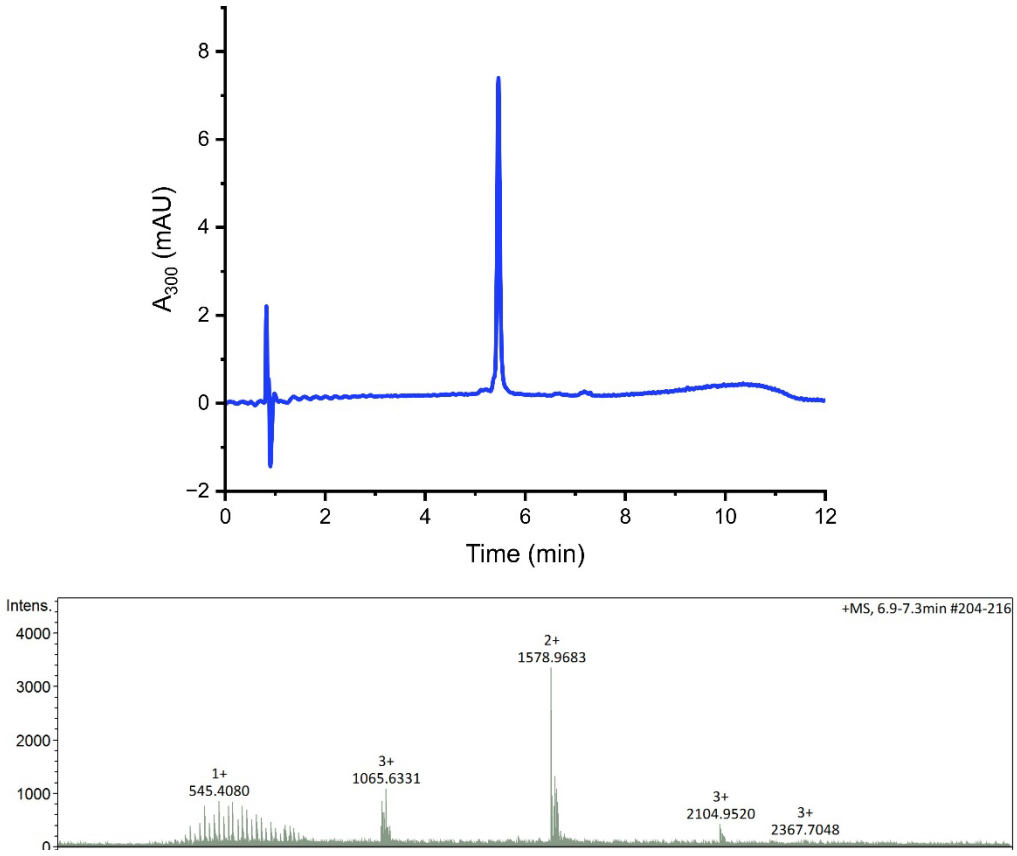

RP-HPLC chromatogram and ESI-MS spectrum of **AOF-1SL**.

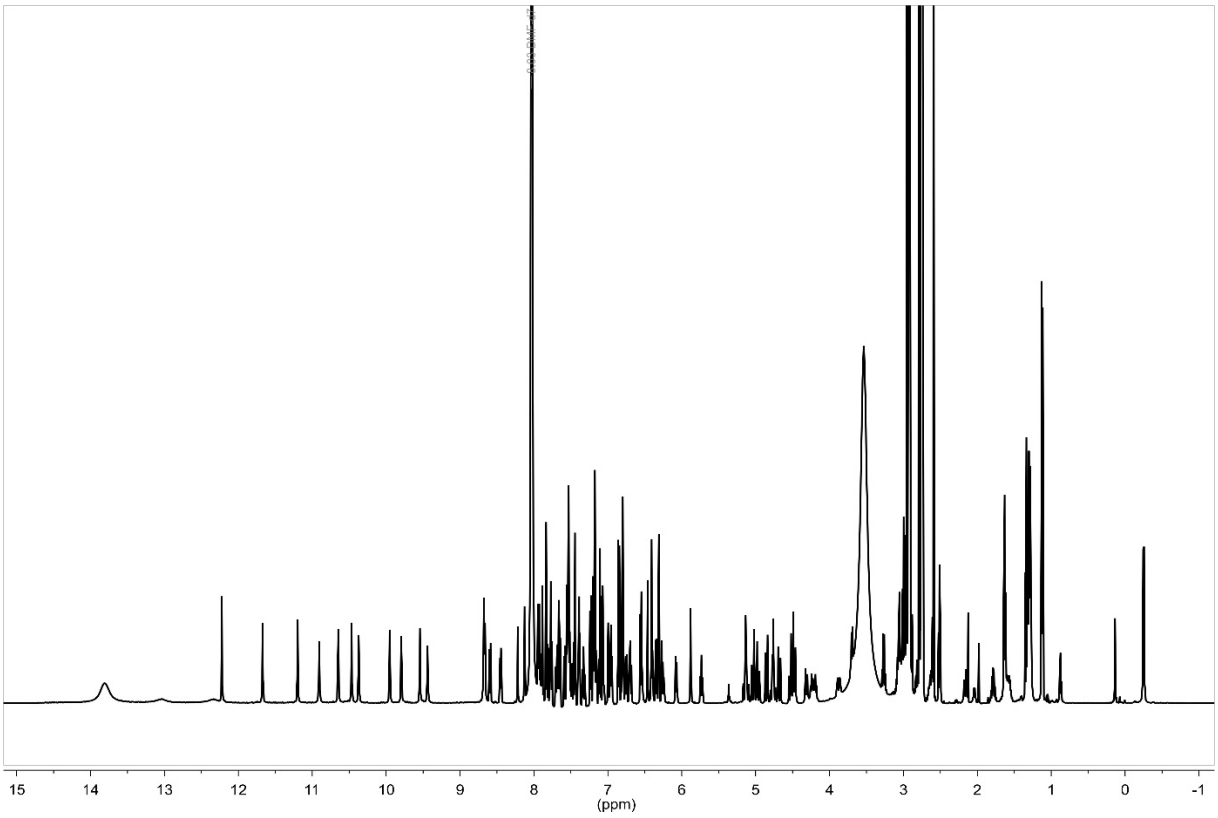

^{1}H-NMR spectrum (500 MHz, DMF-d_7, 25 °C) of **AOF-1SL**.

8.6.5.2. AOF-2SL

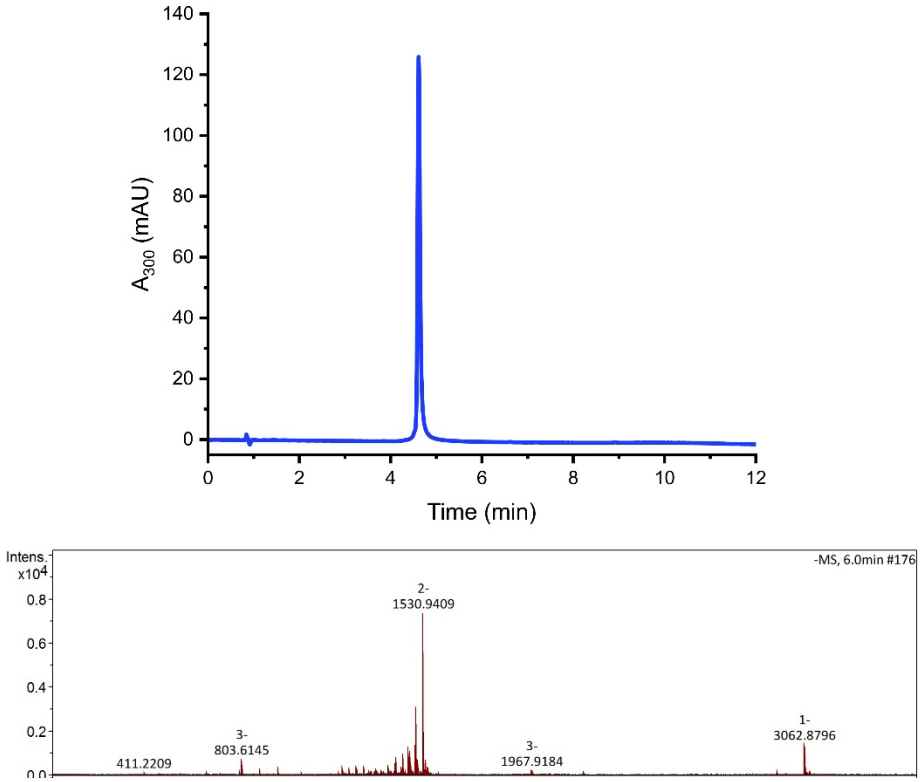

RP-HPLC chromatogram and ESI-MS spectrum of **AOF-2SL**.

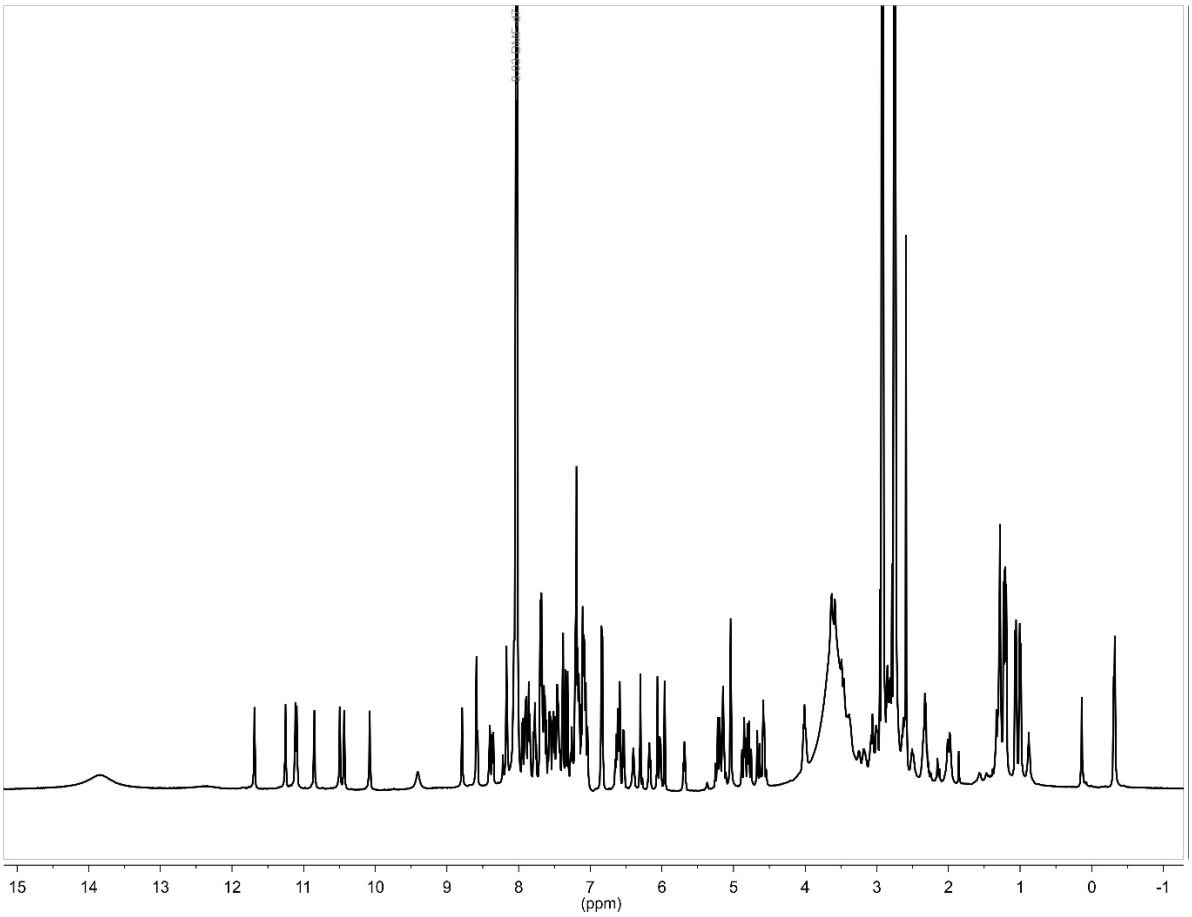

^{1}H-NMR spectrum (500 MHz, DMF-d_7, 25 °C) of **AOF-2SL**.

8.6.5.3. AOF-3SL

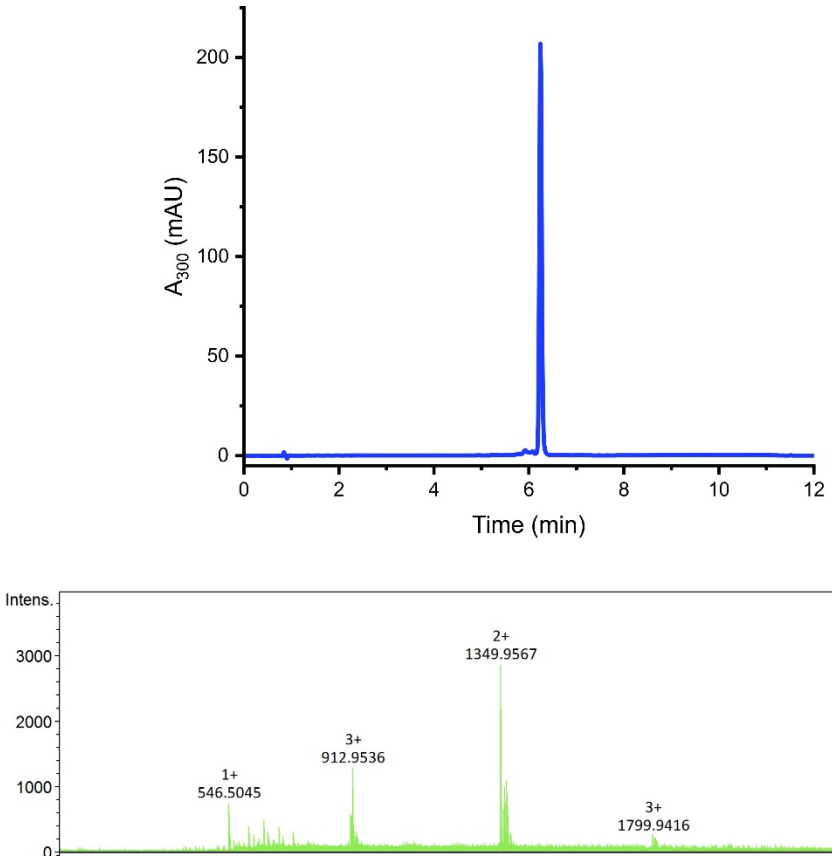

RP-HPLC chromatogram and ESI-MS spectrum of **AOF-3SL**.

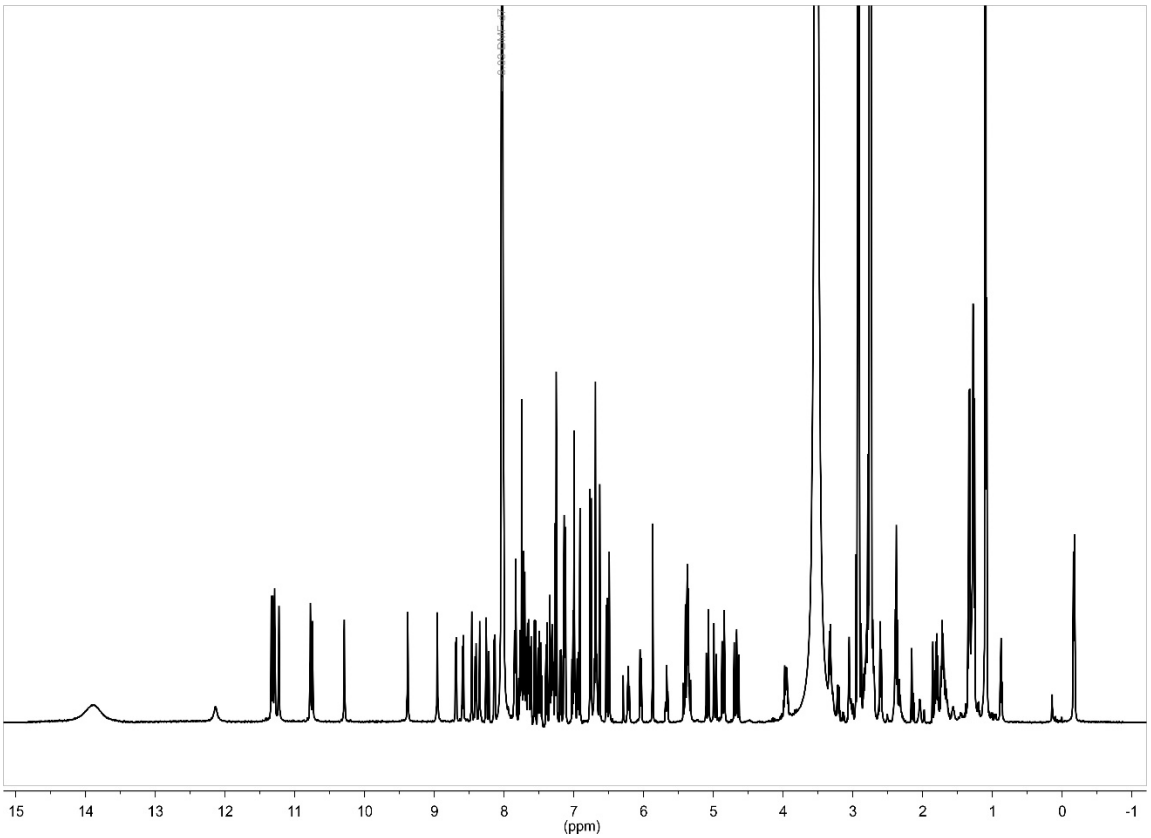

^{1}H-NMR spectrum (500 MHz, DMF-d_7, 25 °C) of **AOF-3SL**.

8.6.5.4. AOF-4LL

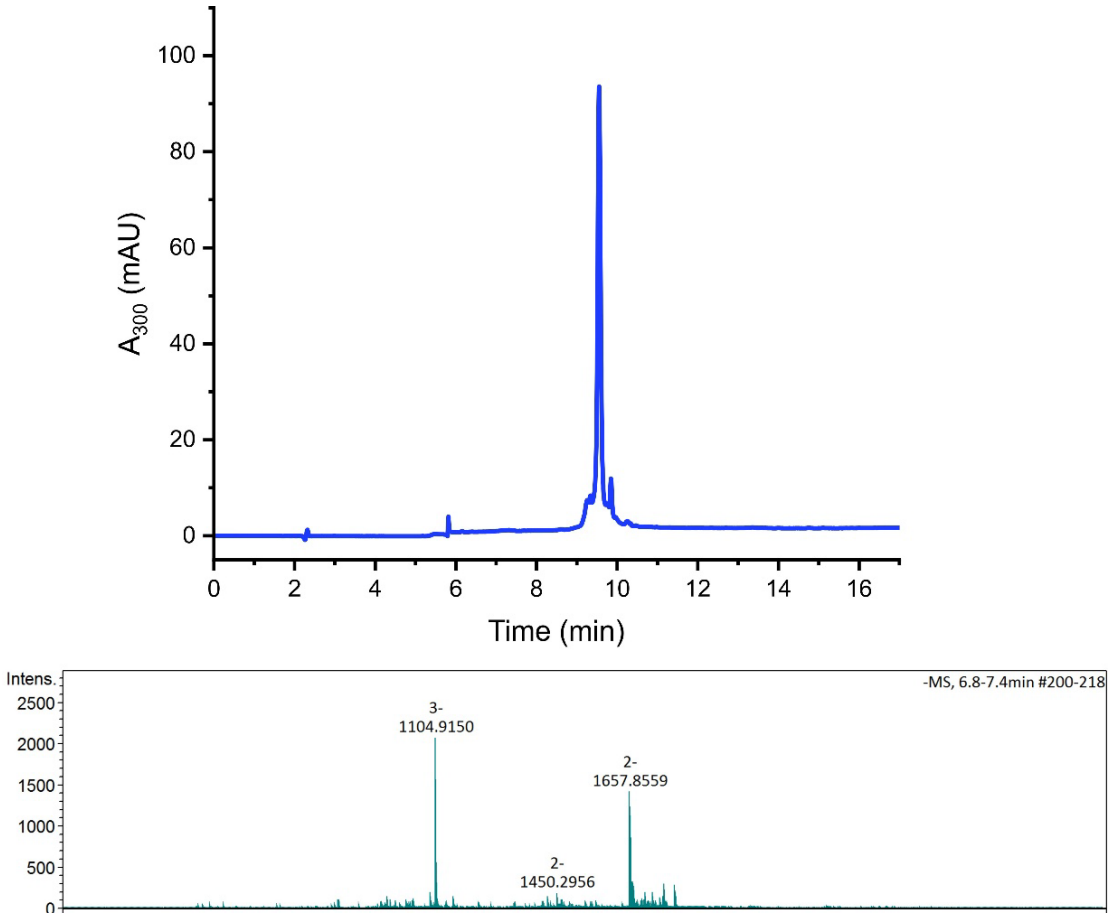

RP-HPLC chromatogram and ESI-MS spectrum of **AOF-4LL**.

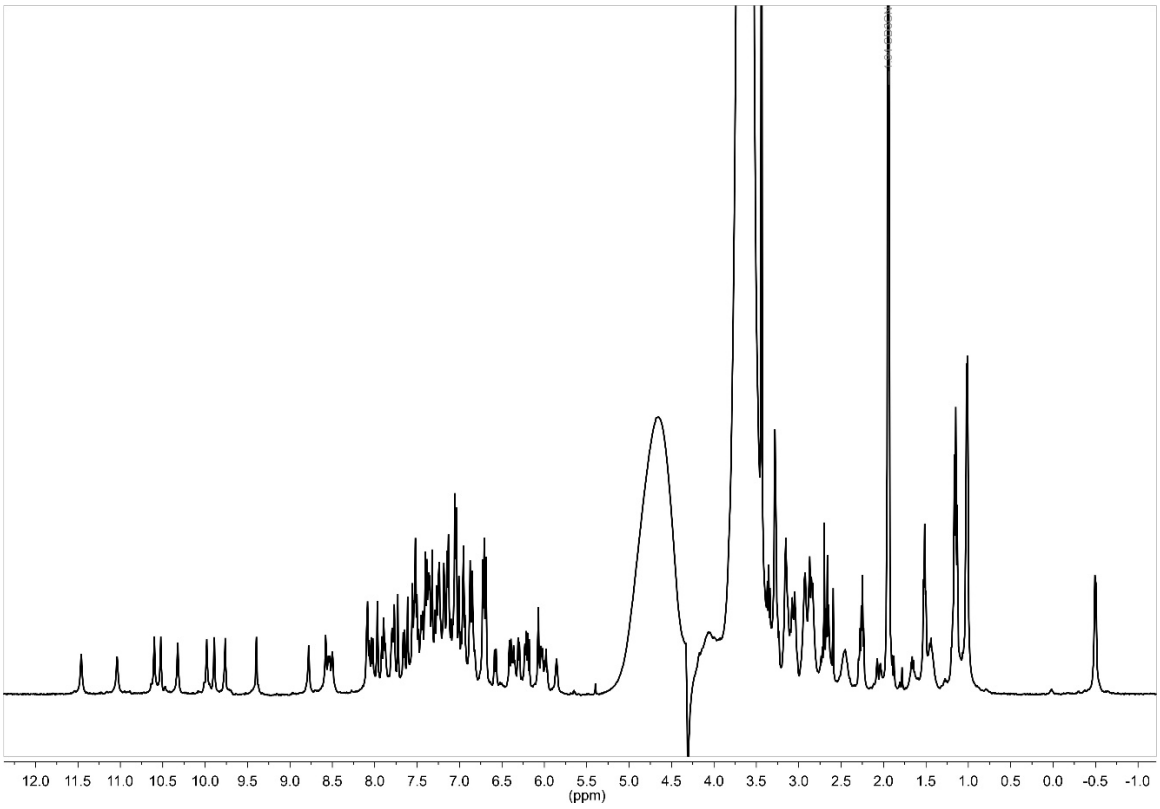

^{1}H-NMR spectrum (500 MHz, $CDCl_3/H_2O$, 25 °C) of **AOF-4LL**.

8.6.5.5. AOF-5LL

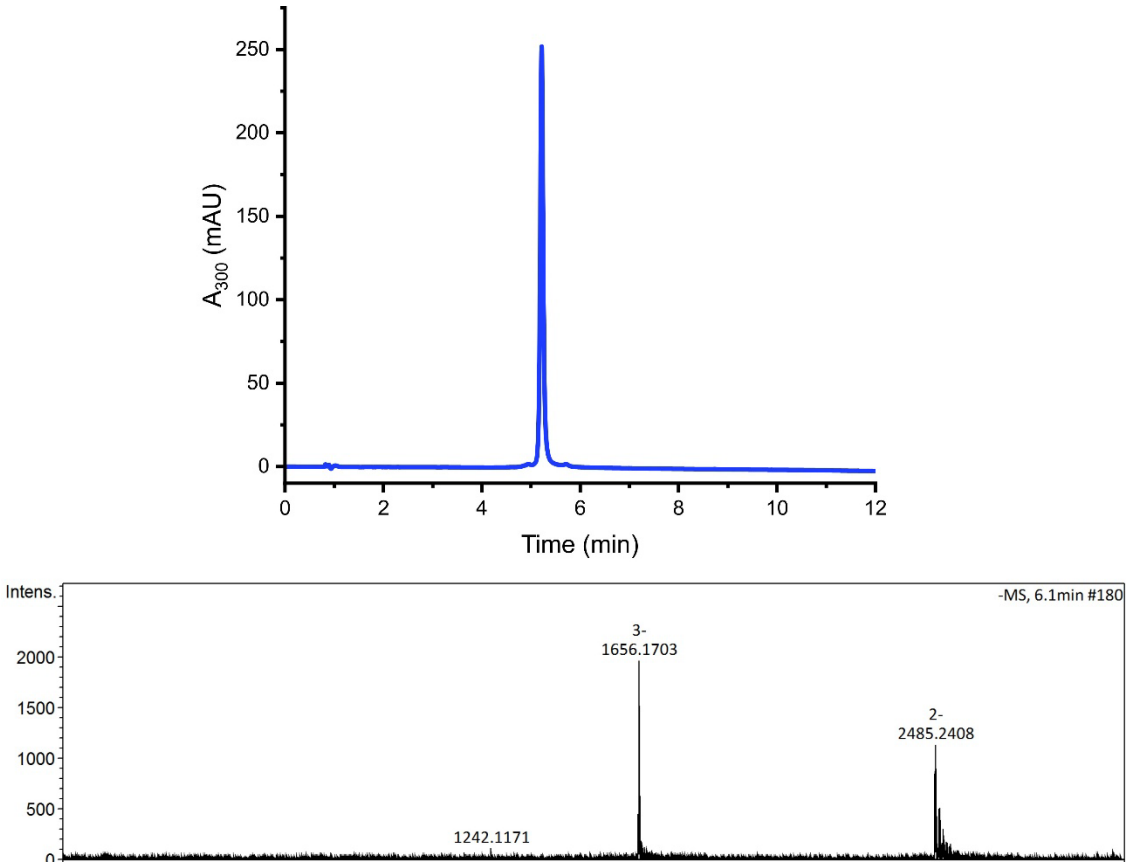

RP-HPLC chromatogram and ESI-MS spectrum of **AOF-5LL**.

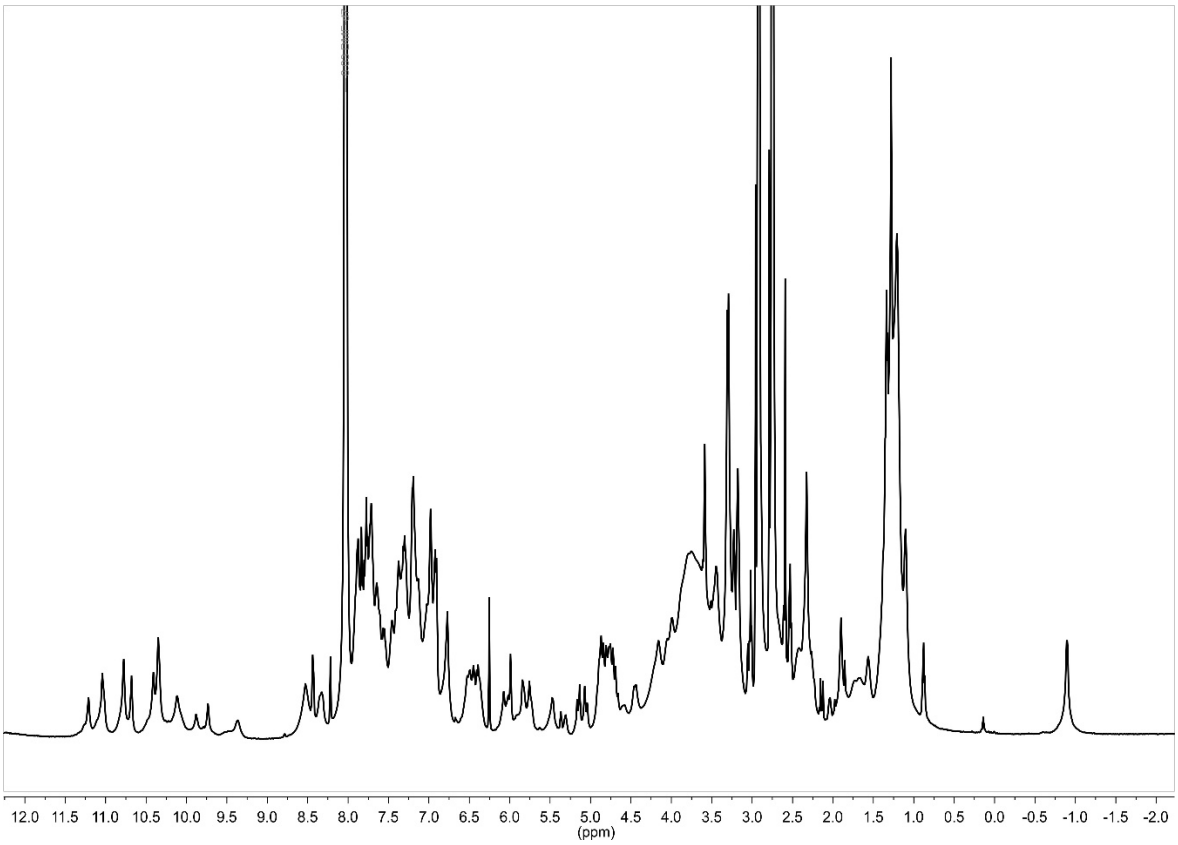

^{1}H-NMR spectrum (500 MHz, DMF-d_7, 25 °C) of **AOF-5LL**.

8.7. Experimental part: protein expression

8.7.1. Material and general methods

All chemicals were purchased from commercial suppliers (*Fischer Scientific*, *Thermo Fischer Scientific*, *Sigma Aldrich*/*Merck*) in bio-grade quality and used without further purification. Tris-buffered saline (50 mM tris, 300 mM NaCl; TBS) was freshly prepared from the respective compounds dissolved in ultra-pure water (dispensed from OmniaPure xs^{basic}, *Stakpure*), and pH was adjusted using a SevenCompact pH-meter (*Mettler Toledo*). Sterilisation of buffers and stock solutions was achieved by vacuum filtration or syringe filtration through 0.2 µm polyvinylidene fluoride (PVDF) membranes. Concentration of protein solutions and foldamer solutions were determined by measuring absorbance at the respective absorption maxima (280 nm for proteins, 375 nm for foldamers) on a NanoDrop™ OneC photo spectrometer (*ThermoFischer Scientific*) and calculation via extinction coefficients. OD_{600} of bacterial cultures were monitored on the same device using 1 cm disposable cuvettes. Centrifugal concentrator units Pierce™ (*ThermoFischer Scientific*) with suitable molecular weight cut-offs were used to concentrate protein solutions. For buffer exchange Slide-A-Lyzer™ (*ThermoFischer Scientific*) dialysis cassettes were used.

All work with bacteria was performed under antiseptic conditions next to a Bunsen burner flame. Pipette tips and liquid containers were sterilised by autoclaving at 121 °C. Transformation medium SOC (Super Optimal broth with Catabolite repression) was purchased pre-prepared (*Sigma Adlrich*), LB medium for bacterial growth cultures was prepared from solid LB broth (*CarlRoth*) and ultra-pure water and sterilised by autoclaving at 121 °C. Kanamycin weas used as 1000 x stock solutions in respective dilution. Competent *E. coli* BL21(DE3) cells were purchased as cryo-stocks (*New England BioLabs*, *ThermoFischer Scientific*), stored at -80 °C and handled on ice during usage.

Plasmids were purchased as lyophilised solids (*Genescript*) and dissolved in autoclaved water to a final concentration of 200 ng/µL. Bacterial colony selection on LB-agarose culture plates, containing 50 µg/mL of antibiotic were conducted overnight at 37 °C. Cryo-stocks of selected colonies were produced by small culture growth overnight and liquid nitrogen flash freezing 600 µL of the growth media mixed 1:1 with 60% v/v sterile glycerol solution. IPTG for expression induction was used as 1 M sterile filtered stock solution in respective dilution. Pelleting of expression cultures was achieved by centrifugation in an Avanti JXN-26 (*Beckman Coulter*) centrifuge. Cell lysis was performed on an UP200St (*Hielscher*) ultrasonic homogeniser.

HisPur™ Ni-NTA resin (*ThermoFischer Scientific*) was used for affinity chromatography of the His-tagged proteins.

SDS-PAGE gels were casted using commercially available SureCast™ (*ThermoFischer Scientific*) stacking and resolving buffers, aqueous acrylamide solution (40 vol%), APS and TMED, according to the manufacturer's composition guide for the desired volume-percentage of acrylamide. Protein samples were mixed with 4× sample loading buffer (0.2 M Tris-HCl, 8% v/v SDS, 6 mM bromophenol blue, 4.3 M glycerol) and heated to 95 °C for 10 min prior to loading. Protein marker color prestained protein standard broad range 10-250 kDa (*New England BioLabs*) was loaded in the marker lane (3 µL). Electrophoresis was performed with 1x SDS running buffer in a Mini-PROTEAN® Tetra Cell (*BioRad*) at 125 W/0.03 A, delivered by a PowerPac HC (*BioRad*) power supply. Separated proteins were stained with Brilliant Blue R Concentrate (*Sigma-Aldrich*) for 15 min under shaking and SDS-PAGE gels were subsequently destained in a H_2O/AcOH/MeOH (6:3:1) solution.
Protein purification by FPLC-SEC was performed on a modular Azura system (*Knauer*) with a MWD 2.1L UV-detector, equipped with HiLoad 16/600 Superdex 75 and 200 pg SEC gel filtration columns (*Cytiva*) or on an Äkta Go system (*Cytiva*) with a UV on 9L Cpl, equipped with a HiLoad 26/600 Superdex 200 pg SEC gel filtration column (*Cytiva*). Chromatographic monitoring was performed at λ = 280 nm. Data was processed in OriginPro V.2019b (*OriginLab*).

8.7.2. Expression and purification of proteins

- *Standard recombinant protein expression*

Proteins were expressed using either the pET-9a or pET-28(+) vector systems, encoding for the target sequence N-terminally fused to a TEV cleavage site with a 6×His tag. Plasmids were transformed into competent *E. coli* BL21(DE3) cells by mixing 1 µL of plasmid stock solution with one tube of bacteria stock (50 µL), incubation on ice for 10 min and subsequent heat-shock at 42 °C for 30 s. The transformed cells were cooled on ice for 5 minutes, mixed with 600 mL S.O.C. medium and incubated at 37 °C for 1 h under shaking (600 rpm). The mixture was spread on LB-Kan agarose plates and incubated over-night at 37 °C. Subsequently, starter cultures were grown from single colonies in 10-50 mL LB medium containing the antibiotic (Kan: 50 µg/mL) at 37 °C overnight. Starter cultures showing visible growth were used for inoculation (1:100 Vol%) of 100 mL-4 L LB-Kan medium and cells were grown at 37 °C under shaking (200 rpm) until an OD600 of ~ 0.6 was reached. For pET-28a(+) construct, expression was induced by adding IPTG (1 mM final concentration) and continued for 3 h at 37 °C. After the expression cells were harvested by centrifugation at 8000 × g for 15 – 20 min at 4 °C. The supernatant was discarded, and cell pellets were either frozen at −20 °C or used directly in the next step.

- *Large-scale protein purification*

Harvested or frozen cell pellets were re-suspended in lysis buffer (TBS, 25 mM imidazole, pH = 7.4). Cells were sonicated in 4-5 rounds of 3 min each on ice (Frequency = 90%; Amplitude = 100%, Power = max) with 10 minutes breaks between rounds to prevent sample overheating. The resulting suspension was centrifuged at 45000 × g for 45 min at 4 °C and the supernatant was incubated with Ni-NTA resin (5 mL suspension per 1 L of expression) at 4°C for 30 min to 1 h. The incubated resin was loaded onto a gravity-flow column, washed with 10 CVs of lysis buffer, 3 CVs of wash buffer (TBS, 50 mM imidazole, pH = 7.4) and the target fusion protein was lastly eluted with elution buffer (TBS, 300 mM imidazole, pH = 7.4). The UV_{280} was monitored using a Nanodrop photo spectrometer to track protein elution and assist with sample collection during the washing and elution steps. The elution fractions were combined, TEV protease (1 u/100 µg) was added and the mixture was dialysed against lysis buffer (TBS, 25 mM imidazole, pH = 7.4) overnight. The cleavage mixture was incubated with Ni-NTA resin for 30 min at 4 °C and subsequently loaded on a gravity-flow column and the flow-through, containing the cleaved target protein was collected and concentrated for SEC purification in TBS. Fractions containing the target protein were pooled, concentrated and either used directly in subsequent experiments or aliquoted and stored at -80 °C.

8.7.3. Protein expressions and adduct characterisation

8.7.3.1. Expression of Ub(H68C)

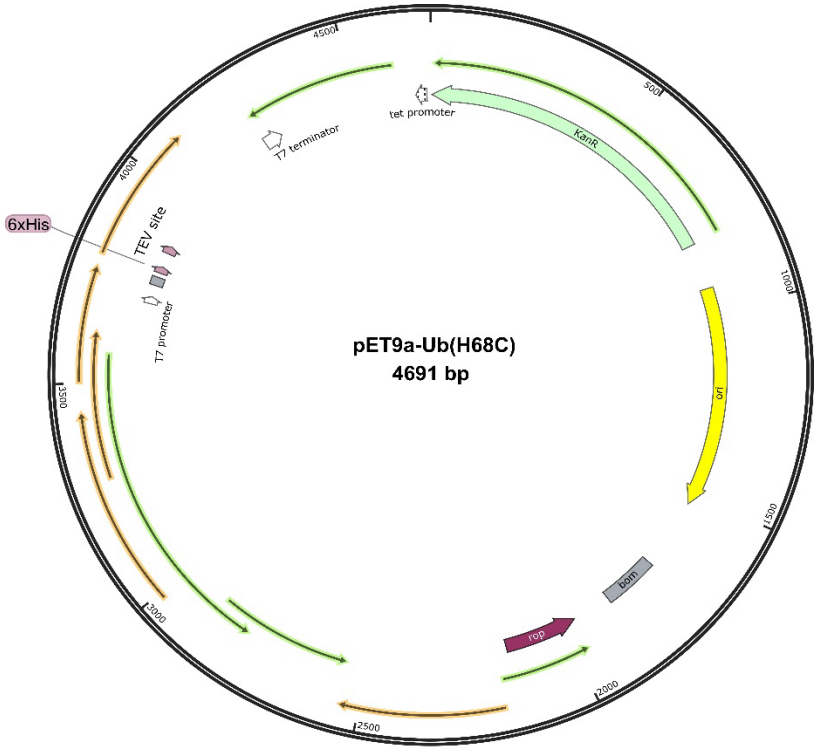

MKHHHHHHPMSDYDIPTTENLYFQGAMGMQIFVKTLTGKTITLEVEPSDTIE
NVKAKIQDKEGIPPDQQRLIFAGKQLEDGRTLSDYNIQKESTLCLVLRLRGG

Expression vector used for the expression of Ub(H68C). The protein sequence is highlighted in green, the cleavage site for TEV is coloured in red and the polyhistidine tag in blue.

8.7.3.2. Expression of diUb(H68C)

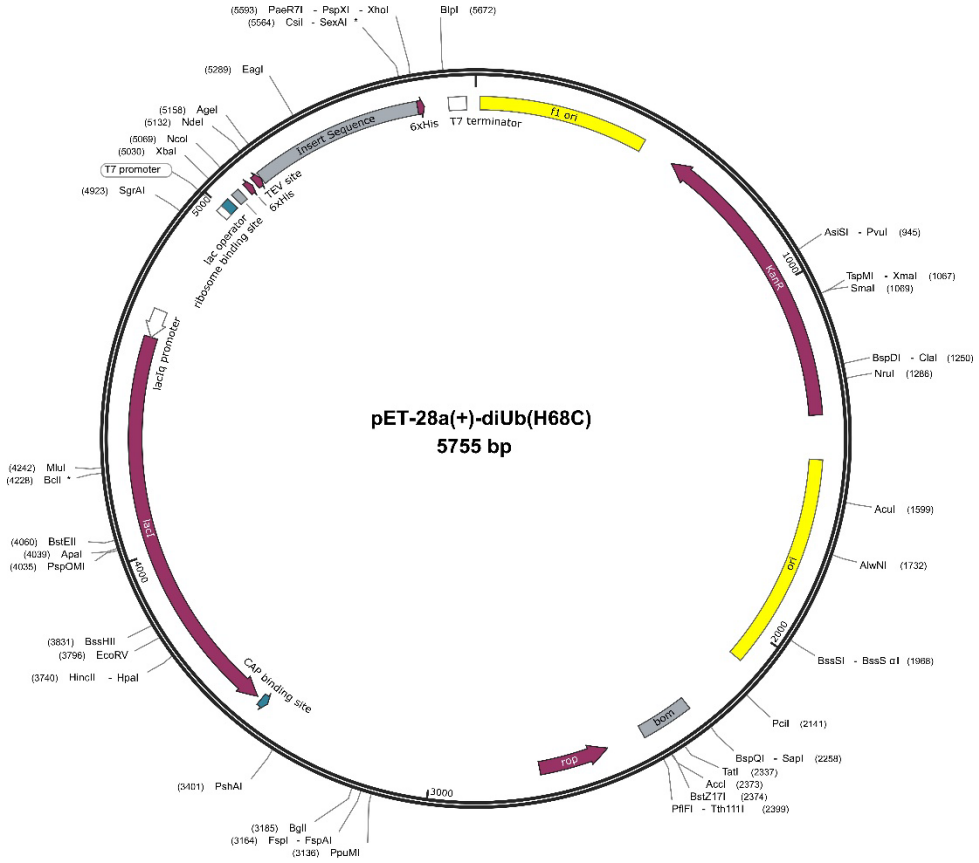

HHHHHHSSGENLYFQGHMQIFVKTLTGKTITLEVEPSDTIE
NVKAKIQDKEGIPPDQQRLIFAGKQLEDGRTLSDYNIQKES
TLCLVLRLRGGMQIFVKTLTGKTITLEVEPSDTIENVKAKI
QDKEGIPPDQQRLIFAGKQLEDGRTLSDYNIQKESTLHLVLR

Expression vector used for the expression of diUb(H68C). The protein sequence is highlighted in green, the cleavage site for TEV is coloured in red and the polyhistidine tag in blue.

8.7.3.3. Adduct Ub(H68C)-1SL

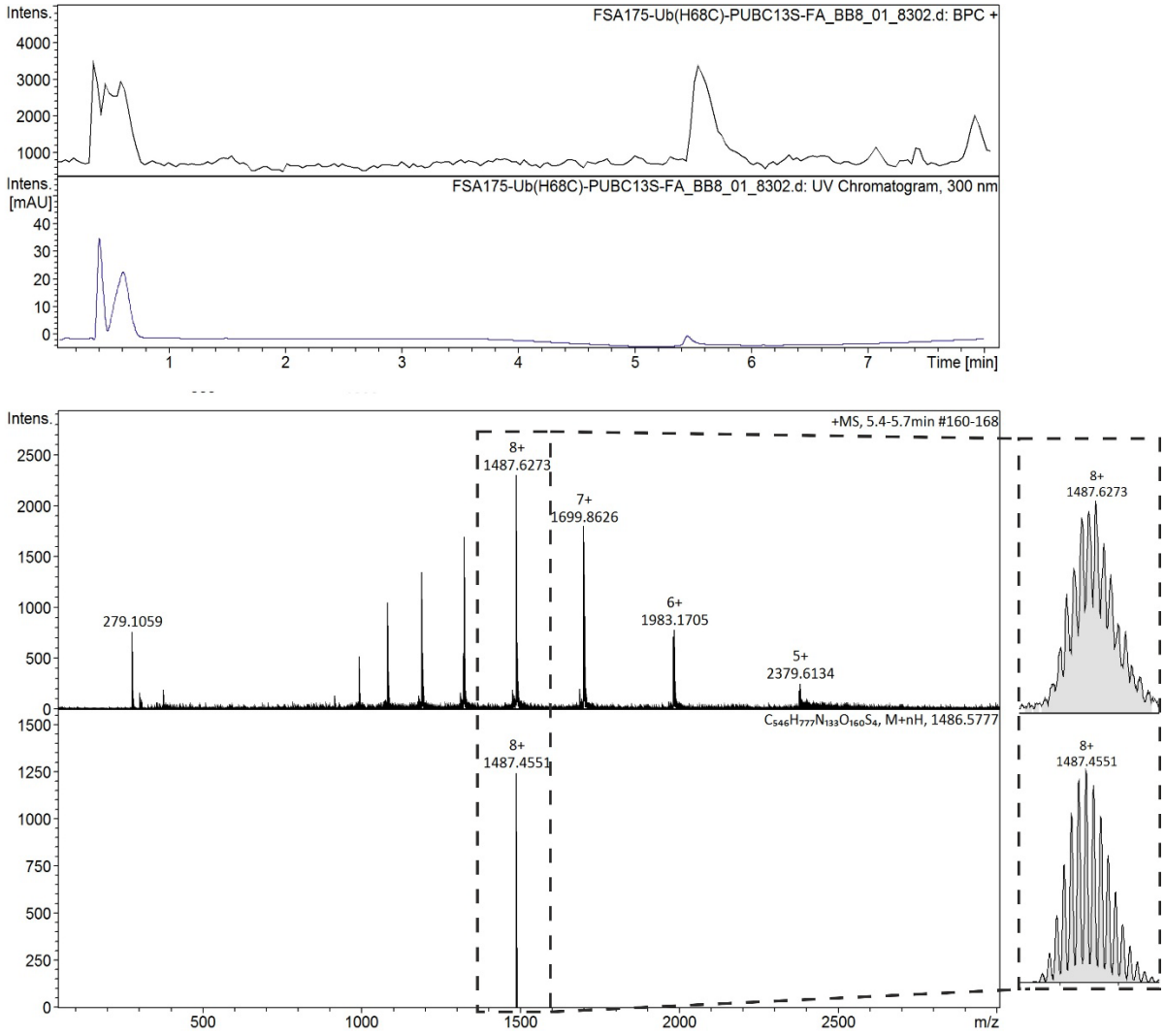

RP-HPLC chromatogram and ESI-MS spectrum of Ub(H68C)-**AOF-1SL**.

HRMS (ESI⁺): *m/z* calculated for $C_{546}H_{777}N_{133}O_{160}S_4$ 1487.4551 $[M+8H]^{8+}$; found 1487.6273 $[M+8H]^{8+}$.

8.7.3.4. Adduct Ub(H68C)-2SL

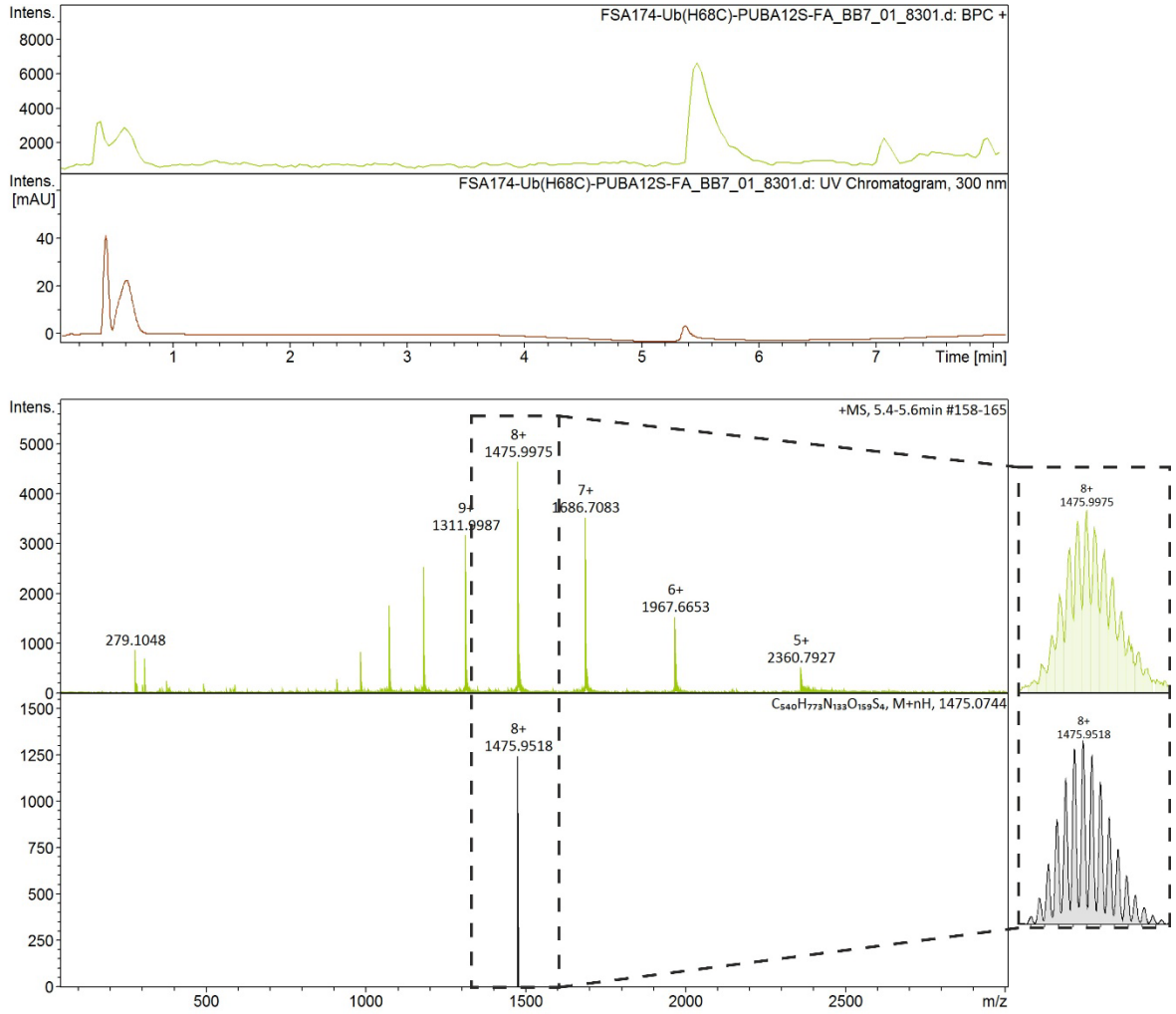

RP-HPLC chromatogram and ESI-MS spectrum of Ub(H68C)-**AOF-2SL**.

HRMS (ESI$^+$): *m/z* calculated for $C_{540}H_{773}N_{133}O_{159}S_4$ 1475.9518 $[M+8H]^{8+}$; found 1475.9975 $[M+8H]^{8+}$.

8.7.3.5. Adduct Ub(H68C)-3SL

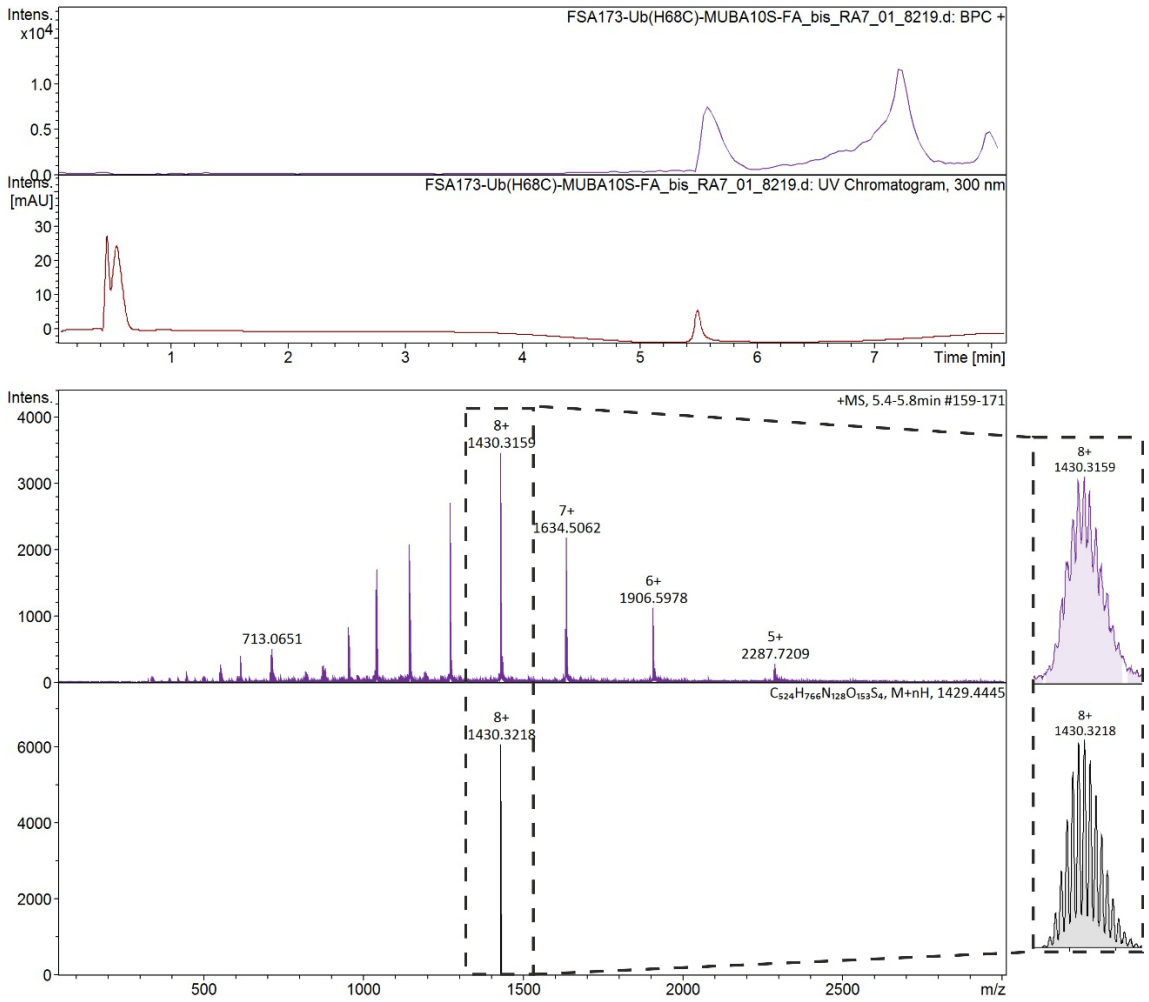

RP-HPLC chromatogram and ESI-MS spectrum of Ub(H68C)-**AOF-3SL**.

HRMS (ESI$^+$): *m/z* calculated for $C_{524}H_{766}N_{128}O_{153}S_4$ 1430.3218 $[M+8H]^{8+}$; found 1430.3159 $[M+8H]^{8+}$.

8.7.3.6. Adduct Ub(H68C)-4LL

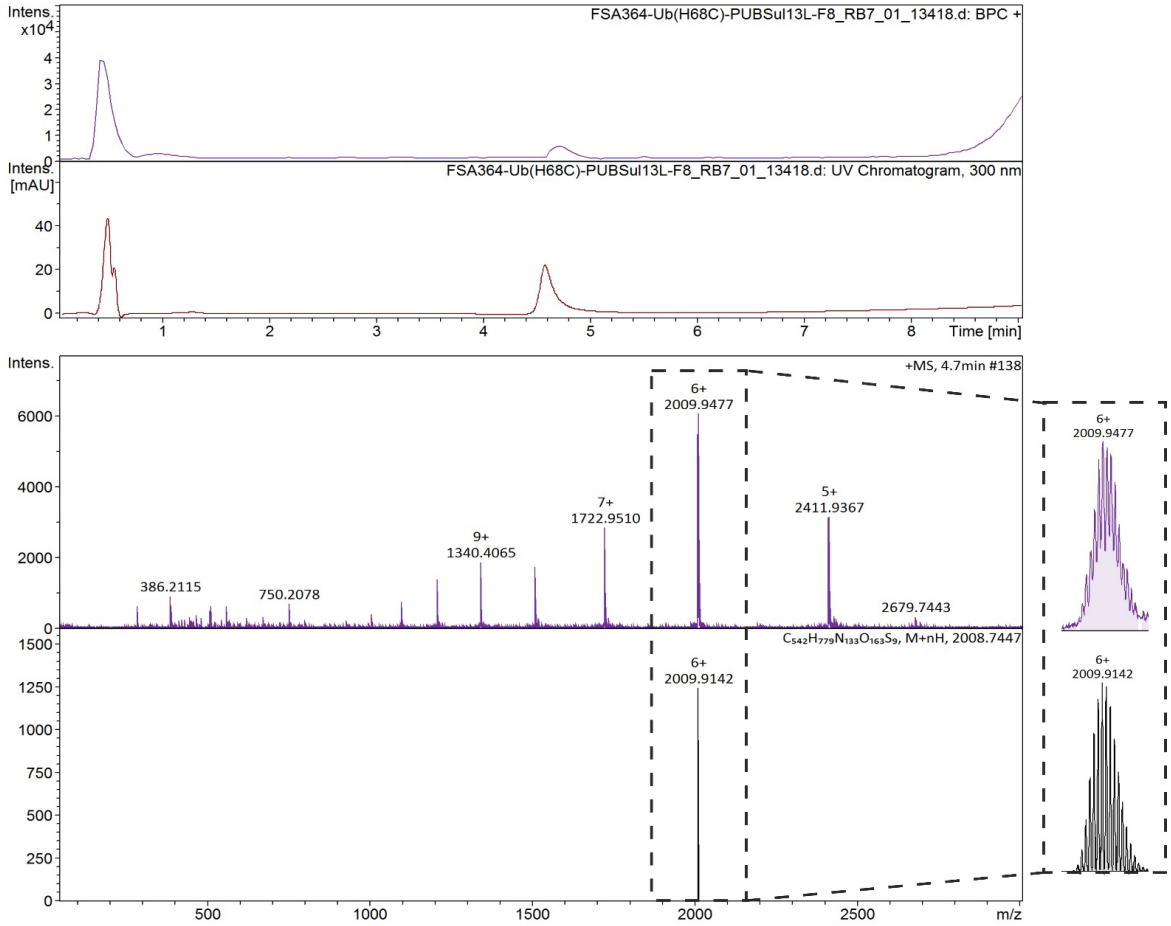

RP-HPLC chromatogram and ESI-MS spectrum of Ub(H68C)-**AOF-4LL**.

HRMS (ESI$^+$): *m/z* calculated for $C_{542}H_{779}N_{133}O_{163}S_9$ 2009.9142 $[M+6H]^{6+}$; found 2009.9477 $[M+6H]^{6+}$.

8.7.3.7. Adduct diUb(H68C)-5LL

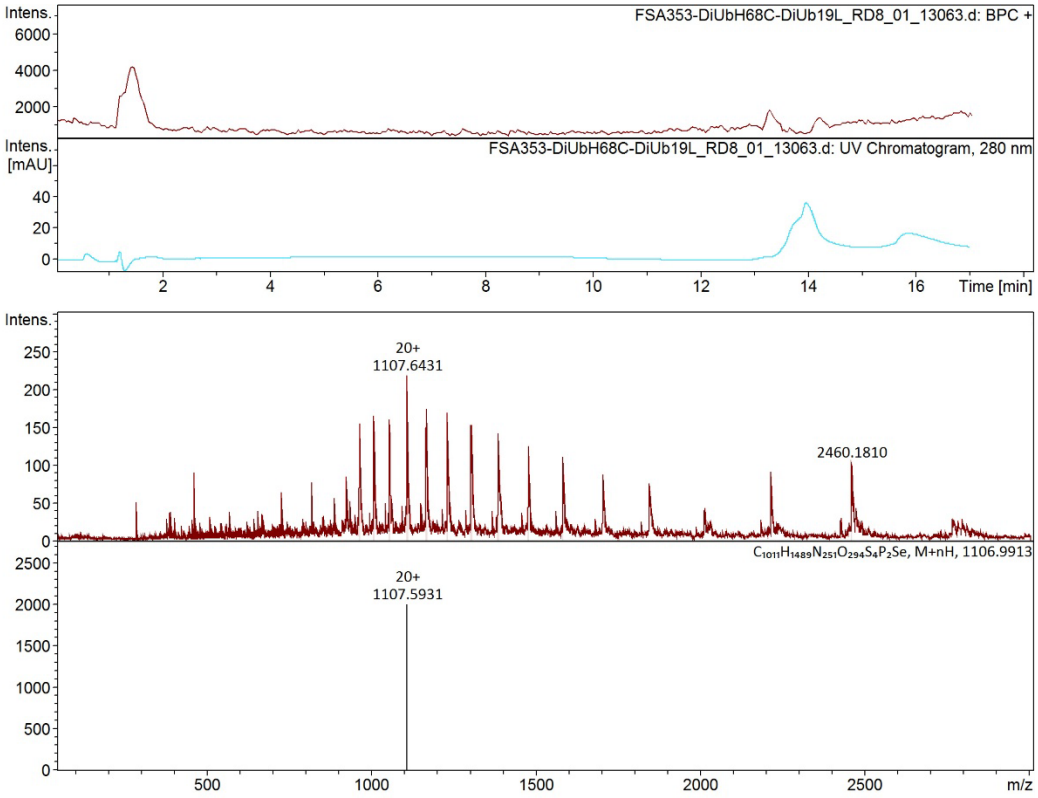

RP-HPLC chromatogram and ESI-MS spectrum of diUb(H68C)-**AOF-5LL**.

HRMS (ESI$^+$): *m/z* calculated for $C_{1011}H_{1489}N_{251}O_{294}S_4P_2Se$ 1107.5931 $[M+20H]^{20+}$; found 1107.6431 $[M+20H]^{+20}$.

8.7.4. Adduct characterisation via NMR

8.7.4.1. ^{15}N-HSQC of Ub(H68C)

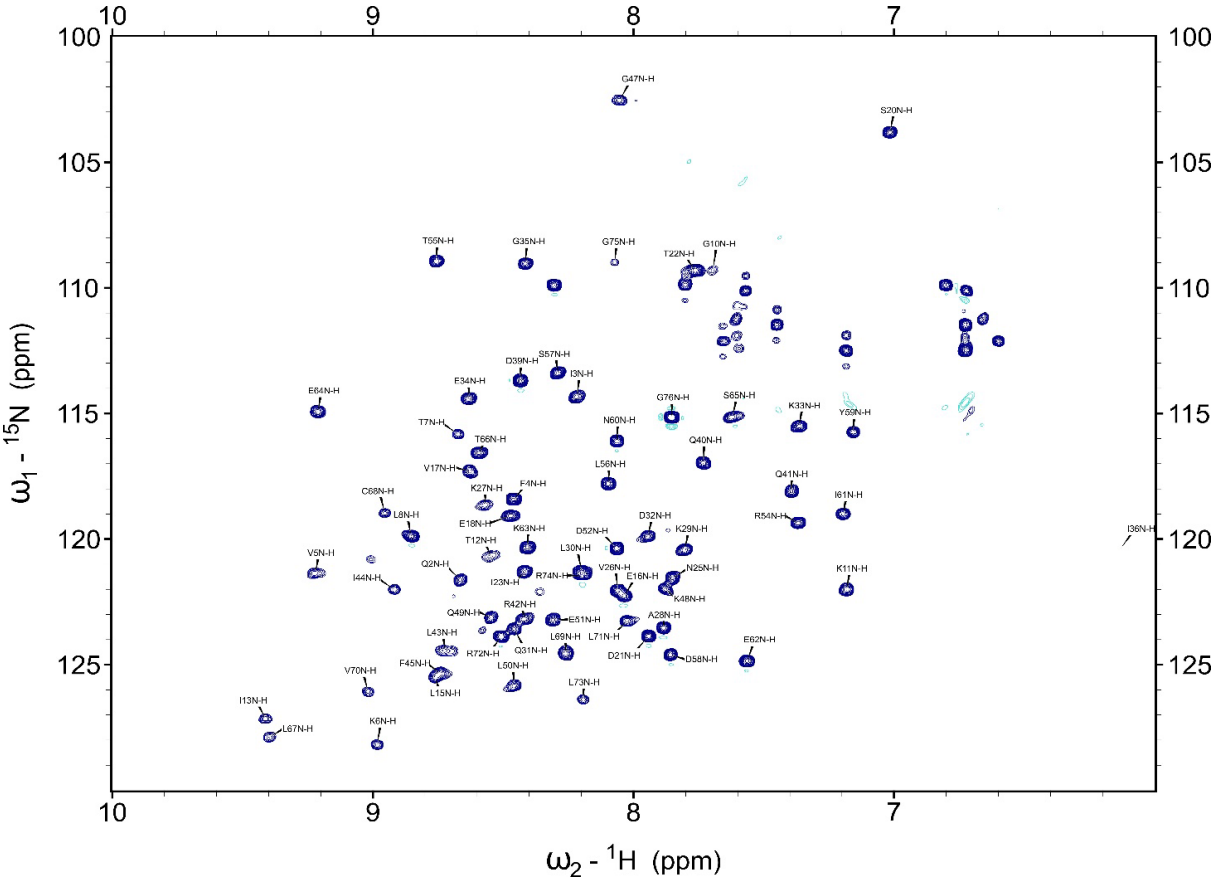

^{1}H,^{15}N-HSQC spectrum at 500 µM of [^{13}C,^{15}N]-Ub(H68C) in TBS at 298K.

8.7.4.2. ^{15}N-HSQC of Ub(H68C)-AOF-1SL

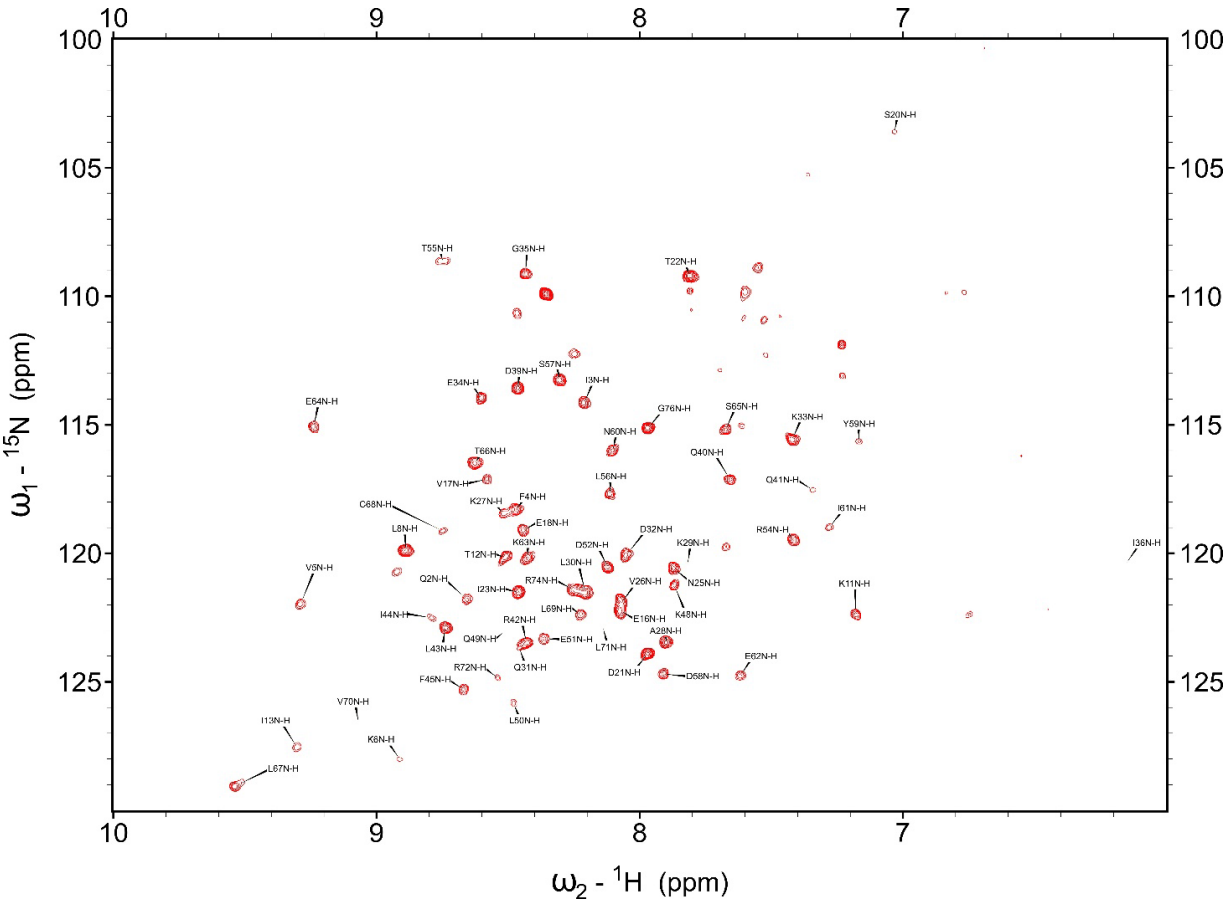

^{1}H,^{15}N-HSQC spectrum at 500 µM of [^{13}C,^{15}N]-Ub(H68C)-**AOF-1SL** in TBS at 298K with 10% (v/v) D_2O.

8.7.4.3. ^{15}N-HSQC of Ub(H68C)-AOF-1SL

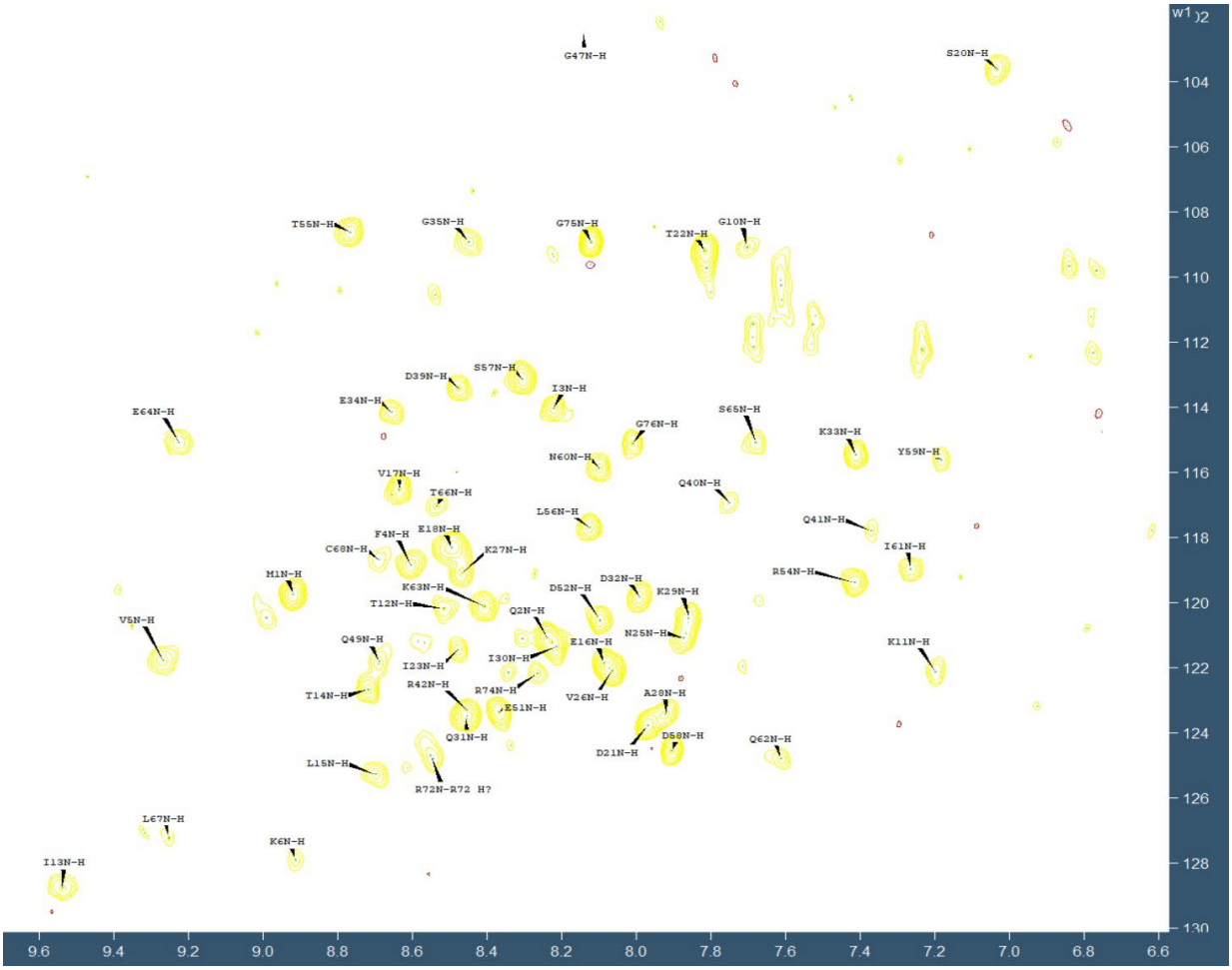

^{1}H,^{15}N-HSQC spectrum at 500 µM of [^{13}C,^{15}N]-Ub(H68C)-**AOF-2SL** in TBS at 298K with 10% (v/v) D_2O.

8.7.4.4. ^{15}N-HSQC of Ub(H68C)-AOF-3SL

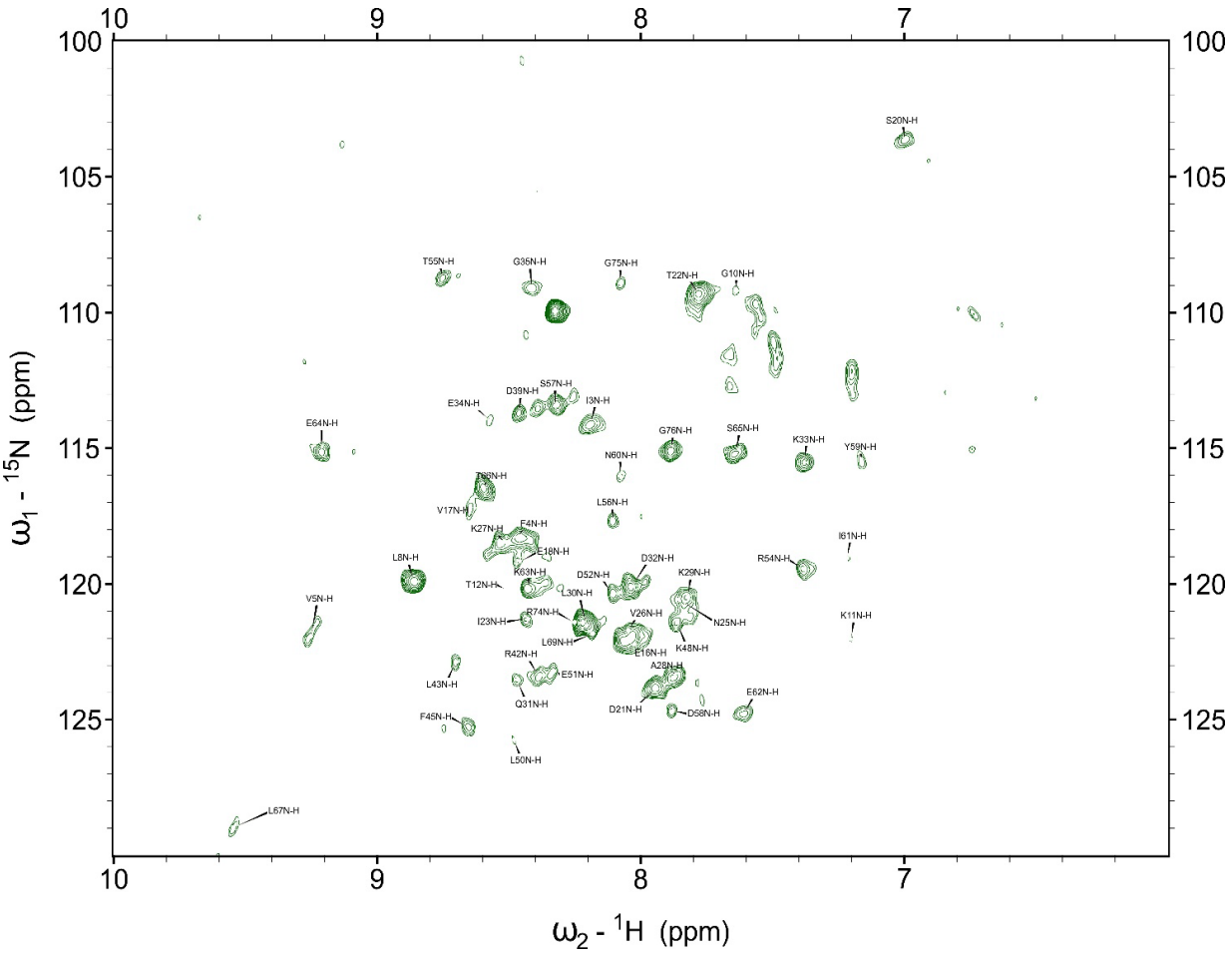

^{1}H,^{15}N-HSQC spectrum at 500 µM of [^{13}C,^{15}N]-Ub(H68C)-**AOF-3SL** in TBS at 298K with 10% (v/v) D_2O.

8.8. References

[1] Z. J. Chen, *Nature Cell Biology* **2005**, *7*, 758-765.

[2] O. M. Siggs, M. Berger, P. Krebs, C. N. Arnold, C. Eidenschenk, C. Huber, E. Pirie, N. G. Smart, K. Khovananth, Y. Xia, G. McInerney, G. B. Karlsson Hedestam, D. Nemazee, B. Beutler, *Proceedings of the National Academy of Sciences* **2010**, *107*, 3046-3051.

[3] C.-J. Wu, in *Cells, Vol. 14*, **2025**.

[4] M. Tsesmelis, U. F. G. Büttner, M. Gerstenlauer, U. Manfras, K. Tsesmelis, Z. Du, N. Sperb, S. E. Weissinger, P. Möller, T. F. E. Barth, H. J. Maier, L. K. Chan, T. Wirth, *Molecular Cancer* **2024**, *23*, 103.

[5] Y.-C. Lo, S.-C. Lin, C. C. Rospigliosi, D. B. Conze, C.-J. Wu, J. D. Ashwell, D. Eliezer, H. Wu, *Molecular Cell* **2009**, *33*, 602-615.

[6] A. Yoshikawa, Y. Sato, M. Yamashita, H. Mimura, A. Yamagata, S. Fukai, *FEBS Letters* **2009**, *583*, 3317-3322.

[7] S. Rahighi, F. Ikeda, M. Kawasaki, M. Akutsu, N. Suzuki, R. Kato, T. Kensche, T. Uejima, S. Bloor, D. Komander, F. Randow, S. Wakatsuki, I. Dikic, *Cell* **2009**, *136*, 1098-1109.

[8] C.-K. Ea, L. Deng, Z.-P. Xia, G. Pineda, Z. J. Chen, *Molecular Cell* **2006**, *22*, 245-257.

[9] C.-J. Wu, D. B. Conze, T. Li, S. M. Srinivasula, J. D. Ashwell, *Nature Cell Biology* **2006**, *8*, 398-406.

[10] S. Bloor, G. Ryzhakov, S. Wagner, P. J. G. Butler, D. L. Smith, R. Krumbach, I. Dikic, F. Randow, *Proceedings of the National Academy of Sciences* **2008**, *105*, 1279-1284.

[11] K. Clark, S. Nanda, P. Cohen, *Nature Reviews Molecular Cell Biology* **2013**, *14*, 673-685.

[12] R. Agrata, D. Komander, *Molecular Cell* **2025**, *85*, 323-346.

[13] S. Vijay-Kumar, C. E. Bugg, W. J. Cook, *Journal of Molecular Biology* **1987**, *194*, 531-544.

[14] S. Rahighi, F. Ikeda, M. Kawasaki, M. Akutsu, N. Suzuki, R. Kato, T. Kensche, T. Uejima, S. Bloor, D. Komander, F. Randow, S. Wakatsuki, I. Dikic, *Cell* **2009**, *136*, 1098-1109.

[15] M. Zwillinger, P. S. Reddy, B. Wicher, P. K. Mandal, M. Csékei, L. Fischer, A. Kotschy, I. Huc, *Chemistry – A European Journal* **2020**, *26*, 17366-17370.

[16] M. Zwillinger, P. Sőregi, F. Sanchez, C. Douat, M. Csékei, I. Huc, A. Kotschy, *The Journal of Organic Chemistry* **2025**, *90*, 3043-3052.

[17] V. Corvaglia, F. Sanchez, F. S. Menke, C. Douat, I. Huc, *Chemistry – A European Journal* **2023**, *29*, e202300898.

[18] M. Vallade, M. Jewginski, L. Fischer, J. Buratto, K. Bathany, J.-M. Schmitter, M. Stupfel, F. Godde, C. D. Mackereth, I. Huc, *Bioconjugate Chemistry* **2019**, *30*, 54-62.

[19] L. Wang, C. Douat, J. Sigl, P. Sai Reddy, L. Fischer, B. L. d'Estaintot, Z. Liu, V. Pophristic, Y. Yang, Y. Zhang, I. Huc, *Chemical Science* **2025**, *16*, 12385-12396.

[20] P. H. Zwart, R. W. Grosse-Kunstleve, P. D. Adams, **2005**.

[21] G. Bunkoczi, N. Echols, A. J. McCoy, R. D. Oeffner, P. D. Adams, R. J. Read, *Acta Crystallographica Section D* **2013**, *69*, 2276-2286.

[22] X. Hu, S. J. Dawson, P. K. Mandal, X. de Hatten, B. Baptiste, I. Huc, *Chemical Science* **2017**, *8*, 3741-3749.

[23] B. Baptiste, C. Douat-Casassus, K. Laxmi-Reddy, F. Godde, I. Huc, *The Journal of Organic Chemistry* **2010**, *75*, 7175-7185.

[24] M. Vallade, P. Sai Reddy, L. Fischer, I. Huc, *European Journal of Organic Chemistry* **2018**, *2018*, 5489-5498.

[25] D. Bindl, E. Heinemann, P. K. Mandal, I. Huc, *Chemical Communications* **2021**, *57*, 5662-5665.

[26] L. Wang, J. M. Rogers, S. J. Dawson, L. M. Langhorn, R. T. Howard, S. Kwon, C. Douat, H. Suga, I. Huc, *Organic & Biomolecular Chemistry* **2025**, *23*, 4641-4647.

[27] D. Bindl, P. K. Mandal, I. Huc, *Chemistry – A European Journal* **2022**, *28*, e202200538.

[28] S. Kwon, V. Morozov, L. Wang, P. K. Mandal, S. Chaignepain, C. Douat, I. Huc, *Organic & Biomolecular Chemistry* **2024**, *22*, 9342-9347.

9. Conclusion and perspectives

9.1. Summary of the thesis projects

The projects presented in this thesis underscore the potential and versatility of aromatic oligoamide foldamers (AOFs) for protein recognition and for targeting biologically relevant molecules. Leveraging the chemical robustness of organic quinoline precursors, which can withstand extensive modifications, we developed a new library of building blocks designed to promote protein interaction via newly synthesised biogenic side chains. These side chains span a range of chemical properties, including cationic, anionic, hydrophobic, and polar neutral functionalities.

We explored multiple synthetic routes to obtain monomers substituted at various positions on the quinoline ring, thereby increasing the likelihood of effective protein interaction. Notably, the inclusion of di-substituted monomers allowed for enhanced side chain density within the AOF backbone. Using this expanded library, we successfully optimised oligomer synthesis on an automated synthesiser.

Through investigation of the mechanistic challenges encountered under *in situ* conditions, we were able to standardise protocols for the rapid production of long oligomers with high purity. These advances significantly improve access to longer and more diverse AOF sequences, broadening the scope for targeting complex biological systems.

Using our robust AOFs as target candidates, we demonstrated their ability to bind two structurally distinct protein scaffolds: a β-sheet-based protein (C10) and a three-α-helix bundle (G02), each identified through independent display selections. Solution-phase techniques (NMR, CD, and BLI), alongside structural studies (X-ray crystallography), revealed that binding occurs in an enantioselective manner and is primarily driven by the hydrophobic cross-section of the foldamer.

Crystallographic analysis of the G02 complex, complemented by scanning mutagenesis experiments, confirmed the contribution of key protein residues and specific AOF side chains in modulating binding affinity. Building on these insights, and to test our ability to rationally predict and design molecular interactions, we synthesised a series of AOF variants. These were engineered to selectively discriminate between the two protein targets by incorporating targeted mutations on the AOF side chains, with the goal of enhancing affinity for one scaffold while reducing it for the other. Although no AOF has yet been identified for this specific purpose, ongoing investigations continue with the aim of

discovering strong candidates capable of discriminating binding interactions between the two selected proteins.

In an effort to target a bio-relevant protein complex between linear di-ubiquitin and the coiled-coil domain of NEMO, we modelled and designed AOF candidates to mimic the interaction interface between coiled-coil NEMO and the ubiquitin surface. Each AOF was equipped with covalent linkers installed via triphosgene activation and featured an activated disulphide for chemical ligation to the protein.

Solution-state NMR studies confirmed that the AOF candidates, once ligated to the protein surface, exerted an influence on the local environment. However, crystallisation of these adducts was unsuccessful. Incorporating a longer covalent linker and different solvent-exposed side chains into one of the AOF designs led to highly reproducible crystal formation. Unfortunately, due to limited diffraction resolution and a large asymmetric unit, the structure of this covalent adduct could not be solved.

Further investigation of the Ub(H68C)-AOF adduct remains promising, with sulphur-SAD phasing considered as a potential strategy for future structural determination. Current efforts have refocused on the original target, linear di-ubiquitin, employing extended AOF candidates with newly designed building blocks to explore the boundaries of automated synthesis. Crystallisation screening is ongoing and may yield the first structural insights into mimicking the side-chain arrangement of coiled-coil NEMO.

9.2. Perspectives

This work has demonstrated the potential of AOF scaffolds to engage in protein interactions, and while we successfully characterised several protein-AOF complexes with different scaffolds, a recurring challenge remains: the aromatic cross-section of our AOFs continues to dominate binding, limiting the contribution of side chains to overall affinity.

To address this, we initiated the design of a second generation AOF, guided by a broader library of building-block monomers described in **section 5**. By exploring new substitution patterns on the quinoline ring, we developed a candidate that presents a flat surface decorated with proteinogenic side chains, offering a wider landscape for interaction. A strategic shift was also made in the anchoring approach, which was to change from N-terminal biotinylation to a side-chain-based biotin anchor. This required the development of a new monomer with selective acid lability, allowing precise on-resin deprotection and biotin moiety coupling (**Figure 22**).

To further reduce non-desired interactions and improve solubility, long tetraethyleneglycol chains were introduced on different faces of the AOF, while other side chains were chosen for their solubilising properties. To eliminate aromatic cross-section bias, which was the main goal, both termini were capped with sterically hindering moieties: aminoisobutyric acid (Aib) at the C-terminus and an ethyleneglycol-based group (PEG) at the N-terminus.

This AOF candidate was submitted to phage display selection against a large affibody library, following the story outlined in **section 7**. The selection yielded a promising affibody clone, E02. While solution and solid-state studies are still ongoing, they hold the potential to reveal an affibody-AOF complex driven by side-chain interactions rather than aromatic cross-section.

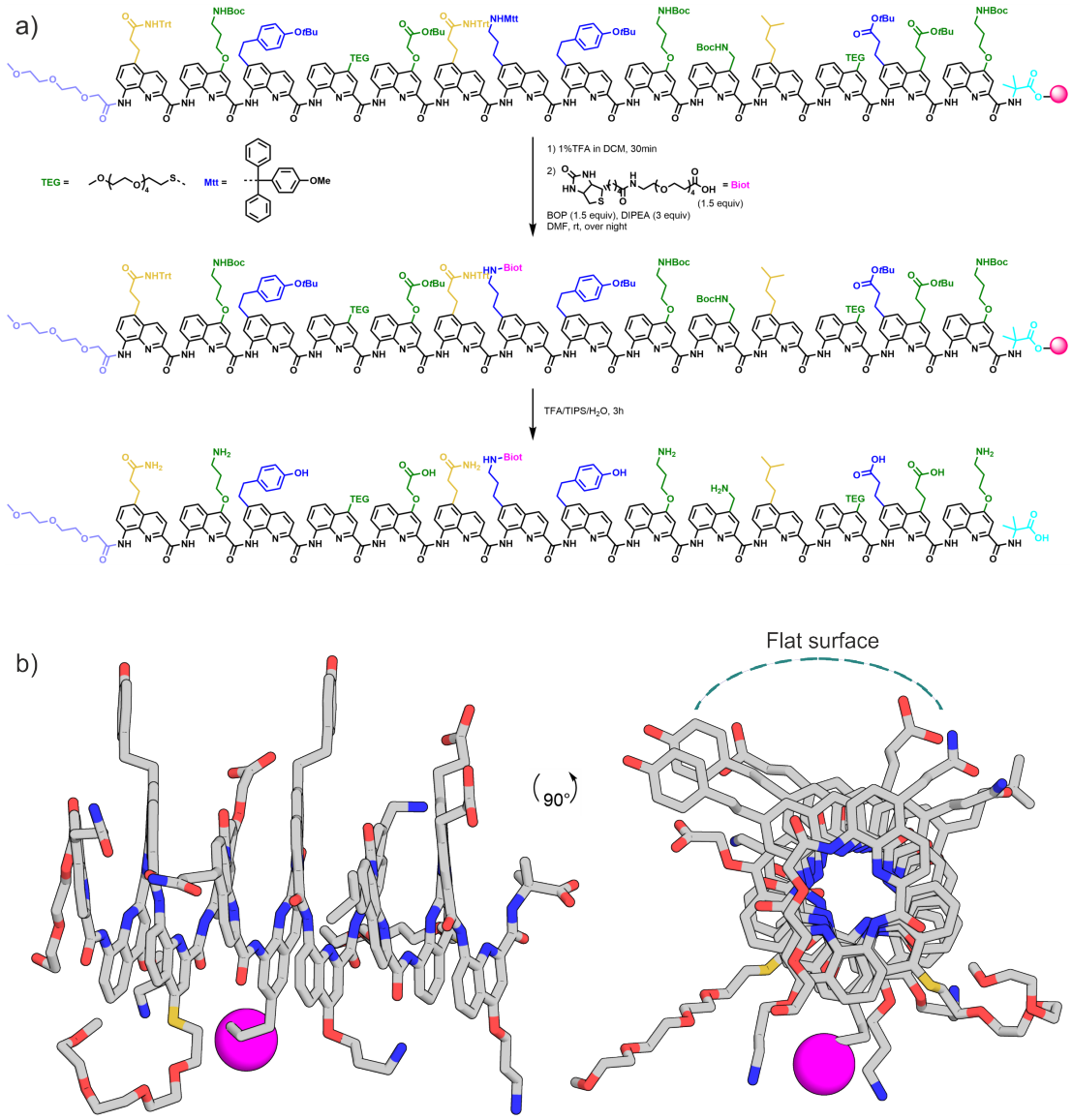

Figure 22. a) Schematic description of the synthesis of new AOF candidate with selective deprotection of Mtt group, followed by coupling of biotin-linker coupling. b) Model of target AOF candidate in side and top view, the pink sphere represent the biotin linker added. The flat surface is highlighted on the top view on the right.

These efforts mark a meaningful step toward designing more selective and bio-relevant protein binders. The results of these investigations will be published in due course and will hopefully contribute to the broader understanding of molecular recognition with AOFs.

As this chapter closes, the tools, strategies, and insights developed here lay strong basis for future exploration, toward more refined molecular architectures, and deeper control over protein-ligand interactions.